NTIS # PB2008-

SSC-451

MECHANICAL COLLAPSE TESTING ON ALUMINUM STIFFENED PANELS FOR MARINE APPLICATIONS

SHIP STRUCTURE COMMITTEE
2008

Ship Structure Committee

RADM Brian M. Salerno
U. S. Coast Guard Assistant Commandant,
Assistant Commandant for Marine Safety, Security and Stewardship
Chairman, Ship Structure Committee

{Name}
{Title}
Naval Sea Systems Command

Dr. Roger Basu
Senior Vice President
American Bureau of Shipping

Mr. Joseph Byrne
Director, Office of Ship Construction
Maritime Administration

Mr. William Nash
Director General, Marine Safety,
Safety & Security
Transport Canada

Mr. Kevin Baetsen
Director of Engineering
Military Sealift Command

Dr. Neil Pegg
Group Leader - Structural Mechanics
Defence Research & Development Canada - Atlantic

CONTRACTING OFFICER TECHNICAL REP.
Mr. Chao Lin / MARAD
Mr. Glenn Ashe / ABS
DRDC / USCG

EXECUTIVE DIRECTOR
Lieutenant Commander, Jason Smith
U. S. Coast Guard

SHIP STRUCTURE SUB-COMMITTEE

AMERICAN BUREAU OF SHIPPING

Mr. Glenn Ashe
Mr. Derek Novak
Mr. Phil Rynn
Mr. Balji Menon

DEFENCE RESEARCH & DEVELOPMENT CANADA ATLANTIC
Dr. David Stredulinsky
Mr. John Porter

MARITIME ADMINISTRATION
Mr. Chao Lin
Mr. Carl Setterstrom
Mr. Richard Sonnenschein

MILITARY SEALIFT COMMAND
Mr. Michael W. Touma
Mr. Paul Handler

ONR / NAVY/ NSWCCD
{Name}
{Name}
{Name}
{Name}

TRANSPORT CANADA
Paul Denis Vallee

US COAST GUARD

CDR Charles Rawson
Mr. James Person
Mr. Rubin Sheinberg

SOCIETY OF NAVAL ARCHITECTS AND MARINE ENGINEERS
Mr. Jaideep Sirkar
Mr. Al Rowen
Mr. Norman Hammer

Address Correspondence to:

Executive Director
Ship Structure Committee
U.S. Coast Guard (CG-5212/SSC)
2100 2nd Street, SW
Washington, D.C. 20593-0001
Web site: http://www.shipstructure.org

SSC – 451
SR – 1446

OCTOBER 3, 2008

MECHANICAL COLLAPSE TESTING ON ALUMINUM STIFFENED PANELS FOR MARINE APPLICATIONS

The benefits of using aluminum alloys are well recognized, particularly for the design and construction of warships and high speed vessels. The size of such ships is increasing, causing various related design challenges compared to vessels with shorter length.

Unlike steel structures, for aluminum structures there are no refined ultimate limit state (ULS) design methods involving local and overall ULS assessment. Theoretical and numerical methodologies for ULS design must be validated prior to their general applications.

The aim of this research project was to investigate the ultimate strength characteristics of aluminum stiffened plate structures considering the effects of weld induced initial imperfections. A total of 78 aluminum single and multi bay stiffened plate prototype structures were used in this project. Such a large scale SSC project would not have been possible without the support of Alcan Marine, France for providing the material and Hanjin Heavy Industries, Korea for providing the fabrication of the test panels. The database and insights developed from the project will be useful for Ultimate Limit State (ULS) design and strength assessment of aluminum stiffened plate structures often used in very large high speed ships.

BRIAN M. SALERNO
Rear Admiral, U.S. Coast Guard
Chairman, Ship Structure Committee

Technical Report Documentation Page

<table>
<tr><td>1. Report No.
SSC - 451</td><td>2. Government Accession No.</td><td colspan="2">3. Recipient's Catalog No.</td></tr>
<tr><td colspan="2" rowspan="2">4. Title and Subtitle
Mechanical Collapse Testing on Aluminum Stiffened Panels for Marine Applications</td><td colspan="2">5. Report Date
March. 1, 2007</td></tr>
<tr><td colspan="2">6. Performing Organization Code</td></tr>
<tr><td colspan="2">7. Author(s)
J.K.Paik, A K Thayamballi, J Y Ryu, J H Jang, J K Seo, S W Park, S K Soe, C Renaud, and N I Kim</td><td colspan="2">8. Performing Organization Report No.
SR-1446</td></tr>
<tr><td colspan="2" rowspan="2">9. Performing Organization Name and Address
National Pusan University</td><td colspan="2">10. Work Unit No. (TRAIS)</td></tr>
<tr><td colspan="2">11. Contract or Grant No.</td></tr>
<tr><td colspan="2" rowspan="2">12. Sponsoring Agency Name and Address
Ship Structure Committee
C/O Commandant (CG-3PSE/SSC)
United States Coast Guard
2100 2nd Street, SW
Washington, DC 20593-0001</td><td colspan="2">13. Type of Report
Final Report</td></tr>
<tr><td colspan="2">14. Sponsoring Agency Code
CG - 5</td></tr>
<tr><td colspan="4">15. Supplementary Notes
Sponsored by the Ship Structure Committee and its member agencies</td></tr>
<tr><td colspan="4">**16. Abstract**
The ultimate strength characteristics of 78 aluminum stiffened prototype panels under axial compressive loads are investigated experimentally and numerically. The objective of this research is to develop a marine application for ULS design methodology of aluminum stiffened panels.

High strength aluminum alloys are increasingly being used for building high-speed vessels as well as other types of weight-critical structures. In the past, criteria and procedures for the design of aluminum-plated structures were primarily based on allowable stresses and simplified buckling checks for structural components. However, the ULS is a much better basis for structural design because it is difficult to determine the real safety margin of any structure using linear elastic methods alone. It is of crucial importance to determine the true ultimate limit state if one is to obtain consistent measures of safety which can then form a fairer basis for comparisons of structures of different sizes, types, and characteristics.

This SSC study was undertaken at Pusan National University, Korea with generous support provided by Alcan Marine, France who provided all the material and Hanjin Heavy Industries, Korea who created the 78 prototype panels.</td></tr>
<tr><td colspan="2">17. Key Words</td><td colspan="2">18. Distribution Statement
Distribution Available From:
National Technical Information Service
U.S. Department of Commerce
Springfield, VA 22151
Ph. (703) 605-6000</td></tr>
<tr><td>19. Security Classif. (of this report)
Unclassified</td><td>20. Security Classif. (of this page)
Unclassified</td><td>21. No. of Pages</td><td>22. Price</td></tr>
</table>

CONVERSION FACTORS
(Approximate conversions to metric measures)

To convert from	to	Function	Value
LENGTH			
inches	meters	divide	39.3701
inches	millimeters	multiply by	25.4000
feet	meters	divide by	3.2808
VOLUME			
cubic feet	cubic meters	divide by	35.3149
cubic inches	cubic meters	divide by	61,024
SECTION MODULUS			
$inches^2$ $feet^2$	$centimeters^2$ $meters^2$	multiply by	1.9665
$inches^2$ $feet^2$	$centimeters^3$	multiply by	196.6448
$inches^4$	$centimeters^3$	multiply by	16.3871
MOMENT OF INERTIA			
$inches^2$ $feet^2$	$centimeters^2$ meters	divide by	1.6684
$inches^2$ $feet^2$	$centimeters^4$	multiply by	5993.73
$inches^4$	$centimeters^4$	multiply by	41.623
FORCE OR MASS			
long tons	tonne	multiply by	1.0160
long tons	kilograms	multiply by	1016.047
pounds	tonnes	divide by	2204.62
pounds	kilograms	divide by	2.2046
pounds	Newtons	multiply by	4.4482
PRESSURE OR STRESS			
$pounds/inch^2$	$Newtons/meter^2$ (Pascals)	multiply by	6894.757
kilo $pounds/inch^2$	mega $Newtons/meter^2$ (mega Pascals)	multiply by	6.8947
BENDING OR TORQUE			
foot tons	meter tons	divide by	3.2291
foot pounds	kilogram meters	divide by	7.23285
foot pounds	Newton meters	multiply by	1.35582
ENERGY			
foot pounds	Joules	multiply by	1.355826
STRESS INTENSITY			
kilo $pound/inch^2$ $inch^{½}$(ksi√in)	mega Newton $MNm^{3/2}$	multiply by	1.0998
J-INTEGRAL			
kilo pound/inch	$Joules/mm^2$	multiply by	0.1753
kilo pound/inch	kilo $Joules/m^2$	multiply by	175.3

Table of Contents

List of Figures

List of Tables

Acknowledgements

The present work was supported by the Ship Structure Committee (http://www.shipstructure.org), a North American based interagency research and development committee, in association with SR-1446 project, together with Alcan Marine, France. The author is very pleased to acknowledge their support.

The author likes to thank the members of the SSC Project Technical Committee - H.P. Cojeen (Chairman), Y.S. Choo, M.D. Collette, P. Franklin, P.A. Frieze, P. Hess III, W. Mish, J. Sirkar, A. Tunik, and X. Wang, who provided valuable comments and suggestions.

This work was undertaken at the Ship and Offshore Structural Mechanics Laboratory (SSML) at Pusan National University, Korea, which is a National Research Laboratory funded by the Korea Ministry of Science and Technology. The author is pleased to thank graduate students at the SSML, for their efforts regarding mechanical model testing and numerical computations. Sincere thanks are also due to Hanjin Heavy Industries & Construction Company which carried out the MIG welding fabrication of all test structures studied in the present study.

Executive Summary

The present report describes the results and insights developed from the SR-1446 research project, sponsored by the Ship Structure Committee, together with the support of Alcan Marine, France. The shipyard of Hanjin Heavy Industries & Construction Company, Korea built the entire test structures used for the present project.

During the last decade, high strength aluminum alloys have been increasingly applied for the design and construction of high speed vessels; and over the same time the size of high speed vessels has grown and their operation has moved into increasingly harsher ocean-going environments. Subsequently, the design and building process to ensure the structural safety of aluminum high speed vessels has become more complex in terms of strength or reliability analysis and fabrication quality control.

During their lifetime, the structures are subjected to various types of loading which is for the most part operational, but may in some cases be extreme or even accidental. In the past, criteria and procedures for the design of aluminum plated structures were primarily based on allowable working stresses and simplified buckling checks for structural components. However, it is now well recognized that the ultimate limit state (ULS) approach is a much better basis for structural design and strength assessment, because it is not possible to determine the true margin of safety as long as the ultimate limit state remains unknown.

It also readily follows that it is of crucial importance to determine the true ULS (or ultimate strength) if one is to obtain consistent measures of structural safety which can then form a fairer basis for comparisons of structures of different sizes, types and characteristics. An ability to better assess the true margin of structural safety would also inevitably lead to improvements in related regulations and design requirements as well.

An aluminum plated structure is typically composed of plate panels and extruded support members (stiffeners). The overall failure of the structure is certainly affected and can be governed by the buckling and plastic collapse of these individual members. In ULS design, therefore, a primary task is to accurately calculate the ultimate strength of such structural components.

In contrast to steel stiffened plate structures which have plentiful information about the weld induced initial imperfections, the related information of aluminum structures is very lacking so far. The lack of related database can make the structural design and strength assessment results uncertain. Therefore, it is very important to develop database of weld induced initial imperfections which can occur during fabrication of aluminum structures. This was one of the major multiple motives that the present project was initiated.

Until now, the mechanical test database on buckling collapse of aluminum stiffened plate structures is very lacking specifically on full scale prototype structures, in contrast to steel stiffened plate structures which have relatively plentiful information. It is recognized that the buckling collapse characteristics of aluminum stiffened plate structures differ from those of steel counterparts. This is partly due to the fact that the softening in the heat affected zone (HAZ) as well as other influential parameters such as initial imperfections, geometric and material properties is a primary parameter affecting the buckling collapse characteristics of aluminum structures unlike steel structures.

Also, due to lack of information about initial imperfections of welded aluminum structures, the ULS design formulations available for steel structures cannot be directly applied to aluminum structures even though the corresponding material properties are properly accounted for. Therefore, the ULS design formulae suitable for aluminum structural components should be developed separately against steel structural components.

Previously, most studies in the areas of the ultimate strength of aluminum ship panels were undertaken for the standard aluminum alloys such as 5083. While it is recognized that 5383 alloy developed by Alcan Marine, France is a better material than the standard aluminum alloys in terms of welded mechanical properties, among other factors, and as such is considered as the foremost material for building high speed vessels, related studies on the ultimate strength of 5383 alloy panels are needed to complete the characterization of this alloy.

The aims and scope of the present research project cover the following aspects:

(1) Develop the relevant design database in terms of the statistics of initial imperfections that occur during welding fabrication of aluminum stiffened plate structures for marine applications,

(2) Develop the mechanical test database on buckling collapse behavior of aluminum stiffened plate structures obtained using full scale prototype models,

(3) Compare the nonlinear finite element method solutions for the prototype test structures with experimental results,

(4) Develop closed-form ULS design formulae for aluminum stiffened plate structures under predominantly axial compressive actions.

In the present research project, a total of 78 single and multi-bay aluminum stiffened plate (ship-shaped) structures, which are full scale equivalent to sub-structures of an 80m long all aluminum high speed vessel, are constructed by metal inert gas (MIG) welding. The material of plating and stiffeners is varied, using 5083-H116 (rolled), 5383-H116 (rolled), 5383-H112 (extruded) and 6082-T6 (extruded) aluminum alloys which are today the most popular types of aluminum material for marine applications. The types and dimensions of the structures are also varied with different types of stiffeners (flat, built-up T-bar, extruded T-bar), stiffener web height, thickness of plating and stiffener, and principal panel dimensions, in addition to the number of -frame bays.

The database and insights developed from the present research project will be very useful for design and building of welded aluminum ocean-going high-speed ship structures in association with reliability analyses and code calibrations of ULS strength and fabrication quality assurance.

Nomenclature

A = cross sectional area of stiffener with attached plating
a = plate length between transverse frames
b = plate breadth between longitudinal stiffeners
t = thickness of plating
b_f = breadth of stiffener flange
b_t = breadth of tensile residual stress block
b'_p = breadth of the HAZ in plating
b'_s = breadth of the HAZ in stiffener web
E = modulus of elasticity (Young's modulus)
h_w = height of stiffener web
I = moment of inertia of stiffener with attached plating
L = a = plate length between transverse frames
$r = \sqrt{I/A}$ = radius of gyration of a plate-stiffener combination
t = plate thickness
t_f = thickness of stiffener flange
t_w = thickness of stiffener web
w_o = initial distortion of plating
w_{o1} = amplitude of one half wave initial distortion of plating
w_{ob} = $w_{opl} - w_{o1}$ = amplitude of local distortion of plating
w_{om} = amplitude of buckling half wave initial distortion of plating
w_{opl} = maximum initial distortion of plating
w_o^c = column type initial distortion of stiffener
w_{oc} = maximum column type initial distortion of stiffener
w_{o1}^c = amplitude of one half wave column type initial distortion of stiffener
w_o^s = sideways initial distortion of stiffener
w_{os} = maximum sideways initial distortion of stiffener
w_{o1}^s = amplitude of one half wave sideways initial distortion of stiffener
β = non-dimensional plate slenderness ratio $= (b/t)\sqrt{\sigma_Y/E}$
$\lambda' = \frac{a}{\pi r}\sqrt{\frac{\sigma_{Yeq}}{E}}$ = column slenderness ratio
ε_f = fracture strain
σ_{rcx} = compressive residual stress in the x direction
σ_{rtx} = tensile residual stress in the x direction
σ_T = ultimate tensile stress
σ_Y = σ_{Yp} = yield stress of plating
$\sigma_{Yeq} = \left[bt\sigma_{Yp} + (h_w t_w + b_f t_f)\sigma_{Ys}\right]/A$ = equivalent yield stress of the entire stiffened panel
σ_{Ys} = yield stress of stiffener
ν = Poisson's ratio

Chapter 1 Introduction

The use of high strength aluminum alloys in shipbuilding provides many benefits but also presents many challenges. The benefits of using aluminum versus steel include lighter weight, which helps increase cargo capacity and/or reduce power requirements, excellent corrosion resistance and low maintenance. Challenges include reduced stiffness causing greater sensitivity to deformation, buckling, and plastic collapse and different welding practices.

The benefits noted above are now well recognized, particularly for the design and construction of war ships, littoral surface crafts and littoral combat ships as well as high-speed passenger ships. The size of such ships is increasing, causing various related design challenges compared to vessels with shorter length. In addition to aluminum alloys being less stiff than mild steel, no refined ultimate limit state (ULS) design methods involving local and overall ULS assessment exist unlike steel structures where the necessary information is plentiful.

Lack of information on fabrication related initial imperfections, including initial distortions, residual stresses and material softening in the heat affected zone (HAZ) due to welding, can in particular make the design and building process for aluminum vessels relatively more uncertain than their steel counterparts which have plentiful information. Theoretical and numerical methodologies for ULS design must of course be validated prior to their general applications by comparisons with appropriate experimental databases, taking into account the influences of fabrication related initial imperfections. For reliability analyses and code calibrations in association with ultimate limit states, fabrication related initial imperfections must be defined in a more appropriate way as precisely as possible.

The aim of the present research project is to investigate the buckling ultimate strength characteristics of aluminum stiffened plate structures considering the effects of weld-induced initial imperfections. Theoretical and experimental investigations in the literature have demonstrated that strength and stiffness of structures are significantly influenced by initial imperfections that can occur during welding fabrication of aluminum stiffened plate structures for marine applications.

In welded steel structures, a relatively large pool of information describing the characteristics of weld-induced initial imperfections in the form of initial distortions and residual stresses are found in the literature. This is beneficial in terms of developing relevant strength criteria taking into account the influence of initial imperfections.

On the other hand, the characteristics of fabrication related initial imperfections in welded aluminum structures are more complex than those in welded steel structures and the related information is so far very lacking. In addition to initial distortions and residual stresses, the complexity arises partly from the fact that during welding, the aluminum material in the HAZ is typically softened, resulting in the reduction of strength properties of the HAZ material unlike welded steel structures.

Related to the study of fabrication related initial imperfections in welded steel structures, extensive surveys of weld induced initial distortions of steel plating used for ships and box girder bridges have been undertaken in terms of the initial distortion statistics and their effects on plate strength and stiffness. These include Kmiecik (1970), Bradfield (1974), Ellis (1977), Faulkner (1975), Czujko & Kmiecik (1975), Somerville et al. (1977), Carlsen & Czujko (1978), Antoniou (1980), Masubuchi (1980), Kmiecik (1981), Antoniou et al. (1984), Smith & Dow (1984), Ueda & Yao (1985), Kmiecik (1986-1987), Smith et al. (1988), Kmiecik et al. (1995), and Paik & Pedersen (1996). In addition, the ISSC (International Ship and Offshore Structures Congress) has constituted a specialist committee on fabrication technology, contain comprehensive surveys of fabrication related initial imperfections of marine structures.

It was shown from these investigations that the shape of initial distortions as well as their magnitude can have a considerable effect on the strength and stiffness of structures, and that the effect on the strength behavior of plating will depend on the applied loading types (uniaxial compression, biaxial compression or other types of load combinations) among other factors. For example, it has been demonstrated by many investigators (e.g., Paik et al. 2004) that the influence of initial deflection shape on the plate collapse behavior under predominantly transverse axial compression or biaxial compression can differ from that under predominantly longitudinal axial compression.

In contrast to the plate initial distortions, the investigation of stiffener initial distortions is relatively lacking, and further study is certainly required since the initial distortions of stiffeners or support members can significantly affect the failure of stiffened plate structures, with particular regard to beam-column type collapse and flexural-torsional buckling of stiffeners (Paik & Thayamballi 2003, 2007).

Surveys of weld-induced residual stresses in steel plating support members or stiffeners have also been performed by many investigators (e.g., Kmiecik 1970, Somerville et al. 1977, Masubuchi 1980, and Cheng et al. 1996). It is recognized that in a plate welded at both edges the tensile residual stresses develop along the weld lines and/ in the HAZ while the compressive residual stresses develop further away in the middle of the plate to achieve an equilibrium condition of internal forces. It was also shown in the literature that the maximum tensile residual stress in a mild steel plate may well reach the material yield stress, implying that the material in the HAZ is essentially not softened.

The studies related to initial imperfection surveys for welded aluminum structures have mostly been performed in conjunction with mechanical collapse test programs. In the early 1980s, a series of 76 aluminum un-stiffened plate collapse tests were carried out by Mofflin (1983) and Mofflin & Dwight (1984) at the University of Cambridge, UK; and these are regarded as perhaps one of the largest and most relevant test programs for the collapse strength of aluminum plating (un-stiffened plates) until now. After TIG (tungsten inert gas) welding in the longitudinal direction and MIG (metal inert gas) welding in the transverse direction, weld-induced initial distortions and residual stresses were measured and their influences on the plate collapse behavior were studied on two of the most common aluminum alloys used for the construction of high-speed vessels, i.e., 5083 and 6082 alloys.

In the late 1980s, Clarke & Swan (1985) and Clarke (1987) at the Admiralty Research Establishment (ARE), UK carried out the buckling collapse tests on a total of five aluminum stiffened plate structures. This one of the earliest collapse, test programs to use ship-shaped aluminum stiffened plate structures using full scale prototype models of all-welded construction with multiple-frame bays. All material of the test structures was equivalent to 5083 aluminum alloy.

Over a decade after the ARE tests, several collapse test programs on aluminum stiffened plate structures constructed by welding were carried out together with various surveys of weld-induced initial imperfections. These include Hopperstad et al. (1998, 1999), Tanaka & Matsuoka (1997), Matsuoka et al. (1999), Zha et al. (2000), Zha & Moan (2001, 2003) and Aalberg et al. (2001). The material of most test structures was 5083 aluminum alloy for plating and 6082 aluminum alloy for stiffeners. Except perhaps for those by Tanaka & Matsuoka (1997) and Matsuoka et al. (1999) which were full scale prototype models with multiple-frame bays, most of these test structures were small scale models composed of a single stiffener with attached plating or a thin-walled cruciform structure.

Although the nature and extent of initial imperfection measurements were somewhat limited, these test results were still very useful in studying the statistics of weld-induced initial imperfections as well as the compressive collapse strength characteristics themselves. Very recently, Collette (2005) developed a comprehensive literature survey report including his own important insights on the ultimate strength and reliability of aluminum stiffened plate structures.

Even in light of existing excellent research results on the weld-induced initial imperfections and ultimate strength of aluminum structures noted above, more studies are certainly required, because a systematic survey of the initial imperfection and buckling collapse characteristics is very lacking for a variety of aluminum alloy types and structural dimensions typical of ship-shaped full scale prototype structures considering the recent trends in the application of aluminum marine structures.

A significant motive for initiating the present research project was to contribute to resolving the issue noted above to a good degree, by developing relevant design database on fabrication related initial imperfections and ultimate strength of welded aluminum stiffened plate structures for marine applications.

In the present research project, therefore, a total of 78 ship-shaped full scale prototype aluminum structures which are equivalent to sub-structures of a 80m long all aluminum high-speed vessel are constructed by MIG (metal inert gas) welding in a major shipyard in Korea, which has experienced in building of aluminum high-speed vessel structures. The material of plating and stiffeners is varied among 5083-H116 (rolled), 5383-H116 (rolled), 5383-H112 (extruded) and 6082-T6 (extruded) aluminum alloys, which are today the most popular for marine applications.

The statistics of weld-induced initial imperfections in plating and stiffeners are obtained by direct measurements of the prototype structures. Six types of primary forms of initial imperfections caused by welding, namely initial distortion of plating (between stiffeners), column type initial distortion of stiffeners, sideways initial distortion of stiffeners, residual stresses of plating, residual stresses of stiffener web and softening of the heat affected zone are measured.

A statistical analysis of measured database is performed to determine mean and coefficient of variation (COV) of each imperfection parameter using Weibull probability density function, which has been proven to reasonably well reflect their statistical characteristics. Three (slight, average and severe) levels of each of the six imperfection parameters are then obtained on a statistical basis and proposed for applications to ultimate limit strength assessment of welded aluminum marine structures. The databases of the test structures and initial imperfection measurements, which could be a good source for future investigations are presented.

Buckling collapse tests of the structures under predominantly axial compressive actions were performed until and after the ULS is reached. The load versus axial compressive displacement (shortening) for each of all test structures was recorded during each of the tests. Collapse modes of stiffened plate structures tested were observed. Elastic-plastic large deflection nonlinear finite element analyses were undertaken for each of all test structures. Closed-form empirical ULS formulae for aluminum stiffened plate structures under axial compressive loads were derived by the regression analysis of experimental and numerical results.

Chapter 2 Aluminum Alloys for Marine Applications

Table 2.1 compares the properties of an aluminum alloy and steel. The density of the aluminum alloy is typically one thirds that of steel, and the elastic modulus of aluminum alloy is one thirds that of steel. . Table 2.2 indicates designation of aluminum alloy groups. The 5xxx and 6xxx series whose yield strength is in the range of 200~350MPa comparable in this regard to the strength of mild steel, and are hence widely considered for marine applications.

The temper is a significant aspect in terms of the nonlinear structural behavior of aluminum structures. The basic temper designations consist of letters and numerals followed by the letter. Three types of the letter are usually relevant, namely

- F – as fabricated with no special control related to thermal or strain-hardening treatments;
- O – fully annealed to obtain the target strength conditions;
- H – strain-hardened to improve the strength, with or without thermal treatments;
- T – thermally treated to produce stable tempers other than F, O or H.

H or T tempers are typically adopted for aluminum alloys for marine applications. The H designation is always followed by two or more digits. The first digit representing the alloy production method is usually given as with either 1 – strain-hardened only, 2 – strain-hardened and then partially annealed, or 3 – strain-hardened and then thermally stabilized. The second digit representing the degree of strain-hardening in the final temper state is given by a numeral such as 1 – eighth hard, 2 – quarter hard, 4 – half hard, 6 – three quarter hard, 8 – hard, and 9 – extra hard. A third digit may be included to indicate specific conditions of the two basic tempers result in a significant difference in mechanical properties.

The T temper designation is always followed by one or two digits. The first digit represents the degree of heat or ageing treatments, such as 1 – cooled from an elevated temperature shaping process (extrusion), 3 – heat-treated, cold-worked and the naturally aged, 4 – heat-treated and naturally aged, 5 – cooled from an elevated temperature shaping process and then artificially aged, 6 – heat-treated and then artificially aged, 8 – heat-treated, cold-worked and then artificially aged, and 9 – heat-treated, artificially aged and then cold-worked. An additional digit may be included to represent a specifically temper condition combination resulting in significant differences in the alloy properties.

The material of aluminum stiffened plate structures for marine applications is often different for plate and stiffeners, where 5xxx series alloys are most common for plating in the form of rolled products and 6xxx (and occasionally 5xxx or even 7xxx) alloys for stiffeners in the form of extrusions. One typical standard material type for plating has been 5083, while that for stiffeners is 6082, where H116 tempers are typically applied for plating, and T6 tempers are taken for stiffeners.

It is however interesting to note that 5083 was not developed originally for marine applications, but was developed for applications to land-based structures and other types. Because the operational environments of marine structures, e.g., exposed to acidic attack from certain types of corrosion, are different from those of land-based structures, a new material, 5383 has been developed by Alcan, France under the brand name ‘Sealium®’.

This is an advanced alloy that has been specifically optimized to be suitable under marine environments. The base metal mechanical properties of Sealium® are slightly better than 5083 as indicated in Table 2.3. For Sealium® (5383), H116 temper is usually taken for sheets and plating, while H112 temper is taken for extruded stiffeners.

Figure 2.1 compares the hardness at welds and base metal for 5083 and Sealium® (Raynaud 1995). Figure 2.2 compares the resistance against acid attack such as from certain types of corrosion for 5083 and Sealium® (Raynaud 1995). It is evident from Figs. 2.1 and 2.2 that, in comparative terms, Sealium® is attractive for marine applications than the basic 5083.

Chapter 3 Aluminum Stiffened Plate Structures for Marine Applications

Figure 3.1 shows a stiffened plate structure for marine applications, composed of plating and support members (longitudinal stiffeners, longitudinal girders and transverse frames), typical for aluminum high-speed vessels as well as steel plated structures. Due to the relatively low stiffness of aluminum as compared to steel and in consideration of response to global hull bending loads, most aluminum vessels are longitudinally stiffened, that is, the plating between longitudinal girders and transverse frames is rigidified with a number of extruded sections in the longitudinal (ship's length) direction.
The yield stress (at 0.2% offset) is denoted by σ_{Yp} for plating and σ_{Ys} for stiffeners. The ultimate tensile stress of material is σ_T and fracture strain is ε_f. The elastic modulus is E and the Poisson ratio is ν.

T
The entire length of a stiffened plate structure is denoted by L; and the spacing of longitudinal girders, transverse frames and longitudinal stiffeners are B, a and b, respectively, as shown in Fig.3.2. The thickness of plating is denoted t. The panel has n_s stiffeners in the longitudinal direction. Unlike steel stiffeners that are usually built up from rectangular sections, aluminum stiffeners are extruded into optimized shapes as shown in the inset to Fig.3.3, where the extruded stiffener is attached to the plate with fillet welds, while an integrated extrusion may sometimes be applied as well.

In specific cases, it is to be recommended that all dimensions and properties to a plate and stiffener combination with extruded stiffener geometry be obtained from the manufacturer. For our study, the geometry of stiffeners will be idealized into one of three types as indicated in Fig.3.3, where the height and thickness of the stiffener web are h_w and t_w, respectively. The breadth and thickness of the stiffener flange are b_f and t_f, respectively.

Chapter 4 Design and Construction of Full Scale Prototype Structures

A total of 78 prototype aluminum structures which are full scale equivalent to sub-structures of an 80m long all aluminum high speed vessel are studied. They are designed in terms of single and multi-bay stiffened plate structures as those shown in Fig.4.1. To cover the possible diverse range of in-service aluminum marine structures representative of collapse failure modes, a variety of structural dimensions, material types, plate thicknesses, stiffener types and stiffener web heights are considered as follows:

- Panel breadth: B = 1000 mm;
- Stiffener spacing: b = 300 mm;
- Panel length: 1000 mm (one-bay structure), 1200 mm (one-bay structure), 3000 mm (three-bay structure of 1000 mm length);
- Material types: plate – 5083-H116 (rolled), 5383-H116 (rolled), stiffeners – 5083-H116 (rolled), 5383-H112 (extruded), 5383-H116 (rolled), 6082-T6 (extruded);
- Thickness: plate – 5 mm, 6 mm, 8 mm, and stiffeners – 4 mm, 5 mm, 6 mm, 8 mm;
- Stiffener types: flat bar, built-up T-bar, extruded T-bar;
- Stiffener web height: 60 mm, 70 mm, 80 mm, 90 mm, 100 mm, 120 mm, 140 mm.

All aluminum alloy sheets (plates) and extrusions necessary for the construction of prototype structures have been supplied by Alcan Marine, France who is one of the world's largest manufacturers of aluminum alloys. The virgin aluminum alloy sheets transported from France were cut by laser cutting machine in Korea. Tensile coupon tests on specimen designed by ASTM standards was undertaken to investigate the mechanical properties (e.g., elastic modulus, yield stress, ultimate tensile stress, fracture strain) of each type of (base or un-welded) material sheets.

Figure 4.2 shows a typical set of the tensile test specimen for aluminum alloys used for the prototype structures. The coupons have been taken from each type of the aluminum alloy sheet in the three directions, i.e., lengthwise (L), crosswise (C), and diagonal (D) directions.

Figure 4.3 and Table 4.1 present the mechanical properties of aluminum alloys used for the construction of the prototype structures, as those obtained by the tensile coupon tests undertaken in the present study. It is clear that the material properties are affected by temper as well. 6082-T6 alloy has a higher yield stress while elongation is shorter than other alloys.

Table 4.2 indicates the list of test structures including a total of 75 one-frame bay structures and a total of 3 three-frame bay structures. Table 4.3 represents the structural dimensions and related properties of all prototype structures. An effective flange thickness t_f of an extruded section was calculated based on the moment of inertia of the actual extruded section. When the extruded section is welded to the plate, the weld itself is not part of any effective dimension calculations (i.e., t_w is the real nominal web thickness value).

Various methods for fabricating aluminum ship structures are today relevant, namely metal inert gas (MIG) welding, tungsten inert gas (TIG) welding, laser welding and friction stir welding (FSW), but the present test program adopts the MIG welding technique, which is now one of the most popular methods of welding aluminum ship construction. Prototype structures have been fabricated using a MIG welding robot at the shipyard of Hanjin Heavy Industries & Construction Company in Korea.

Table 4.3 indicates the welding conditions applied for fabrication of the test structures. In Table 4.3, the 1st pass indicates the fillet welding along one side of the stiffener while the 2nd pass indicates the fillet welding along the other side of the stiffener. The welding speed was kept at 42cpm regardless of the plate thickness although a greater welding intensity was applied for a thicker plate. Filler metal employed for the welding is 5183 aluminum alloy with 1.2mm diameter. Shield gas of Ar99.9% was used. Torch angle of welding machine was set at 45 degrees, while welding progress angle was 68 degrees. A six axes multi-pivot welding robot made by IGM Robotic Systems, Inc. was employed together with the welding machine of max. 500A pulse MIG made by Fronius, Inc. Figure 4.4 shows the order of welding for fabrication of one-frame bay structure, and Figure 4.5 presents pictures showing the MIG welding.

Chapter 5 Mechanisms and Idealizations of Weld Induced Initial Imperfections

Similar to steel structures, welding is usually used for the construction of aluminum marine structures. When structural steels or aluminum alloys are locally heated, the heated part will expand but because of adjacent cold part it will be subjected to compressive stress and distortion. When the heated part is cooled down, it will tend to locally shrink and thus now be subjected to a tensile stress.

While the same happens in steel structures as well, it is the case that in aluminum structures the material in the HAZ is typically softened and subsequently the strength (yield stress) of the HAZ are generally reduced, which is termed a material softening phenomenon.

Figure 5.1 represents a profile of the weld-induced initial distortions in a stiffened plate structure, where stiffeners distort in the direction of web and also sideways and plating deflects in the lateral direction. Due to welding, tensile residual stresses remain in the HAZ, and compressive residual stresses develop in the other areas to be in equilibrium of internal forces as shown in Fig.5.2. The distribution of residual stresses in plating which is welded along multiple stiffener lines or edges may differ from that in stiffener web itself as shown in Fig.5.3.

Figure 5.4 shows idealized schematics of softened regions in the HAZ. In the plating, since stiffeners are assumed to be welded in this case along all four edges, the softening zones develop along all edges as indicated. Its counterpart in the stiffener attached by welding is also shown. In terms of structural behavior in association with softening in the HAZ, the breadth of the softening zones together with the reduction of yield strength plays a primary role in strength characterization.

While weld-induced initial imperfections described above should be minimized by application of proper welding procedures and fabrication methods, it is nevertheless important to realize that their levels in specific cases can have a remarkable influence on the strength and stiffness of the structures. Hence their levels must be dealt with as parameters of influence in the analysis of load-carrying capacity. This means that such initial imperfection parameters must be properly determined in advance and accounted for in the design process including reliability analyses and code calibrations.

For aluminum stiffened plate structures constructed by welding, the following six types of initial imperfections will generally be pertinent, namely

- Initial distortion of plating between stiffeners;
- Column type initial distortion of stiffener;
- Sideways initial distortion of stiffener;
- Residual stresses of plating between stiffeners;
- Residual stresses of stiffener web;
- Softening in the HAZ in terms of reduction of the HAZ material yield stress and breadth of softened zone.

In the following, the mechanisms and idealizations for each of the above six imperfection parameters are described.

5.1 Initial Distortion of Plating between Stiffeners

The measurements of initial distortion of aluminum or steel plating between stiffeners show that depending on the case, one or more waves may develop in the two orthogonal directions; in Figs.5.5(a) and 5.5(b).

Buckling of a long rectangular plate subject to axial compression in the long direction occurs in a mode with multiple sinusoidal half-waves of length approximately equal to the plate breadth b (which is often termed buckling mode deflection), while buckling under axial compression in the short direction takes place with a single half-wave in both directions (Timoshenko & Gere 1961, Timoshenko & Woinowsky-Krieger 1981, Paik & Pedersen 1996).

Hence for long imperfect plates, an isolated or periodic distortion of amplitude w_{ob} with half-wave length b' equal or somewhat less than the plate breadth b as shown in Fig.5.6

may be considered to play a significant role when axial compression is applied predominantly in the long (x) direction, while a single half-wave of amplitude w_{o1} over the plate length plays a more important role for a plate when axial compression in the short (y) direction is predominant.

The values of parameters such as w_{o1} and w_{ob} as well as the maximum plate initial distortion amplitude w_{opl} can be obtained once the geometric configuration of plate initial distortions is known. With the measurements of plate initial distortions available, the following Fourier series function can be used to express the common and very useful case of plate initial distortions with a multi-wave shape in the long direction and a single half-wave in the short direction, namely

$$\frac{w_o}{w_{opl}} = \sum_{i=1}^{M} B_{oi} \sin\frac{i\pi x}{a} \sin\frac{\pi y}{b} \tag{5.1}$$

where a = plate length, b = plate breadth. B_{oi} = initial distortion coefficients normalized by the maximum initial distortion w_{opl}. The subscripts i denote the corresponding half wave number in the x (plate length) direction.

In Eq.(5.1), B_{o1}, i.e., B_{oi} at $i=1$, corresponds to w_{o1}/w_{opl} as indicated in Fig.9. w_{ob} can then be determined as a difference between w_{opl} and w_{o1}, as follows

$$w_{o1} = B_{o1} w_{opl} \tag{5.2}$$

$$w_{ob} = \left| w_{opl} - w_{o1} \right| \tag{5.3}$$

Admittedly, it is known that a buckling (eigen value) mode initial distortion is more likely to govern the buckling collapse behavior of imperfect plates, e.g., Paik & Pedersen (1996) and Paik & Thayamballi (2003, 2007). While the buckling half-wave number m of plating under predominantly transverse compression in the short (y) direction is 1, m in general can be determined as an integer satisfying the following equation when longitudinal compression in the long (x) direction is predominant, namely

$$\frac{a}{b} \le \sqrt{m(m+1)} \tag{5.4}$$

where a/b = plate aspect ratio, m = buckling half-wave number of plating in the long (x) direction. For combined biaxial compression in both x and y directions, a similar criterion as a function of the plate aspect ratio is relevant (Paik & Thayamballi 2003, 2007).

Once the buckling half-wave number of a plate is determined from Eq.(5.4), the buckling mode initial distortion can be obtained as follows

$$w_{om} = B_{om} w_{opl} \tag{5.5}$$

where w_{om} = buckling mode initial distortion of plating, B_{0m} = initial distortion coefficient as defined by Eq.(5.1).

If measured data for the initial distortion of plating are available, the initial distortion amplitudes of Eq.(5.1) can be determined by expanding Eq.(5.1) appropriately using a selected number of terms M, depending on the complexity of the initial distortion shape. In practice, M in Eq.(5.1) may be taken as an integer which corresponds to about three or more times the plate aspect ratio (a/b) greater than 1 (Paik & Pedersen 1996).

From data for steel ship plates, Smith et al. (1988) have suggested the following representative values for the maximum plate initial distortion amplitude w_{opl}, namely

$$\frac{w_{opl}}{t} = \begin{cases} 0.025\beta^2 & \text{for slight level} \\ 0.1\beta^2 & \text{for average level} \\ 0.3\beta^2 & \text{for severe level} \end{cases} \tag{5.6}$$

where $\beta = \frac{b}{t}\sqrt{\frac{\sigma_{Yp}}{E}}$ = plate slenderness ratio. Eq.(5.6) gives an excellent guideline for defining the initial distortion level of welded steel plating at the practical design stage. One important intention behind developing the present study is to derive some similar guidelines for welded aluminum structures as well.

5.2 Column Type Initial Distortion of Stiffeners

The column type initial distortion of stiffeners indicates the initial deflection of the stiffeners in the direction of the stiffener web, with maximum deflection amplitude w_{oc} (w_{ocx} in the x-stiffener and w_{ocy} in the y-stiffener as shown in Figs. 5.1 and 5.2). It significantly affects the collapse behavior of a stiffened panel when a column or beam-column type collapse mode is predominant in a plate-stiffener combination (Paik & Thayamballi 2003).

An expression to Eq.(5.1) can be used for obtaining the geometrical configuration of column type initial distortions of stiffeners as follows

$$\frac{w_o^c}{w_{oc}} = \sum_{i=1}^{M} B_{oi}^c \sin\frac{i\pi x}{a} \tag{5.7}$$

where w_o^c = column type initial distortion of stiffener, w_{0c} = maximum amplitude of the stiffener column type initial distortion, B_{oi}^c = stiffener column type initial distortion amplitude in mode 'i'. For practical design purposes, single half-wave amplitude $w_{o1}^c = B_{o1}^c w_{oc}$ as well as the maximum amplitude w_{oc} is typically used as parameters of influence in the collapse strength analysis of stiffened panels. For steel stiffeners, an average level of w_{oc} is often taken as 0.0015a (Paik & Thayamballi 2003).

5.3 Sideways Initial Distortion of Stiffeners

The sideways initial distortion of stiffeners indicates the initial deflection of stiffeners in the lateral direction of stiffener web as shown in Fig.5.7. It significantly affects the tripping failure (lateral-torsional buckling) of stiffeners. The geometrical configuration of the stiffener sideways initial distortion can again be expressed as follows

$$\frac{w_o^s}{w_{os}} = \sum_{i=1}^{M} B_{oi}^s \sin\frac{i\pi x}{a} \tag{5.8}$$

where w_o^s = sideways initial distortion of stiffener, w_{os} = maximum amplitude of the stiffener sideways initial distortion, B_{oi}^s = stiffener sideways initial distortion amplitudes.

For practical design purposes, single half-wave amplitude $w_{o1}^s = B_{o1}^s w_{os}$ as well as the maximum amplitude w_{oc} is used as parameters of influence in the collapse strength analysis of stiffened panels. For steel stiffeners, an average level of w_{0c} is often taken as 0.0015a (Paik & Thayamballi 2003).

5.4 Residual Stress of Plating between Stiffeners

As shown in Fig.5.3, residual stress distributions in welded steel or aluminum plates represent the tensile residual stresses that develop in the HAZ and the compressive residual stresses that must also exist to achieve self-equilibrium among of internal forces in the plane of the plate since no external forces have been applied. Admittedly, buckling collapse behavior of plating is governed by the compressive residual stress rather than the tensile residual stress.

For practical design purposes, the weld-induced residual stress distributions of a plate between support members for which welding has been carried out along its four edges may be idealized to be composed of tensile and compressive stress blocks, as those shown in Fig.5.8. Among them, Fig.5.8(c) is the most typical idealization of the welding residual stress distribution in a plate.

Along the weld line, tensile residual stresses are usually developed with magnitude σ_{rtx} in the x direction and σ_{rty} in the y direction, the welding being normally performed in both x and y directions, see Fig.5.9. To obtain equilibrium of internal forces, the corresponding compressive residual stresses with magnitude σ_{rcx} in the x direction and σ_{rcy} in the y direction are developed in the middle part of the plate. From the equilibrium considerations, the breadth or length of the related tensile residual stress blocks in the x and y directions can be shown to be as follows

$$2b_t = \frac{\sigma_{rcx}}{\sigma_{rcx} - \sigma_{rtx}} b, \quad 2a_t = \frac{\sigma_{rcy}}{\sigma_{rcy} - \sigma_{rty}} a \tag{5.9}$$

Once the magnitudes of the compressive and tensile residual stresses are defined, breadths of the tensile residual stress blocks can be determined from Eq.(5.9). One can then define the residual stress distributions in the x and y directions as follows

$$\sigma_{rx} = \begin{cases} \sigma_{rtx} & \text{for } 0 \le y < b_t \\ \sigma_{rcx} & \text{for } b_t \le y < b - b_t \\ \sigma_{rtx} & \text{for } b - b_t \le y \le b \end{cases}, \quad \sigma_{ry} = \begin{cases} \sigma_{rty} & \text{for } 0 \le x < a_t \\ \sigma_{rcy} & \text{for } a_t \le x < a - a_t \\ \sigma_{rty} & \text{for } a - a_t \le x \le a \end{cases} \tag{5.10}$$

The magnitude of post-weld residual stresses in the longer direction will normally be larger because the weld length is longer. The residual stresses of plates in either the unloaded or the shorter direction are often neglected. However, where needed, the transverse (plate breadth direction) residual stresses may be approximated pessimistically as follows

$$\sigma_{rcy} = c \frac{b}{a} \sigma_{rcx} \tag{5.11}$$

where c = correction factor which typically takes a value less than 1.0 in steel or aluminum plates. When the applied stress is predominant in the x direction, $c = 0$ is often assumed.

From data related to measurements for steel ship plates, Smith et al. (1988) suggest the following representative values for the overall strength off-setting effect of weld-induced compressive residual stress of steel plates in the longitudinal (x) direction (taking compressive stress as negative), namely

$$\frac{\sigma_{rcx}}{\sigma_{Yp}} = \begin{cases} -0.05 & \text{for slight level} \\ -0.15 & \text{for average level} \\ -0.3 & \text{for severe level} \end{cases} \tag{5.12}$$

Again, Eq.(5.12) gives an excellent guideline for defining a relevant residual stress level of steel ship plating welded at edges in the stage of the plate load-carrying capacity analysis. One important intention behind developing the present study is to derive some similar guidelines for welded aluminum structures.

5.5 Residual Stress of Stiffener Web

In aluminum marine structures, an extruded T-type of stiffener is mostly applied, while built-up T-bars are often used for steel marine structures. As shown in Fig.5.3, an extruded stiffener will be welded at one edge along the intersection with plating so that residual stress distributions in stiffener web differ from those in plates which are welded along all four edges in typical marine structure construction. In this case, the representative parameters of residual stresses in stiffener web are tensile residual stress σ_{rt}^{s} and compressive residual stress σ_{rc}^{s}.

The HAZ extent can again be obtained from equilibrium condition of internal forces inside the stiffener web. The stiffener failure in the beam-column type collapse or tripping mode is governed by the compressive residual stress σ_{rc}^{s} rather than the tensile residual stress when axial compression is applied.

5.6 Softening in the HAZ

For welded aluminum structures, softening phenomenon arising from welding typically occurs in the HAZ as previously discussed. While the softening features of aluminum material may vary with the welding process and the thickness of the plate, among other factors, the primary parameters affecting the panel strength behavior are considered to be the HAZ extent (breadth of softening) and the reduced yield stress in the HAZ.

In an aluminum plate welded along all (four) edges as shown in Fig.5.4, the softening regions develop on four edges. When axial tension is applied, the response of the plate with softened regions will be affected by strain concentration in the HAZ because the strains of the HAZ material and the base material will increase at the same rates but the stress versus strain characteristics of each differ from one another because of different yield stress. Subsequently, fracture associated with strain concentration can potentially take place in the HAZ prior to gross yielding over the plate. The risk of fracture tends to increase as the HAZ extent becomes smaller because strains are more likely to concentrate in the HAZ with smaller extent.

On the other hand, the plate collapse behavior under predominantly axial compression is affected by the reduction of yield strength in the HAZ; The larger the HAZ extent the smaller the load-carrying capacity. In this regard, a complexity associated with softening phenomenon is that assuming large HAZ breadths gives a conservative evaluation of collapse strength but it may give an optimistic assessment of fracture strength. This implies that the HAZ extent must be defined in a more appropriate way as well, as precisely as possible.

For the purposes of simplicity, the HAZ extent (i.e., softening breadth) can be determined from Eq.(5.9) once the tensile residual stress σ_{rt} (σ_{rtx} in the x direction, σ_{rty} in the y direction) and the compressive residual stress σ_{rc} (σ_{rcx} in the x direction and σ_{rcy} in the y direction) are obtained by direct measurements or other methods. It is often assumed that the yield stress (strength) of the HAZ material is approximately equal to the tensile residual stress σ_{rt}, considering that the tensile residual stress in the HAZ may well reach the material yield stress.

Chapter 6 Statistics of Weld Induced Initial Imperfections

6.1 Measurements of Initial Imperfections in Prototype Structures

Six types of weld-induced initial imperfections are measured for the prototype structures. Three types of initial distortions, namely initial distortions of plating between stiffeners, column type initial distortions of stiffeners and sideways initial distortions of stiffeners are measured for all plating and stiffeners of all prototype structures.

6.1.1 Initial Distortion Measurements

Figure 6.1 shows photographs of the initial distortion measurement set-up where the distortions can be detected with precision in order of 1 μm. Table 6.1 shows the summaries of initial distortion measuring for plating and stiffeners. Figure 6.2 shows three dimensional displays of selected prototype structures including the geometrical configuration of measured initial distortions (with the amplification factor of 30).

6.1.2 Residual Stress Measurements

The residual stress measurements were made using a precision machine which applies the so-called hole drilling technique where the strain release(s) after drilling a tiny hole near each measuring point are detected by strain gauges which have been attached to the plate or web in advance.

Residual stresses are selectively measured for some representative structures in terms of geometry, the dimensions and material types where prototype structures having more realistic scantlings of actual high-speed vessels together with each type of different aluminum alloys are selected. It is noted that the holes to measure the welding residual stresses were drilled through the plate thickness up to 3mm at the bottom surface of the plate.

It is interesting to note that the strain gauges which can detect strains in all principal directions must be used. The number of measuring points of strain releases or holes drilled is 1 or 2 in the HAZ and 2 or 3 in the middle of the plate, the former being a tensile residual stress zone and the latter being a compressive residual stress zone. From the view of Eqs.(5.9) or (5.10), the number of strain measuring points adopted in the present study is sufficient enough as long as the residual stress distribution is idealized as case (c) of Fig.5.9.

Once the principal strains at many measuring points in a plate or web are known, the distribution of the corresponding stresses can be theoretically determined using classical theory of structural mechanics using the relationship between elastic stress and strain. Also, the HAZ extent can be readily obtained from Eq.(5.9) since the tensile and compressive residual stresses are known by the measurements.

Figure 6.3(a) shows the hole drilling machine and Figure 6.3(b) shows a strain gauge for detecting strain releases after hole drilling. Figures 6.3(c) and 6.3(d) show photographs of strain release measurements in progress for a plate and a stiffener web, respectively. It is also worthwhile to mention here that the accuracy of the present residual stress measuring method has been proven by calibrations with the results obtained by other measuring techniques such as x-ray diffraction method, magnetic method, sectioning method and electronic speckle pattern interferometry method and/or numerical simulations (Masubuchi 1980).

Both the tensile residual stresses and the compressive residual stresses over the plate between stiffeners or the stiffener web have been obtained for selected prototype structures. Figure 6.4 shows selected examples of the residual stress distributions at plating and stiffener web obtained by the measurements. The HAZ extent in association with softening can be determined from Eq.(5.9) with the measured residual stresses known.

The amount of the statistics in the residual stresses and the HAZ extent is relatively limited, as compared to the statistics of initial distortions in this regard, but it was considered that the present limited measurements well represent the residual stress pattern and the HAZ extent for different types of aluminum alloys as will be described later.

6.2 Statistical Analysis of Initial Imperfection Measurements

The statistical analysis of the extensive initial imperfections measurement data obtained is now performed. It is certain that the statistical characteristics of initial imperfections cannot be reflected by the normal distribution function. After a confirmation that the use of the Weibull probability density function is suitable together with its flexibility in fitting varied sets of data, therefore, mean value and standard deviation of random initial imperfection parameters was calculated by the following,

$$f(x) = \frac{\lambda}{\alpha}\left(\frac{x - x_0}{\alpha}\right)^{\lambda-1} \exp\left[-\left(\frac{x - x_0}{\alpha}\right)^{\lambda}\right] \tag{6.1}$$

where $f(x)$ = probability density function, λ = shape parameter, α = scale parameter, x_o = location parameter (which is taken as $x_0 = 0$ in the present study).

The mean value and standard deviation of the random variable can then be determined as follows

$$\mu = \int_0^{\infty} x f(x) dx = \alpha\Gamma\left(1 + \frac{1}{\lambda}\right) \tag{6.2}$$

$$\sigma = \sqrt{\int_0^{\infty} (x - \mu)^2 f(x) dx} = \alpha\sqrt{\Gamma\left(1 + \frac{2}{\lambda}\right) - \left\{\Gamma\left(1 + \frac{1}{\lambda}\right)\right\}^2} \tag{6.3}$$

$$\mathrm{COV} = \frac{\sigma}{\mu} \tag{6.4}$$

where μ = mean value, σ = standard deviation, $\Gamma(\ )$ = gamma function, COV = coefficient of variation.

As Smith et al. (1988) discussed, three types of any initial imperfection parameter levels may be relevant, namely slight, average and severe levels. An ‘average’ level of any initial imperfection parameter may reflect usual phenomena of the initial imperfections and thus all measurement data will be included in the statistical analysis.

For the slight level analysis, however, measured data at a specified percentile point and below will be used, while those at a specified percentile point and above will be employed for the severe level analysis. For example, the 5% and below band data will be used for the slight level analysis, while the 95% and above band data is employed for the severe level analysis, as illustrated in Fig.6.5.

6.2.1 Plate Initial Distortions

For initial distortions of plating between stiffeners, four types of parameters, namely w_{opl}, w_{o1}, w_{ob} and w_{0m} are necessary to be considered. Figure 6.6 shows a sample plot of the relative frequency versus the maximum plate initial distortions for the average level analysis, with a total of 252 measurements of w_{opl}. It is confirmed from Fig.6.6 that the approximation of the Weibull probability density function applied for the present study is largely successful in terms of cumulated probability representation.

A similar analysis of the statistical data was carried out for w_{o1}, w_{ob} and w_{om} to determine the average level of each parameter. For the slight level analysis of w_{0pl}, three different percentile points, namely 5%, 15% and 30% were considered with their below specified value data band, while the corresponding percentile points, namely 95%, 85% and 70% were considered for the severe level analysis with their above specified value data band. For the slight level analyses of w_{01}, w_{0b} and w_{om}, 5% and below band data are used, while 95% and above band data are employed for the severe level analyses.

For the statistical analyses of w_{o1}, w_{ob} and w_{om}, the measured initial distortions of all plate elements are approximated by Fourier series function of Eq.(5.1), where M is taken as 11. Figure 6.7 shows a selected result of the Fourier series function approximation for plate initial distortion configuration of the prototype structure ID1, together with the plate initial distortion coefficients of Eq.(5.1) for the same structures. For the first plate element (i.e., at y = 150mm), w_{o1} can be determined as w_{o1} = 0.8545 w_{opl} = 2.831mm from Eq.(2), where w_{opl} = 3.313 from Table 5.3 in Chapter 5.

Therefore, w_{ob} is obtained from Eq.(5.3) as $w_{ob} = 0.1455 w_{0pl}$ =0.4820mm. Since the aspect ratio of the plate element is $a/b = 4$, the buckling half-wave number is taken as $m = 4$

from Eq.(5.4). The buckling mode initial deflection w_{om} is then determined as $w_{om} = B_{o4} w_{opl}$ = 0.0407 w_{opl} = 0.1348mm. A similar process can be adopted for w_{om} of each of all plate elements, but it is noted that the buckling half-wave number of the plate elements of ID 73 to 78 is set to be 3 because of the different plate aspect ratio.

Figures 6.8(a) to 6.8(c) show the best fit of the Weibull probability density function for the average level analysis of w_{o1}, w_{ob} and w_{om}, respectively. Tables 6.2(a) to 6.2(d) summarize the statistical analysis results for plate initial distortions of w_{opl}, w_{o1}, w_{ob} and w_{om}, respectively. Three different levels of plate initial distortions obtained by appropriately varying the statistical data bands are indicated in the tables. The three levels of w_{opl} for aluminum plating are compared with those for steel plating suggested by Smith et al. (1988) in Table 6.2(a). It is interesting to note that the characteristics of w_{opl} for both aluminum and steel plating are similar, but the former tends to be slightly smaller than those of the latter.

6.2.2 Column Type Initial Distortions of Stiffeners

The statistical analyses for column type initial distortions of stiffeners are now performed. Column type initial distortion configuration of stiffener can be approximated by the Fourier series function of Eq.(5.7) when M is taken as M=11. Figure 6.9 shows a selected result of the column type initial distortion configuration of stiffener for all prototype structures ID 1, by the Fourier series function, together with the column type initial distortion coefficients of stiffeners as approximated by Eq.(5.7). It is confirmed that the approximations are very successful.

Similar to the statistical analysis of w_{opl} based on presumed Weibull probability density function, slight, average and severe levels of w_{oc} and w_{01}^{c} can be determined. Figures 6.10(a) and 6.10(b) show the best fits of the Weibull function for the average level analysis of w_{oc} and w_{o1}^{c}, which were performed for a total of 336 stiffener column type initial distortion data. Tables 6.3(a) and 6.3(b) present the three levels of column type initial distortions of stiffener, obtained for w_{oc} and w_{o1}^{c}, respectively.

6.2.3 Sideways Initial Distortions of Stiffeners

The sideways initial distortion configuration of stiffeners can also be approximated by the Fourier series function of Eq.(5.8). Figure 6.11 shows a selected result of the sideways initial distortion configuration of stiffeners for all prototype structures ID1, by the Fourier series function, together with the sideways initial distortions of stiffeners as approximated by Eq.(5.8). The statistical analyses can then be performed for w_{os} and w^s_{o1}.

Figures 6.12(a) and 6.12(b) show the best fits of the Weibull probability density function for the average level analysis of w_{os} and w^s_{o1} respectively, which were carried out for a total of 336 stiffener sideways initial distortion data. Tables 6.4(a) and 6.4(b) present the three levels of sideways type initial distortions of stiffener for w_{os} and w^s_{o1}, respectively.

6.2.4 Residual Stresses of Plating

Residual stress distribution inside welded plating has tensile residual stress blocks and compressive residual stress blocks, see Fig.5.8. The magnitude of tensile residual stress typically located in the HAZ approximately equals the yield stress of the HAZ material, considering that the tensile residual stress well reaches the material yield stress in mild steel (Masubuchi 1980, Paik & Thayamballi 2003). Therefore, the tensile residual stress characteristics in the HAZ will be dealt with as an aspect of the HAZ softening.

On the other hand, the statistics of compressive residual stresses in plating can be analyzed. Figure 6.13 shows the best fit of the Weibull probability density function for the average level analysis of the compressive residual stress inside welded plating which was carried out for a total of 29 measurements. It is noted that the statistical analysis was done for the compressive residual stresses normalized by minimum material yield stress values specified by classification societies (DNV 2003), considering that the yield stress of aluminum alloys can of course differ depending on the material types. Table 6.5 indicates the slight, average and severe levels of compressive residual stress inside welded plating.

6.2.5 Residual Stresses of Stiffener Web

The characteristics of compressive residual stress inside stiffener web are now investigated when welding is carried out along the intersection between attached plating and extruded stiffener, see Fig.5.3. Figure 6.14 shows the best fit of the Weibull probability density function for the average level analysis of the compressive residual stress inside stiffener web.

Table 6.6 indicates the resulting values of the slight, average and severe levels for the compressive residual stress inside stiffener web. Again, the compressive residual stress in the statistical analysis is normalized by yield stress of stiffener web.

6.2.6 Softening in the HAZ

In investigating the softening characteristics of the welding HAZ, it is required to determine the reduction of the HAZ yield stress and also the breadth of the HAZ, because the nonlinear structural response analysis involving material nonlinearity as well as geometrical nonlinearity is significantly affected by these two parameters among others. It is also important to realize that the softening characteristics, specifically in terms of the HAZ yield stress reduction can differ depending on aluminum alloy type.

6.2.6.1 Yield Stress of the HAZ Material

The HAZ yield stresses are needed to be investigated separately for different aluminum alloys. In the present study, it is assumed that the HAZ yield stress is equivalent to the HAZ residual stress.

Figures 6.15(a) to 6.15(d) show the best fits of the Weibull probability density function for the average level analysis of the HAZ residual stress for 5083-H116, 5383-H116, 5383-H112 and 6082-T6, respectively. Table 6.7 indicates slight, average and severe levels of the HAZ residual stress measured for 5083-H116, 5383-H116, 5383-H112 and 6082-T6, respectively. In this case, the slight level was determined for 95% and above band data, while the severe level was obtained for 5% and below band data.

6.2.6.2 Breadth of the HAZ

The breadth of tensile residual stress block can be obtained from Eq.(5.9) with the residual stress distribution known. It is approximated that the breadth of the HAZ equals the breadth of tensile residual stress block, i.e., $b_p' \approx b_s' \approx b_t$, see Fig.5.4 for nomenclature.

Figure 6.16 shows the best fit of the Weibull probability density function for the average level analysis of the HAZ breadth. Table 6.8 indicates the slight, average and severe levels of the HAZ breadth obtained by the statistical analysis of measurements.

6.3 Suggestions for Reference Levels of Weld Induced Initial Imperfections

Based on the statistical analyses of the extensive initial imperfection measurements undertaken in the present study, the levels of initial imperfection parameters useful for design as well as reliability analyses and code calibrations can be suggested when 5% and below band data is applied for the slight level analysis and 95% and above band data is applied for the severe level analysis, as follows

Maximum initial distortion of plating:

$$w_{opl} = \begin{cases} 0.018\beta^2 t & \text{for slight level} \\ 0.096\beta^2 t & \text{for average level} \\ 0.252\beta^2 t & \text{for severe level} \end{cases} \tag{6.1}$$

One half-wave initial distortion amplitude of plating:

$$w_{o1} = \begin{cases} 0.0059\beta^2 t & \text{for slight level} \\ 0.093\beta^2 t & \text{for average level} \\ 0.269\beta^2 t & \text{for severe level} \end{cases} \tag{6.2}$$

Localized initial distortion of plating:

$$w_{ob} = \begin{cases} 0.00033\beta^2 t & \text{for slight level} \\ 0.0101\beta^2 t & \text{for average level} \\ 0.0365\beta^2 t & \text{for severe level} \end{cases} \tag{6.3}$$

<u>Buckling mode initial distortion of plating:</u>

$$w_{om} = \begin{cases} 0.0 & \text{for slight level} \\ 0.00552\beta^2 t & \text{for average level} \\ 0.0468\beta^2 t & \text{for severe level} \end{cases} \tag{6.4}$$

<u>Maximum column type initial distortion of stiffener:</u>

$$w_{oc} = \begin{cases} 0.00016a & \text{for slight level} \\ 0.0018a & \text{for average level} \\ 0.0056a & \text{for severe level} \end{cases} \tag{6.5}$$

<u>One half-wave column type initial distortion of stiffener:</u>

$$w_{o1}^{c} = \begin{cases} 0.0 & \text{for slight level} \\ 0.00155a & \text{for average level} \\ 0.00525a & \text{for severe level} \end{cases} \tag{6.6}$$

<u>Maximum sideways initial distortion of stiffener:</u>

$$w_{os} = \begin{cases} 0.00019a & \text{for slight level} \\ 0.001a & \text{for average level} \\ 0.0024a & \text{for severe level} \end{cases} \tag{6.7}$$

One half-wave sideways initial distortion of stiffener:

$$w_{o1}^{s} = \begin{cases} 0.0 & \text{for slight level} \\ 0.000574a & \text{for average level} \\ 0.0018a & \text{for severe level} \end{cases} \tag{6.8}$$

Yield stress of the HAZ material for 5083-H116:

$$\frac{\sigma_{YHAZ}}{\sigma_Y} = \begin{cases} 0.906 & \text{for slight level} \\ 0.777 & \text{for average level} \\ 0.437 & \text{for severe level} \end{cases} \tag{6.9}$$

where σ_Y = 215 N/mm^2.

Yield stress of the HAZ material for 5383-H116:

$$\frac{\sigma_{YHAZ}}{\sigma_Y} = \begin{cases} 0.820 & \text{for slight level} \\ 0.774 & \text{for average level} \\ 0.640 & \text{for severe level} \end{cases} \tag{6.10}$$

where σ_Y = 220 N/mm^2.

Yield stress of the HAZ material for 5383-H112:

$$\frac{\sigma_{YHAZ}}{\sigma_Y} = 0.891 \text{ for average level} \tag{6.11}$$

where σ_Y = 190 N/mm^2.

Yield stress of the HAZ material for 6082-T6:

$$\frac{\sigma_{YHAZ}}{\sigma_Y} = 0.703 \text{ for average level} \tag{6.12}$$

where σ_Y = 240 N/mm^2.

<u>Compressive residual stress at plating:</u>

$$\sigma_{rcx} = \begin{cases} -0.110\sigma_{Yp} & \text{for slight level} \\ -0.161\sigma_{Yp} & \text{for average level} \\ -0.216\sigma_{Yp} & \text{for severe level} \end{cases} \tag{6.13}$$

<u>Compressive residual stress at stiffener web:</u>

$$\sigma_{rcx} = \begin{cases} -0.078\sigma_{Ys} & \text{for slight level} \\ -0.137\sigma_{Ys} & \text{for average level} \\ -0.195\sigma_{Ys} & \text{for severe level} \end{cases} \tag{6.14}$$

<u>Breadth of the HAZ:</u>

$$b'_p = b'_s = \begin{cases} 11.3\,\text{mm} & \text{for slight level} \\ 23.1\,\text{mm} & \text{for average level} \\ 29.9\,\text{mm} & \text{for severe level} \end{cases} \tag{6.15}$$

Chapter 7 Experiments

This chapter presents the experimental results for the test structures under axial compressive loads, together with selected photographs showing typical collapse modes.

7.1 Test Set-up

Figure 7.1 shows the set-up of the physical collapse tests on the stiffened plate structures. The loaded edges are simply supported and the axial compressive loading is applied at the neutral axis of the panel cross section. A rigid circular bar at each side of loaded edges was inserted as shown in Fig.7.2 to reflect simply supported edge conditions along the loaded edges, i.e., by minimizing the rotational restraints.

Two types of unloaded edge condition are considered, namely free and simple support conditions, as shown in Figs.7.1. For the latter condition shown in Fig.7.1(b), a set of supporting jigs was attached to keep the unloaded edges straight. This condition was considered to reflect the behavior of stiffened panels in a continuous stiffened plate structure.

A total of 10 test structures with flat bar type stiffeners, namely ID40, 41, 42, 44, 45, 58, 59, 60, 62 and 63 were tested without the supporting jigs at unloaded edges, indicating a free edge condition.

7.2 Test Results and Discussions

Figures 7.3 to 7.80 show the test results including the load-axial displacement curves. Theoretically, six primary modes of stiffened panel collapse under predominantly axial compressive loads are pertinent, namely (Paik & Thayamballi 2003)

- Mode I: Overall collapse of plating and stiffeners as a unit;
- Mode II: Collapse under predominantly biaxial compression;

- Mode III: Beam-column type collapse;
- Mode IV: Local buckling of stiffener web;
- Mode V: Tripping of stiffener;
- Mode VI: Gross yielding.

Mode I typically represent the collapse pattern when the stiffeners are relatively weak. In this case, the stiffeners can buckle together with plating as a unit.

Mode II represents the collapse pattern wherein the panel collapses by yielding along the plate-stiffener intersection at the panel edges with no stiffener failure. This type of collapse can be important in some cases when the panel is predominantly subjected to biaxial compressive loads.

Mode III indicates a collapse pattern in which the ultimate strength is reached by yielding of the plate-stiffener combination at mid-span.

Mode IV can occur when the ultimate strength is reached subsequent to local compressive buckling of the stiffener web, Mode V represents a collapse pattern in which the panel collapses by tripping of stiffeners.

Mode VI typically takes place when the panel is very stocky and/or the panel is predominantly subjected to axial tensile loading so that neither local nor overall buckling occurs until the panel cross-section yields entirely.

Figure 7.81 shows selected photographs showing typical collapse modes of the test structures. The test structures ID1 and ID41 reached the ultimate limit state by Mode III. Mode IV occurred for ID42 and Mode V occurred for ID2 and ID8. It is interesting to note that Modes III and IV occurred almost simultaneously just before the test structure ID3 collapsed. The test structure ID4 showed a combined mode of IV and V.

Table 7.1 indicates the summary of the ultimate strengths obtained for all test structures together with the collapse modes that occurred.

Figures 7.82 and 7.83 shows the variations of the ultimate strength as a function of plate slenderness ratio and column slenderness ratio of the test structures with flat bars or T-bars, respectively. It was observed that the panel collapse patterns were clearly different depending on the panel geometries. For the ratio of stiffener web height to web thickness is relatively large, the stiffened panel mostly collapsed by lateral torsional buckling or tripping (Mode V), while the beam-column type collapse (Mode III) took place for panels with a smaller web height. For some panels with high T-bars, local web buckling (Mode IV) tends to occur.

From Fig.7.82, it is interesting to note that the ultimate strength of the structures with flat-bars decreases significantly when the column slenderness ratio is small. This is because the lateral-torsional buckling of stiffener web is more likely to take place when the stiffener web height is very large with subsequently small column slenderness ratio.

On the other hand, the ultimate strength of stiffened plate structures with T-bars becomes larger as the column slenderness ratio decreases or the stiffener web height increases as shown in Fig.7.83. It is to be noted that the stiffener web and flange of built-up T-bars could have more severe initial imperfections than those of extruded types. However, the variation of the ultimate strength for built-up T-bars is similar to that for extruded T-types.

The three-frame bay structures, namely ID 76, 77 and 78 were tested to investigate the effect of rotational restraints along the transverse frames. These are corresponding to the one-frame bay structures, namely ID 73, 74 and 75, respectively. It is found that the ultimate strength of the three-frame bay structures (except for ID 77) is slightly greater than the corresponding one-frame bay structures (except for ID 74), by 1.4~2.5%. On the other hand, the ultimate strength of ID 77 is rather smaller than that of ID74, by 3.7%.

As a matter of fact, a more severe level of initial imperfections occurred during the fabrication of the 3-bay structures than the corresponding 1-bay structures as described in Chapter 6. It is considered that the reduction of the ultimate strength due to more severe initial imperfections was more significant than the increase of the ultimate strength due to rotational restraints along the transverse frames in these specific prototype structures.

However, it can be said with certainty that the rotational restraints along the transverse frames can of course contribute to the ultimate strength of the structures to some extent and also the structural idealizations with 1-bay models may give somewhat pessimistic assessment of the stiffened panel ultimate strength as long as the level of initial imperfections is the same.

Chapter 8 Nonlinear Finite Element Analyses

8.1 Structural Modeling

Nonlinear finite element analysis (FEA) using ANSYS (2006) was carried out on each of all test structures by a comparison with FEA and test results. Since some arguments in terms of selecting relevant FEA modeling techniques still remain, 8 types of FEA modeling are in the present study considered with varying the extent of analysis and the direction of column type initial deflection of stiffeners (with the abbreviations of CIP = compression in plate side, CIS = compression in stiffener side, SPM = stiffened panel model, PSC = plate-stiffener combination model), namely

- 1 bay SPM with initial deflection in CIP
- 1 bay SPM with initial deflection in CIS
- 2 bay SPM with initial deflection in CIP
- 2 bay SPM with initial deflection in CIS
- 1 bay PSC with initial deflection in CIP
- 1 bay PSC with initial deflection in CIS
- 2 bay PSC with initial deflection in CIP
- 2 bay PSC with initial deflection in CIS

In addition to the 8 types of modeling noted above, another 2 bay FE model was considered by reflecting the unloaded edges as being simply supported keeping them straight, namely

- 2 bay SPM with all (four) edges simply supported

While the test structures are primarily 1 bay system, i.e., considering the longitudinally stiffened panels between two transverse frames, 2 bay system including transverse frames as shown in Fig.8.1 are also considered in the present FEA to reflect the continuity support condition along the transverse frames in a continuous plate structure.

All of the 1 bay models are analyzed by a load control, while the 2 bay models are loaded by a displacement control, because of easier handling for the load application with regard to the neutral axis at the panel cross section.

After some convergence studies, the FE mesh size adopted has one plate-shell element representing the HAZ at plating and at the stiffener web. 10 plate-shell elements represent the plating between stiffeners and six elements model stiffener web, including the elements in the HAZ.

The softening in the HAZ is considered in the FEA, where the reduced yield stress ratio in the HAZ is set by the guidance of classification societies, i.e., 0.67 for 5083 and 0.7 for 5383. The welding induced residual stresses are also considered in the FEA with the measured values.

While some details of the nonlinear FEA in terms of FE meshing and material stress-strain relation idealization may be found from Paik & Duran (2004), Figure 8.2 shows the modeling effects of material stress-strain relationship on the aluminum panel ultimate strength behavior, where three different models including real stress-strain curve usage. The same characteristics of HAZ softening were considered in this comparison.

It is seen from Figs.8.2(b) and 8.2(c) that the elastic-perfectly plastic material model neglecting the strain-hardening effect does not provide more conservative results than the case of the real material properties.

This is in contrast to steel plated structures where the elastic-perfectly plastic material approximation always gives lower ultimate strength estimates than the case with real material stress-strain relationship. This is because the elastic-plastic regime of material after the proportional limit (before the yield point) plays a role in the collapse behavior of aluminum structures unlike steel structures where it can be neglected.

For practical fast ULS calculations of aluminum structures, however, it is considered that the elastic-perfectly plastic material approximation neglecting the elastic-plastic effect after the proportional limit (before the yield point) and also the strain-hardening effect (after the yield point) may be acceptable alike for steel structures as long as the softening effect in the

HAZ is accounted for, i.e., by considering the reduced yield stress in the HAZ.

Figure 8.3 compares FEA solutions obtained by the 9 types of FE modeling noted above together with test data for two selected test panels until and after the ULS is reached.

It is to be noted in Fig.8.3 that all FEA except for No. 10 were undertaken considering that the unloaded edges are free as in the actual testing, while No.10 was considered that the unloaded edges (as well as the loaded edges) are simply supported keeping them straight.

In the testing, the test panel ID 40 collapsed by column type collapse (Mode III) and ID 63 collapsed by stiffener tripping (Mode V). As would be expected, it is evident that the direction of column type initial deflection of stiffener significantly affects the FE solutions. It is also seen that the 2 bay FEA always gives a larger ULS than 1 bay FEA. This is because the 2 bay FEA involves the rotational restraint effects along the transverse frames in the continuous plate structures.

It is to be noted that the different FE modeling approaches give quite different solutions. It is of vital importance to correctly reflect all of the influential parameters in the FE modeling in this regard. It is important to realize that the direction of column type initial deflections of stiffeners, among other factors may significantly affect the ultimate strength behavior when the magnitude of initial deflections is substantially large.

Also, it is evident that the model type or extent taken for the FE analysis must be determined carefully, while the real material stress-strain relationship rather than the elastic-perfectly plastic material approximation must always be employed unlike the ULS assessment of steel structures. Since softening in the HAZ plays a significant role on the welded aluminum plate structures, it must be carefully dealt with as well. These aspects definitely make the aluminum panel ULS evaluation works cumbersome.

In this regard, the present study adopts the following four types of FEA models for the test structures, namely

- 1 bay PSC model in CIP

- 1 bay PSC model in CIS
- 2 bay PSC model in CIP
- 2 bay PSC model in CIS

It is assumed that the material follows the elastic-perfectly plastic behavior without strain-hardening effect. An average level of initial imperfections including initial distortions, welding residual stresses and HAZ softening as measured for the test structures is applied for the FEA. The mechanical properties (e.g., elastic modulus, yield stress) of aluminum alloys used for the present FEA were defined from the minimum values of classification society rules rather than actual values obtained from the tensile coupon tests.

8.2 Finite Element Analysis Results and Discussions

Figures 8.4 to 8.81 show the load-axial displacement curves of the test structures, as obtained by FEA. The experimental results are compared with the FEA solutions.

Table 8.1 summarizes the ultimate strengths of test structures together with collapse modes obtained by nonlinear FEA. The experimental results are also compared in the table. Figures 8.82 and 8.83 show the variations of the ultimate strength as a function of plate slenderness ratio and column slenderness ratio.

As will be described later in Chapter 9, some additional FEA for stiffened plate structures with different plate slenderness ratio and column slenderness ratio from those of prototype structures tested in the present study were undertaken to develop closed-form empirical formulae. Table 8.2 summarizes the additional FEA solutions.

It is observed that the 2-bay FEA models give greater ultimate strength values than the 1-bay FEA models because the effect of rotational restraints along the transverse frames is taken into account in the 2-bay FEA models. Based on some observations obtained from the present study on ULS of aluminum stiffened plate structures, the following conclusions can be drawn:

- It is evident that the nonlinear elastic-plastic large deflection FEA can give quite different ULS solutions depending on the difference of structural modeling as would be expected. If FE structural modeling is not relevant in terms of reflecting the reality in association with boundary condition and initial imperfections as well as geometric / material properties and loading application, then the FEA may of course give wrong results of the ultimate strength behavior and thus one should be careful in this regard.

- FEA solutions are significantly affected by the direction of column type initial deflections of stiffeners as well as their amplitude, among other factors. For instance, the direction of column type initial deflection of stiffeners, e.g., compression in plate side (CIP) or compression in stiffener side (CIS) can govern the direction of panel buckling deflection, leading to a different collapse pattern.

- By considering the continuity of stiffened panels in a continuous plate structure and the related rotational restraints along transverse frames, 2 bay FEA modeling is more recommendable.

- It is seen that the elastic-perfectly plastic material model may not give conservative ULS solutions but its effect is small. For practical purpose, therefore, the stress-strain relationship of aluminum alloy can be approximated by the elastic-perfectly plastic model.

- The effect of softening in the HAZ is very significant on the ultimate strength behavior of aluminum panels. Therefore, the reduced yield stress in the HAZ must be considered for FEA or other analytical approaches.

Chapter 9 Closed-form Empirical ULS Formulae

In ship design, the hull girder strength of ships is often governed by the buckling collapse behavior of deck or bottom panels. Hence the calculation of the buckling collapse strength of stiffened panels in deck and bottom structures under axial compressive loads which are a primary load component due to ship's hull girder actions is an essential task.

In this chapter, closed-form empirical ULS formulae for aluminum stiffened plate structures under axial compressive loads are derived by the regression analysis of experimental and numerical database obtained from the present study.

As previously described in Chapter 8, some additional FEA were undertaken for stiffened plate structures with different plate slenderness ratio and column slenderness ratio from those of prototype structures tested in the present study so as to cover a wider range of plate slenderness ratio and column slenderness ratio in the developed ULS formulae.

When the continuous stiffened plate structure is modeled as an assembly of plate-stiffener combinations, it is recognized that the ultimate compressive strength of the representative plate-stiffener combination is expressible as follows (Paik & Thayamballi 1997, 2003)

$$\frac{\sigma_u}{\sigma_{Yeq}} = \left[C_1 + C_2\lambda^2 + C_3\beta^2 + C_4\lambda^2\beta^2 + C_5\lambda^4\right]^{-0.5} \le \frac{1}{\lambda^2} \tag{9.1}$$

where $C_1 \sim C_5$ = coefficients to be determined from database.

For steel stiffened plate structures with an average level of weld induced initial imperfections, Paik and Thayamballi (1997, 2003) determined the coefficients of Eq.(9.1) by the least square method based on the experimental database as follows

$$\frac{\sigma_u}{\sigma_{Yeq}} = \left[0.995 + 0.936\lambda^2 + 0.170\beta^2 + 0.188\lambda^2\beta^2 - 0.067\lambda^4\right]^{-0.5} \le \frac{1}{\lambda^2} \tag{9.2}$$

It is to be noted that σ_{Yeq}/λ^2 is the elastic buckling stress of a column member simply supported at both ends, and the ultimate strength of a column member should not be greater than the elastic buckling stress. Eq.(9.2) is useful for predicting the ultimate compressive strength of steel stiffened panels with Tee, angle or flat bars, the last type of stiffeners having relatively large column slenderness ratio, when an average level of initial imperfections is applied.

For aluminum stiffened plate structures, the use of a similar approach to steel stiffened plate structures is attempted but with different formulae for different types of stiffeners. We then suggest the following constants for aluminum stiffened plate structures with extruded or built-up T-bars when an average level of weld induced initial imperfections are applied, namely

$$\frac{\sigma_u}{\sigma_{Yeq}} = \left[1.318 + 2.759\lambda^2 + 0.185\beta^2 - 0.177\lambda^2\beta^2 + 1.003\lambda^4\right]^{-0.5} \le \frac{1}{\lambda^2} \qquad (9.3)$$

Figure 9.1 checks the accuracy of Eq.(9.1) with the coefficients in Eq.(9.3). Eq.(9.1) with the coefficients of Eq.(9.2) for steel stiffened plate structures is also plotted in Fig.9.1. Tables 9.1 and 9.2 also summarize the formula solutions. Figure 9.2 indicates the bias and COV (coefficient of variation) for the formula, Eq.(9.3).

On the other hand, the ultimate strength of aluminum stiffened plate structures with flat bars can be given as a smaller value of the following two formula solutions, when an average level of initial imperfections is applied, namely

$$\frac{\sigma_u}{\sigma_{Yeq}} = \text{Min.}\begin{cases} \left[2.500 - 0.588\lambda^2 + 0.084\beta^2 + 0.069\lambda^2\beta^2 + 1.217\lambda^4\right]^{-0.5} \le \dfrac{1}{\lambda^2} \\ \left[-16.297 + 18.776\lambda + 17.716\beta - 22.507\lambda\beta\right]^{-0.5} \end{cases} \qquad (9.4)$$

Figure 9.3 checks the accuracy of Eq.(9.4) by a comparison with experimental and numerical results. Tables 9.1 and 9.2 also summarize the formula predictions using Eq.(9.4). Figure 9.4 indicates the bias and COV analyses for the formula solutions using Eq.(9.4). Figure 9.5 shows the bias and COV analyses for both Eqs.(9.3) and (9.4) by a comparison with experimental and numerical results.

Considering the uncertainty associated with initial imperfections and structural modeling techniques, among other factors, it is interesting to see the upper and lower limits of the panel ultimate strength with relevant deviations. Figures 9.6 and 9.7 show the panel ultimate strength variations with constant deviations, namely $\pm 10\%$ and $\pm 20\%$, together with the mean values for T- and flat bars, respectively. Except for very thick panels with T-bars, i.e., with $\beta = 2.08$ and 2.10, all experimental and numerical data of the panel ultimate strength are located in the range of $\pm 20\%$ deviations.

Chapter 10 Concluding Remarks

During the last decade, the application of aluminum alloys to marine structures such as high speed vessels and littoral surface crafts has been rapidly increasing. To operate in increasingly harsher environments, the size of high speed vessels has also grown. Subsequently, the structural design and building process to ensure the structural safety has become more complex in terms of limit state strength assessment and fabrication quality control among others.

During welding fabrication of aluminum ship structures, six different types of initial imperfections which significantly affect the load-carrying capacity and the structural performance will develop. Therefore, it is of crucial importance to precisely define the corresponding levels of initial imperfections and deal with these fabrication related initial imperfections as parameters of influence in the strength calculations in association with reliability analyses and code calibrations.

In contrast to steel structures, available information and database of the pertinent weld-induced initial imperfections for aluminum structures is very limited. This can cause great uncertainty upon the ultimate limit design and strength assessment of welded aluminum structures. The primary motive of initiating the present study was then to make some related and potentially useful contributions by the systematic investigation of weld-induced initial imperfection characteristics of aluminum stiffened plate structures for marine applications.

In so doing, the relevant levels of initial imperfections which are expected to occur during the construction of the object structure could be defined for use at the stage of structural design and strength assessment so that more accurate safety assessment is possible.

For ship design, the ultimate strength of stiffened plate structures which are major strength parts of ship structures must be calculated. In contrast to steel stiffened plate structures where a plenty of information on ultimate strength test results is available, the related information is also very lacking in aluminum stiffened plate structures. For the ultimate strength based reliability assessment and code calibration of ship structures, closed-form

ULS formulae are required.

The aims of the present study have also been to develop database of experimental and numerical results on the ultimate strength for aluminum stiffened plate structures, and also to develop closed-form empirical ULS formulae.

A total of 78 full scale prototype aluminum structures which are equivalent to sub-structures of an 80m long aluminum high-speed vessel were constructed by MIG welding and a total of 6 types of fabrication related initial imperfections which govern the load-carrying capacity were measured.

By statistical analyses of initial imperfection measurements, three different levels (i.e., slight, average and severe levels) of each of the six type initial imperfection parameters were determined which can be used as reference levels of initial imperfections in ultimate limit strength assessment in association with reliability analyses and code calibrations for welded aluminum marine structures. The statistics of initial imperfections obtained in the present study could also constitute a good source of database for use by other investigators and thus they are documented.

Buckling collapse testing on the prototype structures was undertaken. The load-axial displacement curve was obtained until and after the ultimate strength is reached. Nonlinear elastic-plastic large deflection finite element analyses were performed for the prototype structures. The ultimate strength characteristics of the structures together with collapse modes were investigated in terms of plate slenderness ratio and column slenderness ratio as well as initial imperfections.

Closed-form empirical ULS formulas for aluminum stiffened plate structures were developed by the regression analysis of experimental and numerical ultimate strength database obtained from the present study.

It is believed and hoped that the database and insights developed from the present research project will be very useful for ultimate limit state design and strength assessment of aluminum stiffened plate structures which are used for building high speed passenger ships, war ships, littoral surface or combat ships.

Table 2.1 Comparison of the properties between aluminum alloy and steel

Property	Density (kg/m^3)	Electrical conductivity (%)	Thermal conductivity (W/m^oC)	Thermal expansion ($10^{-6}/^oC$)	Specific heat (J/kg^oC)	Melting point (^oC)	Elastic modulus (N/mm^2)
Aluminum	2,700	62	222	23.6	940	660	70,000
Steel	7,850	10	46	12.6	496	1,350	207,000

Table 2.2 Classification of aluminum alloys

Alloy	Major alloying element	Alloy number
Pure aluminum	-	1xxx
Aluminum alloy	Copper	2xxx
	Manganese	3xxx
	Silicon	4xxx
	Magnesium	5xxx
	Magnesium and silicon	6xxx
	Zinc	7xxx
	Other elements	8xxx
Experimental alloy	-	9xxx

Table 2.3 Minimum values of mechanical properties of aluminum alloys used for the construction of prototype structures (DNV 2003)

Alloy and temper	Yield strength of base metal (N/mm^2)	Tensile strength of base metal (N/mm^2)	Elongation of base metal (%)	Remark	Yield strength of welded material (N/mm^2)
5083-H116	215	305	10	Rolled	125
5383-H116	220	305	10	Rolled	145
5383-H112	190	310	13	Extruded	145
6082-T6	240	290	5	Extruded	100

Table 4.1 Mechanical properties of aluminum alloys used for the construction of the prototype structures, obtained by tensile coupon tests

Thickness(mm)	Alloy and temper	E(MPa)	σ_Y (MPa)	σ_T (MPa)	ε_f (%)
6	5083-H116(C)	73129	238.93	353.05	21.4
8	5083-H116(C)	69393	232.26	352.28	20.6
	5083-H116(C)	79320	233.96	354.22	20.3
	5083-H116(C)	72317	237.18	353.91	21.7
Average		73540	235.58	353.37	21.0
5	5383-H116(D)	78820	246.61	364.86	20.5
6	5383-H116(D)	69331	206.14	340.85	24.1
	5383-H116(L)	77566	219.07	353.83	16.6
	5383-H116(C)	77353	217.77	347.56	20.8
8	5383-H116(D)	68127	240.66	350.23	20.8
	5383-H116(L)	76713	273.84	382.21	12.3
	5383-H116(C)	65359	258.12	369.83	19.3
Average		73324	237.46	358.48	19.2
6	5383-H112(L)	76772	196.60	326.03	14.7
6	6082-T6(L)	78194	324.97	345.38	14.0

Note: L: length-wise, C: cross-wise, D: diagonal.

Table 4.2 Overall characteristics of the 78 prototype structures

One-frame bay test plate structures (1200 mm × 1000 mm) with no replications:

ID	Plate		Stiffener					
	t(mm)	Alloy and temper	Type	h_w(mm)	t_w(mm)	b_f(mm)	t_f(mm)	Alloy and temper
1	5	5083-H116	Extruded Tee	55.7	3.7	40	(6.7)	5383-H112
2	5	5083-H116	Extruded Tee	66.1	4	40	(5.7)	5383-H112
3	5	5083-H116	Extruded Tee	76.8	4	45	(5.6)	5383-H112
4	5	5083-H116	Extruded Tee	135	6	55	(8.2)	5383-H112
5	6	5083-H116	Extruded Tee	55.7	3.7	40	(6.7)	5383-H112
6	6	5083-H116	Extruded Tee	66.1	4	40	(5.7)	5383-H112
7	6	5083-H116	Extruded Tee	76.8	4	45	(5.6)	5383-H112
8	6	5083-H116	Extruded Tee	135	6	55	(8.2)	5383-H112
9	8	5083-H116	Extruded Tee	55.7	3.7	40	(6.7)	5383-H112
10	8	5083-H116	Extruded Tee	66.1	4	40	(5.7)	5383-H112
11	8	5083-H116	Extruded Tee	76.8	4	45	(5.6)	5383-H112
12	8	5083-H116	Extruded Tee	135	6	55	(8.2)	5383-H112
13	5	5083-H116	Extruded Tee	55.7	3.7	40	(6.7)	6082-T6
14	5	5083-H116	Extruded Tee	66.1	4	40	(5.7)	6082-T6
15	5	5083-H116	Extruded Tee	76.8	4	45	(5.6)	6082-T6
16	5	5083-H116	Extruded Tee	135	6	55	(8.2)	6082-T6
17	6	5083-H116	Extruded Tee	55.7	3.7	40	(6.7)	6082-T6
18	6	5083-H116	Extruded Tee	66.1	4	40	(5.7)	6082-T6
19	6	5083-H116	Extruded Tee	76.8	4	45	(5.6)	6082-T6
20	6	5083-H116	Extruded Tee	135	6	55	(8.2)	6082-T6
21	8	5083-H116	Extruded Tee	55.7	3.7	40	(6.7)	6082-T6
22	8	5083-H116	Extruded Tee	66.1	4	40	(5.7)	6082-T6
23	8	5083-H116	Extruded Tee	76.8	4	45	(5.6)	6082-T6
24	8	5083-H116	Extruded Tee	135	6	55	(8.2)	6082-T6
25	5	5383-H116	Extruded Tee	55.7	3.7	40	(6.7)	5383-H112
26	5	5383-H116	Extruded Tee	66.1	4	40	(5.7)	5383-H112
27	5	5383-H116	Extruded Tee	76.8	4	45	(5.6)	5383-H112
28	5	5383-H116	Extruded Tee	135	6	55	(8.2)	5383-H112
29	6	5383-H116	Extruded Tee	55.7	3.7	40	(6.7)	5383-H112
30	6	5383-H116	Extruded Tee	66.1	4	40	(5.7)	5383-H112

31	6	5383-H116	Extruded Tee	76.8	4	45	(5.6)	5383-H112
32	6	5383-H116	Extruded Tee	135	6	55	(8.2)	5383-H112
33	8	5383-H116	Extruded Tee	55.7	3.7	40	(6.7)	5383-H112
34	8	5383-H116	Extruded Tee	66.1	4	40	(5.7)	5383-H112
35	8	5383-H116	Extruded Tee	76.8	4	45	(5.6)	5383-H112
36	8	5383-H116	Extruded Tee	135	6	55	(8.2)	5383-H112
37	5	5083-H116	Flat	60	5	-	-	5083-H116
38	5	5083-H116	Flat	90	5	-	-	5083-H116
39	5	5083-H116	Flat	120	5	-	-	5083-H116
40	6	5083-H116	Flat	60	6	-	-	5083-H116
41	6	5083-H116	Flat	90	6	-	-	5083-H116
42	6	5083-H116	Flat	120	6	-	-	5083-H116
43	8	5083-H116	Flat	60	8	-	-	5083-H116
44	8	5083-H116	Flat	90	8	-	-	5083-H116
45	8	5083-H116	Flat	120	8	-	-	5083-H116
46	5	5083-H116	Flat	60	5	-	-	5383-H116
47	5	5083-H116	Flat	90	5	-	-	5383-H116
48	5	5083-H116	Flat	120	5	-	-	5383-H116
49	6	5083-H116	Flat	60	6	-	-	5383-H116
50	6	5083-H116	Flat	90	6	-	-	5383-H116
51	6	5083-H116	Flat	120	6	-	-	5383-H116
52	8	5083-H116	Flat	60	8	-	-	5383-H116
53	8	5083-H116	Flat	90	8	-	-	5383-H116
54	8	5083-H116	Flat	120	8	-	-	5383-H116
55	5	5383-H116	Flat	60	5	-	-	5383-H116
56	5	5383-H116	Flat	90	5	-	-	5383-H116
57	5	5383-H116	Flat	120	5	-	-	5383-H116
58	6	5383-H116	Flat	60	6	-	-	5383-H116
59	6	5383-H116	Flat	90	6	-	-	5383-H116
60	6	5383-H116	Flat	120	6	-	-	5383-H116
61	8	5383-H116	Flat	60	8	-	-	5383-H116
62	8	5383-H116	Flat	90	8	-	-	5383-H116
63	8	5383-H116	Flat	120	8	-	-	5383-H116
64	5	5083-H116	Built-up Tee	80	5	60	5	5083-H116

65	6	5083-H116	Built-up Tee	60	5	60	5	5083-H116
66	8	5083-H116	Built-up Tee	100	5	60	5	5083-H116
67	5	5083-H116	Built-up Tee	80	5	60	5	5383-H116
68	6	5083-H116	Built-up Tee	60	5	60	5	5383-H116
69	8	5083-H116	Built-up Tee	100	5	60	5	5383-H116
70	5	5383-H116	Built-up Tee	80	5	60	5	5383-H116
71	6	5383-H116	Built-up Tee	60	5	60	5	5383-H116
72	8	5383-H116	Built-up Tee	100	5	60	5	5383-H116

One-frame bay test plate structures (1000 mm × 1000 mm):

ID	Plate		Stiffener					
	t(mm)	Alloy and temper	Type	h_w(mm)	t_w(mm)	b_f(mm)	t_f(mm)	Alloy and temper
73	6	5083-H116	Extruded Tee	76.8	4	45	(5.6)	6082-T6
74	8	5083-H116	Extruded Tee	100	6	55	(8.2)	6082-T6
75	8	5383-H116	Extruded Tee	100	6	55	(8.2)	5383-H112

Three-frame bay test plate structures (3000 mm × 1000 mm):

ID	Plate		Stiffener					
	t(mm)	Alloy and temper	Type	h_w(mm)	t_w(mm)	b_f(mm)	t_f(mm)	Alloy and temper
76	6	5083-H116	Extruded Tee	76.8	4	45	(5.6)	6082-T6
77	8	5083-H116	Extruded Tee	100	6	55	(8.2)	6082-T6
78	8	5383-H116	Extruded Tee	100	6	55	(8.2)	5383-H112

Notes: t = plate thickness, h_w = web height (excluding flange thickness), t_w = web thickness, b_f = flange breadth, t_f = flange thickness, t_f where given in brackets indicates the effective value of for an idealized plate-stiffener combination with the same moment of inertia as the actual case.

Table 4.3 Structural dimensions and related properties of the prototype structures

ID	L (mm)	B (mm)	a (mm)	B (mm)	t (mm)	h_w (mm)	t_w (mm)	b_f (mm)	t_f (mm)	σ_{Yp} (MPa)	σ_{Ys} (MPa)	β	λ'
1	1208	1000	1200	300	5	55.7	3.7	40	(6.7)	215	220	3.33	0.94
2	1208	1000	1200	300	5	66.1	4	40	(5.7)	215	220	3.33	0.84
3	1208	1000	1200	300	5	76.8	4	45	(5.6)	215	220	3.33	0.71
4	1208	1000	1200	300	5	135	6	55	(8.2)	215	220	3.33	0.37
5	1208	1000	1200	300	6	55.7	3.7	40	(6.7)	215	220	2.77	0.99
6	1208	1000	1200	300	6	66.1	4	40	(5.7)	215	220	2.77	0.88
7	1208	1000	1200	300	6	76.8	4	45	(5.6)	215	220	2.77	0.74
8	1208	1000	1200	300	6	135	6	55	(8.2)	215	220	2.77	0.38
9	1208	1000	1200	300	8	55.7	3.7	40	(6.7)	215	220	2.08	1.06
10	1208	1000	1200	300	8	66.1	4	40	(5.7)	215	220	2.08	0.95
11	1208	1000	1200	300	8	76.8	4	45	(5.6)	215	220	2.08	0.80
12	1208	1000	1200	300	8	135	6	55	(8.2)	215	220	2.08	0.40
13	1208	1000	1200	300	5	55.7	3.7	40	(6.7)	215	260	3.33	0.96
14	1208	1000	1200	300	5	66.1	4	40	(5.7)	215	260	3.33	0.86
15	1208	1000	1200	300	5	76.8	4	45	(5.6)	215	260	3.33	0.73
16	1208	1000	1200	300	5	135	6	55	(8.2)	215	260	3.33	0.39
17	1208	1000	1200	300	6	55.7	3.7	40	(6.7)	215	260	2.77	1.00
18	1208	1000	1200	300	6	66.1	4	40	(5.7)	215	260	2.77	0.90
19	1208	1000	1200	300	6	76.8	4	45	(5.6)	215	260	2.77	0.76
20	1208	1000	1200	300	6	135	6	55	(8.2)	215	260	2.77	0.39
21	1208	1000	1200	300	8	55.7	3.7	40	(6.7)	215	260	2.08	1.08
22	1208	1000	1200	300	8	66.1	4	40	(5.7)	215	260	2.08	0.96
23	1208	1000	1200	300	8	76.8	4	45	(5.6)	215	260	2.08	0.81
24	1208	1000	1200	300	8	135	6	55	(8.2)	215	260	2.08	0.41
25	1208	1000	1200	300	5	55.7	3.7	40	(6.7)	220	220	3.36	0.95
26	1208	1000	1200	300	5	66.1	4	40	(5.7)	220	220	3.36	0.85
27	1208	1000	1200	300	5	76.8	4	45	(5.6)	220	220	3.36	0.72
28	1208	1000	1200	300	5	135	6	55	(8.2)	220	220	3.36	0.38
29	1208	1000	1200	300	6	55.7	3.7	40	(6.7)	220	220	2.80	0.99
30	1208	1000	1200	300	6	66.1	4	40	(5.7)	220	220	2.80	0.89
31	1208	1000	1200	300	6	76.8	4	45	(5.6)	220	220	2.80	0.75
32	1208	1000	1200	300	6	135	6	55	(8.2)	220	220	2.80	0.38

33	1208	1000	1200	300	8	55.7	3.7	40	(6.7)	220	220	2.10	1.07
34	1208	1000	1200	300	8	66.1	4	40	(5.7)	220	220	2.10	0.96
35	1208	1000	1200	300	8	76.8	4	45	(5.6)	220	220	2.10	0.81
36	1208	1000	1200	300	8	135	6	55	(8.2)	220	220	2.10	0.40
37	1208	1000	1200	300	5	60	5	-	-	215	215	3.33	1.50
38	1208	1000	1200	300	5	90	5	-	-	215	215	3.33	0.90
39	1208	1000	1200	300	5	120	5	-	-	215	215	3.33	0.63
40	1208	1000	1200	300	6	60	6	-	-	215	215	2.77	1.48
41	1208	1000	1200	300	6	90	6	-	-	215	215	2.77	0.89
42	1208	1000	1200	300	6	120	6	-	-	215	215	2.77	0.62
43	1208	1000	1200	300	8	60	8	-	-	215	215	2.08	1.44
44	1208	1000	1200	300	8	90	8	-	-	215	215	2.08	0.87
45	1208	1000	1200	300	8	120	8	-	-	215	215	2.08	0.62
46	1208	1000	1200	300	5	60	5	-	-	215	220	3.33	1.51
47	1208	1000	1200	300	5	90	5	-	-	215	220	3.33	0.90
48	1208	1000	1200	300	5	120	5	-	-	215	220	3.33	0.63
49	1208	1000	1200	300	6	60	6	-	-	215	220	2.77	1.49
50	1208	1000	1200	300	6	90	6	-	-	215	220	2.77	0.89
51	1208	1000	1200	300	6	120	6	-	-	215	220	2.77	0.62
52	1208	1000	1200	300	8	60	8	-	-	215	220	2.08	1.45
53	1208	1000	1200	300	8	90	8	-	-	215	220	2.08	0.88
54	1208	1000	1200	300	8	120	8	-	-	215	220	2.08	0.62
55	1208	1000	1200	300	5	60	5	-	-	220	220	3.36	1.52
56	1208	1000	1200	300	5	90	5	-	-	220	220	3.36	0.91
57	1208	1000	1200	300	5	120	5	-	-	220	220	3.36	0.63
58	1208	1000	1200	300	6	60	6	-	-	220	220	2.80	1.50
59	1208	1000	1200	300	6	90	6	-	-	220	220	2.80	0.90
60	1208	1000	1200	300	6	120	6	-	-	220	220	2.80	0.63
61	1208	1000	1200	300	8	60	8	-	-	220	220	2.10	1.46
62	1208	1000	1200	300	8	90	8	-	-	220	220	2.10	0.88
63	1208	1000	1200	300	8	120	8	-	-	220	220	2.10	0.62
64	1208	1000	1200	300	5	80	5	60	5	215	215	3.33	0.66
65	1208	1000	1200	300	6	60	5	60	5	215	215	2.77	0.89
66	1208	1000	1200	300	8	100	5	60	5	215	215	2.08	0.58
67	1208	1000	1200	300	5	80	5	60	5	215	220	3.34	0.66

68	1208	1000	1200	300	6	60	5	60	5	215	220	2.78	0.90
69	1208	1000	1200	300	8	100	5	60	5	215	220	2.08	0.59
70	1208	1000	1200	300	5	80	5	60	5	220	220	3.36	0.66
71	1208	1000	1200	300	6	60	5	60	5	220	220	2.80	0.90
72	1208	1000	1200	300	8	100	5	60	5	220	220	2.10	0.59
73	1000	1000	992	300	6	76.8	4	45	(5.6)	215	260	2.84	0.63
74	987	1000	979	300	8	100	6	55	(8.2)	215	260	2.14	0.44
75	1000	1000	992	300	8	100	6	55	(8.2)	220	220	2.10	0.44
76	3000	1000	992	300	6	76.8	4	45	(5.6)	215	260	2.84	0.63
77	2961	1000	979	300	8	100	6	55	(8.2)	215	260	2.14	0.44
78	3000	1000	992	300	8	100	6	55	(8.2)	220	220	2.10	0.44

Note: $\beta = \frac{b}{t}\sqrt{\frac{\sigma_{Yp}}{E}}$, $\lambda' = \frac{a}{\pi r}\sqrt{\frac{\sigma_{Yeq}}{E}}$, $r = \sqrt{\frac{I}{A}}$, $\sigma_{Yeq} = \frac{bt\sigma_{Yp} + (h_w t_w + b_f t_f)\sigma_{Ys}}{A}$ = equivalent yield stress, A = cross sectional area of stiffener with attached plating, I = moment of inertia of stiffener with attached plating

Table 4.4 Welding conditions for fabrication of prototype test structures

Thickness	1st Pass	2nd Pass
Plate 5mm, stiffener 6mm	165A, 22.3V, 42cpm	170A, 22.7V, 42cpm
Plate 6mm, stiffener 6mm	167A, 22.5V, 42cpm	172A, 22.8V, 42cpm
Plate 8mm, stiffener 6mm	189A, 23.4V, 42cpm	197A, 23.5V, 42cpm

Note: 1st pass = fillet welding along one side of stiffener, 2nd pass = fillet welding along the other side of stiffener, cpm = cm per minutes.

Table 6.1 Measured data for plate initial distortions, column type initial distortions of stiffeners and sideways initial distortion of stiffeners

ID	t (mm)	β	a (mm)	w_{opl} (mm)	w_{oc} (mm)	w_{os} (mm)	$w_{opl}/(t\beta^2)$	w_{oc}/a	w_{os}/a
1	5	3.33	1200	3.313	1.443	0.658	0.060	0.00120	0.00055
				4.852	2.171	0.993	0.088	0.00181	0.00083
				4.001	2.717	0.578	0.072	0.00226	0.00048
				-	1.496	0.525	-	0.00125	0.00044
2	5	3.33	1200	3.259	1.267	1.772	0.059	0.00106	0.00148
				4.290	1.913	1.179	0.077	0.00159	0.00098
				3.013	1.700	1.879	0.054	0.00142	0.00157
				-	1.023	2.118	-	0.00085	0.00176
3	5	3.33	1200	3.302	1.856	1.939	0.060	0.00155	0.00162
				3.472	1.796	2.105	0.063	0.0015	0.00175
				3.069	1.550	2.172	0.055	0.00129	0.00181
				-	1.272	1.686	-	0.00106	0.00141
4	5	3.33	1200	2.827	1.642	1.254	0.051	0.00137	0.00105
				3.168	1.909	1.427	0.057	0.00159	0.00119
				2.942	2.058	1.531	0.053	0.00171	0.00128
				-	1.891	1.611	-	0.00158	0.00134
5	6	2.77	1200	3.501	1.539	1.092	0.076	0.00128	0.00091
				4.442	2.454	1.146	0.096	0.00205	0.00096
				2.709	2.245	0.541	0.059	0.00187	0.00045
				-	0.808	1.098	-	0.00067	0.00092
6	6	2.77	1200	3.444	2.008	0.388	0.075	0.00167	0.00032
				3.999	2.214	0.497	0.087	0.00184	0.00041
				2.645	1.860	0.979	0.057	0.00155	0.00082
				-	1.126	0.623	-	0.00094	0.00052
7	6	2.77	1200	3.468	1.879	0.502	0.075	0.00157	0.00042
				4.057	1.985	0.736	0.088	0.00165	0.00061
				2.941	1.885	0.293	0.064	0.00157	0.00024
				-	1.245	0.873	-	0.00104	0.00073
8	6	2.77	1200	3.056	1.991	0.972	0.066	0.00166	0.00081
				3.346	1.639	0.852	0.073	0.00137	0.00071
				2.581	1.720	0.825	0.056	0.00143	0.00069
				-	1.021	1.352	-	0.00085	0.00113

9	8	2.08	1200	2.475	0.865	1.915	0.072	0.00072	0.00160
				3.363	1.279	1.980	0.097	0.00107	0.00165
				2.256	1.036	1.052	0.065	0.00086	0.00088
				-	1.237	1.916	-	0.00103	0.00160
10	8	2.08	1200	2.456	0.871	1.450	0.071	0.00073	0.00121
				3.568	1.606	1.420	0.103	0.00134	0.00118
				2.457	1.350	1.432	0.071	0.00112	0.00119
				-	1.202	0.914	-	0.00100	0.00076
11	8	2.08	1200	2.412	0.871	1.099	0.070	0.00073	0.00092
				3.496	1.606	0.935	0.101	0.00134	0.00078
				2.444	1.350	1.248	0.071	0.00112	0.00104
				-	1.202	0.766	-	0.00100	0.00064
12	8	2.08	1200	2.582	1.620	1.517	0.075	0.00135	0.00126
				2.987	1.644	0.620	0.086	0.00137	0.00052
				2.227	1.848	1.233	0.064	0.00154	0.00103
				-	1.736	0.910	-	0.00145	0.00076
13	5	3.33	1200	3.061	0.875	1.774	0.055	0.00073	0.00148
				3.667	1.596	1.465	0.066	0.00133	0.00122
				2.784	1.482	1.758	0.050	0.00123	0.00147
				-	0.614	1.247	-	0.00051	0.00104
14	5	3.33	1200	2.479	0.867	0.495	0.045	0.00072	0.00041
				3.421	1.452	0.810	0.062	0.00121	0.00068
				2.104	1.191	0.827	0.038	0.00099	0.00069
				-	0.288	1.147	-	0.00024	0.00096
15	5	3.33	1200	2.794	1.017	0.409	0.050	0.00085	0.00034
				3.650	1.243	1.127	0.066	0.00104	0.00094
				2.584	1.370	0.880	0.047	0.00114	0.00073
					0.452	1.274		0.00038	0.00106
16	5	3.33	1200	2.517	0.600	0.980	0.045	0.00050	0.00082
				2.992	0.536	1.161	0.054	0.00045	0.00097
				2.266	0.334	1.368	0.041	0.00028	0.00114
				-	0.318	1.219	-	0.00027	0.00102
17	6	2.77	1200	2.601	0.262	1.414	0.057	0.00022	0.00118
				3.491	1.268	1.746	0.076	0.00106	0.00146
				2.572	1.417	0.919	0.056	0.00118	0.00077

				-	0.466	0.807	-	0.00039	0.00067
18	6	2.77	1200	2.301	1.523	1.139	0.050	0.00127	0.00095
				2.922	1.447	1.332	0.063	0.00121	0.00111
				2.790	2.154	1.822	0.061	0.00180	0.00152
					1.396	0.894		0.00116	0.00075
19	6	2.77	1200	3.313	1.443	1.292	0.072	0.00120	0.00108
				4.852	2.171	0.466	0.105	0.00181	0.00039
				4.001	2.717	0.367	0.087	0.00226	0.00031
				-	1.496	0.659	-	0.00125	0.00055
20	6	2.77	1200	2.390	0.207	1.146	0.052	0.00017	0.00095
				2.756	0.148	0.235	0.060	0.00012	0.00020
				2.073	0.276	1.131	0.045	0.00023	0.00094
				-	0.378	1.493	-	0.00032	0.00124
21	8	2.08	1200	2.578	1.344	0.965	0.074	0.00112	0.00080
				3.261	1.557	0.698	0.094	0.00130	0.00058
				2.316	2.084	1.291	0.067	0.00174	0.00108
				-	1.497	0.681	-	0.00125	0.00057
22	8	2.08	1200	2.948	1.467	1.444	0.085	0.00122	0.00120
				3.326	1.853	0.436	0.096	0.00154	0.00036
				3.036	1.897	0.830	0.088	0.00158	0.00069
				-	1.176	0.511	-	0.00098	0.00043
23	8	2.08	1200	3.376	1.583	0.801	0.098	0.00132	0.00067
				3.926	2.135	0.561	0.113	0.00178	0.00047
				3.471	2.088	1.049	0.100	0.00174	0.00087
				-	1.375	0.391	-	0.00115	0.00033
24	8	2.08	1200	2.980	1.374	0.620	0.086	0.00115	0.00052
				3.394	1.920	1.851	0.098	0.00160	0.00154
				3.146	1.941	0.978	0.091	0.00162	0.00082
				-	1.584	0.372	-	0.00132	0.00031
25	5	3.36	1200	0.953	0.915	0.234	0.017	0.00076	0.00019
				0.991	1.373	1.277	0.018	0.00114	0.00106
				1.053	1.618	0.542	0.019	0.00135	0.00045
				-	0.655	2.765	-	0.00055	0.00230
26	5	3.36	1200	1.610	0.925	0.521	0.029	0.00077	0.00043
				2.234	1.050	0.274	0.040	0.00088	0.00023

				1.845	1.045	0.927	0.033	0.00087	0.00077
				-	0.818	1.521	-	0.00068	0.00127
27	5	3.36	1200	1.521	1.178	0.800	0.027	0.00098	0.00067
				1.915	2.033	0.837	0.034	0.00169	0.00070
				1.794	1.925	0.417	0.032	0.00160	0.00035
				-	1.055	0.386	-	0.00088	0.00032
28	5	3.36	1200	0.981	1.744	1.606	0.017	0.00145	0.00134
				0.993	1.741	1.550	0.018	0.00145	0.00129
				0.957	1.669	1.650	0.017	0.00139	0.00138
				-	2.383	1.897	-	0.00199	0.00158
29	6	2.80	1200	2.987	1.298	3.200	0.063	0.00108	0.00267
				4.388	2.639	0.887	0.093	0.00220	0.00074
				3.264	2.316	1.790	0.069	0.00193	0.00149
				-	1.938	1.549	-	0.00161	0.00129
30	6	2.80	1200	2.347	0.969	1.411	0.050	0.00081	0.00118
				3.008	1.132	2.162	0.064	0.00094	0.00180
				2.438	1.152	1.892	0.052	0.00096	0.00158
				-	0.866	2.330	-	0.00072	0.00194
31	6	2.80	1200	2.445	0.816	1.058	0.052	0.00068	0.00088
				3.199	0.913	0.601	0.068	0.00076	0.00050
				2.904	1.173	0.489	0.062	0.00098	0.00041
				-	1.328	1.146	-	0.00111	0.00095
32	6	2.80	1200	3.103	0.899	0.474	0.066	0.00075	0.00040
				3.896	1.057	1.005	0.083	0.00088	0.00084
				3.427	1.415	1.053	0.073	0.00118	0.00088
				-	1.799	0.822	-	0.00150	0.00069
33	8	2.10	1200	2.662	1.255	1.381	0.075	0.00105	0.00115
				3.711	1.485	0.610	0.105	0.00124	0.00051
				2.916	1.952	1.313	0.083	0.00163	0.00109
				-	1.594	0.758	-	0.00133	0.00063
34	8	2.10	1200	2.781	1.382	0.620	0.079	0.00115	0.00052
				4.435	1.990	0.600	0.126	0.00166	0.00050
				3.366	2.562	0.876	0.095	0.00213	0.00073
				-	1.911	0.828	-	0.00159	0.00069
35	8	2.10	1200	3.353	1.762	0.669	0.095	0.00147	0.00056

				4.367	2.685	2.319	0.124	0.00224	0.00193
				3.417	2.074	0.629	0.097	0.00173	0.00052
				-	2.804	0.719	-	0.00234	0.00060
36	8	2.10	1200	3.230	1.599	0.534	0.092	0.00133	0.00045
				4.125	1.520	1.302	0.117	0.00127	0.00108
				3.107	1.576	0.920	0.088	0.00131	0.00077
				-	1.870	0.582	-	0.00156	0.00048
37	5	3.33	1200	1.646	0.813	0.999	0.030	0.00068	0.00083
				3.371	1.185	0.455	0.061	0.00099	0.00038
				1.641	1.021	0.563	0.030	0.00085	0.00047
				-	0.732	1.146	-	0.00061	0.00096
38	5	3.33	1200	2.193	0.678	0.634	0.040	0.00057	0.00053
				3.252	1.112	0.722	0.059	0.00093	0.00060
				2.173	1.070	0.485	0.039	0.00089	0.00040
				-	0.706	0.681	-	0.00059	0.00057
39	5	3.33	1200	2.817	0.532	3.134	0.051	0.00044	0.00261
				3.800	0.755	1.493	0.069	0.00063	0.00124
				2.911	1.240	0.537	0.053	0.00103	0.00045
				-	0.814	1.232	-	0.00068	0.00103
40	6	2.77	1200	2.160	0.387	0.701	0.047	0.00032	0.00058
				4.440	1.909	0.387	0.096	0.00159	0.00032
				2.574	2.440	0.725	0.056	0.00203	0.00060
				-	0.205	0.157	-	0.00017	0.00013
41	6	2.77	1200	2.646	0.954	0.701	0.057	0.00080	0.00058
				4.632	2.597	0.942	0.101	0.00216	0.00079
				3.234	2.501	0.797	0.070	0.00208	0.00066
				-	1.329	0.374	-	0.00111	0.00031
42	6	2.77	1200	2.028	1.341	0.749	0.044	0.00112	0.00062
				2.832	1.691	0.507	0.062	0.00141	0.00042
				2.076	1.401	0.338	0.045	0.00117	0.00028
				-	1.546	0.495	-	0.00129	0.00041
43	8	2.08	1200	3.984	2.452	0.532	0.115	0.00204	0.00044
				3.328	2.948	2.488	0.096	0.00246	0.00207
				1.520	1.691	2.102	0.044	0.00141	0.00175
				-	1.377	2.935	-	0.00115	0.00245

44	8	2.08	1200	1.368	1.522	2.525	0.040	0.00127	0.00210
				1.720	1.897	2.621	0.050	0.00158	0.00218
				1.112	1.305	1.631	0.032	0.00109	0.00136
				-	1.365	2.428	-	0.00114	0.00202
45	8	2.08	1200	2.496	1.643	1.377	0.072	0.00137	0.00115
				2.712	1.244	0.580	0.078	0.00104	0.00048
				2.112	0.532	1.305	0.061	0.00044	0.00109
				-	1.582	0.834	-	0.00132	0.00069
46	5	3.33	1200	1.735	0.483	1.125	0.031	0.00040	0.00094
				2.161	0.575	1.061	0.039	0.00048	0.00088
				1.680	0.326	1.049	0.030	0.00027	0.00087
				-	0.316	2.464	-	0.00026	0.00205
47	5	3.33	1200	2.511	1.253	0.504	0.045	0.00104	0.00042
				3.266	1.303	1.750	0.059	0.00109	0.00146
				2.837	1.690	1.131	0.051	0.00141	0.00094
				-	1.690	1.341	-	0.00141	0.00112
48	5	3.33	1200	3.003	1.626	0.578	0.054	0.00136	0.00048
				3.753	1.626	0.772	0.068	0.00136	0.00064
				3.512	1.759	0.386	0.063	0.00147	0.00032
				-	2.415	0.644	-	0.00201	0.00054
49	6	2.77	1200	2.850	0.930	0.906	0.062	0.00078	0.00076
				4.344	1.981	1.027	0.094	0.00165	0.00086
				2.532	1.546	1.619	0.055	0.00129	0.00135
				-	0.727	0.519	-	0.00061	0.00043
50	6	2.77	1200	2.743	1.459	0.620	0.060	0.00122	0.00052
				4.190	2.345	0.374	0.091	0.00195	0.00031
				3.169	2.263	0.352	0.069	0.00189	0.00029
				-	1.449	0.598	-	0.00121	0.00050
51	6	2.77	1200	2.670	1.607	1.220	0.058	0.00134	0.00102
				3.714	1.401	0.411	0.081	0.00117	0.00034
				2.832	1.546	0.338	0.062	0.00129	0.00028
				-	1.498	0.652	-	0.00125	0.00054
52	8	2.08	1200	1.840	0.495	1.051	0.053	0.00041	0.00088
				2.336	0.399	0.495	0.067	0.00033	0.00041
				1.712	0.302	0.338	0.049	0.00025	0.00028

				-	0.592	0.942	-	0.00049	0.00079
53	8	2.08	1200	2.544	1.196	0.314	0.074	0.00100	0.00026
				3.640	1.764	1.546	0.105	0.00147	0.00129
				2.688	2.054	0.834	0.078	0.00171	0.00069
				-	1.727	1.063	-	0.00144	0.00089
54	8	2.08	1200	2.408	1.486	1.353	0.070	0.00124	0.00113
				2.968	1.280	0.399	0.086	0.00107	0.00033
				2.536	0.785	0.592	0.073	0.00065	0.00049
				-	1.196	1.329	-	0.00100	0.00111
55	5	3.36	1200	2.990	1.389	1.957	0.053	0.00116	0.00163
				3.386	1.226	1.265	0.060	0.00102	0.00105
				2.380	0.814	0.891	0.042	0.00068	0.00074
				-	0.914	0.978	-	0.00076	0.00082
56	5	3.36	1200	0.902	1.131	0.630	0.016	0.00094	0.00053
				1.153	1.862	0.274	0.020	0.00155	0.00023
				1.104	1.770	0.771	0.020	0.00148	0.00064
				-	2.213	0.884	-	0.00184	0.00074
57	5	3.36	1200	3.889	2.348	0.235	0.069	0.00196	0.00020
				4.136	1.705	0.372	0.073	0.00142	0.00031
				4.550	2.117	1.243	0.081	0.00176	0.00104
				-	2.920	0.977	-	0.00243	0.00081
58	6	2.80	1200	1.896	0.133	1.619	0.040	0.00011	0.00135
				3.366	0.640	0.713	0.072	0.00053	0.00059
				2.220	1.329	0.423	0.047	0.00111	0.00035
				-	0.785	1.111	-	0.00065	0.00093
59	6	2.80	1200	2.508	0.918	0.978	0.053	0.00077	0.00082
				3.966	1.558	0.906	0.084	0.00130	0.00076
				2.598	1.595	0.834	0.055	0.00133	0.00069
				-	1.075	0.882	-	0.00090	0.00073
60	6	2.80	1200	2.580	1.329	0.616	0.055	0.00111	0.00051
				3.540	1.063	0.773	0.075	0.00089	0.00064
				2.292	0.797	1.619	0.049	0.00066	0.00135
				-	1.015	1.148	-	0.00085	0.00096
61	8	2.10	1200	1.648	0.326	0.326	0.047	0.00027	0.00027
				2.784	0.701	0.338	0.079	0.00058	0.00028

				1.680	1.075	1.788	0.048	0.00090	0.00149
				-	0.254	1.848	-	0.00021	0.00154
62	8	2.10	1200	2.352	1.232	1.570	0.067	0.00103	0.00131
				3.400	1.438	0.435	0.096	0.00120	0.00036
				2.224	1.667	0.797	0.063	0.00139	0.00066
				-	0.689	0.797	-	0.00057	0.00066
63	8	2.10	1200	2.872	1.921	0.507	0.081	0.00160	0.00042
				3.400	1.546	0.930	0.096	0.00129	0.00078
				2.032	1.474	1.317	0.058	0.00123	0.00110
				-	1.232	0.519	-	0.00103	0.00043
64	5	3.33	1200	3.109	1.340	0.781	0.056	0.00112	0.00065
				3.406	0.685	1.046	0.061	0.00057	0.00087
				2.913	0.794	1.461	0.053	0.00066	0.00122
				-	0.620	0.234	-	0.00052	0.00020
65	6	2.77	1200	2.999	1.580	0.731	2.999	0.00132	0.00061
				3.249	1.300	0.960	3.249	0.00108	0.00080
				2.576	0.911	1.444	2.576	0.00076	0.00120
				-	0.863	0.542	-	0.00072	0.00045
66	8	2.08	1200	2.416	0.674	1.687	2.416	0.00056	0.00141
				3.006	0.343	0.907	3.006	0.00029	0.00076
				2.594	0.403	1.806	2.594	0.00034	0.00151
				-	0.576	0.806	-	0.00048	0.00067
67	5	3.33	1200	2.727	1.656	0.965	2.727	0.00138	0.00080
				3.135	0.961	1.473	3.135	0.00080	0.00123
				3.058	0.722	1.469	3.058	0.00060	0.00122
				-	1.430	1.097	-	0.00119	0.00091
68	6	2.77	1200	2.110	0.827	1.884	2.110	0.00069	0.00157
				2.868	0.702	1.268	2.868	0.00059	0.00106
				2.710	0.871	1.443	2.710	0.00073	0.00120
				-	1.103	1.223	-	0.00092	0.00102
69	8	2.08	1200	2.177	0.359	1.001	2.177	0.00030	0.00083
				3.038	0.494	0.841	3.038	0.00041	0.00070
				1.829	0.615	1.443	1.829	0.00051	0.00120
				-	0.550	1.647	-	0.00046	0.00137
70	5	3.36	1200	3.833	1.810	1.113	3.833	0.00151	0.00093

				3.916	1.522	1.600	3.916	0.00127	0.00133
				3.952	0.914	1.285	3.952	0.00076	0.00107
				-	1.977	1.469	-	0.00165	0.00122
71	6	2.80	1200	1.301	0.523	0.541	1.301	0.00044	0.00045
				1.922	1.447	1.274	1.922	0.00121	0.00106
				1.790	2.154	0.698	1.790	0.00180	0.00058
				-	1.396	0.709	-	0.00116	0.00059
72	8	2.10	1200	1.843	0.875	1.222	1.843	0.00073	0.00102
				2.676	1.537	1.127	2.676	0.00128	0.00094
				1.430	0.846	0.776	1.430	0.00071	0.00065
				-	1.854	1.830	-	0.00155	0.00153
73	6	2.77	992	3.670	1.198	0.791	0.080	0.00121	0.00080
				3.148	1.448	0.380	0.068	0.00146	0.00038
				3.490	1.336	0.406	0.076	0.00135	0.00041
				-	1.133	0.808	-	0.00114	0.00081
74	8	2.08	979	3.116	2.197	1.011	0.090	0.00224	0.00103
				3.925	1.977	1.585	0.113	0.00202	0.00162
				2.905	1.625	1.151	0.084	0.00166	0.00118
				-	2.302	0.131	-	0.00235	0.00013
75	8	2.10	992	2.917	1.296	0.818	0.083	0.00131	0.00082
				3.516	1.154	0.629	0.100	0.00116	0.00063
				2.711	0.905	0.148	0.077	0.00091	0.00015
				-	0.681	0.061	-	0.00069	0.00006
76	6	2.77	992	8.031	4.886	0.976	0.174	0.00493	0.00098
				8.145	5.583	1.066	0.177	0.00563	0.00107
				7.806	5.209	1.021	0.170	0.00525	0.00103
				-	4.781	1.142	-	0.00482	0.00115
				7.775	5.984	1.812	0.169	0.00603	0.00183
				7.565	5.693	0.589	0.164	0.00574	0.00059
				8.370	4.369	1.384	0.182	0.00440	0.00140
				-	5.233	1.582	-	0.00527	0.00159
				7.720	5.194	0.594	0.168	0.00524	0.00060
				8.637	4.723	1.471	0.188	0.00476	0.00148
				7.793	6.127	1.590	0.169	0.00618	0.00160
				-	5.383	1.583	-	0.00543	0.00160

77	8	2.08	979	7.263	5.662	2.033	0.210	0.00578	0.00208
				8.633	5.226	2.696	0.249	0.00534	0.00275
				8.158	4.882	2.462	0.236	0.00499	0.00252
				-	5.072	1.269	-	0.00518	0.00130
				8.046	5.832	1.372	0.232	0.00596	0.00140
				9.064	4.549	1.153	0.262	0.00465	0.00118
				8.554	6.255	2.154	0.247	0.00639	0.00220
				-	6.608	3.401	-	0.00675	0.00347
				9.001	6.341	1.709	0.260	0.00648	0.00175
				11.231	5.993	1.220	0.324	0.00612	0.00125
				10.386	8.217	2.825	0.300	0.00839	0.00289
				-	7.218	1.529	-	0.00737	0.00156
78	8	2.10	992	6.588	3.207	0.744	0.187	0.00323	0.00075
				8.555	4.092	1.442	0.242	0.00413	0.00145
				8.721	3.677	0.883	0.247	0.00371	0.00089
				-	3.822	1.271	-	0.00385	0.00128
				7.209	6.011	2.190	0.204	0.00606	0.00221
				10.298	3.659	1.207	0.292	0.00369	0.00122
				8.560	3.678	0.824	0.243	0.00371	0.00083
				-	4.711	1.644	-	0.00475	0.00166
				7.433	4.481	0.936	0.211	0.00452	0.00094
				10.482	3.619	0.943	0.297	0.00365	0.00095
				8.693	4.955	1.050	0.246	0.00499	0.00106
				-	3.231	1.048	-	0.00326	0.00106

Table 6.2(a) Slight, average and severe levels of $w_{opl}/(t\beta^2)$ for plating

Level		Mean	Standard deviation	COV	Mean for steel* (Smith et al. 1988)
Slight	5% and below band	0.018	0.0017	0.094	0.025
	15% and below band	0.027	0.0077	0.28	-
	30% and below band	0.046	0.011	0.24	-
Average		0.096	0.055	0.57	0.1
Severe	95% and above band	0.252	0.038	0.15	0.3
	85% and above band	0.220	0.049	0.22	-
	70% and above band	0.210	0.053	0.24	-

Note: * Smith et al. (1988) suggested the three levels of initial distortions for steel.

Table 6.2(b) Slight, average and severe levels of $w_{ol}/(t\beta^2)$ for plating

Level		Mean	Standard deviation	COV
Slight	5% and below band	0.0059	0.00327	0.55
	15% and below band	0.0181	0.00809	0.45
	30% and below band	0.0344	0.0147	0.43
Average		0.093	0.055	0.57
Severe	95% and above band	0.269	0.0358	0.13
	85% and above band	0.243	0.0498	0.20
	70% and above band	0.202	0.0656	0.33

Table 6.2(c) Slight, average and severe levels of $w_{ob}/(t\beta^2)$ for plating

Level		Mean	Standard deviation	COV
Slight	5% and below band	0.00033	0.00025	0.76
	15% and below band	0.00105	0.00072	0.68
	30% and below band	0.00202	0.00139	0.69
Average		0.0101	0.00898	0.89
Severe	95% and above band	0.0365	0.00804	0.22
	85% and above band	0.0299	0.00932	0.31
	70% and above band	0.0198	0.00902	0.46

Table 6.2(d) Slight, average and severe levels of w_{om} for plating

Level		Mean	Standard deviation	COV
Slight	5% and below band	1.36×10^{-5}	5.62×10^{-5}	0.04
	15% and below band	9.15×10^{-5}	4.78×10^{-5}	0.52
	30% and below band	0.00034	1.42×10^{-5}	0.04
Average		0.00552	0.00993	1.80
Severe	95% and above band	0.0468	0.0177	0.38
	85% and above band	0.0382	0.0201	0.53
	70% and above band	0.0320	0.0224	0.70

Table 6.3(a) Slight, average and severe levels of w_{oc}/a for stiffener

Level		Mean	Standard deviation	COV
Slight	5% and below band	0.00016	3.7×10^{-5}	0.23
	15% and below band	0.00033	0.00011	0.32
	30% and below band	0.00058	0.00021	0.35
Average		0.0018	0.0014	0.75
Severe	95% and above band	0.0056	0.0011	0.19
	85% and above band	0.0052	0.0013	0.25
	70% and above band	0.0047	0.0015	0.32

Table 6.3(b) Slight, average and severe levels of w_{ol}^{c}/a for stiffener

Level		Mean	Standard deviation	COV
Slight	5% and below band	6.71×10^{-5}	5.21×10^{-5}	0.78
	15% and below band	0.00015	0.00011	0.78
	30% and below band	0.00038	0.00026	0.69
Average		0.00155	0.00132	0.19
Severe	95% and above band	0.00525	0.001	0.19
	85% and above band	0.00472	0.00113	0.24
	70% and above band	0.00382	0.00148	0.38

Table 6.4(a) Slight, average and severe levels of w_{os}/a for stiffener

Level		Mean	Standard deviation	COV
Slight	5% and below band	0.00019	5.1×10^{-5}	0.27
	15% and below band	0.00034	8.8×10^{-5}	0.26
	30% and below band	0.00046	0.00014	0.31
Average		0.001	0.00054	0.52
Severe	95% and above band	0.0024	0.00047	0.20
	85% and above band	0.0021	0.00051	0.25
	70% and above band	0.0017	0.00051	0.30

Table 6.4(b) Slight, average and severe levels of w_{01}^{s}/a for stiffener

Level		Mean	Standard deviation	COV
Slight	5% and below band	3.5×10^{-5}	1.58×10^{-5}	0.45
	15% and below band	7.98×10^{-5}	4.77×10^{-5}	0.66
	30% and below band	0.00014	8.7×10^{-5}	0.63
Average		0.000574	0.000451	0.79
Severe	95% and above band	0.0018	0.00022	0.12
	85% and above band	0.00139	0.00033	0.24
	70% and above band	0.0011	0.00036	0.33

Table 6.5 Slight, average and severe levels of σ_{rcx}/σ_{Yp} inside welded plating

Level		Mean	Standard deviation	COV
Slight	5% and below band	-0.110	0.004	0.038
Average		-0.161	0.031	0.193
Severe	95% and above band	-0.216	0.007	0.030

Table 6.6 Slight, average and severe levels of σ_{rcx}/σ_{Ys} inside welded plating

Level		Mean	Standard deviation	COV
Slight	5% and below band	-0.078	0.012	0.153
Average		-0.137	0.036	0.260
Severe	95% and above band	-0.195	0.014	0.074

Table 6.7 Slight, average and severe levels of the HAZ tensile residual stress measured for 5083-H116, 5383-H116, 5383-H112 and 6082-T6

Material	Level	Mean (MPa)	Standard deviation (MPa)	COV	Reduction factor (Mean/ σ_Y)*
5083-H116	Slight (95% and above band)	194.707	3.336	0.017	0.906
	Average	167.143	18.617	0.111	0.777
	Severe (5% and below band)	93.886	30.980	0.330	0.437
5383-H116	Slight (95% and above band)	180.397	1.134	0.006	0.820
	Average	170.388	12.865	0.076	0.774
	Severe (5% and below band)	140.875	1.843	0.013	0.640
5383-H112	Slight (95% and above band)	-	-	-	-
	Average	169.379	11.936	0.070	0.891
	Severe (5% and below band)	-	-	-	-
6082-T6	Slight (95% and above band)	-	-	-	-
	Average	168.746	2.807	0.017	0.703
	Severe (5% and below band)	-	-	-	-

Note: * σ_Y = minimum yield stress of the corresponding material which can be taken from Table 3.

Table 6.8 Slight, average and severe levels of the HAZ breadth measured

Level	Mean (mm)	Standard deviation (mm)	COV
Slight (5% and below band)	11.298	1.794	0.159
Average	23.132	4.233	0.183
Severe (95% and above band)	29.922	1.561	0.052

Table 7.1 Summary of the ultimate strengths obtained for all test structures

ID	P_u (KN)	σ_u (MPa)	σ_u/σ_{Yeq}	Collapse mode
ID1	697.01	99.02	0.462	III
ID2	762.32	108.56	0.487	V
ID3	807.52	109.28	0.517	III+IV
ID4	1354.40	131.03	0.546	IV+V
ID5	776.14	96.55	0.448	III
ID6	917.94	114.42	0.530	III
ID7	931.77	111.07	0.516	III
ID8	1513.75	133.53	0.615	V
ID9	1150.05	114.56	0.531	V
ID10	1169.37	116.68	0.407	V
ID11	1179.47	113.53	0.526	V
ID12	1610.44	120.76	0.557	V
ID13	687.79	97.72	0.435	III
ID14	756.83	107.77	0.477	III
ID15	825.86	111.77	0.492	III+IV
ID16	1450.21	140.30	0.596	III+IV
ID17	778.01	96.78	0.431	III
ID18	829.59	103.41	0.460	III
ID19	970.50	115.68	0.513	III+IV
ID20	1659.18	146.36	0.627	III+IV
ID21	1172.99	116.85	0.525	III

ID22	1360.88	135.78	0.610	V
ID23	1511.89	145.53	0.651	IV+V
ID24	1868.24	140.09	0.613	III+IV
ID25	600.32	85.29	0.384	III
ID26	646.31	92.04	0.418	III
ID27	728.29	98.56	0.448	III+IV
ID28	1249.48	120.88	0.549	III+IV
ID29	790.95	98.39	0.447	V
ID30	908.72	113.27	0.515	V
ID31	895.88	106.79	0.494	III+IV
ID32	1367.35	120.62	0.548	III+IV
ID33	1202.51	119.79	0.544	V
ID34	1185.94	118.33	0.538	V
ID35	1123.28	108.12	0.491	V
ID36	1513.75	113.51	0.516	V
ID37	474.31	76.50	0.356	III
ID38	748.59	110.09	0.512	III
ID39	661.12	89.34	0.416	V
ID40	481.47	64.71	0.301	III
ID41	813.02	99.63	0.463	III
ID42	820.37	92.38	0.430	V
ID43	693.28	69.89	0.325	V
ID44	1294.59	118.99	0.553	V
ID45	1414.32	119.45	0.556	V
ID46	479.71	77.37	0.357	III
ID47	743.00	109.27	0.504	V
ID48	512.85	69.30	0.319	V
ID49	435.48	58.53	0.271	III
ID50	987.07	120.97	0.559	V
ID51	985.21	110.95	0.513	V
ID52	953.34	96.10	0.394	III
ID53	1346.17	123.73	0.572	III
ID54	1293.61	109.26	0.506	V
ID55	440.98	71.13	0.323	III
ID56	697.89	102.63	0.467	V

ID57	627.88	84.85	0.386	V
ID58	510.11	68.56	0.312	III
ID59	775.26	95.01	0.432	III
ID60	818.51	92.17	0.419	V
ID61	883.03	89.02	0.405	III
ID62	1643.58	151.07	0.687	V
ID63	1461.19	123.41	0.561	V
ID64	861.85	110.49	0.518	III+IV
ID65	917.06	109.17	0.508	III
ID66	1394.90	124.55	0.579	V
ID67	889.40	114.03	0.526	III+IV
ID68	831.45	98.98	0.466	III+IV
ID69	1214.47	108.44	0.501	V
ID70	818.51	104.94	0.485	III+IV
ID71	849.79	101.17	0.460	III
ID72	1524.73	136.14	0.619	V
ID73	995.31	118.64	0.526	III
ID74	1655.55	134.62	0.589	III+IV
ID75	1602.10	130.27	0.592	III+IV
ID76	1009.14	120.29	0.529	III
ID77	1594.75	129.68	0.563	III+IV
ID78	1642.60	133.57	0.607	III

Note: P_u = ultimate load, σ_u = ultimate stress, σ_{Yeq} = equivalent yield stress considering the difference of yield stresses for both plate and stiffeners.

Table 8.1 Summary of the ultimate strengths of test structures together with collapse modes obtained by FEA and experiment

ID	Exp.		FEA							
			1 bay-CIP		1 bay-CIS		2 bay-CIS		2 bay-CIS	
	σ_u/σ_{Yeq}	Mode	σ_u/σ_{Yeq}	Mode	σ_u/σ_{Yeq}	Mode	σ_u/σ_{Yeq}	Mode	σ_u/σ_{Yeq}	Mode
ID1	0.462	III	0.380	III	0.413	III	0.474	III	0.449	V
ID2	0.487	V	0.426	III	0.459	III	0.508	III	0.471	V
ID3	0.517	III,IV	0.460	III	0.490	III	0.517	III	0.492	V
ID4	0.546	IV,V	0.452	III	0.456	III	0.550	V	0.562	V
ID5	0.448	III	0.434	III	0.482	III	0.478	III	0.471	V
ID6	0.530	III	0.490	III	0.536	III	0.516	III	0.495	V
ID7	0.516	III	0.521	III	0.559	III	0.554	III	0.526	V
ID8	0.615	V	0.554	III	0.560	III	0.604	V	0.590	V
ID9	0.531	V	0.459	III	0.421	V	0.485	III	0.491	V
ID10	0.407	V	0.568	V	0.417	V	0.533	III	0.534	V
ID11	0.526	V	0.589	V	0.467	V	0.590	III	0.581	V
ID12	0.557	V	0.673	III	0.692	III	0.670	V	0.650	V
ID13	0.435	III	0.354	III	0.390	III	0.491	III	0.474	V
ID14	0.477	III	0.399	III	0.434	III	0.531	III	0.479	V
ID15	0.492	III,IV	0.433	III	0.464	III	0.602	III	0.543	V
ID16	0.596	III,IV	0.505	III	0.511	III	0.582	V	0.593	V
ID17	0.431	III	0.402	III	0.452	III	0.506	III	0.491	V
ID18	0.460	III	0.458	III	0.528	III	0.532	III	0.500	V
ID19	0.513	III,IV	0.487	III	0.529	III	0.602	III	0.556	V
ID20	0.627	III,IV	0.503	III	0.514	III	0.575	V	0.582	V
ID21	0.525	III	0.501	III	0.468	V	0.521	III	0.533	V
ID22	0.610	V	0.590	III	0.451	V	0.570	III	0.570	V
ID23	0.651	IV,V	0.622	III	0.514	V	0.662	III	0.647	V
ID24	0.613	III,IV	0.614	III	0.645	III	0.674	V	0.687	V
ID25	0.384	III	0.383	III	0.419	III	0.468	III	0.442	V
ID26	0.418	III	0.430	III	0.464	III	0.501	III	0.464	V
ID27	0.448	III,IV	0.464	III	0.494	III	0.564	III	0.497	V
ID28	0.549	III,IV	0.513	III	0.544	III	0.577	V	0.570	V
ID29	0.447	V	0.433	III	0.485	III	0.486	III	0.475	V
ID30	0.515	V	0.488	III	0.537	III	0.532	III	0.508	V

ID31	0.494	III,IV	0.525	III	0.564	III	0.564	III	0.543	V
ID32	0.548	III,IV	0.552	III	0.590	III	0.608	V	0.594	V
ID33	0.544	V	0.518	III	0.407	V	0.551	III	0.538	V
ID34	0.538	V	0.536	III	0.401	V	0.575	III	0.564	V
ID35	0.491	V	0.564	V	0.448	V	0.612	III	0.600	V
ID36	0.516	V	0.602	III	0.628	III	0.664	V	0.645	V
ID37	0.356	III	0.312	III	0.339	III	0.361	III	0.384	V
ID38	0.512	III	0.471	III	0.460	V	0.513	III	0.510	V
ID39	0.416	V	0.406	III	0.393	V	0.423	III	0.418	V
ID40	0.301	III	0.290	III	0.304	III	0.312	III	0.326	V
ID41	0.463	III	0.457	III	0.465	III	0.523	III	0.482	V
ID42	0.430	V	0.427	III	0.413	V	0.465	III	0.440	V
ID43	0.325	V	0.318	III	0.329	V	0.343	III	0.355	V
ID44	0.553	V	0.543	III	0.570	III	0.577	III	0.566	V
ID45	0.556	V	0.520	III	0.560	V	0.588	III	0.558	V
ID46	0.357	III	0.313	III	0.341	III	0.353	III	0.377	V
ID47	0.504	V	0.472	III	0.483	V	0.514	III	0.516	V
ID48	0.319	V	0.284	III	0.281	V	0.344	III	0.358	V
ID49	0.271	III	0.264	III	0.288	III	0.314	III	0.327	V
ID50	0.559	V	0.522	III	0.545	V	0.567	III	0.569	V
ID51	0.513	V	0.507	III	0.484	V	0.530	III	0.495	V
ID52	0.394	III	0.413	III	0.418	V	0.451	III	0.449	V
ID53	0.572	III	0.572	III	0.559	III	0.581	III	0.583	V
ID54	0.506	V	0.493	III	0.486	V	0.560	III	0.511	V
ID55	0.323	III	0.295	III	0.315	III	0.332	III	0.343	V
ID56	0.467	V	0.440	III	0.411	V	0.476	III	0.450	V
ID57	0.386	V	0.369	III	0.349	V	0.425	III	0.410	V
ID58	0.312	III	0.292	III	0.306	III	0.312	III	0.324	V
ID59	0.432	III	0.436	III	0.446	III	0.472	III	0.447	V
ID60	0.419	V	0.435	III	0.389	V	0.402	III	0.422	V
ID61	0.405	III	0.385	III	0.380	V	0.397	III	0.405	V
ID62	0.687	V	0.575	III	0.635	III	0.616	III	0.621	V
ID63	0.561	V	0.570	III	0.556	V	0.579	III	0.558	V
ID64	0.518	III,IV	0.465	III	0.500	III	0.567	III	0.522	V
ID65	0.508	III	0.468	III	0.500	III	0.510	III	0.486	V

ID66	0.579	V	0.612	III	0.545	V	0.612	III	0.619	V
ID67	0.526	III,IV	0.464	III	0.520	III	0.579	III	0.523	V
ID68	0.466	III,IV	0.467	III	0.523	III	0.510	III	0.487	V
ID69	0.501	V	0.617	III	0.560	V	0.625	III	0.621	V
ID70	0.485	III,IV	0.469	III	0.502	III	0.574	III	0.517	V
ID71	0.460	III	0.472	III	0.531	III	0.505	III	0.480	V
ID72	0.619	V	0.633	III	0.547	V	0.619	III	0.614	V
ID73	0.526	III	0.520	III	0.554	III	-	-	-	-
ID74	0.589	III,IV	0.603	III	0.644	III	-	-	-	-
ID75	0.592	III,IV	0.612	III	0.651	III	-	-	-	-
ID76	0.529	III	-	-	-	-	0.564	III	0.541	V
ID77	0.563	III,IV	-	-	-	-	0.581	III	0.557	V
ID78	0.607	III	-	-	-	-	0.643	III	0.620	V

Notes: III = beam-column type collapse mode, IV = stiffener web buckling mode, V = stiffener tripping mode, σ_u = ultimate compressive strength (stress), σ_{Yeq} = equivalent material yield stress over plating and stiffeners.

Table 8.2 Additional FEA solutions for different plate and column slenderness ratios from the prototype structures

Stiffener Type	β	λ	FEA(σ_u/σ_{Yeq})			
			1 bay-CIP	1 bay-CIS	2 bay-CIP	2 bay-CIS
Tee	2.08	0.26	0.615	0.635	0.696	0.685
Flat	2.08	0.38	0.418	0.374	0.358	0.331
Tee	2.08	1.44	0.316	0.244	0.350	0.352
Flat	2.08	2.06	0.187	0.217	0.220	0.222
Tee	2.08	2.26	0.184	0.148	0.186	0.187
Tee	2.10	0.26	0.606	0.629	0.692	0.680
Flat	2.10	0.39	0.283	0.242	0.255	0.251
Tee	2.10	1.62	0.246	0.193	0.250	0.251
Tee	2.10	2.07	0.177	0.143	0.172	0.173
Flat	2.10	2.08	0.179	0.208	0.210	0.209
Tee	2.77	0.26	0.595	0.601	0.654	0.637
Flat	2.77	0.38	0.260	0.237	0.304	0.322
Tee	2.77	1.32	0.381	0.334	0.355	0.374
Tee	2.77	2.10	0.180	0.185	0.202	0.205
Flat	2.77	2.13	0.161	0.201	0.210	0.213
Tee	2.80	0.26	0.588	0.594	0.649	0.634
Flat	2.80	0.39	0.261	0.237	0.330	0.318
Tee	2.80	1.64	0.282	0.254	0.279	0.283
Tee	2.80	2.13	0.180	0.177	0.192	0.195
Flat	2.80	2.16	0.162	0.196	0.191	0.194
Tee	3.33	0.26	0.506	0.509	0.610	0.621
Flat	3.33	0.39	0.199	0.187	0.271	0.204
Tee	3.33	1.54	0.266	0.311	0.324	0.329
Tee	3.33	2.00	0.177	0.239	0.234	0.238
Flat	3.33	2.18	0.148	0.180	0.190	0.193
Tee	3.36	0.26	0.493	0.497	0.638	0.619
Flat	3.36	0.39	0.207	0.194	0.269	0.196
Tee	3.36	1.56	0.266	0.316	0.289	0.293
Tee	3.36	2.02	0.176	0.216	0.203	0.206
Flat	3.36	2.20	0.152	0.189	0.181	0.184

Table 9.1 Formula predictions of the prototype structures, using Eqs.(9.3) or (9.4)

ID	β	λ	Exp. (σ_u/σ_{Yeq})	FEA (σ_u/σ_{Yeq})				Formula (σ_u/σ_{Yeq})
				1 bay-CIP	1 bay-CIS	2 bay-CIP	2 bay-CIS	
ID1	3.33	0.94	0.462	0.380	0.413	0.474	0.449	0.454
ID2	3.33	0.84	0.487	0.426	0.459	0.508	0.471	0.475
ID3	3.33	0.71	0.517	0.460	0.490	0.517	0.492	0.498
ID4	3.33	0.37	0.546	0.452	0.456	0.550	0.562	0.535
ID5	2.77	0.99	0.448	0.434	0.482	0.478	0.471	0.444
ID6	2.77	0.88	0.530	0.490	0.536	0.516	0.495	0.475
ID7	2.77	0.74	0.516	0.521	0.559	0.554	0.526	0.513
ID8	2.77	0.38	0.615	0.554	0.560	0.604	0.590	0.581
ID9	2.08	1.06	0.531	0.459	0.421	0.485	0.491	0.422
ID10	2.08	0.95	0.407	0.568	0.417	0.533	0.534	0.460
ID11	2.08	0.80	0.526	0.589	0.467	0.590	0.581	0.513
ID12	2.08	0.40	0.557	0.673	0.692	0.670	0.650	0.637
ID13	3.33	0.96	0.435	0.354	0.390	0.491	0.474	0.449
ID14	3.33	0.86	0.477	0.399	0.434	0.531	0.479	0.471
ID15	3.33	0.73	0.492	0.433	0.464	0.602	0.543	0.495
ID16	3.33	0.39	0.596	0.505	0.511	0.582	0.593	0.533
ID17	2.77	1.00	0.431	0.402	0.452	0.506	0.491	0.441
ID18	2.77	0.90	0.460	0.458	0.528	0.532	0.500	0.470
ID19	2.77	0.76	0.513	0.487	0.529	0.602	0.556	0.508
ID20	2.77	0.39	0.627	0.503	0.514	0.575	0.582	0.580
ID21	2.08	1.08	0.525	0.501	0.468	0.521	0.533	0.415
ID22	2.08	0.96	0.610	0.590	0.451	0.570	0.570	0.456
ID23	2.08	0.81	0.651	0.622	0.514	0.662	0.647	0.509
ID24	2.08	0.41	0.613	0.614	0.645	0.674	0.687	0.635
ID25	3.36	0.95	0.384	0.383	0.419	0.468	0.442	0.451
ID26	3.36	0.85	0.418	0.430	0.464	0.501	0.464	0.472
ID27	3.36	0.72	0.448	0.464	0.494	0.564	0.497	0.496
ID28	3.36	0.38	0.549	0.513	0.544	0.577	0.570	0.532
ID29	2.80	0.99	0.447	0.433	0.485	0.486	0.475	0.444
ID30	2.80	0.89	0.515	0.488	0.537	0.532	0.508	0.472
ID31	2.80	0.75	0.494	0.525	0.564	0.564	0.543	0.509
ID32	2.80	0.38	0.548	0.552	0.590	0.608	0.594	0.579

ID33	2.10	1.07	0.544	0.518	0.407	0.551	0.538	0.418
ID34	2.10	0.96	0.538	0.536	0.401	0.575	0.564	0.456
ID35	2.10	0.81	0.491	0.564	0.448	0.612	0.600	0.509
ID36	2.10	0.40	0.516	0.602	0.628	0.664	0.645	0.636
ID37	3.33	1.50	0.356	0.312	0.339	0.361	0.384	0.316
ID38	3.33	0.90	0.512	0.471	0.460	0.513	0.510	0.478
ID39	3.33	0.63	0.416	0.406	0.393	0.423	0.418	0.370
ID40	2.77	1.48	0.301	0.290	0.304	0.312	0.326	0.336
ID41	2.77	0.89	0.463	0.457	0.465	0.523	0.482	0.509
ID42	2.77	0.62	0.430	0.427	0.413	0.465	0.440	0.417
ID43	2.08	1.44	0.325	0.318	0.329	0.343	0.355	0.365
ID44	2.08	0.87	0.553	0.543	0.570	0.577	0.566	0.547
ID45	2.08	0.62	0.556	0.520	0.560	0.588	0.558	0.562
ID46	3.33	1.51	0.357	0.313	0.341	0.353	0.377	0.314
ID47	3.33	0.90	0.504	0.472	0.483	0.514	0.516	0.478
ID48	3.33	0.63	0.319	0.284	0.281	0.344	0.358	0.370
ID49	2.77	1.49	0.271	0.264	0.288	0.314	0.327	0.333
ID50	2.77	0.89	0.559	0.522	0.545	0.567	0.569	0.509
ID51	2.77	0.62	0.513	0.507	0.484	0.530	0.495	0.417
ID52	2.08	1.45	0.394	0.413	0.418	0.451	0.449	0.362
ID53	2.08	0.88	0.572	0.572	0.559	0.581	0.583	0.545
ID54	2.08	0.62	0.506	0.493	0.486	0.560	0.511	0.562
ID55	3.36	1.52	0.323	0.295	0.315	0.332	0.343	0.310
ID56	3.36	0.91	0.467	0.440	0.411	0.476	0.450	0.475
ID57	3.36	0.63	0.386	0.369	0.349	0.425	0.410	0.367
ID58	2.80	1.50	0.312	0.292	0.306	0.312	0.324	0.329
ID59	2.80	0.90	0.432	0.436	0.446	0.472	0.447	0.505
ID60	2.80	0.63	0.419	0.435	0.389	0.402	0.422	0.429
ID61	2.10	1.46	0.405	0.385	0.380	0.397	0.405	0.358
ID62	2.10	0.88	0.687	0.575	0.635	0.616	0.621	0.544
ID63	2.10	0.62	0.561	0.570	0.556	0.579	0.558	0.555
ID64	3.33	0.66	0.518	0.465	0.500	0.567	0.522	0.506
ID65	2.77	0.89	0.508	0.468	0.500	0.510	0.486	0.473
ID66	2.08	0.58	0.579	0.612	0.545	0.612	0.619	0.587
ID67	3.33	0.66	0.526	0.464	0.520	0.579	0.523	0.506

ID68	2.77	0.90	0.466	0.467	0.523	0.510	0.487	0.470
ID69	2.08	0.59	0.501	0.617	0.560	0.625	0.621	0.584
ID70	3.36	0.66	0.485	0.469	0.502	0.574	0.517	0.505
ID71	2.80	0.90	0.460	0.472	0.531	0.505	0.480	0.469
ID72	2.10	0.59	0.619	0.633	0.547	0.619	0.614	0.583
ID73	2.77	0.63	0.526	0.520	0.554	-	-	0.538
ID74	2.08	0.44	0.589	0.603	0.644	-	-	0.627
ID75	2.10	0.44	0.592	0.612	0.651	-	-	0.626
ID76	2.77	0.63	0.529	-	-	0.564	0.541	0.538
ID77	2.08	0.44	0.563	-	-	0.581	0.557	0.627
ID78	2.10	0.44	0.607	-	-	0.643	0.620	0.626

Note: Ultimate strength of the prototype structures with T-bars is calculated by Eq.(9.3), while the value with flat bars is calculated by Eq.(9.4).

Table 9.2 Formula predictions of the additional structures with different plate and column slenderness ratios from the prototype structures, using Eqs.(9.3) or (9.4)

Stiffener Type	β	λ	FEA (σ_u/σ_{Yeq})				Formula
			1 bay-CIP	1 bay-CIS	2 bay-CIP	2 bay-CIS	(σ_u/σ_{Yeq})
Tee	2.08	0.26	0.615	0.635	0.696	0.685	0.666
Flat	2.08	0.38	0.418	0.374	0.358	0.331	0.318
Tee	2.08	1.44	0.316	0.244	0.350	0.352	0.308
Flat	2.08	2.06	0.187	0.217	0.220	0.222	0.206
Tee	2.08	2.26	0.184	0.148	0.186	0.187	0.161
Tee	2.10	0.26	0.606	0.629	0.692	0.680	0.662
Flat	2.10	0.39	0.283	0.242	0.255	0.251	0.320
Tee	2.10	1.62	0.246	0.193	0.250	0.251	0.265
Tee	2.10	2.07	0.177	0.143	0.172	0.173	0.186
Flat	2.10	2.08	0.179	0.208	0.210	0.209	0.202
Tee	2.77	0.26	0.595	0.601	0.654	0.637	0.594
Flat	2.77	0.38	0.260	0.237	0.304	0.322	0.248
Tee	2.77	1.32	0.381	0.334	0.355	0.374	0.349
Tee	2.77	2.10	0.180	0.185	0.202	0.205	0.187
Flat	2.77	2.13	0.161	0.201	0.210	0.213	0.189
Tee	2.80	0.26	0.588	0.594	0.649	0.634	0.590

Flat	2.80	0.39	0.261	0.237	0.330	0.318	0.250
Tee	2.80	1.64	0.282	0.254	0.279	0.283	0.269
Tee	2.80	2.13	0.180	0.177	0.192	0.195	0.184
Flat	2.80	2.16	0.162	0.196	0.191	0.194	0.184
Tee	3.33	0.26	0.506	0.509	0.610	0.621	0.541
Flat	3.33	0.39	0.199	0.187	0.271	0.204	0.219
Tee	3.33	1.54	0.266	0.311	0.324	0.329	0.302
Tee	3.33	2.00	0.177	0.239	0.234	0.238	0.210
Flat	3.33	2.18	0.148	0.180	0.190	0.193	0.177
Tee	3.36	0.26	0.493	0.497	0.638	0.619	0.537
Flat	3.36	0.39	0.207	0.194	0.269	0.196	0.218
Tee	3.36	1.56	0.266	0.316	0.289	0.293	0.299
Tee	3.36	2.02	0.176	0.216	0.203	0.206	0.207
Flat	3.36	2.20	0.152	0.189	0.181	0.184	0.174

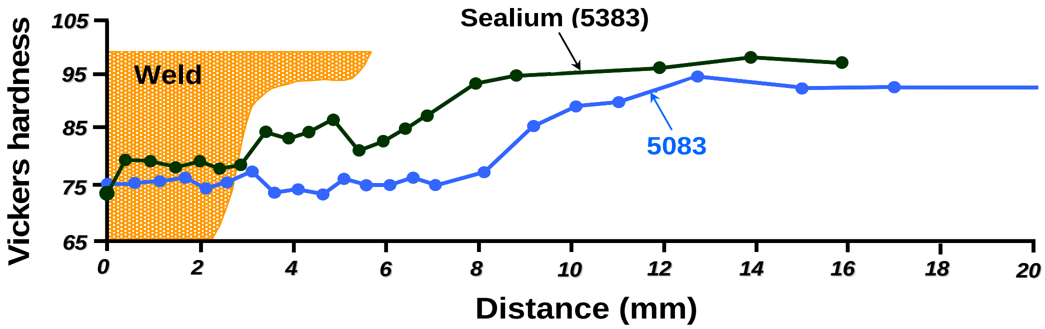

Figure 2.1 Comparison of hardness at weld and base metal for 5083 and Sealium® (5383) (Raynaud 1995)

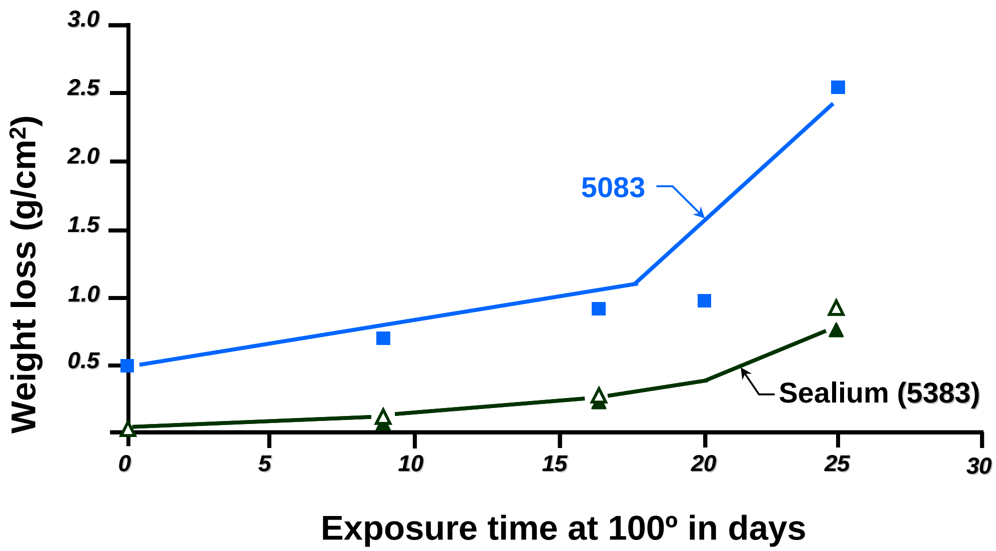

Figure 2.2 Comparison of resistance against acid attack for 5083 and Sealium® (5383) (Raynaud 1995)

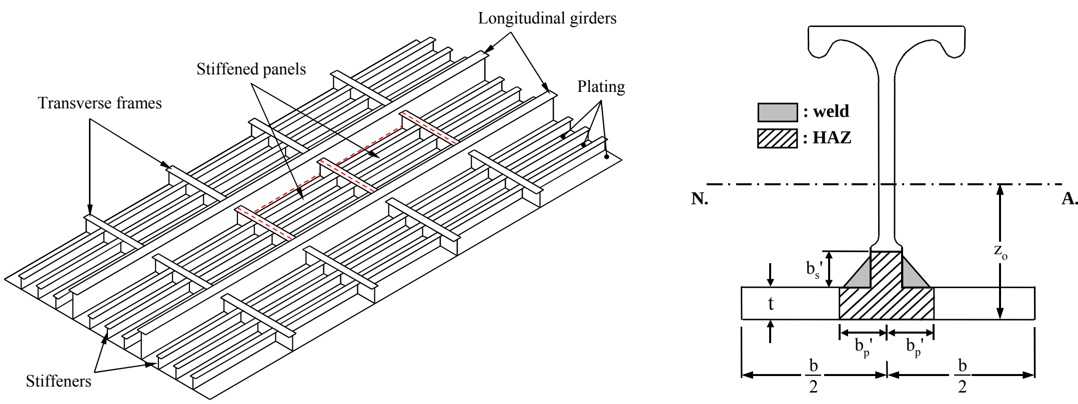

Figure 3.1 A profile of typical aluminum stiffened plate structure with schematic of an extruded stiffener welded to plating, for marine applications (N.A. = neutral axis)

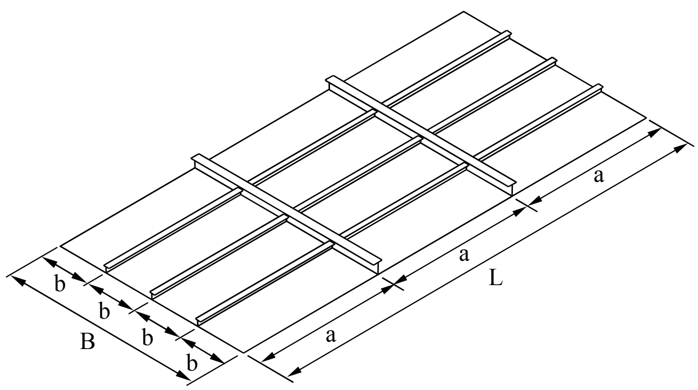

Figure 3.2 Nomenclature for a stiffened plate structure

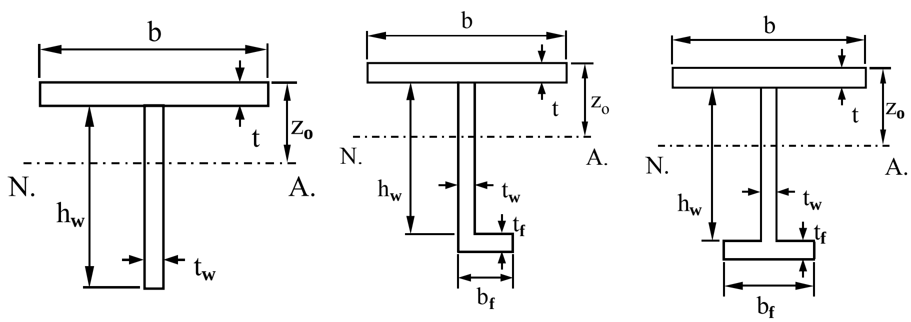

Figure 3.3 Typical types of plate-stiffener combinations (flat bar, angle bar and T-bar)

(a)  (b) 

Figure 4.1 Prototype structures; (a) one-bay, (b) two-bay

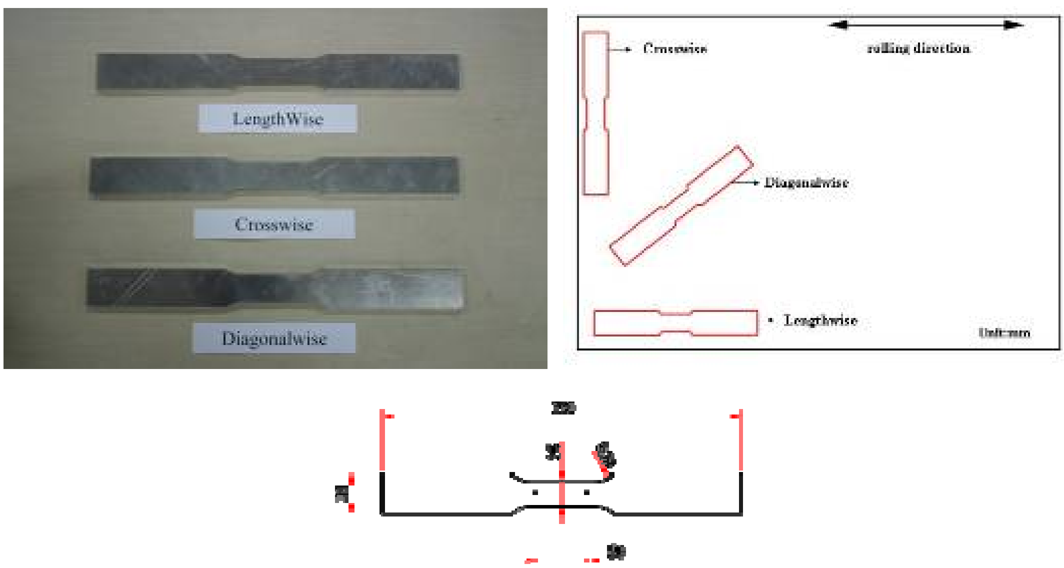

Figure 4.2 A typical set of ASTM tensile coupon test specimen cut out of the aluminum sheet, used for the present study (in mm)

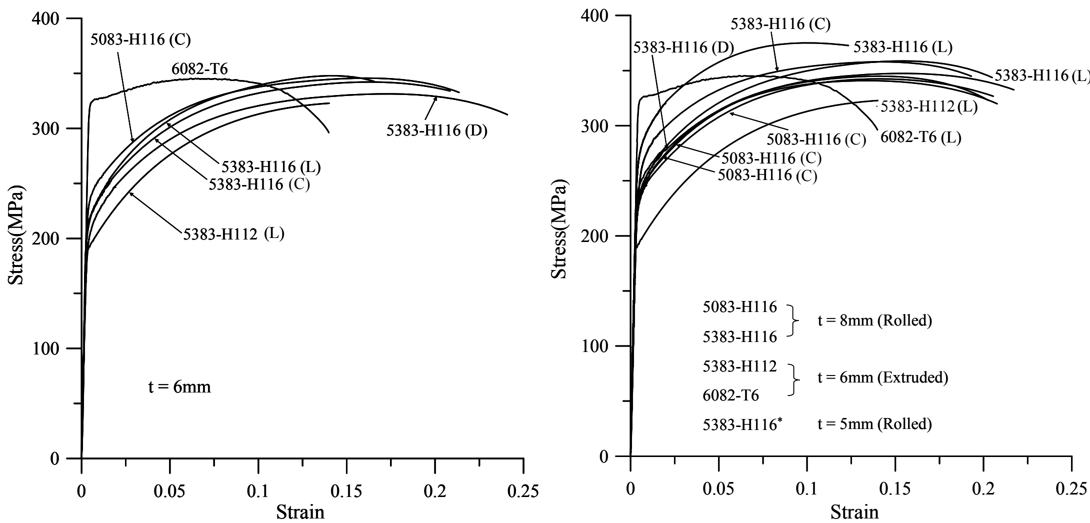

Figure 4.3 Stress versus strain curves of aluminum alloys used for the construction of the prototype structures, obtained by tensile coupon testing (L: length-wise, C: cross-wise, D: diagonal)

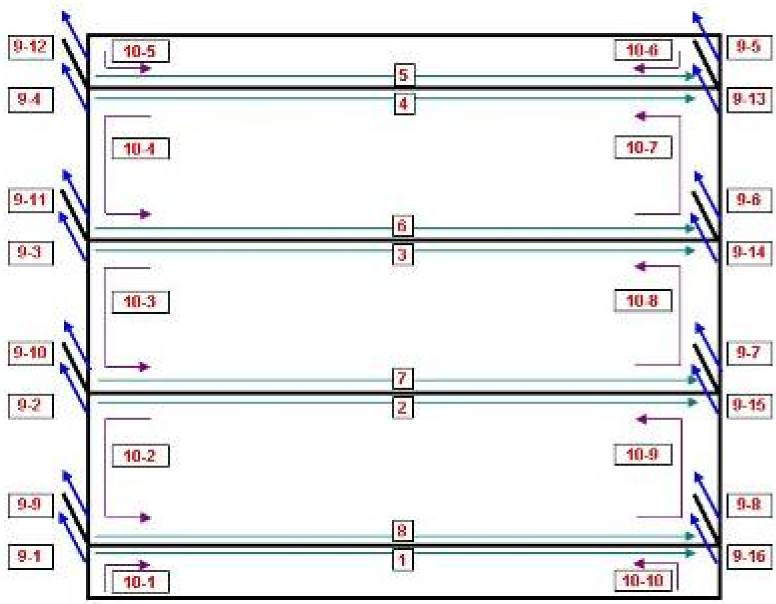

Figure 4.4 The order of welding for fabrication of the test structure

Figure 4.5 Pictures showing the MIG welding

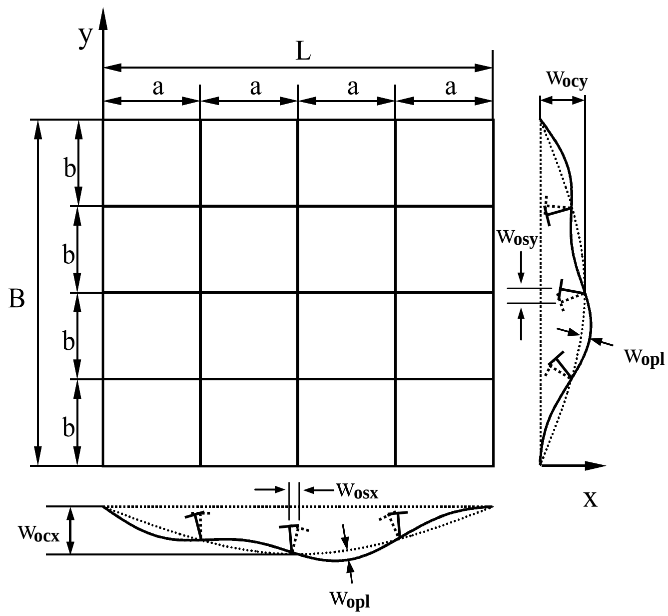

Figure 5.1 A profile of weld induced initial distortions in a stiffened plate structure

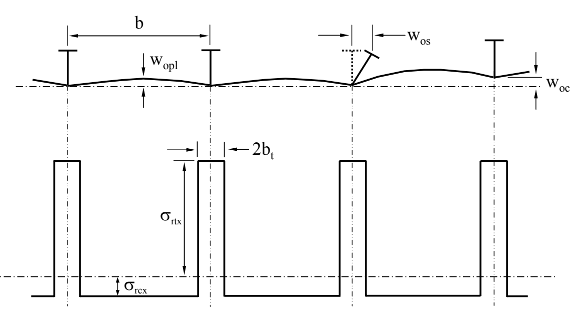

Figure 5.2 Weld induced initial distortions and residual stresses in a stiffened plate structure

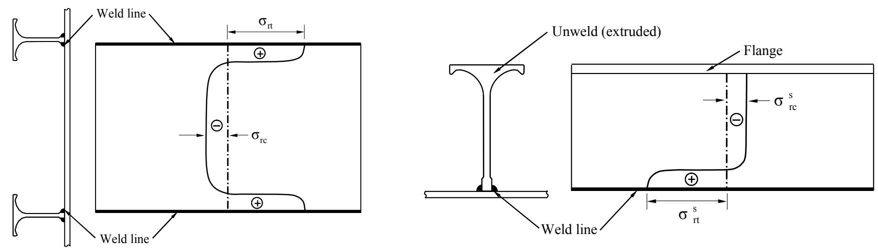

Figure 5.3 Schematics of the distribution of weld induced residual stresses in a plate welded at two edges, and in the stiffener web welded at one edge (left: plating, right: extruded stiffener web; +: tension, -: compression)

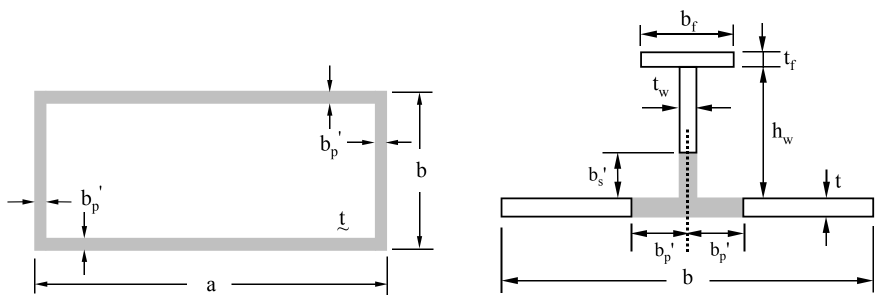

Figure 5.4 Idealized profiles of softening zones inside an aluminum plate welded at four edges, and its counterpart in the stiffener attachment to plating

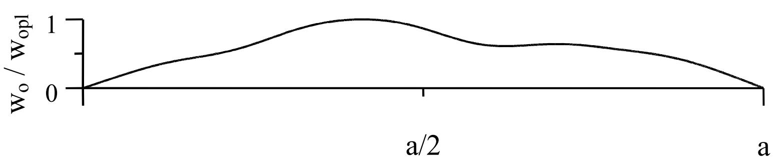

Figure 5.5(a) A specific type of initial distortion in plating between stiffeners in the long (plate length), after welded attachment of stiffeners

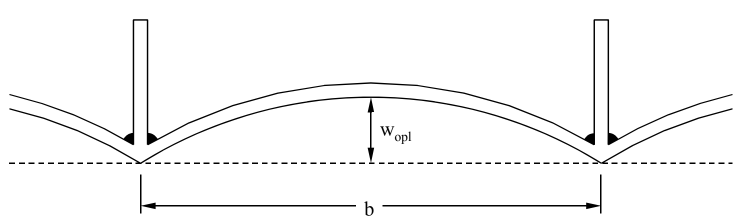

Figure 5.5(b) A specific type of initial distortion in plating between stiffeners in the short (plate breadth) direction, after welded attachment of stiffeners

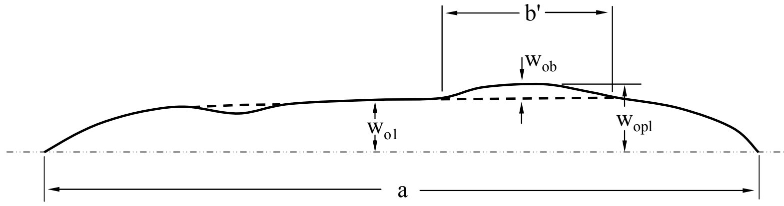

Figure 5.6 A specific profile of plate initial distortion with related nomenclature

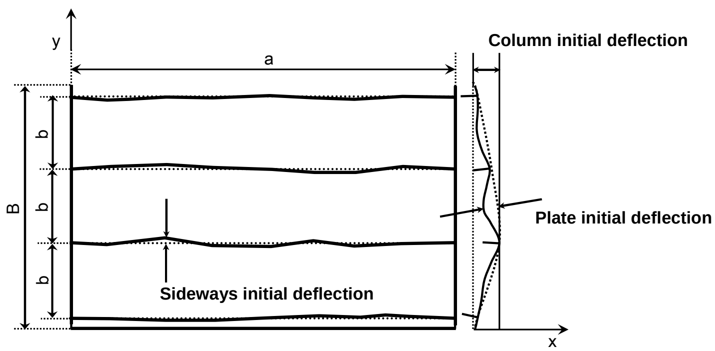

Figure 5.7 Sideways initial distortion of stiffeners

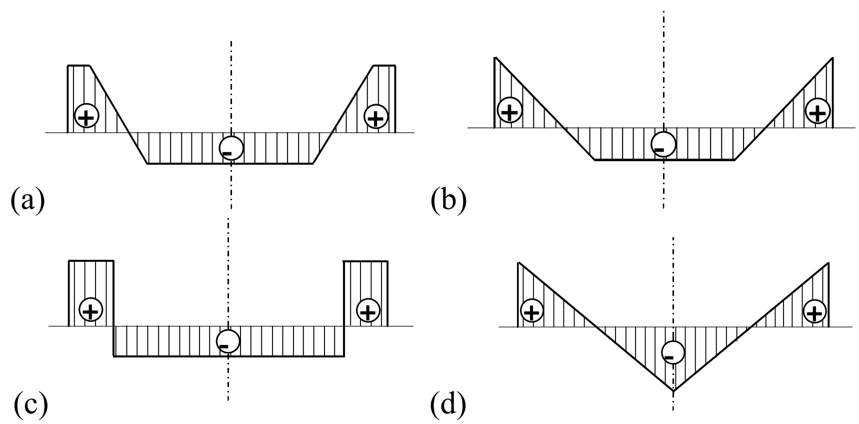

Figure 5.8 Various idealizations of residual stress distribution in a plate element (+: tension, -: compression)

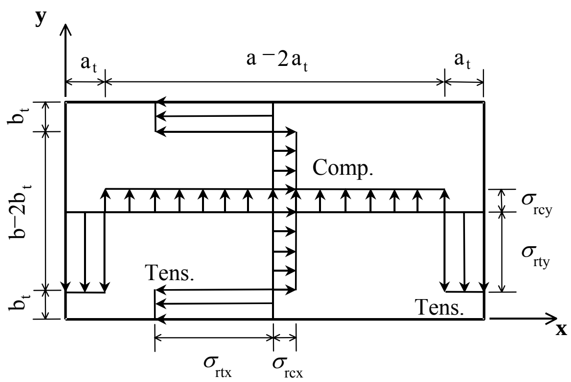

Figure 5.9 A typical idealized welding induced residual stress distribution inside the plate element in the x and y directions; based on case (c) in Fig.5.8

Figure 6.1 Dial gauge and its attachment for initial distortion measurement

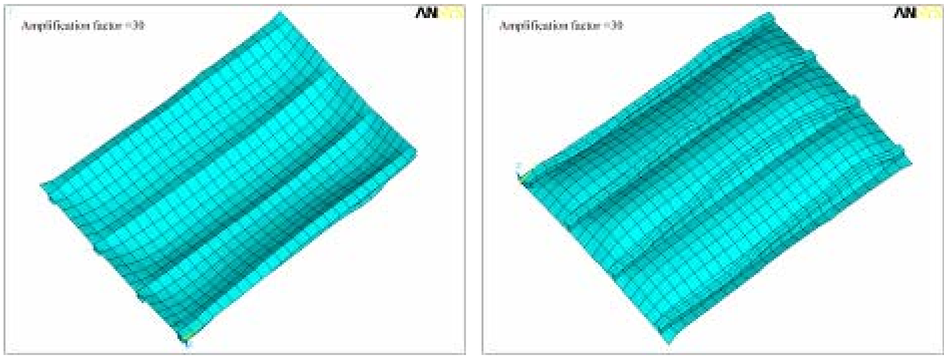

Figure 6.2(a) Three-dimensional displays of the prototype structure distorted after welding (with amplification factor of 30), for ID 17

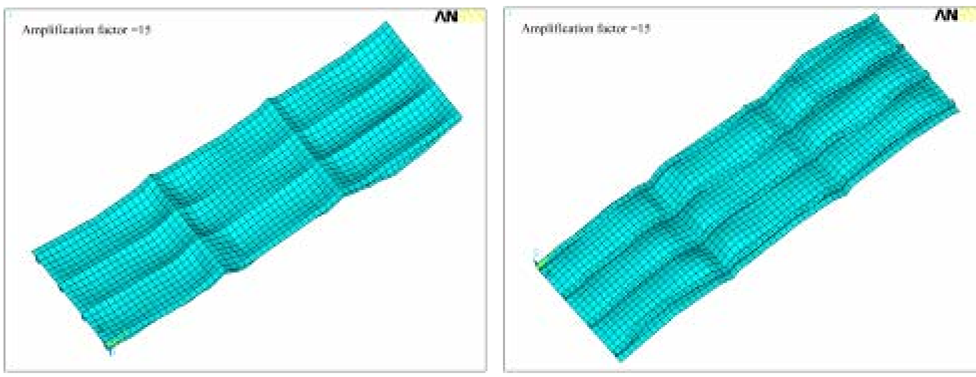

Figure 6.2(b) Three-dimensional displays of the prototype structure distorted after welding (with amplification factor of 30), for ID 76

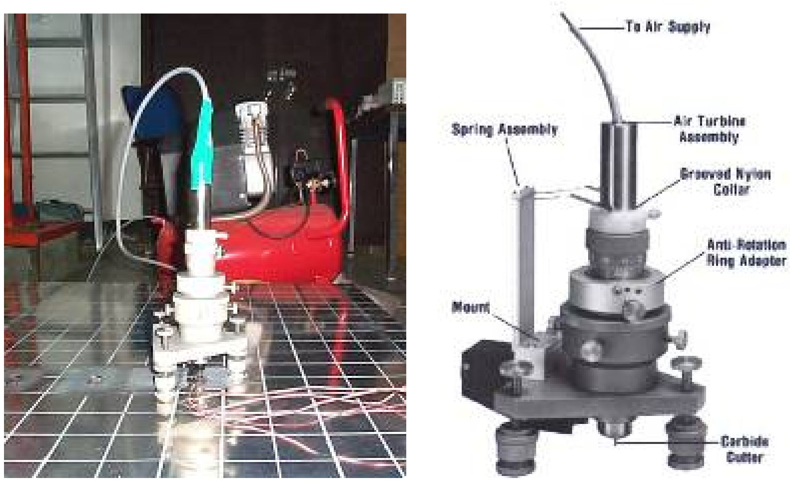

Figure 6.3 Hole drilling machine used for strain release measurement

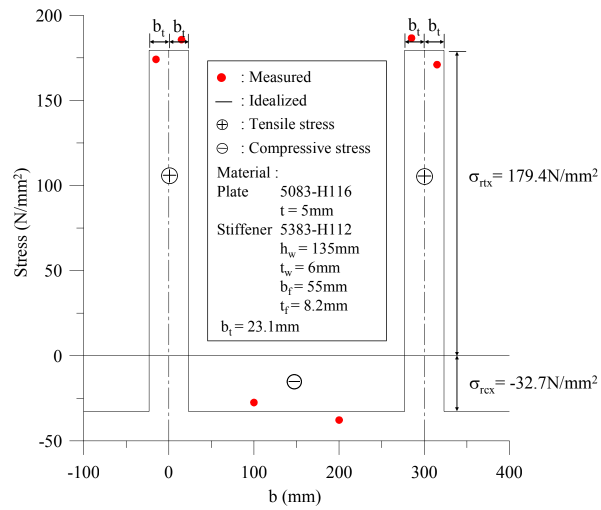

Figure 6.4(a) Residual stress distributions at plating, for ID4 (5083-H116)

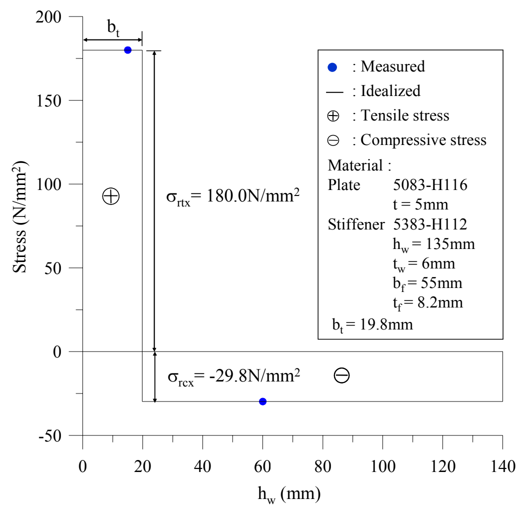

Figure 6.4(b) Residual stress distribution at stiffener web, for ID4 (5083-H116)

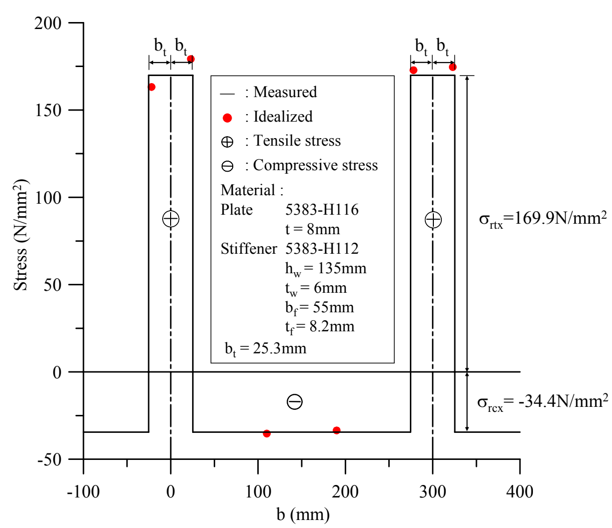

Figure 6.4(c) Residual stress distribution at plating, for ID 36 (5383-H116)

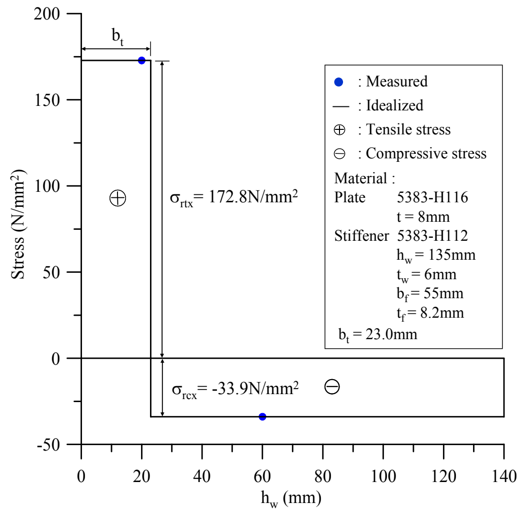

Figure 6.4(d) Residual stress distribution at stiffener web, for ID36 (5383-H116)

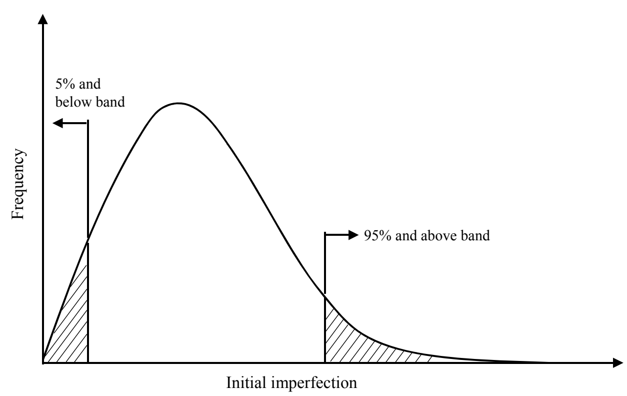

Figure 6.5 5% and below data band for the slight level analysis and 95% and above data band for the severe level analysis

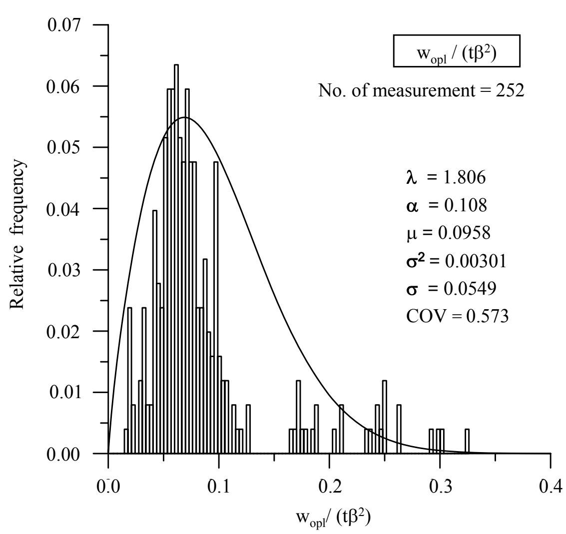

Figure 6.6 The best fit of the Weibull probability density function for the average level analysis of

w_{opl}

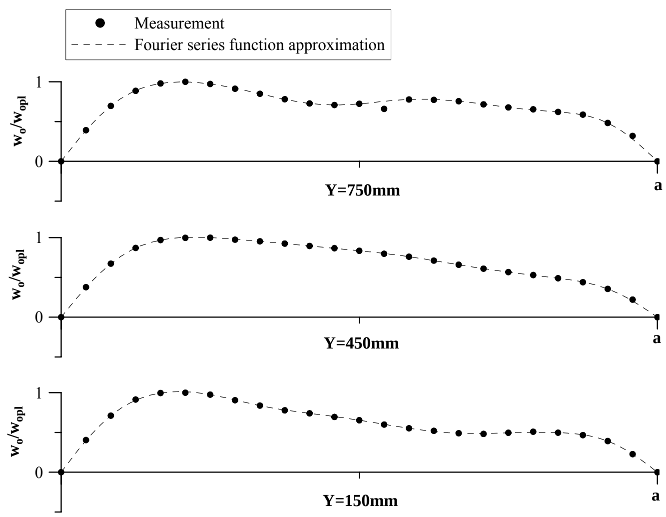

Y(mm)	Bo1	Bo2	Bo3	Bo4	Bo5	Bo6	Bo7	Bo8	Bo9	Bo10	Bo11
750	0.9736	0.1279	0.3023	0.0762	0.0826	-0.0216	0.0379	-0.0001	0.0100	-0.0025	0.0022
450	-0.9896	-0.2216	-0.2150	-0.0532	-0.0804	-0.0033	-0.0245	0.0005	-0.0066	0.0019	-0.0020
150	0.8545	0.2444	0.2911	0.0407	0.1016	0.0047	0.0184	-0.0028	0.0111	0.0001	0.0041

Figure 6.7 Approximation of the plate initial distortion configuration w_{opl} by Fourier series Eq.(5.1), for ID1

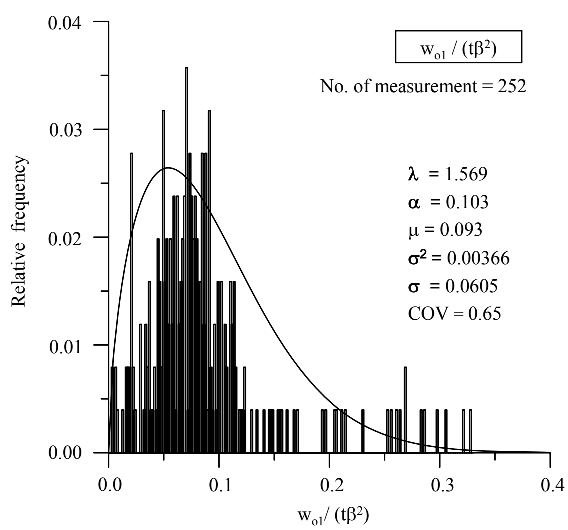

Figure 6.8(a) The best fit of the Weibull probability density function for the average level analysis of w_{o1}

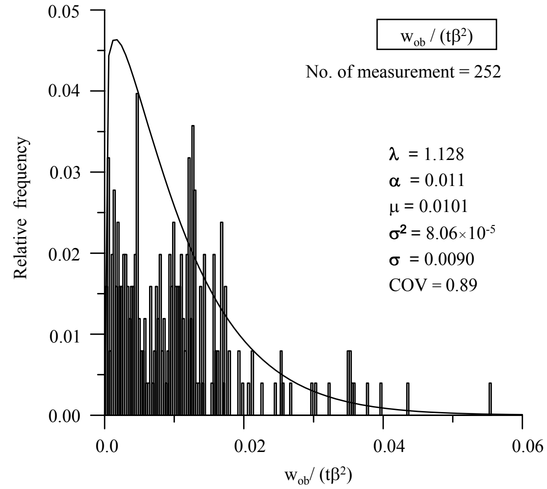

Figure 6.8(b) The best fit of the Weibull probability density function for the average level analysis of w_{ob}

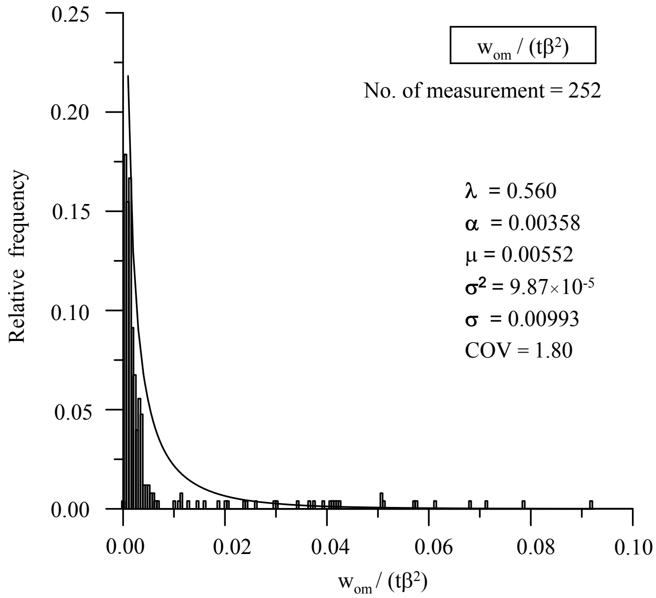

Figure 6.8(c) The best fit of the Weibull probability density function for the average level analysis of w_{om}

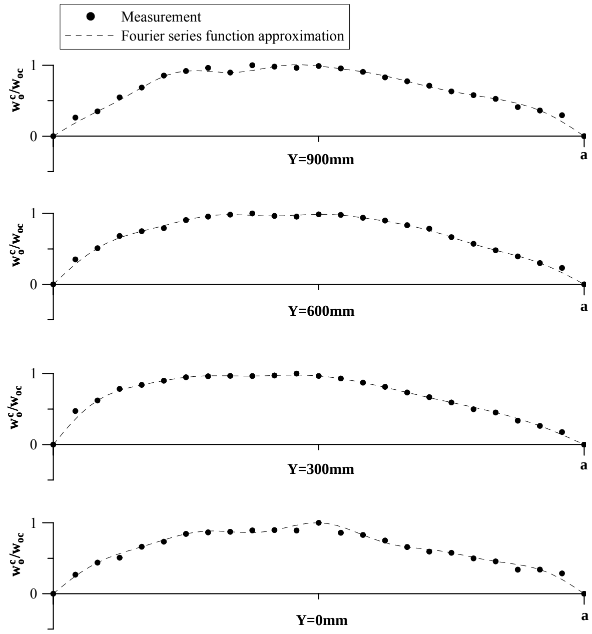

Y(mm)	B_{o1}	B_{o2}	B_{o3}	B_{o4}	B_{o5}	B_{o6}	B_{o7}	B_{o8}	B_{o9}	B_{o10}	B_{o11}
900	1.0239	0.0938	0.0811	-0.0072	0.0380	-0.0376	-0.0112	-0.0176	0.0071	0.0122	0.0104
600	1.0557	0.1199	0.0967	0.0439	0.0318	-0.0009	0.0223	0.0092	0.0158	-0.0007	-0.0027
300	1.0311	0.1874	0.1226	0.0593	0.0636	0.0173	0.0172	0.0146	0.0141	0.0076	0.0026
0	0.9597	0.1193	0.0754	0.0030	0.0711	-0.0167	-0.0064	0.0056	0.0360	-0.0024	-0.0022

Figure 6.9 Approximation of the column type initial distortion configuration of stiffener by Fourier series function of Eq.(5.7), for ID1

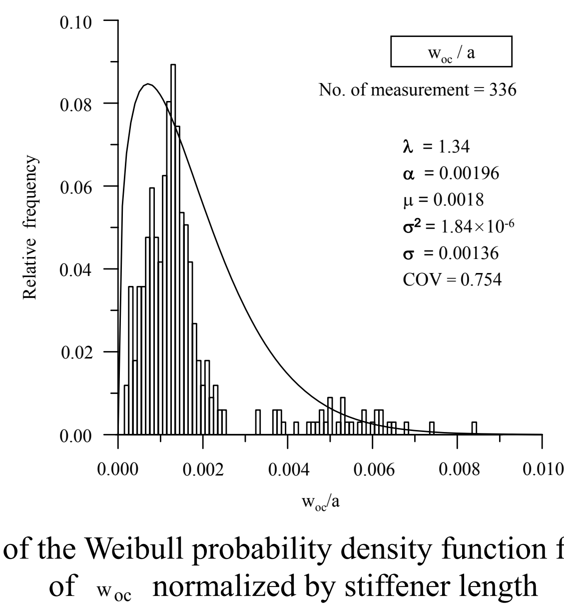

Figure 6.10(a) The best fit of the Weibull probability density function for the average level analysis of w_{oc} normalized by stiffener length

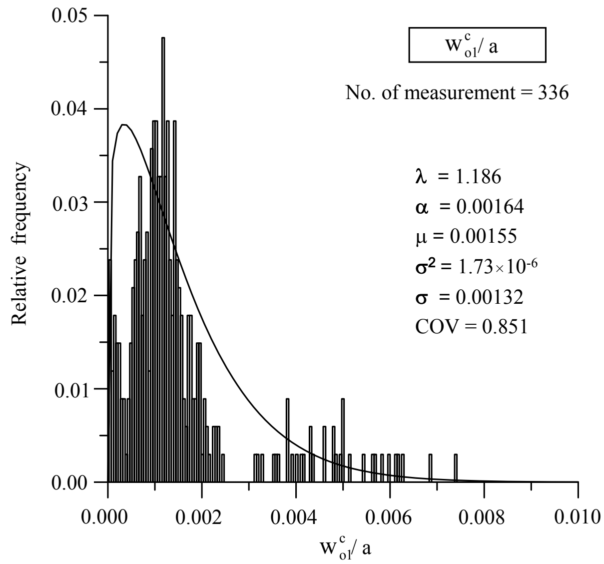

Figure 6.10(b) The best fit of the Weibull probability density function for the average level analysis of w^c_{ol} normalized by stiffener length

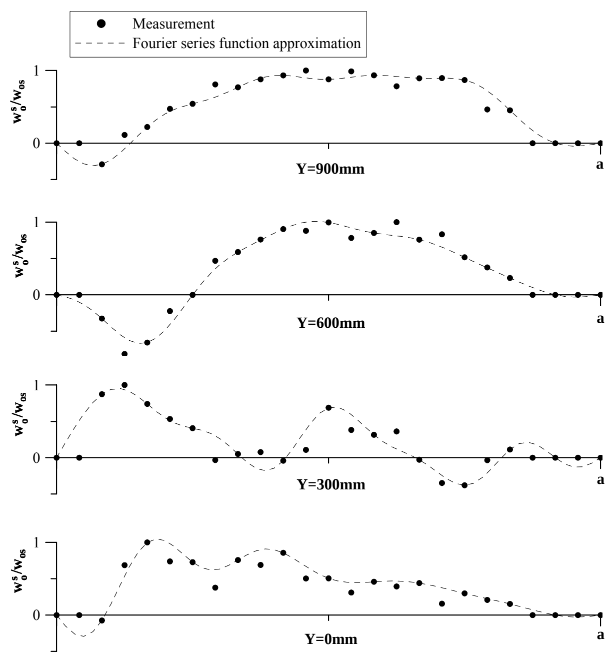

Y(mm)	B_{o1}	B_{o2}	B_{o3}	B_{o4}	B_{o5}	B_{o6}	B_{o7}	B_{o8}	B_{o9}	B_{o10}	B_{o11}
900	0.8972	-0.1299	-0.1219	-0.0571	-0.1696	0.0060	-0.0955	-0.0265	-0.0542	-0.0279	0.0116
600	0.6549	-0.2618	-0.4214	-0.1585	-0.1014	0.0409	0.0263	0.0487	0.0521	0.0439	0.0041
300	0.2737	0.2760	0.1013	0.2568	0.3317	-0.0449	-0.0330	0.0983	0.0461	0.0720	-0.1042
0	0.6828	0.2665	0.0652	0.0083	-0.0687	-0.0175	-0.0836	-0.1446	-0.1508	-0.0694	-0.0237

Figure 6.11 Approximation of the sideways initial distortion configuration of stiffener by Fourier series function of Eq.(5.8), for ID1

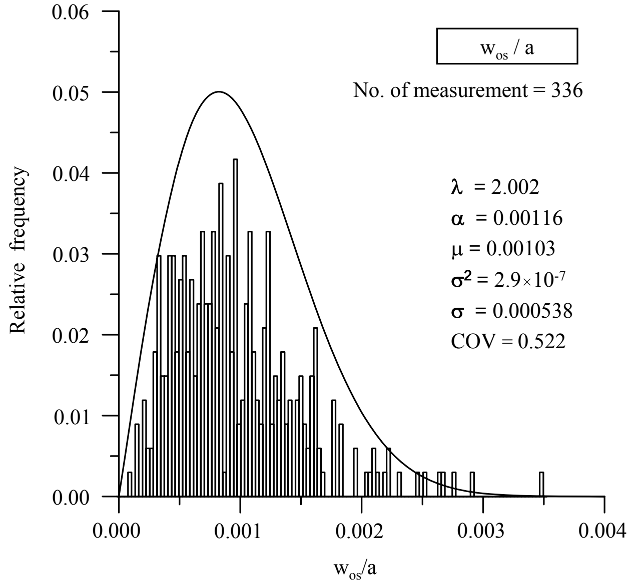

Figure 6.12(a) The best fit of the Weibull probability density function for the average level analysis of w_{os} normalized by stiffener length

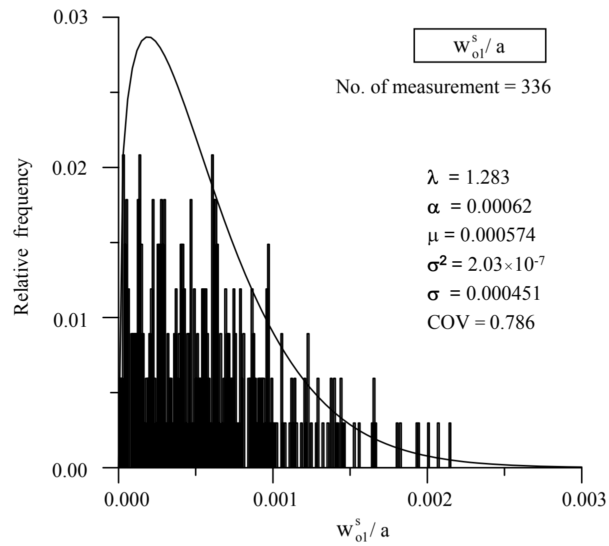

Figure 6.12(b) The best fit of the Weibull probability density function for the average level analysis of w^s_{o1} normalized by stiffener length

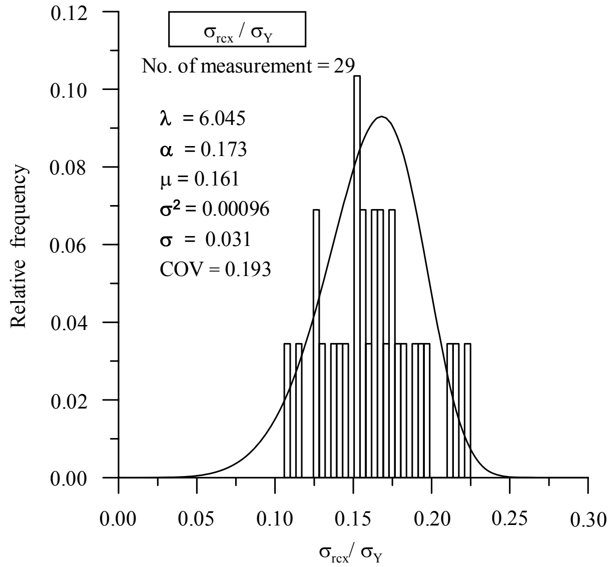

Figure 6.13 The best fit of the Weibull probability density function for the average level analysis of the compressive residual stress inside welded plating

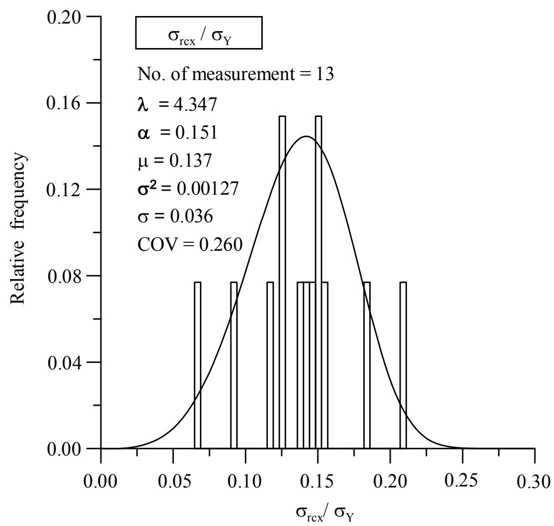

Figure 6.14 The best fit of the Weibull probability density function for the average level analysis of the compressive residual stress inside stiffener web

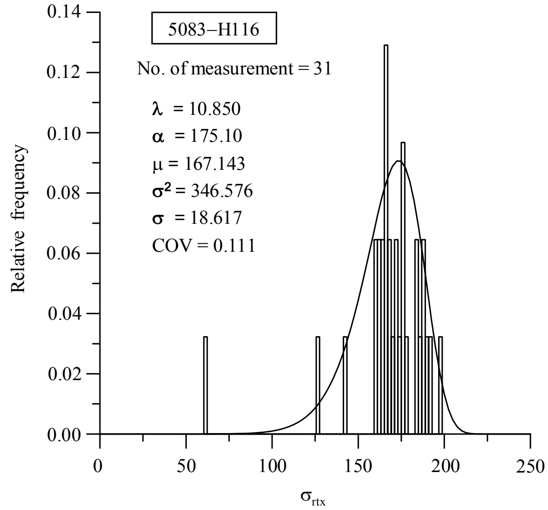

Figure 6.15(a) The best fit of the Weibull probability density function for the average level analysis of the 5083-H116 HAZ residual stress

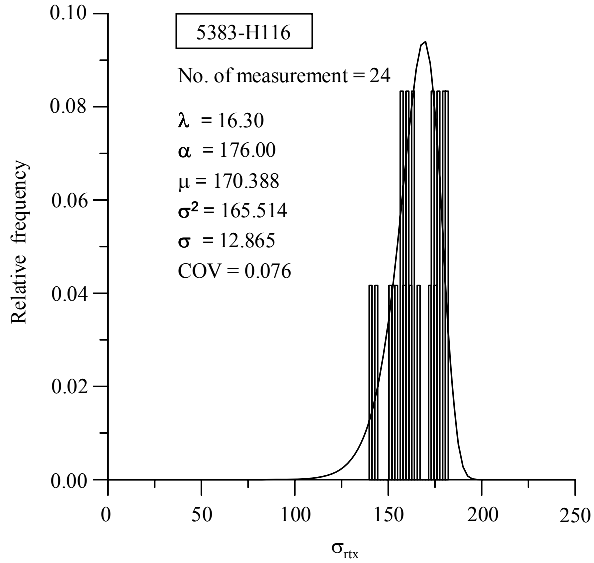

Figure 6.15(b) The best fit of the Weibull probability density function for the average level analysis of the 5383-H116 HAZ residual stress

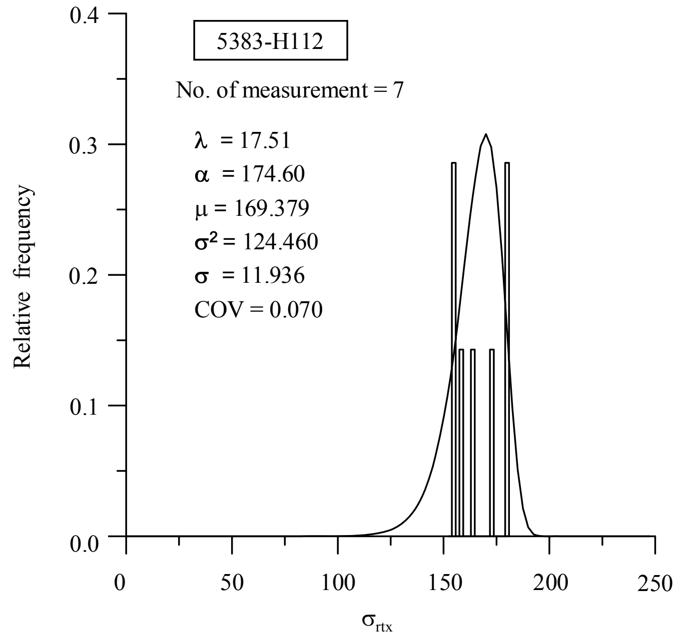

Figure 6.15(c) The best fit of the Weibull probability density function for the average level analysis of the 5383-H112 HAZ residual stress

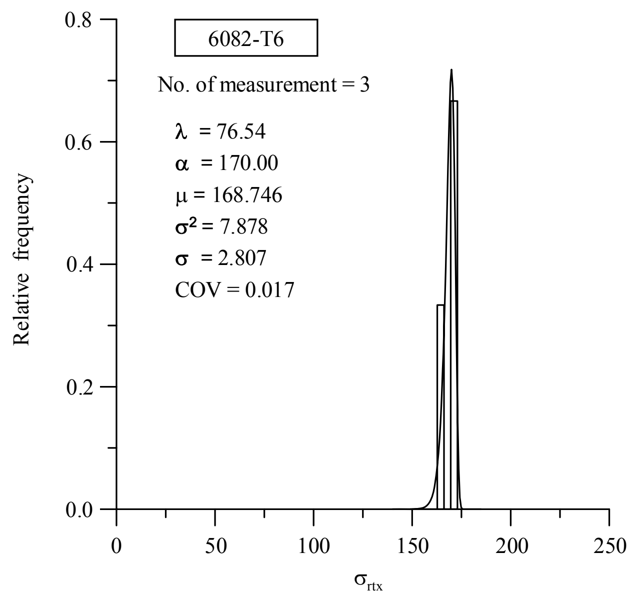

Figure 6.15(d) The best fit of the Weibull probability density function for the average level analysis of the 6082-T6 HAZ residual stress

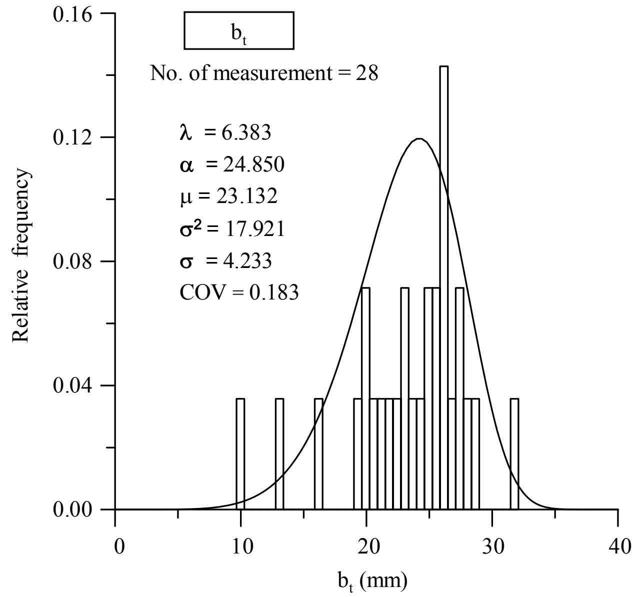

Figure 6.16 The best fit of the Weibull probability density function for the average level analysis of the HAZ breadth

(a)  (b) 

Figure 7.1 Test set-up for collapse testing on stiffened plate structures (a) without supporting jigs at unloaded edges, (b) with supporting jigs at unloaded edges to keep them straight

Figure 7.2 Simply supported condition at loaded edges and axial compressive loading at the neutral axis of the panel cross section

ID 1

Plate		Stiffener				
t	Material	h_w	t_w	b_f	t_f	Material
5 mm	5083-H116	55.7 mm	3.7 mm	40 mm	6.7 mm	5383-H112

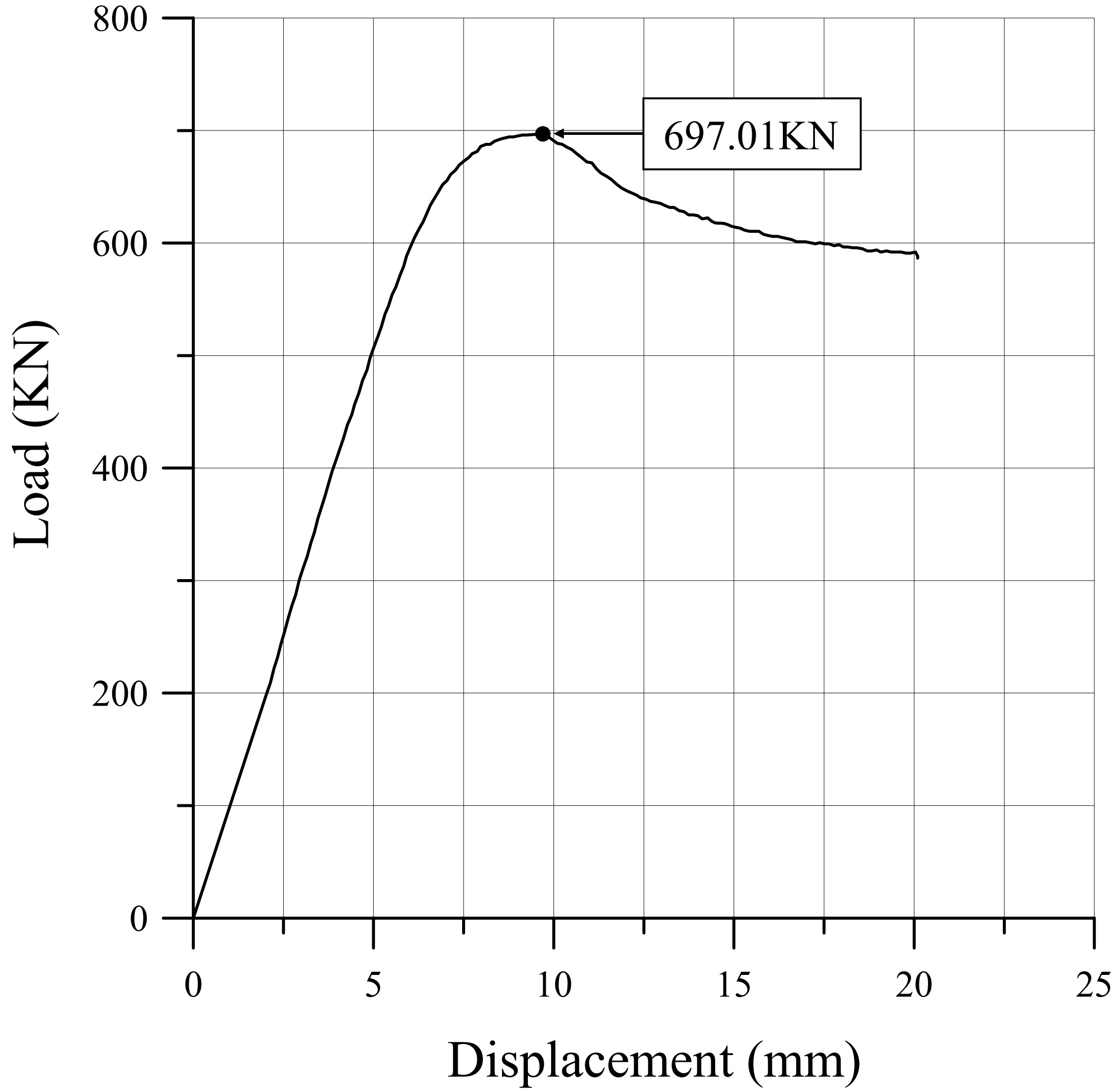

Figure 7.3 The load-axial displacement curve for ID1

ID 2

Plate		Stiffener				
t	Material	h_w	t_w	b_f	t_f	Material
5 mm	5083-H116	66.1 mm	4 mm	40 mm	5.7 mm	5383-H112

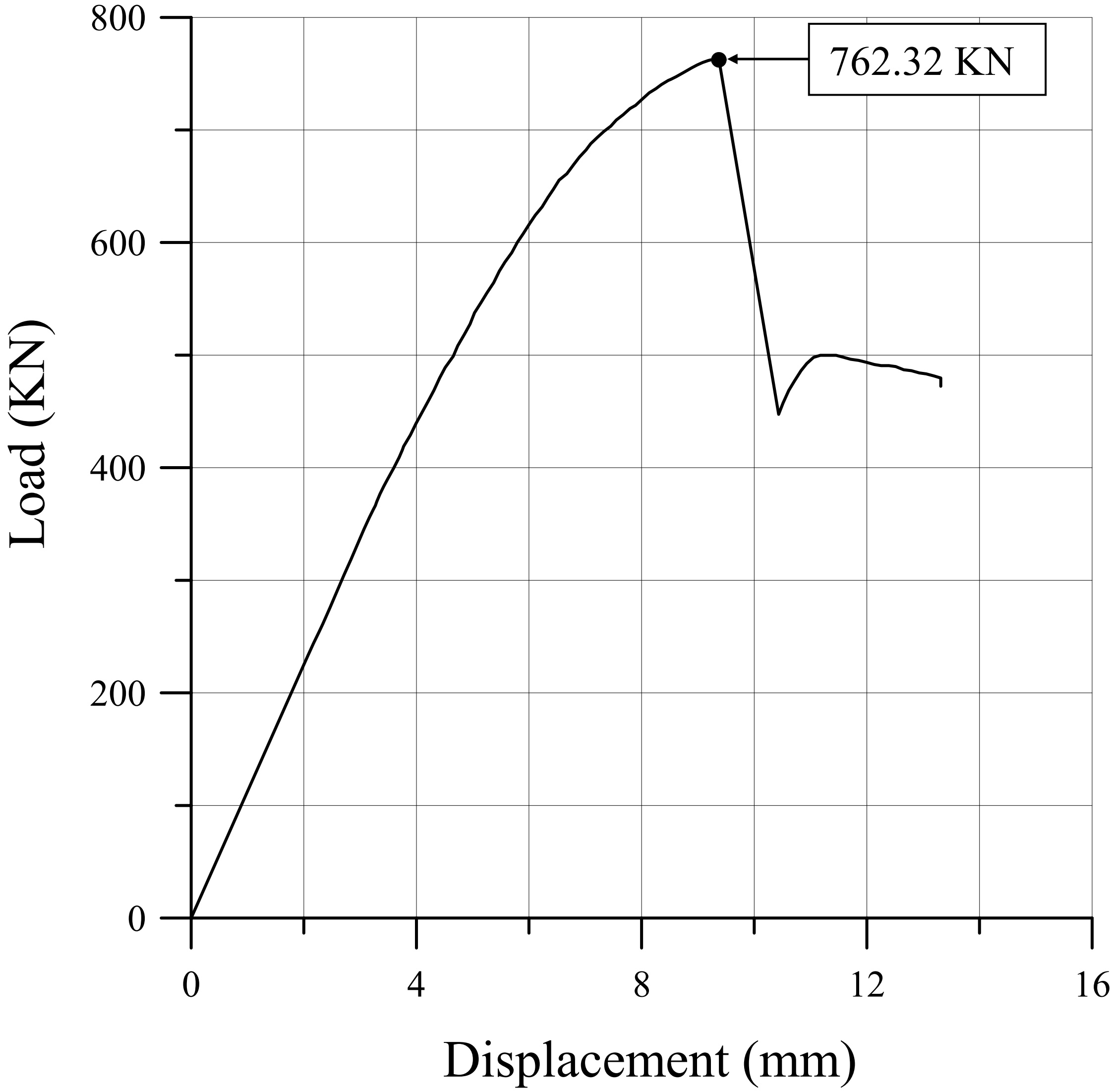

Figure 7.4 The load-axial displacement curve for ID2

ID 3

Plate		Stiffener				
t	Material	h_w	t_w	b_f	t_f	Material
5 mm	5083-H116	76.8 mm	4 mm	45 mm	5.6 mm	5383-H112

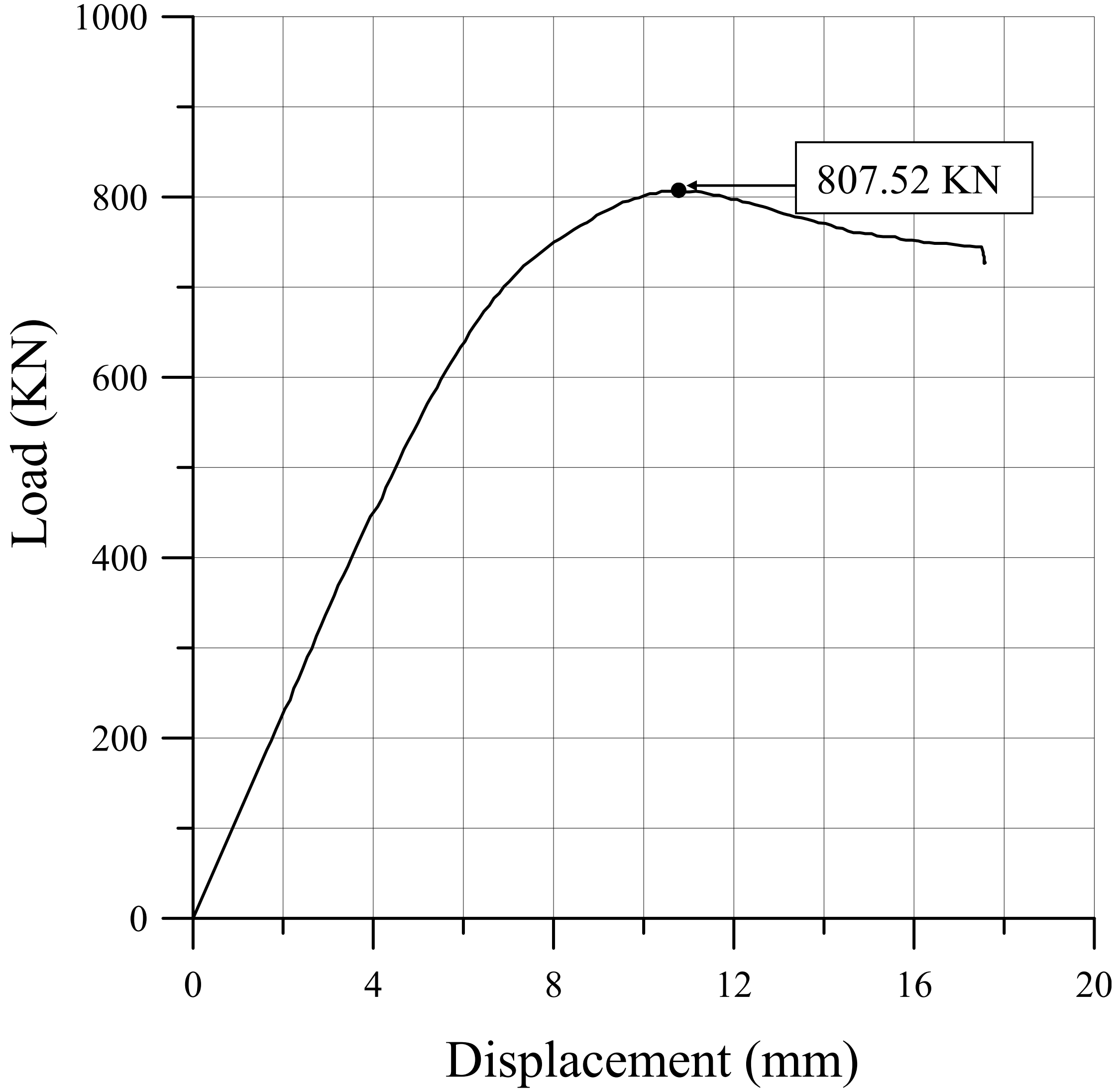

Figure 7.5 The load-axial displacement curve for ID3

ID 4

Plate		Stiffener				
t	Material	h_w	t_w	b_f	t_f	Material
5 mm	5083-H116	135 mm	6 mm	55 mm	8.2 mm	5383-H112

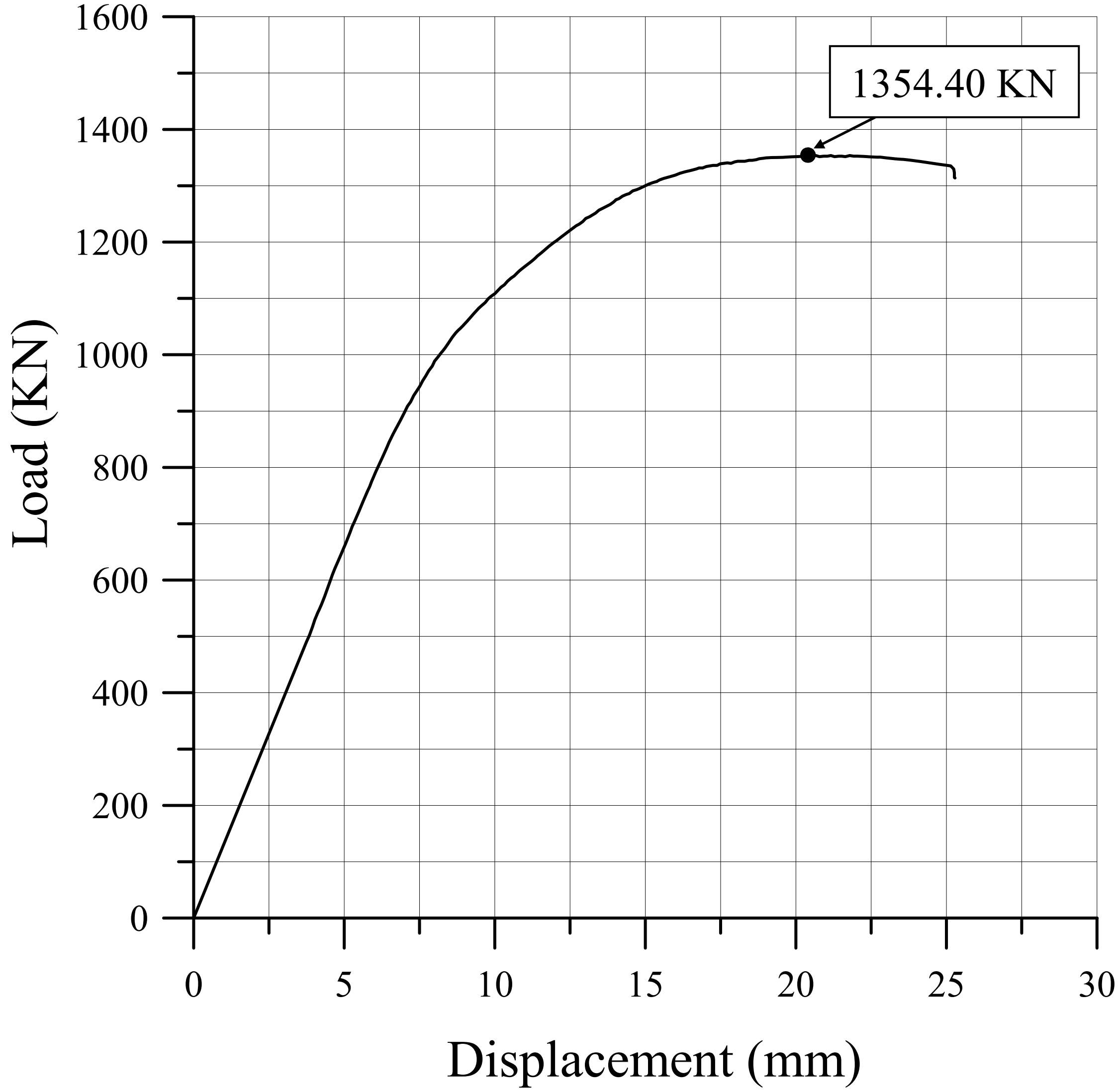

Figure 7.6 The load-axial displacement curve for ID4

ID 5

Plate		Stiffener				
t	Material	h_w	t_w	b_f	t_f	Material
6 mm	5083-H116	55.7 mm	3.7 mm	40 mm	6.7 mm	5383-H112

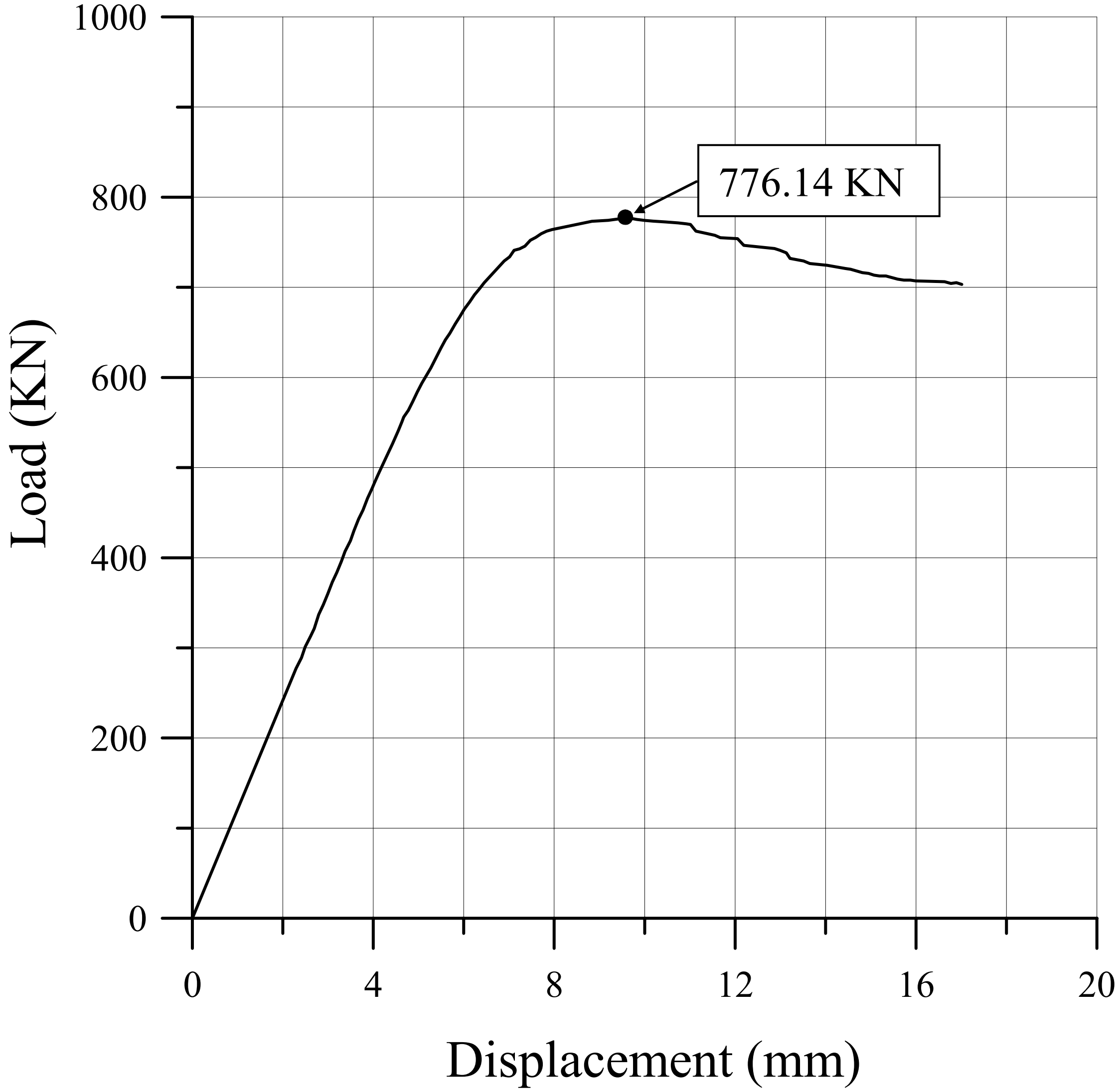

Figure 7.7 The load-axial displacement curve for ID5

ID 6

Plate		Stiffener				
t	Material	h_w	t_w	b_f	t_f	Material
6 mm	5083-H116	66.1 mm	4 mm	40 mm	5.7 mm	5383-H112

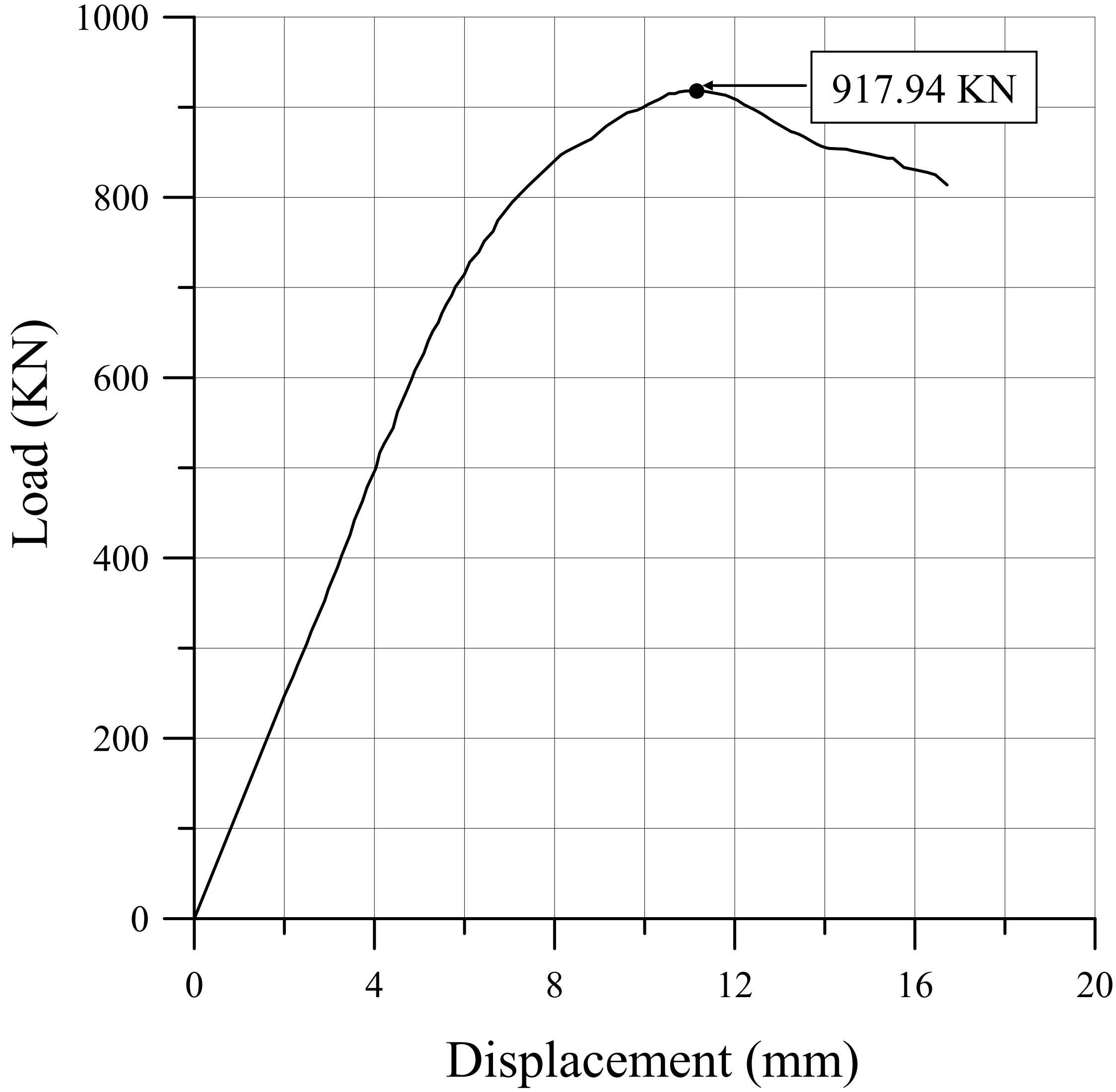

Figure 7.8 The load-axial displacement curve for ID6

ID 7

Plate		Stiffener				
t	Material	h_w	t_w	b_f	t_f	Material
6 mm	5083-H116	76.8 mm	4 mm	45 mm	5.6 mm	5383-H112

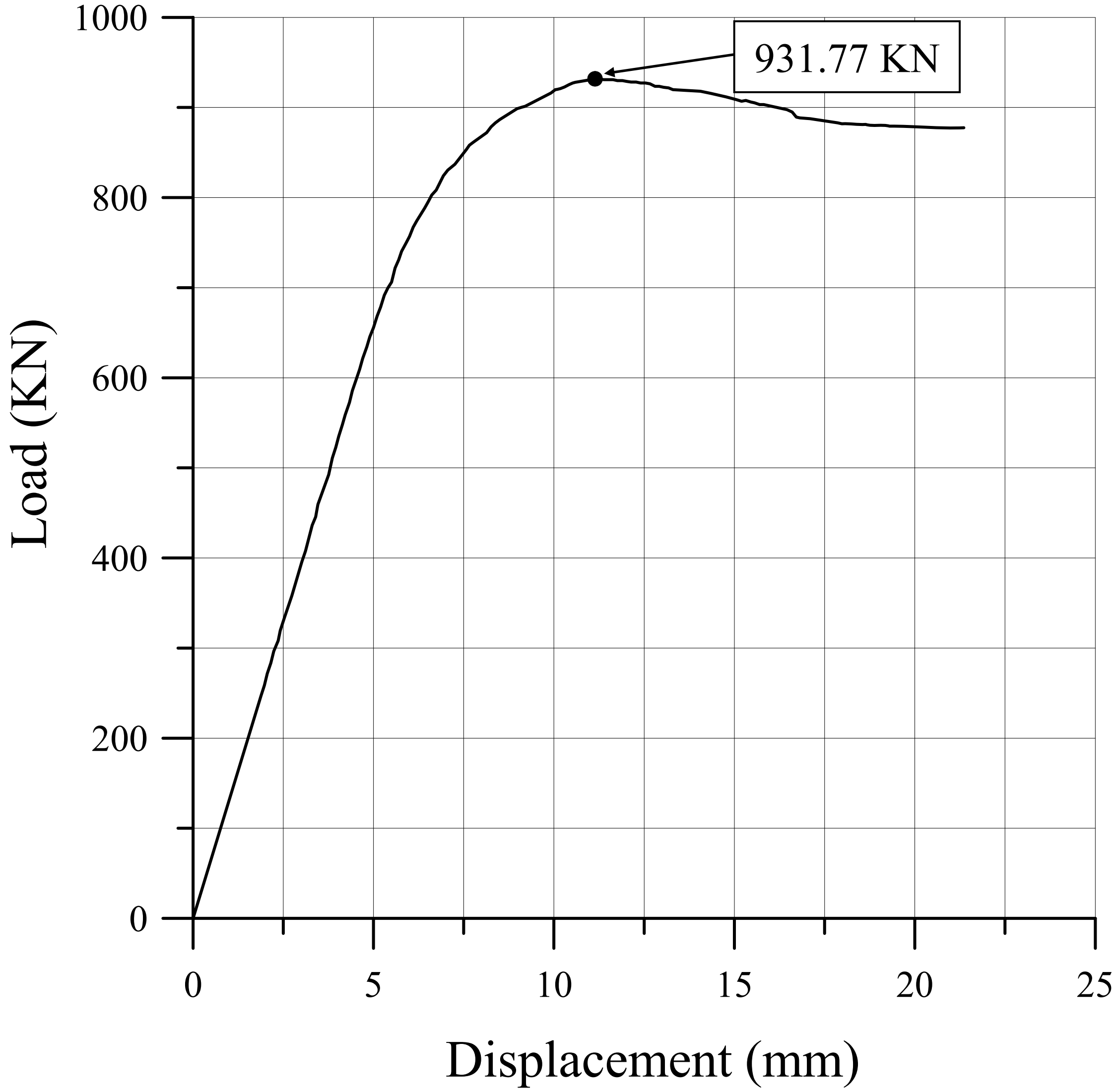

Figure 7.9 The load-axial displacement curve for ID7

ID 8

Plate		Stiffener				
t	Material	h_w	t_w	b_f	t_f	Material
6 mm	5083-H116	135 mm	6 mm	55 mm	8.2 mm	5383-H112

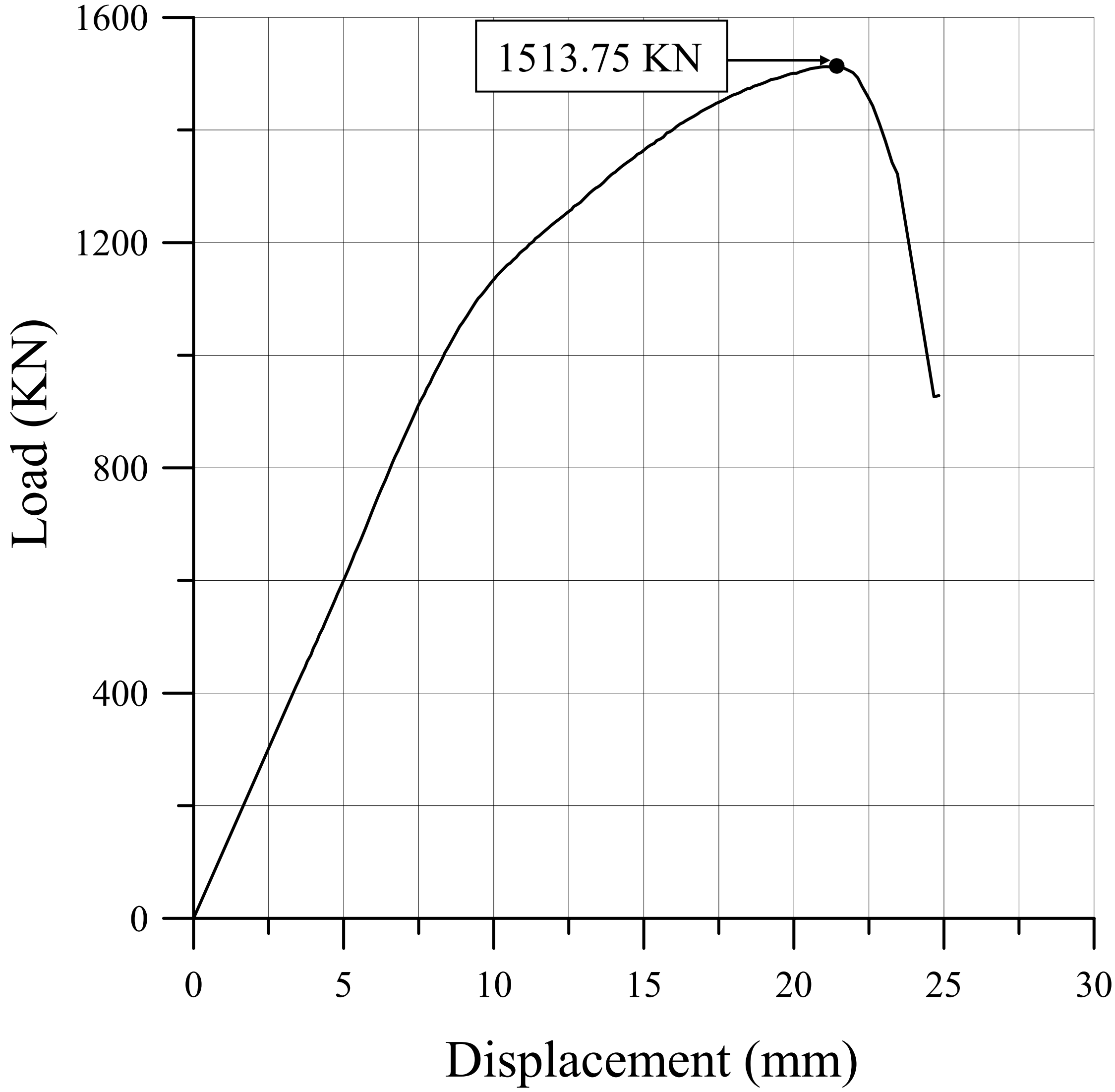

Figure 7.10 The load-axial displacement curve for ID8

ID 9

Plate		Stiffener				
t	Material	h_w	t_w	b_f	t_f	Material
8 mm	5083-H116	55.7 mm	3.7 mm	40 mm	6.7 mm	5383-H112

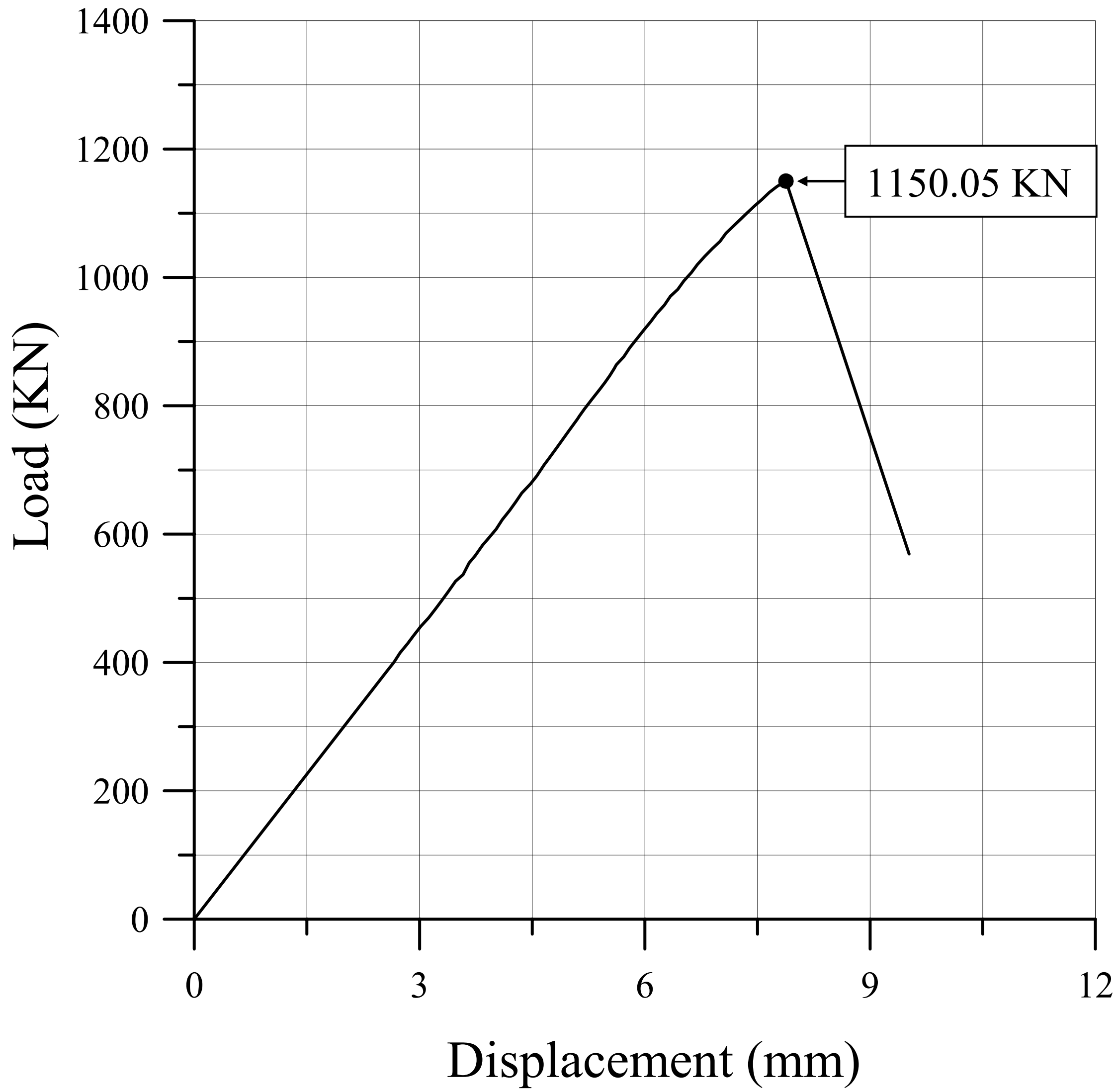

Figure 7.11 The load-axial displacement curve for ID9

ID 10

Plate		Stiffener				
t	Material	h_w	t_w	b_f	t_f	Material
8 mm	5083-H116	66.1 mm	4 mm	40 mm	5.7 mm	5383-H112

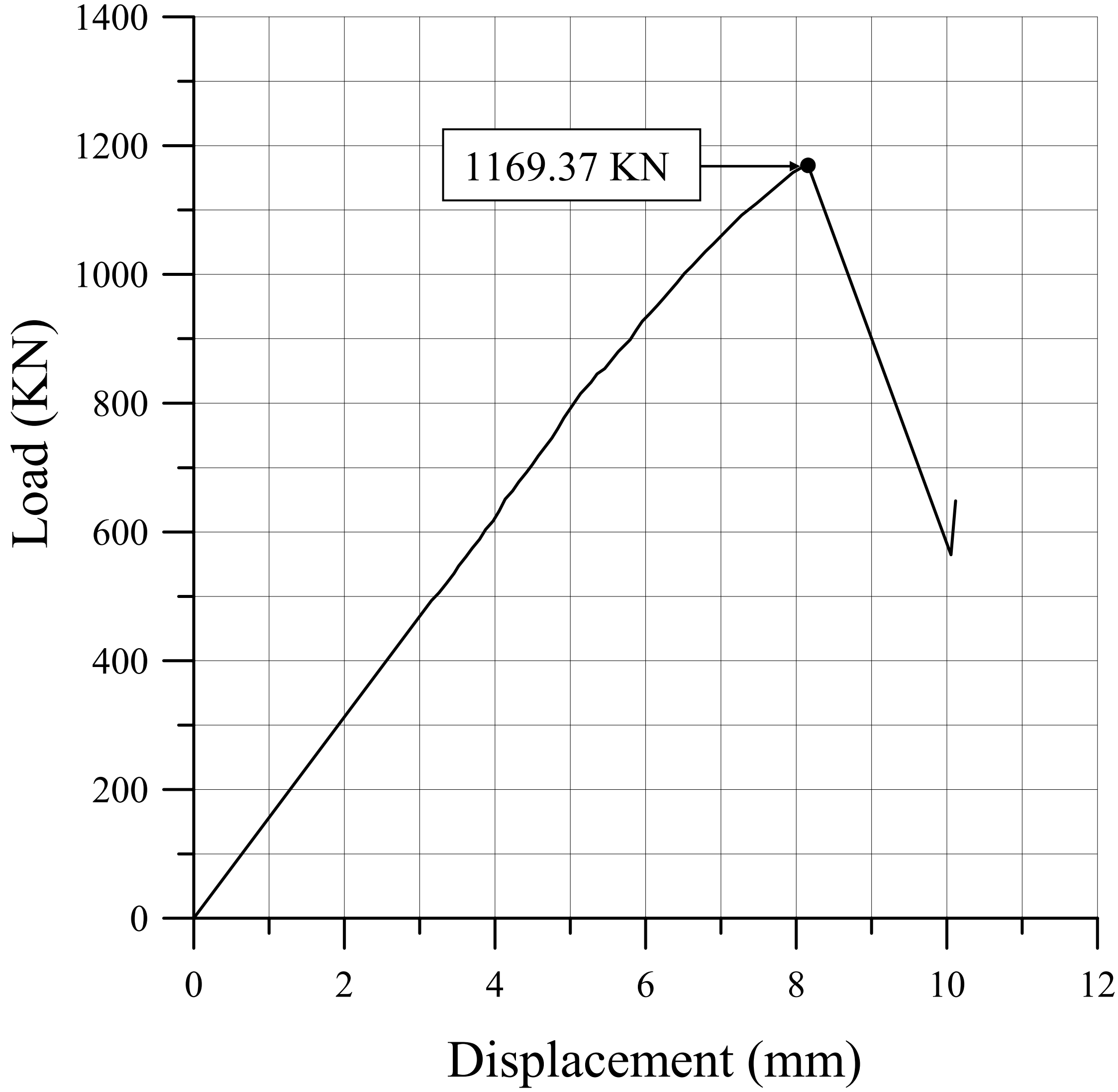

Figure 7.12 The load-axial displacement curve for ID10

ID 11

Plate		Stiffener				
t	Material	h_w	t_w	b_f	t_f	Material
8 mm	5083-H116	76.8 mm	4 mm	45 mm	5.6 mm	5383-H112

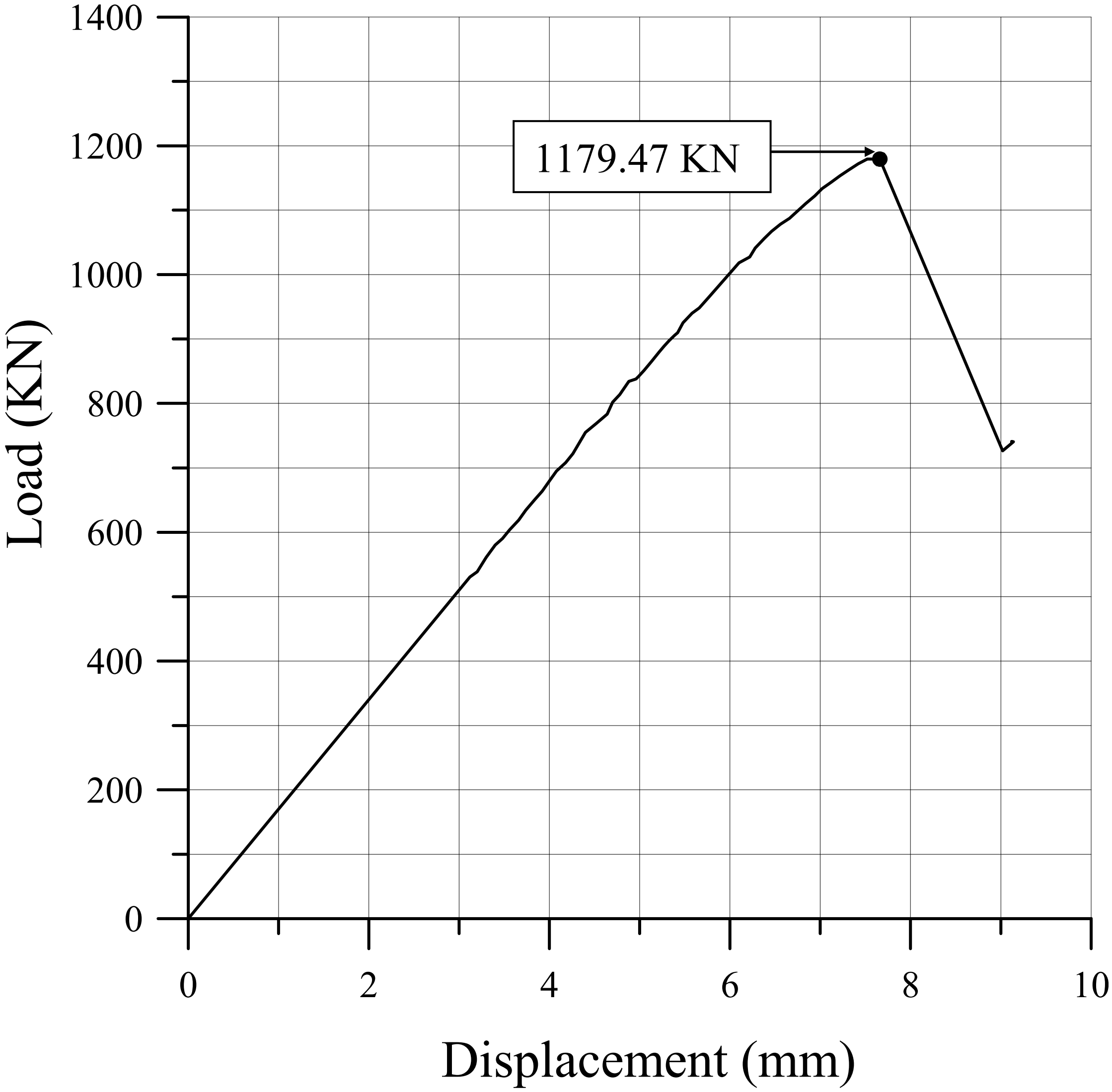

Figure 7.13 The load-axial displacement curve for ID11

ID 12

Plate		Stiffener				
t	Material	h_w	t_w	b_f	t_f	Material
8 mm	5083-H116	135 mm	6 mm	55 mm	8.2 mm	5383-H112

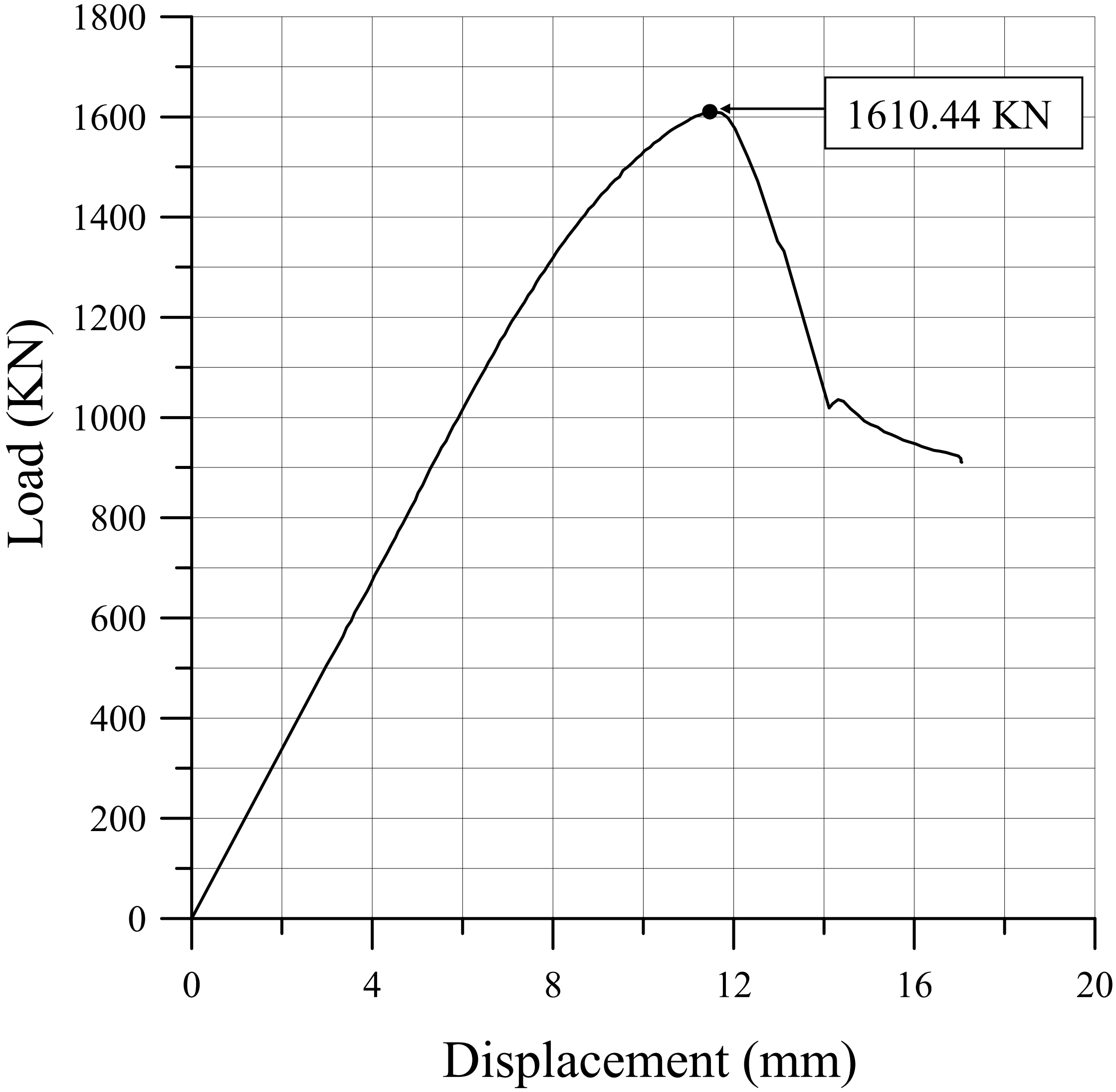

Figure 7.14 The load-axial displacement curve for ID12

ID 13

Plate		Stiffener				
t	Material	h_w	t_w	b_f	t_f	Material
5 mm	5083-H116	55.7 mm	3.7 mm	40 mm	6.7 mm	6082-T6

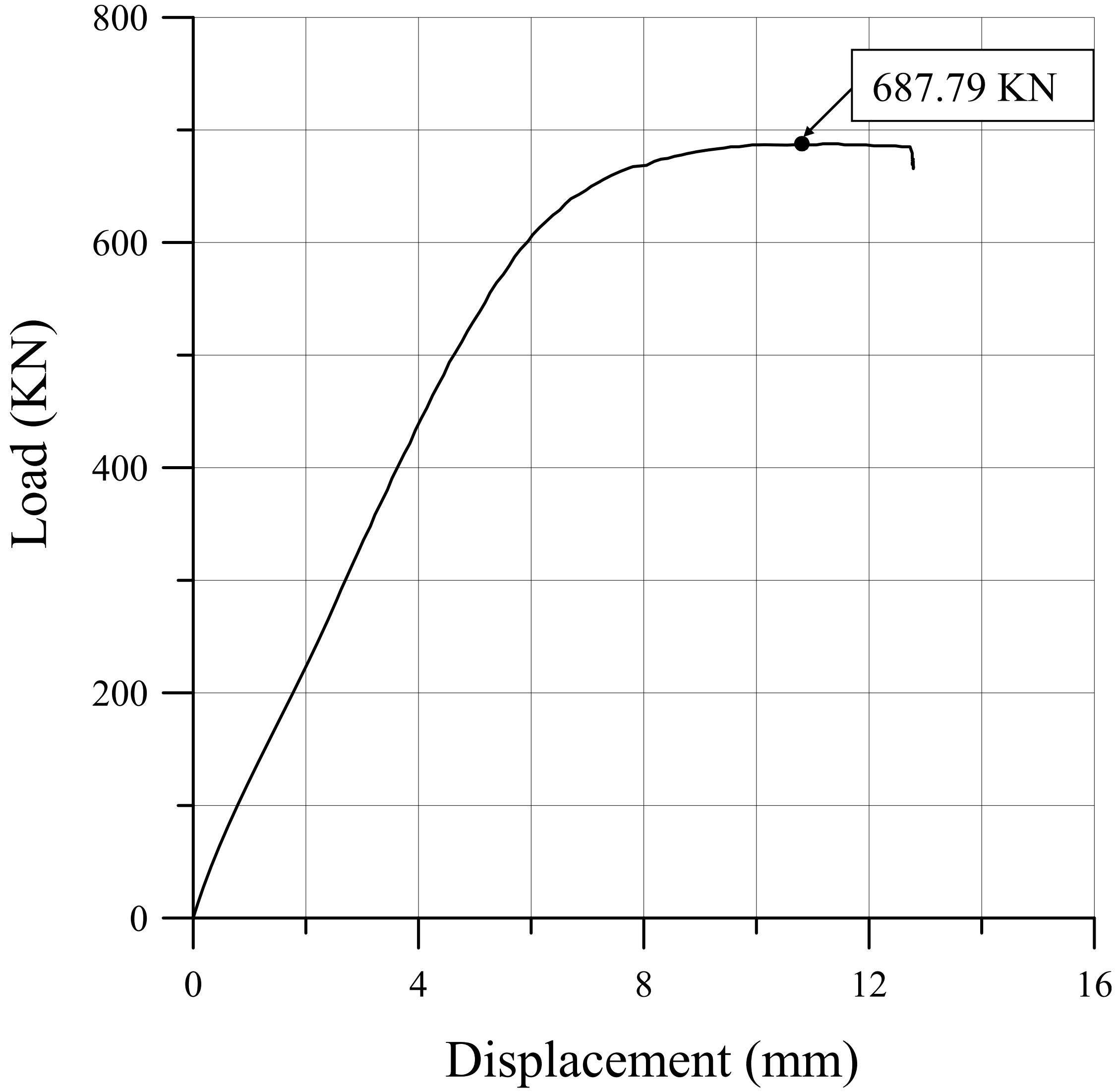

Figure 7.15 The load-axial displacement curve for ID13

ID 14

Plate		Stiffener				
t	Material	h_w	t_w	b_f	t_f	Material
5 mm	5083-H116	66.1 mm	4 mm	40 mm	5.7 mm	6082-T6

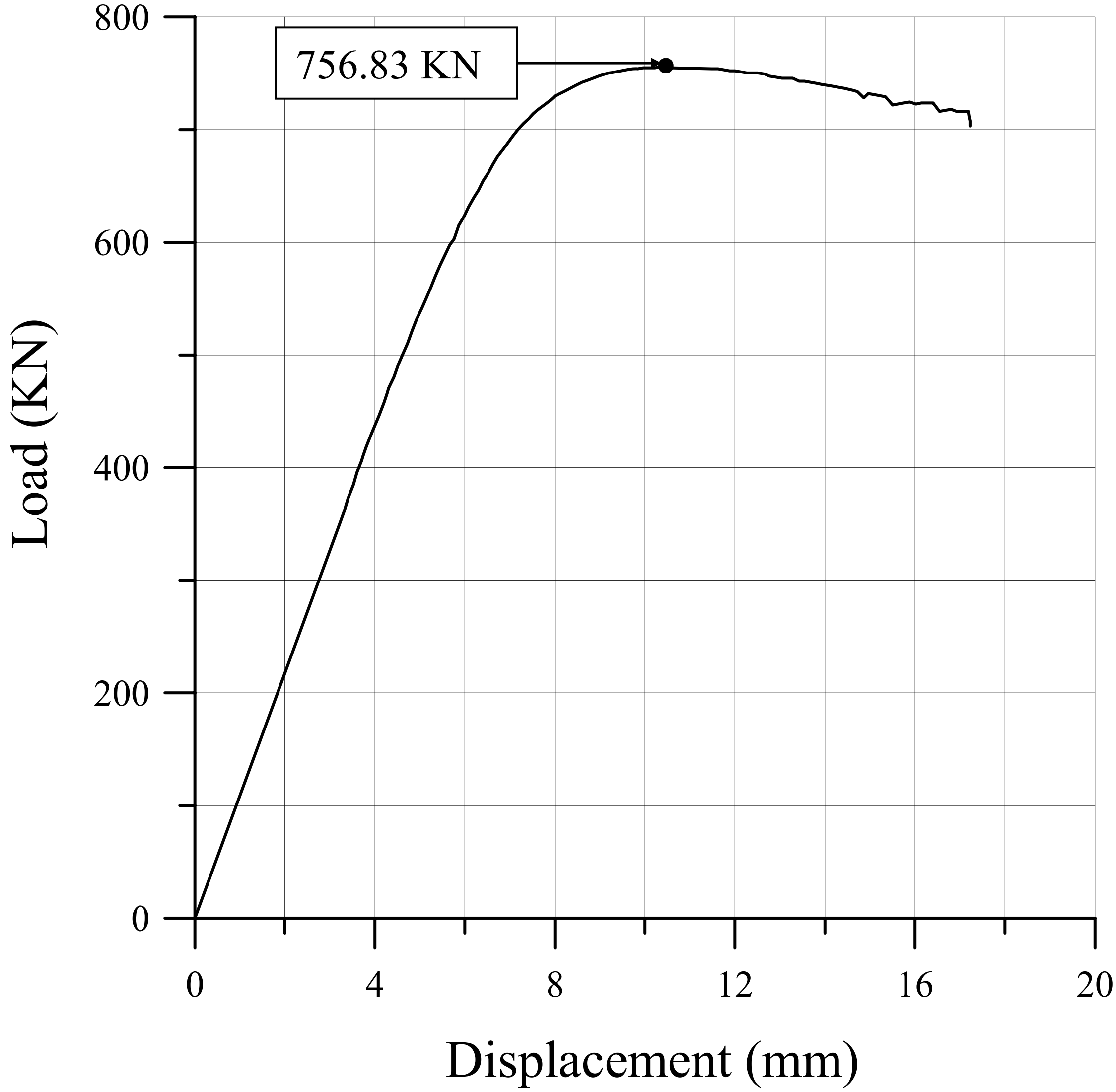

Figure 7.16 The load-axial displacement curve for ID14

ID 15	Plate		Stiffener				
	t	Material	h_w	t_w	b_f	t_f	Material
	5 mm	5083-H116	76.8 mm	4 mm	45 mm	5.6 mm	6082-T6

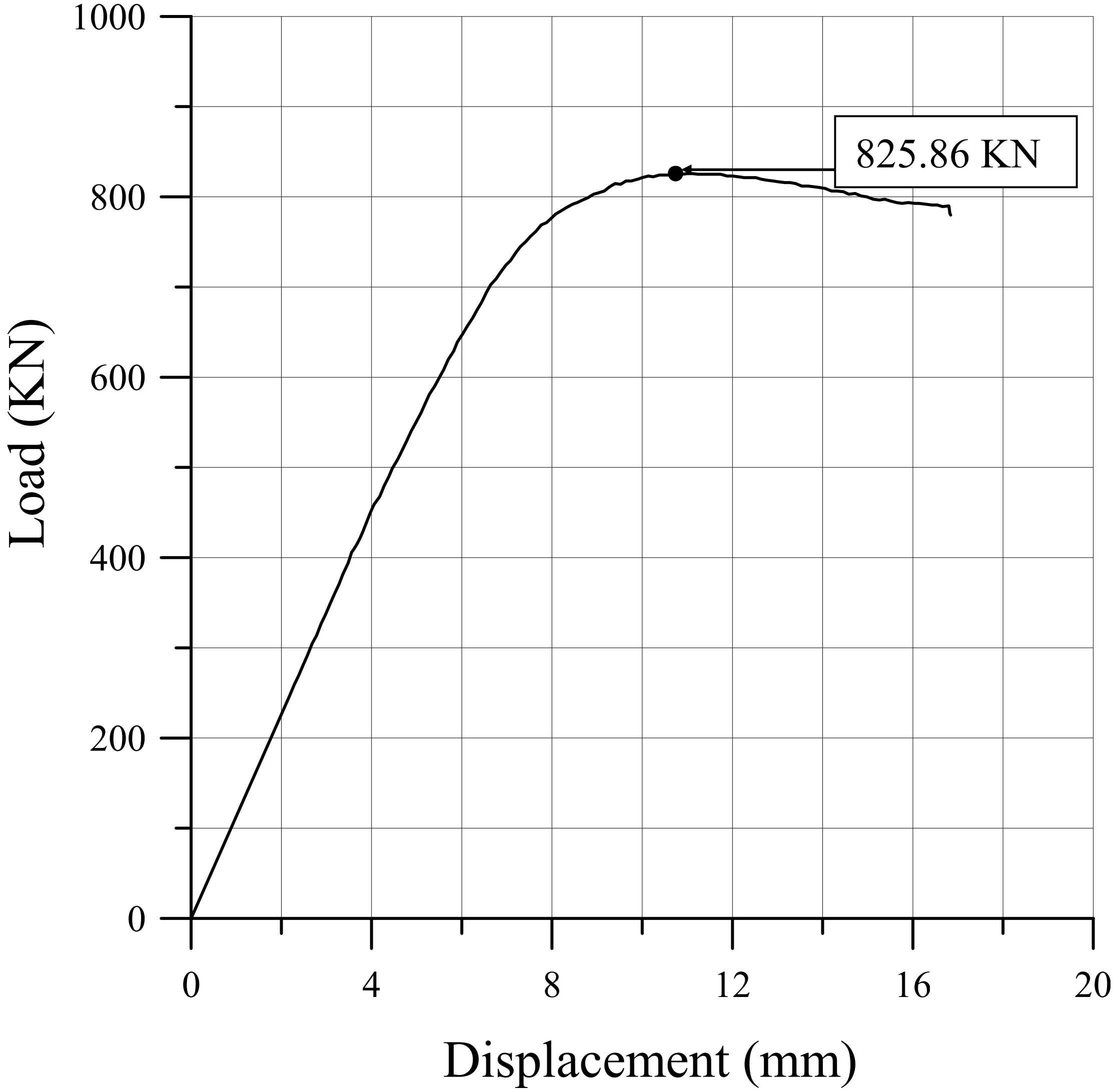

Figure 7.17 The load-axial displacement curve for ID15

ID 16

Plate		Stiffener				
t	Material	h_w	t_w	b_f	t_f	Material
5 mm	5083-H116	135 mm	6 mm	55 mm	8.2 mm	6082-T6

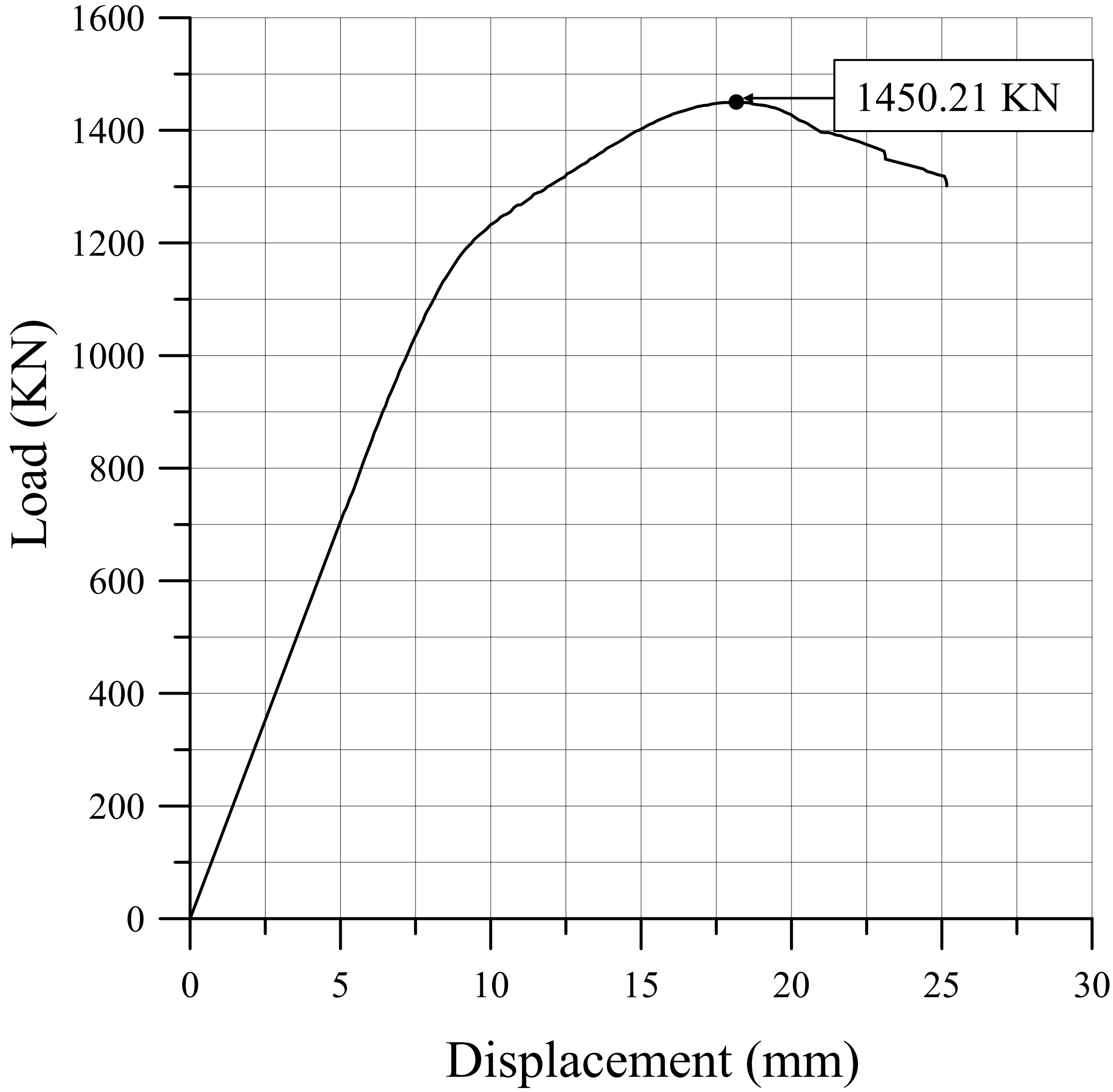

Figure 7.18 The load-axial displacement curve for ID16

ID 17

Plate		Stiffener				
t	Material	h_w	t_w	b_f	t_f	Material
6 mm	5083-H116	55.7 mm	3.7 mm	40 mm	6.7 mm	6082-T6

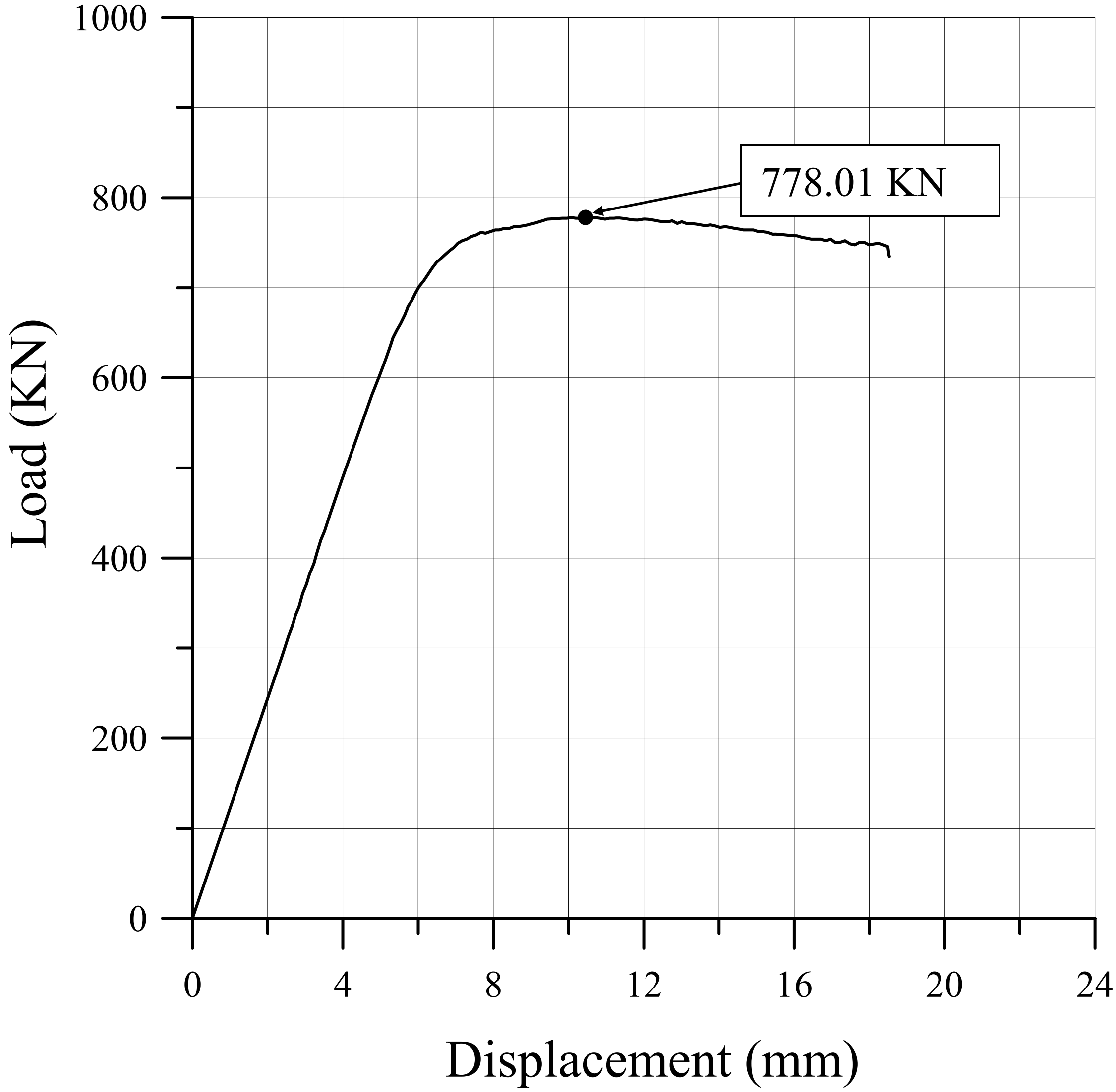

Figure 7.19 The load-axial displacement curve for ID17

ID 18

Plate		Stiffener				
t	Material	h_w	t_w	b_f	t_f	Material
6 mm	5083-H116	66.1 mm	4 mm	40 mm	5.7 mm	6082-T6

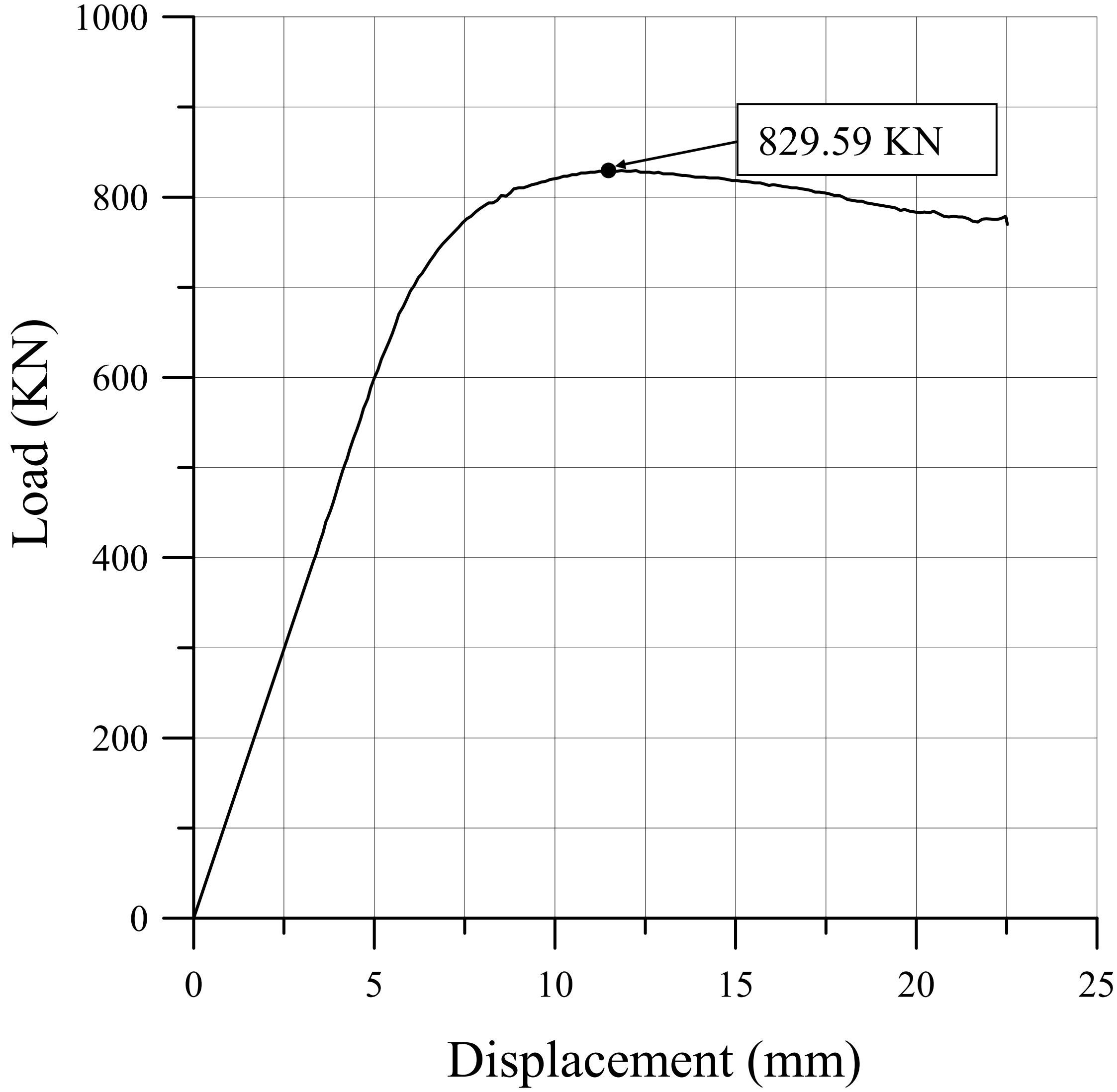

Figure 7.20 The load-axial displacement curve for ID18

ID 19

Plate		Stiffener				
t	Material	h_w	t_w	b_f	t_f	Material
6 mm	5083-H116	76.8 mm	4 mm	45 mm	5.6 mm	6082-T6

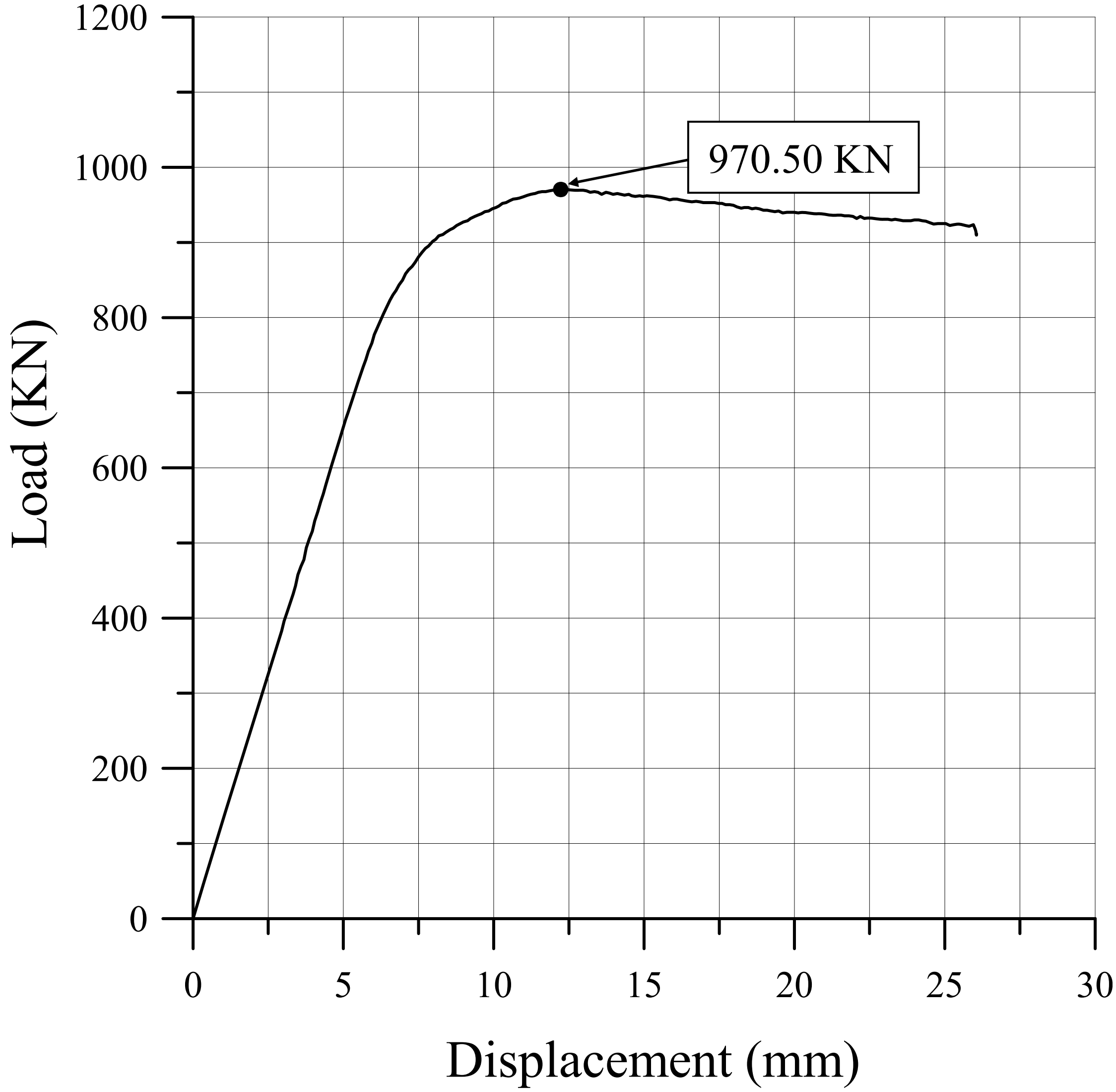

Figure 7.21 The load-axial displacement curve for ID19

ID 20

Plate		Stiffener				
t	Material	h_w	t_w	b_f	t_f	Material
6 mm	5083-H116	135 mm	6 mm	55 mm	8.2 mm	6082-T6

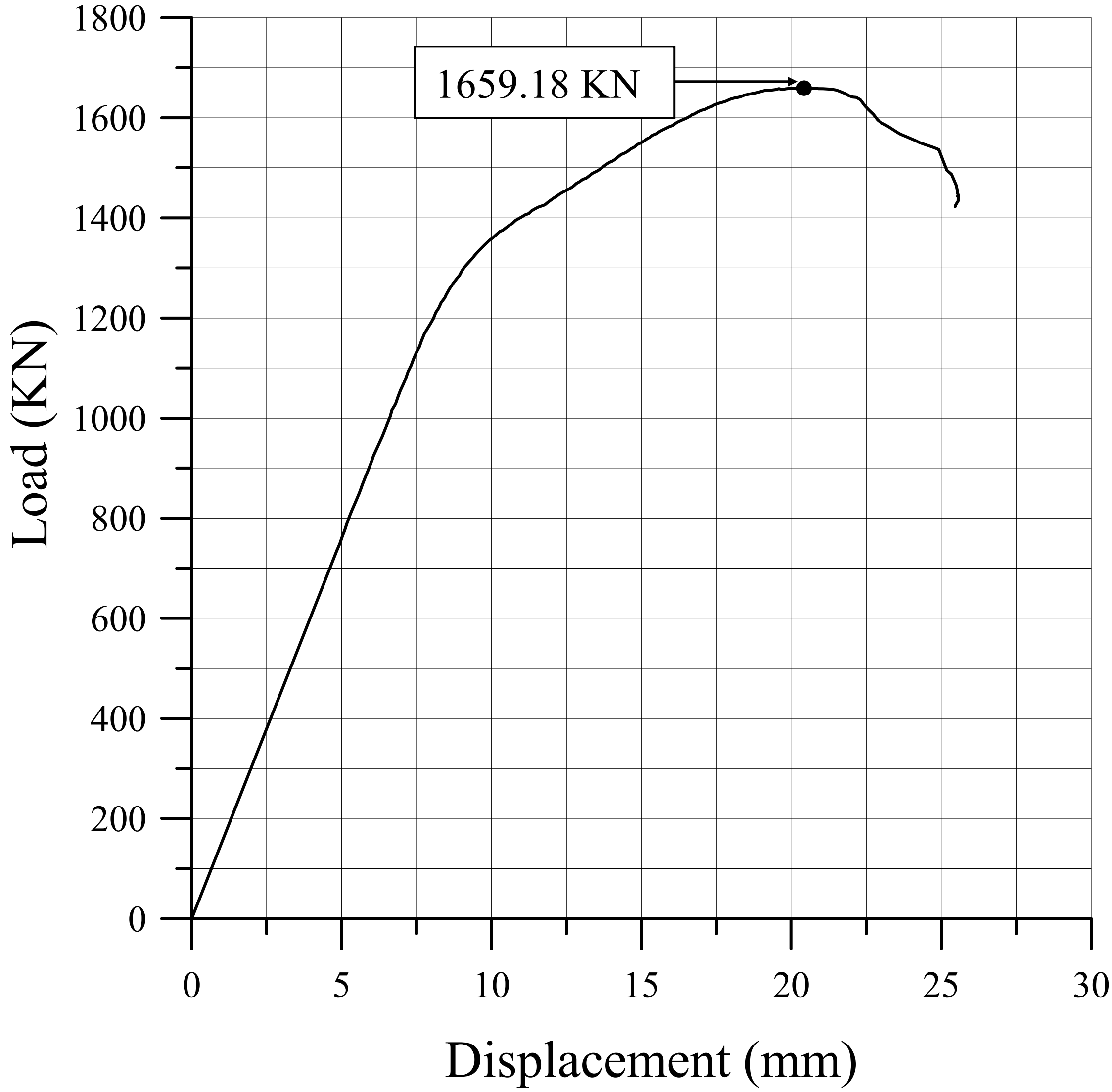

Figure 7.22 The load-axial displacement curve for ID20

ID 21

Plate		Stiffener				
t	Material	h_w	t_w	b_f	t_f	Material
8 mm	5083-H116	55.7 mm	3.7 mm	40 mm	6.7 mm	6082-T6

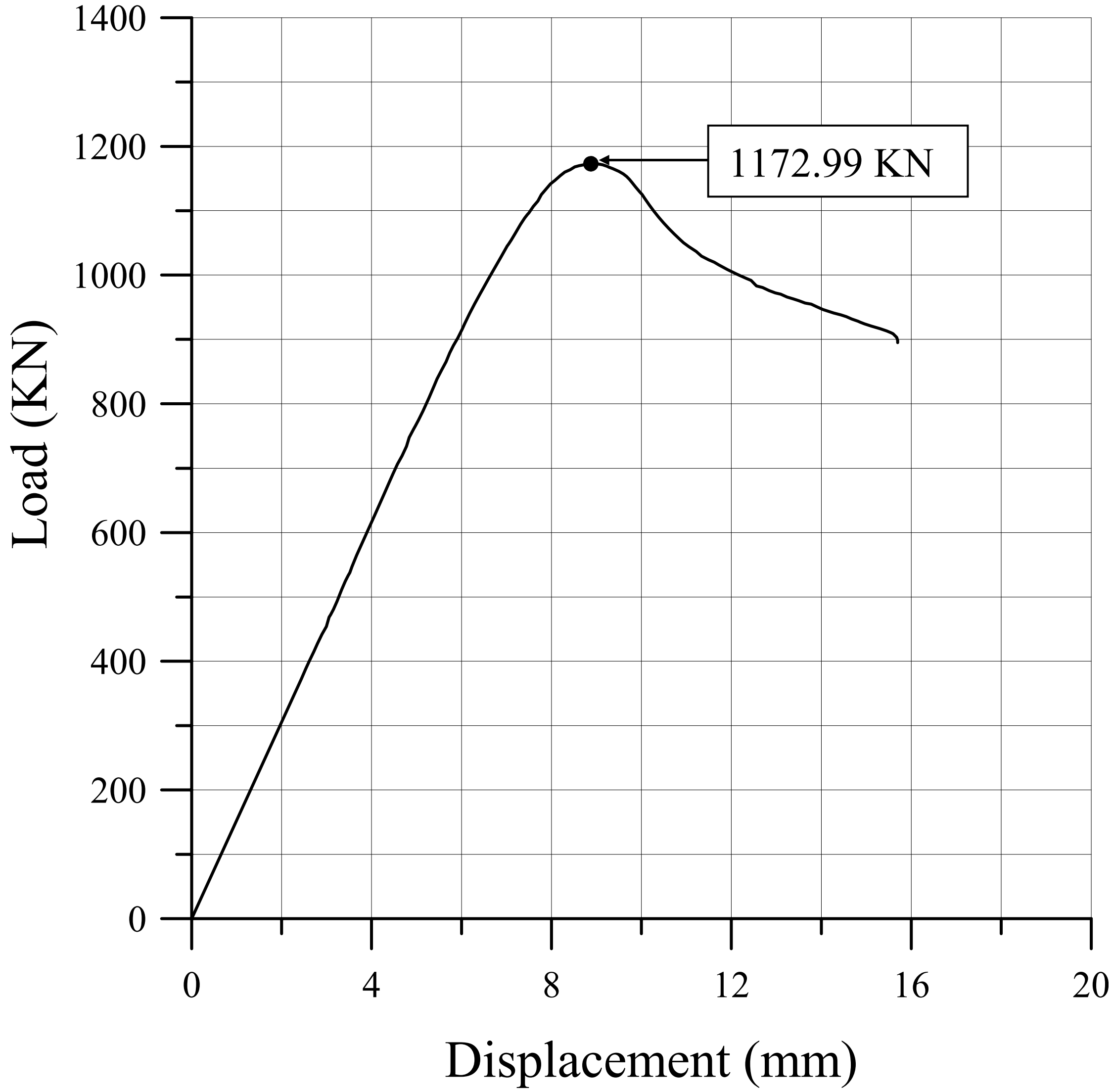

Figure 7.23 The load-axial displacement curve for ID21

ID 22

Plate		Stiffener				
t	Material	h_w	t_w	b_f	t_f	Material
8 mm	5083-H116	66.1 mm	4 mm	40 mm	5.7 mm	6082-T6

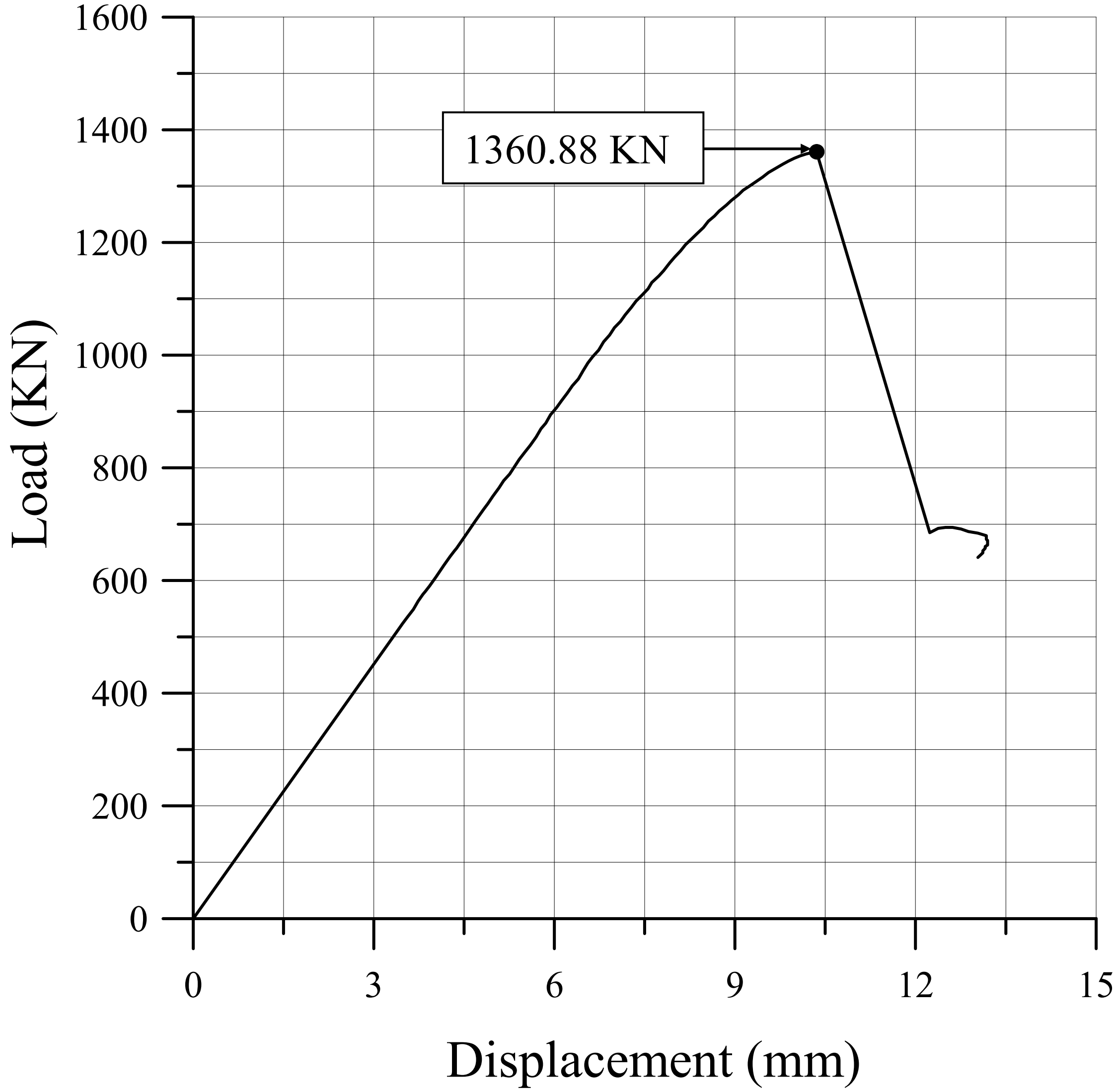

Figure 7.24 The load-axial displacement curve for ID22

ID 23

Plate		Stiffener				
t	Material	h_w	t_w	b_f	t_f	Material
8 mm	5083-H116	76.8 mm	4 mm	45 mm	5.6 mm	6082-T6

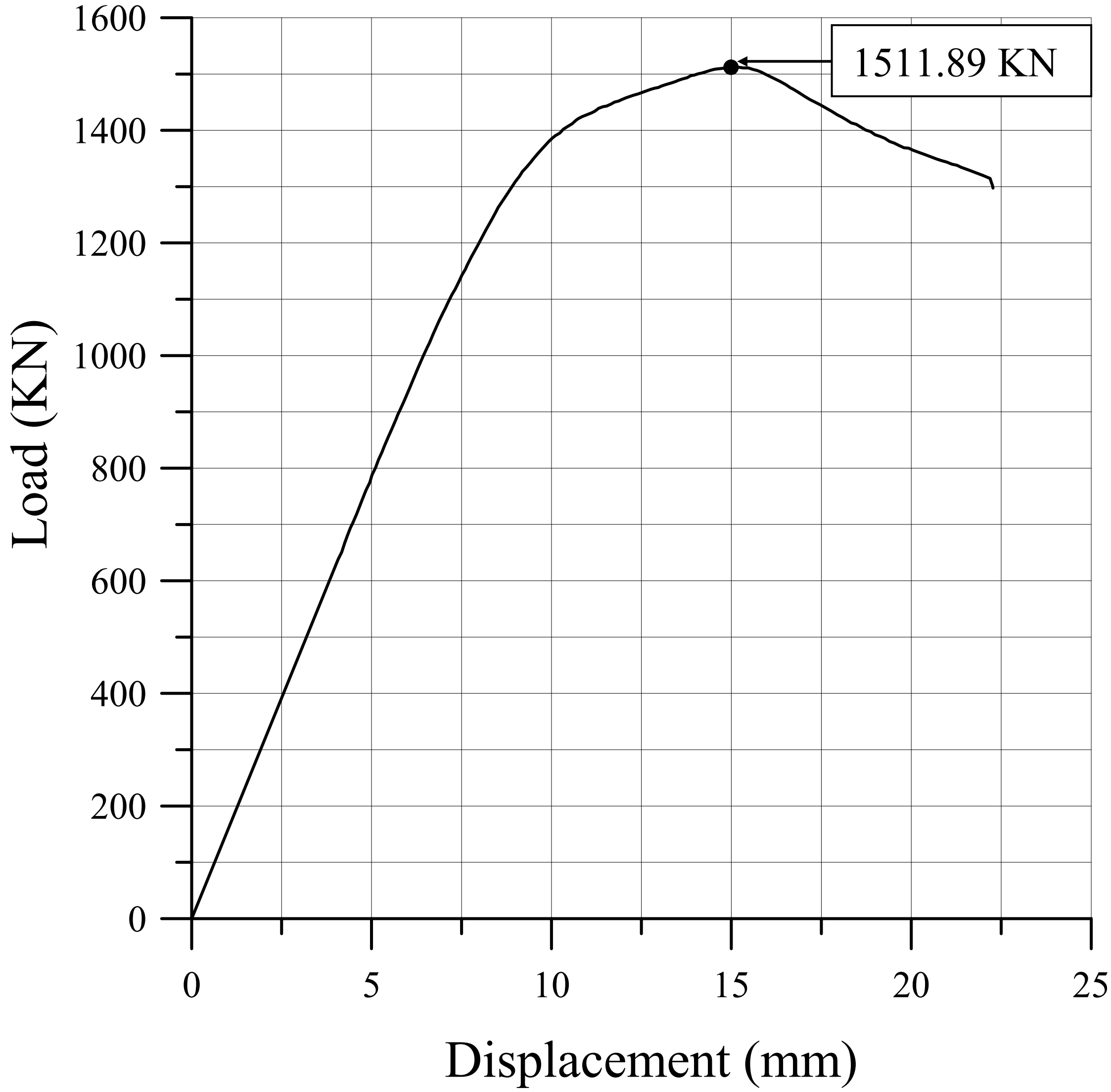

Figure 7.25 The load-axial displacement curve for ID23

ID 24

Plate		Stiffener				
t	Material	h_w	t_w	b_f	t_f	Material
8 mm	5083-H116	135 mm	6 mm	55 mm	8.2 mm	6082-T6

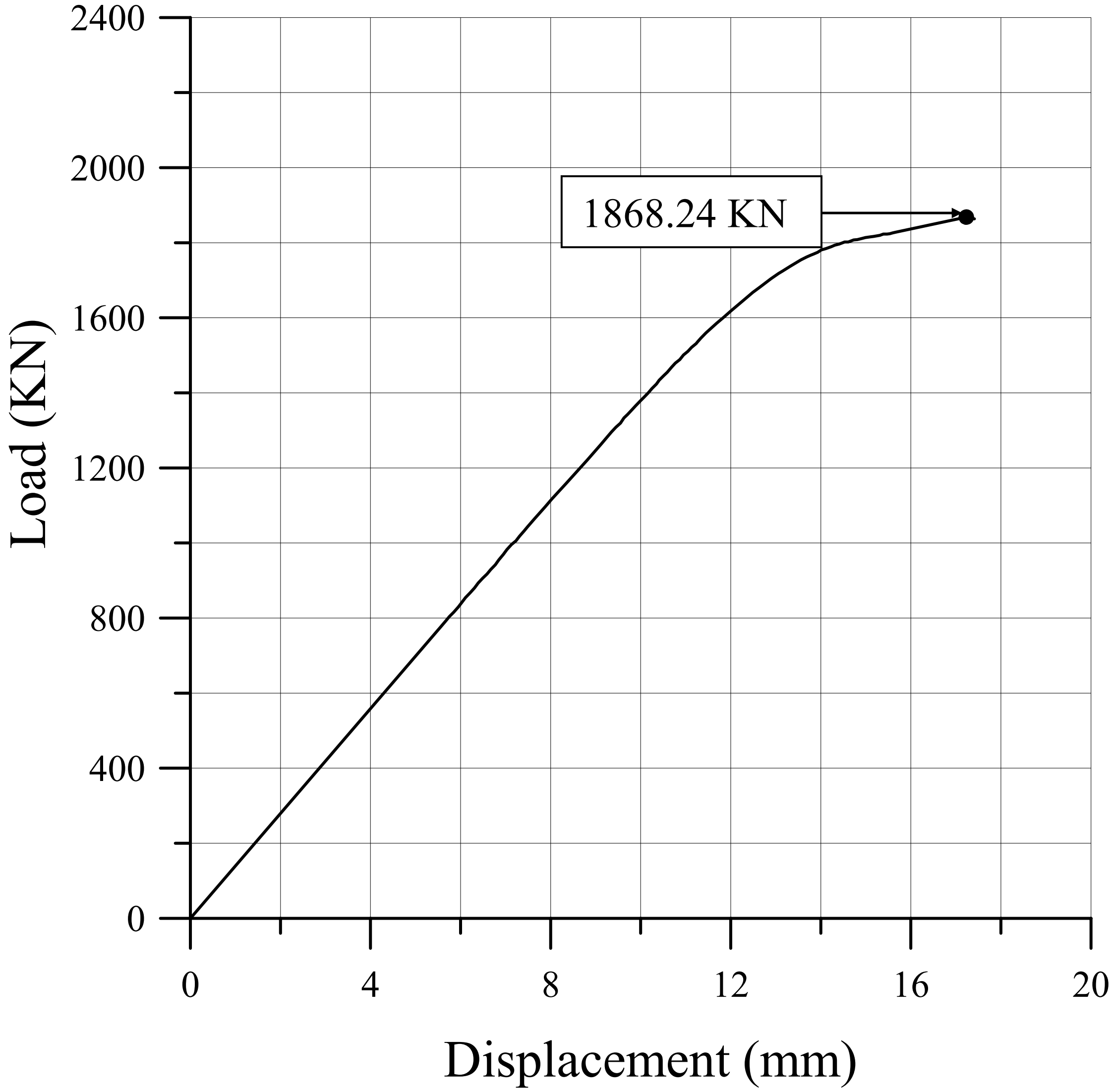

Figure 7.26 The load-axial displacement curve for ID24

ID 25

Plate		Stiffener				
t	Material	h_w	t_w	b_f	t_f	Material
5 mm	5383-H116	55.7 mm	3.7 mm	40 mm	6.7 mm	5383-H112

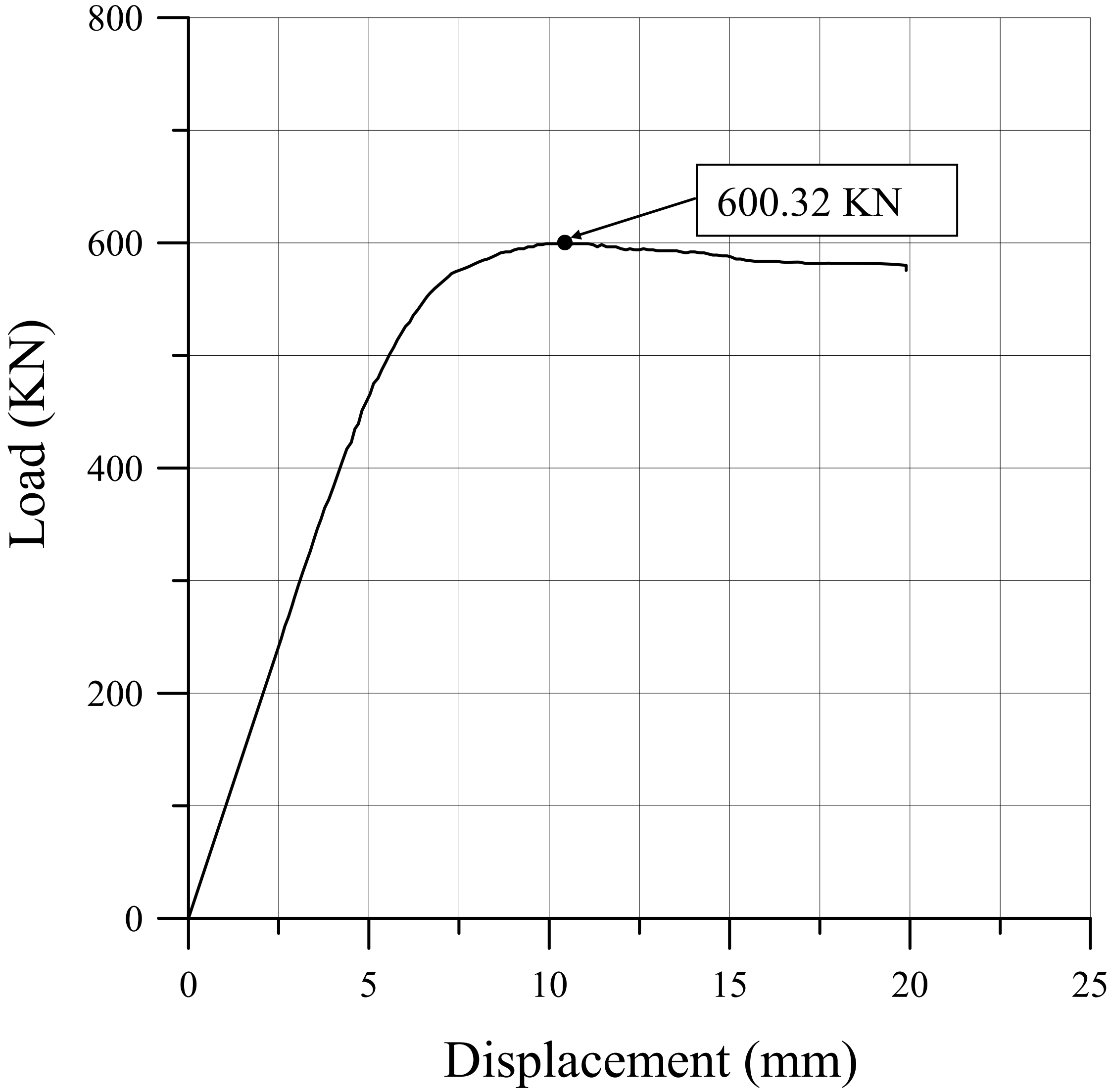

Figure 7.27 The load-axial displacement curve for ID25

ID 26

Plate		Stiffener				
t	Material	h_w	t_w	b_f	t_f	Material
5 mm	5383-H116	66.1 mm	4 mm	40 mm	5.7 mm	5383-H112

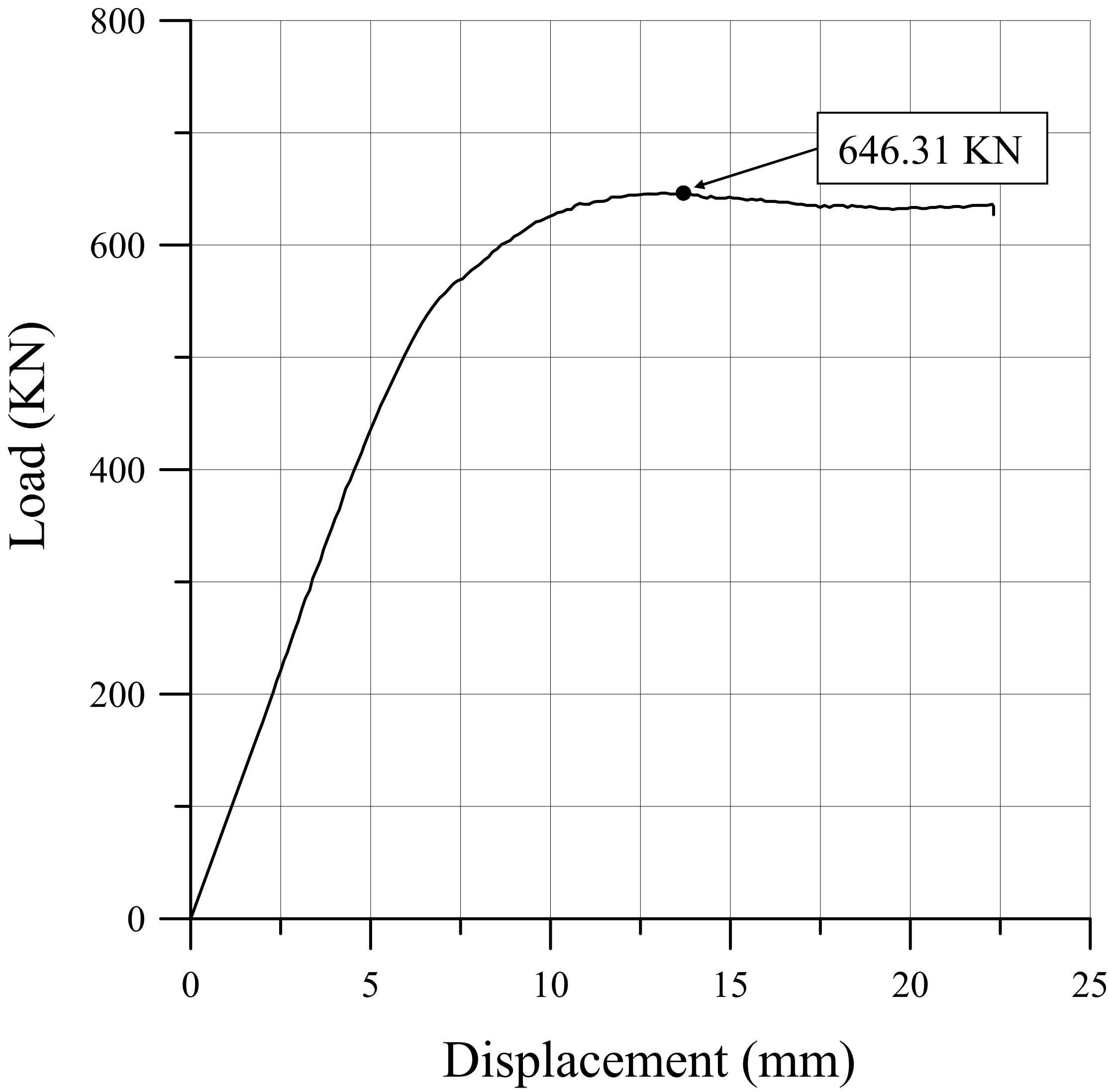

Figure 7.28 The load-axial displacement curve for ID26

ID 27

Plate		Stiffener				
t	Material	h_w	t_w	b_f	t_f	Material
5 mm	5383-H116	76.8 mm	4 mm	45 mm	5.6 mm	5383-H112

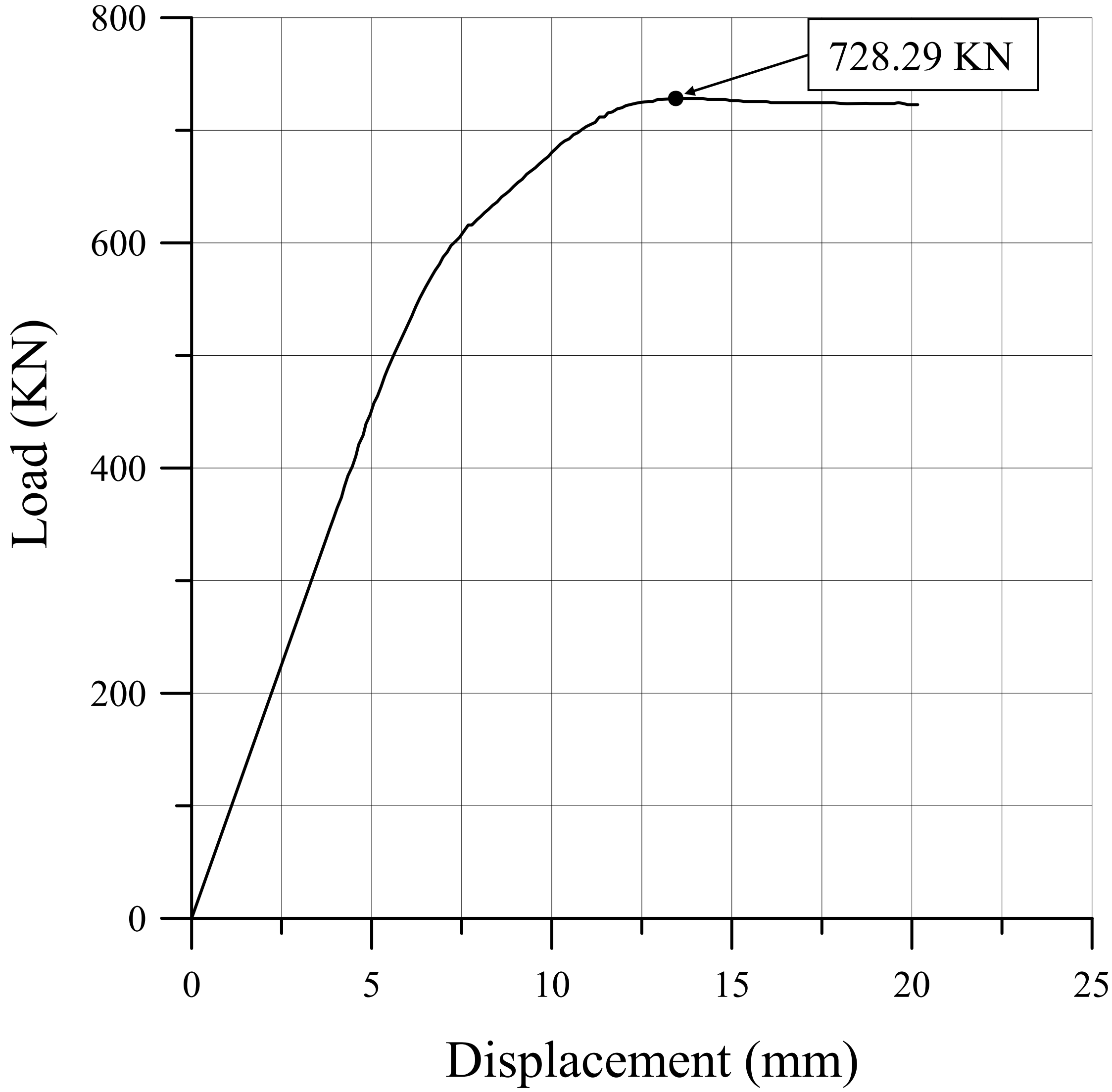

Figure 7.29 The load-axial displacement curve for ID27

ID 28

Plate		Stiffener				
t	Material	h_w	t_w	b_f	t_f	Material
5 mm	5383-H116	135 mm	6 mm	55 mm	8.2 mm	5383-H112

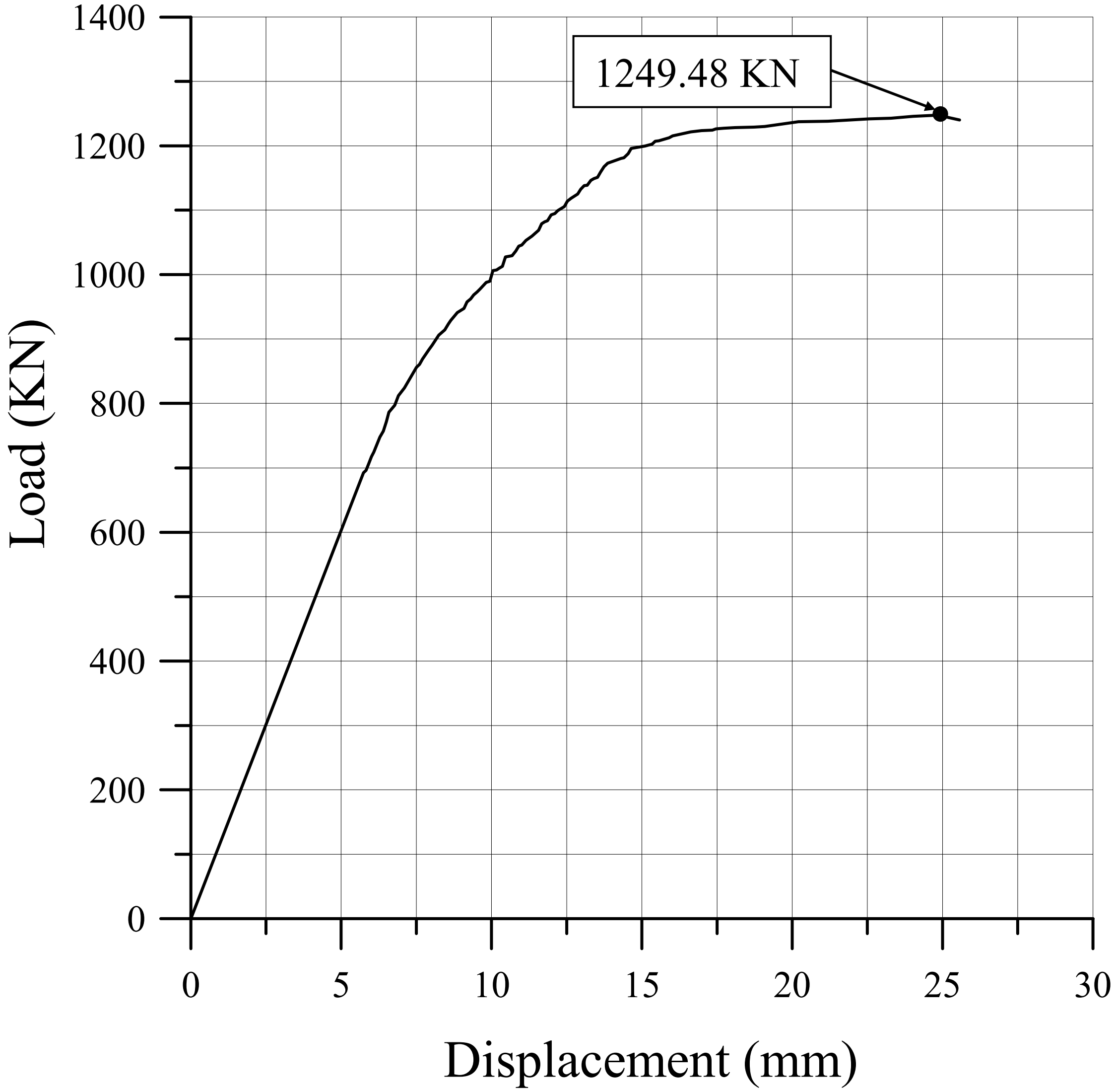

Figure 7.30 The load-axial displacement curve for ID28

ID 29

Plate		Stiffener				
t	Material	h_w	t_w	b_f	t_f	Material
6 mm	5383-H116	55.7 mm	3.7 mm	40 mm	6.7 mm	5383-H112

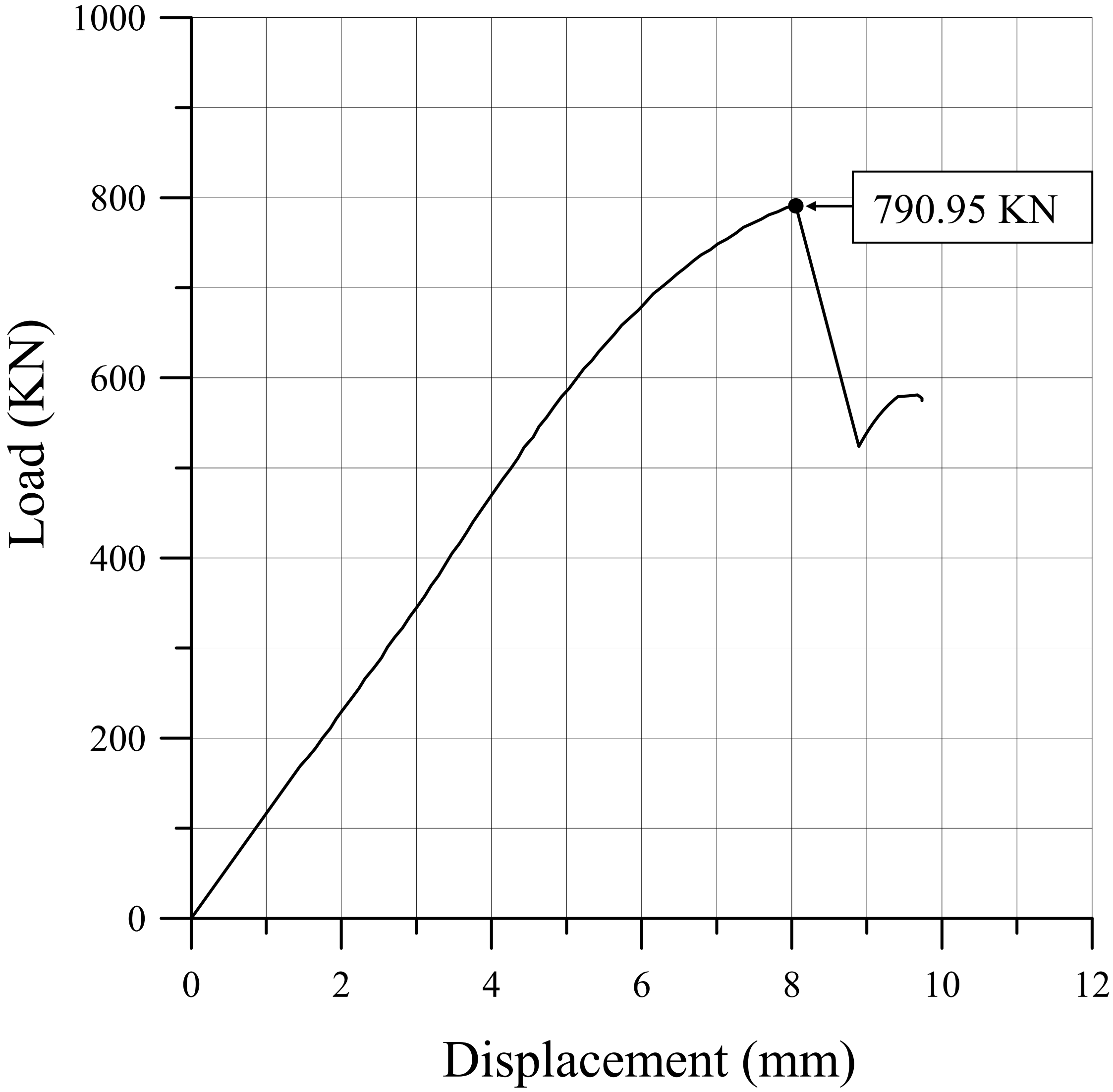

Figure 7.31 The load-axial displacement curve for ID29

ID 30

Plate		Stiffener				
t	Material	h_w	t_w	b_f	t_f	Material
6 mm	5383-H116	66.1 mm	4 mm	40 mm	5.7 mm	5383-H112

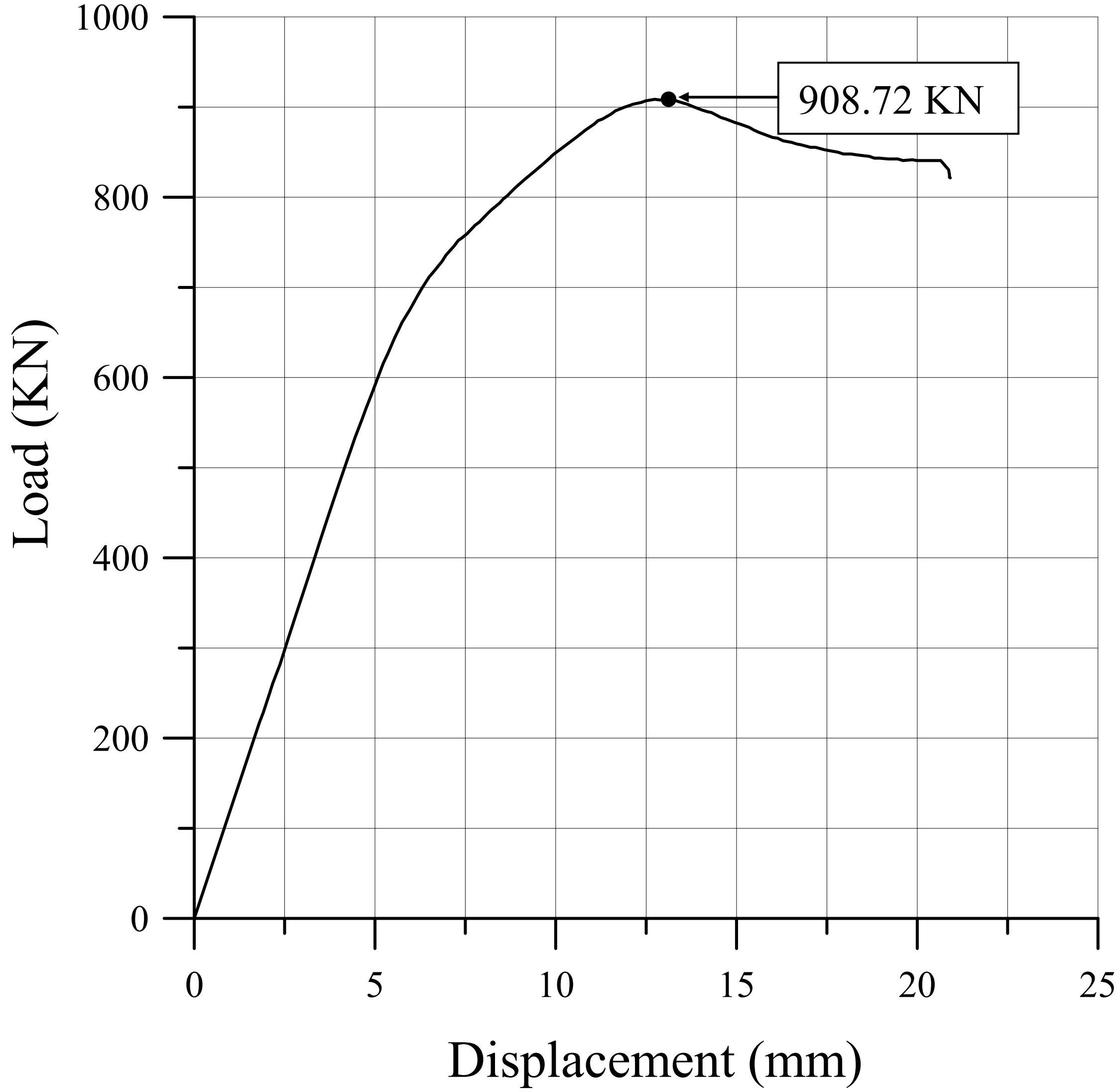

Figure 7.32 The load-axial displacement curve for ID30

ID 31

Plate		Stiffener				
t	Material	h_w	t_w	b_f	t_f	Material
6 mm	5383-H116	76.8 mm	4 mm	45 mm	5.6 mm	5383-H112

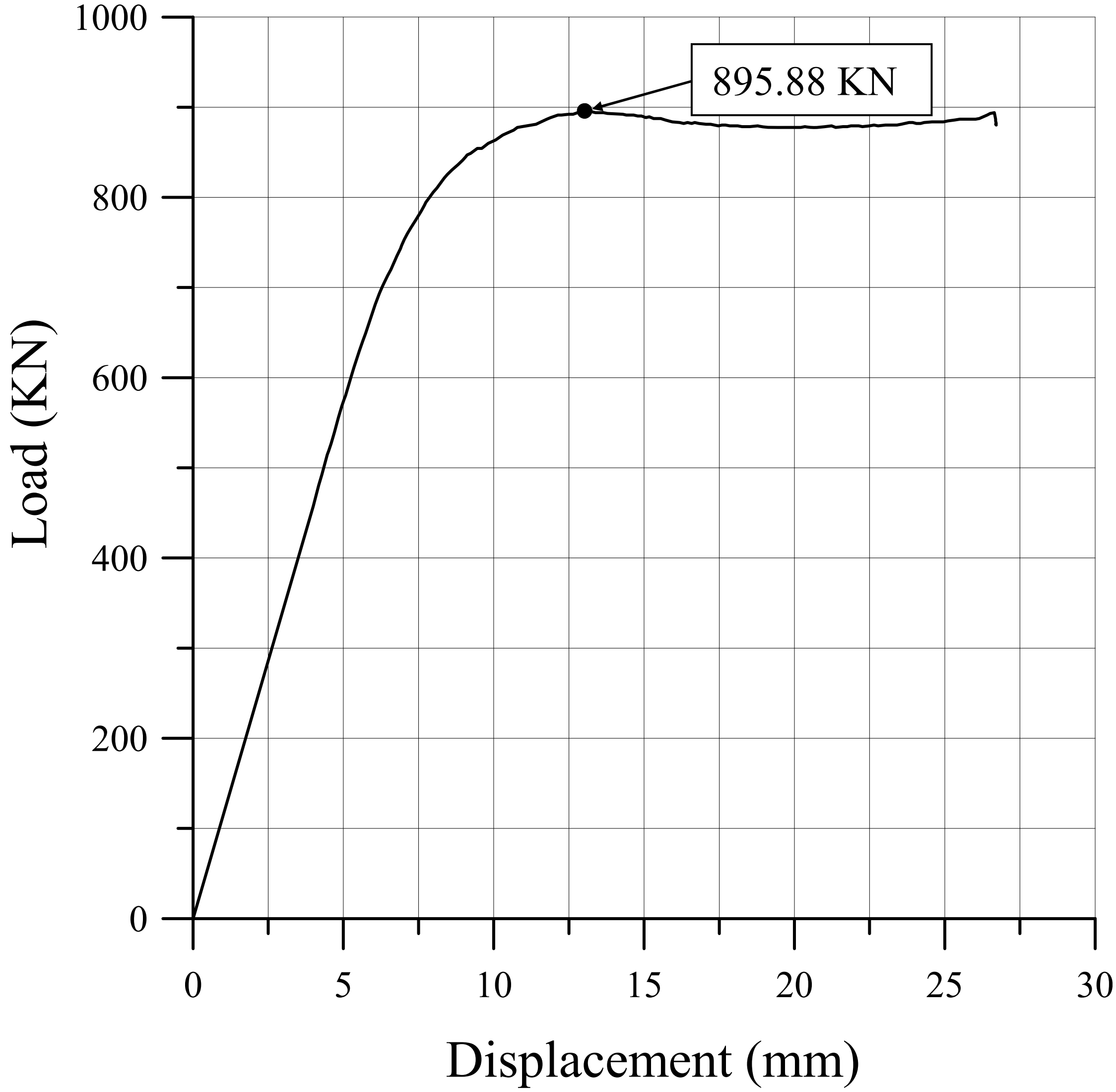

Figure 7.33 The load-axial displacement curve for ID31

ID 32

Plate		Stiffener				
t	Material	h_w	t_w	b_f	t_f	Material
6 mm	5383-H116	135 mm	6 mm	55 mm	8.2 mm	5383-H112

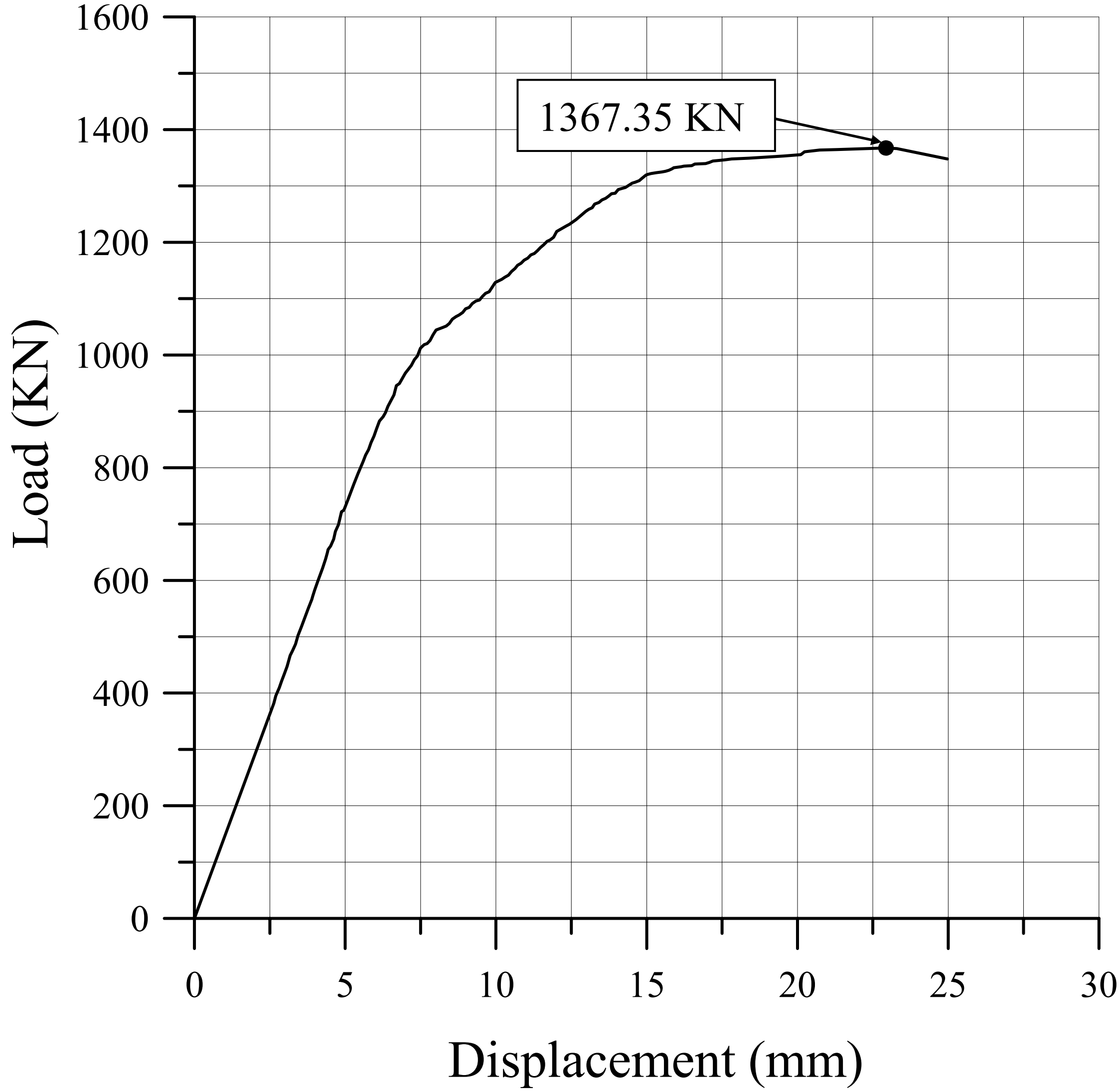

Figure 7.34 The load-axial displacement curve for ID32

ID 33

Plate		Stiffener				
t	Material	h_w	t_w	b_f	t_f	Material
8 mm	5383-H116	55.7 mm	3.7 mm	40 mm	6.7 mm	5383-H112

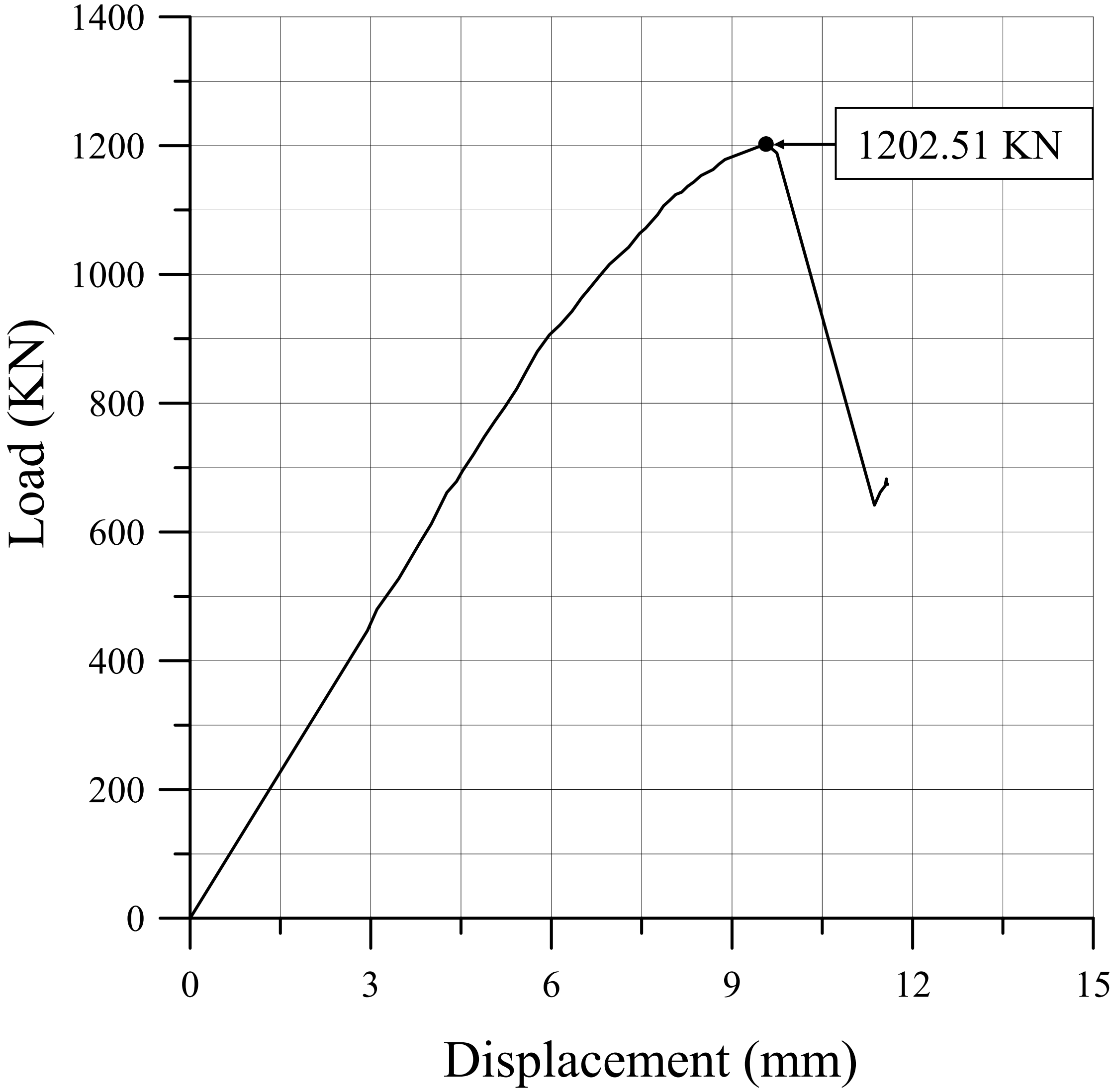

Figure 7.35 The load-axial displacement curve for ID33

ID 34

Plate		Stiffener				
t	Material	h_w	t_w	b_f	t_f	Material
8 mm	5383-H116	66.1 mm	4 mm	40 mm	5.7 mm	5383-H112

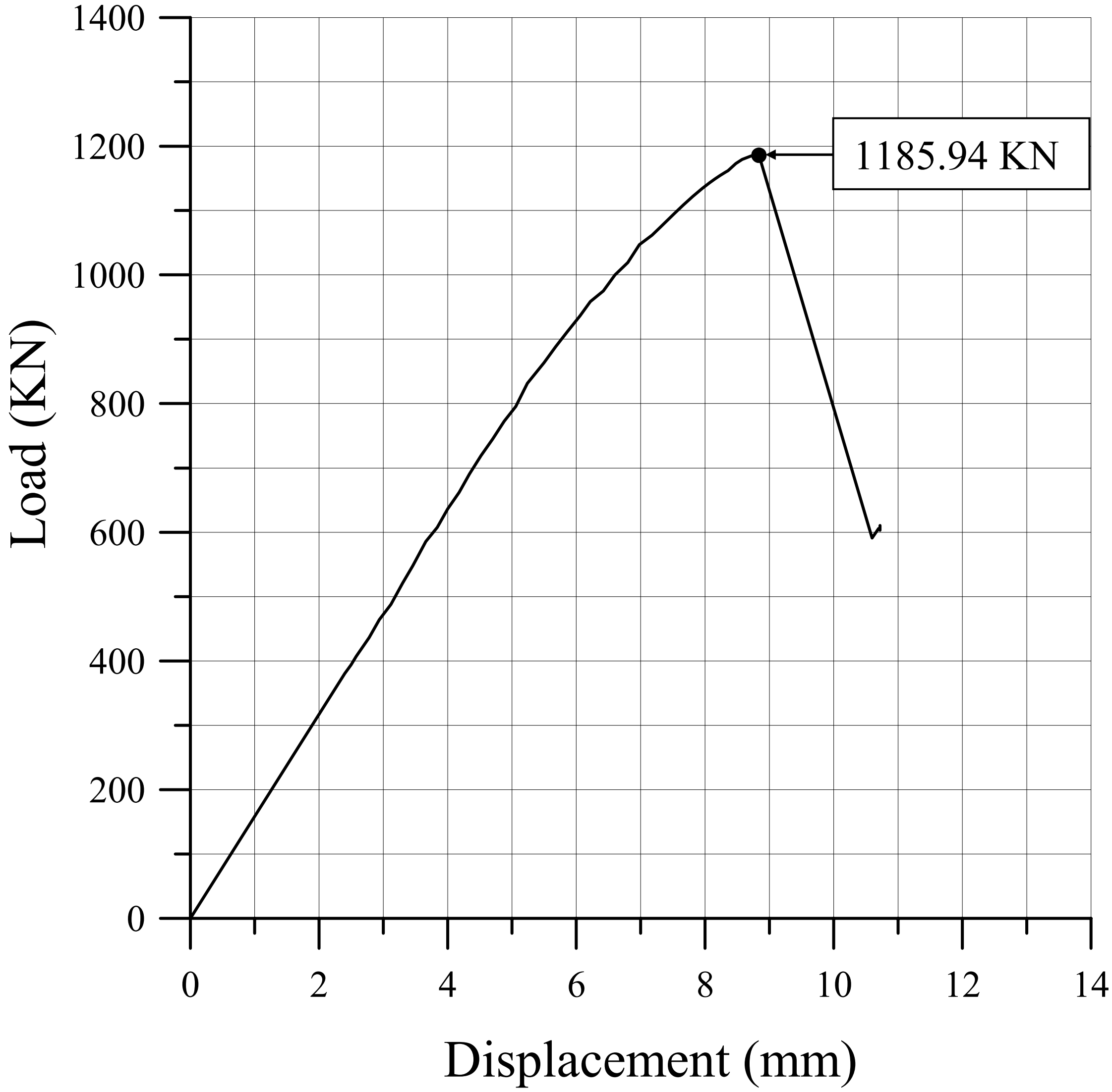

Figure 7.36 The load-axial displacement curve for ID34

ID 35

Plate		Stiffener				
t	Material	h_w	t_w	b_f	t_f	Material
8 mm	5383-H116	76.8 mm	4 mm	45 mm	5.6 mm	5383-H112

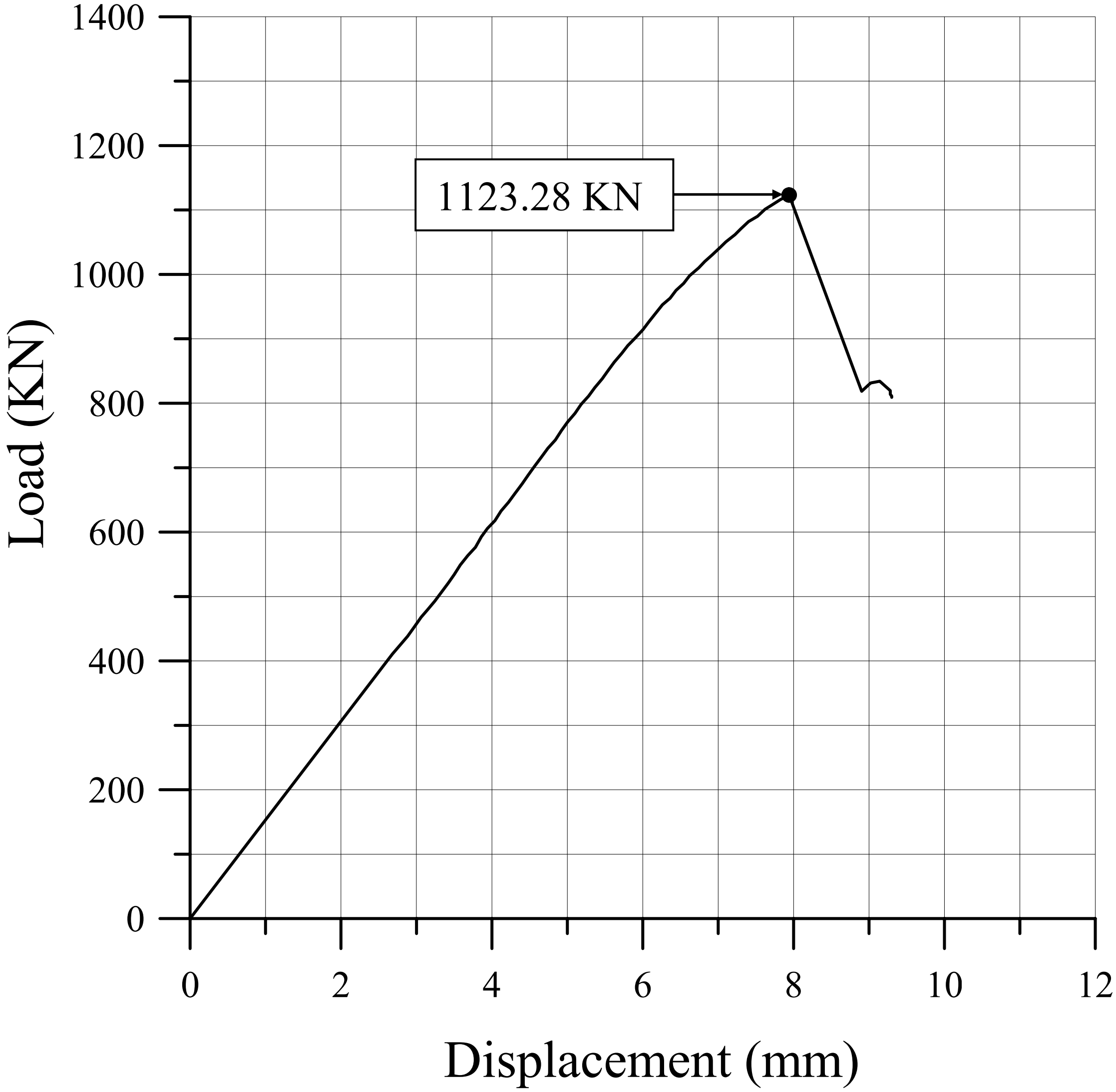

Figure 7.37 The load-axial displacement curve for ID35

ID 36

Plate		Stiffener				
t	Material	h_w	t_w	b_f	t_f	Material
8 mm	5383-H116	135 mm	6 mm	55 mm	8.2 mm	5383-H112

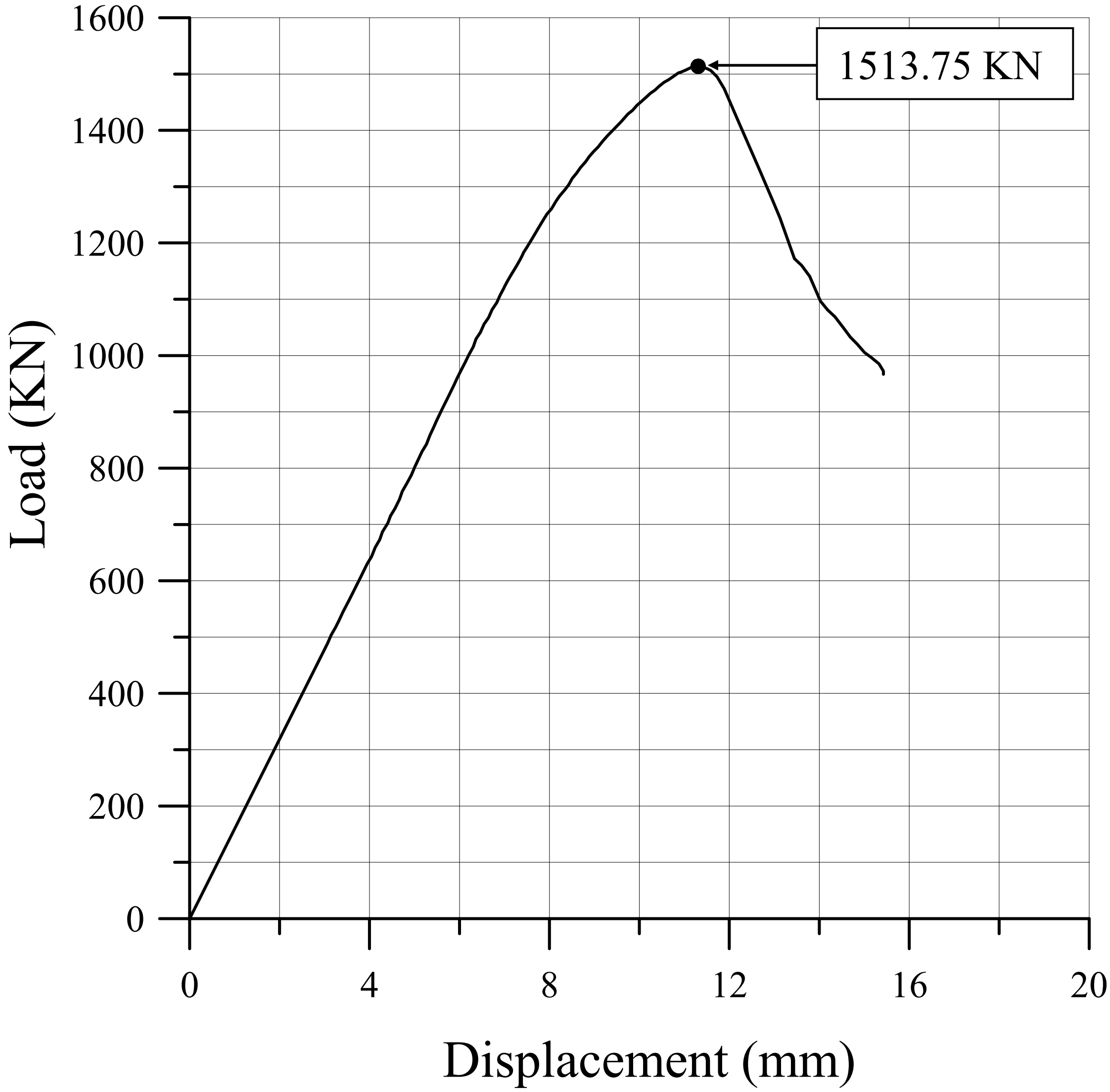

Figure 7.38 The load-axial displacement curve for ID36

ID 37

Plate		Stiffener				
t	Material	h_w	t_w	b_f	t_f	Material
5 mm	5083-H116	60 mm	5 mm	-	-	5083-H116

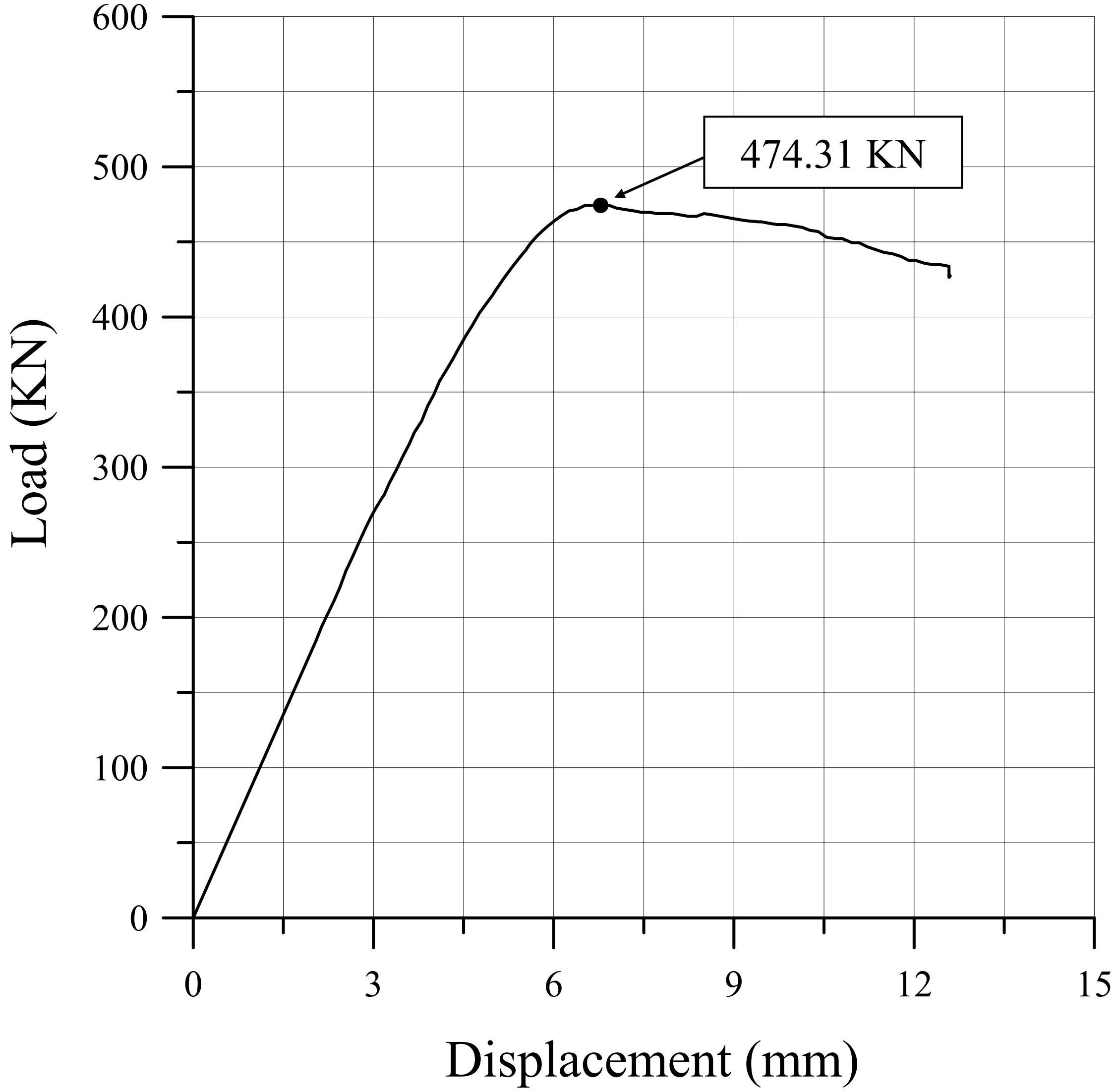

Figure 7.39 The load-axial displacement curve for ID37

ID 38

Plate		Stiffener				
t	Material	h_w	t_w	b_f	t_f	Material
5 mm	5083-H116	90 mm	5 mm	-	-	5083-H116

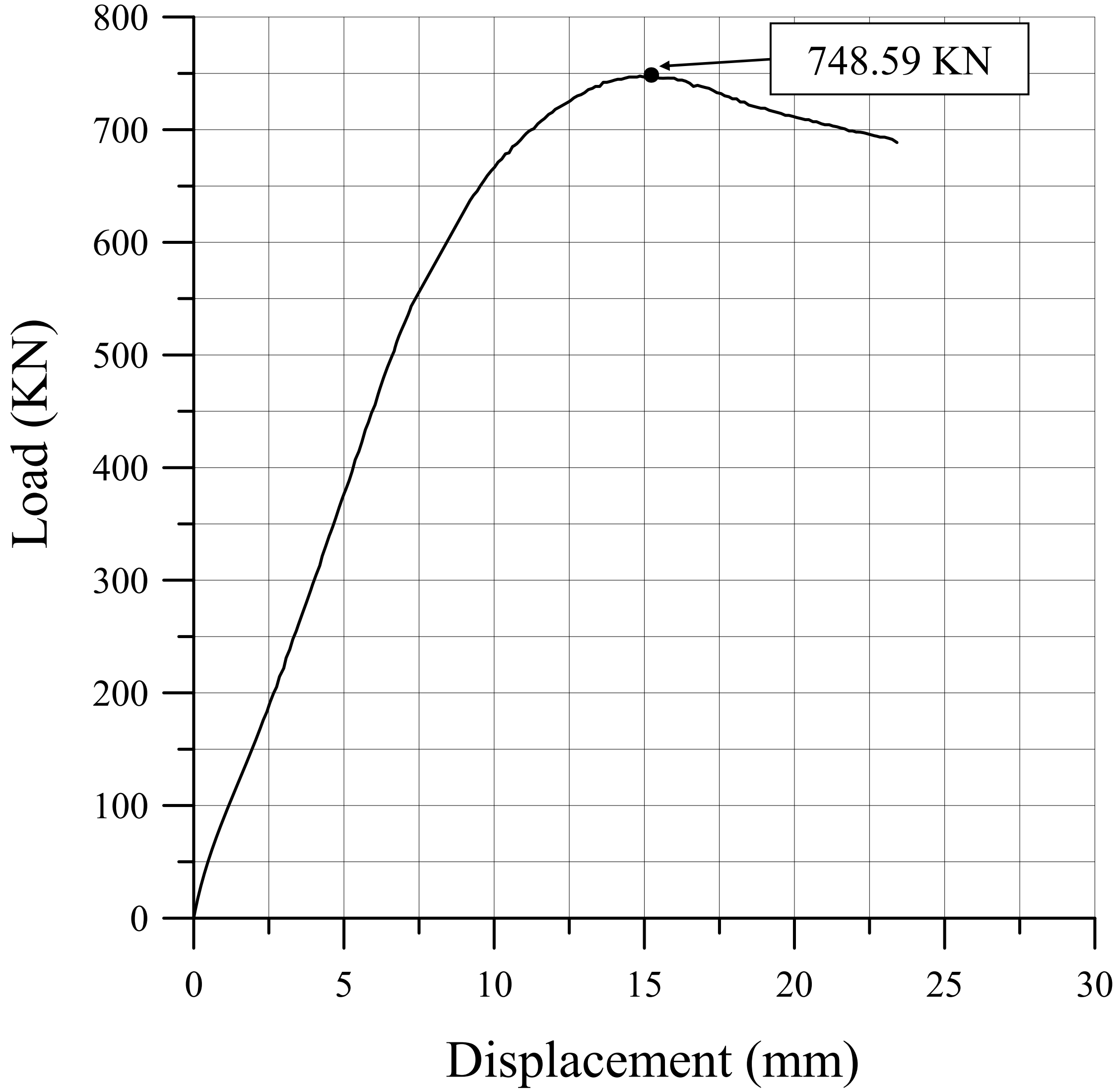

Figure 7.40 The load-axial displacement curve for ID38

ID 39

Plate		Stiffener				
t	Material	h_w	t_w	b_f	t_f	Material
5 mm	5083-H116	120 mm	5 mm	-	-	5083-H116

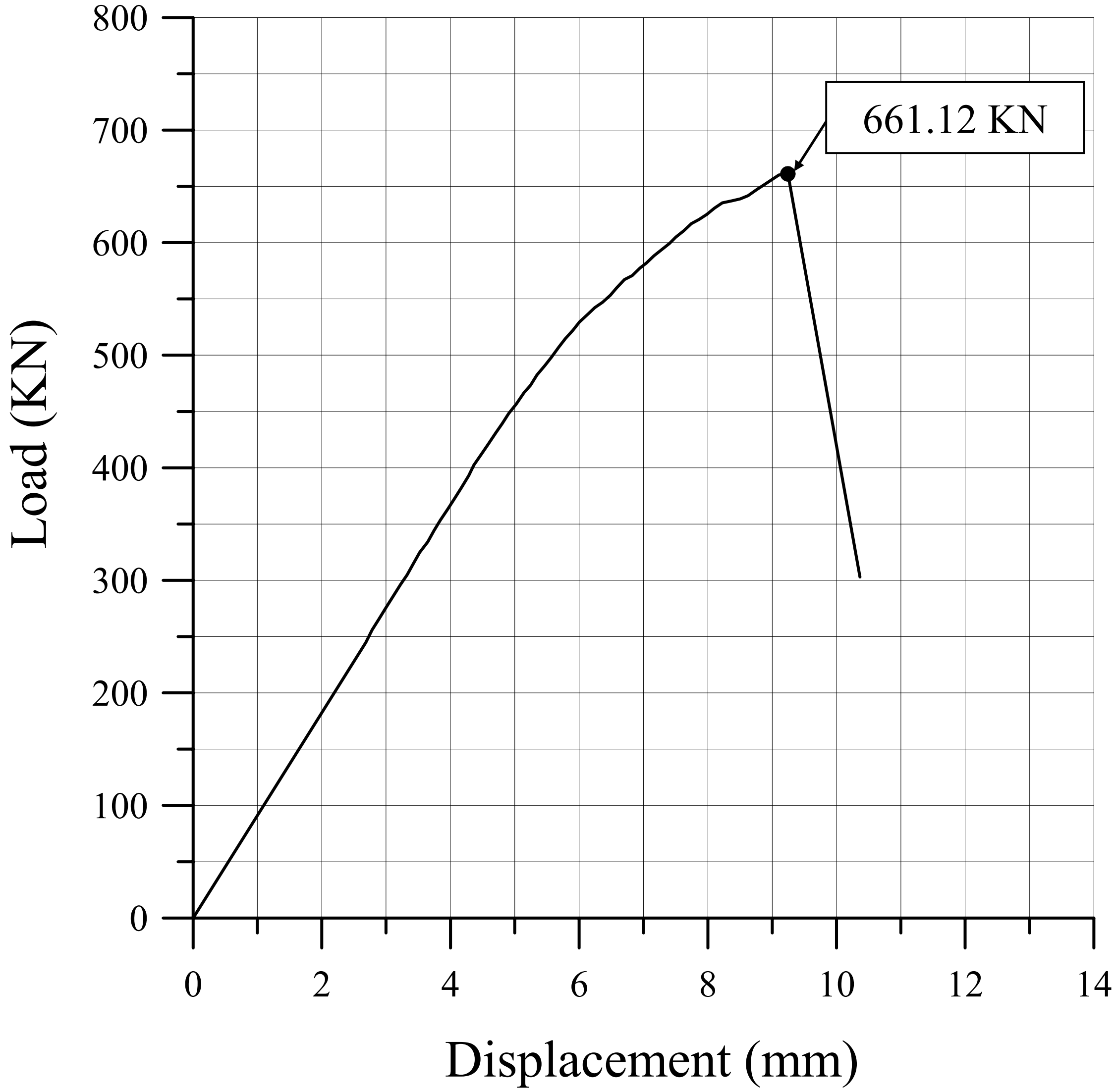

Figure 7.41 The load-axial displacement curve for ID39

ID 40

Plate		Stiffener				
t	Material	h_w	t_w	b_f	t_f	Material
6 mm	5083-H116	60 mm	6 mm	-	-	5083-H116

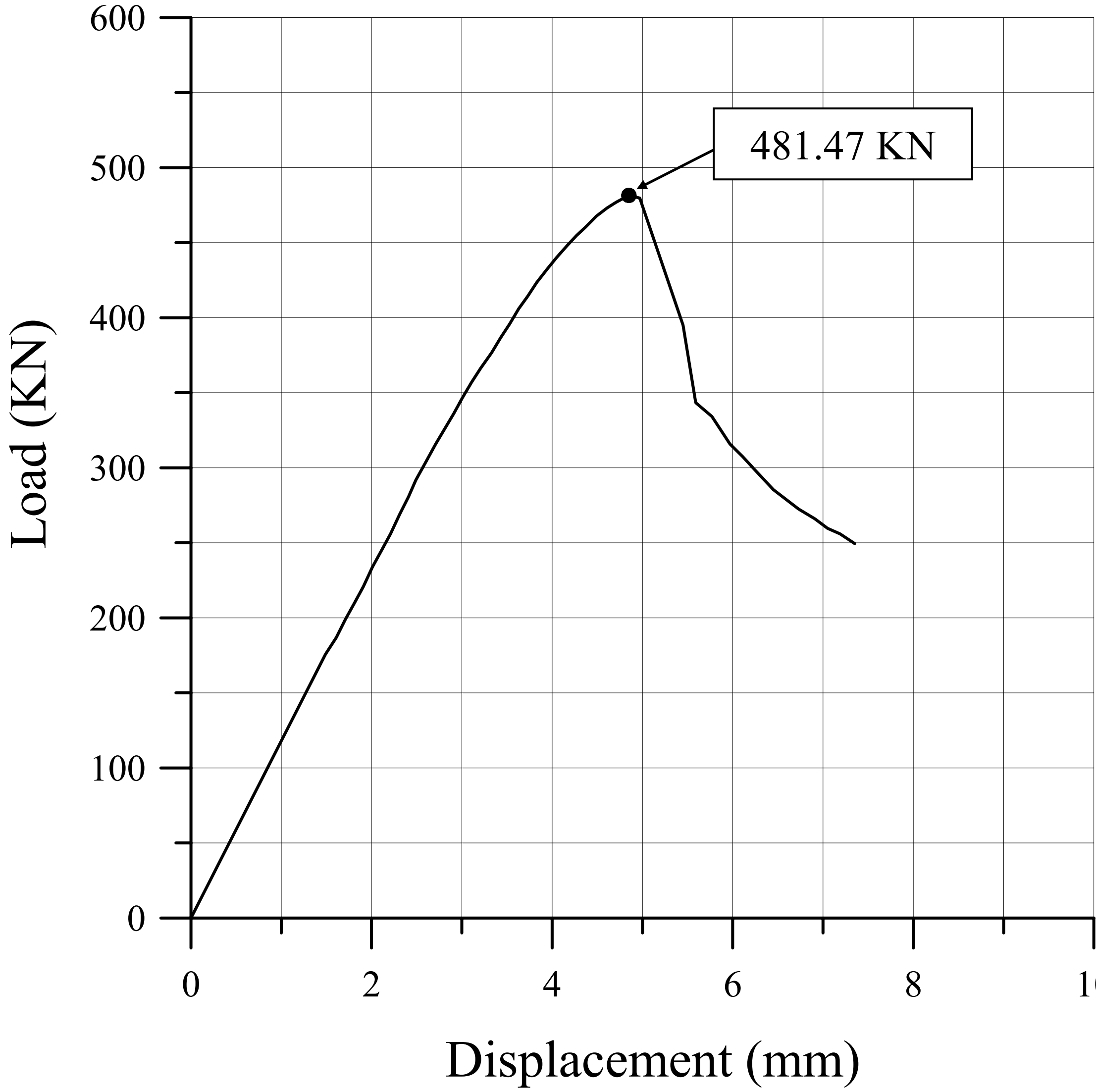

Figure 7.42 The load-axial displacement curve for ID40

ID 41

Plate		Stiffener				
t	Material	h_w	t_w	b_f	t_f	Material
6 mm	5083-H116	90 mm	6 mm	-	-	5083-H116

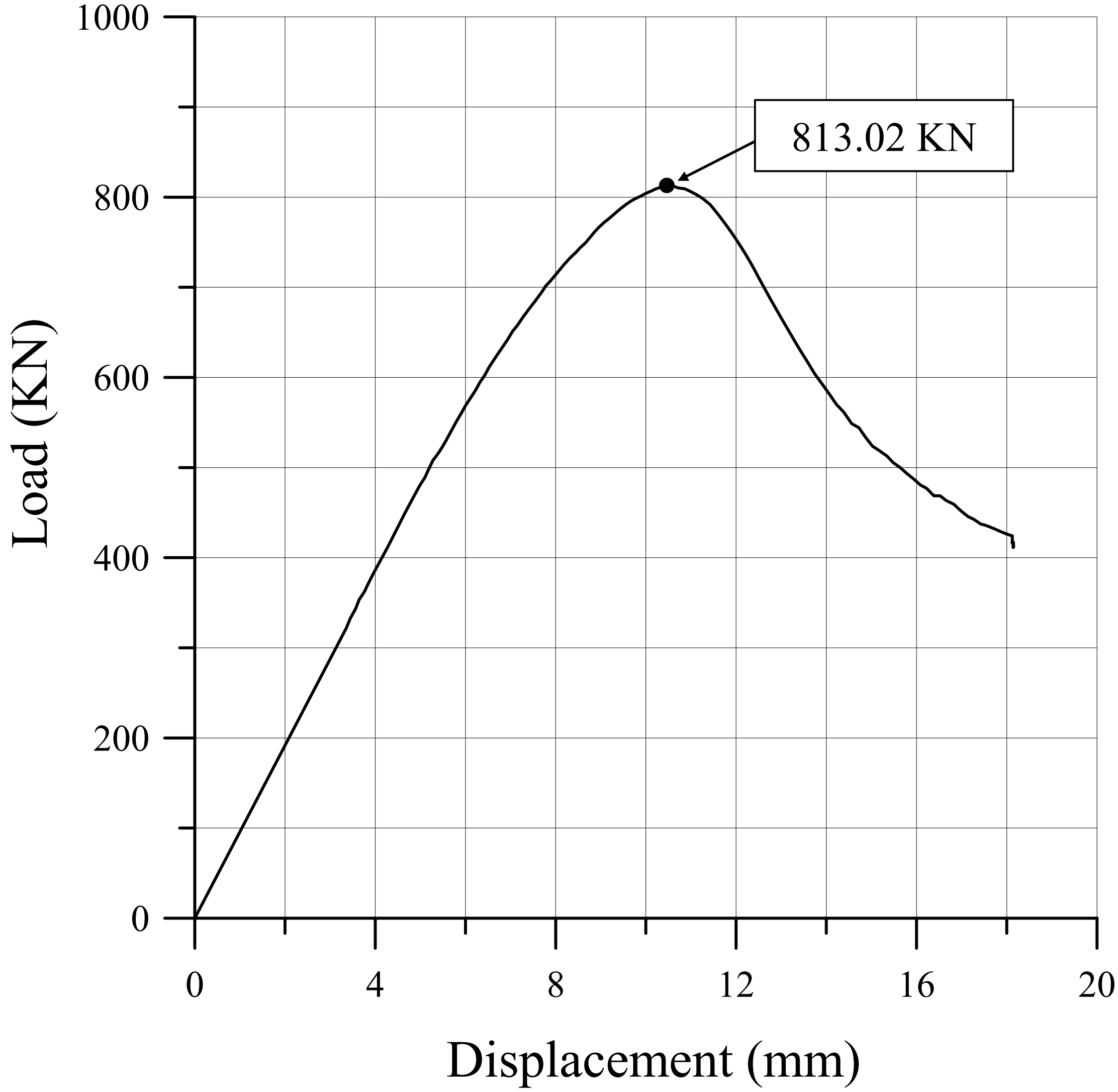

Figure 7.43 The load-axial displacement curve for ID41

ID 42

Plate		Stiffener				
t	Material	h_w	t_w	b_f	t_f	Material
6 mm	5083-H116	120 mm	6 mm	-	-	5083-H116

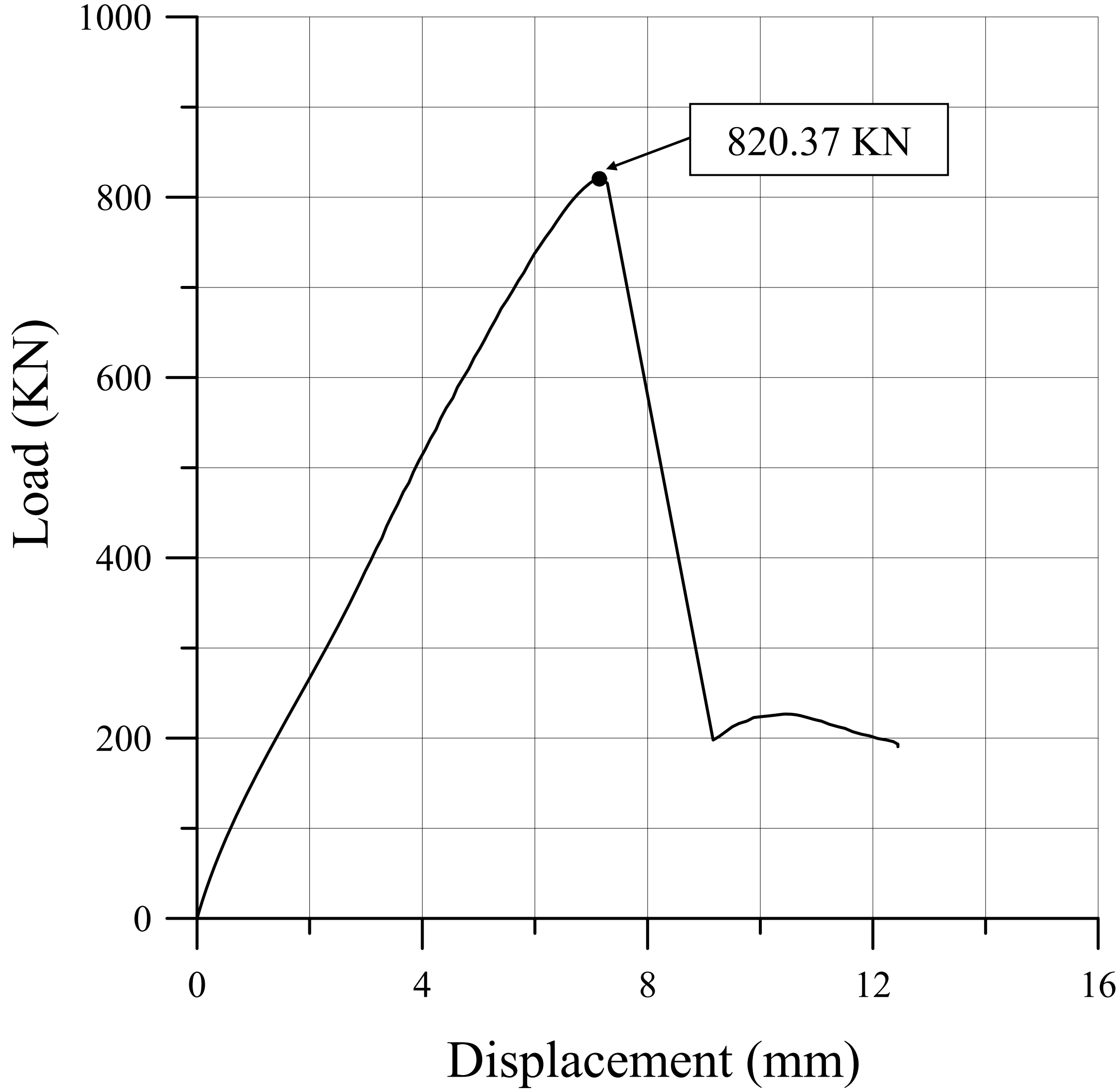

Figure 7.44 The load-axial displacement curve for ID42

ID 43

Plate		Stiffener				
t	Material	h_w	t_w	b_f	t_f	Material
8 mm	5083-H116	60 mm	8 mm	-	-	5083-H116

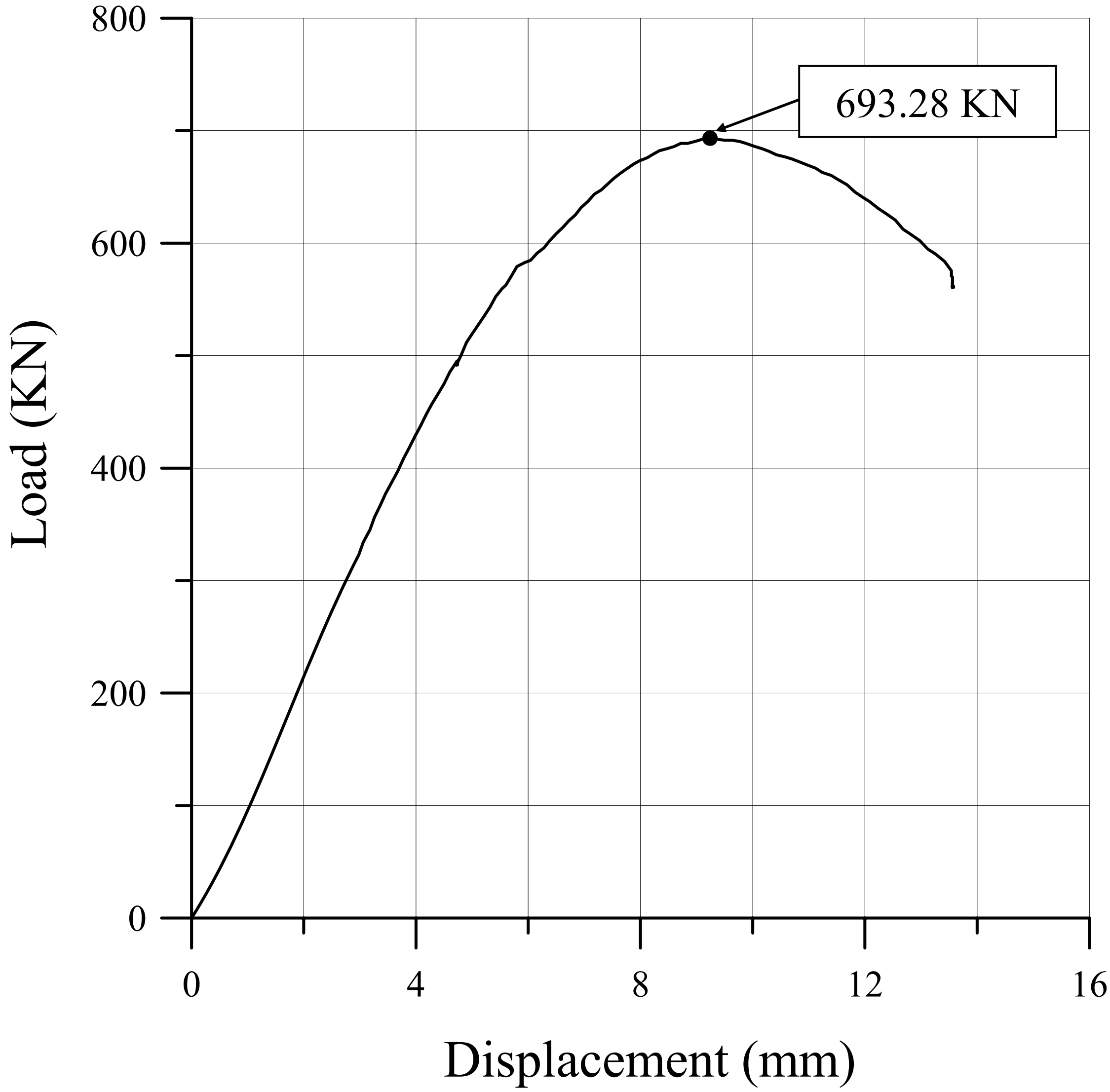

Figure 7.45 The load-axial displacement curve for ID43

ID 44

Plate		Stiffener				
t	Material	h_w	t_w	b_f	t_f	Material
8 mm	5083-H116	90 mm	8 mm	-	-	5083-H116

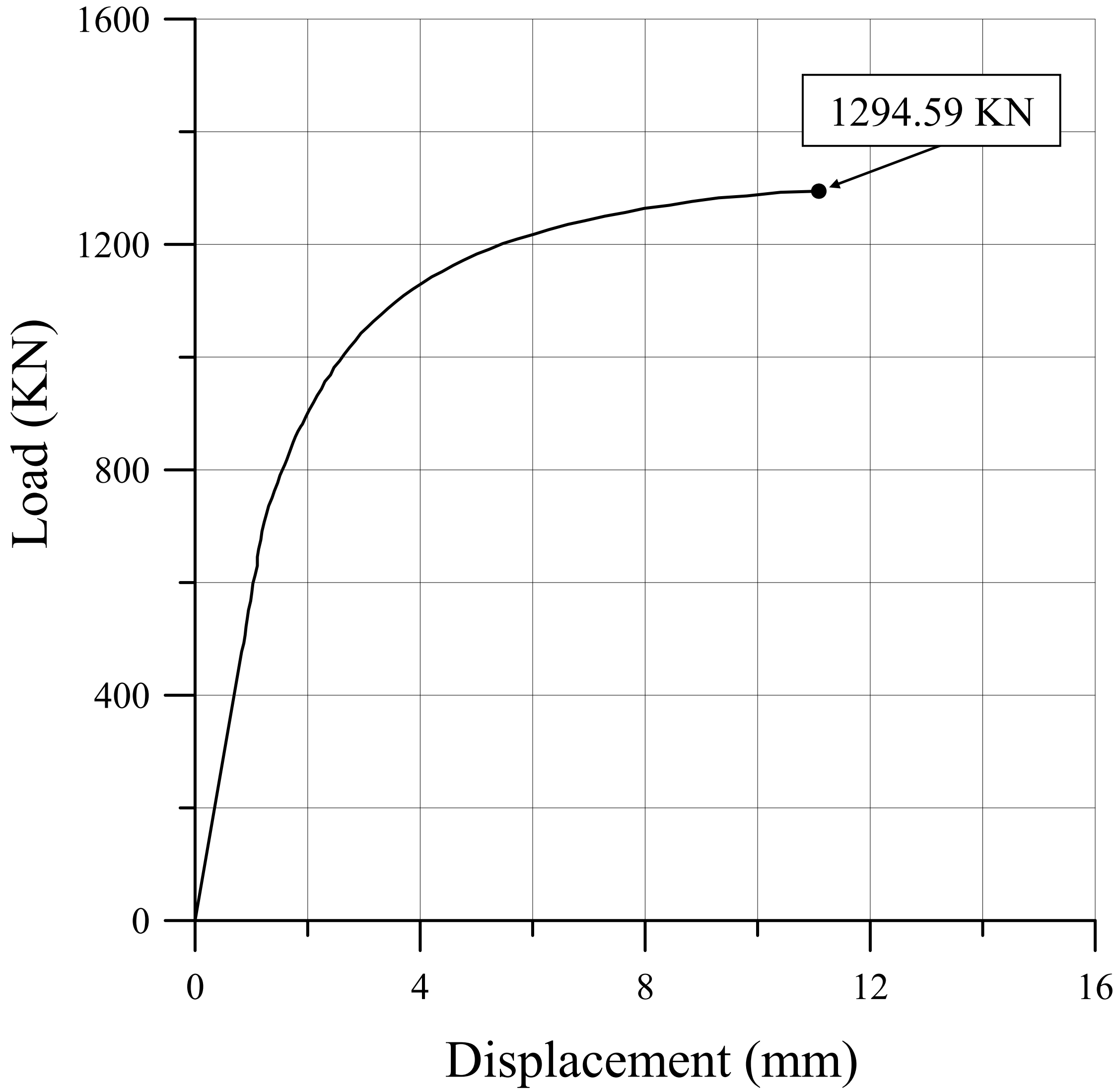

Figure 7.46 The load-axial displacement curve for ID44

ID 45

Plate		Stiffener				
t	Material	h_w	t_w	b_f	t_f	Material
8 mm	5083-H116	120 mm	8 mm	-	-	5083-H116

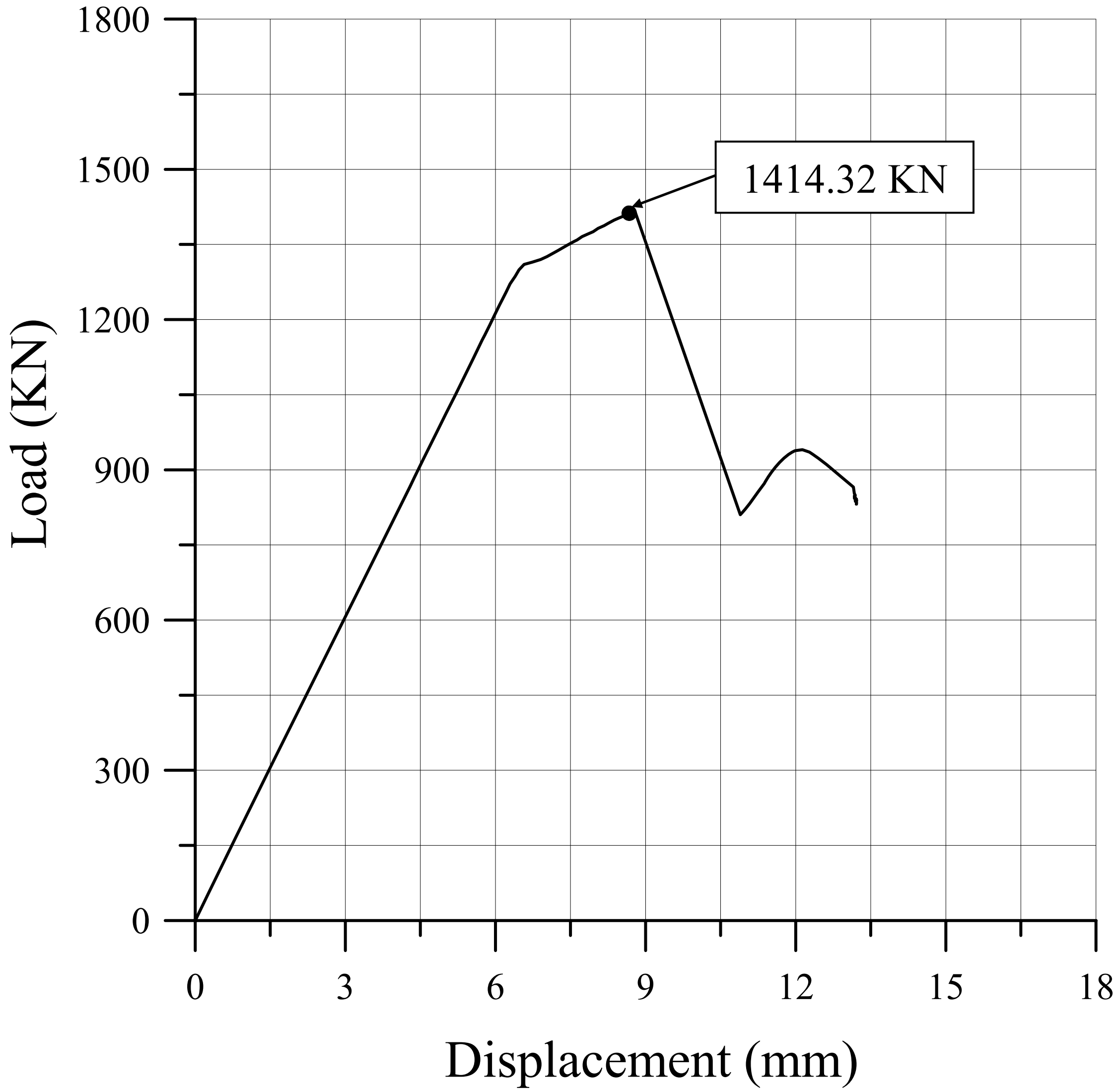

Figure 7.47 The load-axial displacement curve for ID45

ID 46

Plate		Stiffener				
t	Material	h_w	t_w	b_f	t_f	Material
5 mm	5083-H116	60 mm	5 mm	-	-	5383-H116

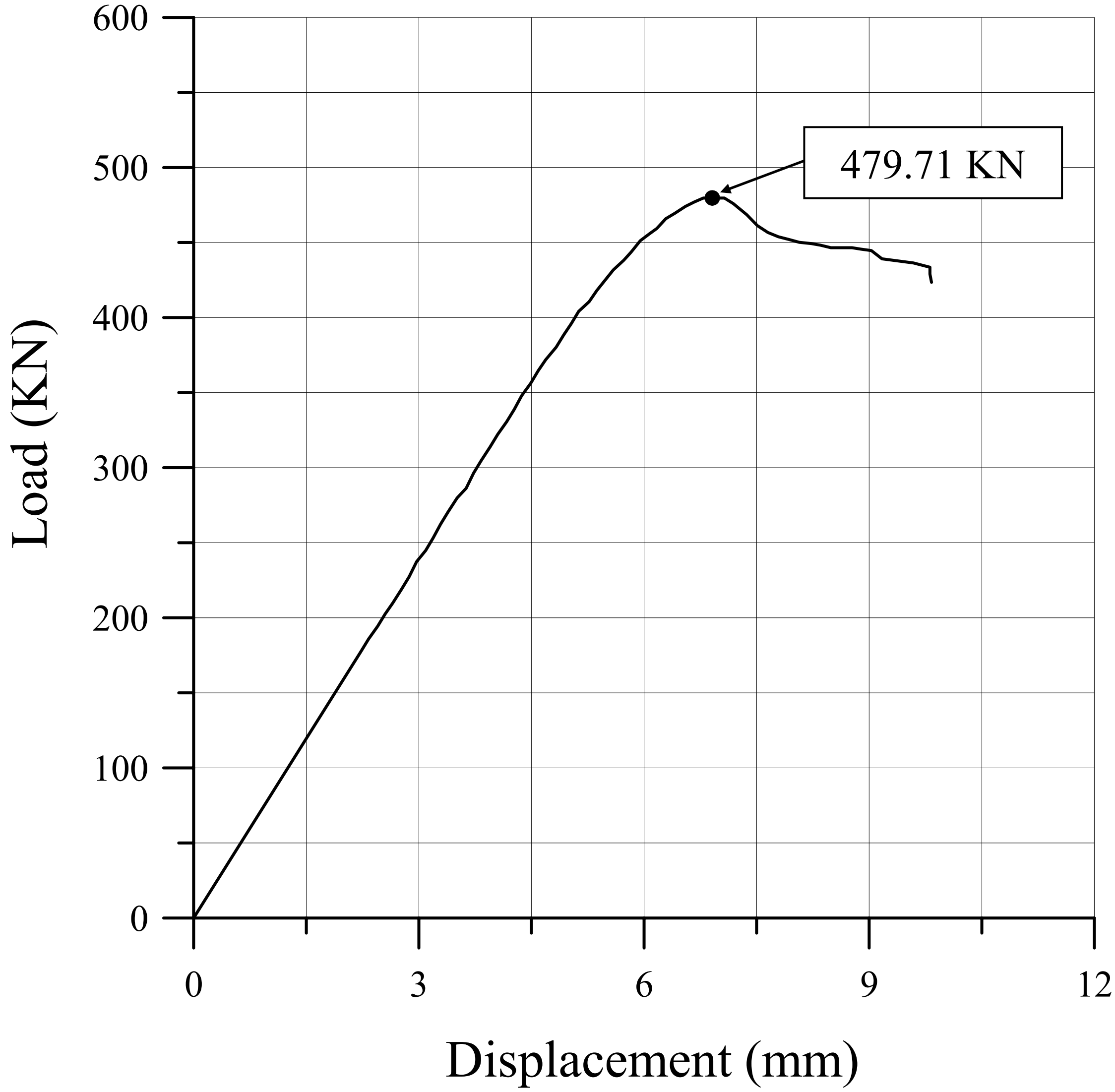

Figure 7.48 The load-axial displacement curve for ID46

ID 47

Plate		Stiffener				
t	Material	h_w	t_w	b_f	t_f	Material
5 mm	5083-H116	90 mm	5 mm	-	-	5383-H116

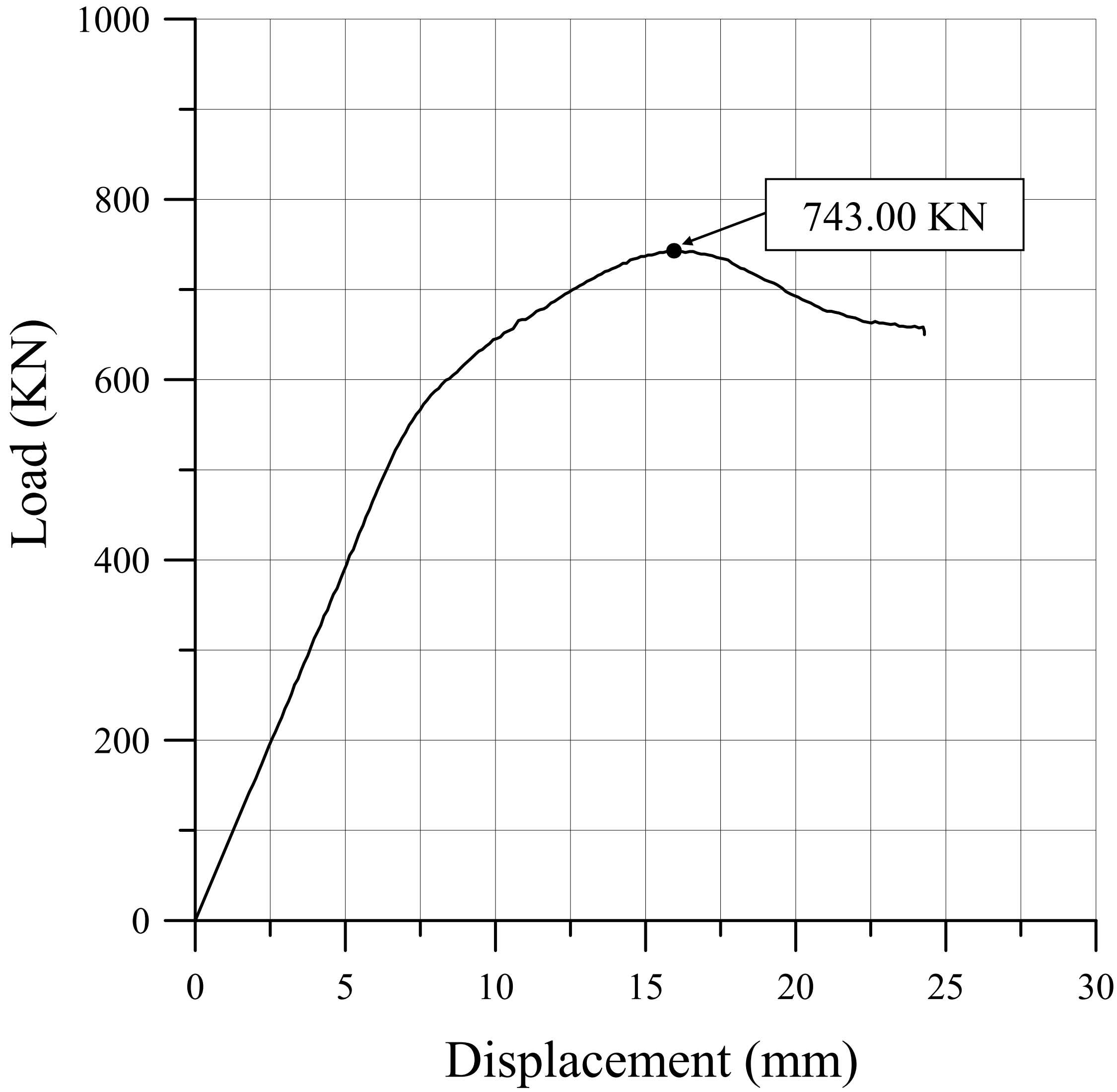

Figure 7.49 The load-axial displacement curve for ID47

ID 48

Plate		Stiffener				
t	Material	h_w	t_w	b_f	t_f	Material
5 mm	5083-H116	120 mm	5 mm	-	-	5383-H116

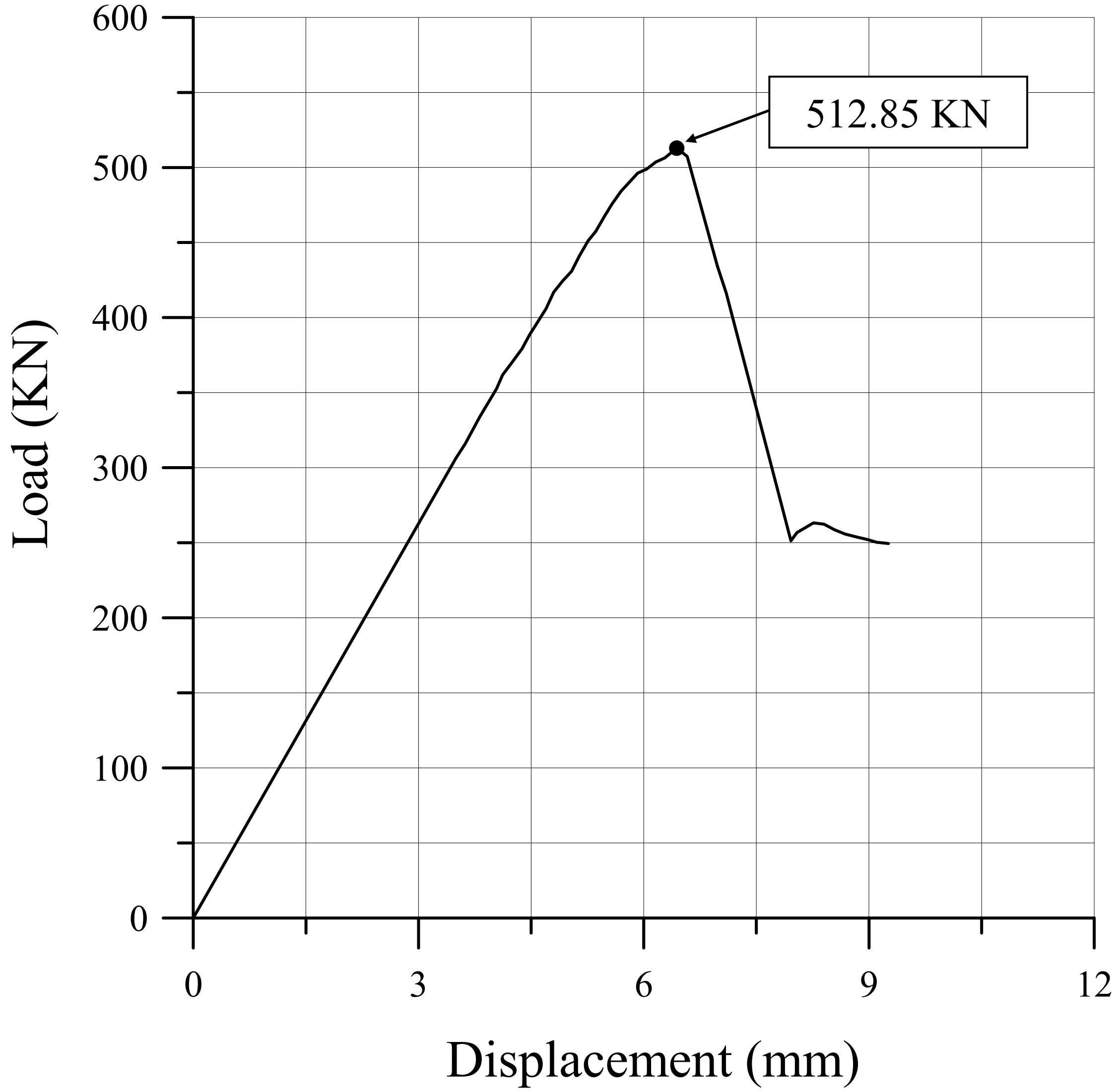

Figure 7.50 The load-axial displacement curve for ID48

ID 49

Plate		Stiffener				
t	Material	h_w	t_w	b_f	t_f	Material
6 mm	5083-H116	60 mm	6 mm	-	-	5383-H116

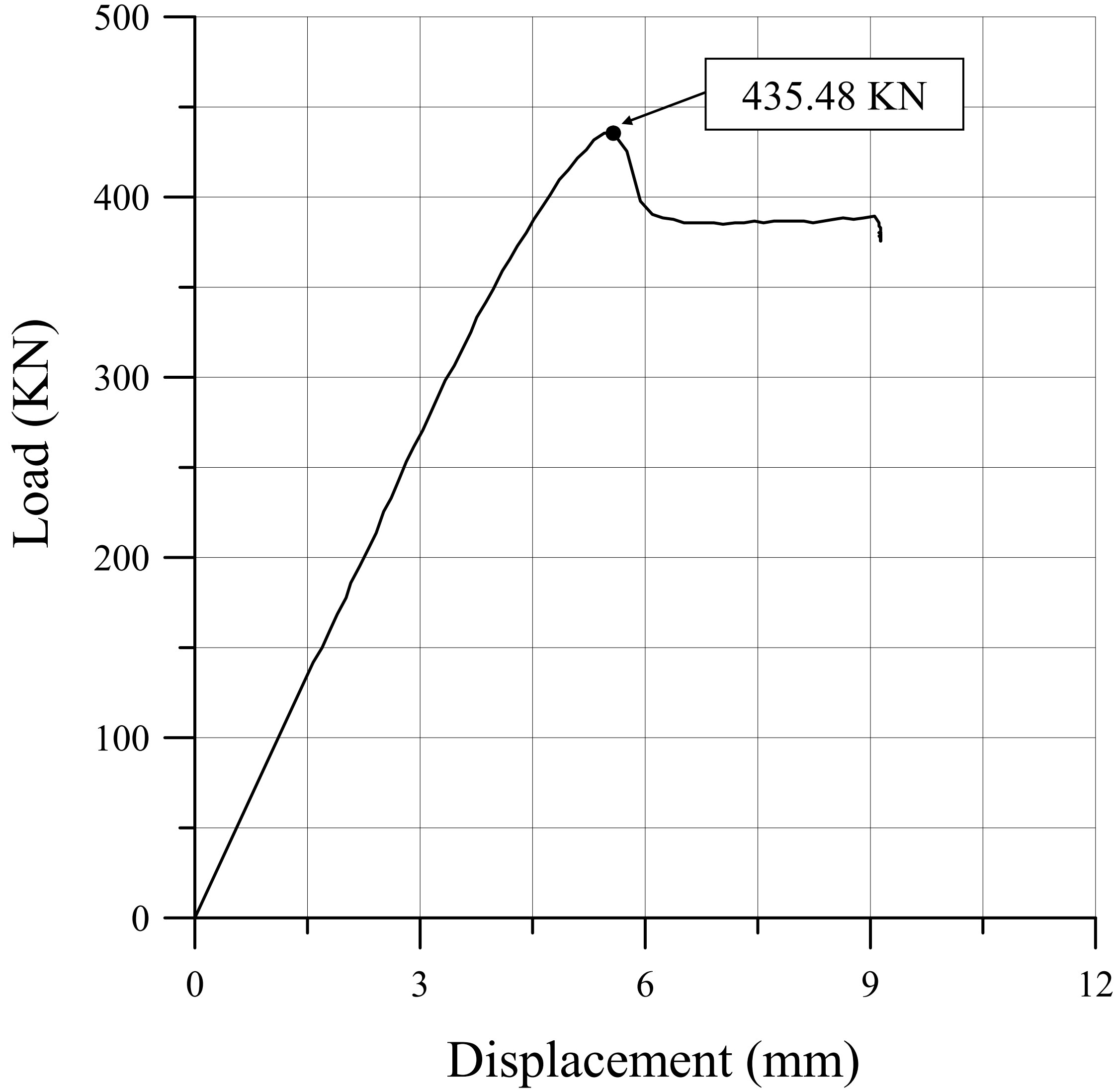

Figure 7.51 The load-axial displacement curve for ID49

ID 50

Plate		Stiffener				
t	Material	h_w	t_w	b_f	t_f	Material
6 mm	5083-H116	90 mm	6 mm	-	-	5383-H116

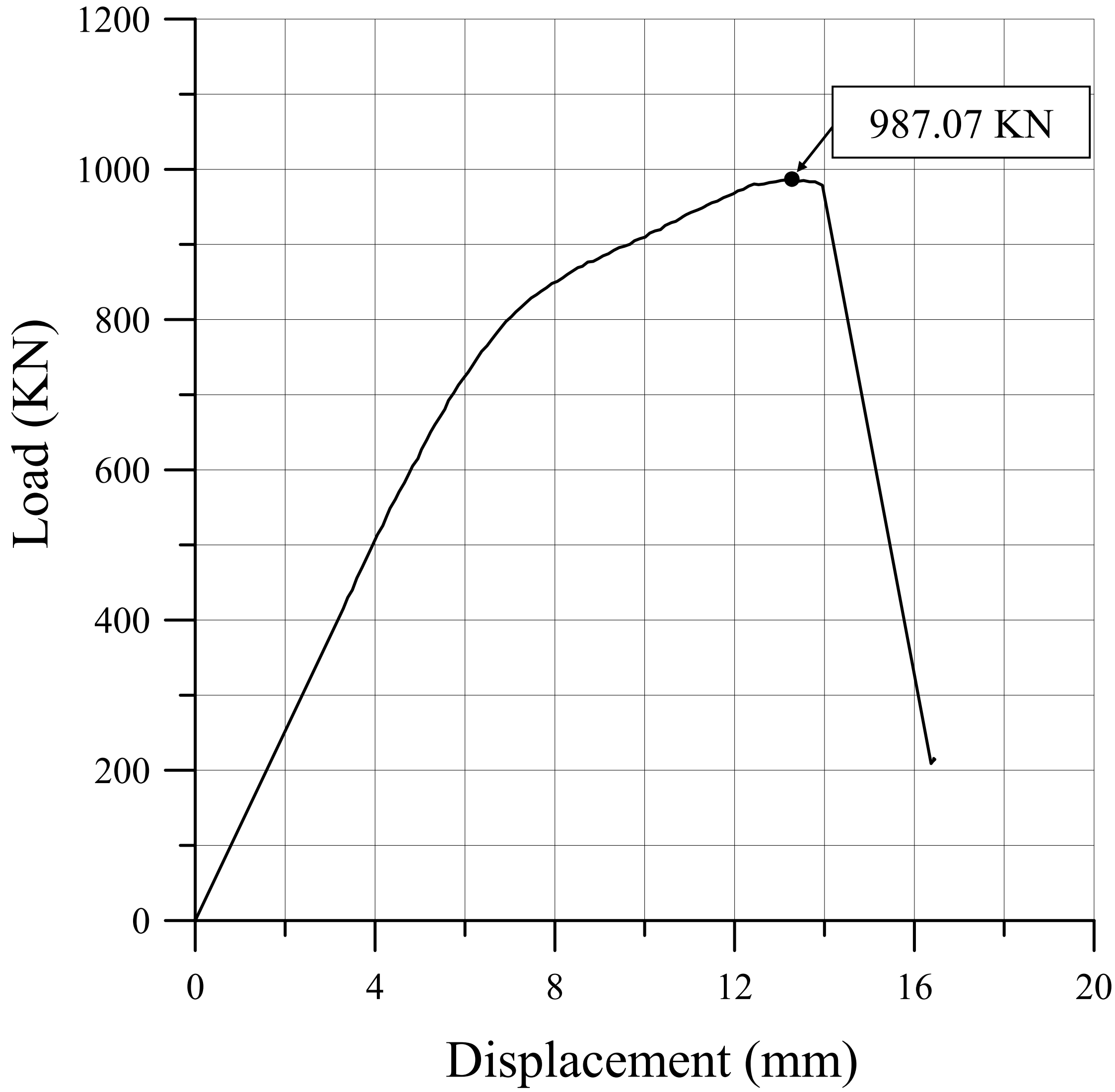

Figure 7.52 The load-axial displacement curve for ID50

ID 51

Plate		Stiffener				
t	Material	h_w	t_w	b_f	t_f	Material
6 mm	5083-H116	120 mm	6 mm	-	-	5383-H116

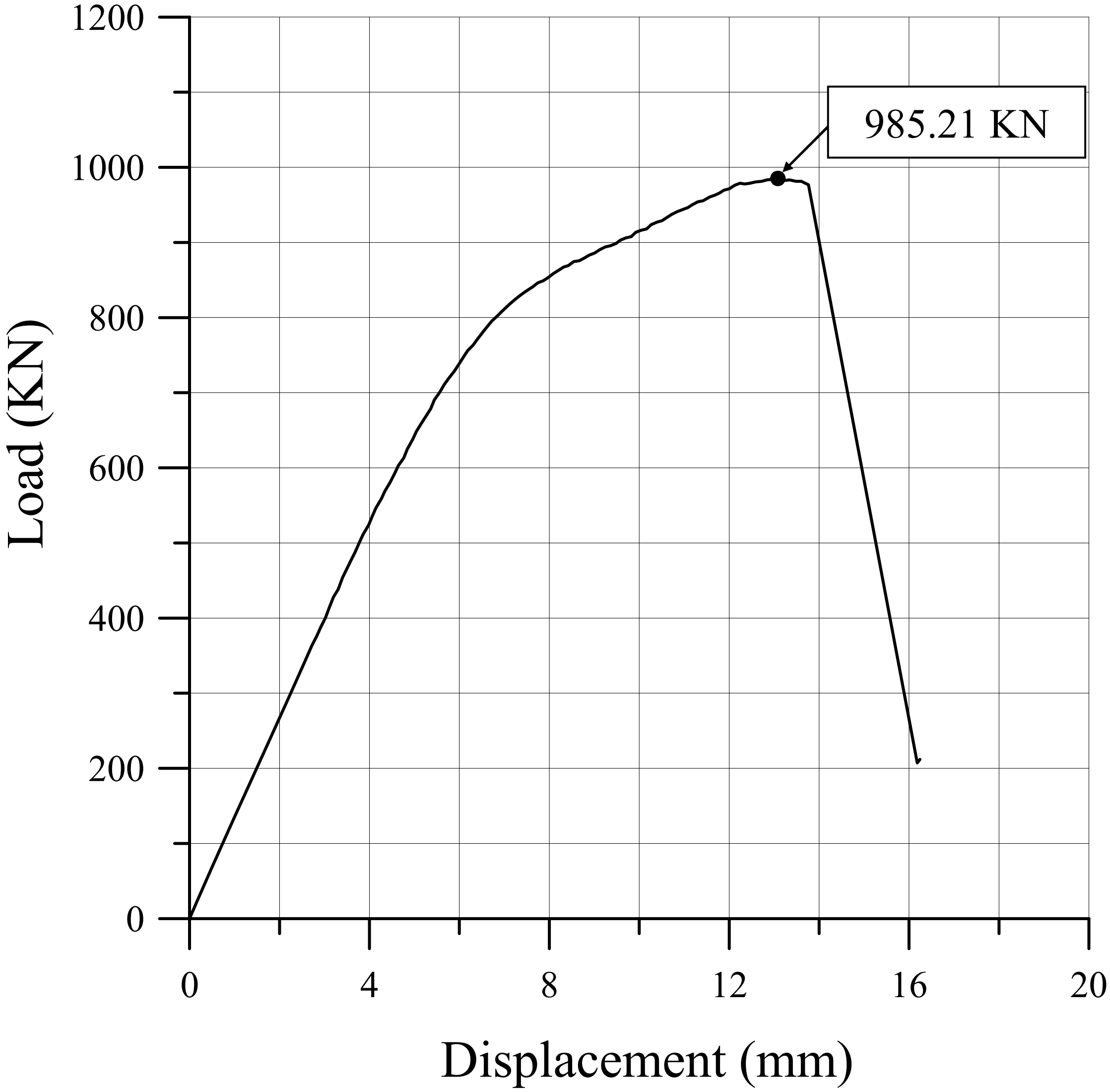

Figure 7.53 The load-axial displacement curve for ID51

ID 52

Plate		Stiffener				
t	Material	h_w	t_w	b_f	t_f	Material
8 mm	5083-H116	60 mm	8 mm	-	-	5383-H116

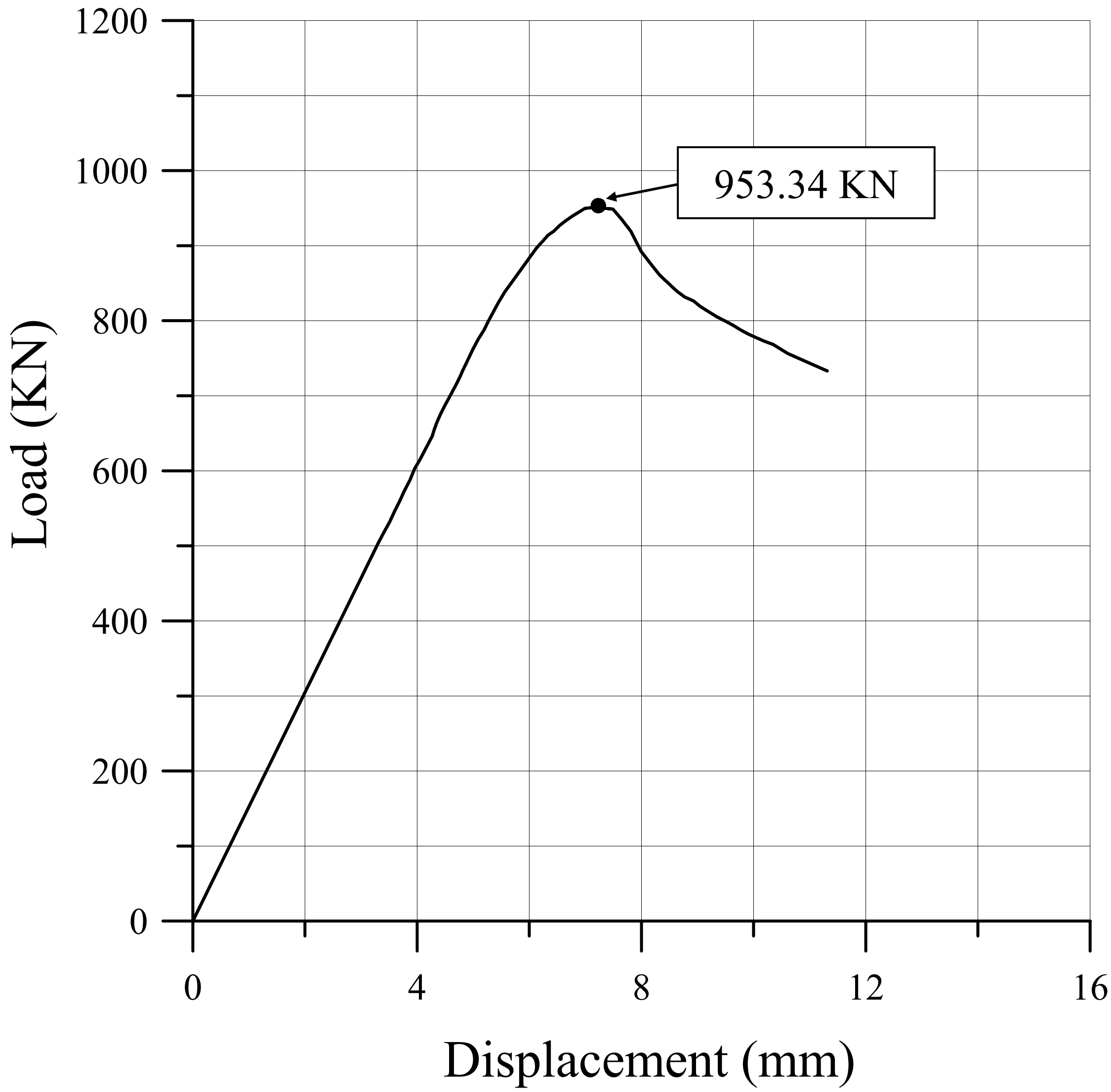

Figure 7.54 The load-axial displacement curve for ID52

ID 53

Plate		Stiffener				
t	Material	h_w	t_w	b_f	t_f	Material
8 mm	5083-H116	90 mm	8 mm	-	-	5383-H116

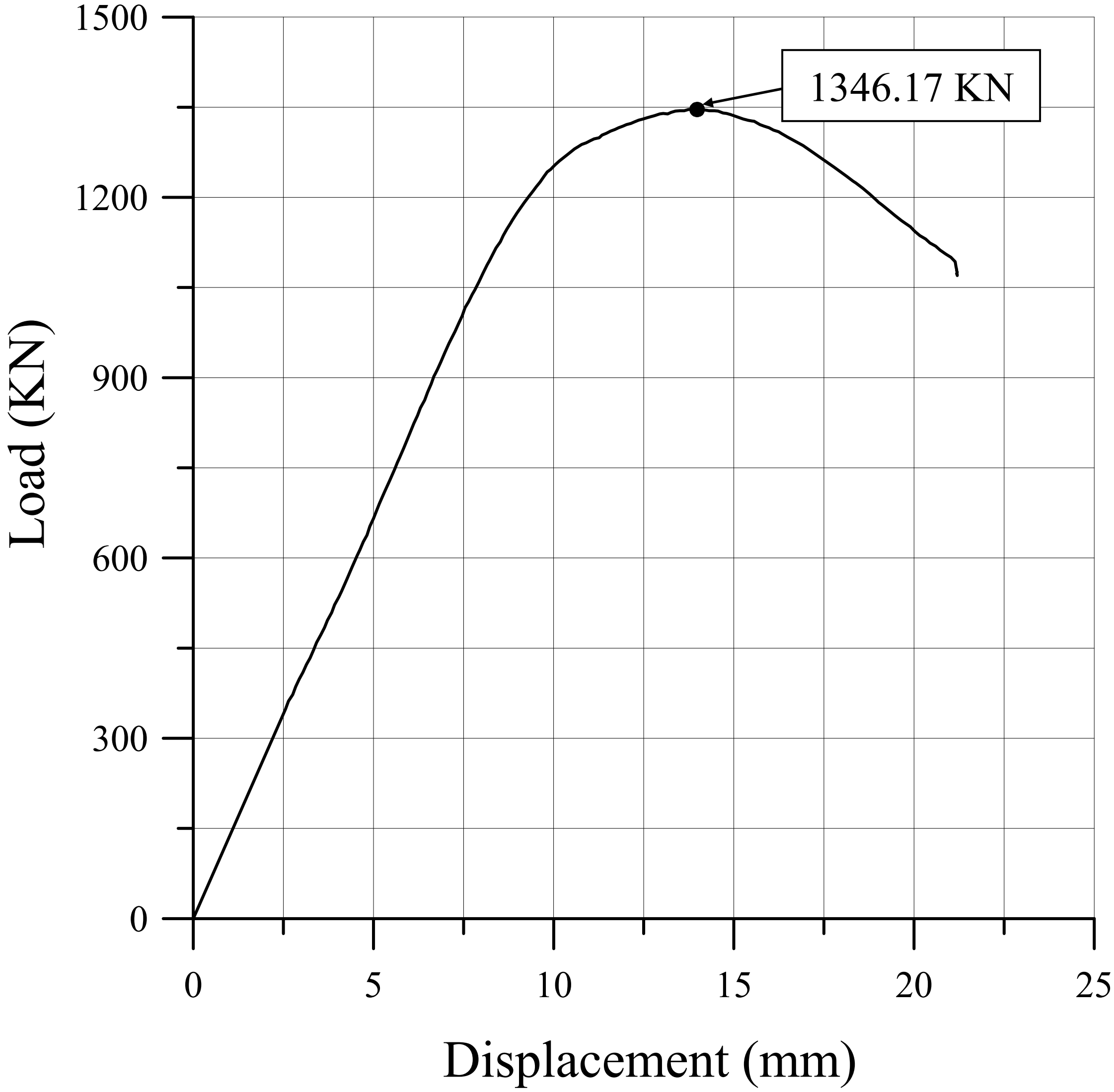

Figure 7.55 The load-axial displacement curve for ID53

ID 54

Plate		Stiffener				
t	Material	h_w	t_w	b_f	t_f	Material
8 mm	5083-H116	120 mm	8 mm	-	-	5383-H116

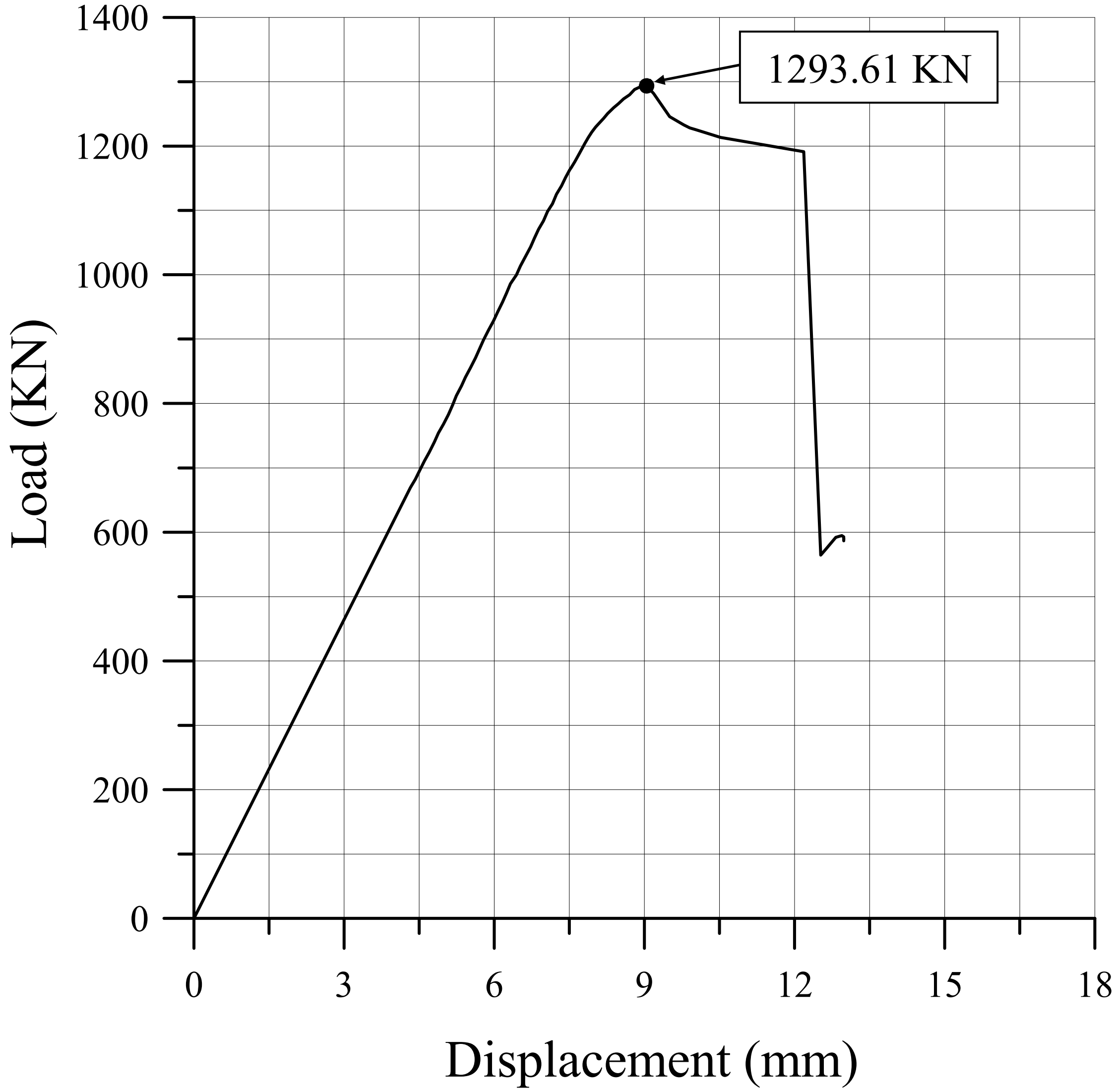

Figure 7.56 The load-axial displacement curve for ID54

ID 55

Plate		Stiffener				
t	Material	h_w	t_w	b_f	t_f	Material
5 mm	5383-H116	60 mm	5 mm	-	-	5383-H116

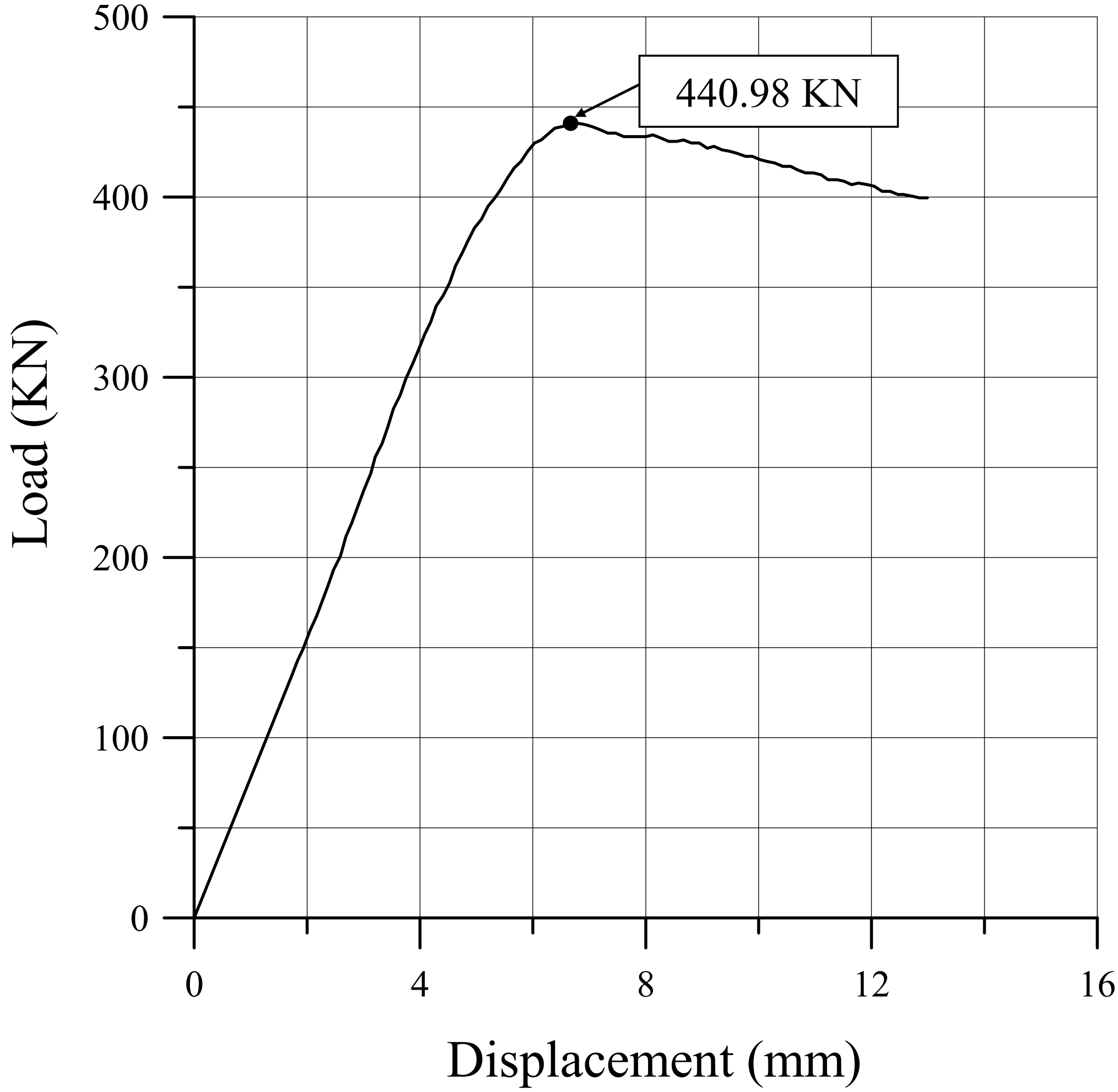

Figure 7.57 The load-axial displacement curve for ID55

ID 56

Plate		Stiffener				
t	Material	h_w	t_w	b_f	t_f	Material
5 mm	5383-H116	90 mm	5 mm	-	-	5383-H116

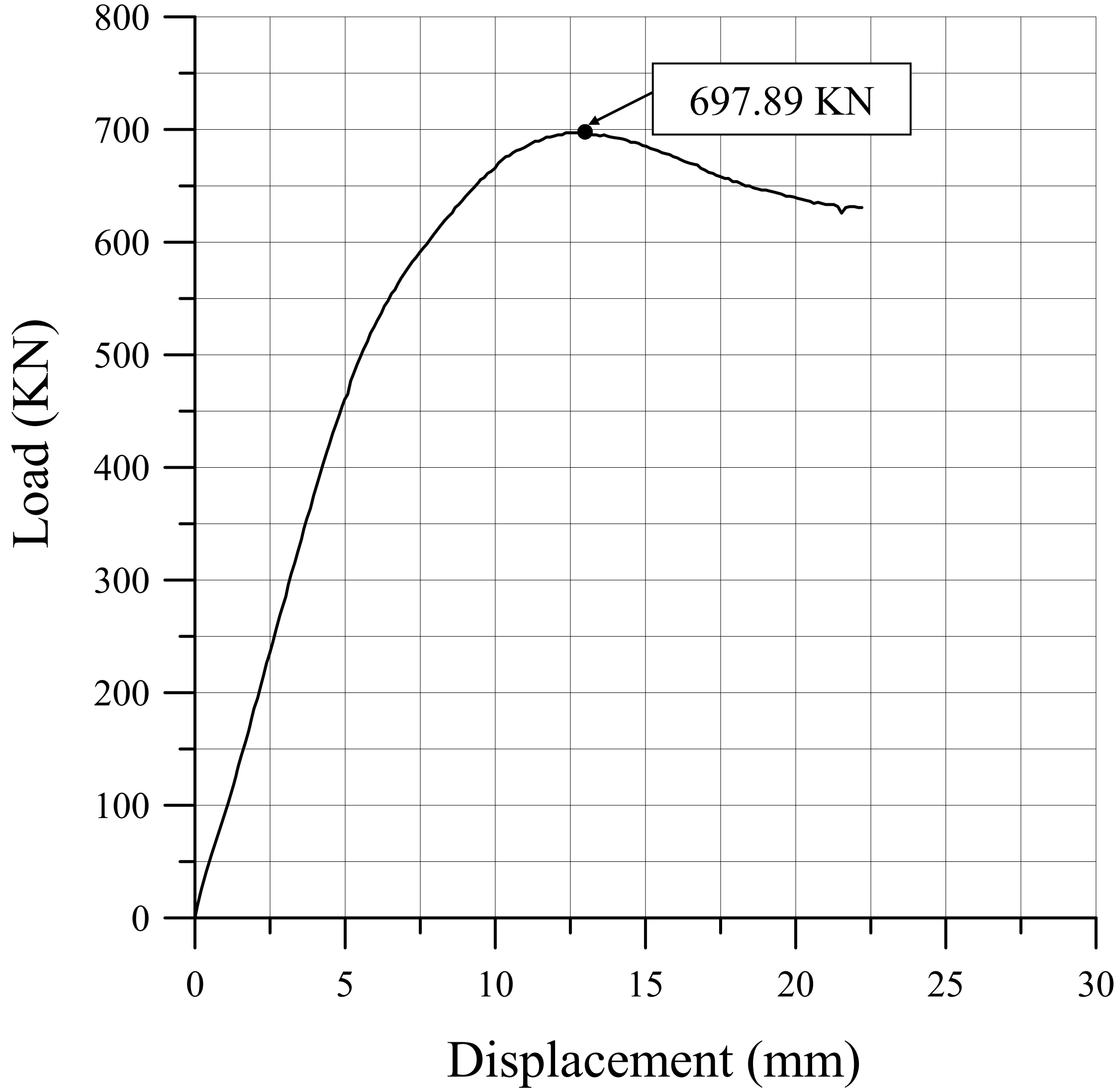

Figure 7.58 The load-axial displacement curve for ID56

ID 57

Plate		Stiffener				
t	Material	h_w	t_w	b_f	t_f	Material
6 mm	5383-H116	120 mm	5 mm	-	-	5383-H116

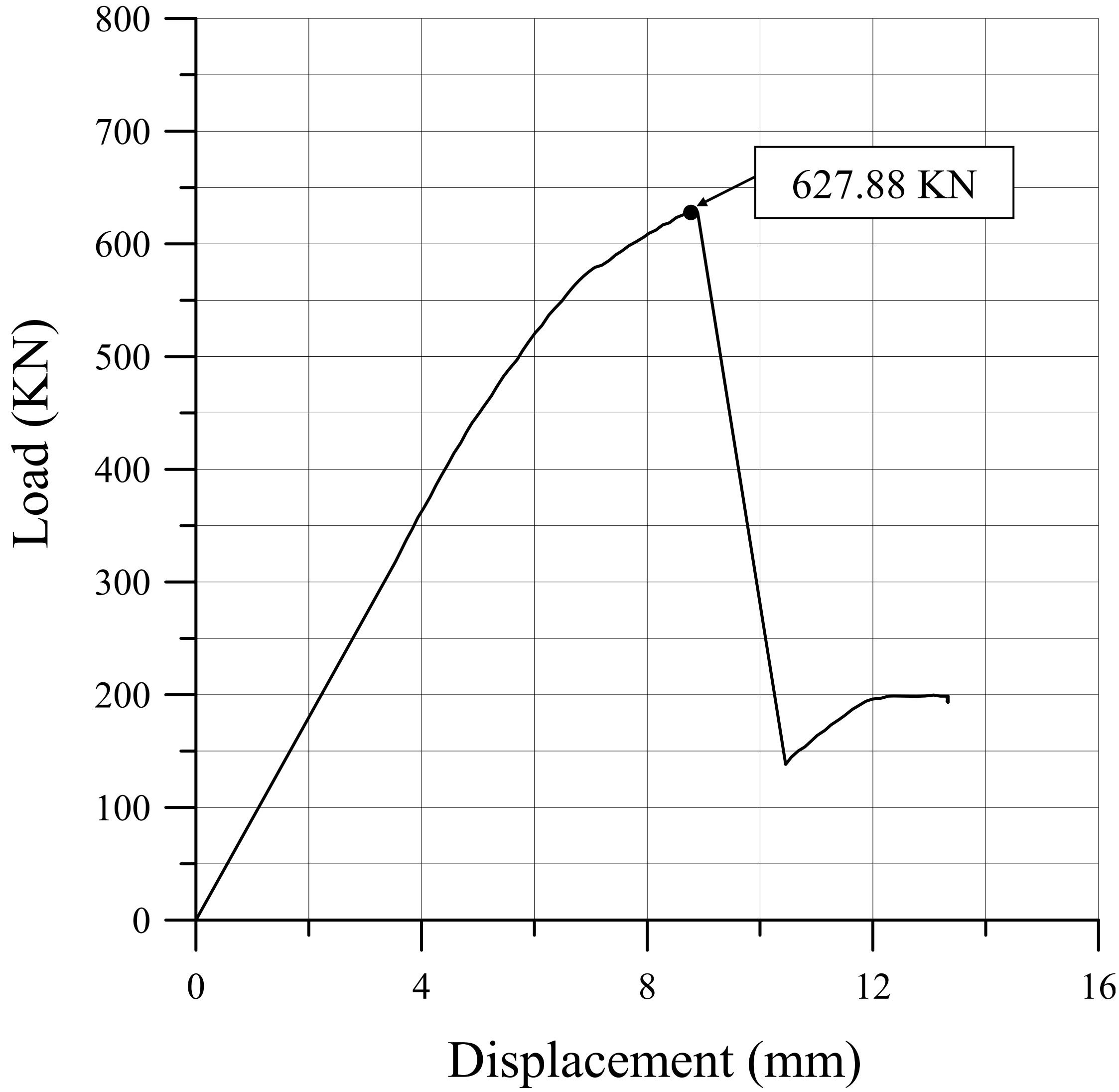

Figure 7.59 The load-axial displacement curve for ID57

ID 58

Plate		Stiffener				
t	Material	h_w	t_w	b_f	t_f	Material
6 mm	5383-H116	60 mm	6 mm	-	-	5383-H116

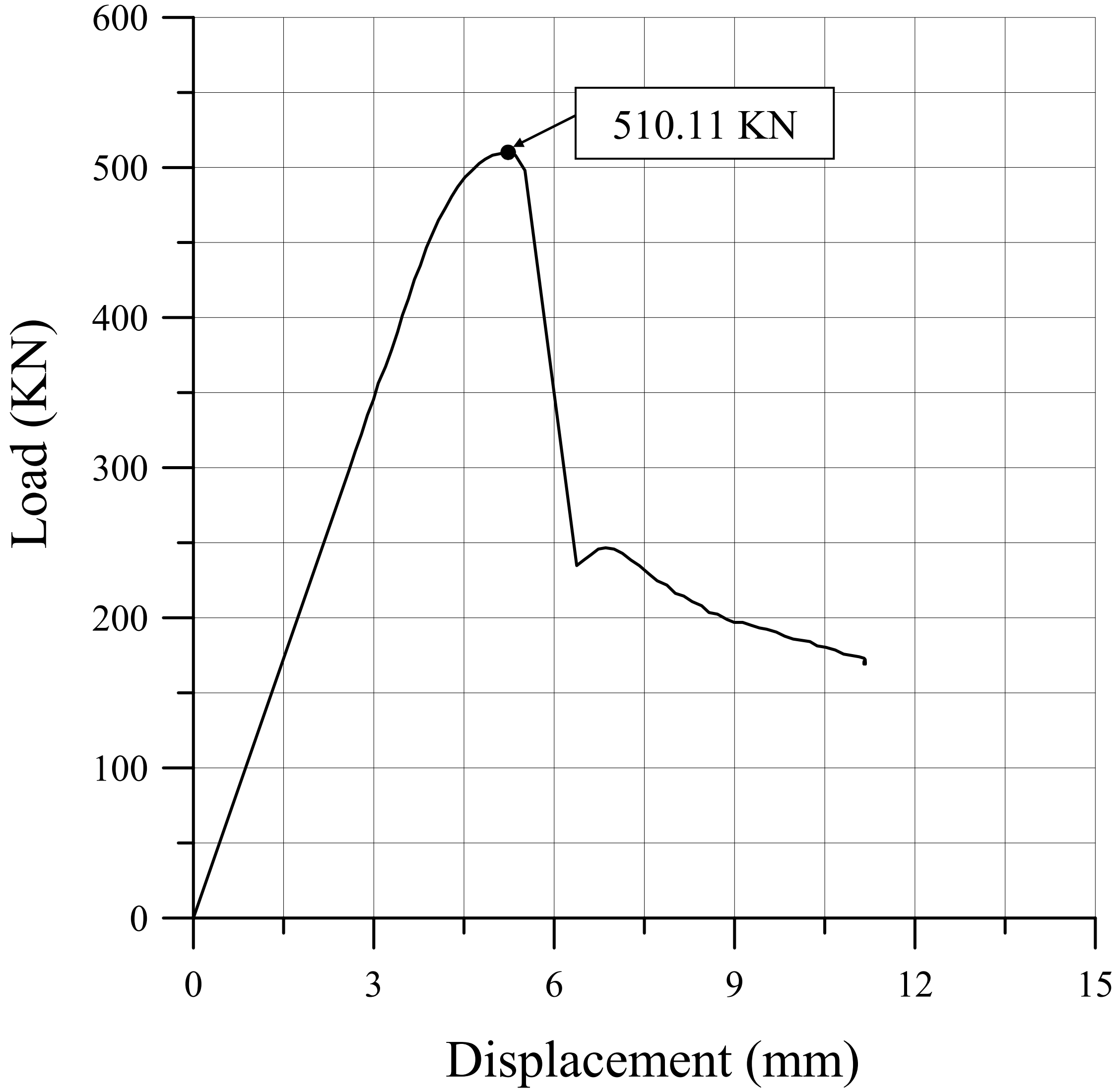

Figure 7.60 The load-axial displacement curve for ID58

ID 59

Plate		Stiffener				
t	Material	h_w	t_w	b_f	t_f	Material
6 mm	5383-H116	90 mm	6 mm	-	-	5383-H116

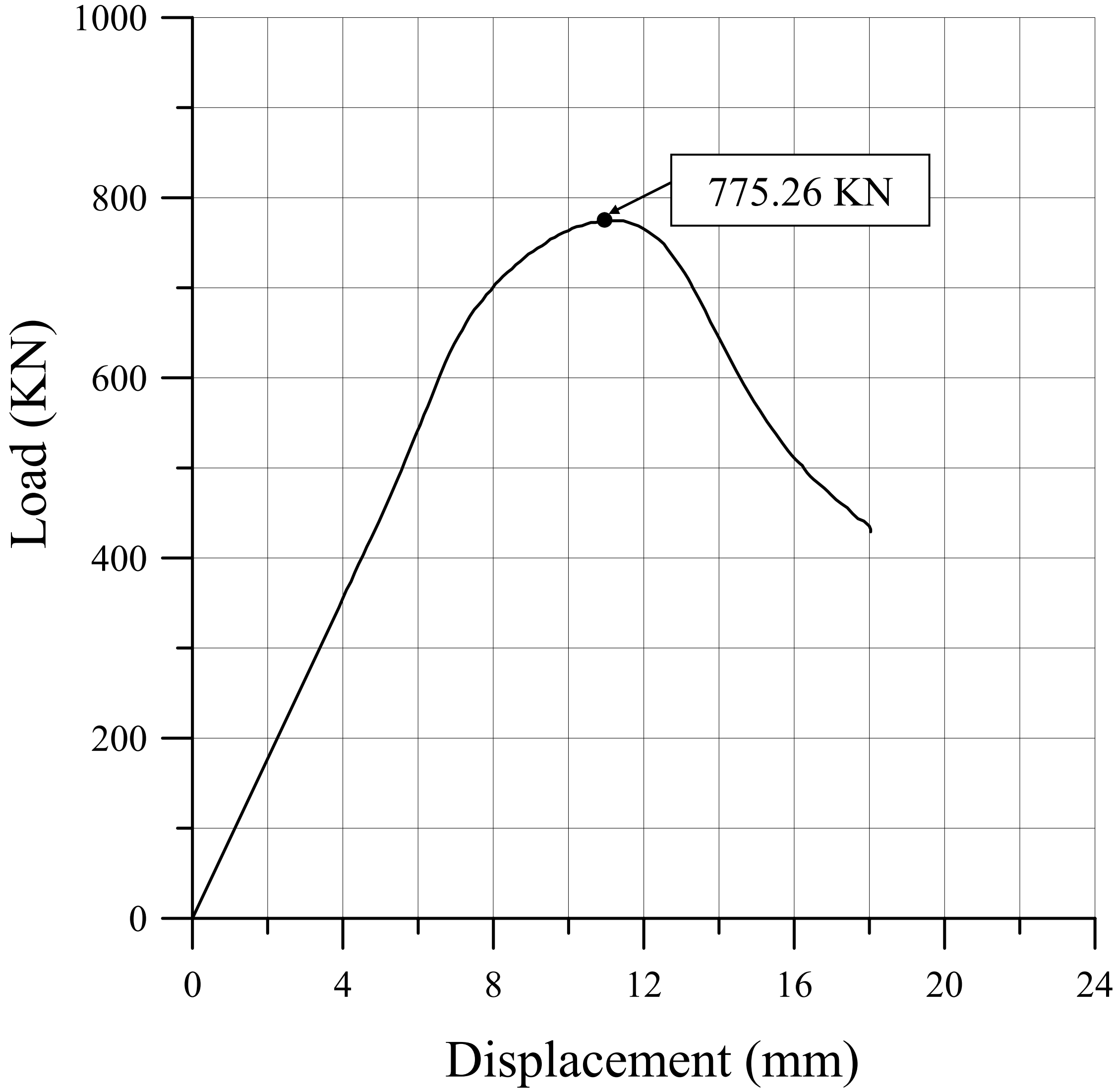

Figure 7.61 The load-axial displacement curve for ID59

ID 60

Plate		Stiffener				
t	Material	h_w	t_w	b_f	t_f	Material
6 mm	5383-H116	120 mm	6 mm	-	-	5383-H116

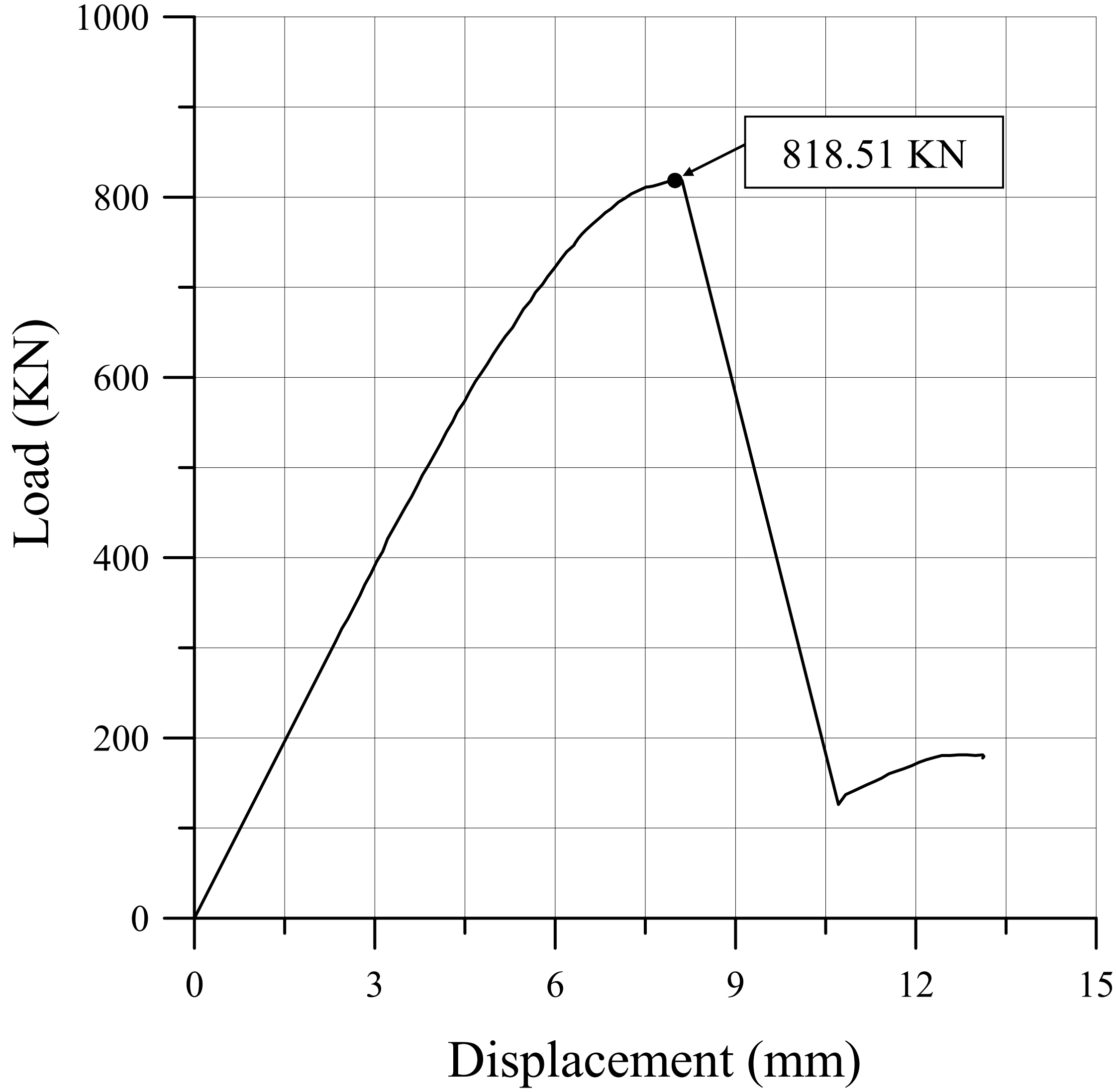

Figure 7.62 The load-axial displacement curve for ID60

ID 61

Plate		Stiffener				
t	Material	h_w	t_w	b_f	t_f	Material
8 mm	5383-H116	60 mm	8 mm	-	-	5383-H116

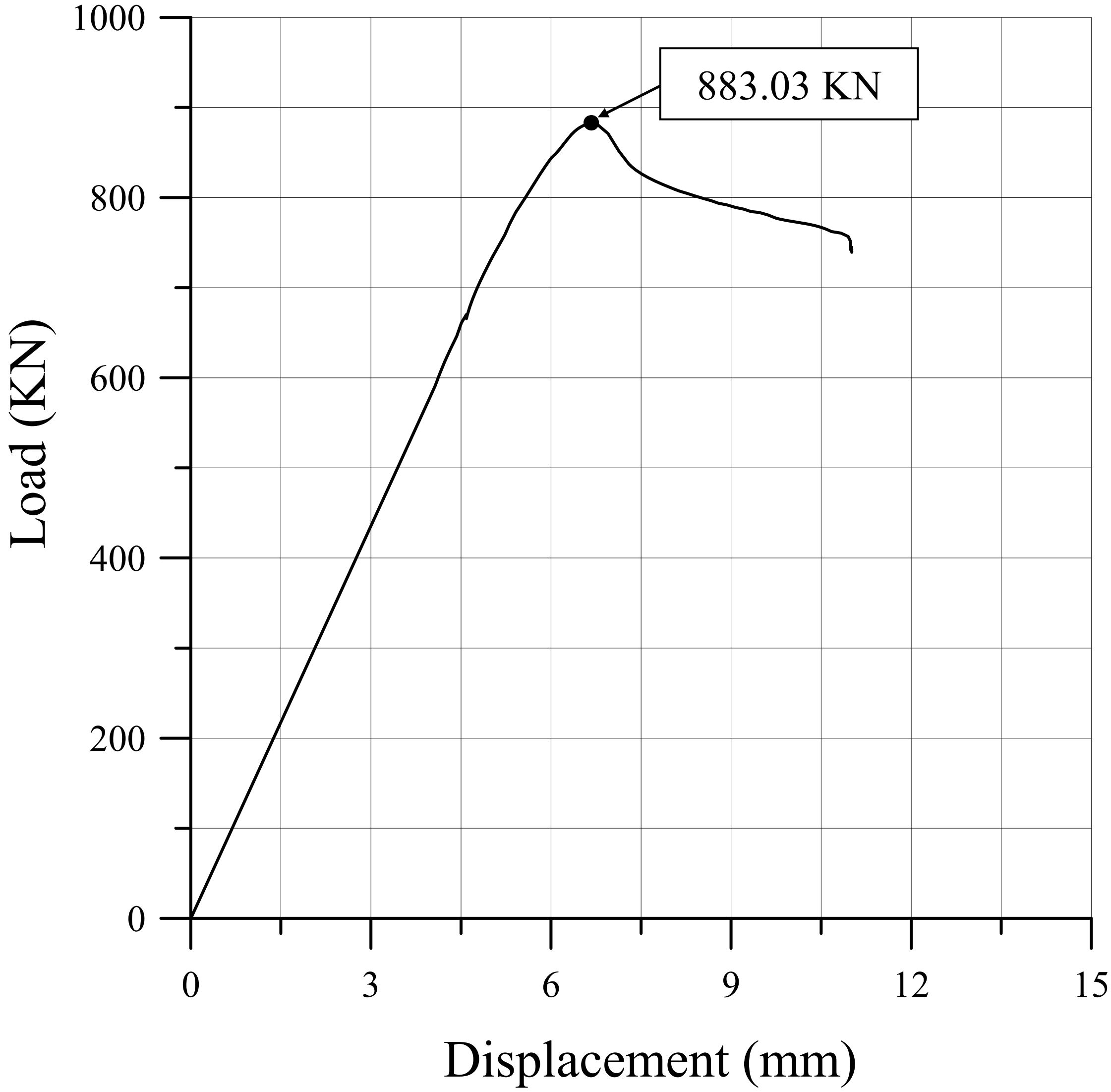

Figure 7.63 The load-axial displacement curve for ID61

ID 62

Plate		Stiffener				
t	Material	h_w	t_w	b_f	t_f	Material
8 mm	5383-H116	90 mm	8 mm	-	-	5383-H116

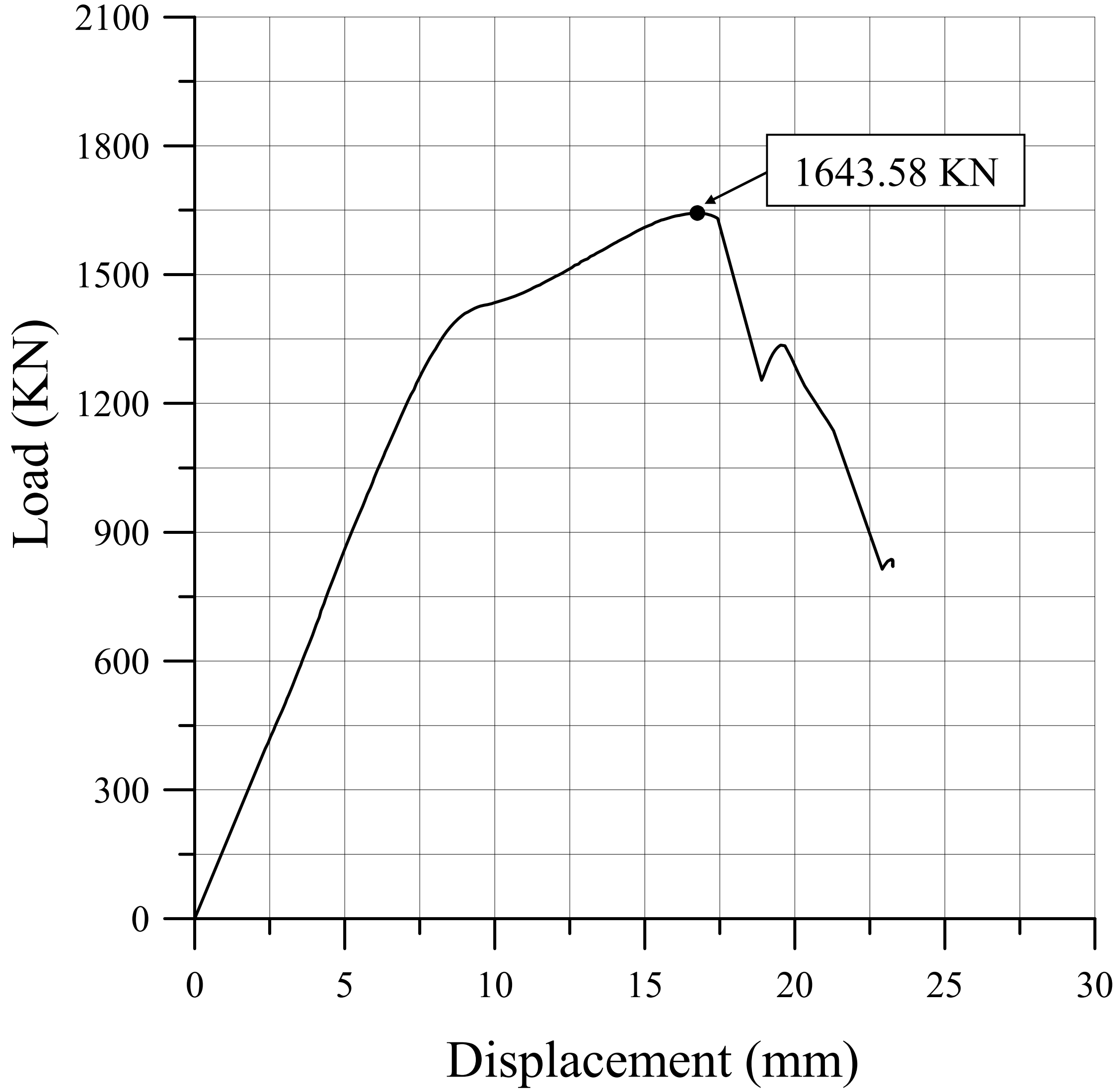

Figure 7.64 The load-axial displacement curve for ID62

ID 63

Plate		Stiffener				
t	Material	h_w	t_w	b_f	t_f	Material
8 mm	5383-H116	120 mm	8 mm	-	-	5383-H116

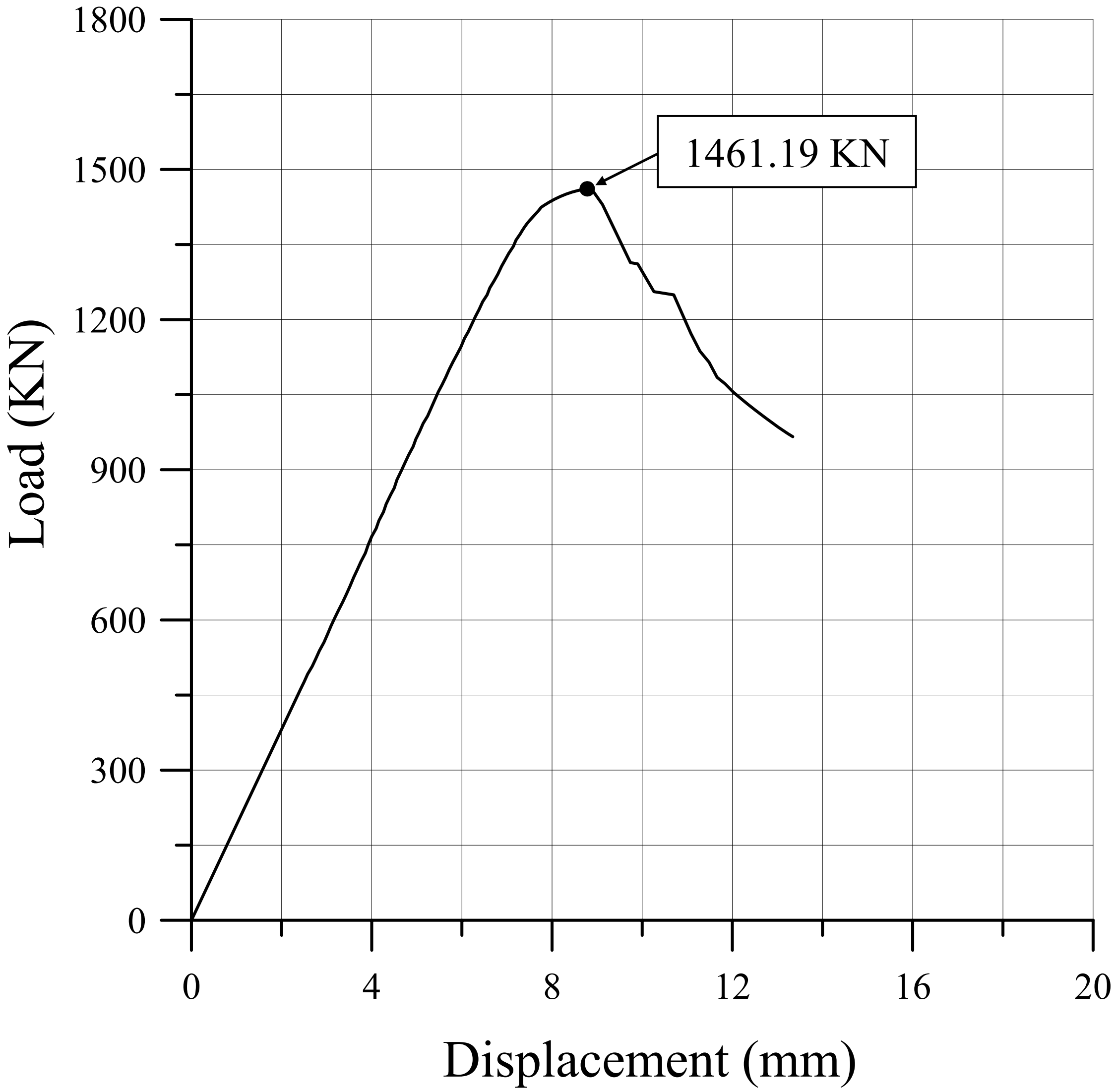

Figure 7.65 The load-axial displacement curve for ID63

ID 64

Plate		Stiffener				
t	Material	h_w	t_w	b_f	t_f	Material
5 mm	5083-H116	80 mm	5 mm	60 mm	5 mm	5083-H116

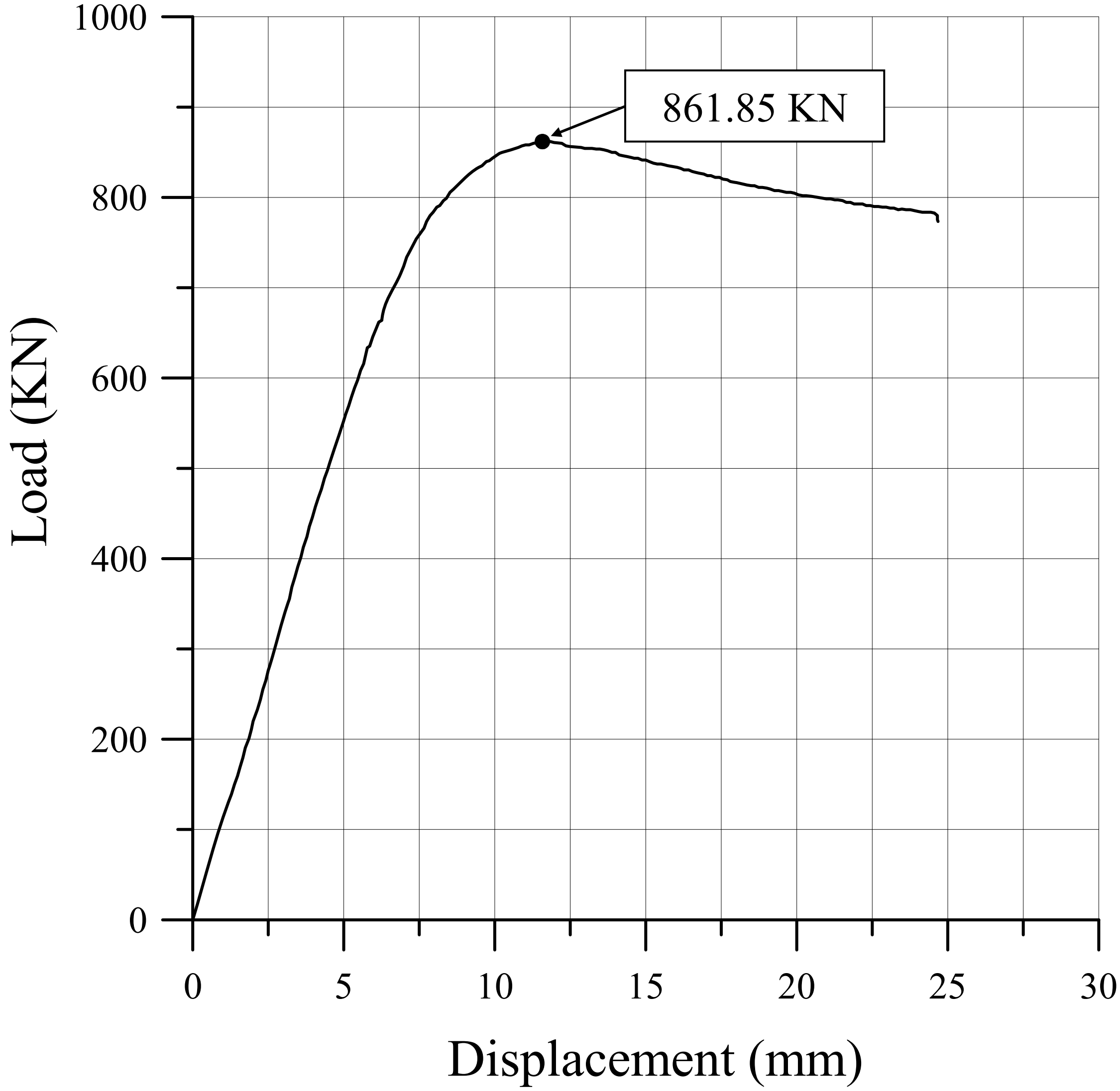

Figure 7.66 The load-axial displacement curve for ID64

ID 65

Plate		Stiffener				
t	Material	h_w	t_w	b_f	t_f	Material
6 mm	5083-H116	60 mm	5 mm	60 mm	5 mm	5083-H116

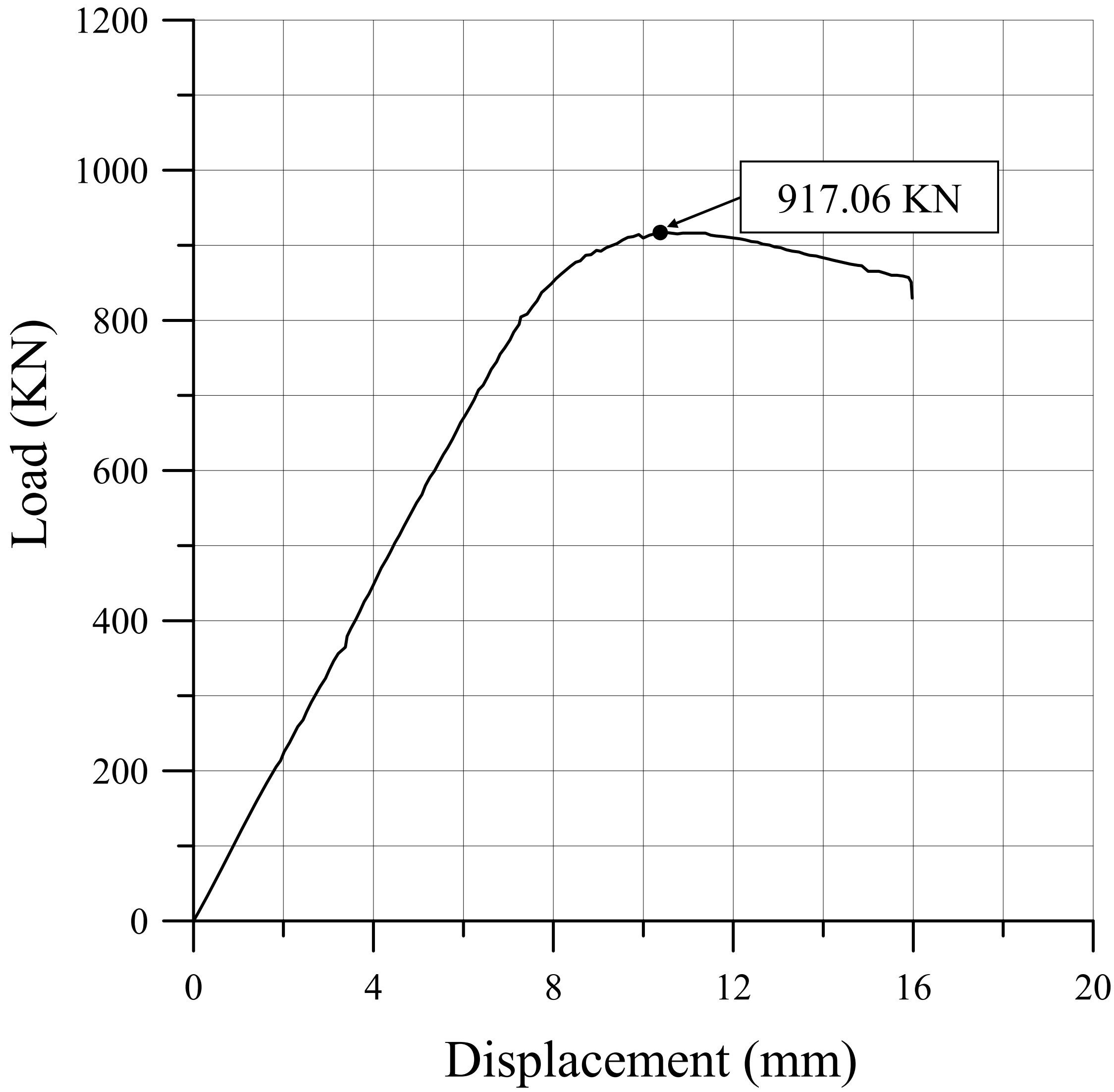

Figure 7.67 The load-axial displacement curve for ID65

ID 66

Plate		Stiffener				
t	Material	h_w	t_w	b_f	t_f	Material
8 mm	5083-H116	100 mm	5 mm	60 mm	5 mm	5083-H116

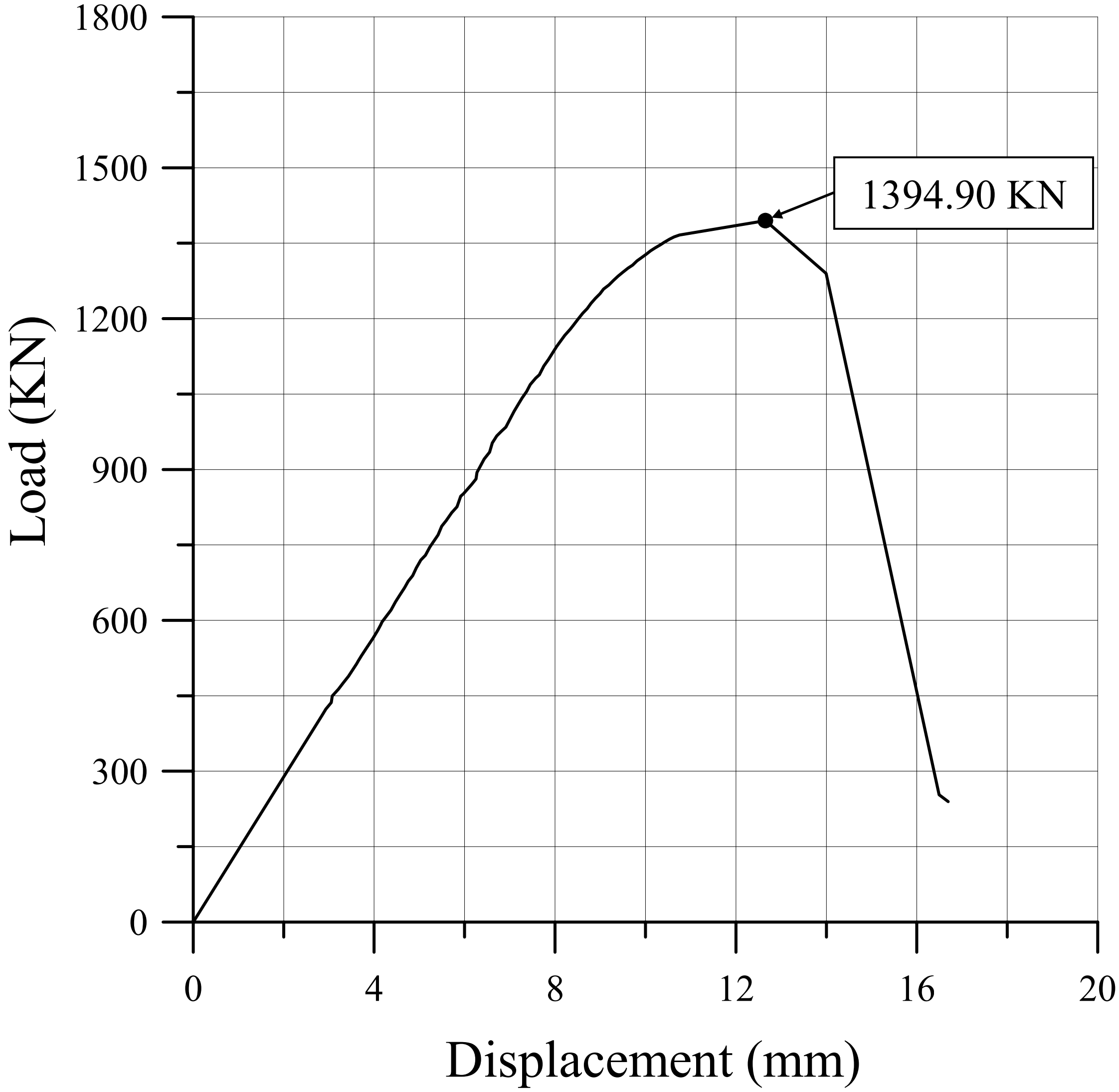

Figure 7.68 The load-axial displacement curve for ID66

ID 67

Plate		Stiffener				
t	Material	h_w	t_w	b_f	t_f	Material
5 mm	5083-H116	80 mm	5 mm	60 mm	5 mm	5383-H116

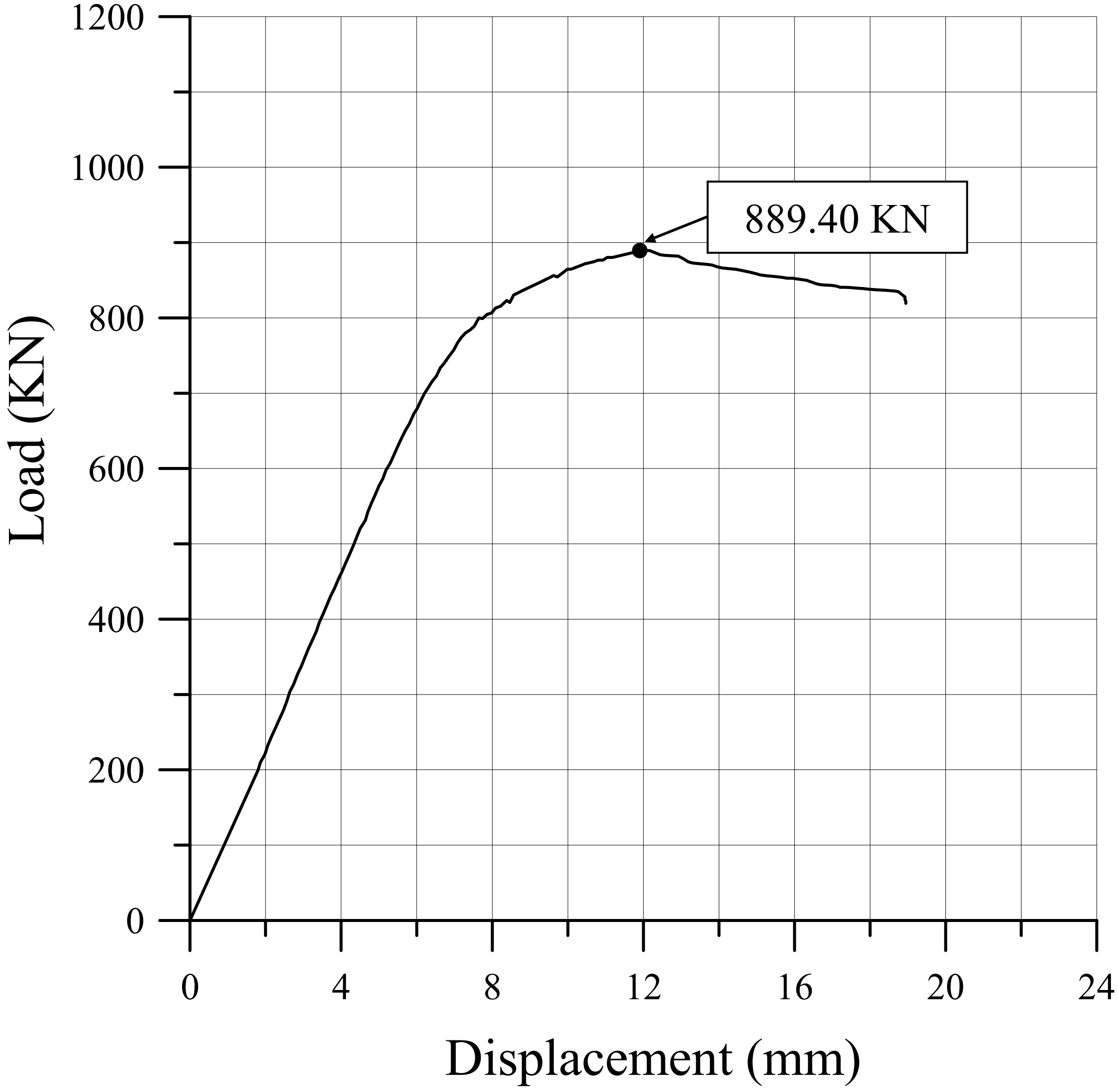

Figure 7.69 The load-axial displacement curve for ID67

ID 68

Plate		Stiffener				
t	Material	h_w	t_w	b_f	t_f	Material
6 mm	5083-H116	60 mm	5 mm	60 mm	5 mm	5383-H116

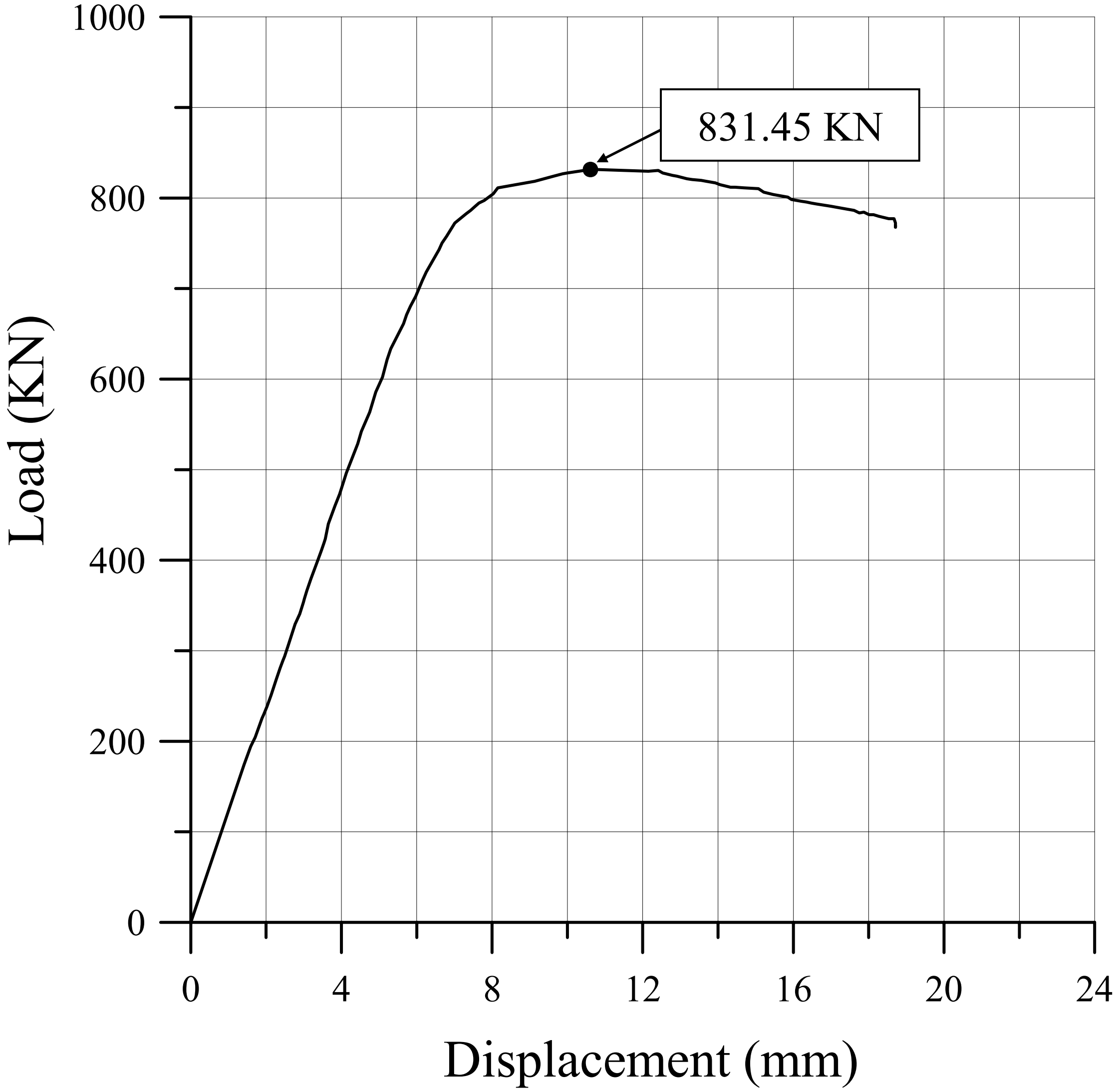

Figure 7.70 The load-axial displacement curve for ID68

ID 69

Plate		Stiffener				
t	Material	h_w	t_w	b_f	t_f	Material
8 mm	5083-H116	100 mm	5 mm	60 mm	5 mm	5383-H116

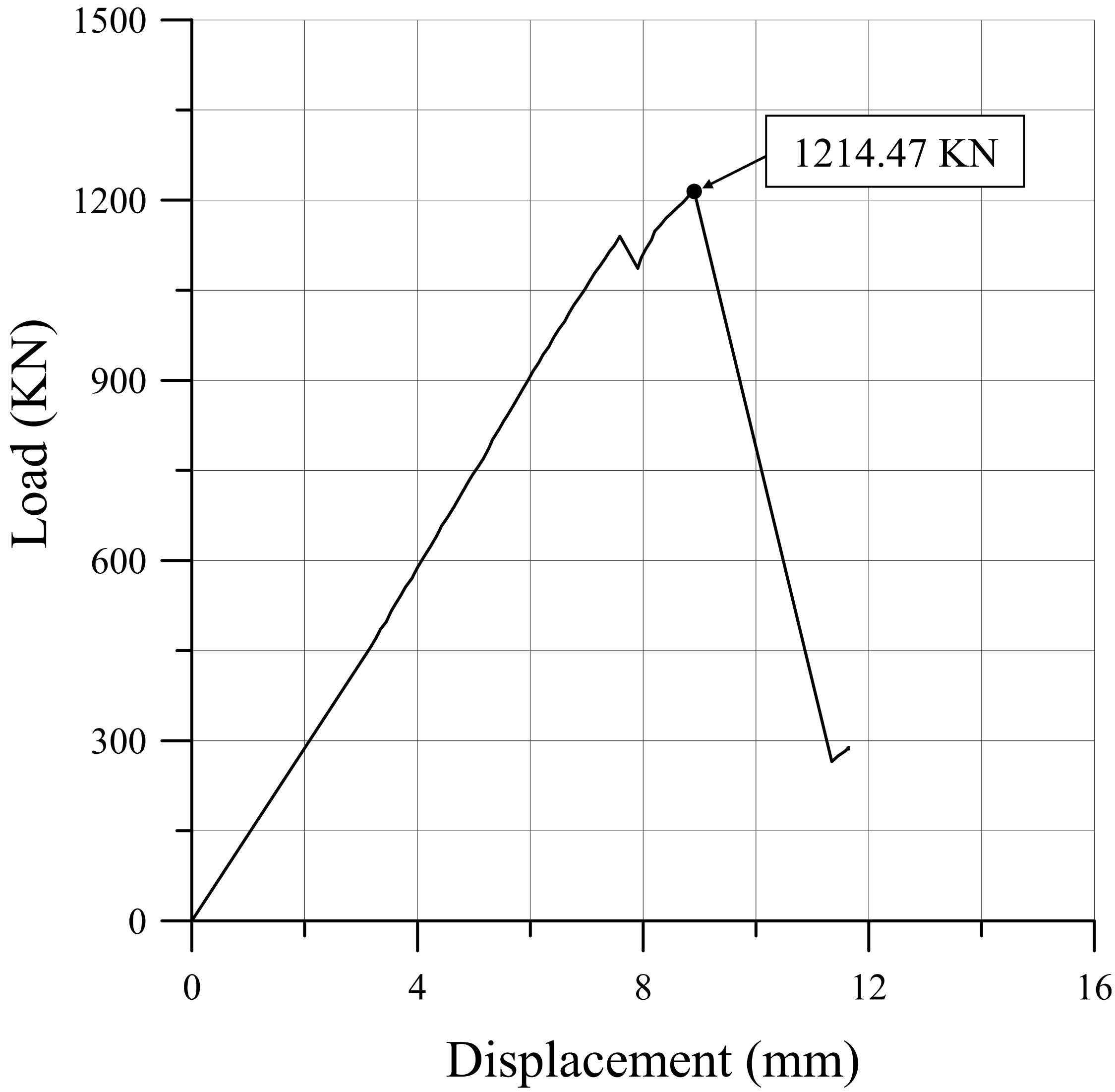

Figure 7.71 The load-axial displacement curve for ID69

ID 70

Plate		Stiffener				
t	Material	h_w	t_w	b_f	t_f	Material
5 mm	5383-H116	80 mm	5 mm	60 mm	5 mm	5383-H116

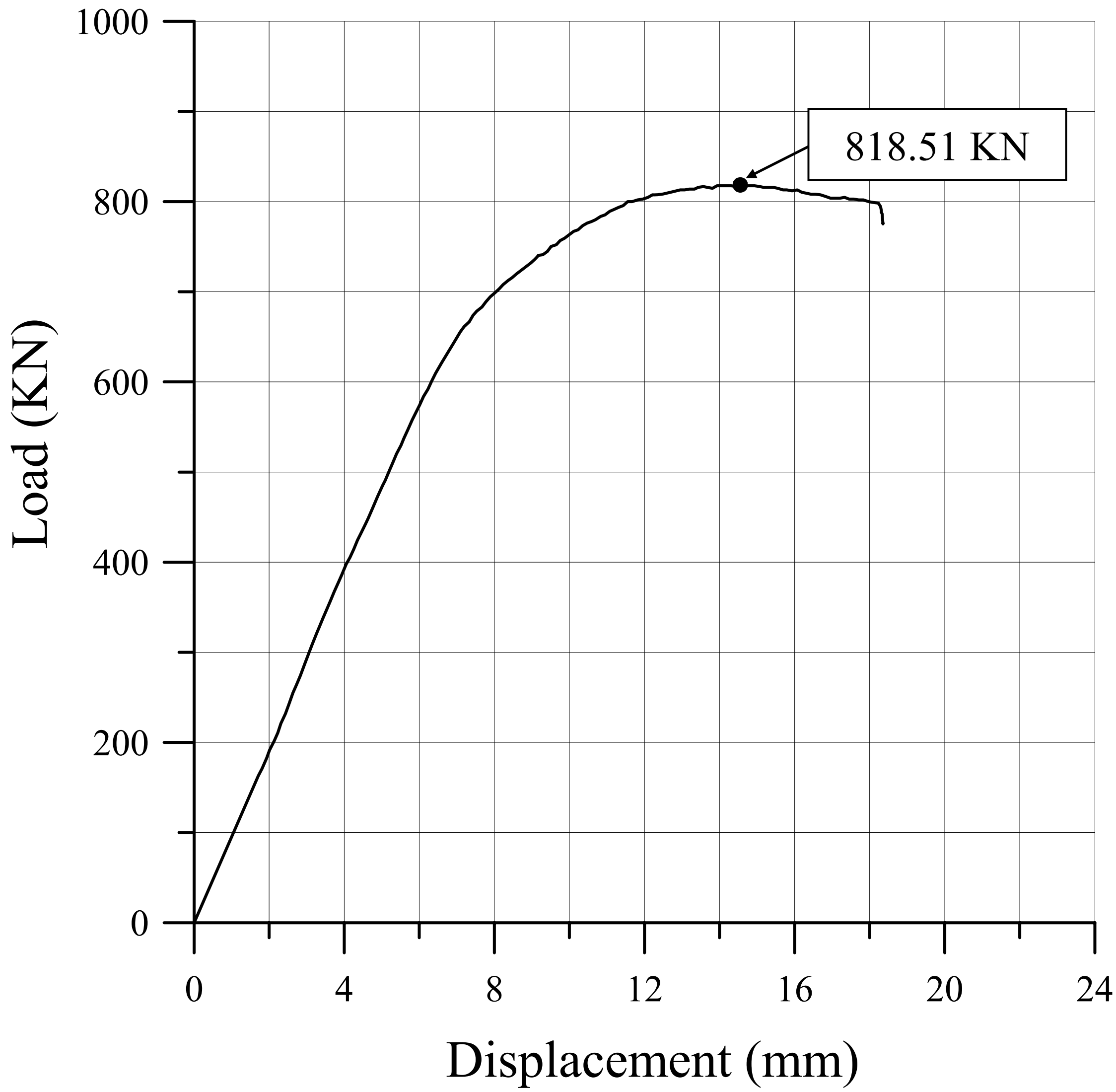

Figure 7.72 The load-axial displacement curve for ID70

ID 71

Plate		Stiffener				
t	Material	h_w	t_w	b_f	t_f	Material
6 mm	5383-H116	60 mm	5 mm	60 mm	5 mm	5383-H116

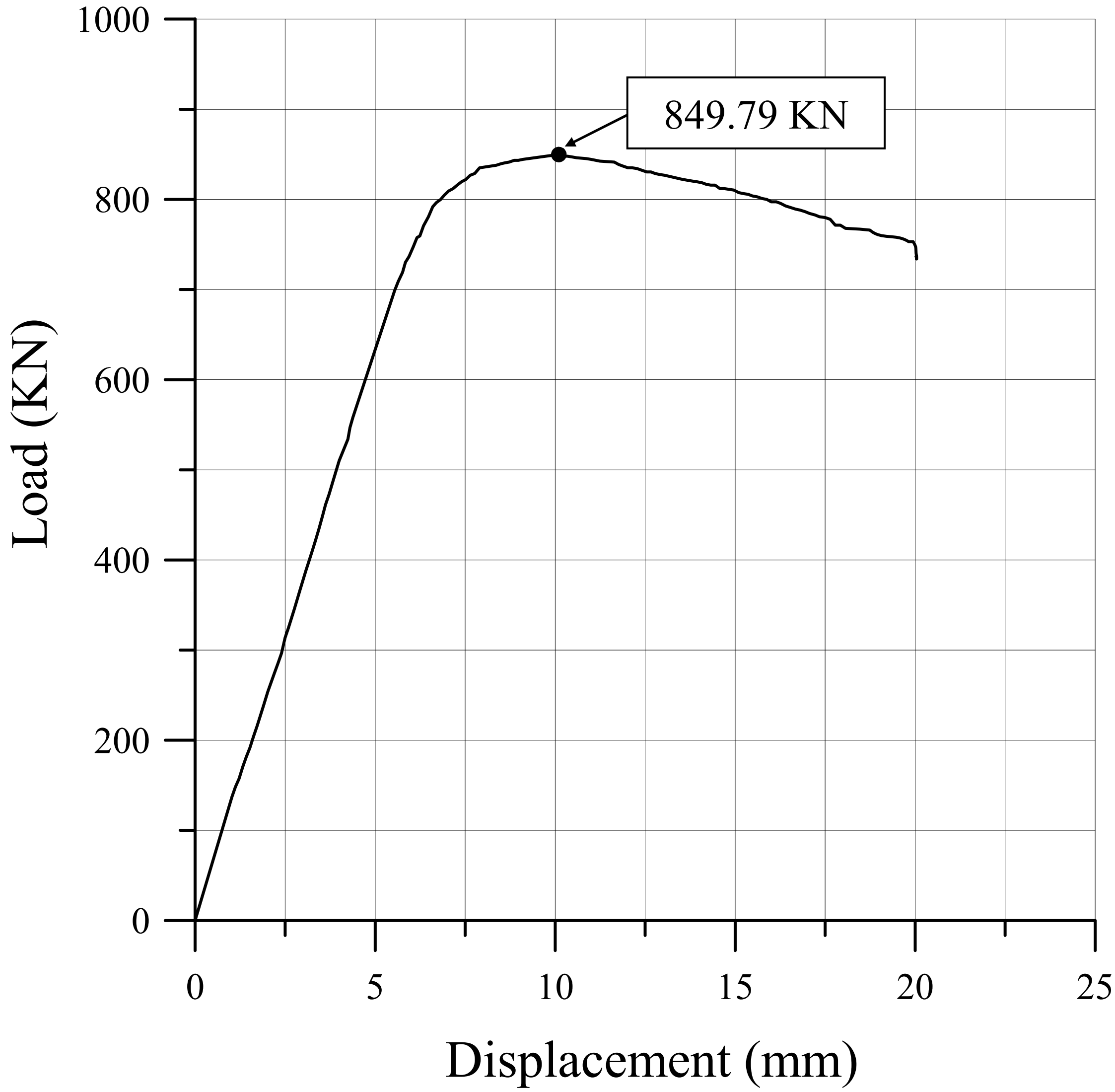

Figure 7.73 The load-axial displacement curve for ID71

ID 72

Plate		Stiffener				
t	Material	h_w	t_w	b_f	t_f	Material
8 mm	5383-H116	100 mm	5 mm	60 mm	5 mm	5383-H116

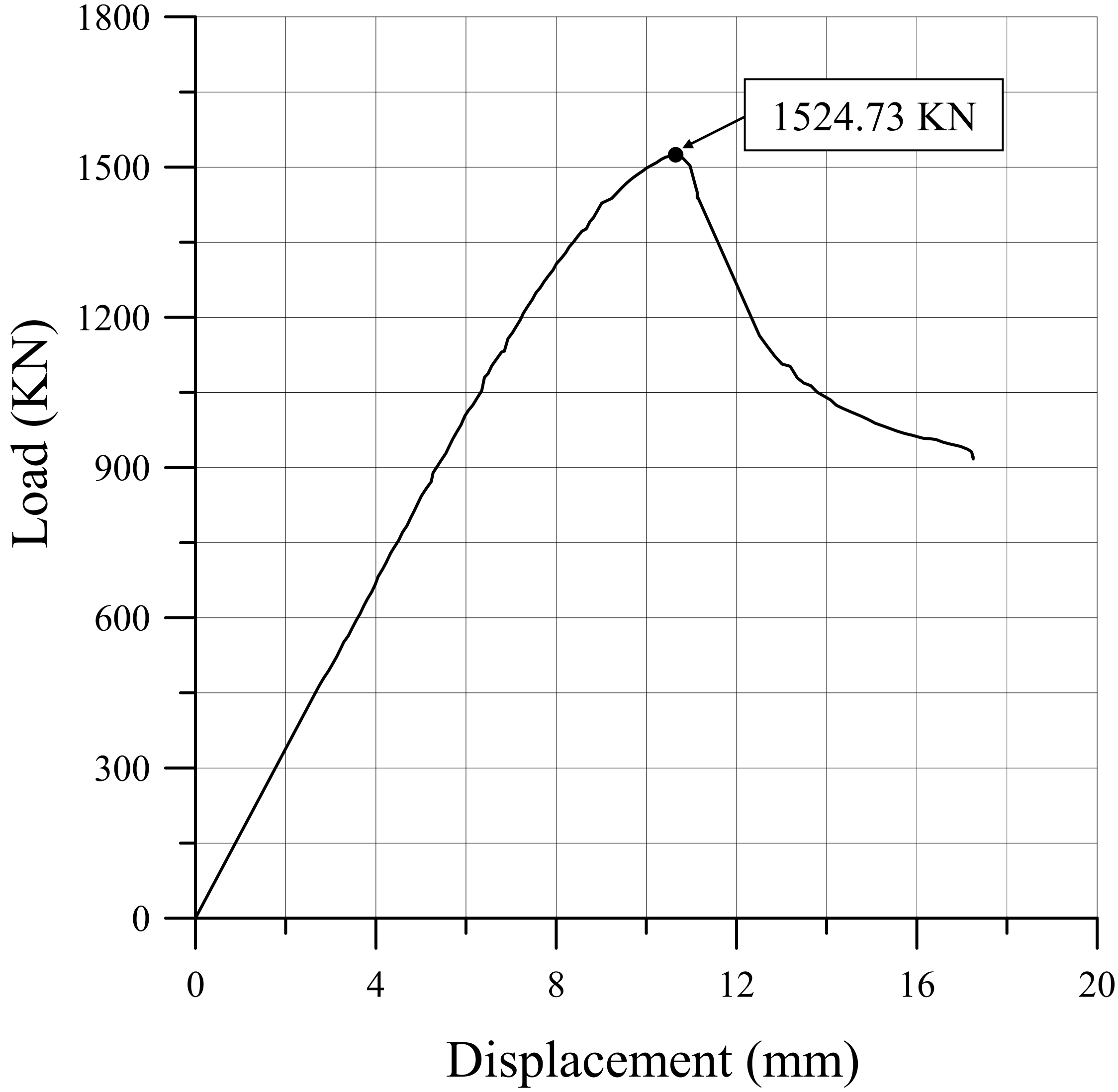

Figure 7.74 The load-axial displacement curve for ID72

ID 73

Plate		Stiffener				
t	Material	h_w	t_w	b_f	t_f	Material
6 mm	5083-H116	76.8 mm	4 mm	45 mm	5.6 mm	6082-T6

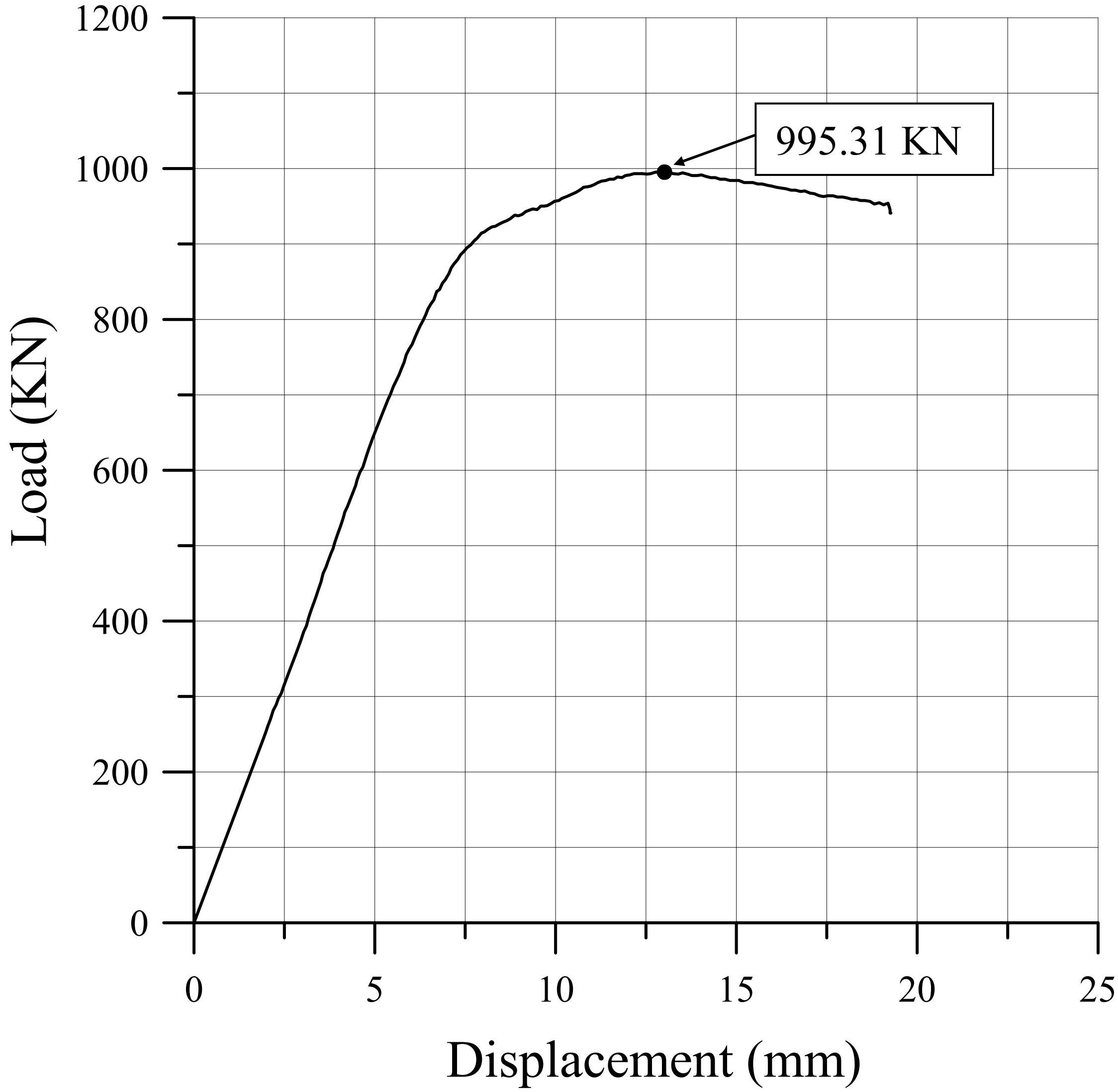

Figure 7.75 The load-axial displacement curve for ID73

ID 74

Plate		Stiffener				
t	Material	h_w	t_w	b_f	t_f	Material
8 mm	5083-H116	100 mm	6 mm	55 mm	8.2 mm	6082-T6

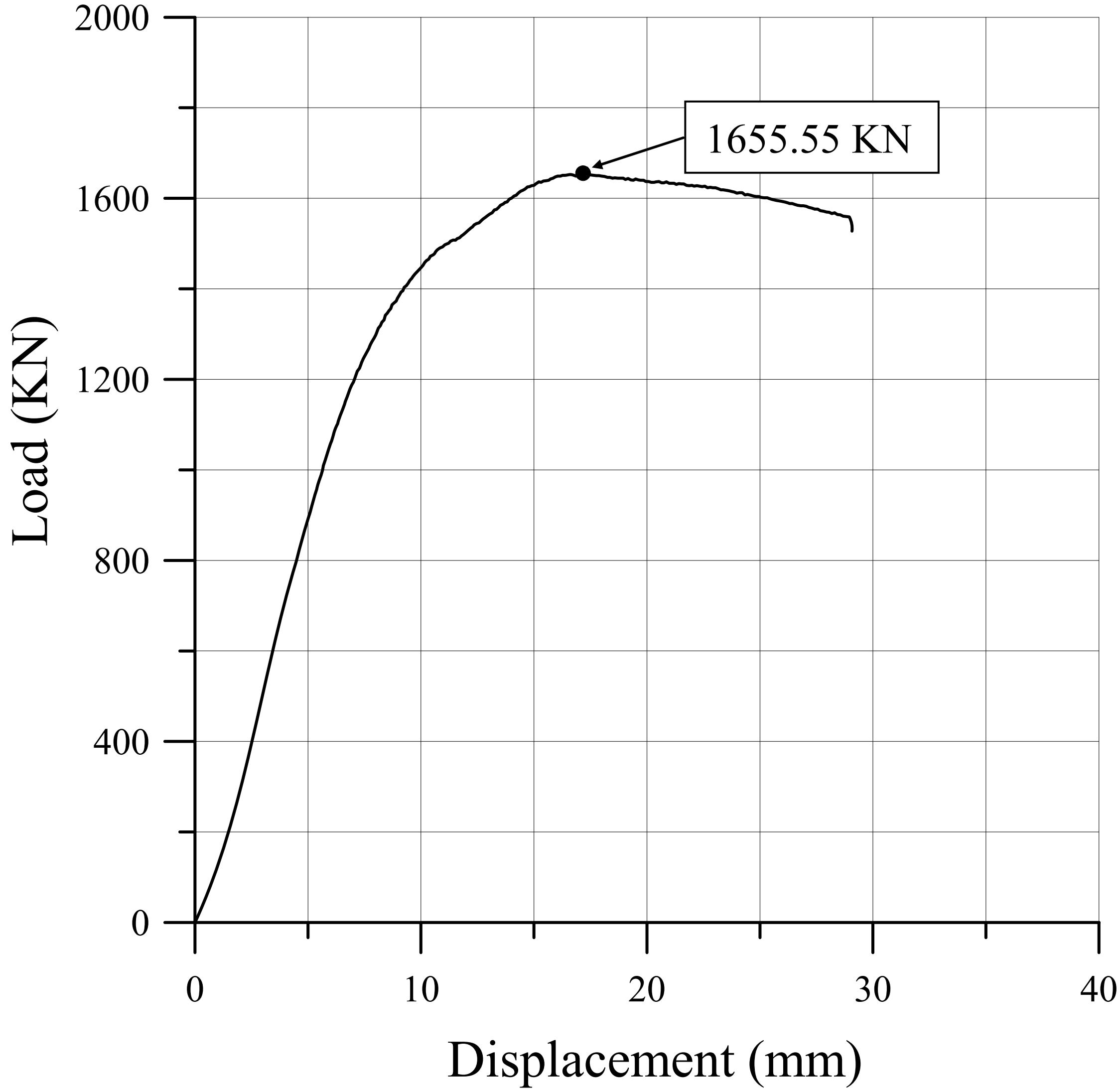

Figure 7.76 The load-axial displacement curve for ID74

ID 75

Plate		Stiffener				
t	Material	h_w	t_w	b_f	t_f	Material
8 mm	5383-H116	100 mm	6 mm	55 mm	8.2 mm	5383-H112

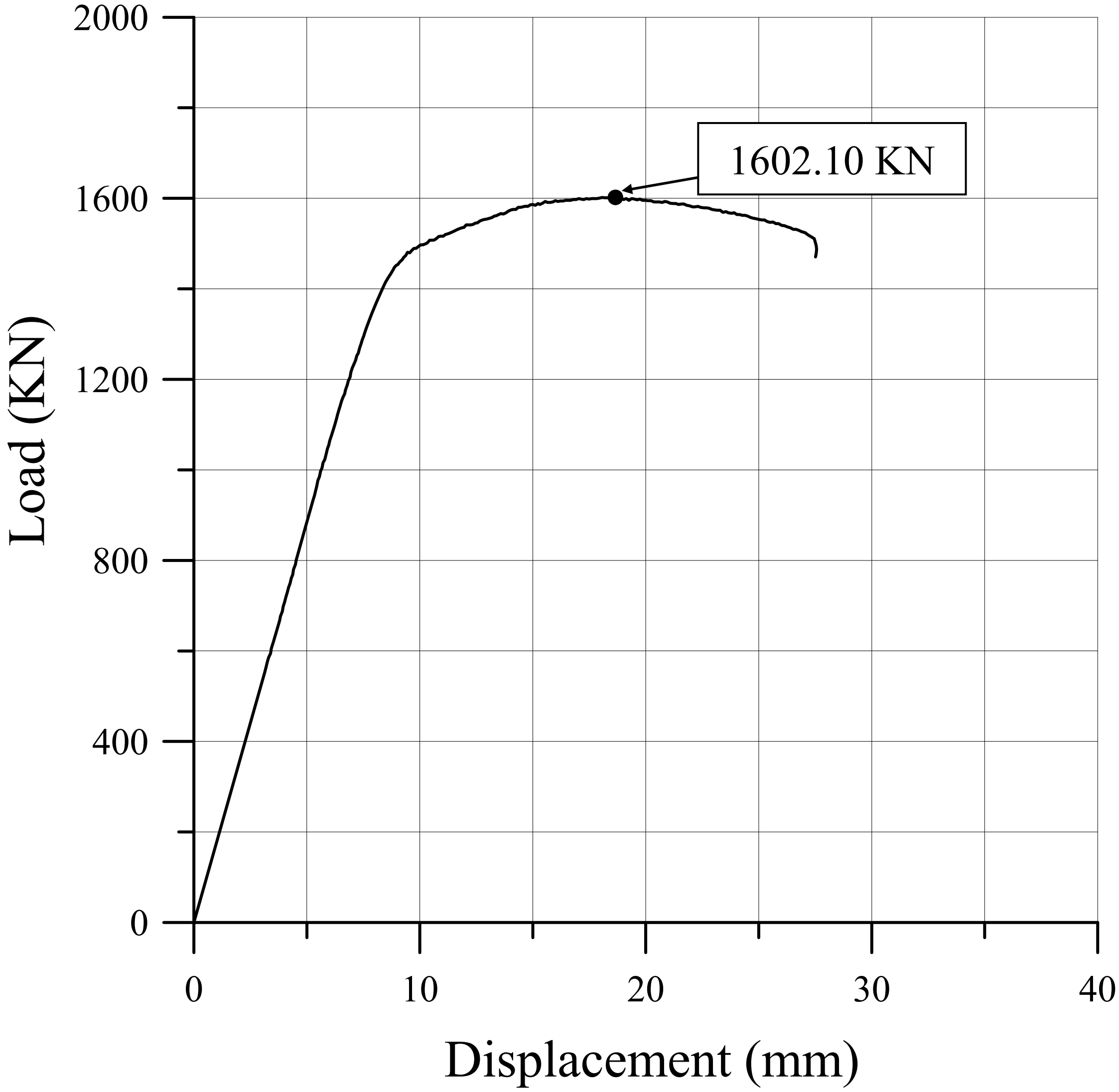

Figure 7.77 The load-axial displacement curve for ID75

ID 76

Plate		Stiffener				
t	Material	h_w	t_w	b_f	t_f	Material
6 mm	5083-H116	76.8 mm	4 mm	45 mm	5.6 mm	6082-T6

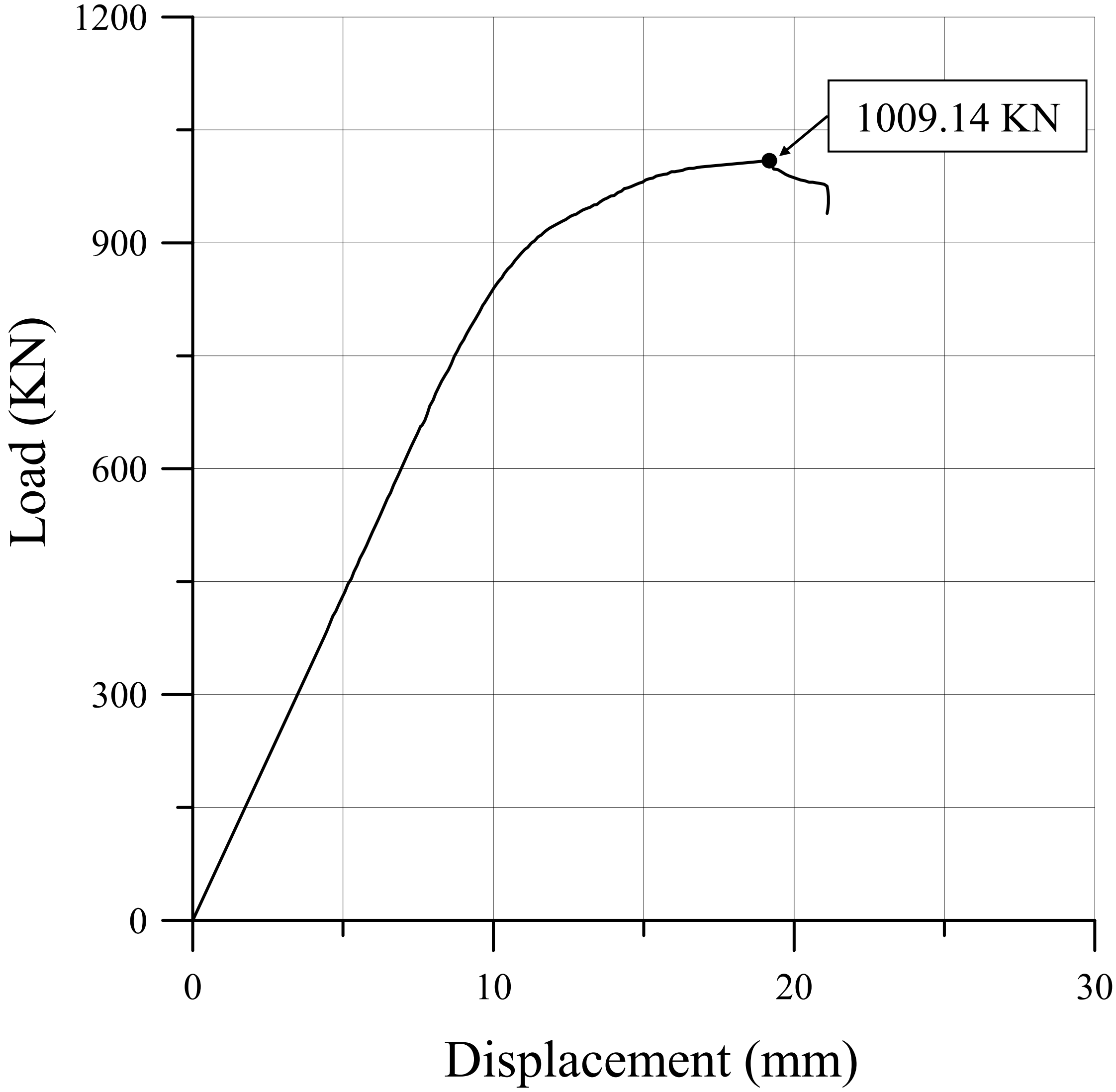

Figure 7.78 The load-axial displacement curve for ID76

ID 77

Plate		Stiffener				
t	Material	h_w	t_w	b_f	t_f	Material
8 mm	5083-H116	100 mm	6 mm	55 mm	8.2 mm	6082-T6

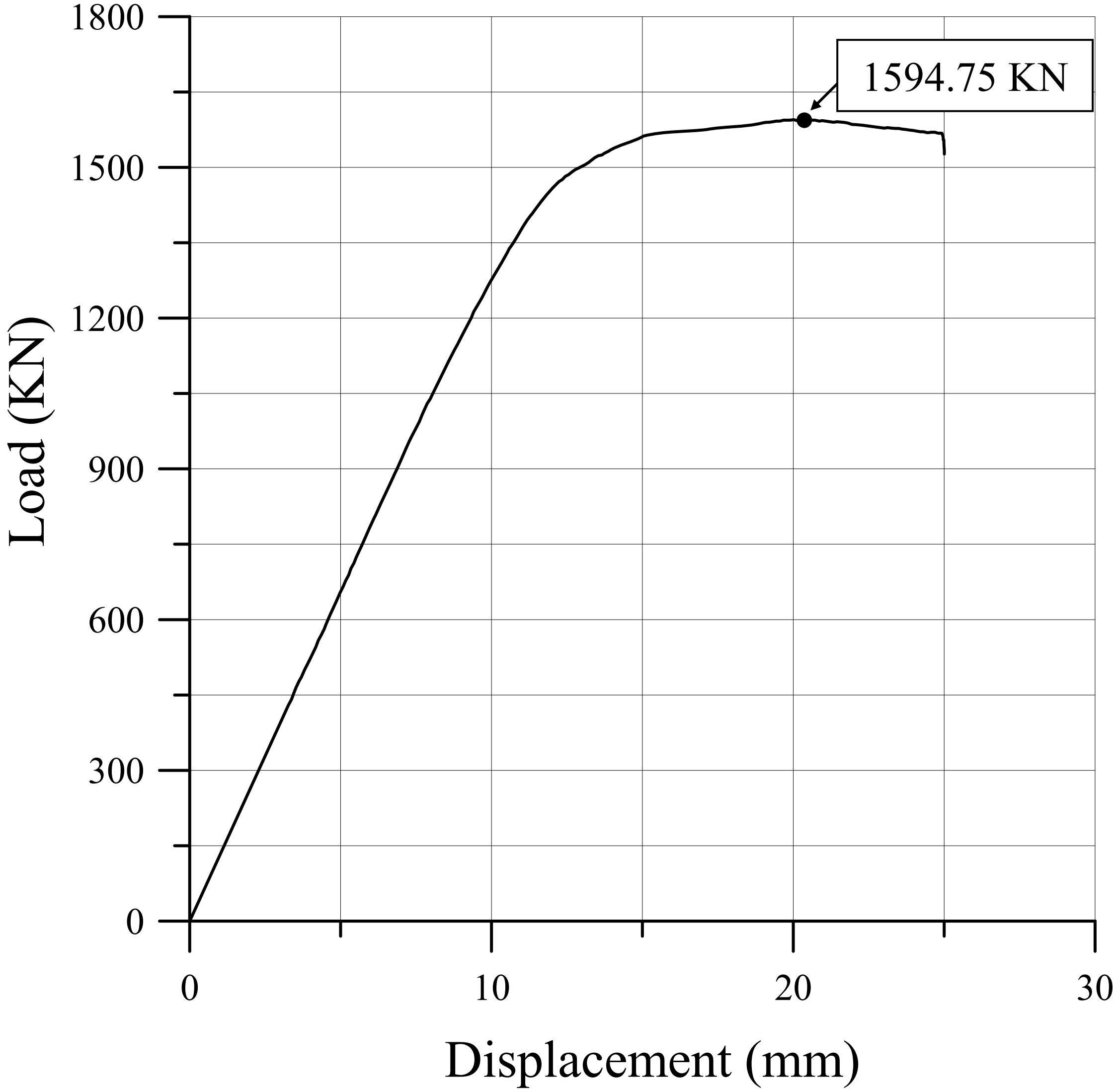

Figure 7.79 The load-axial displacement curve for ID77

ID 78

Plate		Stiffener				
t	Material	h_w	t_w	b_f	t_f	Material
8 mm	5383-H116	100 mm	6 mm	55 mm	8.2 mm	5383-H112

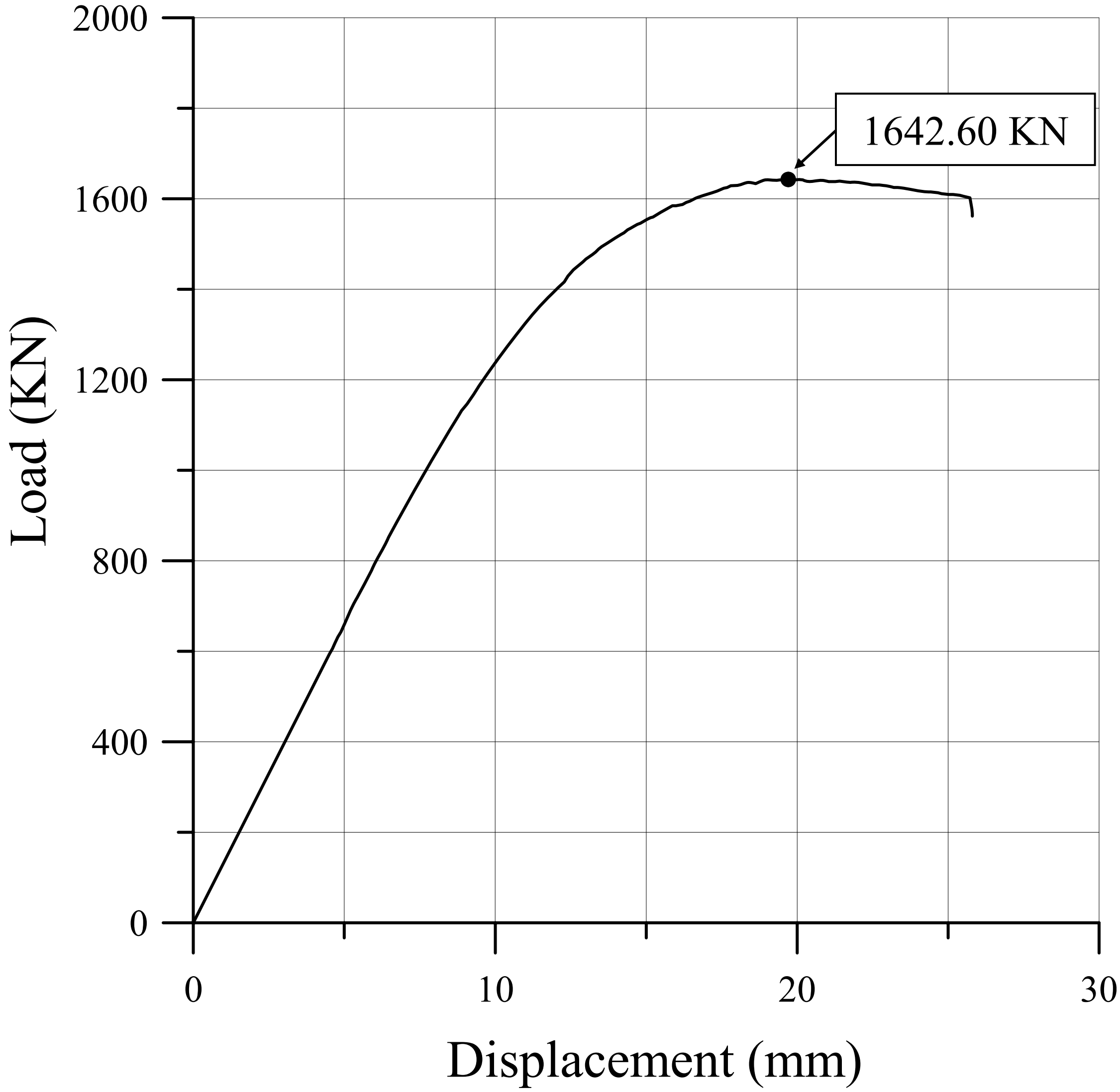

Figure 7.80 The load-axial displacement curve for ID78

Figure 7.81 Selected photos of the test structures showing typical collapse modes
(ID1: Mode III, ID2: Mode V, ID3: Mode III+IV, ID4: Mode IV+V, ID8: Mode V, ID41: Mode III, ID42: Mode IV)

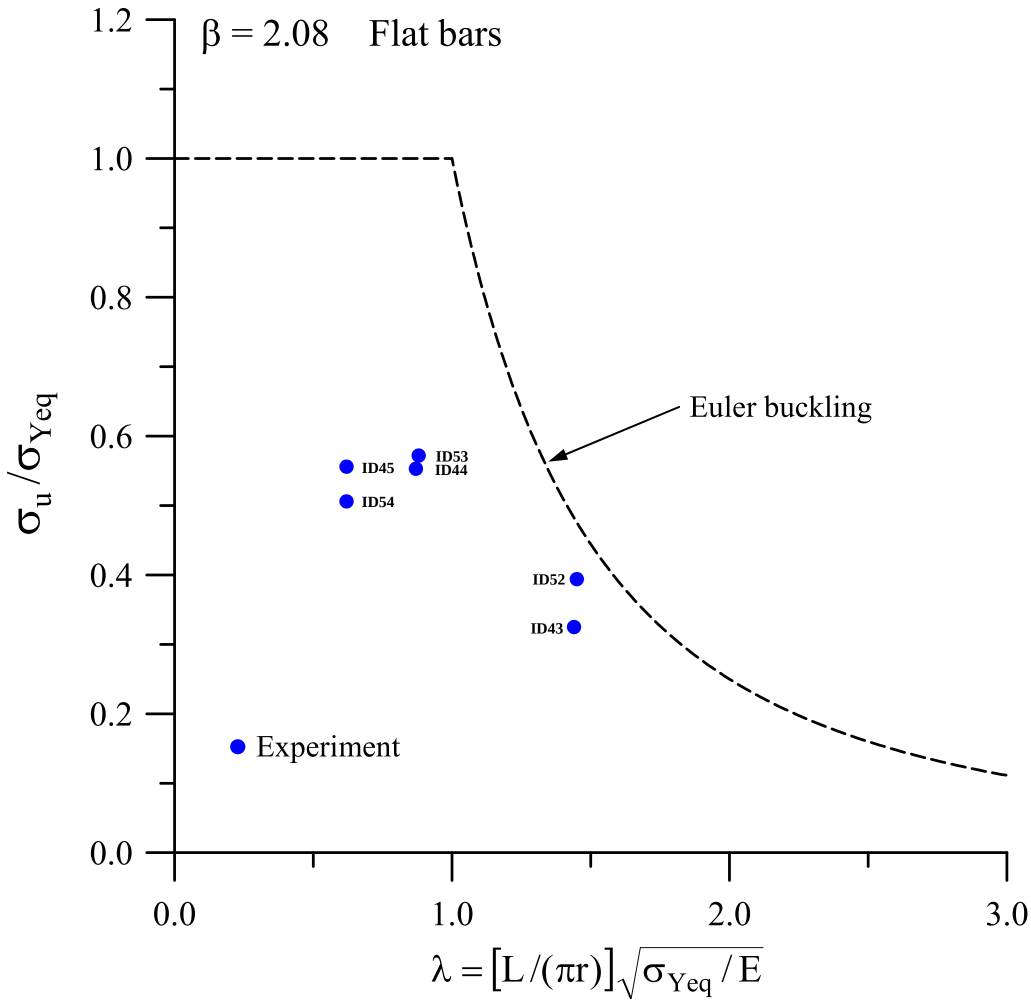

Figure 7.82(a) Variation of the ultimate strength for the test structures with flat-bars, β =2.08

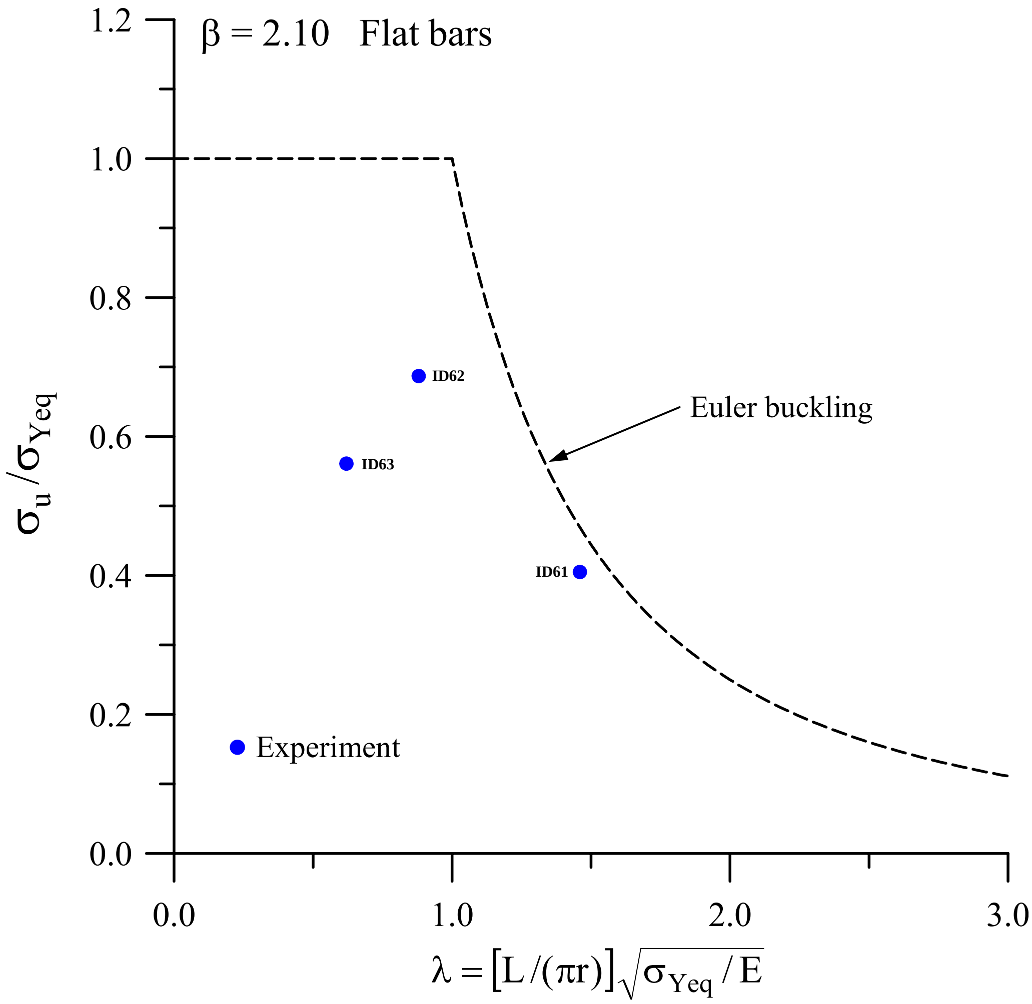

Figure 7.82(b) Variation of the ultimate strength for the test structures with flat-bars, β=2.10

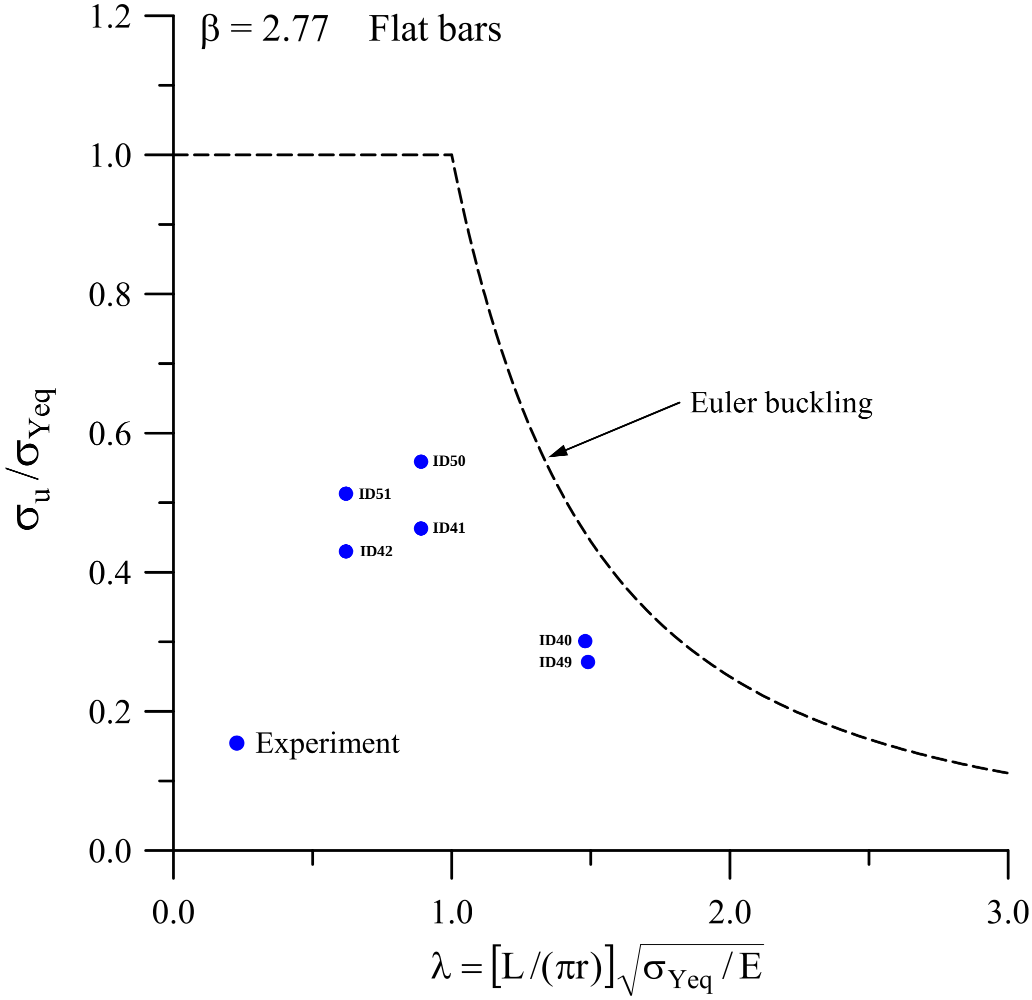

Figure 7.82(c) Variation of the ultimate strength for the test structures with flat-bars, β=2.77

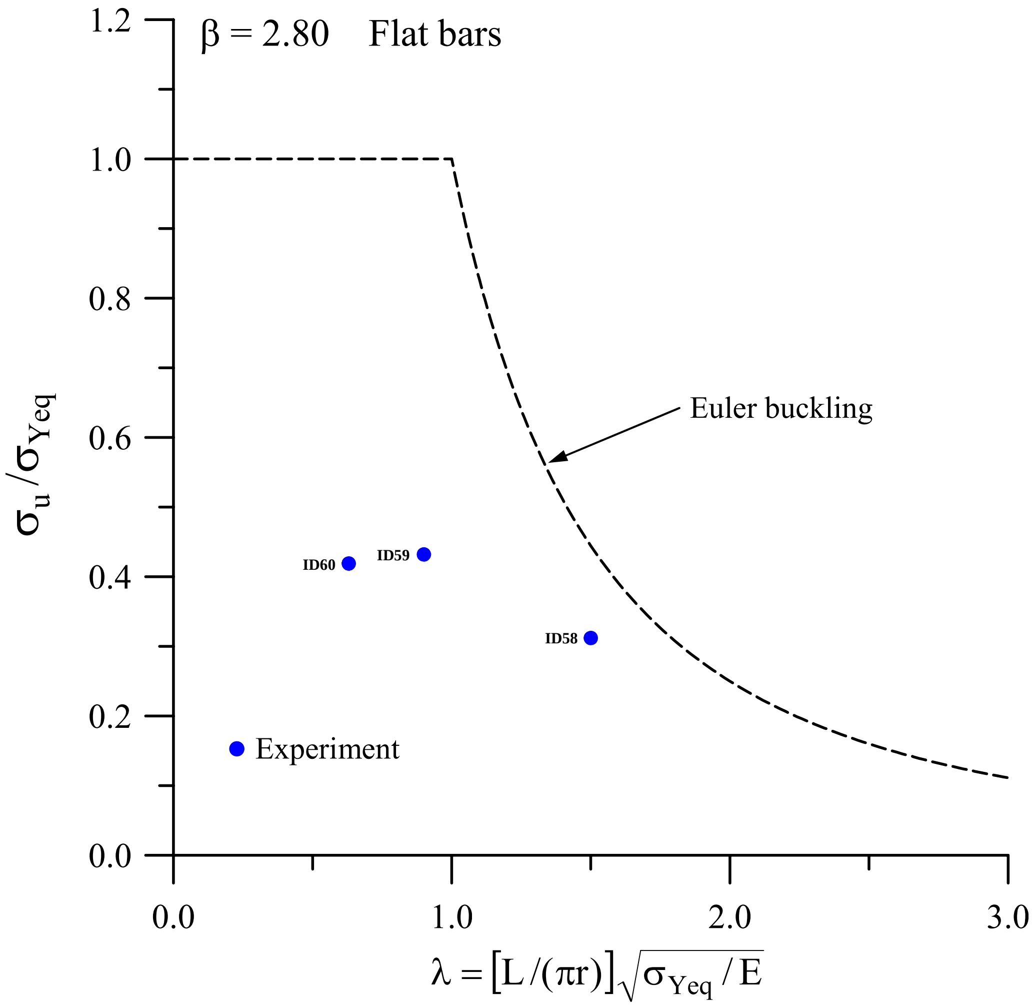

Figure 7.82(d) Variation of the ultimate strength for the test structures with flat-bars, β =2.80

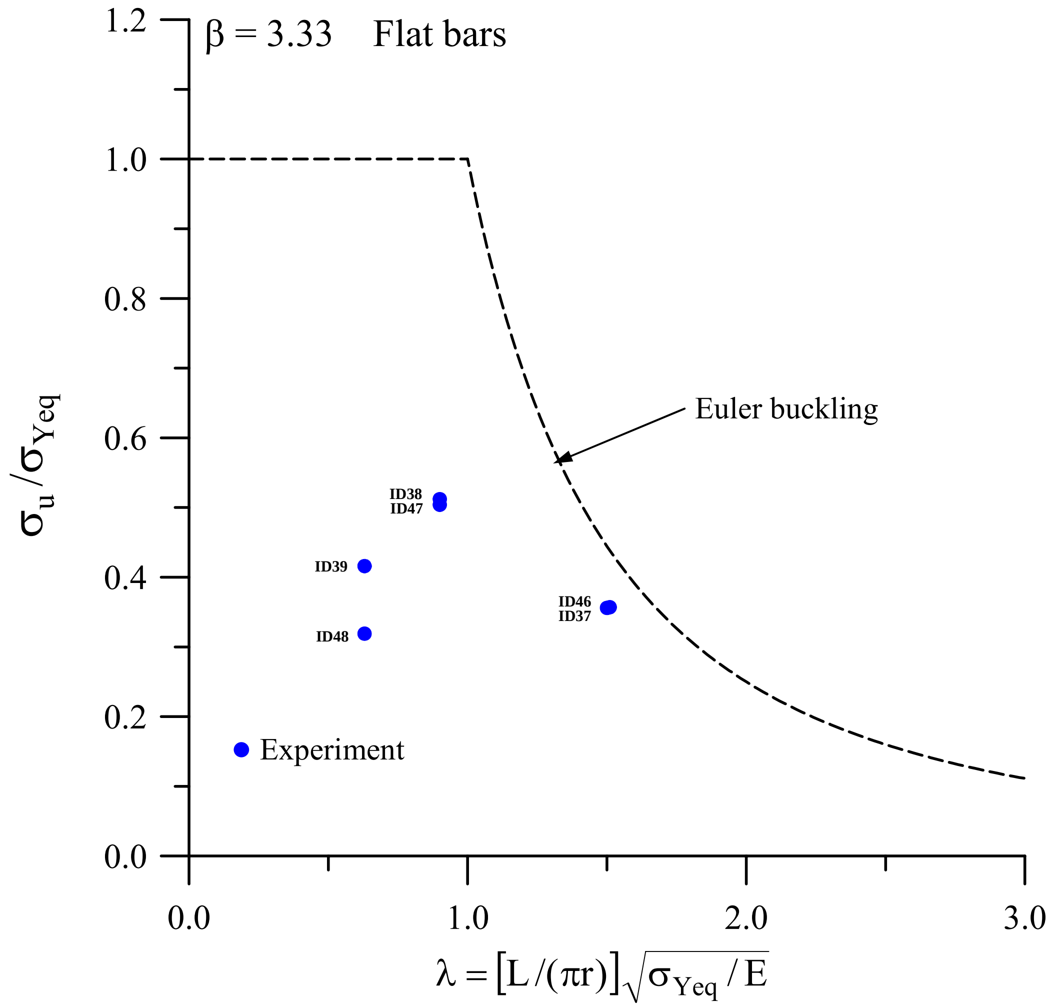

Figure 7.82(e) Variation of the ultimate strength for the test structures with flat-bars, β=3.33

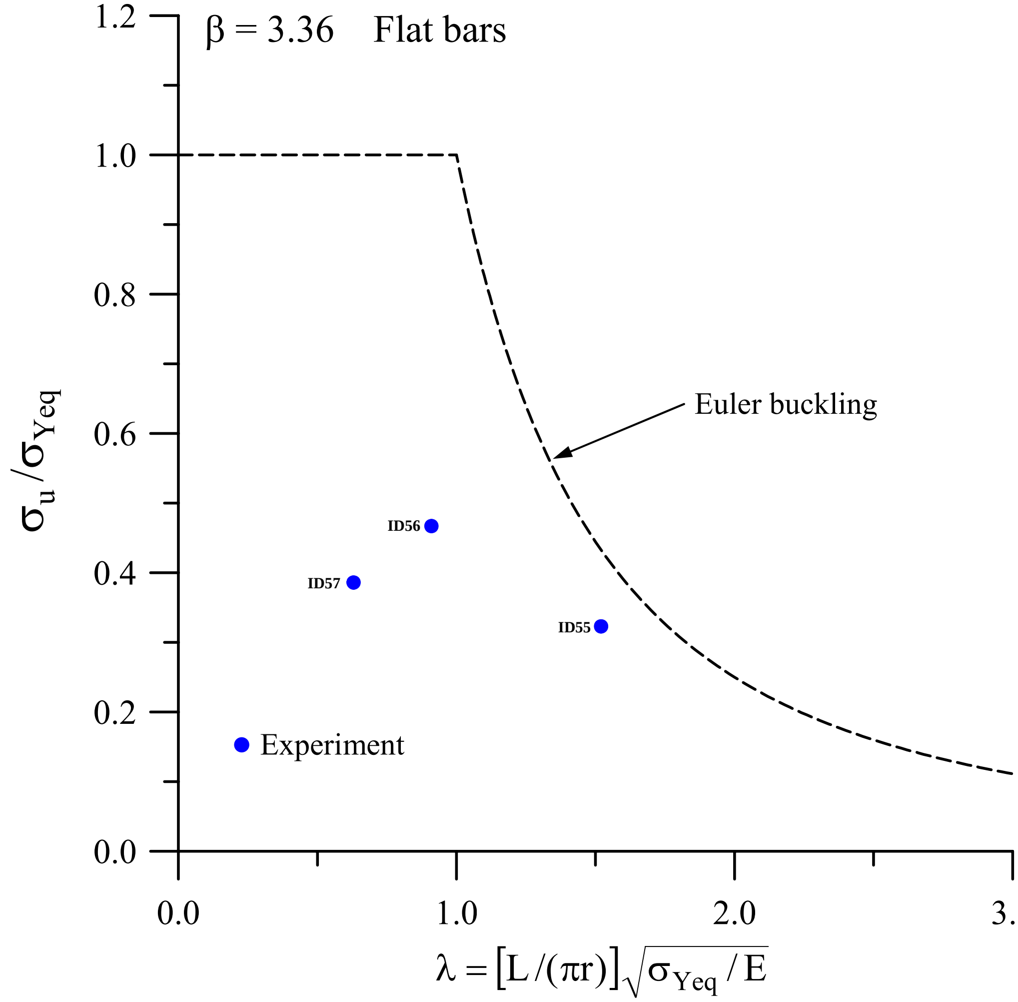

Figure 7.82(f) Variation of the ultimate strength for the test structures with flat-bars, $\beta = 3.36$

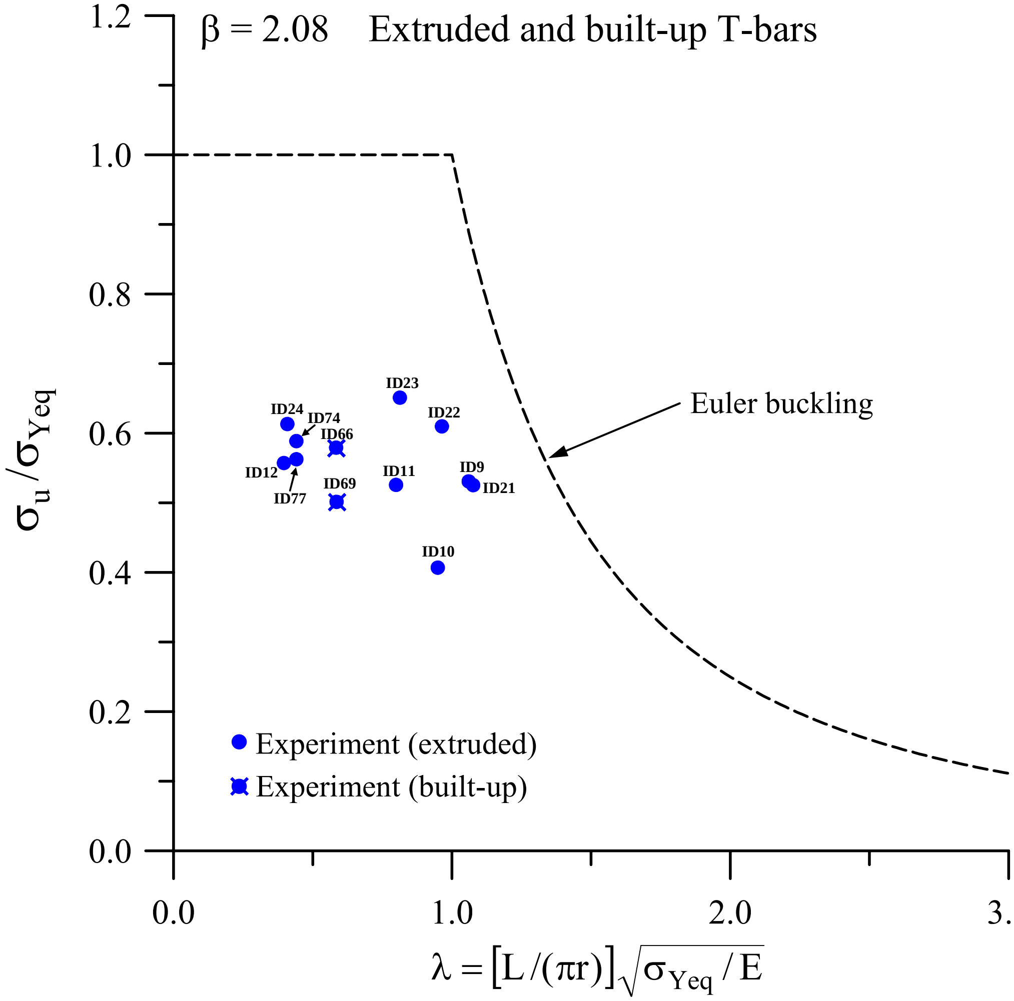

Figure 7.83(a) Variation of the ultimate strength for the test structures with extruded and built-up T-bars, $\beta = 2.08$

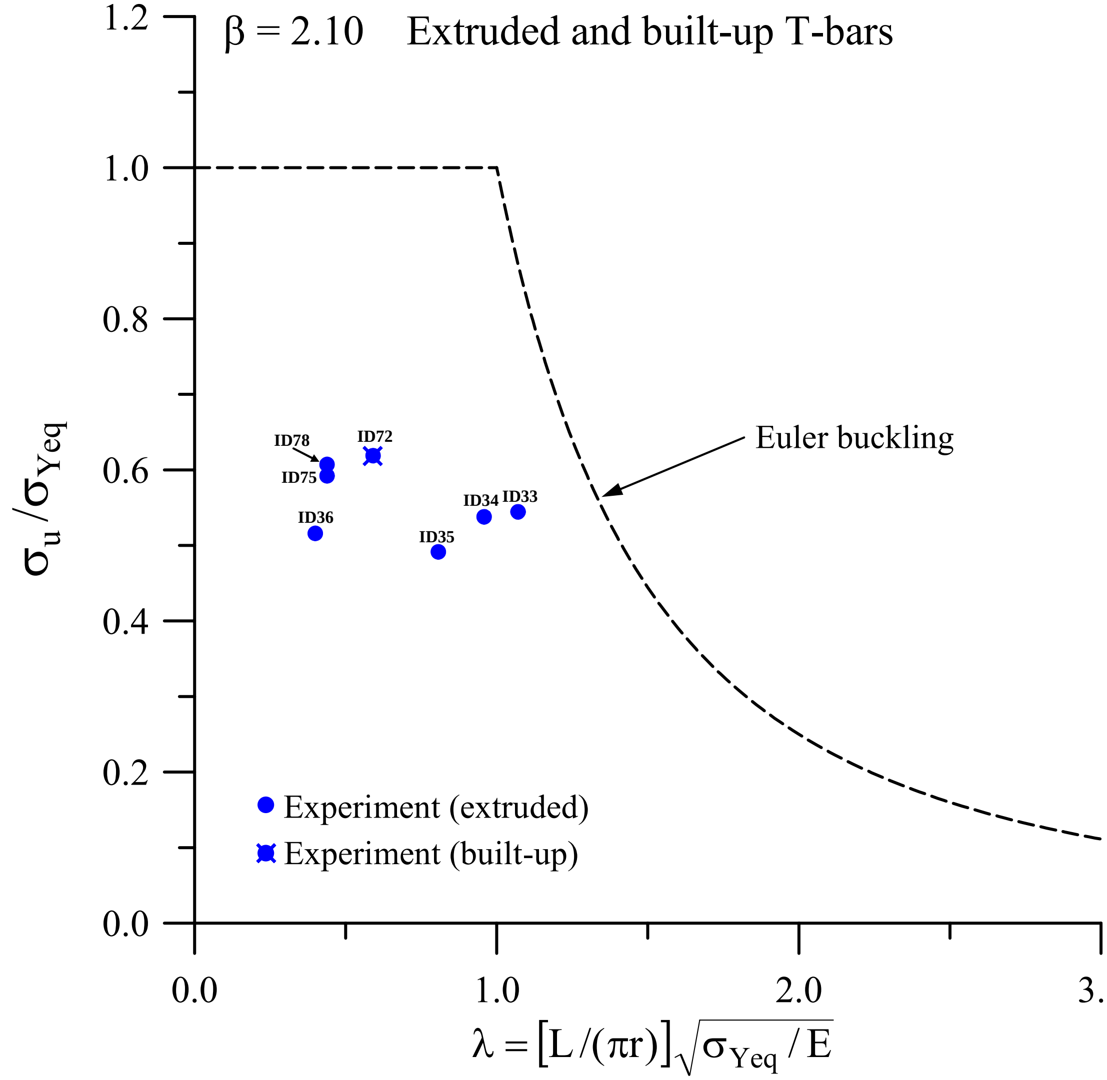

Figure 7.83(b) Variation of the ultimate strength for the test structures with extruded and built-up T-bars, $\beta = 2.10$

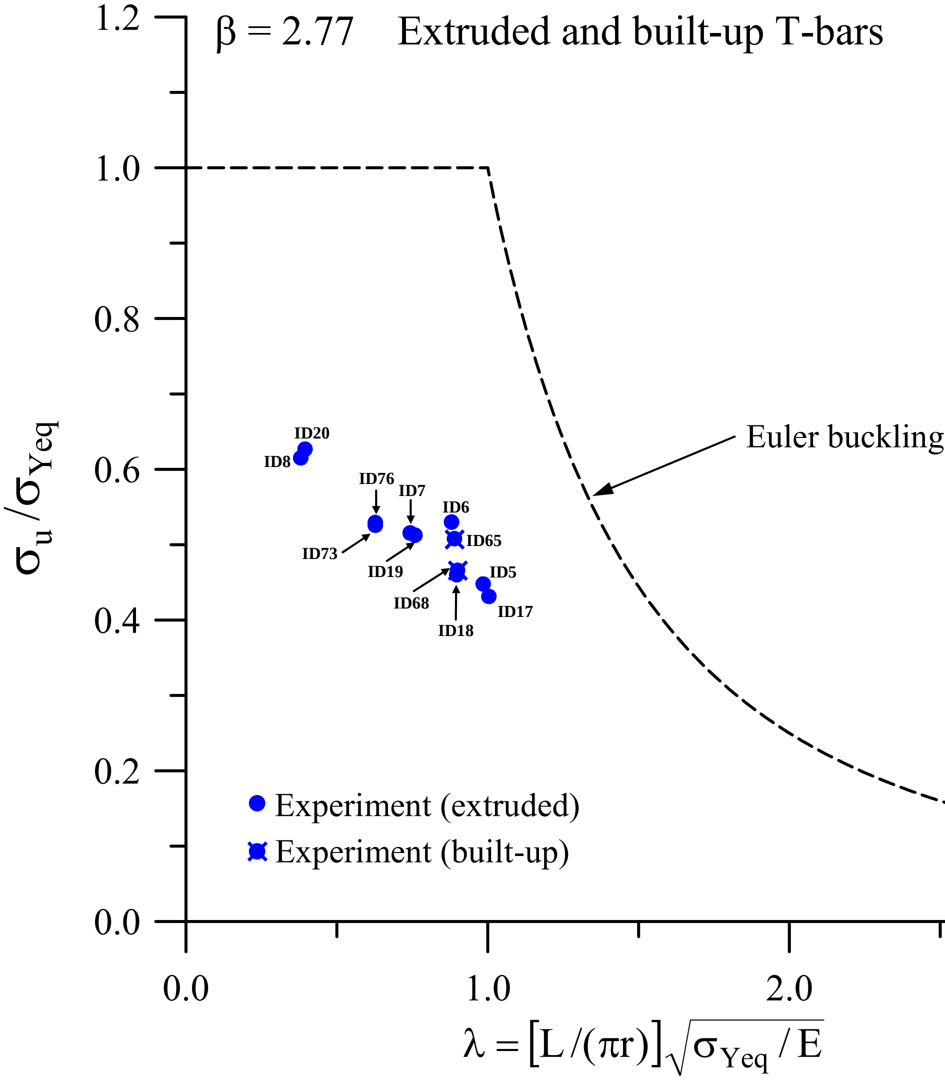

Figure 7.83(c) Variation of the ultimate strength for the test structures with extruded and built-up T-bars, $\beta = 2.77$

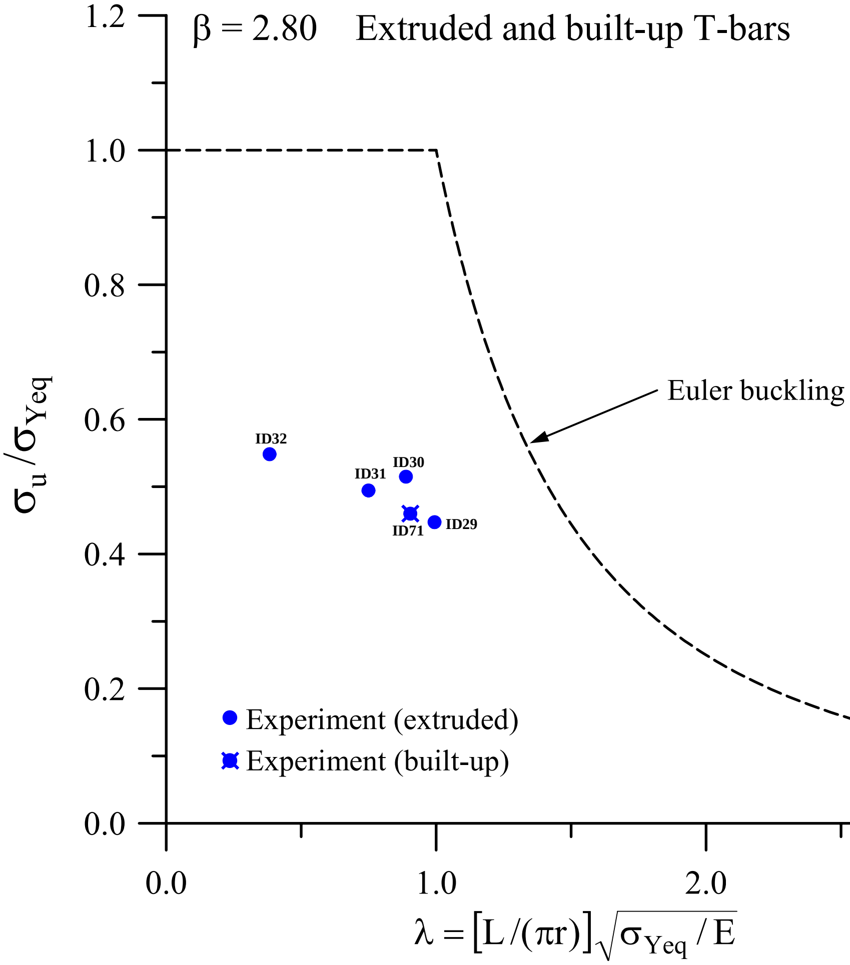

Figure 7.83(d) Variation of the ultimate strength for the test structures with extruded and built-up T-bars, $\beta = 2.80$

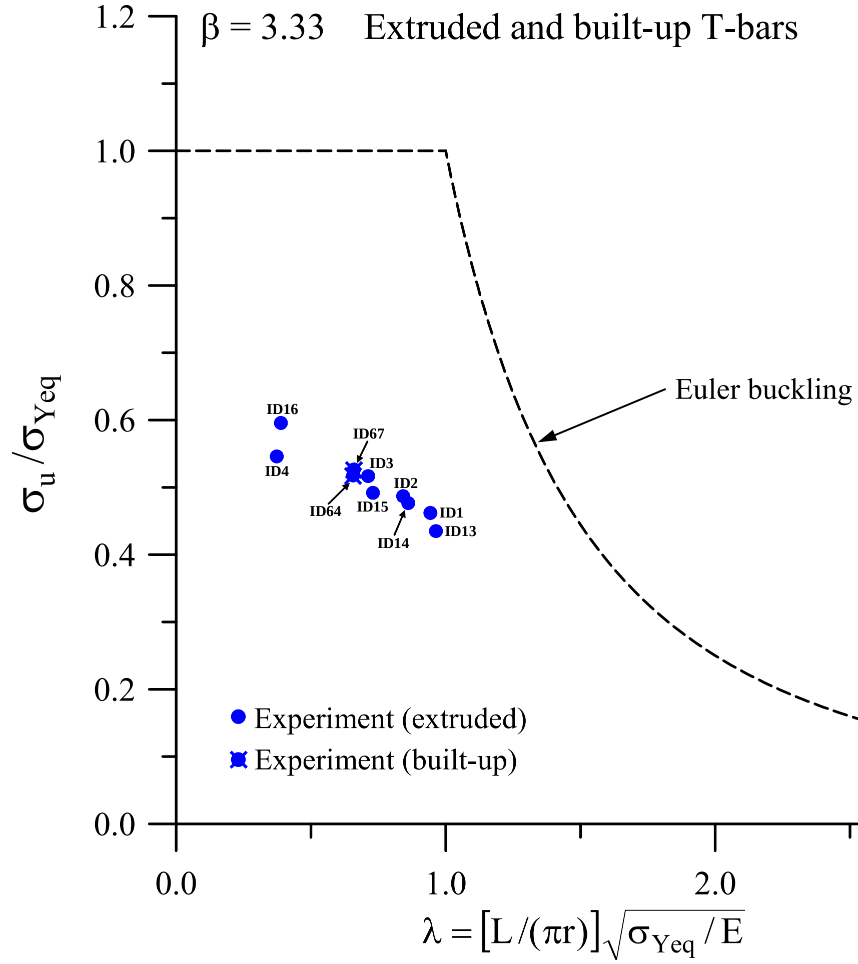

Figure 7.83(e) Variation of the ultimate strength for the test structures with extruded and built-up T-bars, $\beta = 3.33$

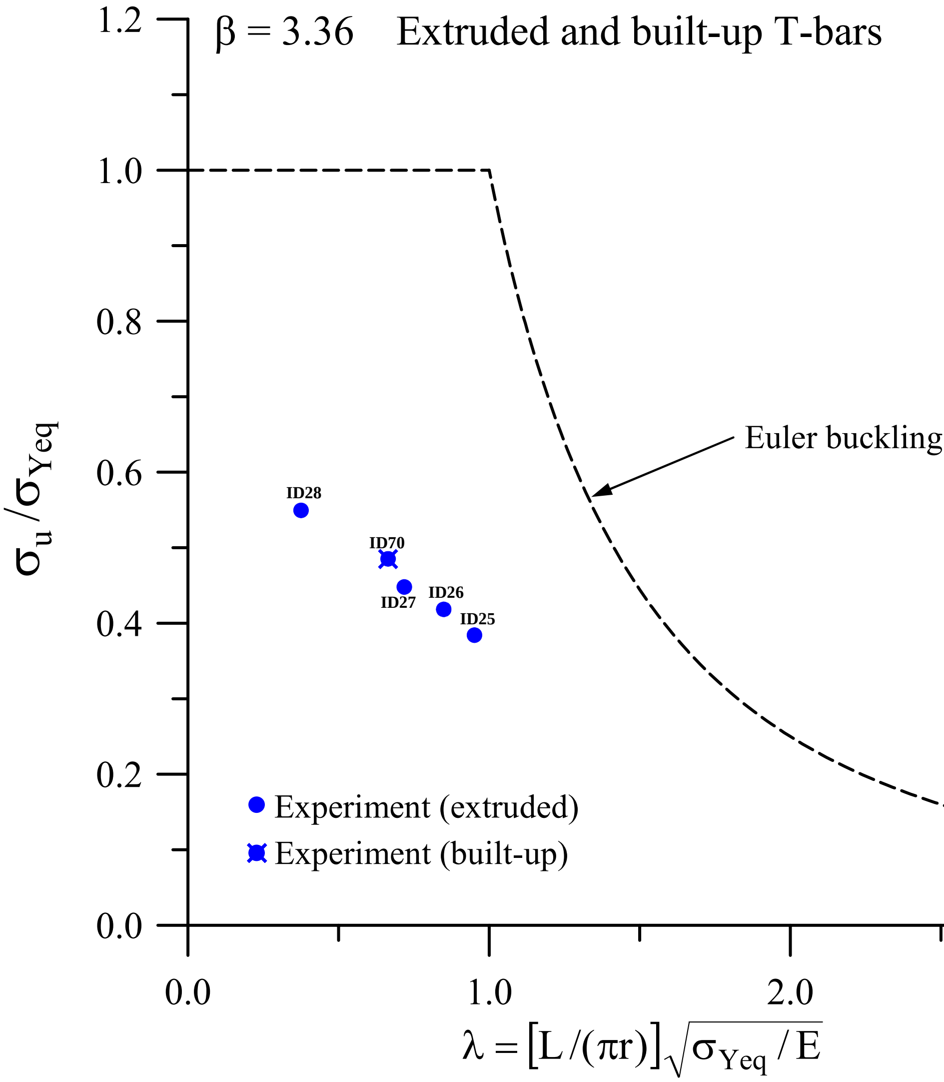

Figure 7.83(f) Variation of the ultimate strength for the test structures with extruded and built-up T-bars, $\beta = 3.36$

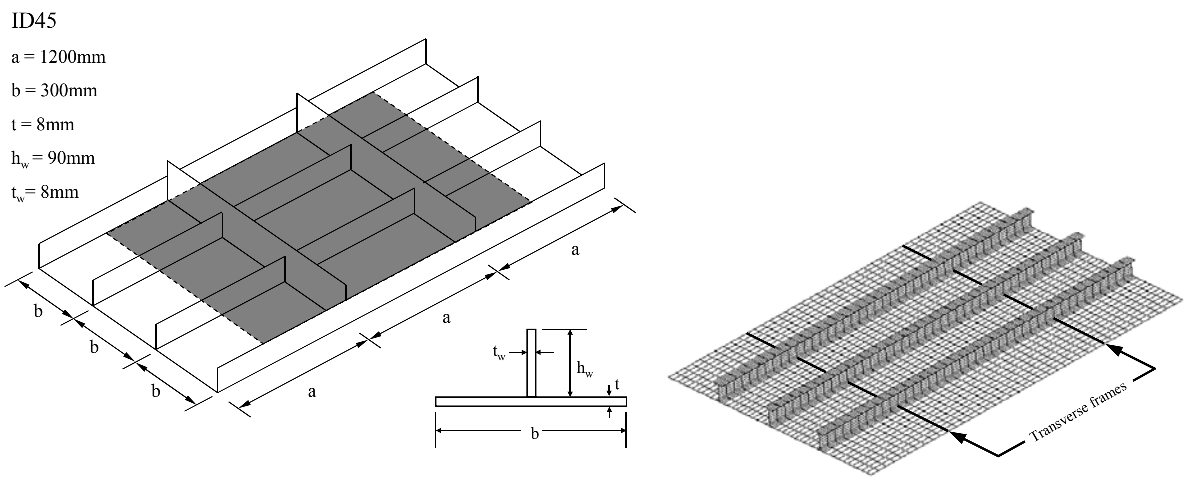

Figure 8.1(a) The extent and structural modeling for the 2 bay stiffened panel model (SPM) FEA

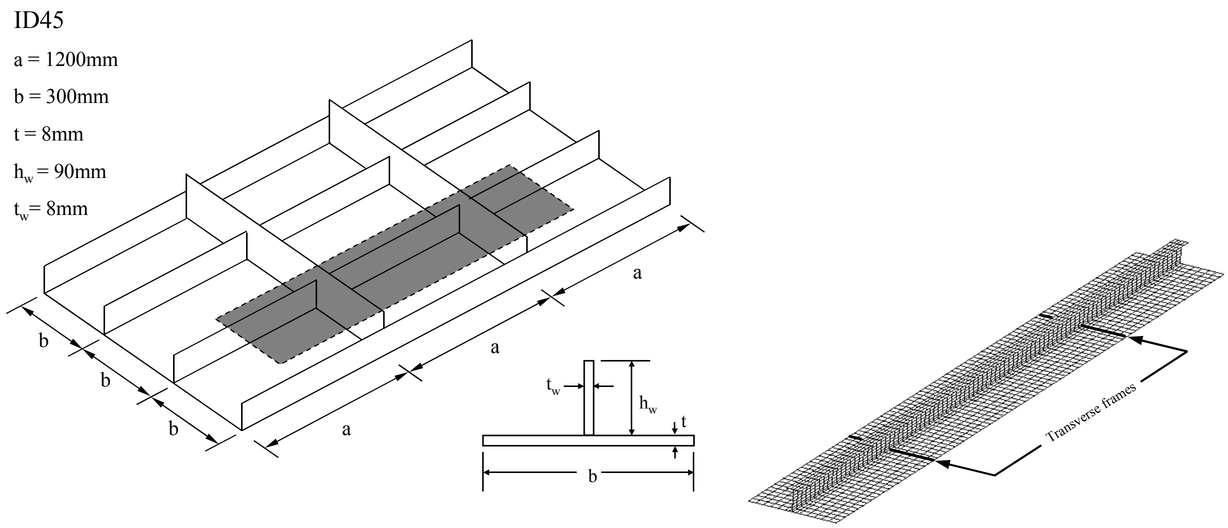

Figure 8.1(b) The extent and structural modeling for the 2 bay plate-stiffener combination (PSC) FEA

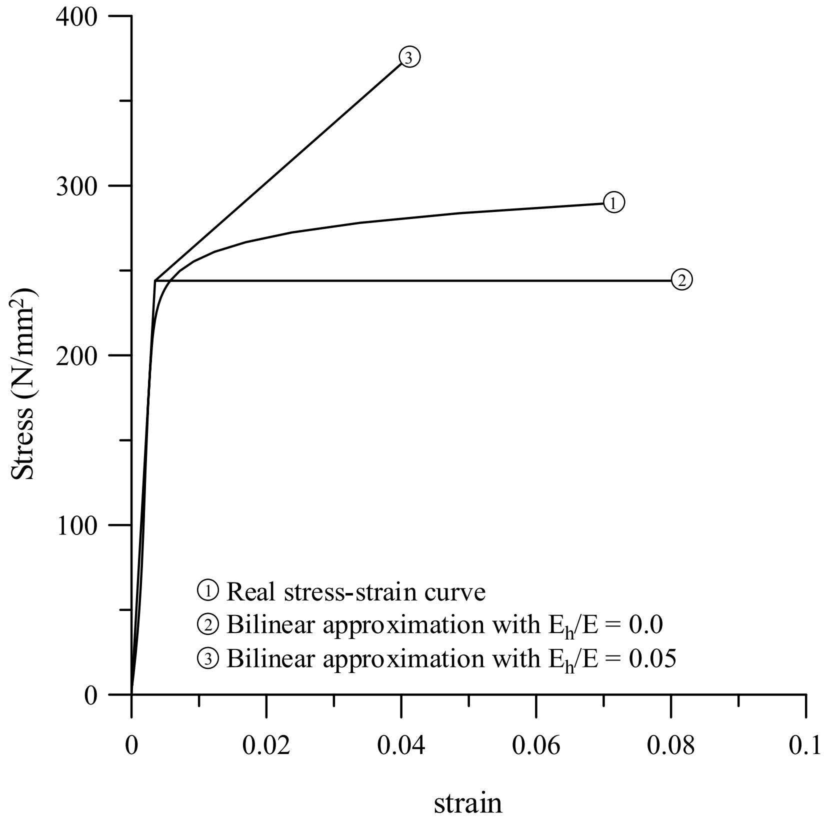

Figure 8.2(a) Three types of material stress-strain relation modeling

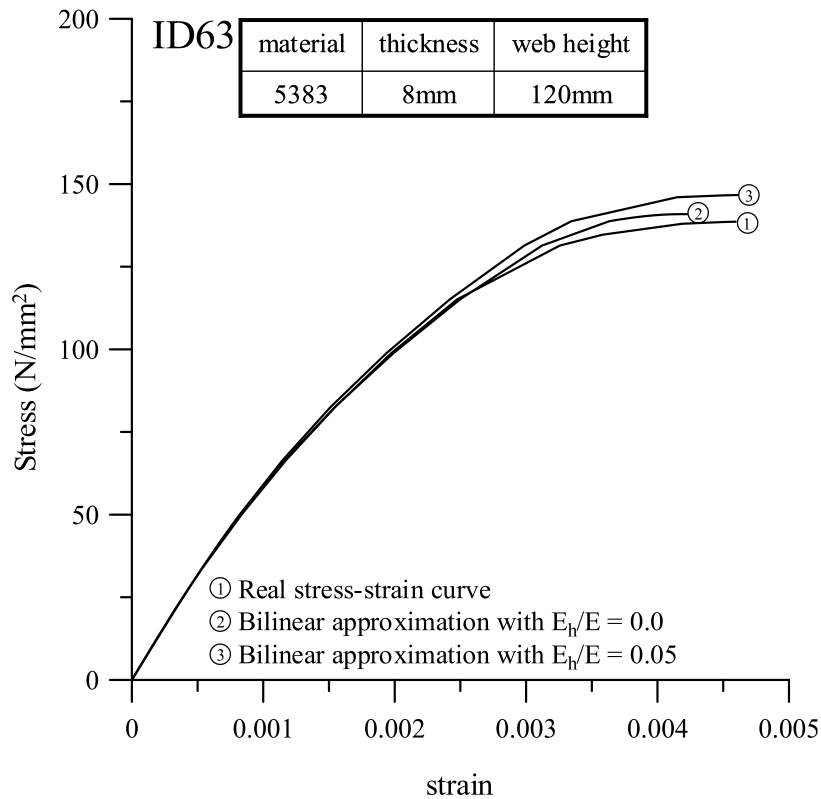

Figure 8.2(b) Effect of material stress-strain relation models on the aluminum panel ultimate strength behavior obtained by 1 bay PSC FEA with initial deflection in CIP

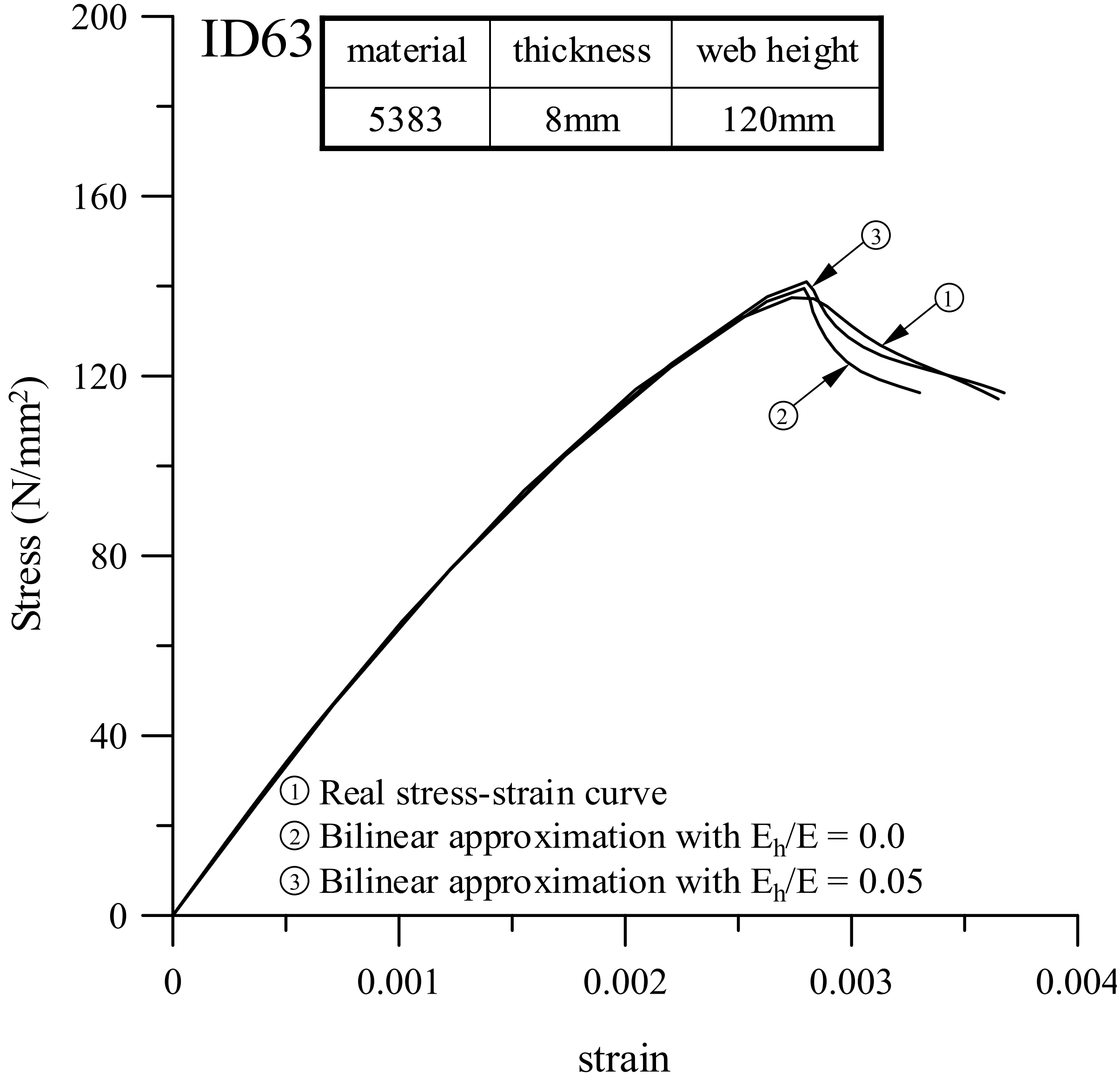

Figure 8.2(c) Effect of material stress-strain relation models on the aluminum panel ultimate strength behavior obtained by the 2 bay SPM FEA with initial deflection in CIS

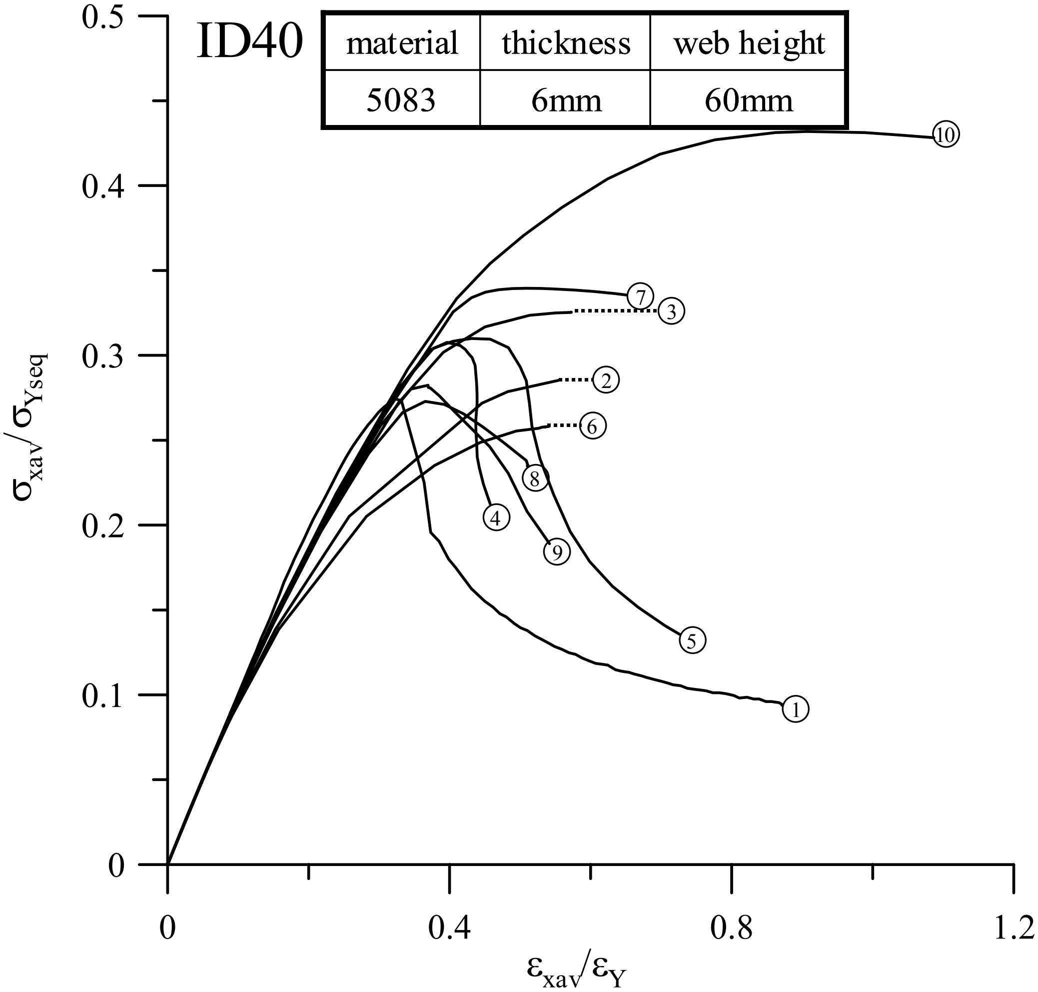

① Experiment, collapse mode III (CIP)

② 1 bay FEA(SPM), collapse mode III (CIP), column type initial deflection with CIP

③ 1 bay FEA(SPM), collapse mode III (CIP), column type initial deflection with CIS

④ 2 bay FEA(SPM), collapse mode III (CIP), column type initial deflection with CIP

⑤ 2 bay FEA(SPM), collapse mode V (CIS), column type initial deflection with CIS

⑥ 1 bay FEA(PSC), collapse mode III (CIP), column type initial deflection with CIP

⑦ 1 bay FEA(PSC), collapse mode III (CIP), column type initial deflection with CIS

⑧ 2 bay FEA(PSC), collapse mode III (CIP), column type initial deflection with CIP

⑨ 2 bay FEA(PSC), collapse mode V (CIS), column type initial deflection with CIS

⑩ 2 bay FEA(SPM), collapse mode III (CIP), column type initial deflection with CIP

(All edges simply supported keeping them straight)

Note: CIP = compression in plate side, CIS = compression in stiffener side

Figure 8.3(a) Comparison of FEA solutions as those obtained by 9 types of FE modeling together with test data for a 5083 panel with 6mm-thick and 60mm-web height (σ_{xav} =average axial stress, σ_{Yseq} =yield stress, ε_{xav} =average axial strain, $\varepsilon_Y = \sigma_{Yseq}/E$, E = elastic modulus)

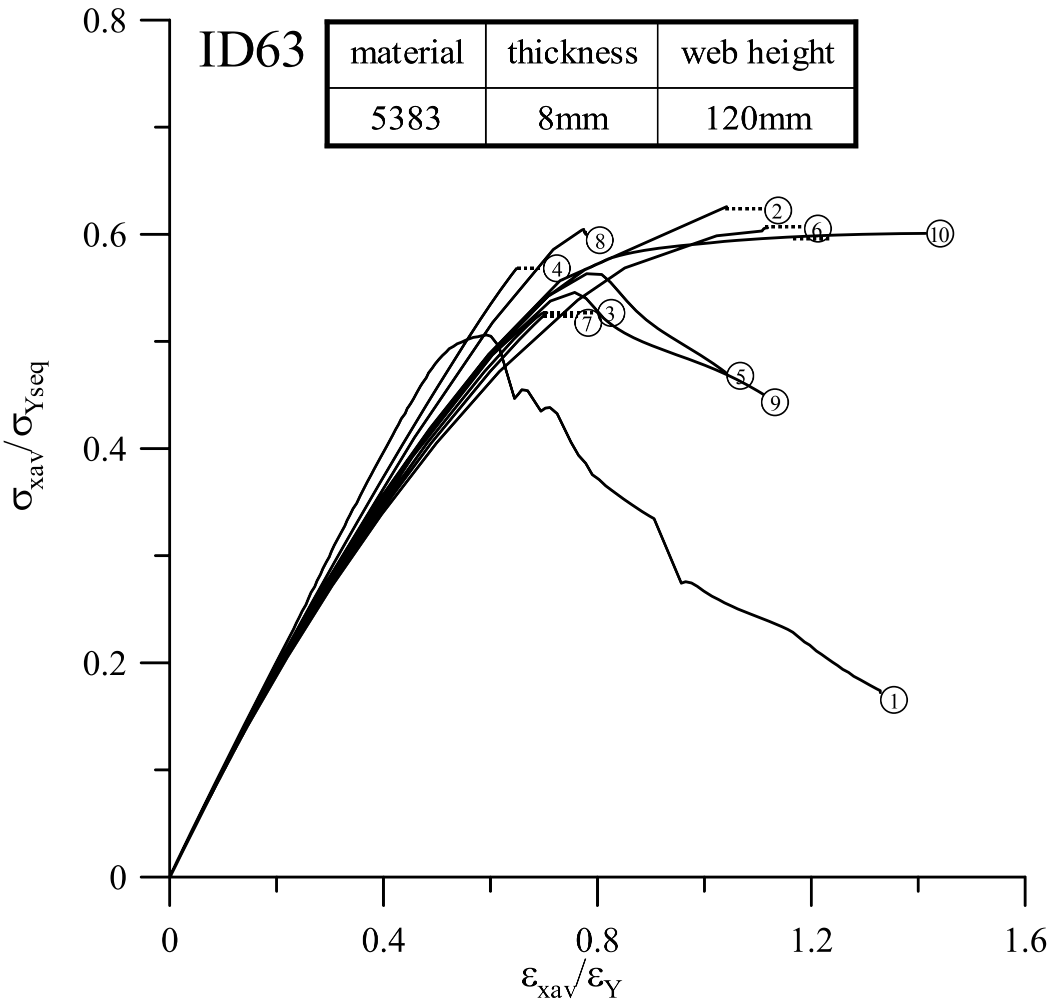

① Experiment, collapse mode V (CIS)

② 1 bay FEA(SPM), collapse mode III (CIP), column type initial deflection with CIP

③ 1 bay FEA(SPM), collapse mode V (CIS), column type initial deflection with CIS

④ 2 bay FEA(SPM), collapse mode III (CIP), column type initial deflection with CIP

⑤ 2 bay FEA(SPM), collapse mode V (CIS), column type initial deflection with CIS

⑥ 1 bay FEA(PSC), collapse mode III (CIP), column type initial deflection with CIP

⑦ 1 bay FEA(PSC), collapse mode V (CIS), column type initial deflection with CIS

⑧ 2 bay FEA(PSC), collapse mode III (CIP), column type initial deflection with CIP

⑨ 2 bay FEA(PSC), collapse mode V (CIS), column type initial deflection with CIS

⑩ 2 bay FEA(SPM), collapse mode V (CIS), column type initial deflection with CIS

(All edges simply supported keeping them straight)

Note: CIP = compression in plate side, CIS = compression in stiffener side

Figure 8.3(b) Comparison of FEA solutions as those obtained by 9 types of FE modeling together with test data for a 5383 panel with 8mm-thick and 120mm-web height (σ_{xav} = average axial stress, σ_{Yseq} = yield stress, ε_{xav} =average axial strain, $\varepsilon_{Y} = \sigma_{Yseq}/E$, E = elastic modulus)

ID 1

Plate		Stiffener				
t	Material	h_w	t_w	b_f	t_f	Material
5 mm	5083-H116	55.7 mm	3.7 mm	40 mm	6.7 mm	5383-H112

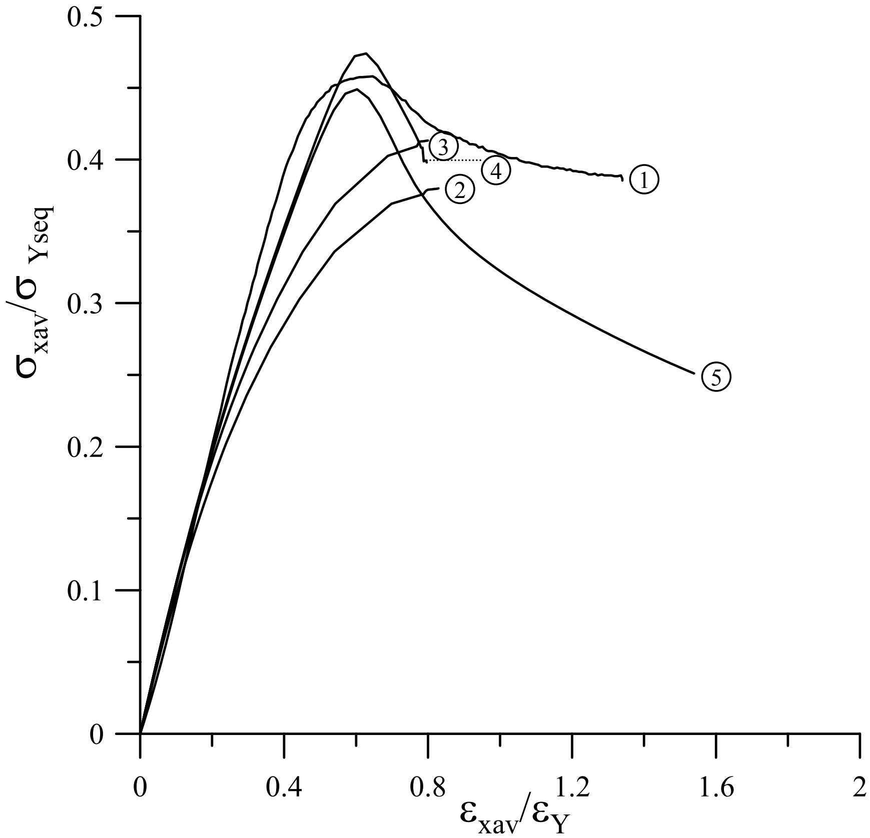

① Exp., collapse mode III (CIP)

② 1 bay FEA(PSC-model), collapse mode III (CIP), column type initial deflection with CIP

③ 1 bay FEA(PSC-model), collapse mode III (CIP), column type initial deflection with CIS

④ 2 bay FEA(PSC-model), collapse mode III (CIP), column type initial deflection with CIP

⑤ 2 bay FEA(PSC-model), collapse mode V (CIS), column type initial deflection with CIS

Note: CIP = compression in plate side, CIS = compression in stiffener side

Figure 8.4 The load-axial displacement curves for ID1

ID 2

Plate		Stiffener				
t	Material	h_w	t_w	b_f	t_f	Material
5 mm	5083-H116	66.1 mm	4 mm	40 mm	5.7 mm	5383-H112

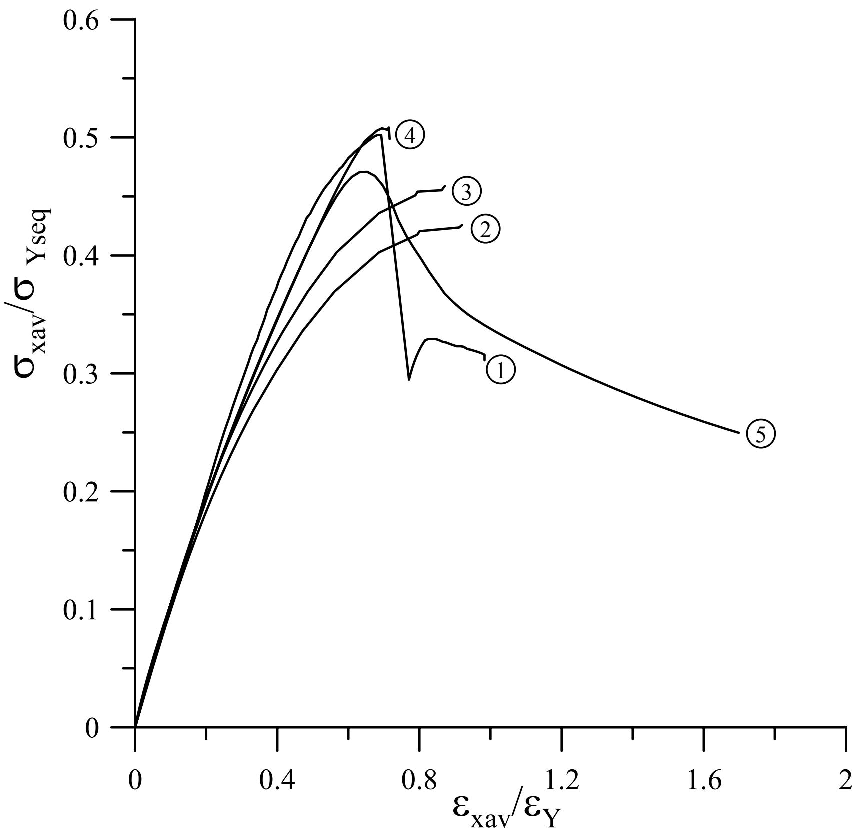

① Exp., collapse mode V (CIS)

② 1 bay FEA(PSC-model), collapse mode III (CIP), column type initial deflection with CIP

③ 1 bay FEA(PSC-model), collapse mode III (CIP), column type initial deflection with CIS

④ 2 bay FEA(PSC-model), collapse mode III (CIP), column type initial deflection with CIP

⑤ 2 bay FEA(PSC-model), collapse mode V (CIS), column type initial deflection with CIS

Note: CIP = compression in plate side, CIS = compression in stiffener side

Figure 8.5 The load-axial displacement curves for ID2

ID 3

Plate		Stiffener				
t	Material	h_w	t_w	b_f	t_f	Material
5 mm	5083-H116	76.8 mm	4 mm	45 mm	5.6 mm	5383-H112

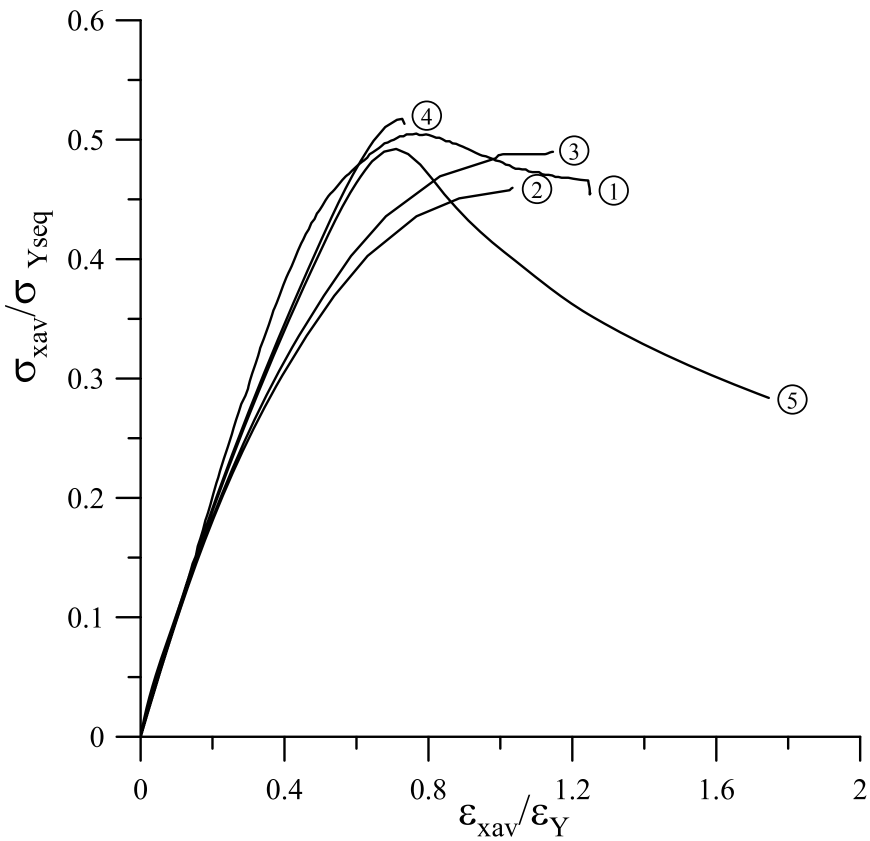

① Exp., collapse mode III (CIP), IV

② 1 bay FEA(PSC-model), collapse mode III (CIP), column type initial deflection with CIP

③ 1 bay FEA(PSC-model), collapse mode III (CIP), column type initial deflection with CIS

④ 2 bay FEA(PSC-model), collapse mode III (CIP), column type initial deflection with CIP

⑤ 2 bay FEA(PSC-model), collapse mode V (CIS), column type initial deflection with CIS

Note: CIP = compression in plate side, CIS = compression in stiffener side

Figure 8.6 The load-axial displacement curves for ID3

ID 4

Plate		Stiffener				
t	Material	h_w	t_w	b_f	t_f	Material
5 mm	5083-H116	135 mm	6 mm	55 mm	8.2 mm	5383-H112

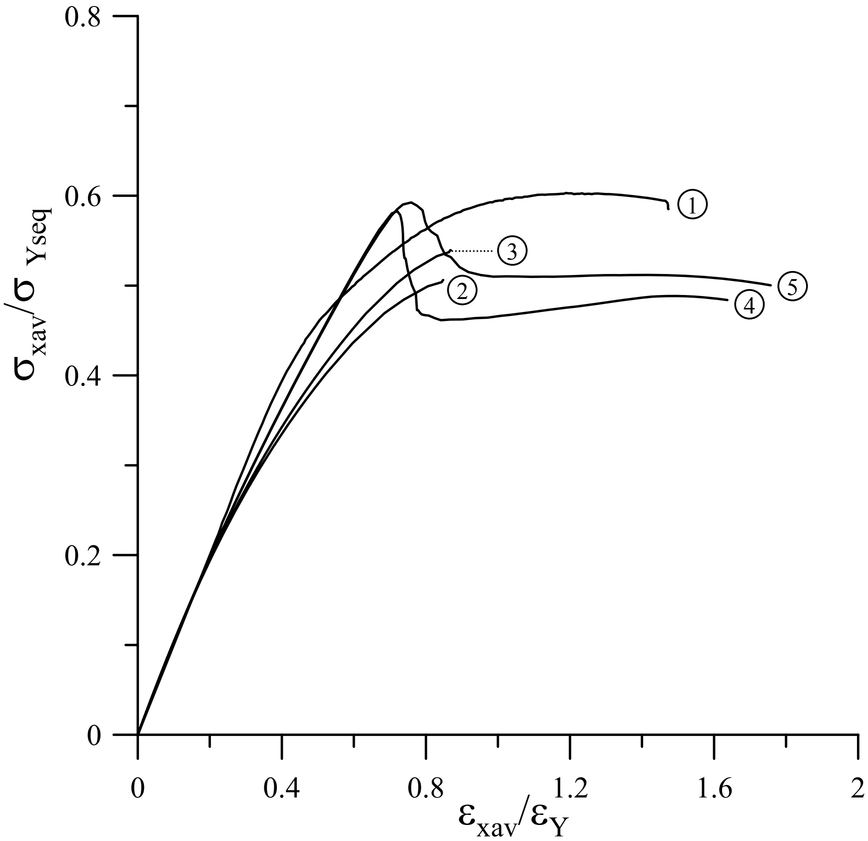

① Exp., collapse mode IV, V (CIS)

② 1 bay FEA(PSC-model), collapse mode III (CIP), column type initial deflection with CIP

③ 1 bay FEA(PSC-model), collapse mode III (CIP), column type initial deflection with CIS

④ 2 bay FEA(PSC-model), collapse mode V (CIS), column type initial deflection with CIP

⑤ 2 bay FEA(PSC-model), collapse mode V (CIS), column type initial deflection with CIS

Note: CIP = compression in plate side, CIS = compression in stiffener side

Figure 8.7 The load-axial displacement curves for ID4

ID 5

Plate		Stiffener				
t	Material	h_w	t_w	b_f	t_f	Material
6 mm	5083-H116	55.7 mm	3.7 mm	40 mm	6.7 mm	5383-H112

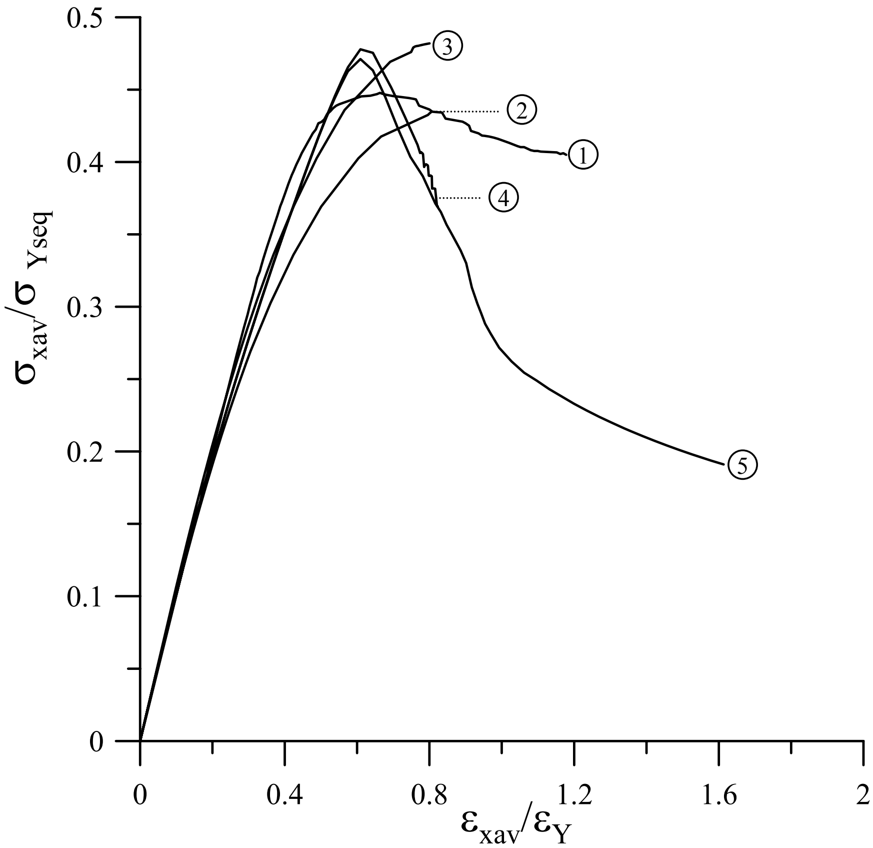

① Exp., collapse mode III (CIP)

② 1 bay FEA(PSC-model), collapse mode III (CIP), column type initial deflection with CIP

③ 1 bay FEA(PSC-model), collapse mode III (CIP), column type initial deflection with CIS

④ 2 bay FEA(PSC-model), collapse mode III (CIP), column type initial deflection with CIP

⑤ 2 bay FEA(PSC-model), collapse mode V (CIS), column type initial deflection with CIS

Note: CIP = compression in plate side, CIS = compression in stiffener side

Figure 8.8 The load-axial displacement curves for ID5

ID 6

Plate		Stiffener				
t	Material	h_w	t_w	b_f	t_f	Material
6 mm	5083-H116	66.1 mm	4 mm	40 mm	5.7 mm	5383-H112

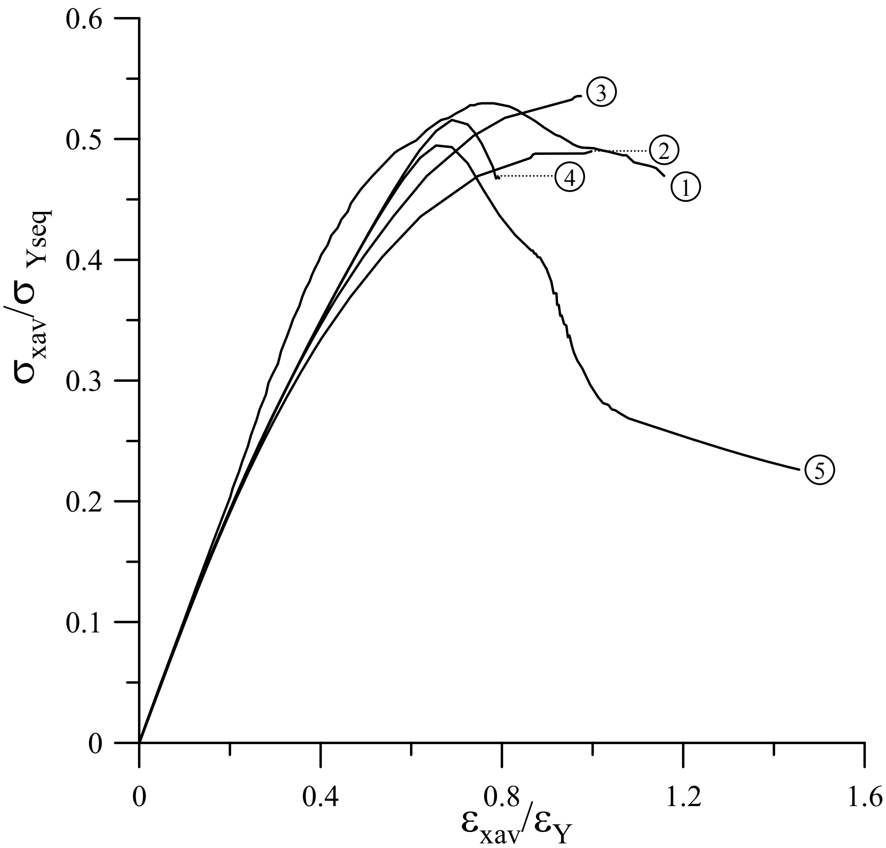

① Exp., collapse mode III (CIP)

② 1 bay FEA(PSC-model), collapse mode III (CIP), column type initial deflection with CIP

③ 1 bay FEA(PSC-model), collapse mode III (CIP), column type initial deflection with CIS

④ 2 bay FEA(PSC-model), collapse mode III (CIP), column type initial deflection with CIP

⑤ 2 bay FEA(PSC-model), collapse mode V (CIS), column type initial deflection with CIS

Note: CIP = compression in plate side, CIS = compression in stiffener side

Figure 8.9 The load-axial displacement curves for ID6

ID 7

Plate		Stiffener				
t	Material	h_w	t_w	b_f	t_f	Material
6 mm	5083-H116	76.8 mm	4 mm	45 mm	5.6 mm	5383-H112

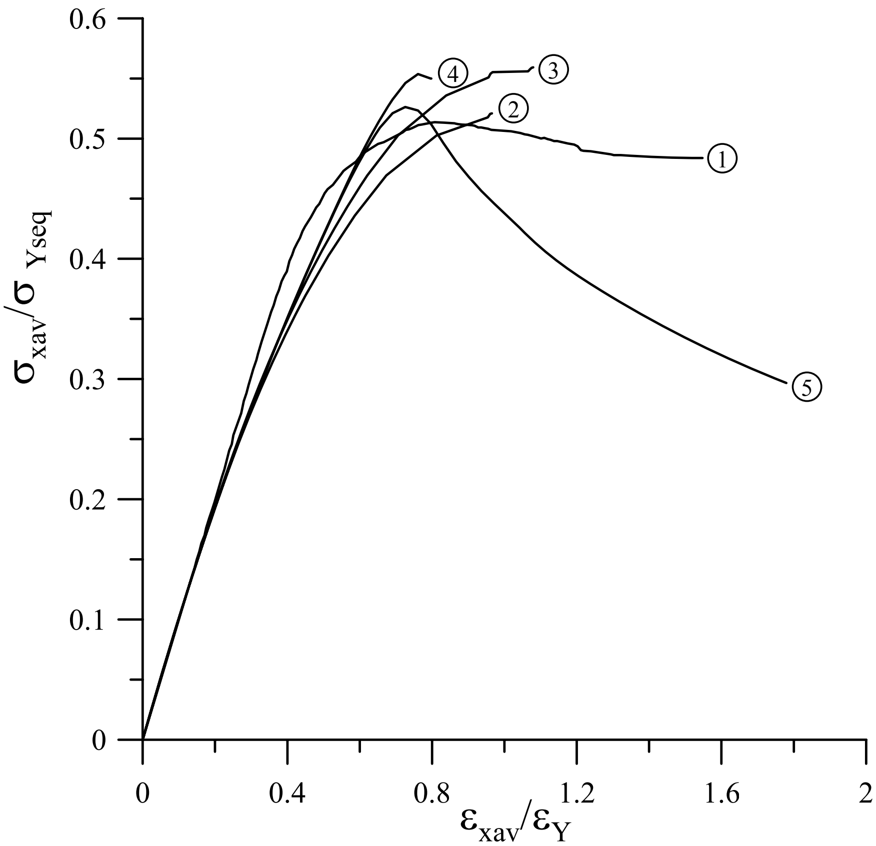

① Exp., collapse mode III (CIP)

② 1 bay FEA(PSC-model), collapse mode III (CIP), column type initial deflection with CIP

③ 1 bay FEA(PSC-model), collapse mode III (CIP), column type initial deflection with CIS

④ 2 bay FEA(PSC-model), collapse mode III (CIP), column type initial deflection with CIP

⑤ 2 bay FEA(PSC-model), collapse mode V (CIS), column type initial deflection with CIS

Note: CIP = compression in plate side, CIS = compression in stiffener side

Figure 8.10 The load-axial displacement curves for ID7

ID 8

Plate		Stiffener				
t	Material	h_w	t_w	b_f	t_f	Material
6 mm	5083-H116	135 mm	6 mm	55 mm	8.2 mm	5383-H112

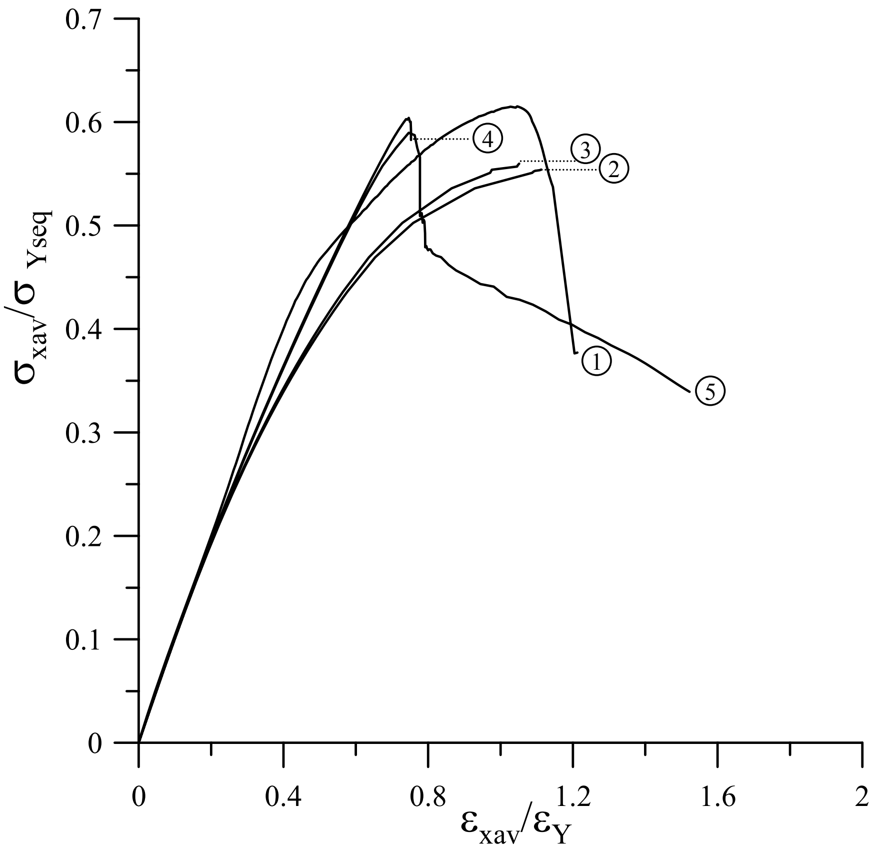

① Exp., collapse mode V (CIS)

② 1 bay FEA(PSC-model), collapse mode III (CIP), column type initial deflection with CIP

③ 1 bay FEA(PSC-model), collapse mode III (CIP), column type initial deflection with CIS

④ 2 bay FEA(PSC-model), collapse mode V (CIS), column type initial deflection with CIP

⑤ 2 bay FEA(PSC-model), collapse mode V (CIS), column type initial deflection with CIS

Note: CIP = compression in plate side, CIS = compression in stiffener side

Figure 8.11 The load-axial displacement curves for ID8

ID 9

Plate		Stiffener				
t	Material	h_w	t_w	b_f	t_f	Material
8 mm	5083-H116	55.7 mm	3.7 mm	40 mm	6.7 mm	5383-H112

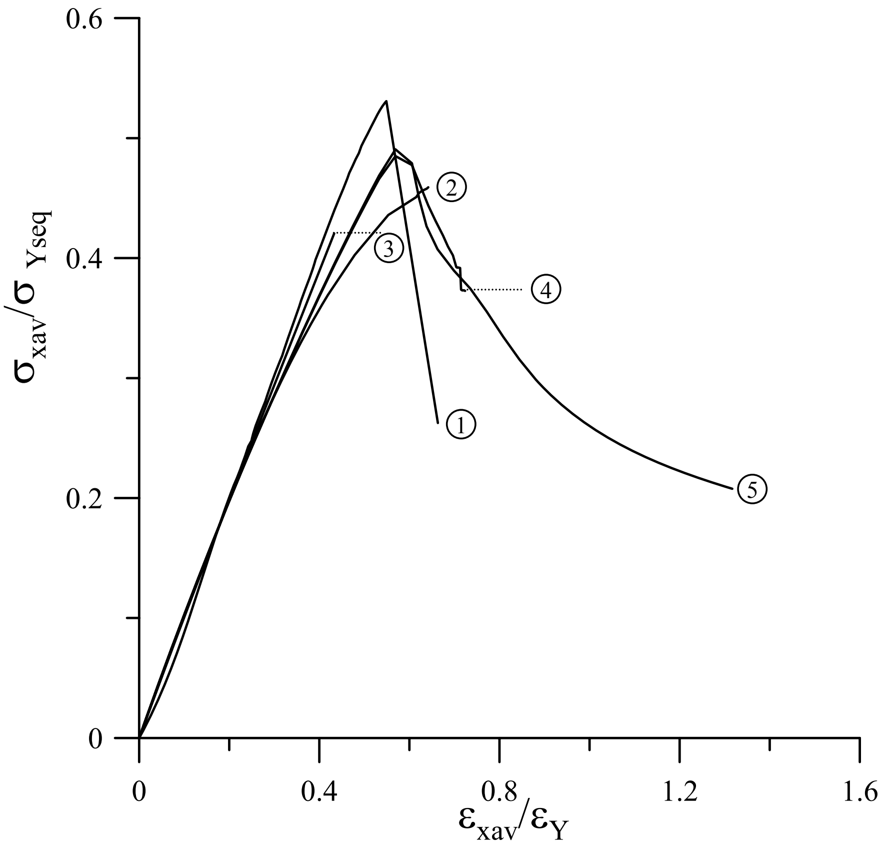

① Exp., collapse mode V (CIS)

② 1 bay FEA(PSC-model), collapse mode III (CIP), column type initial deflection with CIP

③ 1 bay FEA(PSC-model), collapse mode V (CIS), column type initial deflection with CIS

④ 2 bay FEA(PSC-model), collapse mode III (CIP), column type initial deflection with CIP

⑤ 2 bay FEA(PSC-model), collapse mode V (CIS), column type initial deflection with CIS

Note: CIP = compression in plate side, CIS = compression in stiffener side

Figure 8.12 The load-axial displacement curves for ID9

ID 10

Plate		Stiffener				
t	Material	h_w	t_w	b_f	t_f	Material
8 mm	5083-H116	66.1 mm	4 mm	40 mm	5.7 mm	5383-H112

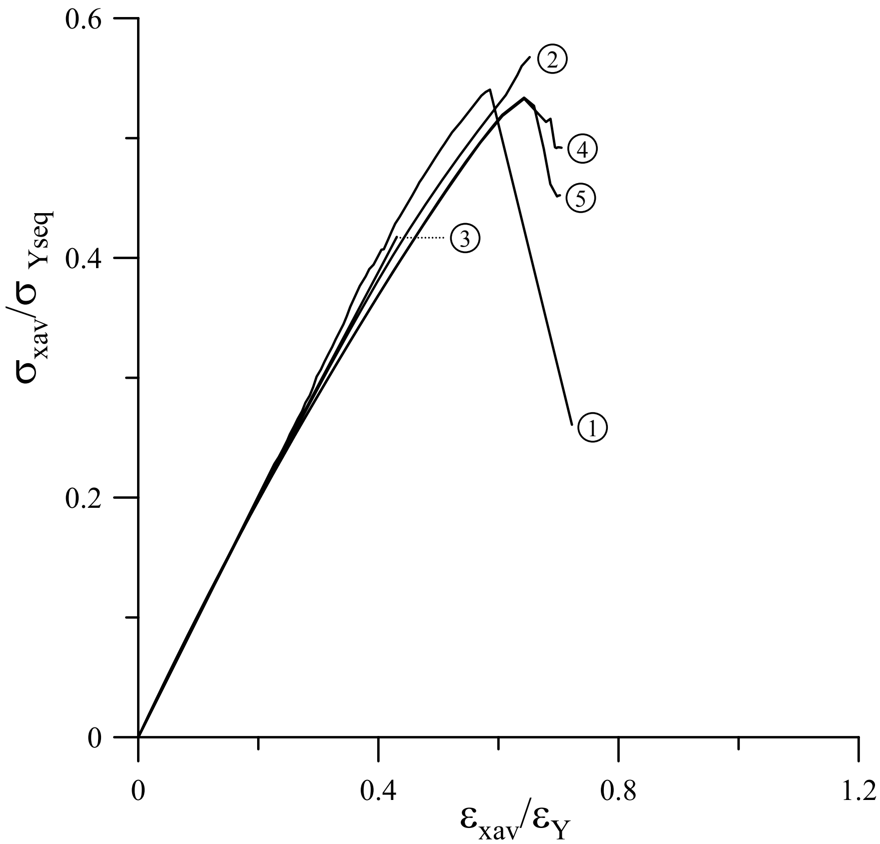

① Exp., collapse mode V (CIS)

② 1 bay FEA(PSC-model), collapse mode V (CIS), column type initial deflection with CIP

③ 1 bay FEA(PSC-model), collapse mode V (CIS), column type initial deflection with CIS

④ 2 bay FEA(PSC-model), collapse mode III (CIP), column type initial deflection with CIP

⑤ 2 bay FEA(PSC-model), collapse mode V (CIS), column type initial deflection with CIS

Note: CIP = compression in plate side, CIS = compression in stiffener side

Figure 8.13 The load-axial displacement curves for ID10

ID 11

Plate		Stiffener				
t	Material	h_w	t_w	b_f	t_f	Material
8 mm	5083-H116	76.8 mm	4 mm	45 mm	5.6 mm	5383-H112

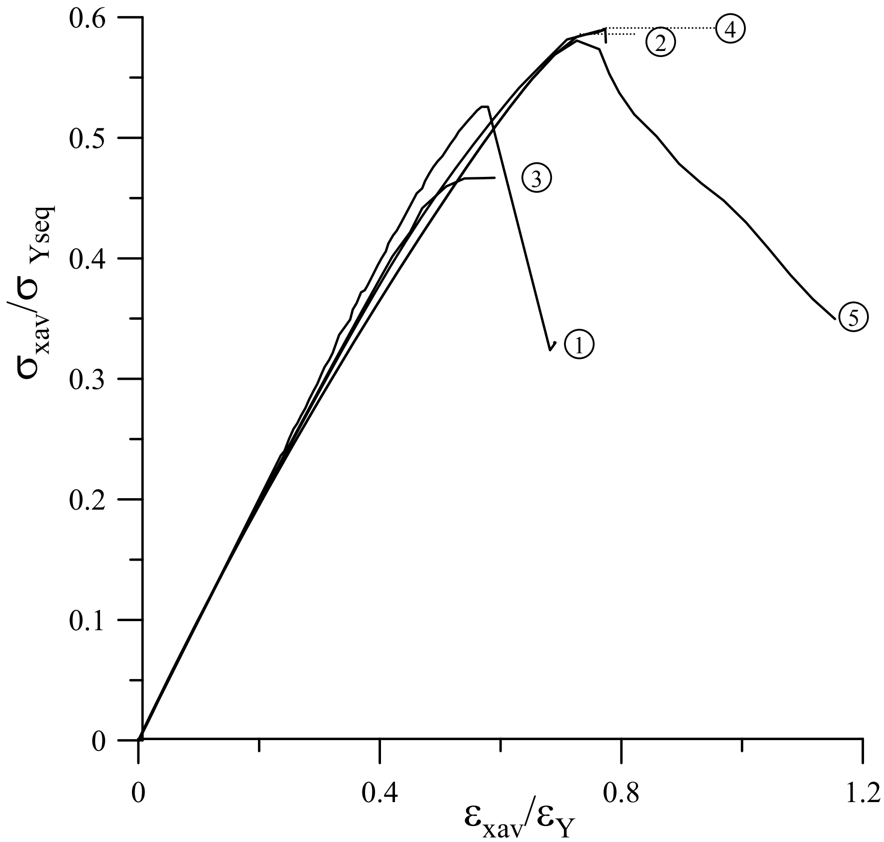

① Exp., collapse mode V (CIS)

② 1 bay FEA(PSC-model), collapse mode V (CIS), column type initial deflection with CIP

③ 1 bay FEA(PSC-model), collapse mode V (CIS), column type initial deflection with CIS

④ 2 bay FEA(PSC-model), collapse mode III (CIP), column type initial deflection with CIP

⑤ 2 bay FEA(PSC-model), collapse mode V (CIS), column type initial deflection with CIS

Note: CIP = compression in plate side, CIS = compression in stiffener side

Figure 8.14 The load-axial displacement curves for ID11

ID 12

Plate		Stiffener				
t	Material	h_w	t_w	b_f	t_f	Material
8 mm	5083-H116	135 mm	6 mm	55 mm	8.2 mm	5383-H112

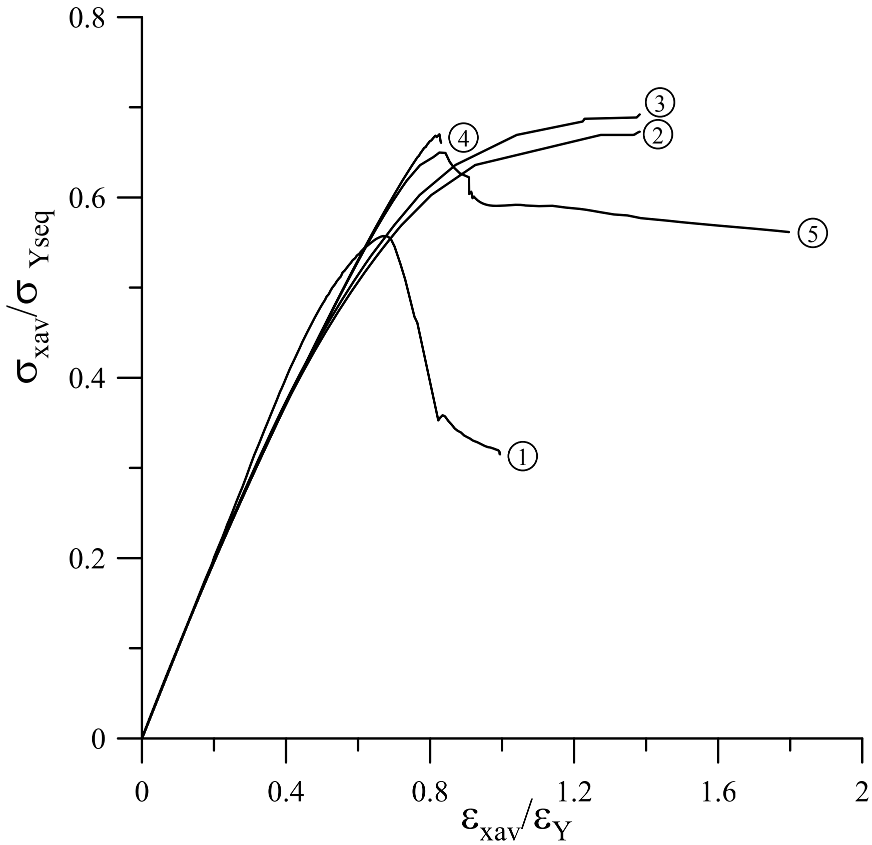

① Exp., collapse mode V (CIS)

② 1 bay FEA(PSC-model), collapse mode III (CIP), column type initial deflection with CIP

③ 1 bay FEA(PSC-model), collapse mode III (CIP), column type initial deflection with CIS

④ 2 bay FEA(PSC-model), collapse mode V (CIS), column type initial deflection with CIP

⑤ 2 bay FEA(PSC-model), collapse mode V (CIS), column type initial deflection with CIS

Note: CIP = compression in plate side, CIS = compression in stiffener side

Figure 8.15 The load-axial displacement curves for ID12

ID 13

Plate		Stiffener				
t	Material	h_w	t_w	b_f	t_f	Material
5 mm	5083-H116	55.7 mm	3.7 mm	40 mm	6.7 mm	6082-T6

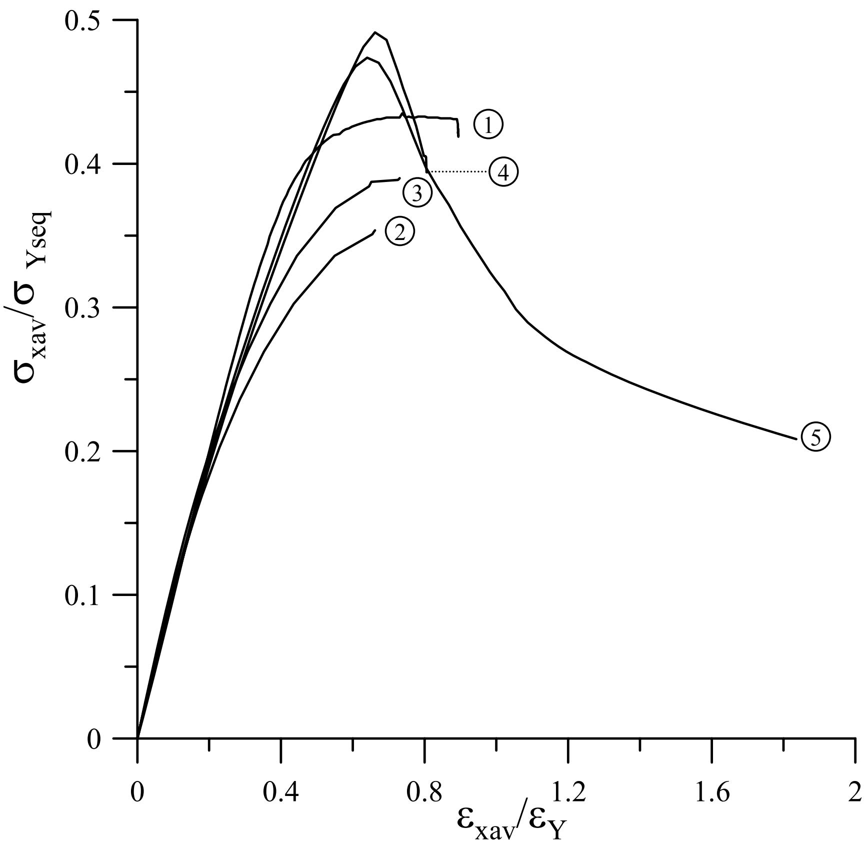

① Exp., collapse mode III (CIP)

② 1 bay FEA(PSC-model), collapse mode III (CIP), column type initial deflection with CIP

③ 1 bay FEA(PSC-model), collapse mode III (CIP), column type initial deflection with CIS

④ 2 bay FEA(PSC-model), collapse mode III (CIP), column type initial deflection with CIP

⑤ 2 bay FEA(PSC-model), collapse mode V (CIS), column type initial deflection with CIS

Note: CIP = compression in plate side, CIS = compression in stiffener side

Figure 8.16 The load-axial displacement curves for ID13

ID 14

Plate		Stiffener				
t	Material	h_w	t_w	b_f	t_f	Material
5 mm	5083-H116	66.1 mm	4 mm	40 mm	5.7 mm	6082-T6

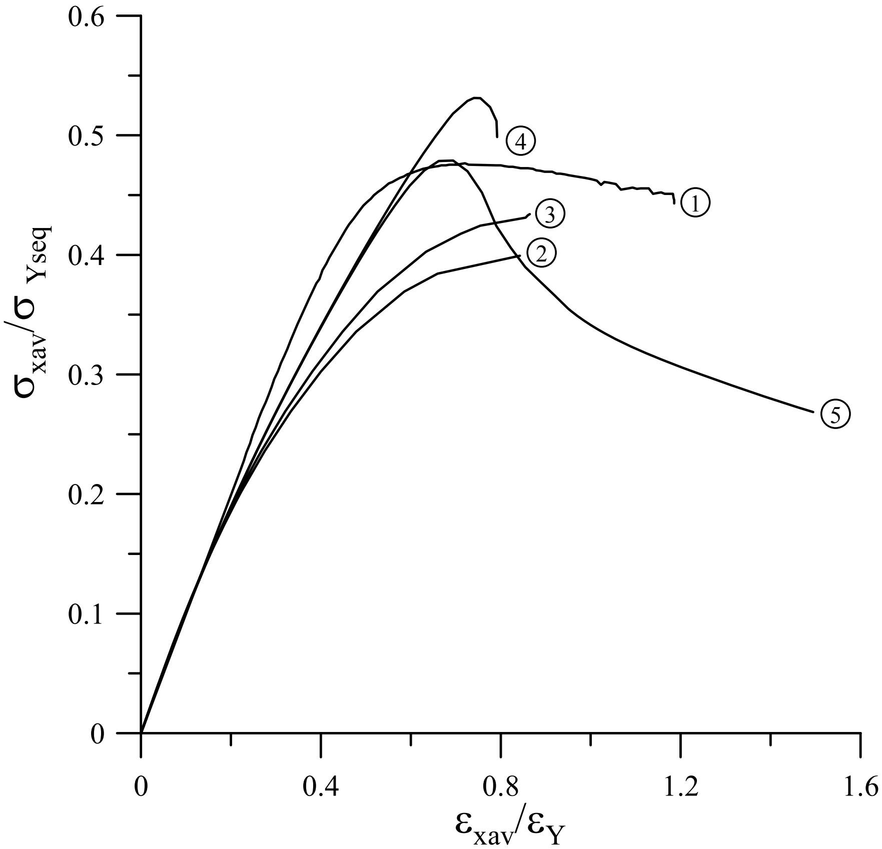

① Exp., collapse mode III (CIP)

② 1 bay FEA(PSC-model), collapse mode III (CIP), column type initial deflection with CIP

③ 1 bay FEA(PSC-model), collapse mode III (CIP), column type initial deflection with CIS

④ 2 bay FEA(PSC-model), collapse mode III (CIP), column type initial deflection with CIP

⑤ 2 bay FEA(PSC-model), collapse mode V (CIS), column type initial deflection with CIS

Note: CIP = compression in plate side, CIS = compression in stiffener side

Figure 8.17 The load-axial displacement curves for ID14

ID 15

Plate		Stiffener				
t	Material	h_w	t_w	b_f	t_f	Material
5 mm	5083-H116	76.8 mm	4 mm	45 mm	5.6 mm	6082-T6

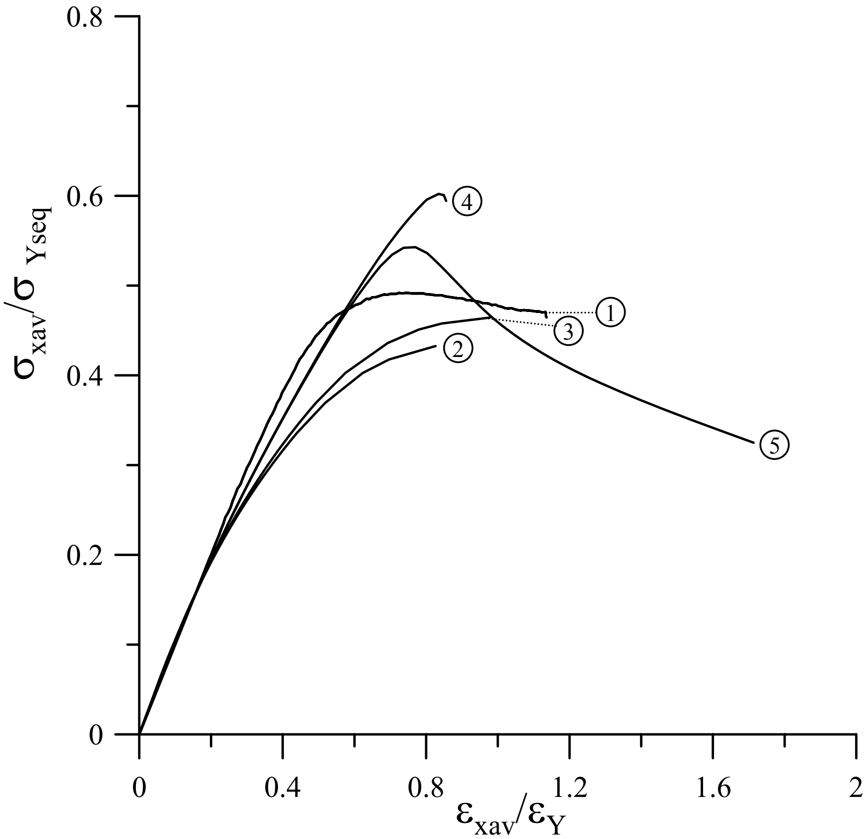

① Exp., collapse mode III (CIP), IV

② 1 bay FEA(PSC-model), collapse mode III (CIP), column type initial deflection with CIP

③ 1 bay FEA(PSC-model), collapse mode III (CIP), column type initial deflection with CIS

④ 2 bay FEA(PSC-model), collapse mode III (CIP), column type initial deflection with CIP

⑤ 2 bay FEA(PSC-model), collapse mode V (CIS), column type initial deflection with CIS

Note: CIP = compression in plate side, CIS = compression in stiffener side

Figure 8.18 The load-axial displacement curves for ID15

ID 16

Plate		Stiffener				
t	Material	h_w	t_w	b_f	t_f	Material
5 mm	5083-H116	135 mm	6 mm	55 mm	8.2 mm	6082-T6

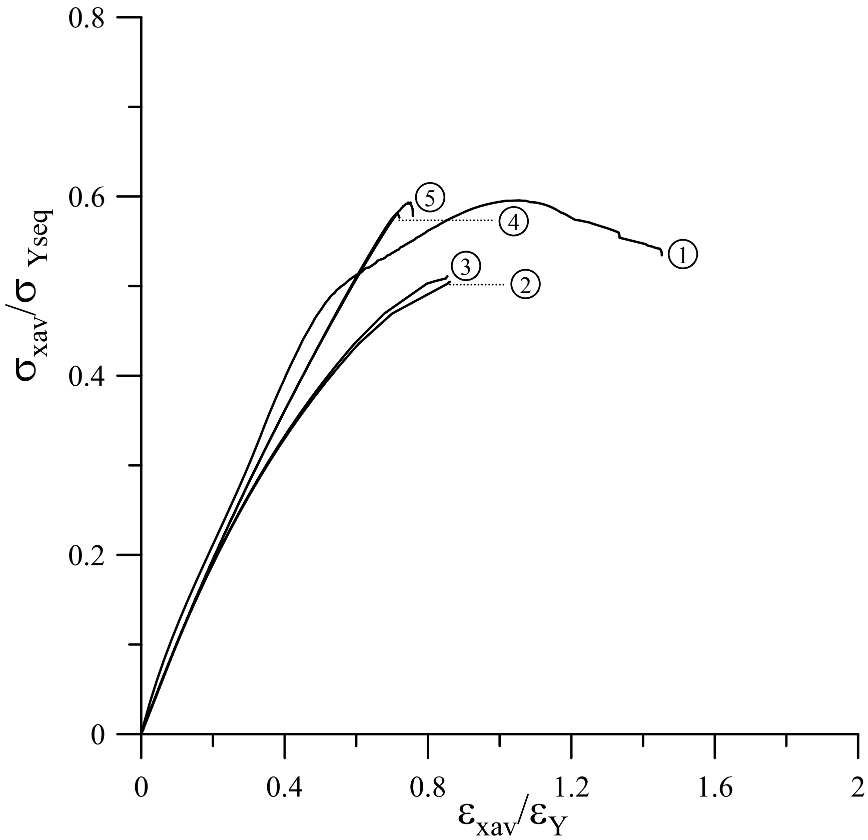

① Exp., collapse mode III (CIP), IV

② 1 bay FEA(PSC-model), collapse mode III (CIP), column type initial deflection with CIP

③ 1 bay FEA(PSC-model), collapse mode III (CIP), column type initial deflection with CIS

④ 2 bay FEA(PSC-model), collapse mode V (CIS), column type initial deflection with CIP

⑤ 2 bay FEA(PSC-model), collapse mode V (CIS), column type initial deflection with CIS

Note: CIP = compression in plate side, CIS = compression in stiffener side

Figure 8.19 The load-axial displacement curves for ID16

ID 17

Plate		Stiffener				
t	Material	h_w	t_w	b_f	t_f	Material
6 mm	5083-H116	55.7 mm	3.7 mm	40 mm	6.7 mm	6082-T6

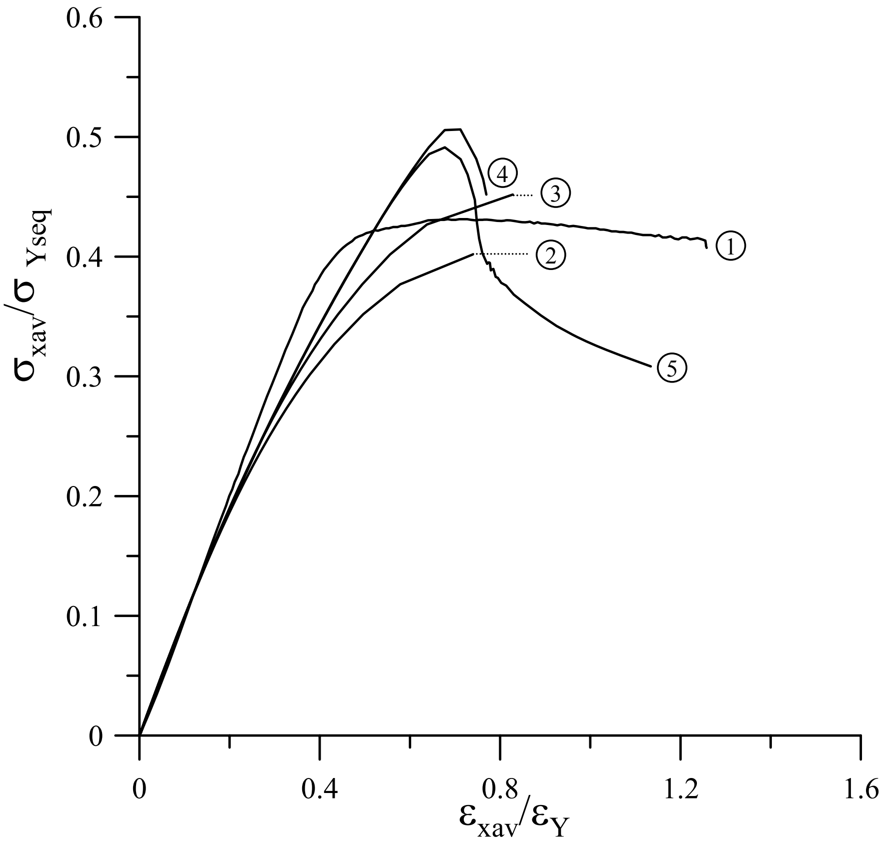

① Exp., collapse mode III (CIP)

② 1 bay FEA(PSC-model), collapse mode III (CIP), column type initial deflection with CIP

③ 1 bay FEA(PSC-model), collapse mode III (CIP), column type initial deflection with CIS

④ 2 bay FEA(PSC-model), collapse mode III (CIP), column type initial deflection with CIP

⑤ 2 bay FEA(PSC-model), collapse mode V (CIS), column type initial deflection with CIS

Note: CIP = compression in plate side, CIS = compression in stiffener side

Figure 8.20 The load-axial displacement curves for ID17

ID 18

Plate		Stiffener				
t	Material	h_w	t_w	b_f	t_f	Material
6 mm	5083-H116	66.1 mm	4 mm	40 mm	5.7 mm	6082-T6

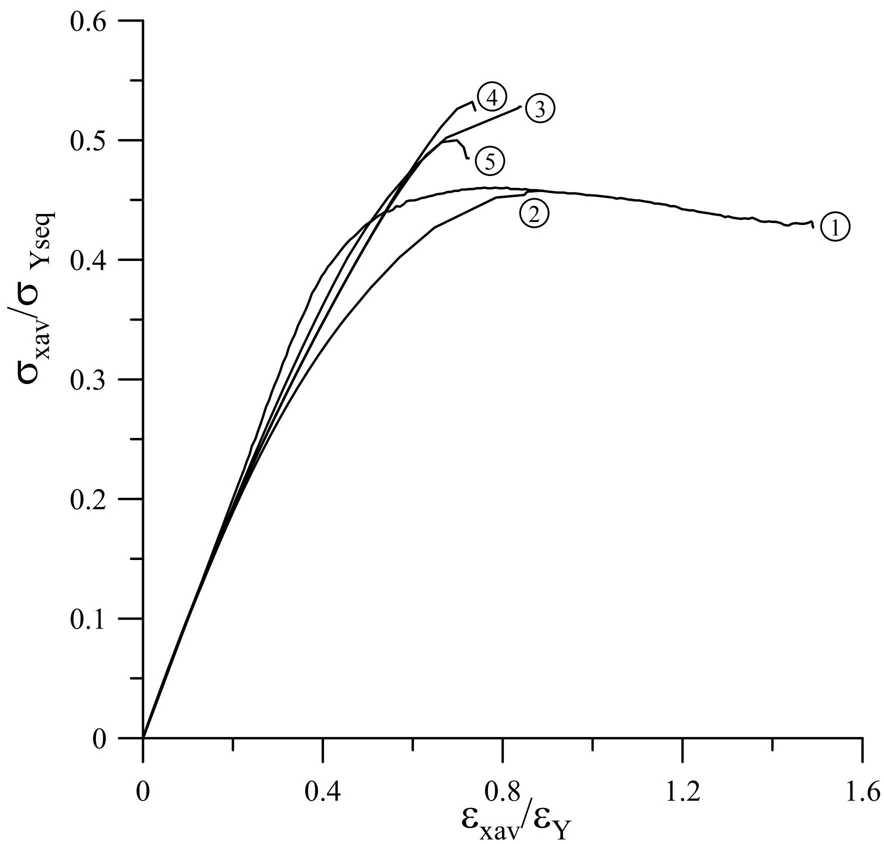

① Exp., collapse mode III (CIP)

② 1 bay FEA(PSC-model), collapse mode III (CIP), column type initial deflection with CIP

③ 1 bay FEA(PSC-model), collapse mode III (CIP), column type initial deflection with CIS

④ 2 bay FEA(PSC-model), collapse mode III (CIP), column type initial deflection with CIP

⑤ 2 bay FEA(PSC-model), collapse mode V (CIS), column type initial deflection with CIS

Note: CIP = compression in plate side, CIS = compression in stiffener side

Figure 8.21 The load-axial displacement curves for ID18

ID 19

Plate		Stiffener				
t	Material	h_w	t_w	b_f	t_f	Material
6 mm	5083-H116	76.8 mm	4 mm	45 mm	5.6 mm	6082-T6

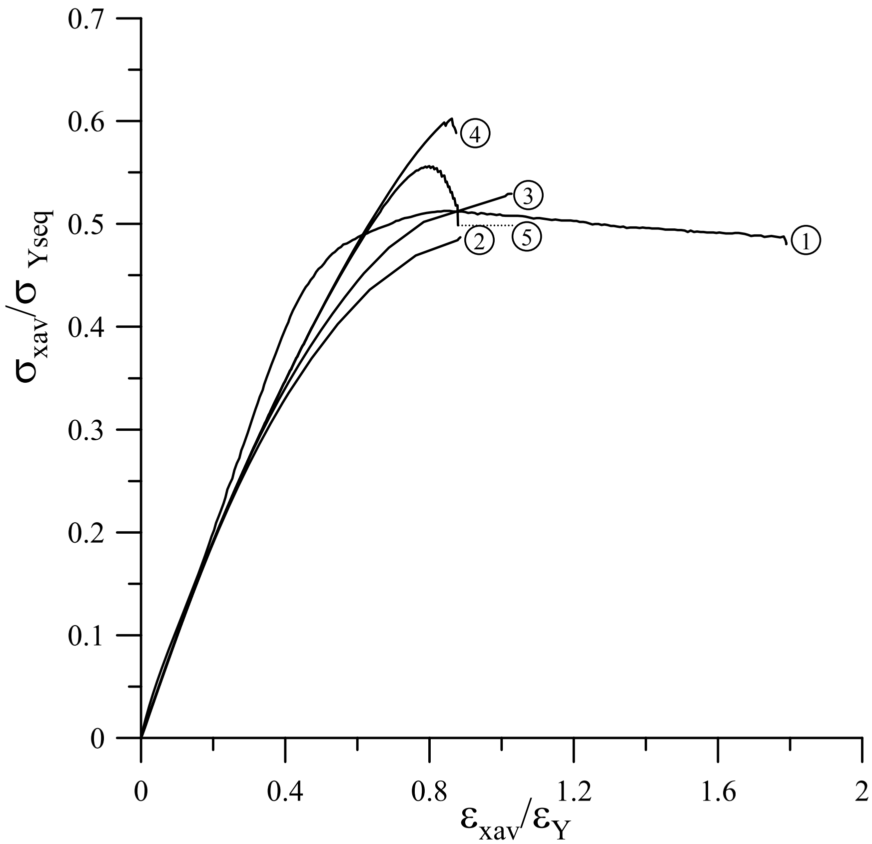

①Exp., collapse mode III (CIP), IV

② 1 bay FEA(PSC-model), collapse mode III (CIP), column type initial deflection with CIP

③ 1 bay FEA(PSC-model), collapse mode III (CIP), column type initial deflection with CIS

④ 2 bay FEA(PSC-model), collapse mode III (CIP), column type initial deflection with CIP

⑤ 2 bay FEA(PSC-model), collapse mode V (CIS), column type initial deflection with CIS

Note: CIP = compression in plate side, CIS = compression in stiffener side

Figure 8.22 The load-axial displacement curves for ID19

ID 20

Plate		Stiffener				
t	Material	h_w	t_w	b_f	t_f	Material
6 mm	5083-H116	135 mm	6 mm	55 mm	8.2 mm	6082-T6

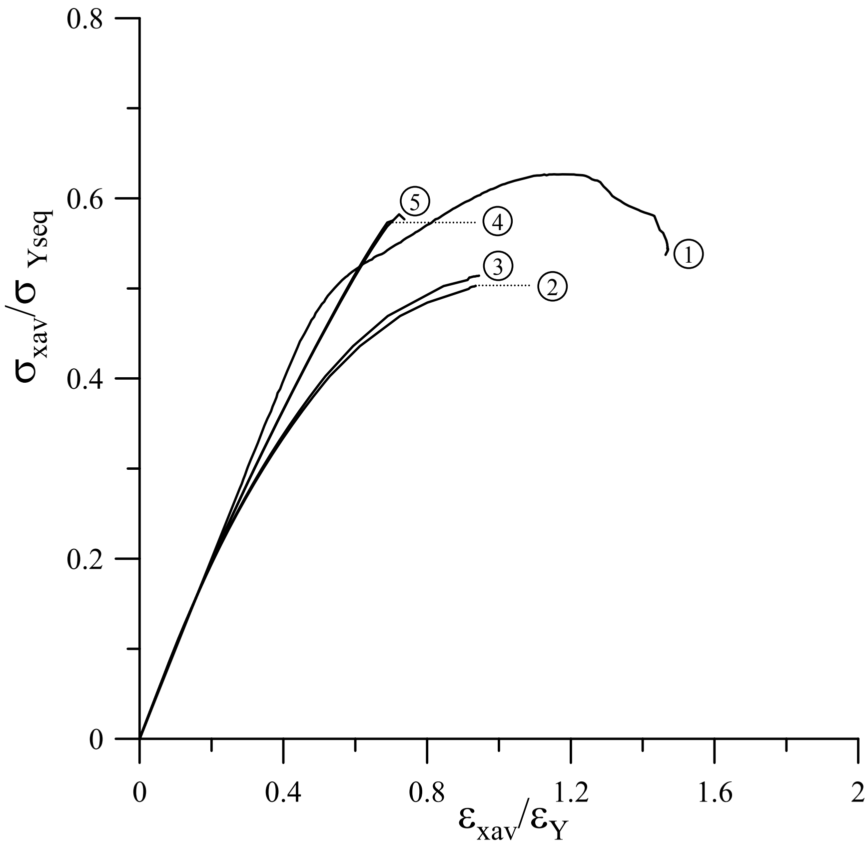

① Exp., collapse mode III (CIP), IV

② 1 bay FEA(PSC-model), collapse mode III (CIP), column type initial deflection with CIP

③ 1 bay FEA(PSC-model), collapse mode III (CIP), column type initial deflection with CIS

④ 2 bay FEA(PSC-model), collapse mode V (CIS), column type initial deflection with CIP

⑤ 2 bay FEA(PSC-model), collapse mode V (CIS), column type initial deflection with CIS

Note: CIP = compression in plate side, CIS = compression in stiffener side

Figure 8.23 The load-axial displacement curves for ID20

ID 21

Plate		Stiffener				
t	Material	h_w	t_w	b_f	t_f	Material
8 mm	5083-H116	55.7 mm	3.7 mm	40 mm	6.7 mm	6082-T6

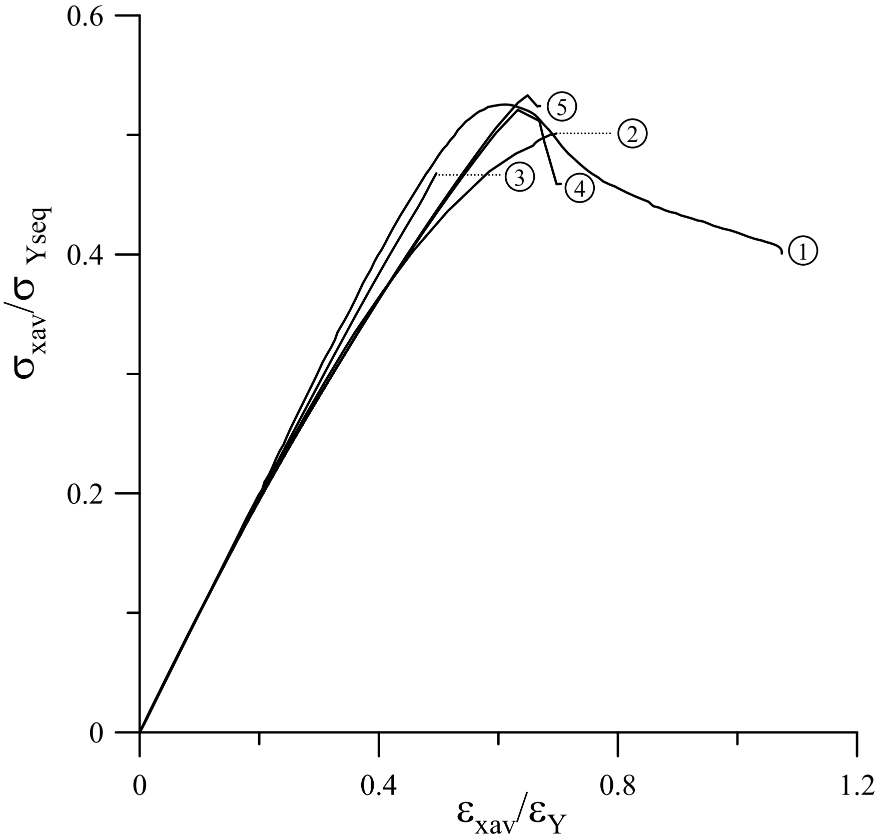

① Exp., collapse mode III (CIP)

② 1 bay FEA(PSC-model), collapse mode III (CIP), column type initial deflection with CIP

③ 1 bay FEA(PSC-model), collapse mode V (CIS), column type initial deflection with CIS

④ 2 bay FEA(PSC-model), collapse mode III (CIP), column type initial deflection with CIP

⑤ 2 bay FEA(PSC-model), collapse mode V (CIS), column type initial deflection with CIS

Note: CIP = compression in plate side, CIS = compression in stiffener side

Figure 8.24 The load-axial displacement curves for ID21

ID 22

Plate		Stiffener				
t	Material	h_w	t_w	b_f	t_f	Material
8 mm	5083-H116	66.1 mm	4 mm	40 mm	5.7 mm	6082-T6

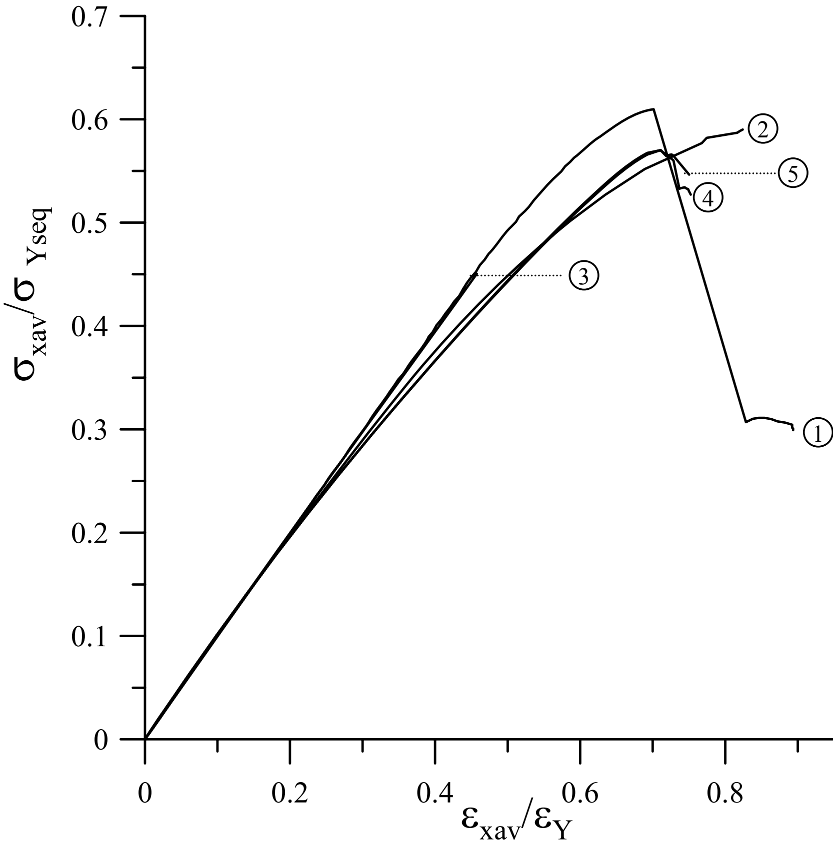

① Exp., collapse mode V (CIS)

② 1 bay FEA(PSC-model), collapse mode III (CIP), column type initial deflection with CIP

③ 1 bay FEA(PSC-model), collapse mode V (CIS), column type initial deflection with CIS

④ 2 bay FEA(PSC-model), collapse mode III (CIP), column type initial deflection with CIP

⑤ 2 bay FEA(PSC-model), collapse mode V (CIS), column type initial deflection with CIS

Note: CIP = compression in plate side, CIS = compression in stiffener side

Figure 8.25 The load-axial displacement curves for ID22

ID 23

Plate		Stiffener				
t	Material	h_w	t_w	b_f	t_f	Material
8 mm	5083-H116	76.8 mm	4 mm	45 mm	5.6 mm	6082-T6

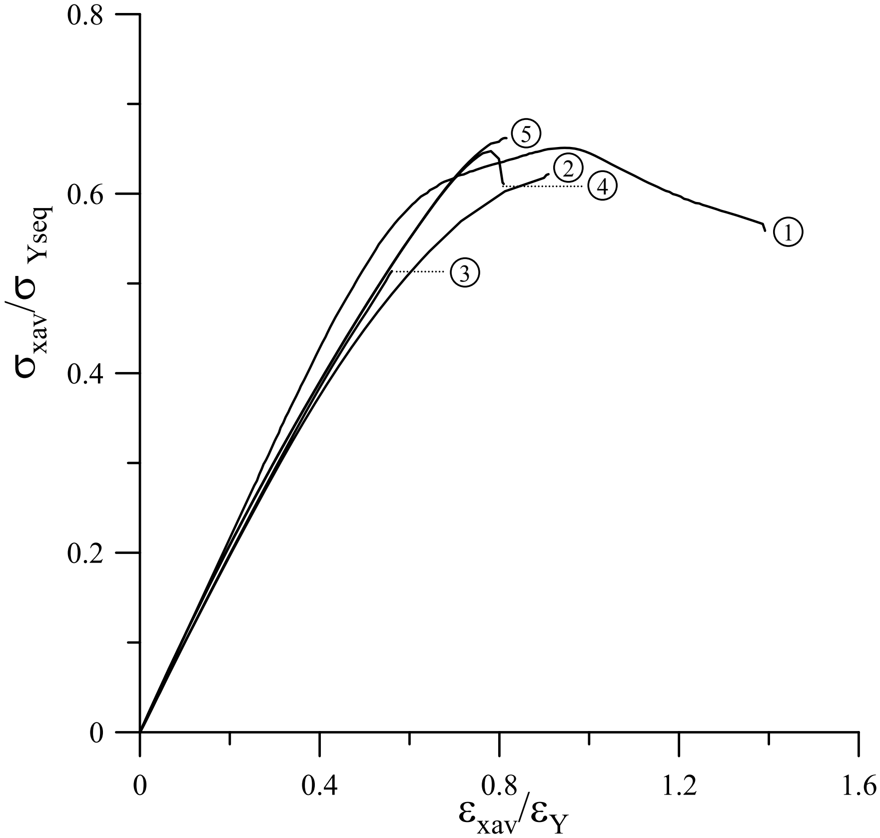

① Exp., collapse mode IV, V (CIS)

② 1 bay FEA(PSC-model), collapse mode III (CIP), column type initial deflection with CIP

③ 1 bay FEA(PSC-model), collapse mode V (CIS), column type initial deflection with CIS

④ 2 bay FEA(PSC-model), collapse mode III (CIP), column type initial deflection with CIP

⑤ 2 bay FEA(PSC-model), collapse mode V (CIS), column type initial deflection with CIS

Note: CIP = compression in plate side, CIS = compression in stiffener side

Figure 8.26 The load-axial displacement curves for ID23

ID 24

Plate		Stiffener				
t	Material	h_w	t_w	b_f	t_f	Material
8 mm	5083-H116	135 mm	6 mm	55 mm	8.2 mm	6082-T6

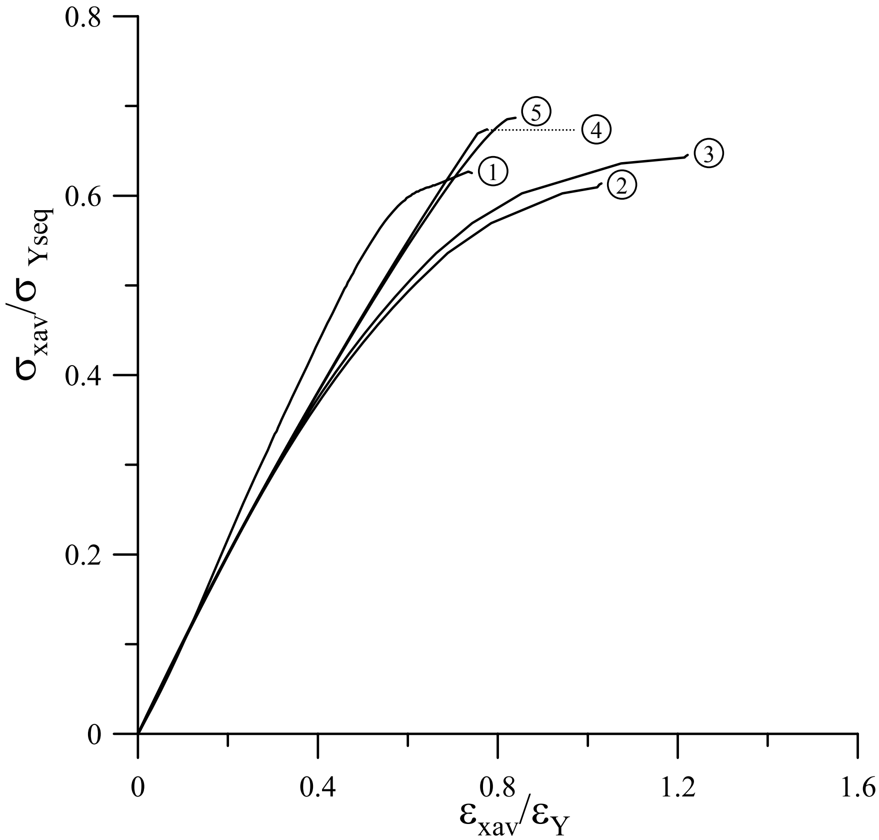

① Exp., collapse mode III (CIP), IV

② 1 bay FEA(PSC-model), collapse mode III (CIP), column type initial deflection with CIP

③ 1 bay FEA(PSC-model), collapse mode III (CIP), column type initial deflection with CIS

④ 2 bay FEA(PSC-model), collapse mode V (CIS), column type initial deflection with CIP

⑤ 2 bay FEA(PSC-model), collapse mode V (CIS), column type initial deflection with CIS

Note: CIP = compression in plate side, CIS = compression in stiffener side

Figure 8.27 The load-axial displacement curves for ID24

ID 25

Plate		Stiffener				
t	Material	h_w	t_w	b_f	t_f	Material
8 mm	5383-H116	55.7 mm	3.7 mm	40 mm	6.7 mm	5383-H112

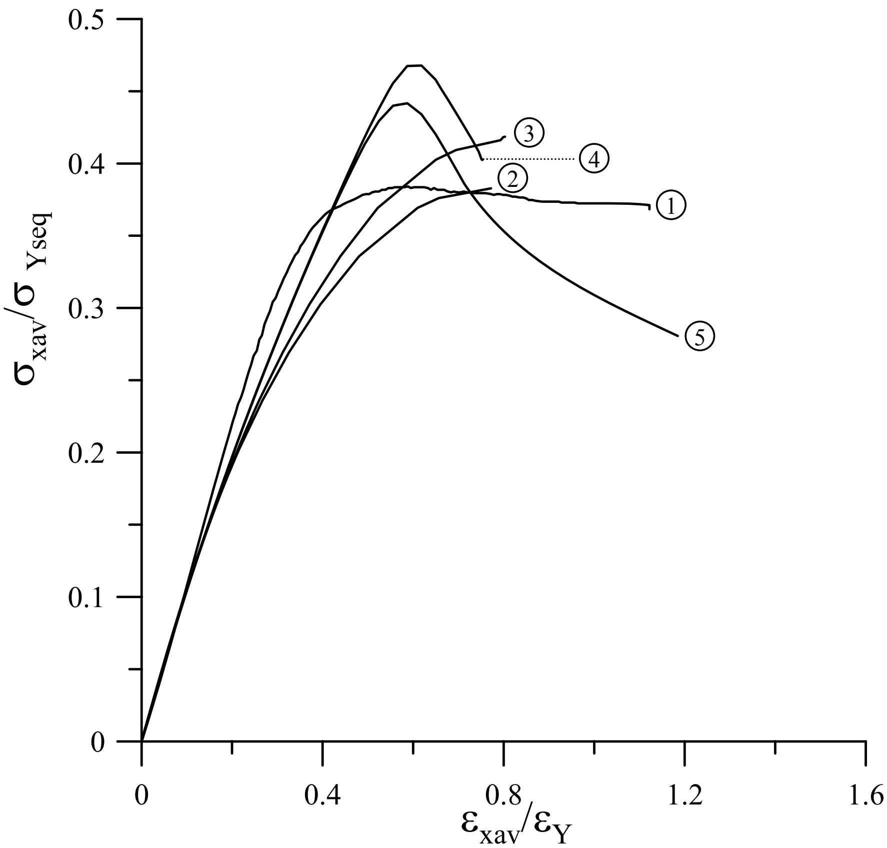

①Exp., collapse mode III (CIP)

②1 bay FEA(PSC-model), collapse mode III (CIP), column type initial deflection with CIP

③1 bay FEA(PSC-model), collapse mode III (CIP), column type initial deflection with CIS

④2 bay FEA(PSC-model), collapse mode III (CIP), column type initial deflection with CIP

⑤2 bay FEA(PSC-model), collapse mode V (CIS), column type initial deflection with CIS

Note: CIP = compression in plate side, CIS = compression in stiffener side

Figure 8.28 The load-axial displacement curves for ID25

ID 26

Plate		Stiffener				
t	Material	h_w	t_w	b_f	t_f	Material
5 mm	5383-H116	66.1 mm	4 mm	40 mm	5.7 mm	5383-H112

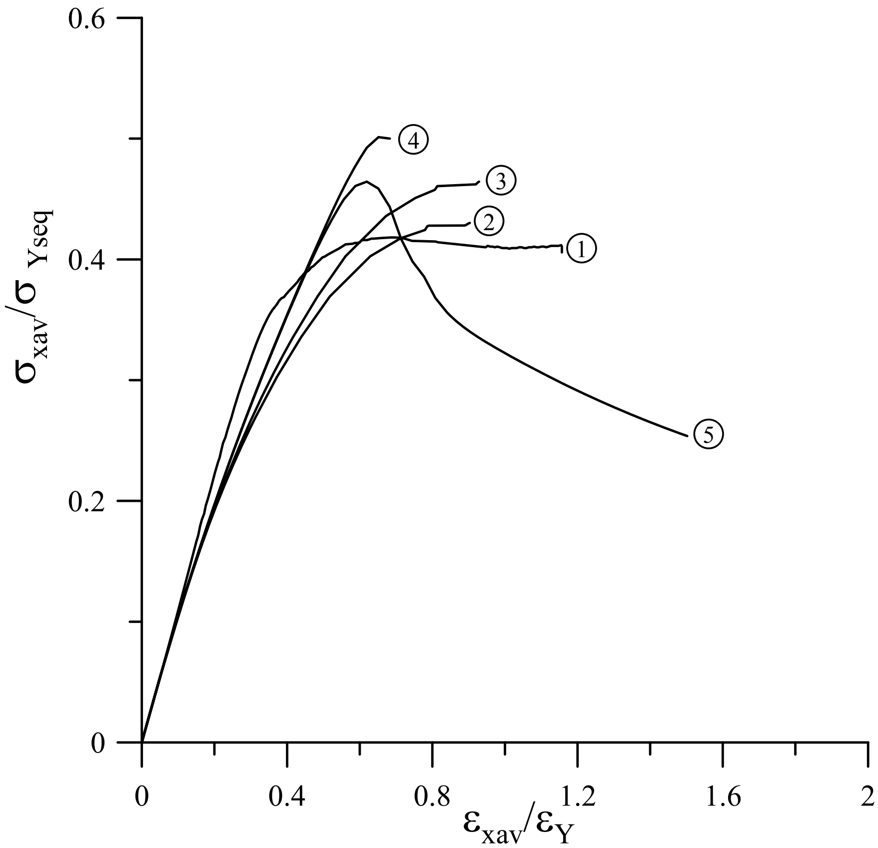

① Exp., collapse mode III (CIP)

② 1 bay FEA(PSC-model), collapse mode III (CIP), column type initial deflection with CIP

③ 1 bay FEA(PSC-model), collapse mode III (CIP), column type initial deflection with CIS

④ 2 bay FEA(PSC-model), collapse mode III (CIP), column type initial deflection with CIP

⑤ 2 bay FEA(PSC-model), collapse mode V (CIS), column type initial deflection with CIS

Note: CIP = compression in plate side, CIS = compression in stiffener side

Figure 8.29 The load-axial displacement curves for ID26

ID 27

Plate		Stiffener				
t	Material	h_w	t_w	b_f	t_f	Material
5 mm	5383-H116	76.8 mm	4 mm	45 mm	5.6 mm	5383-H112

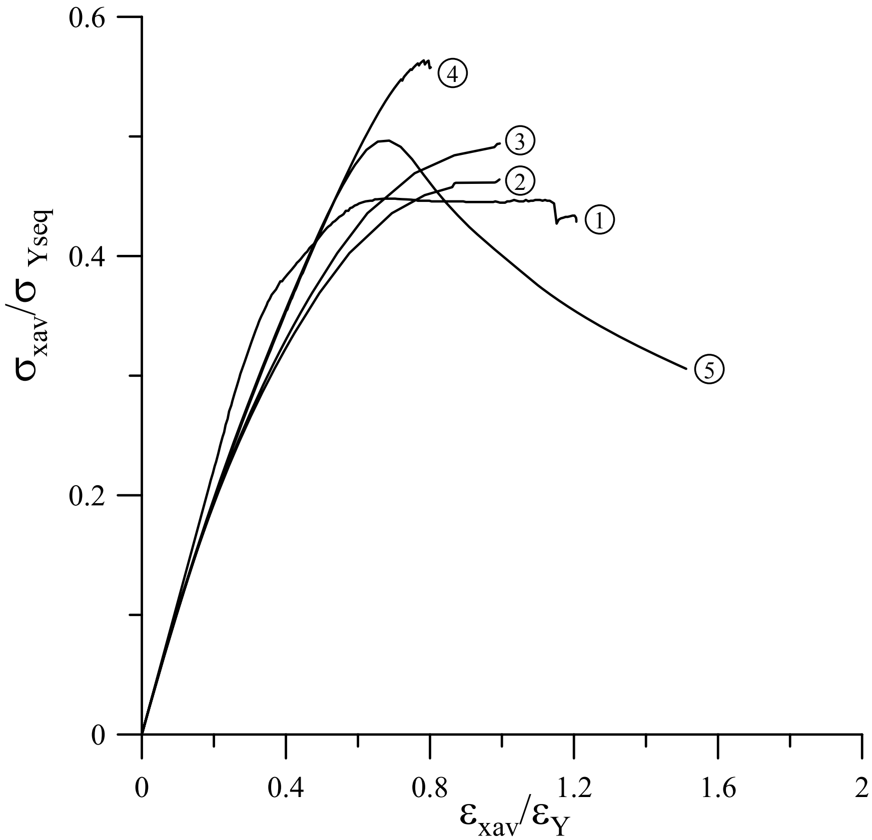

① Exp., collapse mode III (CIP), IV

② 1 bay FEA(PSC-model), collapse mode III (CIP), column type initial deflection with CIP

③ 1 bay FEA(PSC-model), collapse mode III (CIP), column type initial deflection with CIS

④ 2 bay FEA(PSC-model), collapse mode III (CIP), column type initial deflection with CIP

⑤ 2 bay FEA(PSC-model), collapse mode V (CIS), column type initial deflection with CIS

Note: CIP = compression in plate side, CIS = compression in stiffener side

Figure 8.30 The load-axial displacement curves for ID27

ID 28

Plate		Stiffener				
t	Material	h_w	t_w	b_f	t_f	Material
5 mm	5383-H116	135 mm	6 mm	55 mm	8.2 mm	5383-H112

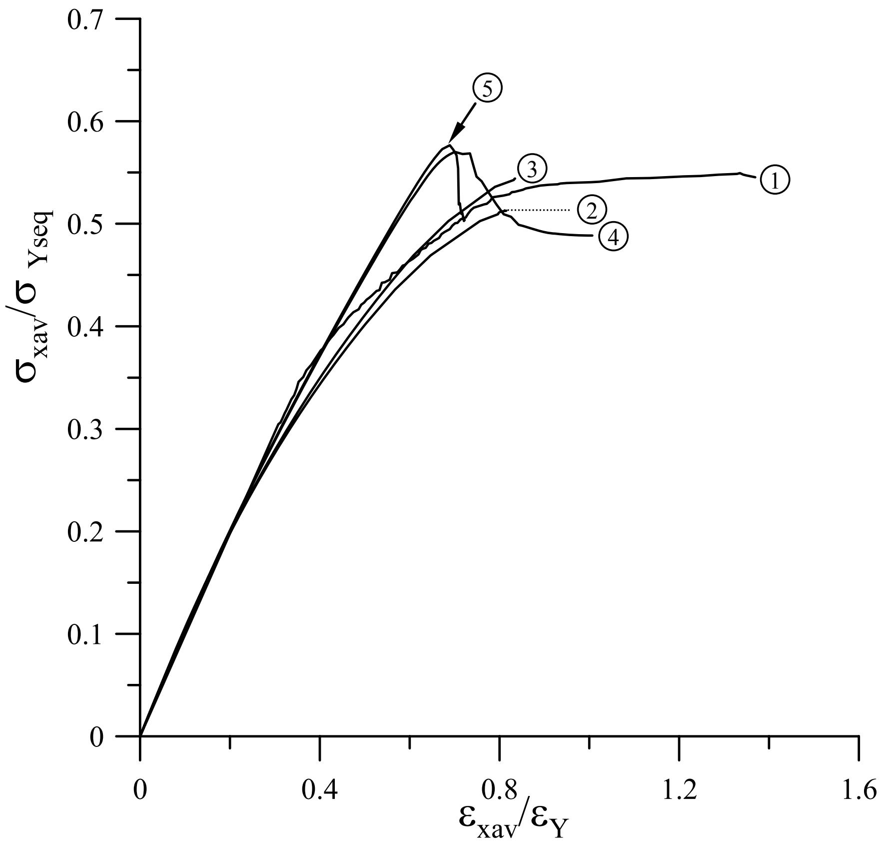

① Exp., collapse mode III (CIP), IV

② 1 bay FEA(PSC-model), collapse mode III (CIP), column type initial deflection with CIP

③ 1 bay FEA(PSC-model), collapse mode III (CIP), column type initial deflection with CIS

④ 2 bay FEA(PSC-model), collapse mode V (CIS), column type initial deflection with CIP

⑤ 2 bay FEA(PSC-model), collapse mode V (CIS), column type initial deflection with CIS

Note: CIP = compression in plate side, CIS = compression in stiffener side

Figure 8.31 The load-axial displacement curves for ID28

ID 29

Plate		Stiffener				
t	Material	h_w	t_w	b_f	t_f	Material
6 mm	5383-H116	55.7 mm	3.7 mm	40 mm	6.7 mm	5383-H112

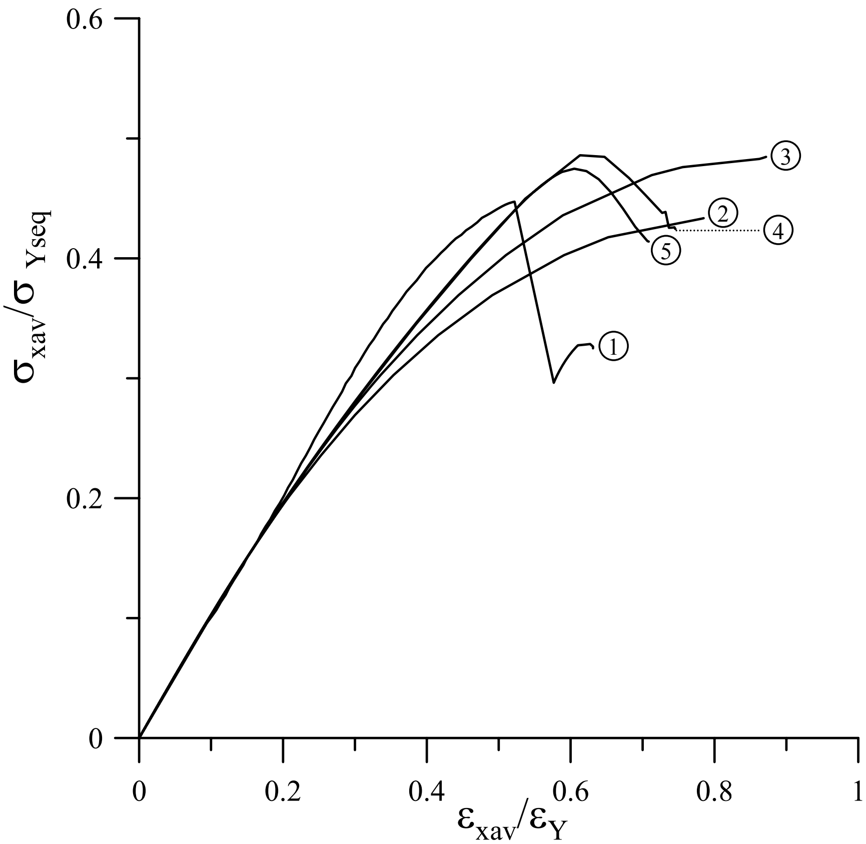

① Exp., collapse mode V (CIS)

② 1 bay FEA(PSC-model), collapse mode III (CIP), column type initial deflection with CIP

③ 1 bay FEA(PSC-model), collapse mode III (CIP), column type initial deflection with CIS

④ 2 bay FEA(PSC-model), collapse mode III (CIP), column type initial deflection with CIP

⑤ 2 bay FEA(PSC-model), collapse mode V (CIS), column type initial deflection with CIS

Note: CIP = compression in plate side, CIS = compression in stiffener side

Figure 8.32 The load-axial displacement curves for ID29

ID 30

Plate		Stiffener				
t	Material	h_w	t_w	b_f	t_f	Material
6 mm	5383-H116	66.1 mm	4 mm	40 mm	5.7 mm	5383-H112

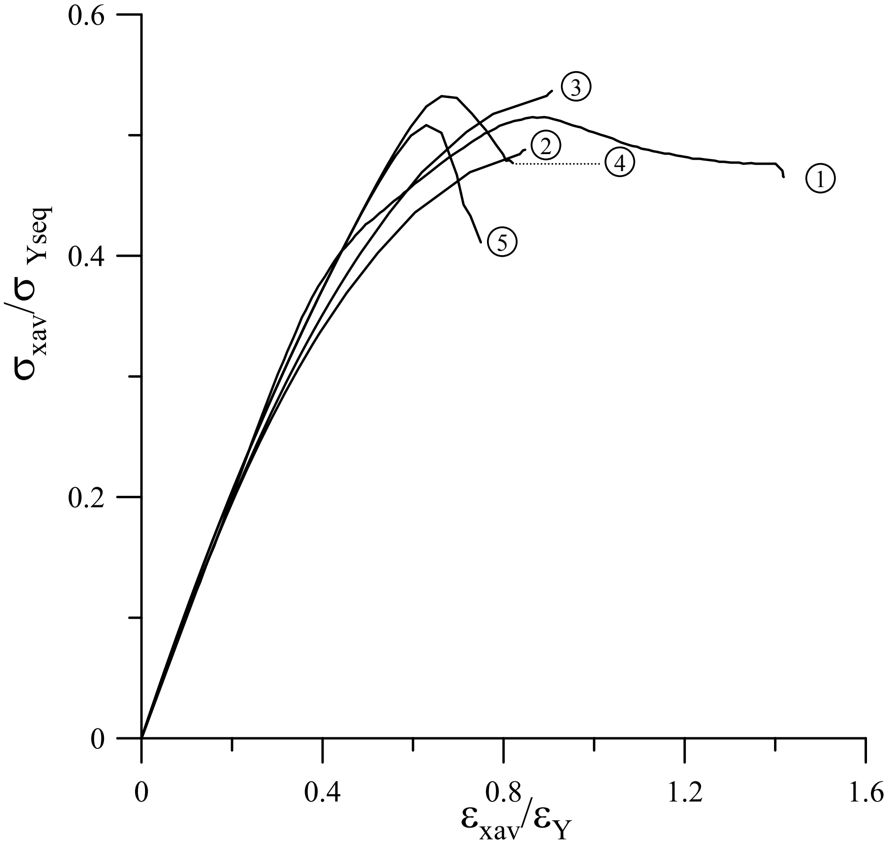

① Exp., collapse mode V (CIS)

② 1 bay FEA(PSC-model), collapse mode III (CIP), column type initial deflection with CIP

③ 1 bay FEA(PSC-model), collapse mode III (CIP), column type initial deflection with CIS

④ 2 bay FEA(PSC-model), collapse mode III (CIP), column type initial deflection with CIP

⑤ 2 bay FEA(PSC-model), collapse mode V (CIS), column type initial deflection with CIS

Note: CIP = compression in plate side, CIS = compression in stiffener side

Figure 8.33 The load-axial displacement curves for ID30

ID 31

Plate		Stiffener				
t	Material	h_w	t_w	b_f	t_f	Material
6 mm	5383-H116	76.8 mm	4 mm	45 mm	5.6 mm	5383-H112

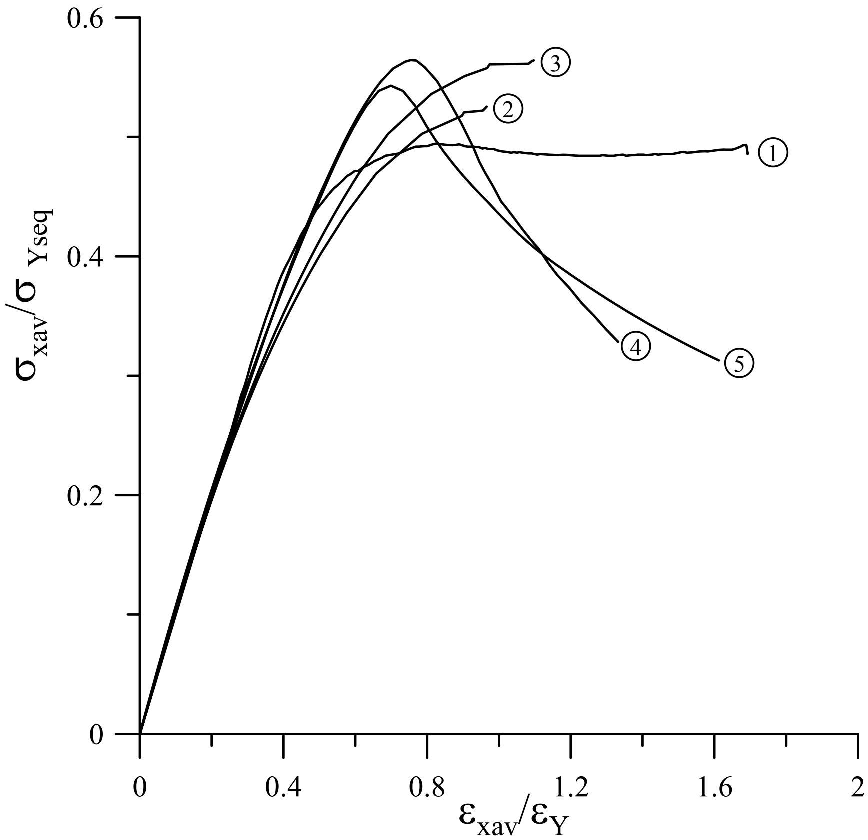

①Exp., collapse mode III (CIP), IV

②1 bay FEA(PSC-model), collapse mode III (CIP), column type initial deflection with CIP

③1 bay FEA(PSC-model), collapse mode III (CIP), column type initial deflection with CIS

④2 bay FEA(PSC-model), collapse mode III (CIP), column type initial deflection with CIP

⑤2 bay FEA(PSC-model), collapse mode V (CIS), column type initial deflection with CIS

Note: CIP = compression in plate side, CIS = compression in stiffener side

Figure 8.34 The load-axial displacement curves for ID31

ID 32

Plate		Stiffener				
t	Material	h_w	t_w	b_f	t_f	Material
6 mm	5383-H116	135 mm	6 mm	55 mm	8.2 mm	5383-H112

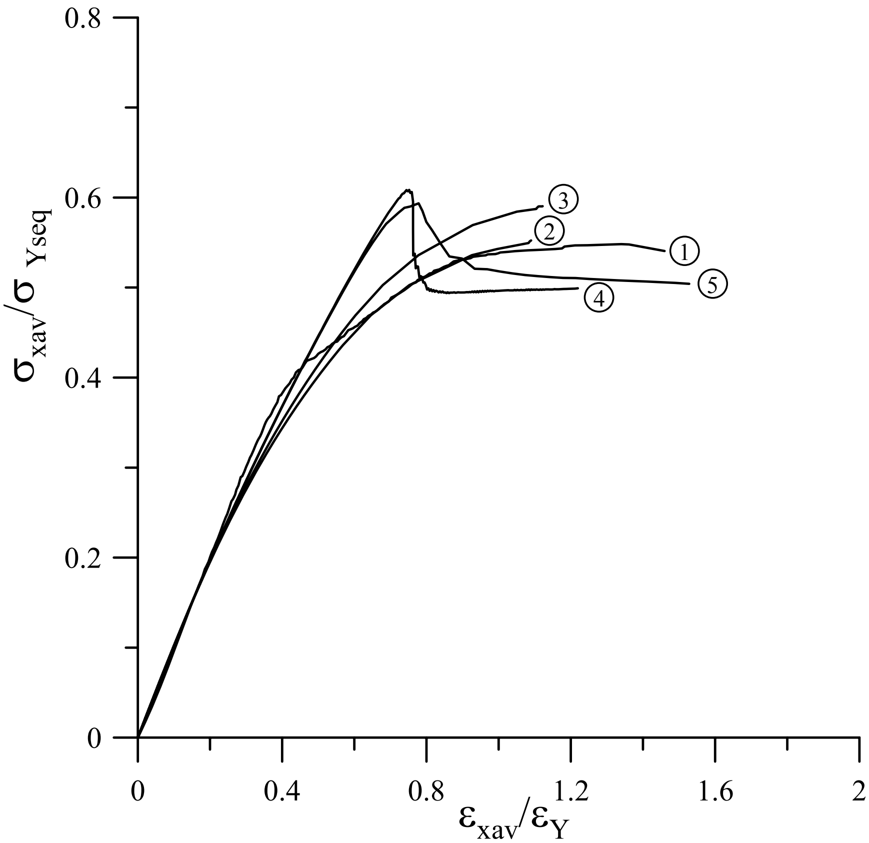

① Exp., collapse mode III (CIP), IV

② 1 bay FEA(PSC-model), collapse mode III (CIP), column type initial deflection with CIP

③ 1 bay FEA(PSC-model), collapse mode III (CIP), column type initial deflection with CIS

④ 2 bay FEA(PSC-model), collapse mode V (CIS), column type initial deflection with CIP

⑤ 2 bay FEA(PSC-model), collapse mode V (CIS), column type initial deflection with CIS

Note: CIP = compression in plate side, CIS = compression in stiffener side

Figure 8.35 The load-axial displacement curves for ID32

ID 33

Plate		Stiffener				
t	Material	h_w	t_w	b_f	t_f	Material
8 mm	5383-H116	55.7 mm	3.7 mm	40 mm	6.7 mm	5383-H112

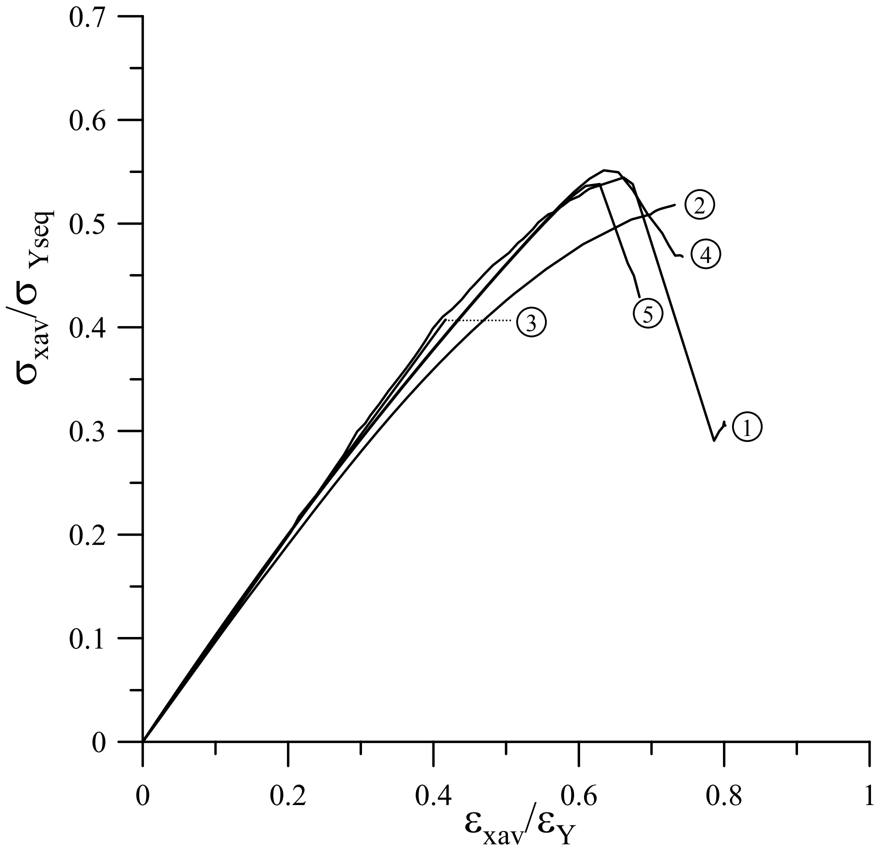

① Exp., collapse mode V (CIS)

② 1 bay FEA(PSC-model), collapse mode III (CIP), column type initial deflection with CIP

③ 1 bay FEA(PSC-model), collapse mode V (CIS), column type initial deflection with CIS

④ 2 bay FEA(PSC-model), collapse mode III (CIP), column type initial deflection with CIP

⑤ 2 bay FEA(PSC-model), collapse mode V (CIS), column type initial deflection with CIS

Note: CIP = compression in plate side, CIS = compression in stiffener side

Figure 8.36 The load-axial displacement curves for ID33

ID 34

Plate		Stiffener				
t	Material	h_w	t_w	b_f	t_f	Material
8 mm	5383-H116	66.1 mm	4 mm	40 mm	5.7 mm	5383-H112

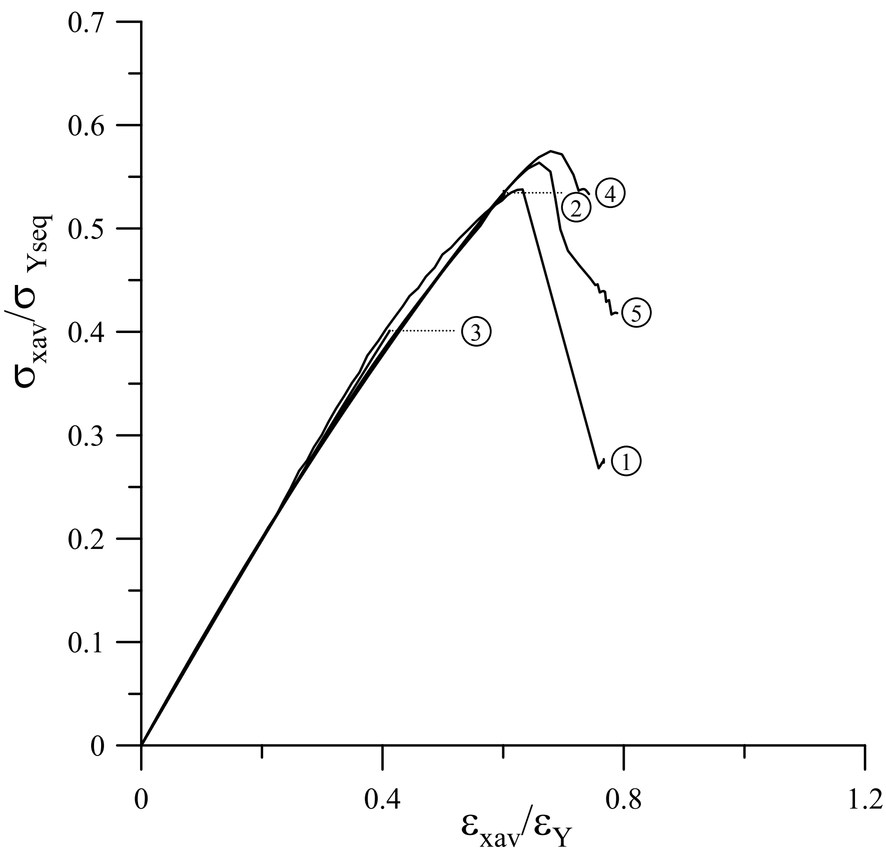

① Exp., collapse mode V (CIS)

② 1 bay FEA(PSC-model), collapse mode III (CIP), column type initial deflection with CIP

③ 1 bay FEA(PSC-model), collapse mode V (CIS), , column type initial deflection with CIS

④ 2 bay FEA(PSC-model), collapse mode III (CIP), column type initial deflection with CIP

⑤ 2 bay FEA(PSC-model), collapse mode V (CIS), column type initial deflection with CIS

Note: CIP = compression in plate side, CIS = compression in stiffener side

Figure 8.37 The load-axial displacement curves for ID34

ID 35

Plate		Stiffener				
t	Material	h_w	t_w	b_f	t_f	Material
8 mm	5383-H116	76.8 mm	4 mm	45 mm	5.6 mm	5383-H112

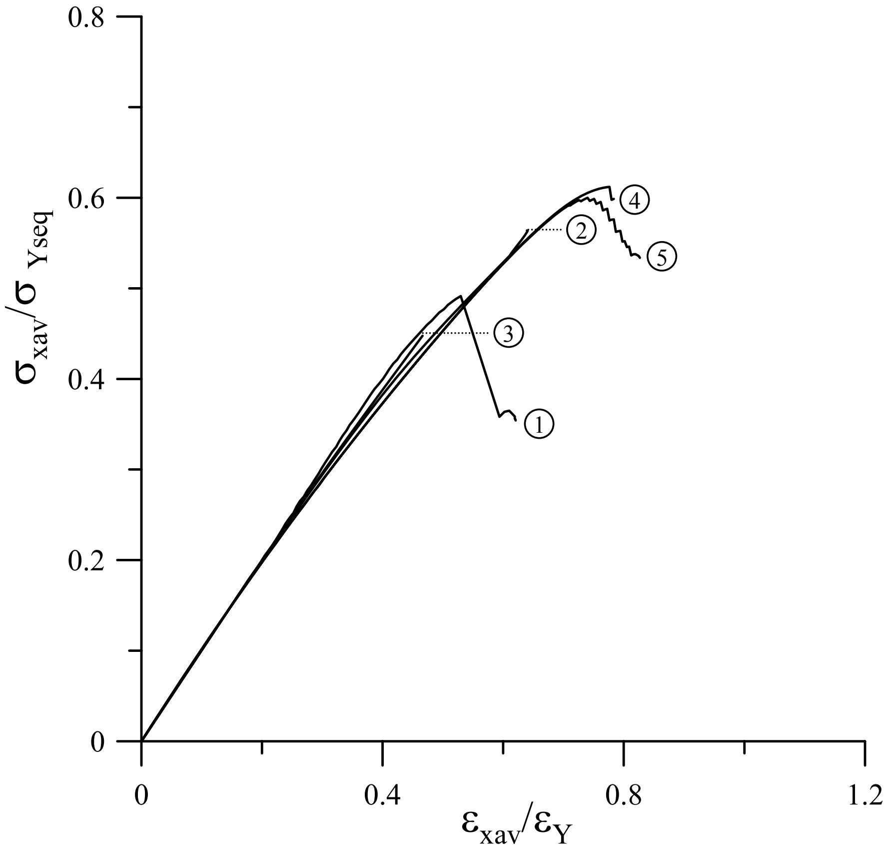

① Exp., collapse mode V (CIS)

② 1 bay FEA(PSC-model), collapse mode V (CIS), column type initial deflection with CIP

③ 1 bay FEA(PSC-model), collapse mode V (CIS), , column type initial deflection with CIS

④ 2 bay FEA(PSC-model), collapse mode III (CIP), column type initial deflection with CIP

⑤ 2 bay FEA(PSC-model), collapse mode V (CIS), column type initial deflection with CIS

Note: CIP = compression in plate side, CIS = compression in stiffener side

Figure 8.38 The load-axial displacement curves for ID35

ID 36

Plate		Stiffener				
t	Material	h_w	t_w	b_f	t_f	Material
8 mm	5383-H116	135 mm	6 mm	55 mm	8.2 mm	5383-H112

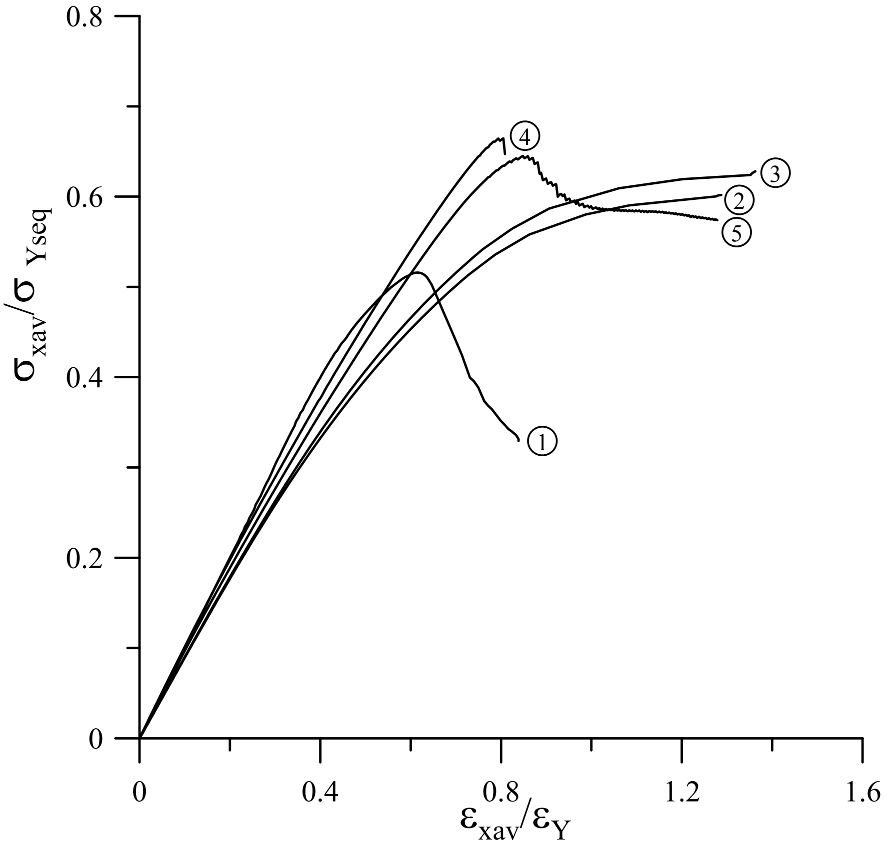

① Exp., collapse mode V (CIS)

② 1 bay FEA(PSC-model), collapse mode III (CIP), column type initial deflection with CIP

③ 1 bay FEA(PSC-model), collapse mode III (CIP), , column type initial deflection with CIS

④ 2 bay FEA(PSC-model), collapse mode V (CIS), column type initial deflection with CIP

⑤ 2 bay FEA(PSC-model), collapse mode V (CIS), column type initial deflection with CIS

Note: CIP = compression in plate side, CIS = compression in stiffener side

Figure 8.39 The load-axial displacement curves for ID36

ID 37

Plate		Stiffener				
t	Material	h_w	t_w	b_f	t_f	Material
5 mm	5083-H116	60 mm	5 mm	-	-	5083-H116

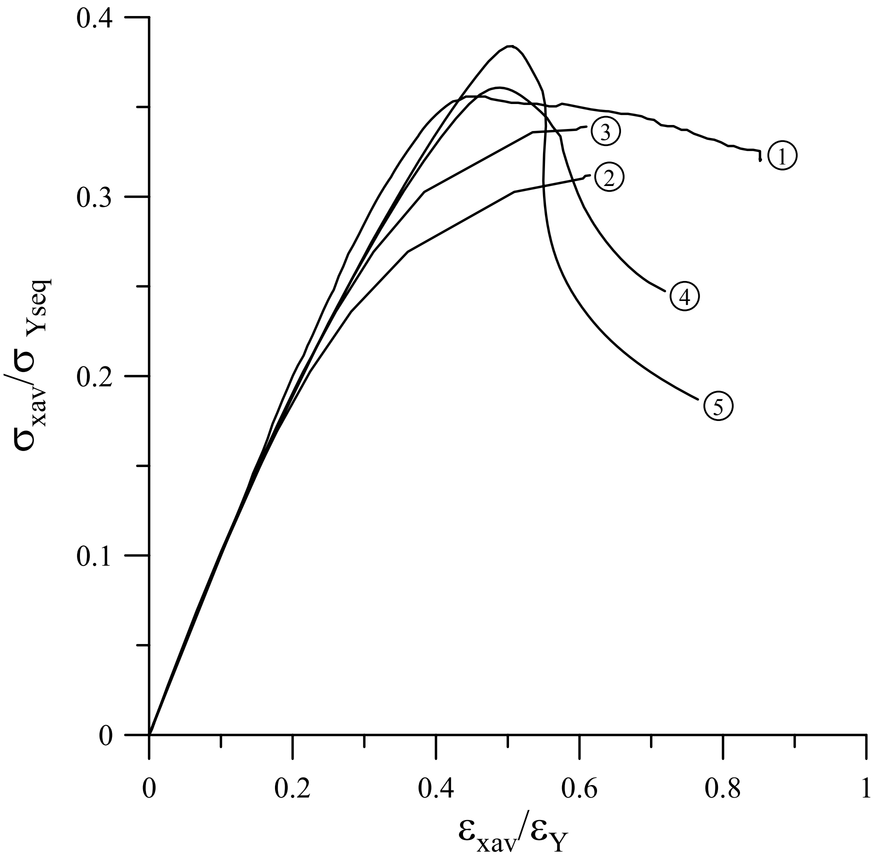

① Exp., collapse mode III (CIP)

② 1 bay FEA(PSC-model), collapse mode III (CIP), column type initial deflection with CIP

③ 1 bay FEA(PSC-model), collapse mode III (CIP), column type initial deflection with CIS

④ 2 bay FEA(PSC-model), collapse mode III (CIP), column type initial deflection with CIP

⑤ 2 bay FEA(PSC-model), collapse mode V (CIS), column type initial deflection with CIS

Note: CIP = compression in plate side, CIS = compression in stiffener side

Figure 8.40 The load-axial displacement curves for ID37

ID 38

Plate		Stiffener				
t	Material	h_w	t_w	b_f	t_f	Material
5 mm	5083-H116	90 mm	5 mm	-	-	5083-H116

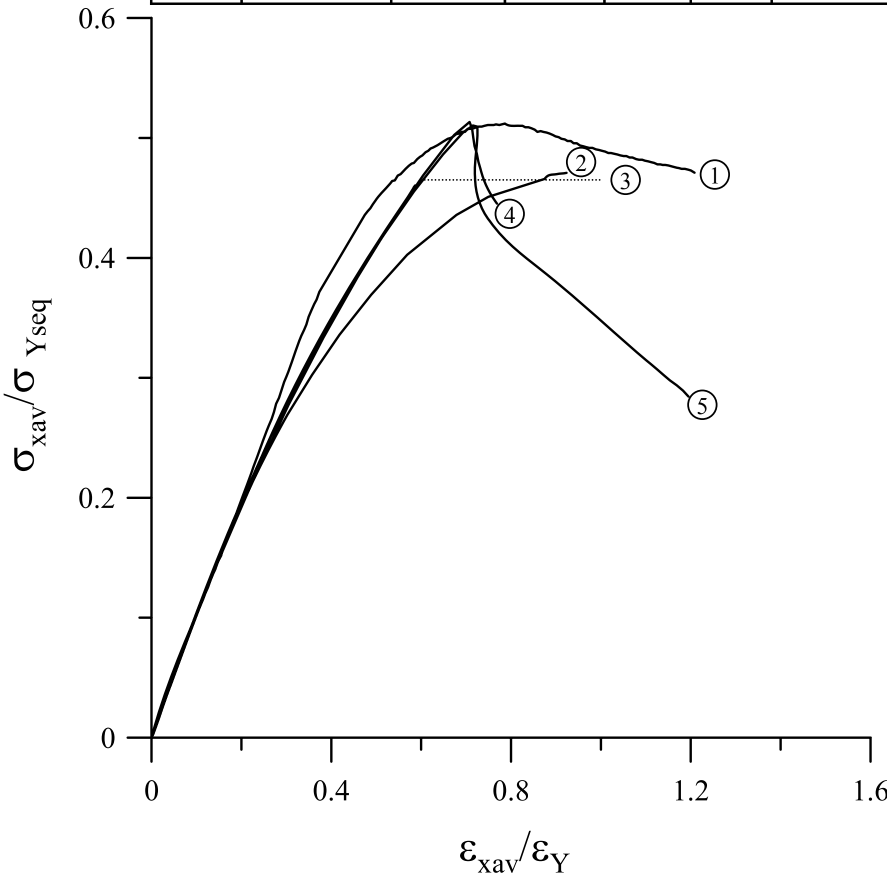

① Exp., collapse mode III (CIP)

② 1 bay FEA(PSC-model), collapse mode III (CIP), column type initial deflection with CIP

③ 1 bay FEA(PSC-model), collapse mode V (CIS), column type initial deflection with CIS

④ 2 bay FEA(PSC-model), collapse mode III (CIP), column type initial deflection with CIP

⑤ 2 bay FEA(PSC-model), collapse mode V (CIS), column type initial deflection with CIS

Note: CIP = compression in plate side, CIS = compression in stiffener side

Figure 8.41 The load-axial displacement curves for ID38

ID 39

Plate		Stiffener				
t	Material	h_w	t_w	b_f	t_f	Material
5 mm	5083-H116	120 mm	5 mm	-	-	5083-H116

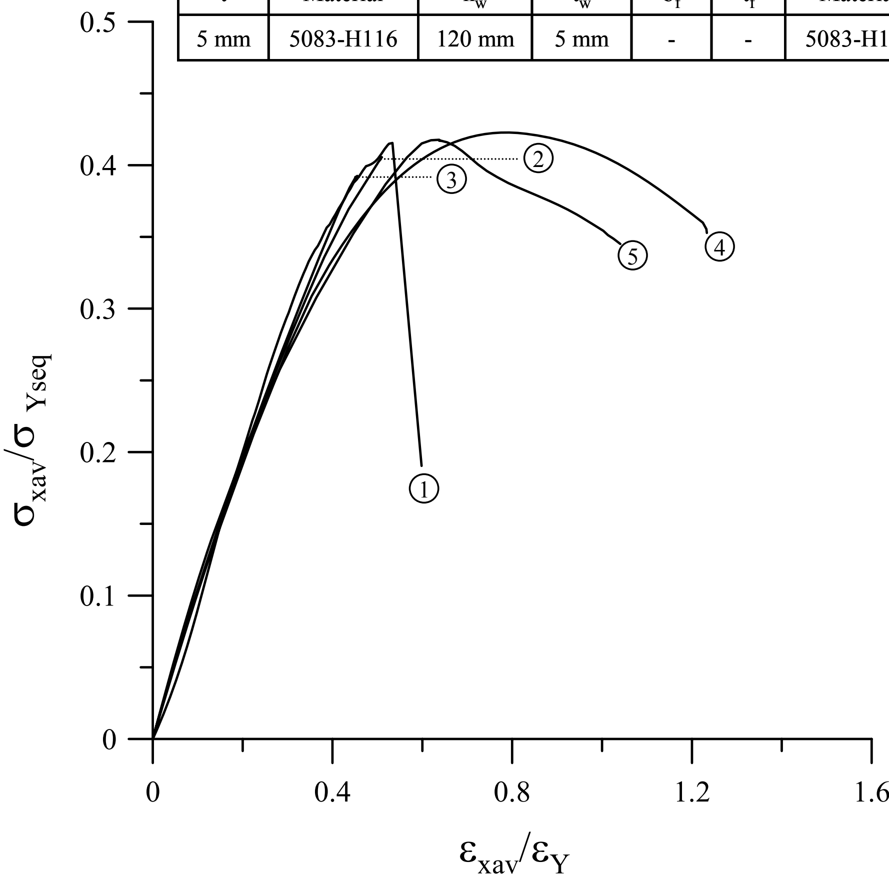

① Exp., collapse mode V (CIS)

② 1 bay FEA(PSC-model), collapse mode III (CIP), column type initial deflection with CIP

③ 1 bay FEA(PSC-model), collapse mode V (CIS), column type initial deflection with CIS

④ 2 bay FEA(PSC-model), collapse mode III (CIP), column type initial deflection with CIP

⑤ 2 bay FEA(PSC-model), collapse mode V (CIS), column type initial deflection with CIS

Note: CIP = compression in plate side, CIS = compression in stiffener side

Figure 8.42 The load-axial displacement curves for ID39

ID 40

Plate		Stiffener				
t	Material	h_w	t_w	b_f	t_f	Material
6 mm	5083-H116	60 mm	6 mm	-	-	5083-H116

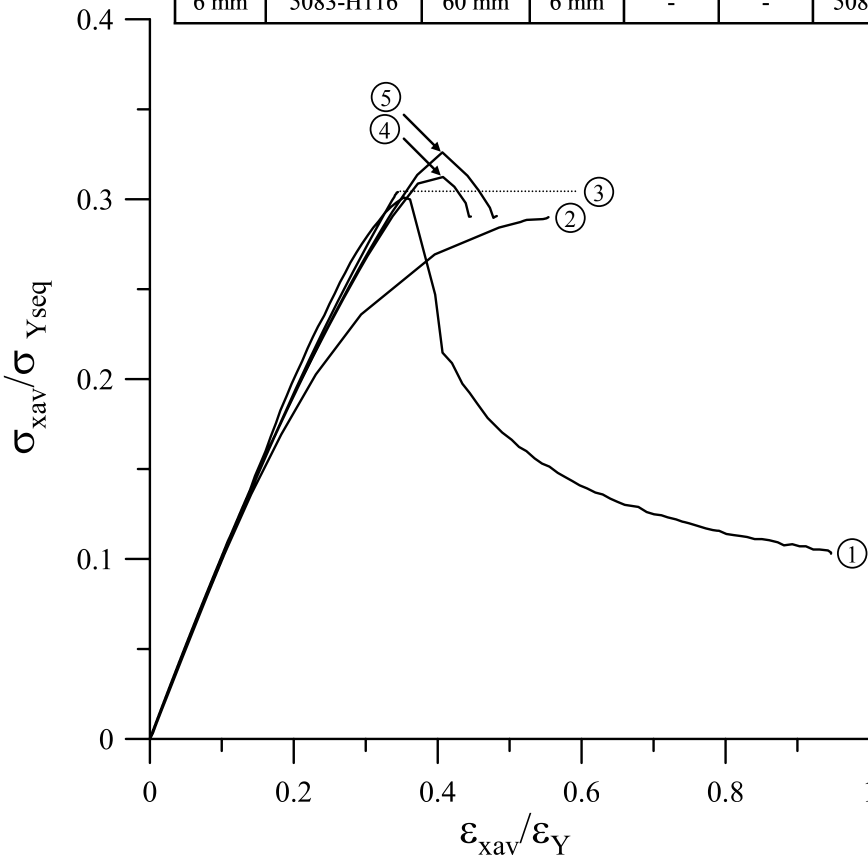

① Exp., collapse mode III (CIP)

② 1 bay FEA(PSC-model), collapse mode III (CIP), column type initial deflection with CIP

③ 1 bay FEA(PSC-model), collapse mode III (CIP), column type initial deflection with CIS

④ 2 bay FEA(PSC-model), collapse mode III (CIP), column type initial deflection with CIP

⑤ 2 bay FEA(PSC-model), collapse mode V (CIS), column type initial deflection with CIS

Note: CIP = compression in plate side, CIS = compression in stiffener side

Figure 8.43 The load-axial displacement curves for ID40

ID 41

Plate		Stiffener				
t	Material	h_w	t_w	b_f	t_f	Material
6 mm	5083-H116	90 mm	6 mm	-	-	5083-H116

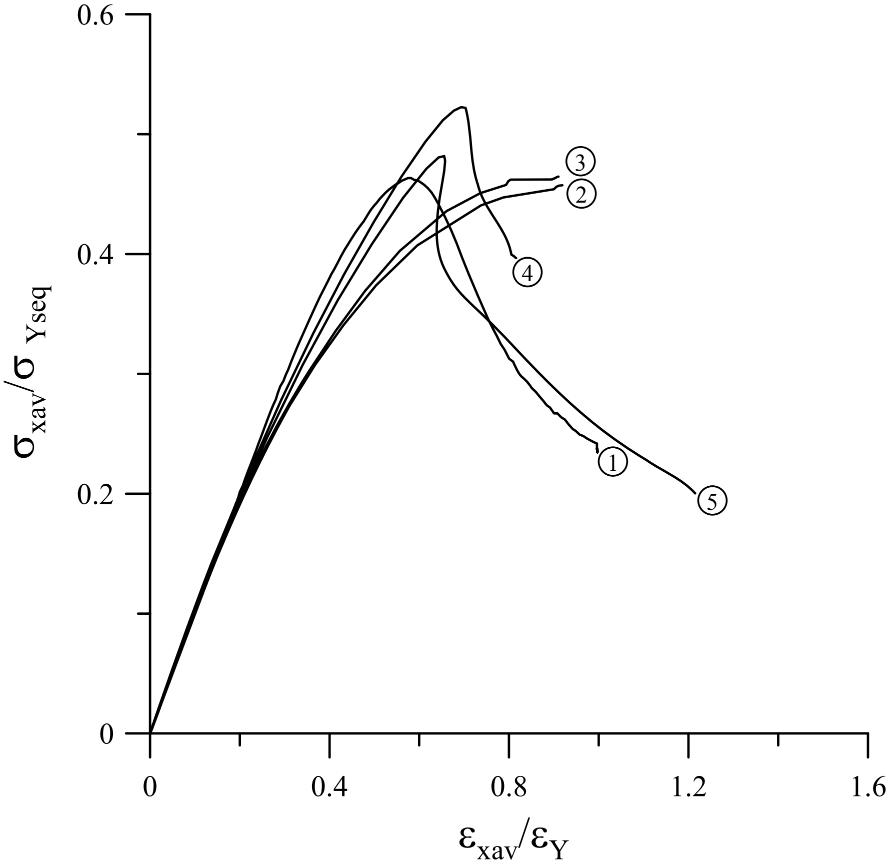

① Exp., collapse mode III (CIP)

② 1 bay FEA(PSC-model), collapse mode III (CIP), column type initial deflection with CIP

③ 1 bay FEA(PSC-model), collapse mode III (CIP), column type initial deflection with CIS

④ 2 bay FEA(PSC-model), collapse mode III (CIP), column type initial deflection with CIP

⑤ 2 bay FEA(PSC-model), collapse mode V (CIS), column type initial deflection with CIS

Note: CIP = compression in plate side, CIS = compression in stiffener side

Figure 8.44 The load-axial displacement curves for ID41

ID 42

Plate		Stiffener				
t	Material	h_w	t_w	b_f	t_f	Material
6 mm	5083-H116	120 mm	6 mm	-	-	5083-H116

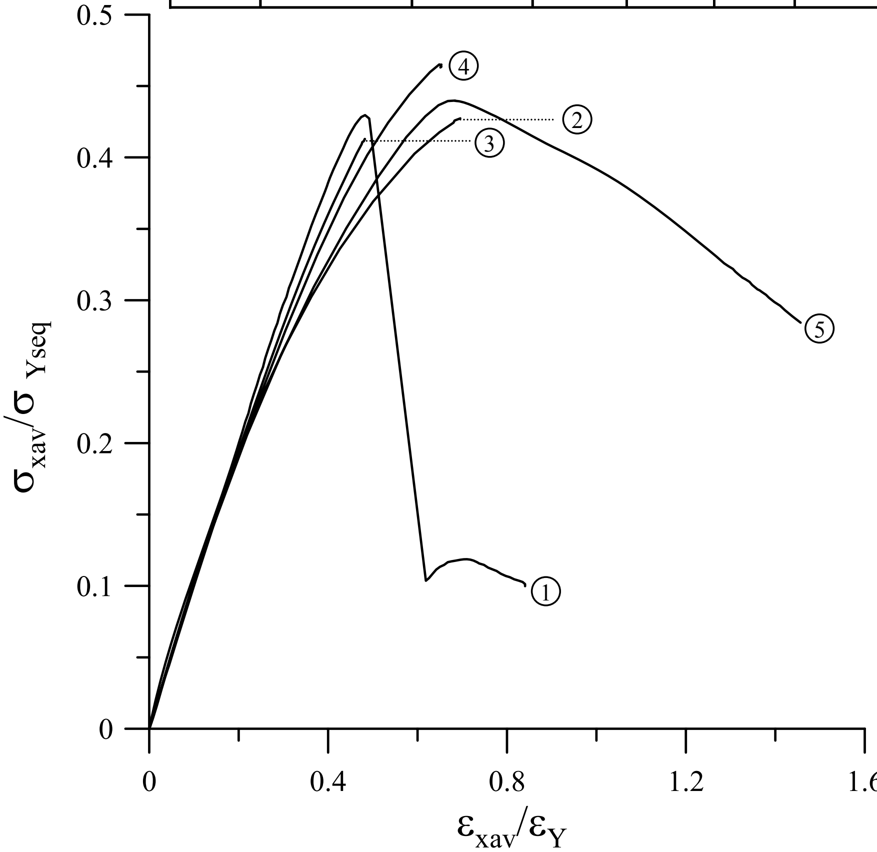

① Exp., collapse mode V (CIS)

② 1 bay FEA(PSC-model), collapse mode III (CIP), column type initial deflection with CIP

③ 1 bay FEA(PSC-model), collapse mode V (CIS), column type initial deflection with CIS

④ 2 bay FEA(PSC-model), collapse mode III (CIP), column type initial deflection with CIP

⑤ 2 bay FEA(PSC-model), collapse mode V (CIS), column type initial deflection with CIS

Note: CIP = compression in plate side, CIS = compression in stiffener side

Figure 8.45 The load-axial displacement curves for ID42

ID 43

Plate		Stiffener				
t	Material	h_w	t_w	b_f	t_f	Material
8 mm	5083-H116	60 mm	8 mm	-	-	5083-H116

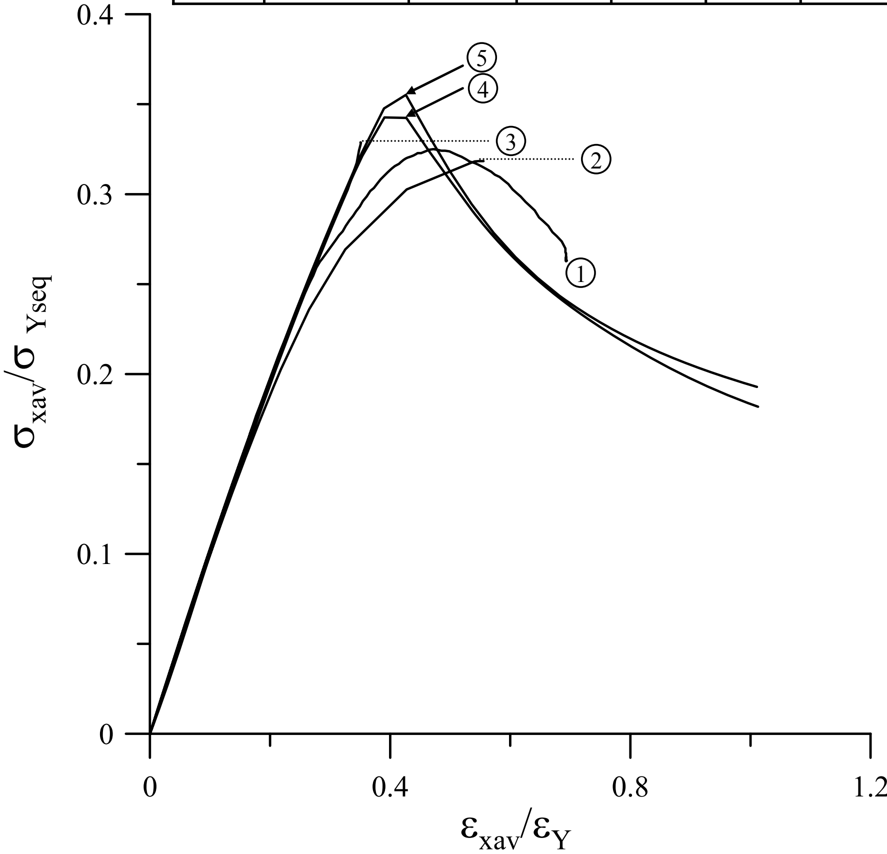

① Exp., collapse mode V (CIS)

② 1 bay FEA(PSC-model), collapse mode III (CIP), column type initial deflection with CIP

③ 1 bay FEA(PSC-model), collapse mode V (CIS), column type initial deflection with CIS

④ 2 bay FEA(PSC-model), collapse mode III (CIP), column type initial deflection with CIP

⑤ 2 bay FEA(PSC-model), collapse mode V (CIS), column type initial deflection with CIS

Note: CIP = compression in plate side, CIS = compression in stiffener side

Figure 8.46 The load-axial displacement curves for ID43

ID 44

Plate		Stiffener				
t	Material	h_w	t_w	b_f	t_f	Material
8 mm	5083-H116	90 mm	8 mm	-	-	5083-H116

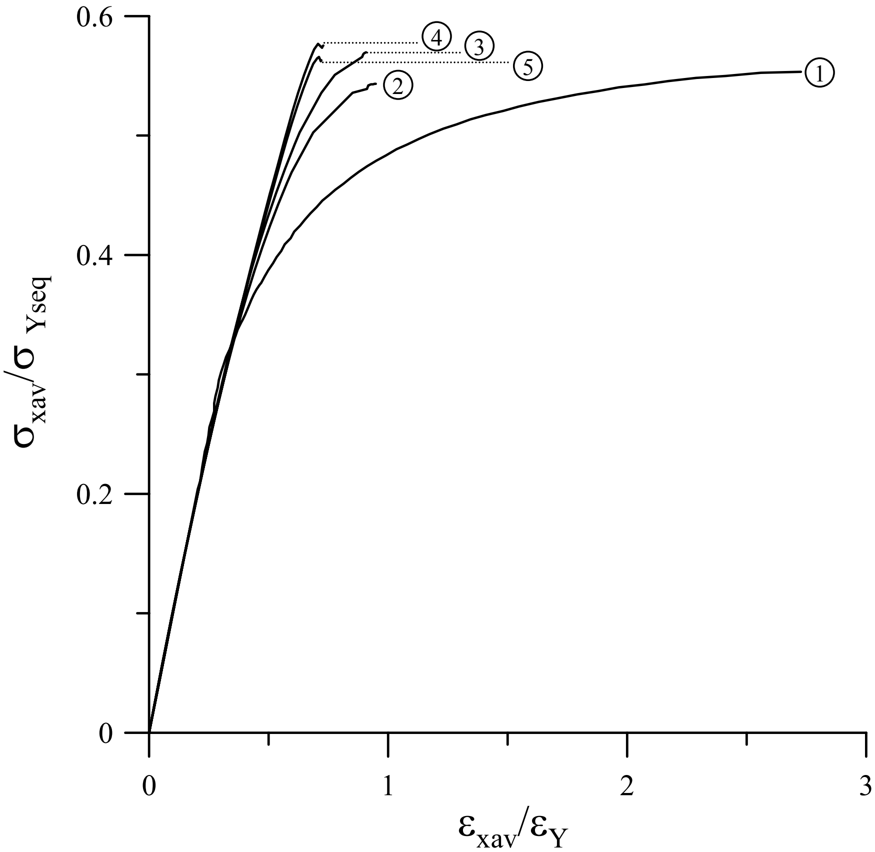

① Exp., collapse mode V (CIS)

② 1 bay FEA(PSC-model), collapse mode III (CIP), column type initial deflection with CIP

③ 1 bay FEA(PSC-model), collapse mode III (CIP), column type initial deflection with CIS

④ 2 bay FEA(PSC-model), collapse mode III (CIP), column type initial deflection with CIP

⑤ 2 bay FEA(PSC-model), collapse mode V (CIS), column type initial deflection with CIS

Note: CIP = compression in plate side, CIS = compression in stiffener side

Figure 8.47 The load-axial displacement curves for ID44

ID 45

Plate		Stiffener				
t	Material	h_w	t_w	b_f	t_f	Material
8 mm	5083-H116	120 mm	8 mm	-	-	5083-H116

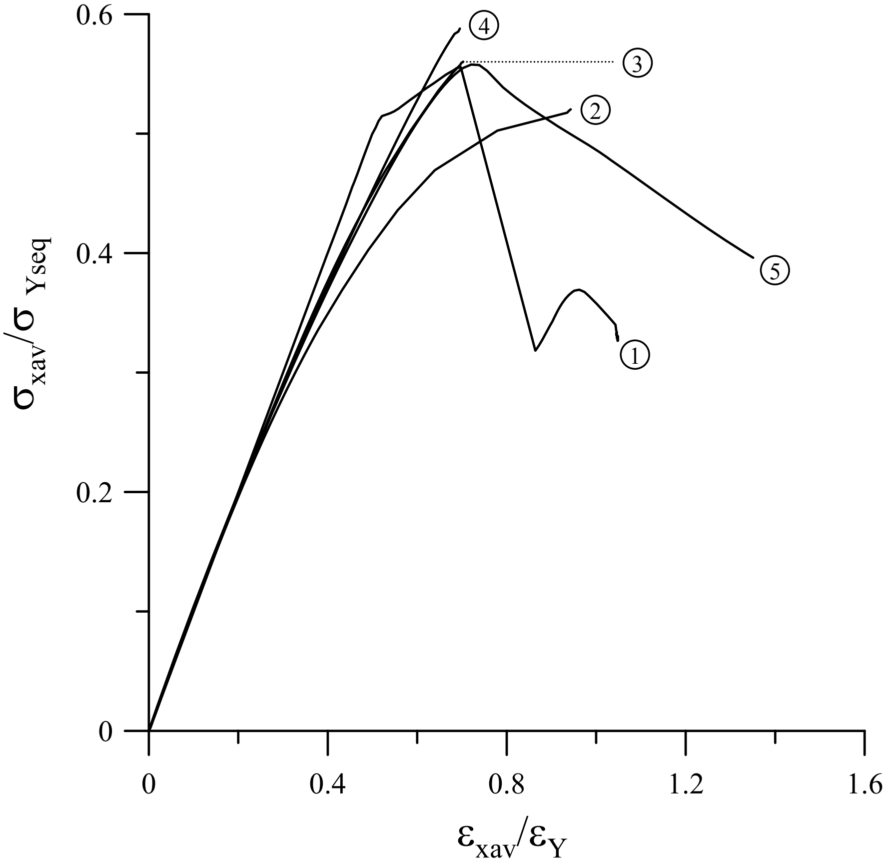

① Exp., collapse mode V (CIS)

② 1 bay FEA(PSC-model), collapse mode III (CIP), column type initial deflection with CIP

③ 1 bay FEA(PSC-model), collapse mode V (CIS), column type initial deflection with CIS

④ 2 bay FEA(PSC-model), collapse mode III (CIP), column type initial deflection with CIP

⑤ 2 bay FEA(PSC-model), collapse mode V (CIS), column type initial deflection with CIS

Note: CIP = compression in plate side, CIS = compression in stiffener side

Figure 8.48 The load-axial displacement curves for ID45

ID 46

Plate		Stiffener				
t	Material	h_w	t_w	b_f	t_f	Material
5 mm	5083-H116	60 mm	5 mm	-	-	5383-H116

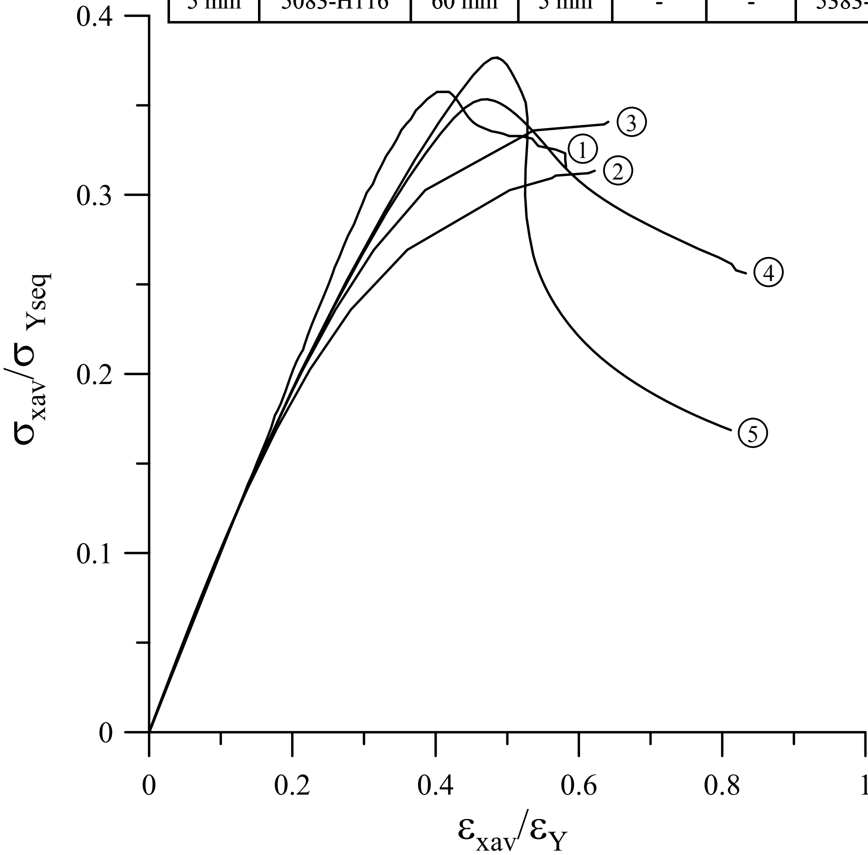

① Exp., collapse mode III (CIP)

② 1 bay FEA(PSC-model), collapse mode III (CIP), column type initial deflection with CIP

③ 1 bay FEA(PSC-model), collapse mode III (CIP), column type initial deflection with CIS

④ 2 bay FEA(PSC-model), collapse mode III (CIP), column type initial deflection with CIP

⑤ 2 bay FEA(PSC-model), collapse mode V (CIS), column type initial deflection with CIS

Note: CIP = compression in plate side, CIS = compression in stiffener side

Figure 8.49 The load-axial displacement curves for ID46

ID 47

Plate		Stiffener				
t	Material	h_w	t_w	b_f	t_f	Material
5 mm	5083-H116	90 mm	5 mm	-	-	5383-H116

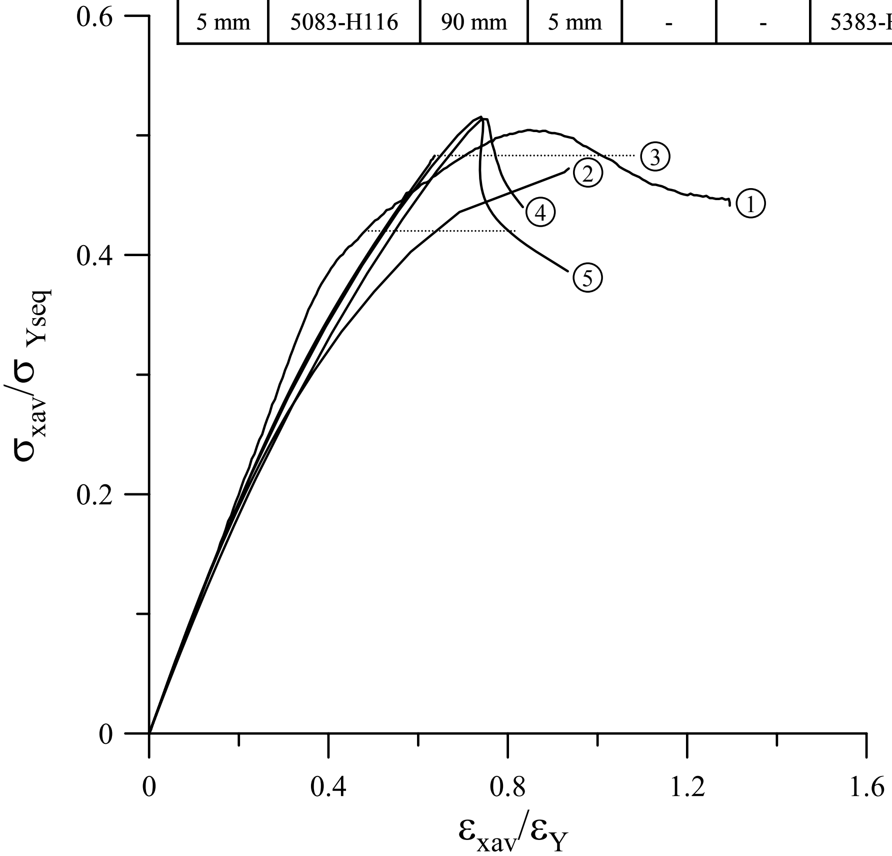

① Exp., collapse mode V (CIS)

② 1 bay FEA(PSC-model), collapse mode III (CIP), column type initial deflection with CIP

③ 1 bay FEA(PSC-model), collapse mode V (CIS), column type initial deflection with CIS

④ 2 bay FEA(PSC-model), collapse mode III (CIP), column type initial deflection with CIP

⑤ 2 bay FEA(PSC-model), collapse mode V (CIS), column type initial deflection with CIS

Note: CIP = compression in plate side, CIS = compression in stiffener side

Figure 8.50 The load-axial displacement curves for ID47

ID 48

Plate		Stiffener				
t	Material	h_w	t_w	b_f	t_f	Material
5 mm	5083-H116	120 mm	5 mm	-	-	5383-H116

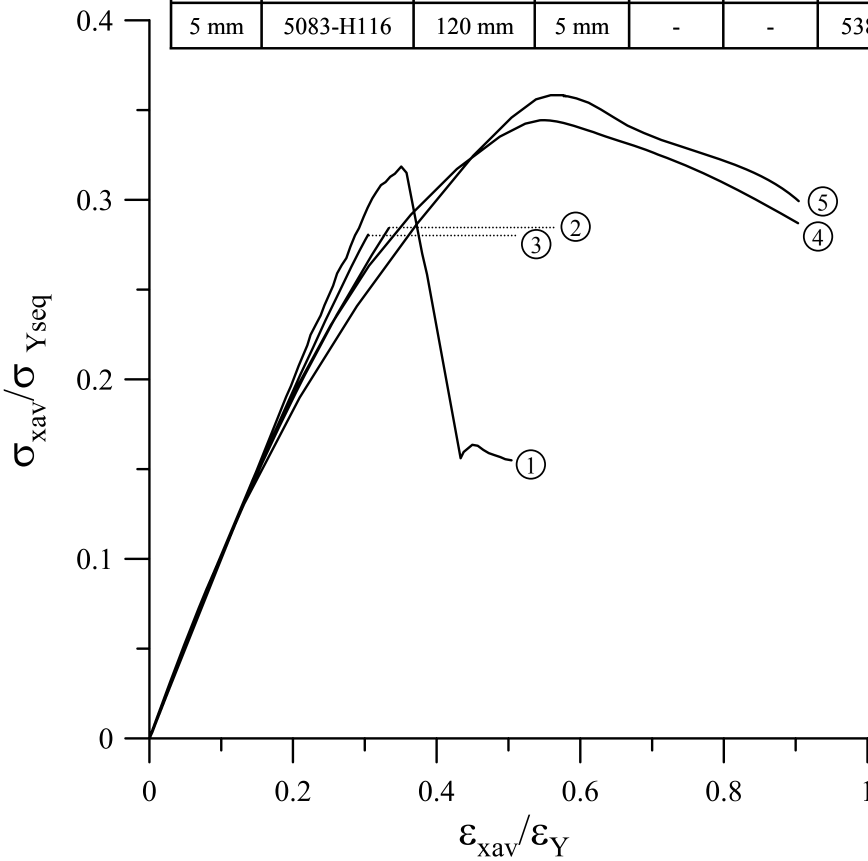

① Exp., collapse mode V (CIS)

② 1 bay FEA(PSC-model), collapse mode III (CIP), column type initial deflection with CIP

③ 1 bay FEA(PSC-model), collapse mode V (CIS), column type initial deflection with CIS

④ 2 bay FEA(PSC-model), collapse mode III (CIP), column type initial deflection with CIP

⑤ 2 bay FEA(PSC-model), collapse mode V (CIS), column type initial deflection with CIS

Note: CIP = compression in plate side, CIS = compression in stiffener side

Figure 8.51 The load-axial displacement curves for ID48

ID 49

Plate		Stiffener				
t	Material	h_w	t_w	b_f	t_f	Material
6 mm	5083-H116	60 mm	6 mm	-	-	5383-H116

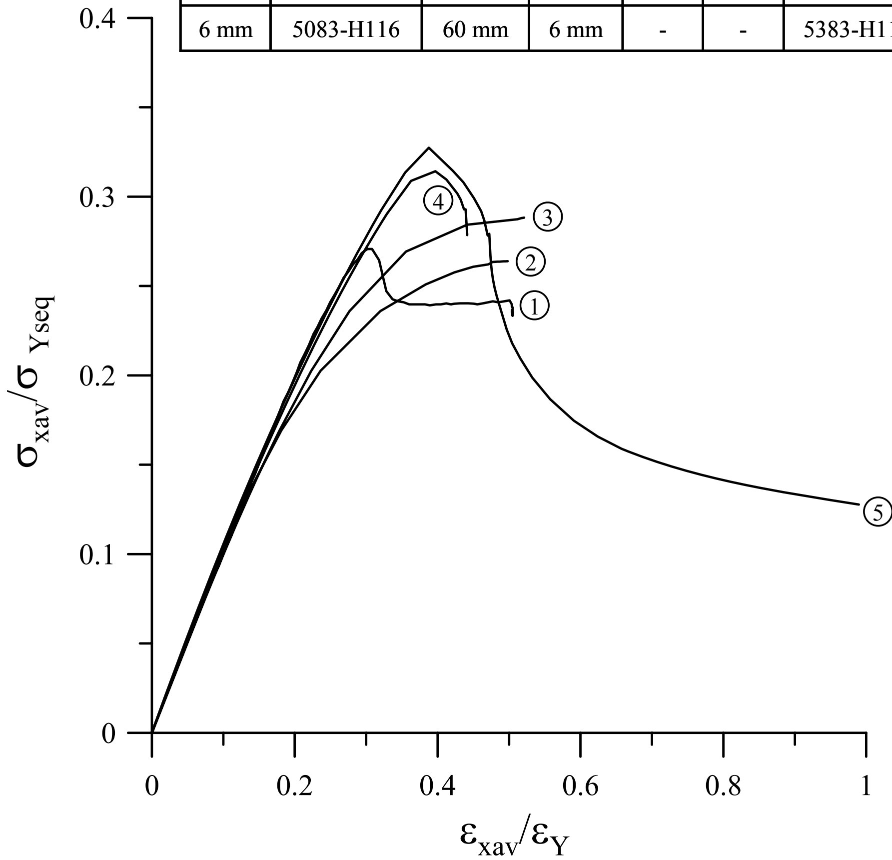

① Exp., collapse mode III (CIP)

② 1 bay FEA(PSC-model), collapse mode III (CIP), column type initial deflection with CIP

③ 1 bay FEA(PSC-model), collapse mode III (CIP), column type initial deflection with CIS

④ 2 bay FEA(PSC-model), collapse mode III (CIP), column type initial deflection with CIP

⑤ 2 bay FEA(PSC-model), collapse mode V (CIS), column type initial deflection with CIS

Note: CIP = compression in plate side, CIS = compression in stiffener side

Figure 8.52 The load-axial displacement curves for ID49

ID 50

Plate		Stiffener				
t	Material	h_w	t_w	b_f	t_f	Material
6 mm	5083-H116	90 mm	6 mm	-	-	5383-H116

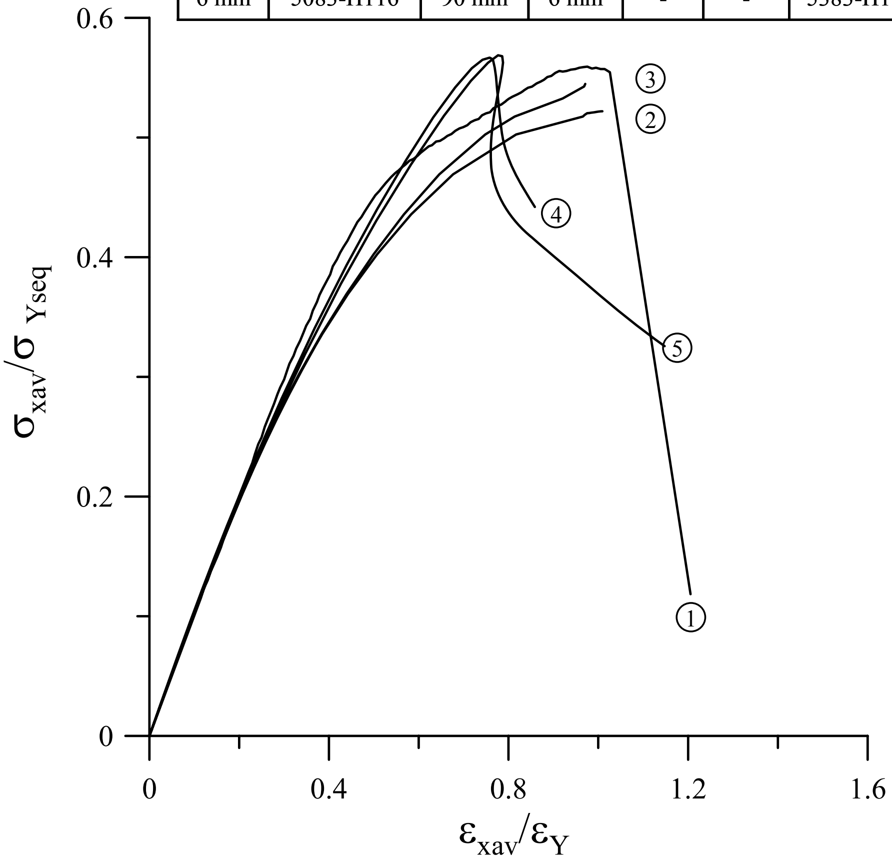

① Exp., collapse mode V (CIS)

② 1 bay FEA(PSC-model), collapse mode III (CIP), column type initial deflection with CIP

③ 1 bay FEA(PSC-model), collapse mode V (CIS), column type initial deflection with CIS

④ 2 bay FEA(PSC-model), collapse mode III (CIP), column type initial deflection with CIP

⑤ 2 bay FEA(PSC-model), collapse mode V (CIS), column type initial deflection with CIS

Note: CIP = compression in plate side, CIS = compression in stiffener side

Figure 8.53 The load-axial displacement curves for ID50

ID 51

Plate		Stiffener				
t	Material	h_w	t_w	b_f	t_f	Material
6 mm	5083-H116	120 mm	6 mm	-	-	5383-H116

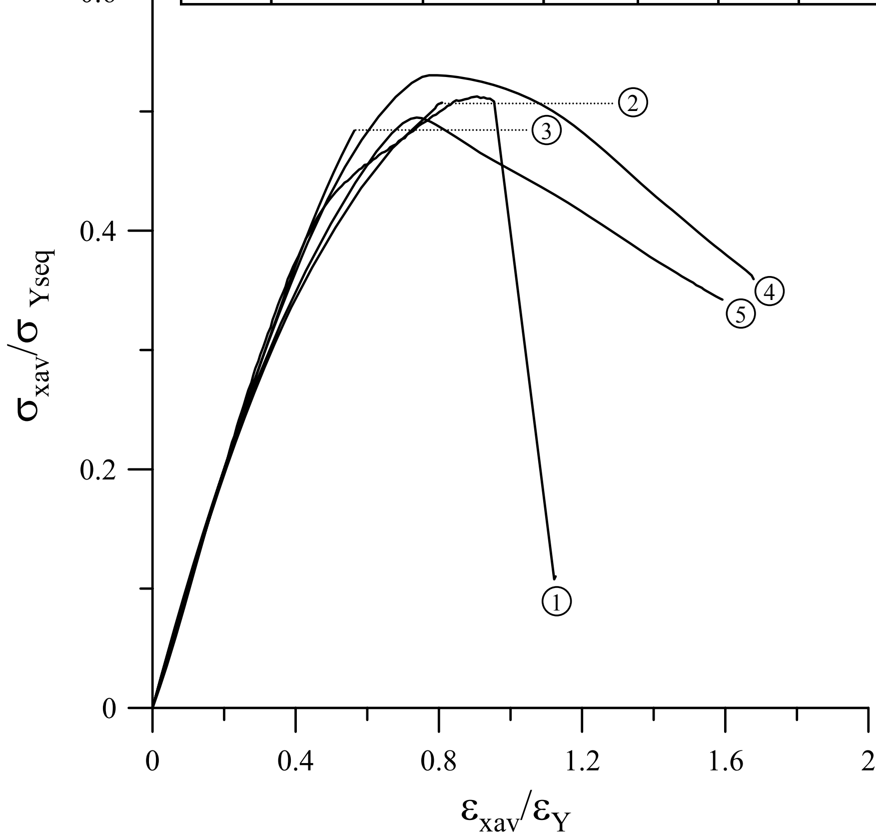

① Exp., collapse mode V (CIS)

② 1 bay FEA(PSC-model), collapse mode III (CIP), column type initial deflection with CIP

③ 1 bay FEA(PSC-model), collapse mode V (CIS), column type initial deflection with CIS

④ 2 bay FEA(PSC-model), collapse mode III (CIP), column type initial deflection with CIP

⑤ 2 bay FEA(PSC-model), collapse mode V (CIS), column type initial deflection with CIS

Note: CIP = compression in plate side, CIS = compression in stiffener side

Figure 8.54 The load-axial displacement curves for ID51

ID 52

Plate		Stiffener				
t	Material	h_w	t_w	b_f	t_f	Material
8 mm	5083-H116	60 mm	8 mm	-	-	5383-H116

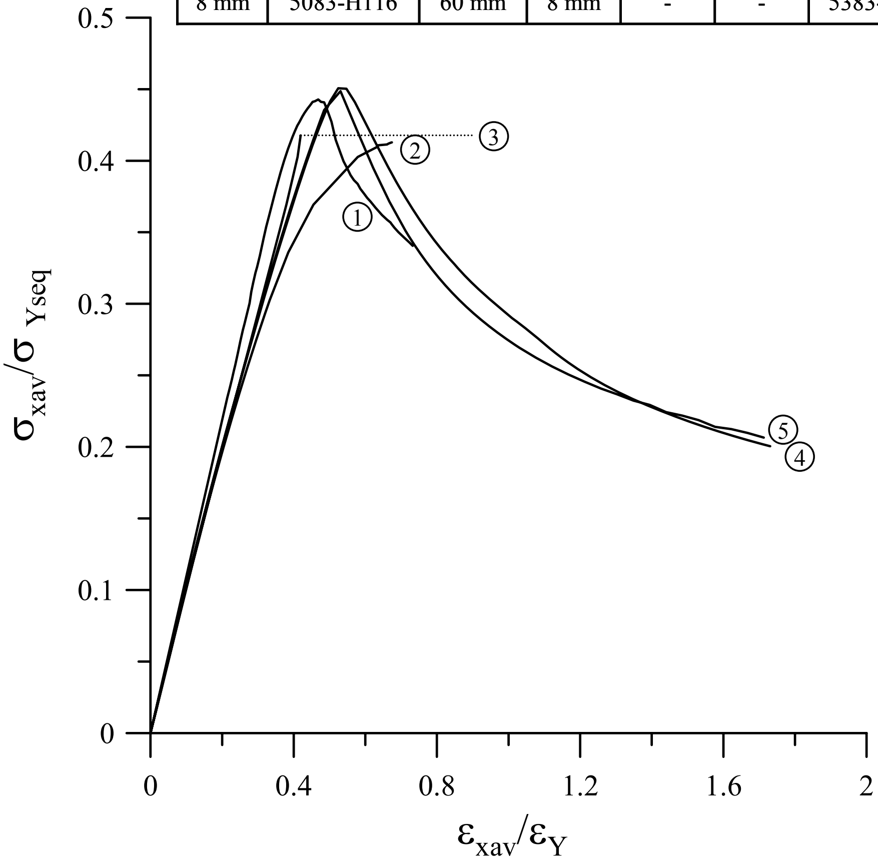

① Exp., collapse mode III (CIP)

② 1 bay FEA(PSC-model), collapse mode III (CIP), column type initial deflection with CIP

③ 1 bay FEA(PSC-model), collapse mode V (CIS), column type initial deflection with CIS

④ 2 bay FEA(PSC-model), collapse mode III (CIP), column type initial deflection with CIP

⑤ 2 bay FEA(PSC-model), collapse mode V (CIS), column type initial deflection with CIS

Note: CIP = compression in plate side, CIS = compression in stiffener side

Figure 8.55 The load-axial displacement curves for ID52

ID 53

Plate		Stiffener				
t	Material	h_w	t_w	b_f	t_f	Material
8 mm	5083-H116	90 mm	8 mm	-	-	5383-H116

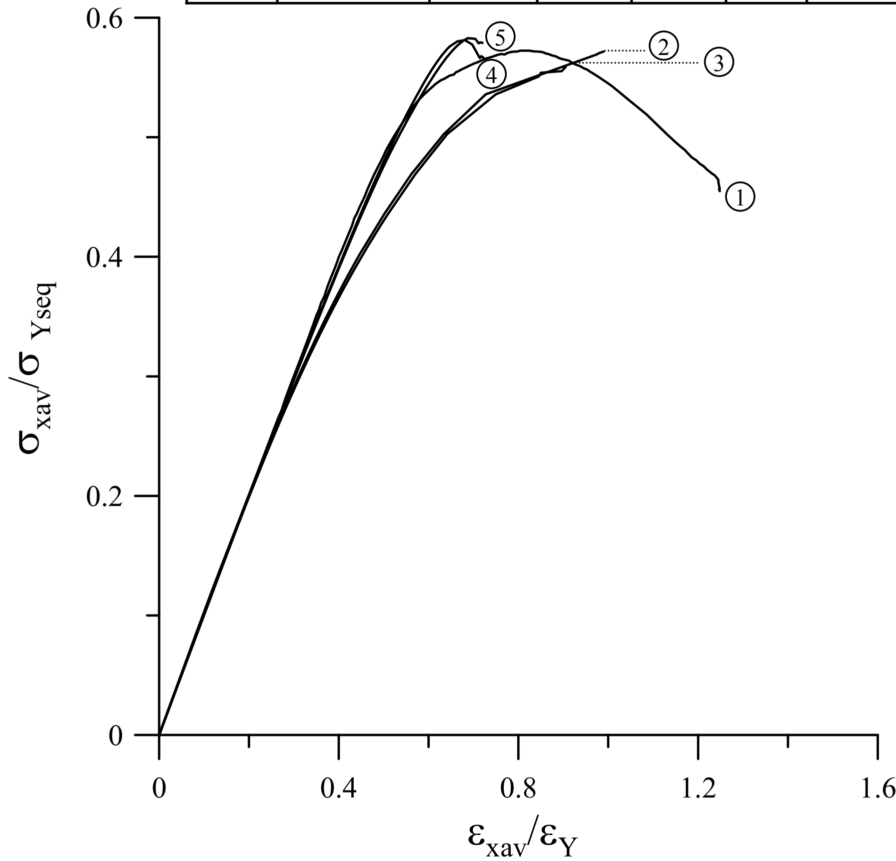

① Exp., collapse mode III (CIP)

② 1 bay FEA(PSC-model), collapse mode III (CIP), column type initial deflection with CIP

③ 1 bay FEA(PSC-model), collapse mode III (CIP), column type initial deflection with CIS

④ 2 bay FEA(PSC-model), collapse mode III (CIP), column type initial deflection with CIP

⑤ 2 bay FEA(PSC-model), collapse mode V (CIS), column type initial deflection with CIS

Note: CIP = compression in plate side, CIS = compression in stiffener side

Figure 8.56 The load-axial displacement curves for ID53

ID 54

Plate		Stiffener				
t	Material	h_w	t_w	b_f	t_f	Material
8 mm	5083-H116	120 mm	8 mm	-	-	5383-H116

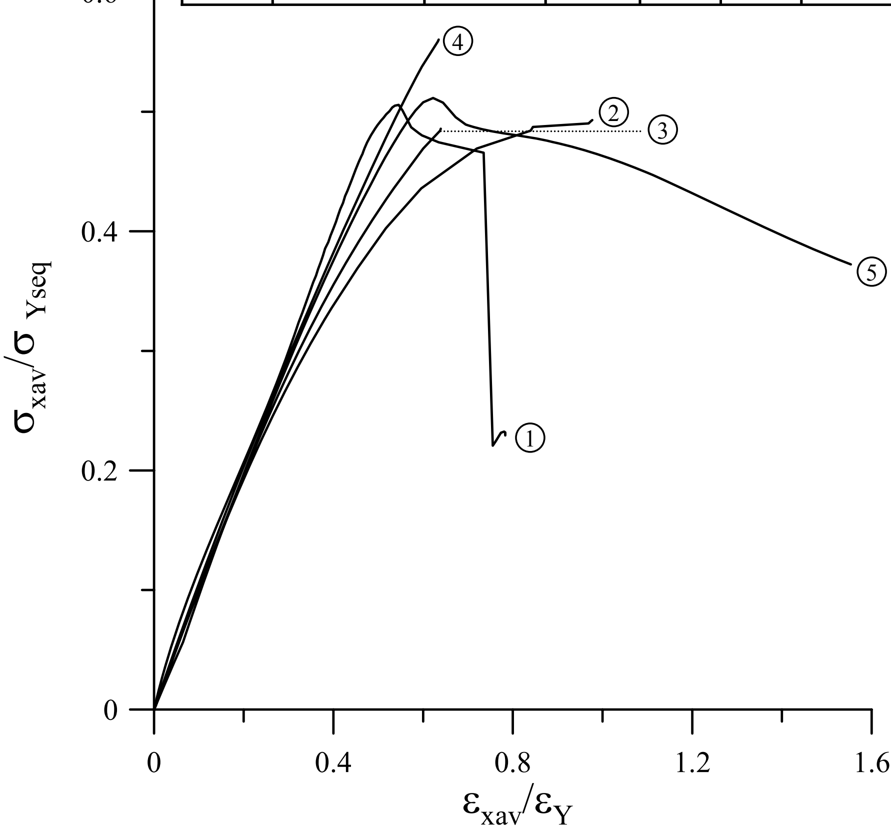

① Exp., collapse mode V (CIS)

② 1 bay FEA(PSC-model), collapse mode III (CIP), column type initial deflection with CIP

③ 1 bay FEA(PSC-model), collapse mode V (CIS), column type initial deflection with CIS

④ 2 bay FEA(PSC-model), collapse mode III (CIP), column type initial deflection with CIP

⑤ 2 bay FEA(PSC-model), collapse mode V (CIS), column type initial deflection with CIS

Note: CIP = compression in plate side, CIS = compression in stiffener side

Figure 8.57 The load-axial displacement curves for ID54

ID 55

Plate		Stiffener				
t	Material	h_w	t_w	b_f	t_f	Material
5 mm	5383-H116	60 mm	5 mm	-	-	5383-H116

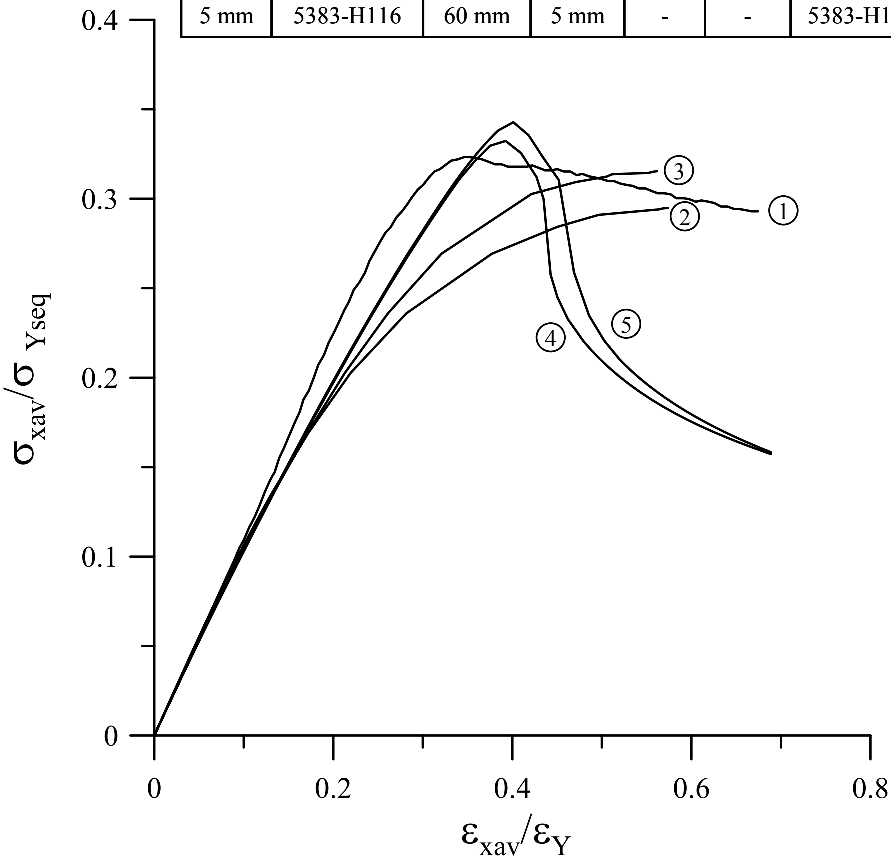

① Exp., collapse mode III (CIP)

② 1 bay FEA(PSC-model), collapse mode III (CIP), column type initial deflection with CIP

③ 1 bay FEA(PSC-model), collapse mode III (CIP), column type initial deflection with CIS

④ 2 bay FEA(PSC-model), collapse mode III (CIP), column type initial deflection with CIP

⑤ 2 bay FEA(PSC-model), collapse mode V (CIS), column type initial deflection with CIS

Note: CIP = compression in plate side, CIS = compression in stiffener side

Figure 8.58 The load-axial displacement curves for ID55

ID 56

Plate		Stiffener				
t	Material	h_w	t_w	b_f	t_f	Material
5 mm	5383-H116	90 mm	5 mm	-	-	5383-H116

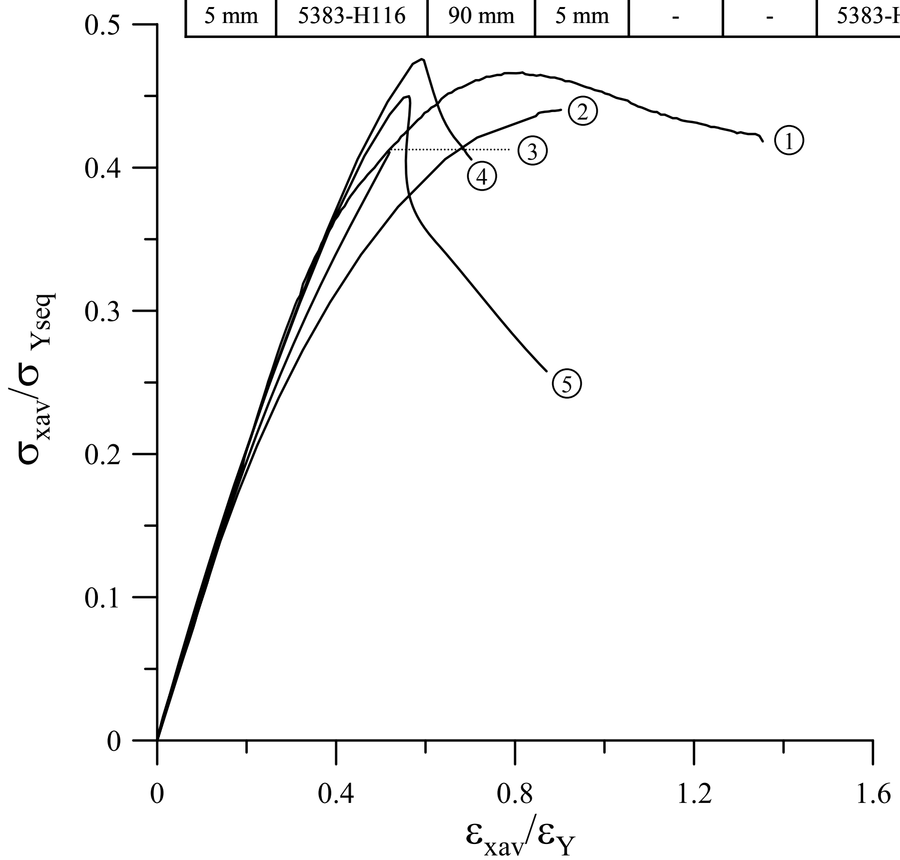

① Exp., collapse mode V (CIS)

② 1 bay FEA(PSC-model), collapse mode III (CIP), column type initial deflection with CIP

③ 1 bay FEA(PSC-model), collapse mode V (CIS), column type initial deflection with CIS

④ 2 bay FEA(PSC-model), collapse mode III (CIP), column type initial deflection with CIP

⑤ 2 bay FEA(PSC-model), collapse mode V (CIS), column type initial deflection with CIS

Note: CIP = compression in plate side, CIS = compression in stiffener side

Figure 8.59 The load-axial displacement curves for ID56

ID 57

Plate		Stiffener				
t	Material	h_w	t_w	b_f	t_f	Material
5 mm	5383-H116	120 mm	5 mm	-	-	5383-H116

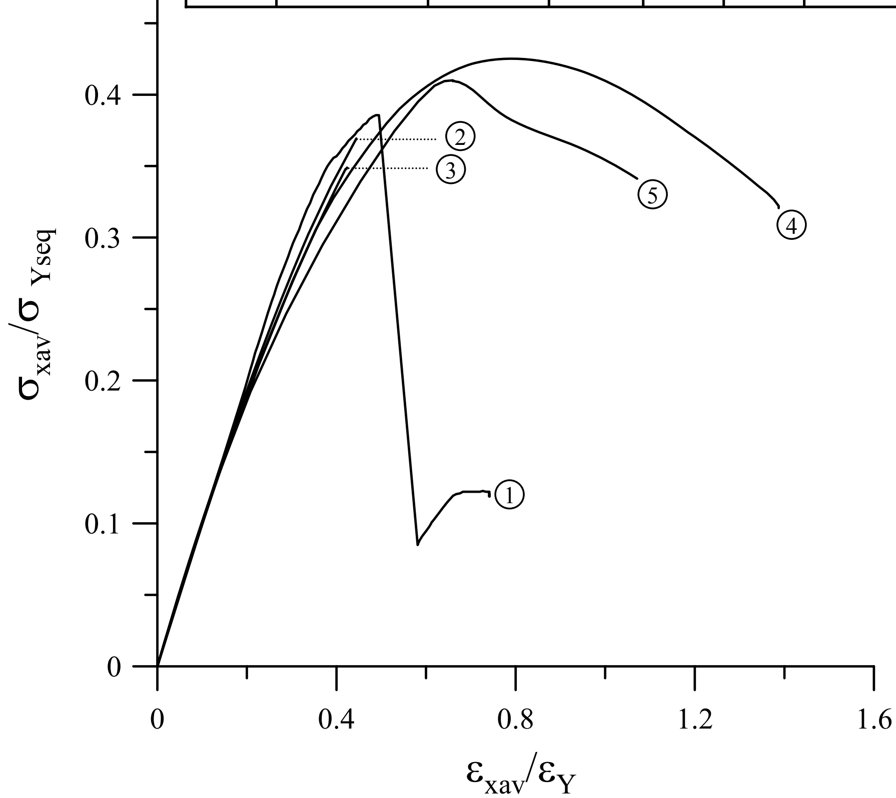

① Exp., collapse mode V (CIS)

② 1 bay FEA(PSC-model), collapse mode III (CIP), column type initial deflection with CIP

③ 1 bay FEA(PSC-model), collapse mode V (CIS), column type initial deflection with CIS

④ 2 bay FEA(PSC-model), collapse mode III (CIP), column type initial deflection with CIP

⑤ 2 bay FEA(PSC-model), collapse mode V (CIS), column type initial deflection with CIS

Note: CIP = compression in plate side, CIS = compression in stiffener side

Figure 8.60 The load-axial displacement curves for ID57

ID 58

Plate		Stiffener				
t	Material	h_w	t_w	b_f	t_f	Material
6 mm	5383-H116	60 mm	6 mm	-	-	5383-H116

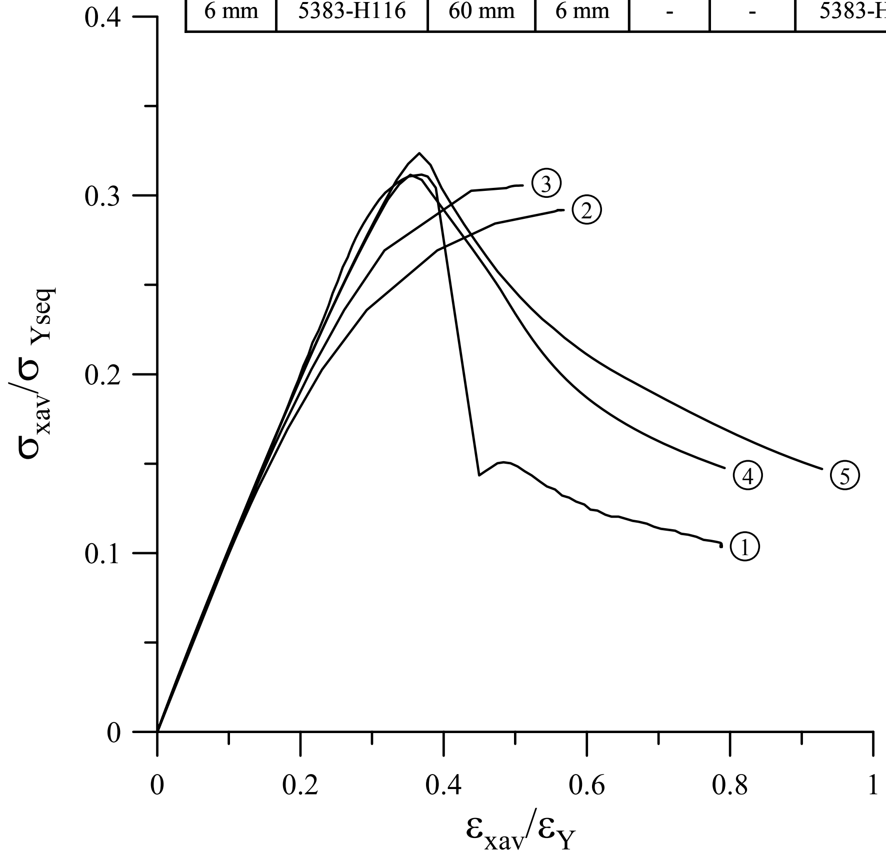

① Exp., collapse mode III (CIP)

② 1 bay FEA(PSC-model), collapse mode III (CIP), column type initial deflection with CIP

③ 1 bay FEA(PSC-model), collapse mode III (CIP), column type initial deflection with CIS

④ 2 bay FEA(PSC-model), collapse mode III (CIP), column type initial deflection with CIP

⑤ 2 bay FEA(PSC-model), collapse mode V (CIS), column type initial deflection with CIS

Note: CIP = compression in plate side, CIS = compression in stiffener side

Figure 8.61 The load-axial displacement curves for ID58

ID 59

Plate		Stiffener				
t	Material	h_w	t_w	b_f	t_f	Material
6 mm	5383-H116	90 mm	6 mm	-	-	5383-H116

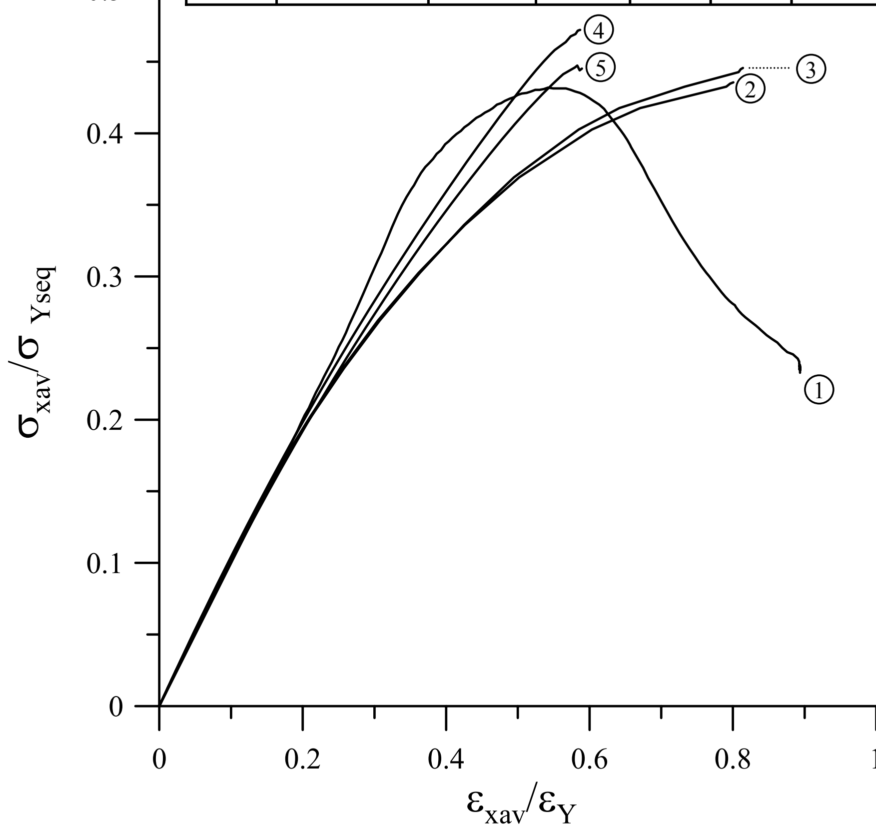

① Exp., collapse mode III (CIP)

② 1 bay FEA(PSC-model), collapse mode III (CIP), column type initial deflection with CIP

③ 1 bay FEA(PSC-model), collapse mode III (CIP), column type initial deflection with CIS

④ 2 bay FEA(PSC-model), collapse mode III (CIP), column type initial deflection with CIP

⑤ 2 bay FEA(PSC-model), collapse mode V (CIS), column type initial deflection with CIS

Note: CIP = compression in plate side, CIS = compression in stiffener side

Figure 8.62 The load-axial displacement curves for ID59

ID 60

Plate		Stiffener				
t	Material	h_w	t_w	b_f	t_f	Material
6 mm	5383-H116	120 mm	6 mm	-	-	5383-H116

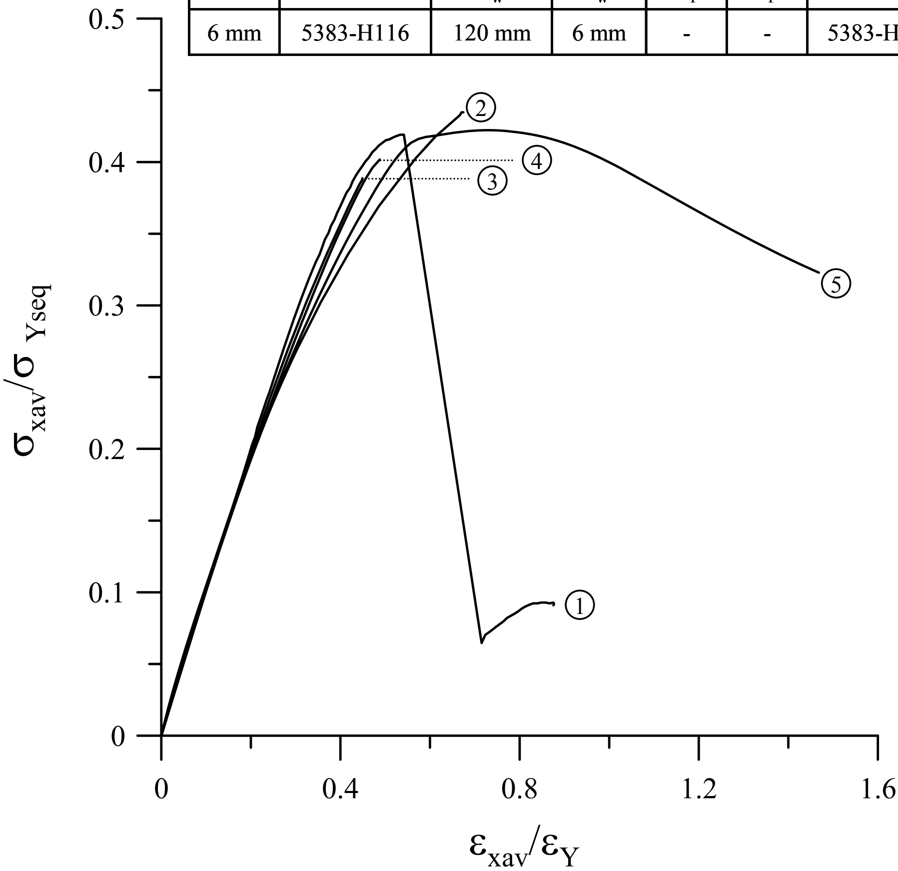

① Exp., collapse mode V (CIS)

② 1 bay FEA(PSC-model), collapse mode III (CIP), column type initial deflection with CIP

③ 1 bay FEA(PSC-model), collapse mode V (CIS), column type initial deflection with CIS

④ 2 bay FEA(PSC-model), collapse mode III (CIP), column type initial deflection with CIP

⑤ 2 bay FEA(PSC-model), collapse mode V (CIS), column type initial deflection with CIS

Note: CIP = compression in plate side, CIS = compression in stiffener side

Figure 8.63 The load-axial displacement curves for ID60

ID 61

Plate		Stiffener				
t	Material	h_w	t_w	b_f	t_f	Material
8 mm	5383-H116	60 mm	8 mm	-	-	5383-H116

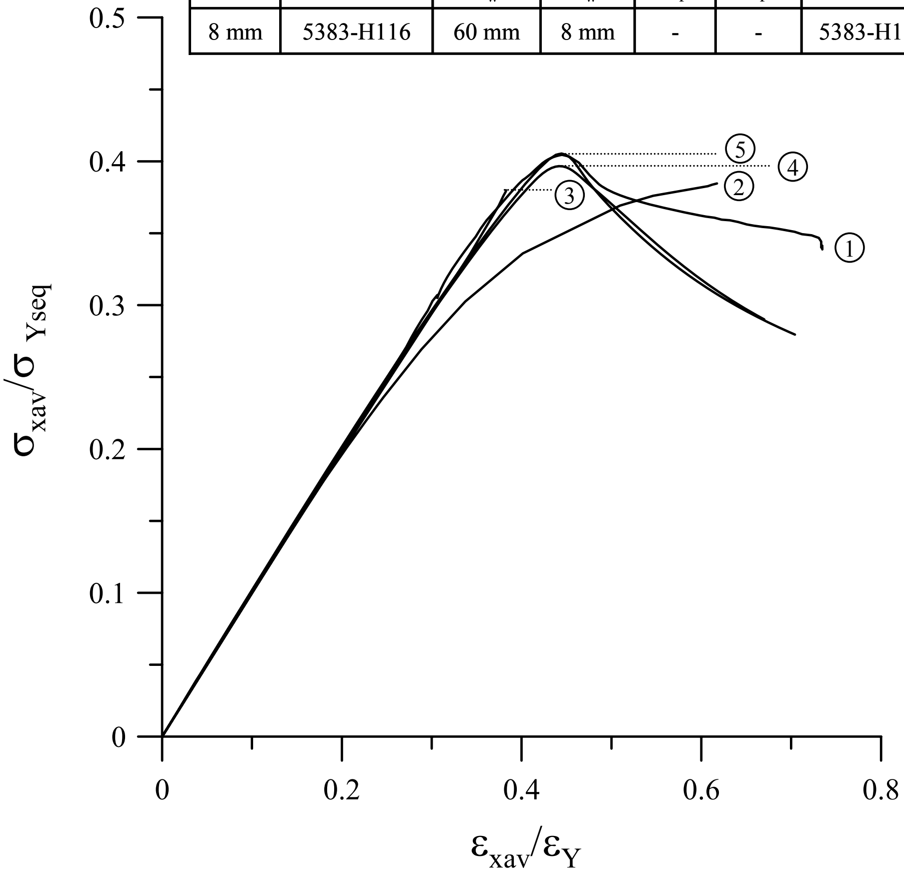

① Exp., collapse mode III (CIP)

② 1 bay FEA(PSC-model), collapse mode III (CIP), column type initial deflection with CIP

③ 1 bay FEA(PSC-model), collapse mode V (CIS), column type initial deflection with CIS

④ 2 bay FEA(PSC-model), collapse mode III (CIP), column type initial deflection with CIP

⑤ 2 bay FEA(PSC-model), collapse mode V (CIS), column type initial deflection with CIS

Note: CIP = compression in plate side, CIS = compression in stiffener side

Figure 8.64 The load-axial displacement curves for ID61

ID 62

Plate		Stiffener				
t	Material	h_w	t_w	b_f	t_f	Material
8 mm	5383-H116	90 mm	8 mm	-	-	5383-H116

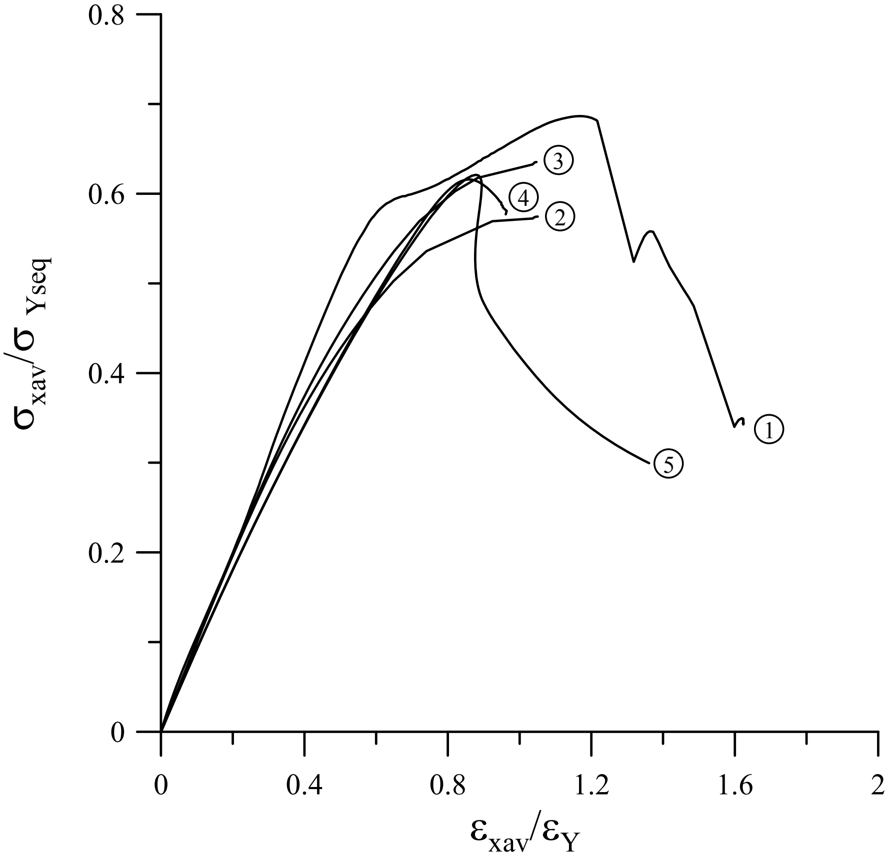

① Exp., collapse mode V (CIS)

② 1 bay FEA(PSC-model), collapse mode III (CIP), column type initial deflection with CIP

③ 1 bay FEA(PSC-model), collapse mode III (CIP), column type initial deflection with CIS

④ 2 bay FEA(PSC-model), collapse mode III (CIP), column type initial deflection with CIP

⑤ 2 bay FEA(PSC-model), collapse mode V (CIS), column type initial deflection with CIS

Note: CIP = compression in plate side, CIS = compression in stiffener side

Figure 8.65 The load-axial displacement curves for ID62

ID 63

Plate		Stiffener				
t	Material	h_w	t_w	b_f	t_f	Material
8 mm	5383-H116	120 mm	8 mm	-	-	5383-H116

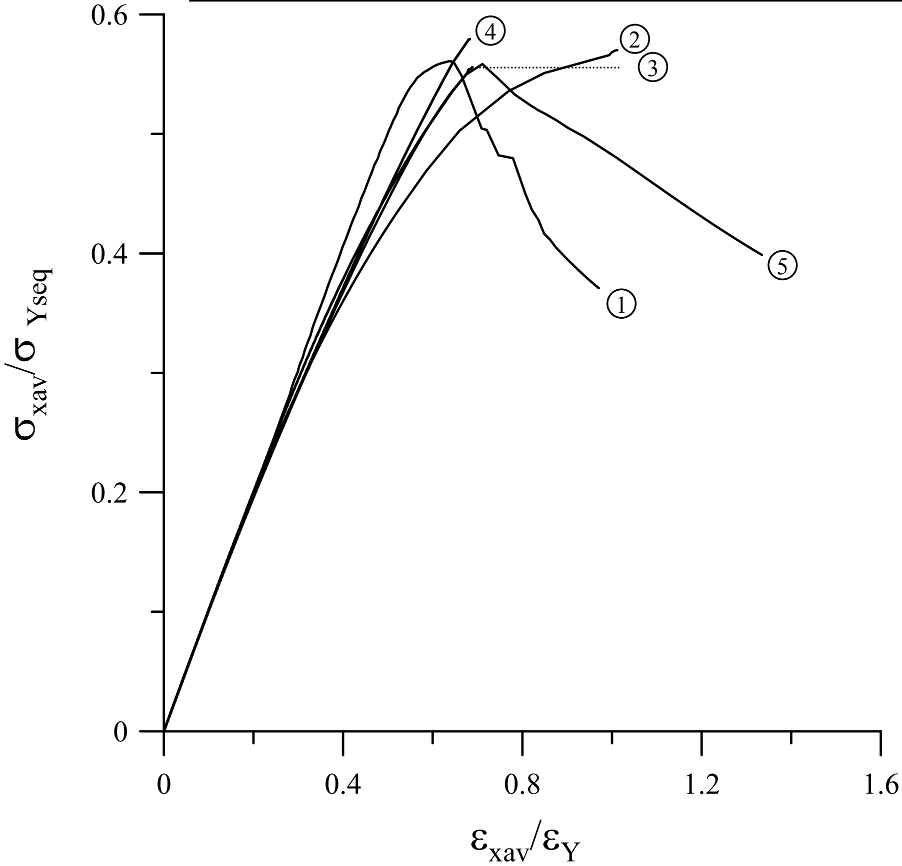

① Exp., collapse mode V (CIS)

② 1 bay FEA(PSC-model), collapse mode III (CIP), column type initial deflection with CIP

③ 1 bay FEA(PSC-model), collapse mode V (CIS), column type initial deflection with CIS

④ 2 bay FEA(PSC-model), collapse mode III (CIP), column type initial deflection with CIP

⑤ 2 bay FEA(PSC-model), collapse mode V (CIS), column type initial deflection with CIS

Note: CIP = compression in plate side, CIS = compression in stiffener side

Figure 8.66 The load-axial displacement curves for ID63

ID 64

Plate		Stiffener				
t	Material	h_w	t_w	b_f	t_f	Material
5 mm	5083-H116	80 mm	5 mm	60 mm	5 mm	5083-H116

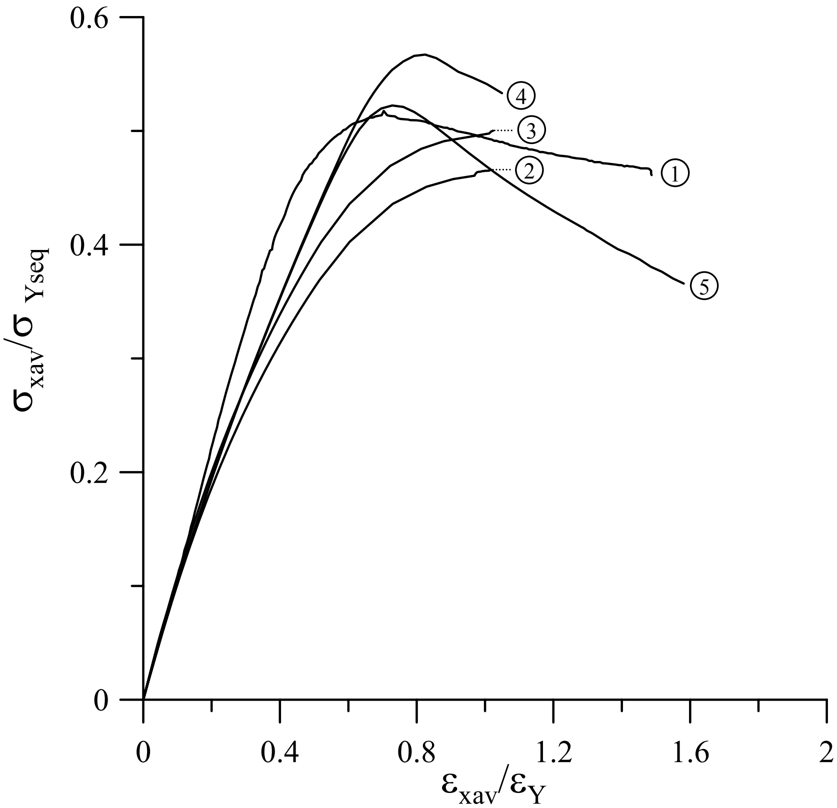

① Exp., collapse mode III (CIP), IV

② 1 bay FEA(PSC-model), collapse mode III (CIP), column type initial deflection with CIP

③ 1 bay FEA(PSC-model), collapse mode III (CIP), column type initial deflection with CIS

④ 2 bay FEA(PSC-model), collapse mode III (CIP), column type initial deflection with CIP

⑤ 2 bay FEA(PSC-model), collapse mode V (CIS), column type initial deflection with CIS

Note: CIP = compression in plate side, CIS = compression in stiffener side

Figure 8.67 The load-axial displacement curves for ID64

ID 65

Plate		Stiffener				
t	Material	h_w	t_w	b_f	t_f	Material
6 mm	5083-H116	60 mm	5 mm	60 mm	5 mm	5083-H116

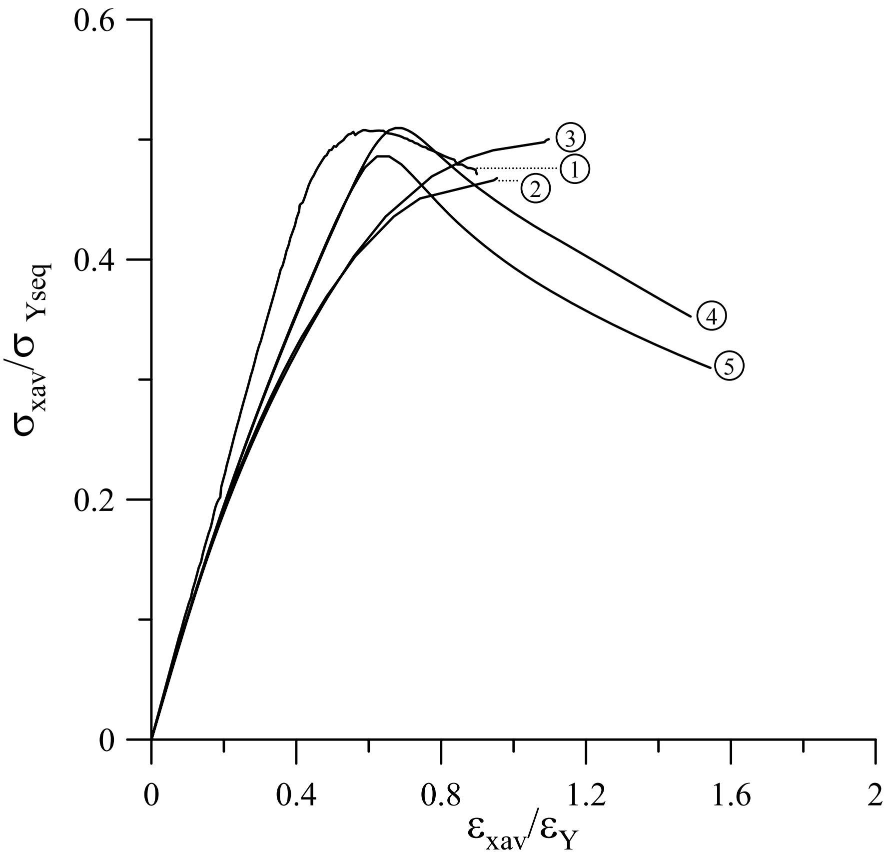

① Exp., collapse mode III (CIP)

② 1 bay FEA(PSC-model), collapse mode III (CIP), column type initial deflection with CIP

③ 1 bay FEA(PSC-model), collapse mode III (CIP), column type initial deflection with CIS

④ 2 bay FEA(PSC-model), collapse mode III (CIP), column type initial deflection with CIP

⑤ 2 bay FEA(PSC-model), collapse mode V (CIS), column type initial deflection with CIS

Note: CIP = compression in plate side, CIS = compression in stiffener side

Figure 8.68 The load-axial displacement curves for ID65

ID 66

Plate		Stiffener				
t	Material	h_w	t_w	b_f	t_f	Material
8 mm	5083-H116	100 mm	5 mm	60 mm	5 mm	5083-H116

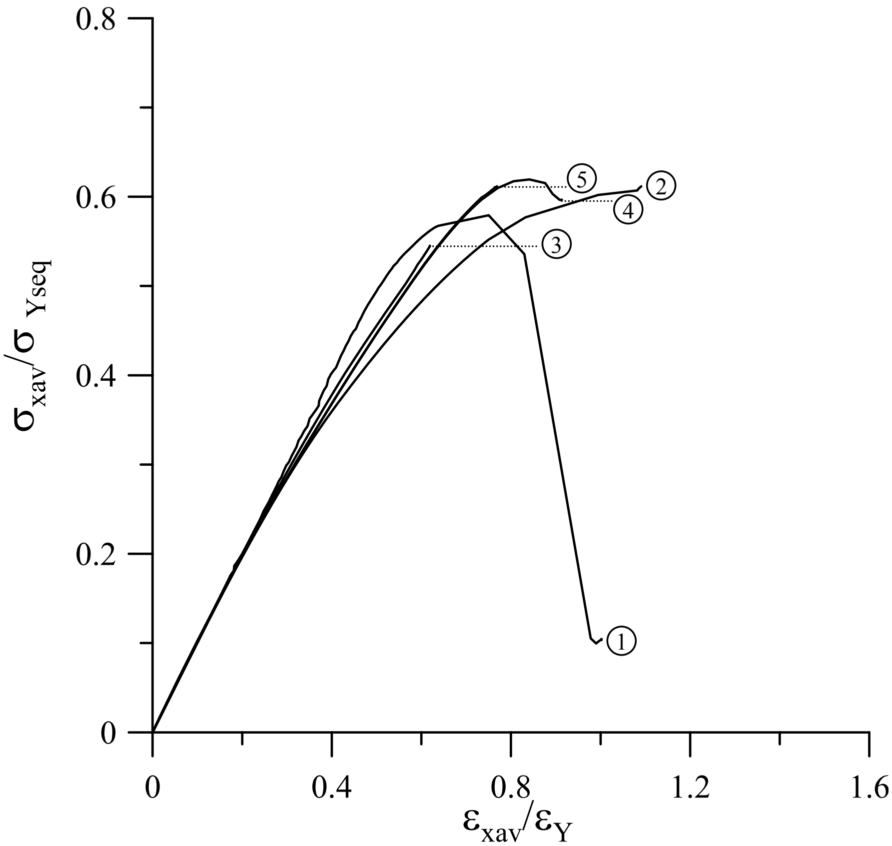

① Exp., collapse mode V (CIS)

② 1 bay FEA(PSC-model), collapse mode III (CIP), column type initial deflection with CIP

③ 1 bay FEA(PSC-model), collapse mode V (CIS), column type initial deflection with CIS

④ 2 bay FEA(PSC-model), collapse mode III (CIP), column type initial deflection with CIP

⑤ 2 bay FEA(PSC-model), collapse mode V (CIS), column type initial deflection with CIS

Note: CIP = compression in plate side, CIS = compression in stiffener side

Figure 8.69 The load-axial displacement curves for ID66

ID 67

Plate		Stiffener				
t	Material	h_w	t_w	b_f	t_f	Material
5 mm	5083-H116	80 mm	5 mm	60 mm	5 mm	5383-H116

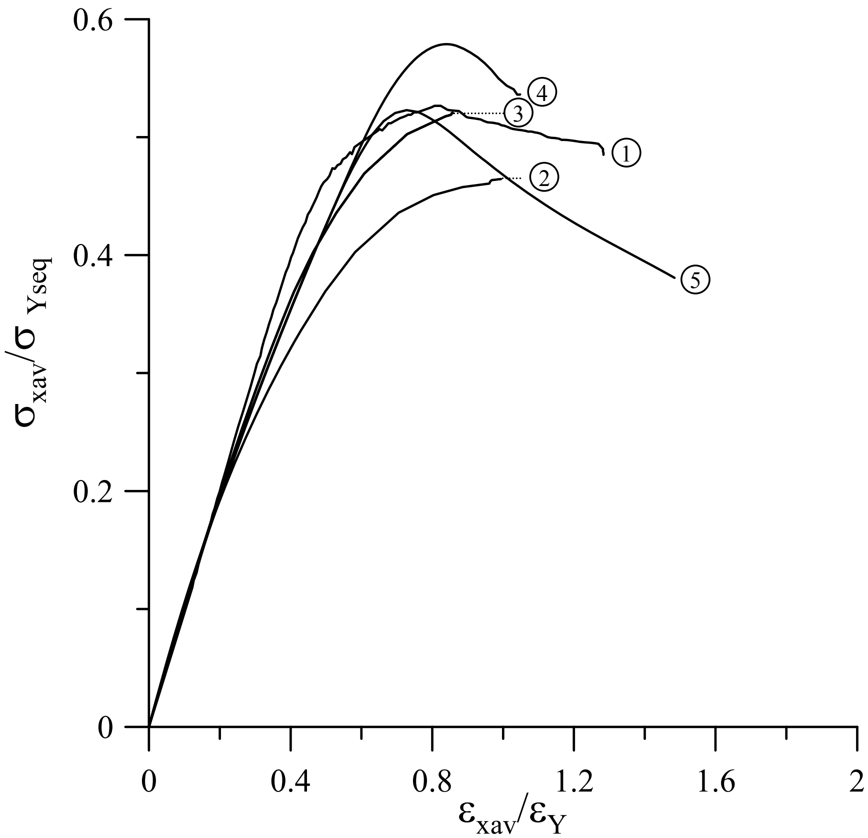

① Exp., collapse mode III (CIP), IV

② 1 bay FEA(PSC-model), collapse mode III (CIP), column type initial deflection with CIP

③ 1 bay FEA(PSC-model), collapse mode III (CIP), column type initial deflection with CIS

④ 2 bay FEA(PSC-model), collapse mode III (CIP), column type initial deflection with CIP

⑤ 2 bay FEA(PSC-model), collapse mode V (CIS), column type initial deflection with CIS

Note: CIP = compression in plate side, CIS = compression in stiffener side

Figure 8.70 The load-axial displacement curves for ID67

ID 68

Plate		Stiffener				
t	Material	h_w	t_w	b_f	t_f	Material
6 mm	5083-H116	60 mm	5 mm	60 mm	5 mm	5383-H116

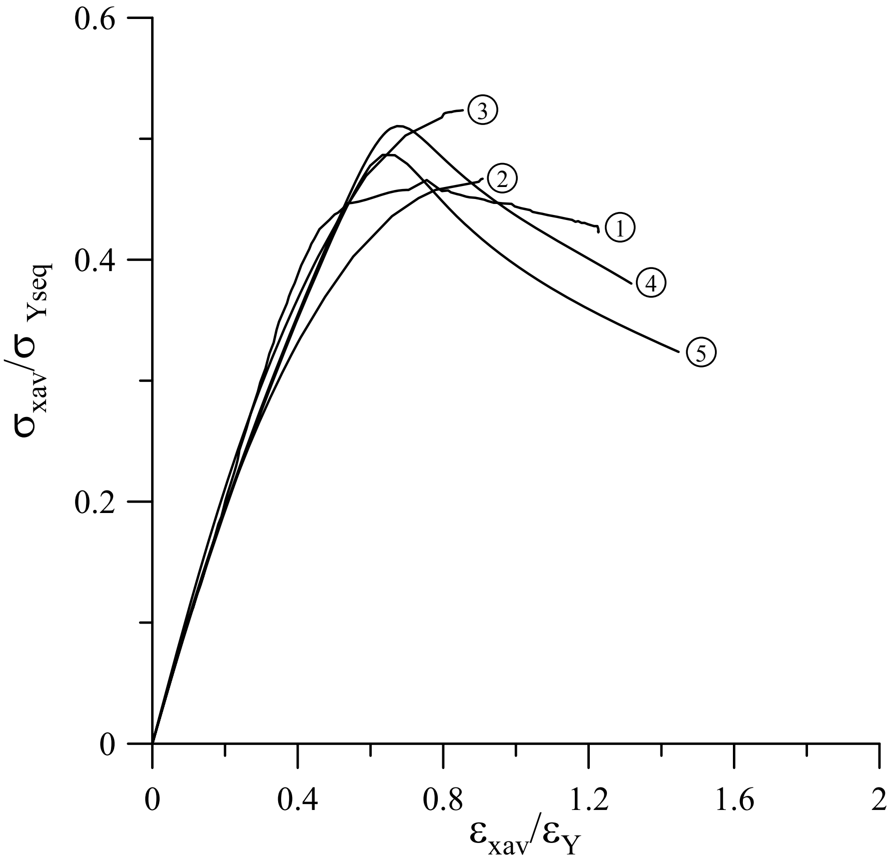

① Exp., collapse mode III (CIP), IV

② 1 bay FEA(PSC-model), collapse mode III (CIP), column type initial deflection with CIP

③ 1 bay FEA(PSC-model), collapse mode III (CIP), column type initial deflection with CIS

④ 2 bay FEA(PSC-model), collapse mode III (CIP), column type initial deflection with CIP

⑤ 2 bay FEA(PSC-model), collapse mode V (CIS), column type initial deflection with CIS

Note: CIP = compression in plate side, CIS = compression in stiffener side

Figure 8.71 The load-axial displacement curves for ID68

ID 69

Plate		Stiffener				
t	Material	h_w	t_w	b_f	t_f	Material
8 mm	5083-H116	100 mm	5 mm	60 mm	5 mm	5383-H116

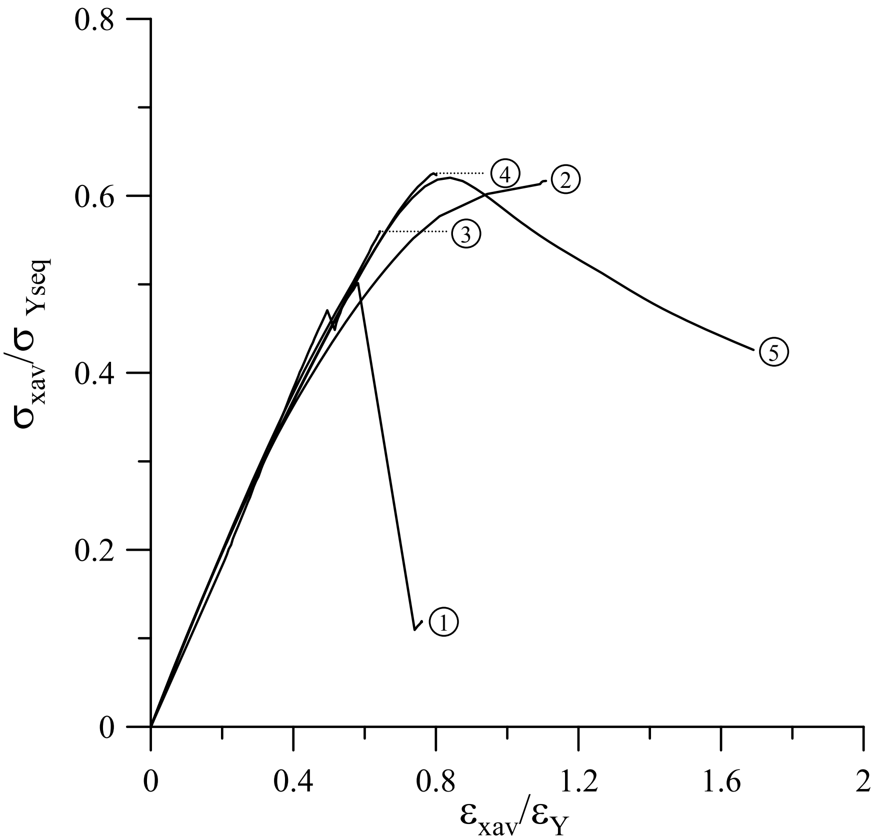

① Exp., collapse mode V (CIS)

② 1 bay FEA(PSC-model), collapse mode III (CIP), column type initial deflection with CIP

③ 1 bay FEA(PSC-model), collapse mode V (CIS), column type initial deflection with CIS

④ 2 bay FEA(PSC-model), collapse mode III (CIP), column type initial deflection with CIP

⑤ 2 bay FEA(PSC-model), collapse mode V (CIS), column type initial deflection with CIS

Note: CIP = compression in plate side, CIS = compression in stiffener side

Figure 8.72 The load-axial displacement curves for ID69

ID 70

Plate		Stiffener				
t	Material	h_w	t_w	b_f	t_f	Material
5 mm	5383-H116	80 mm	5 mm	60 mm	5 mm	5383-H116

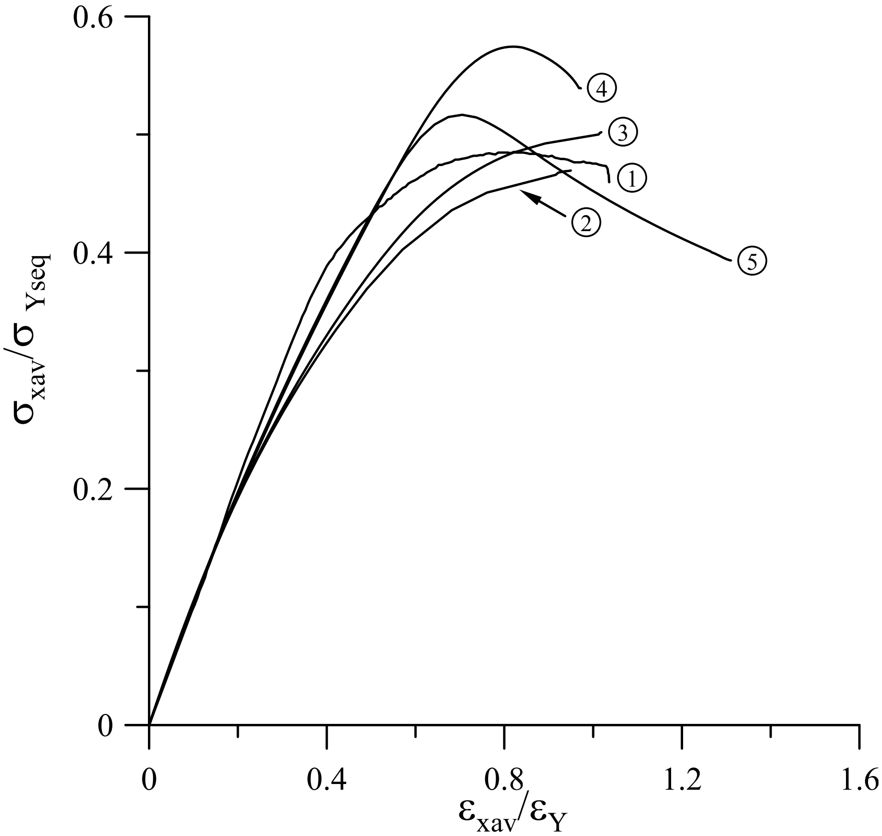

① Exp., collapse mode III (CIP), IV

② 1 bay FEA(PSC-model), collapse mode III (CIP), column type initial deflection with CIP

③ 1 bay FEA(PSC-model), collapse mode III (CIP), column type initial deflection with CIS

④ 2 bay FEA(PSC-model), collapse mode III (CIP), column type initial deflection with CIP

⑤ 2 bay FEA(PSC-model), collapse mode V (CIS), column type initial deflection with CIS

Note: CIP = compression in plate side, CIS = compression in stiffener side

Figure 8.73 The load-axial displacement curves for ID70

ID 71

Plate		Stiffener				
t	Material	h_w	t_w	b_f	t_f	Material
6 mm	5383-H116	60 mm	5 mm	60 mm	5 mm	5383-H116

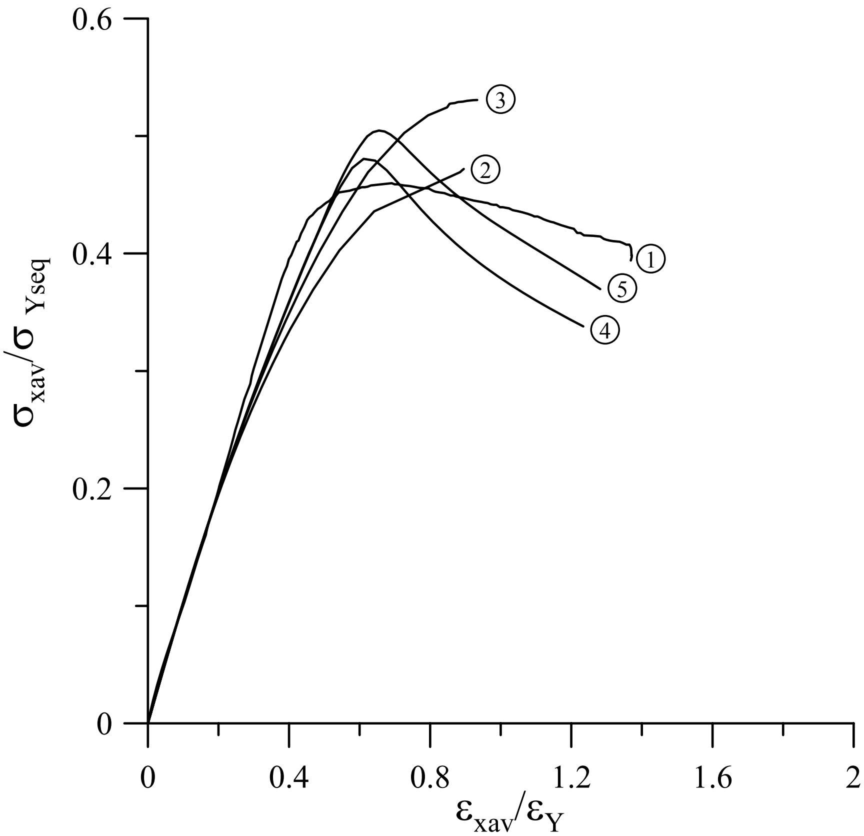

① Exp., collapse mode III (CIP)

② 1 bay FEA(PSC-model), collapse mode III (CIP), column type initial deflection with CIP

③ 1 bay FEA(PSC-model), collapse mode III (CIP), column type initial deflection with CIS

④ 2 bay FEA(PSC-model), collapse mode III (CIP), column type initial deflection with CIP

⑤ 2 bay FEA(PSC-model), collapse mode V (CIS), column type initial deflection with CIS

Note: CIP = compression in plate side, CIS = compression in stiffener side

Figure 8.74 The load-axial displacement curves for ID71

ID 72

Plate		Stiffener				
t	Material	h_w	t_w	b_f	t_f	Material
8 mm	5383-H116	100 mm	5 mm	60 mm	5 mm	5383-H116

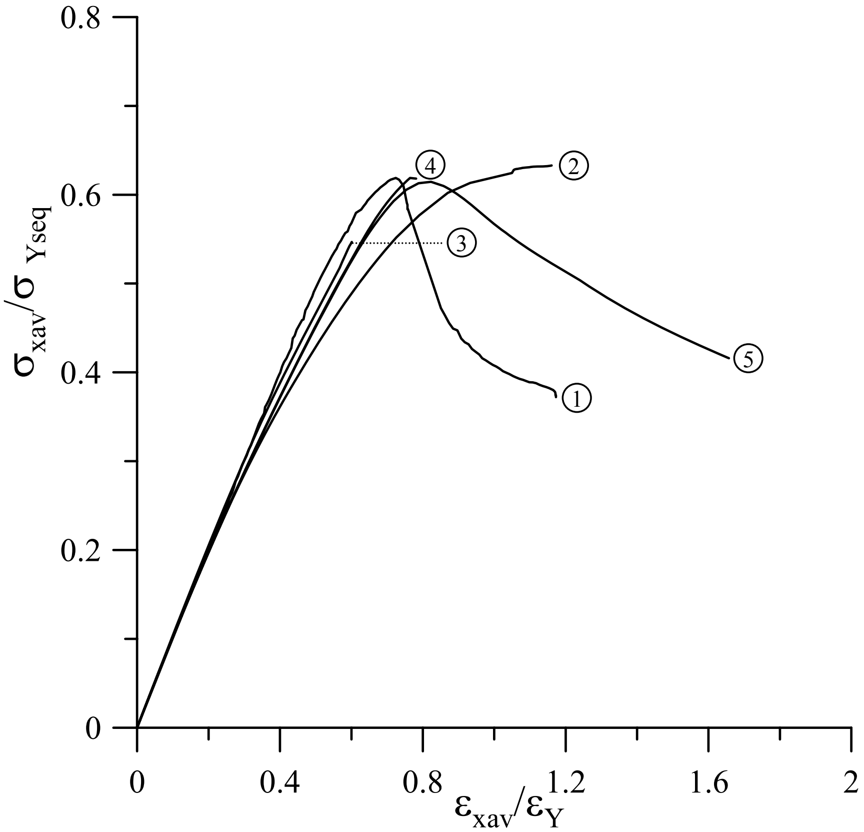

① Exp., collapse mode V (CIS)

② 1 bay FEA(PSC-model), collapse mode III (CIP), column type initial deflection with CIP

③ 1 bay FEA(PSC-model), collapse mode V (CIS), column type initial deflection with CIS

④ 2 bay FEA(PSC-model), collapse mode III (CIP), column type initial deflection with CIP

⑤ 2 bay FEA(PSC-model), collapse mode V (CIS), column type initial deflection with CIS

Note: CIP = compression in plate side, CIS = compression in stiffener side

Figure 8.75 The load-axial displacement curves for ID72

ID 73

Plate		Stiffener				
t	Material	h_w	t_w	b_f	t_f	Material
6 mm	5083-H116	76.8 mm	4 mm	45 mm	5.6 mm	6082-T6

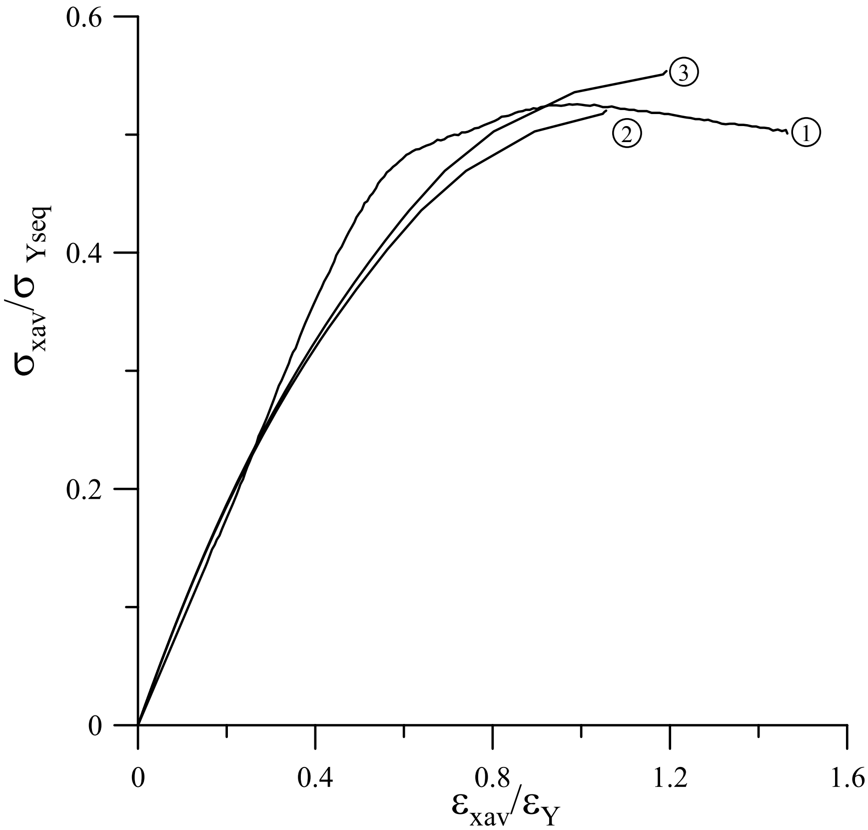

① Exp., collapse mode III (CIP)

② 1 bay FEA(PSC-model), collapse mode III (CIP), column type initial deflection with CIP

③ 1 bay FEA(PSC-model), collapse mode III (CIP), column type initial deflection with CIS

Note: CIP = compression in plate side, CIS = compression in stiffener side

Figure 8.76 The load-axial displacement curves for ID73

ID 74

Plate		Stiffener				
t	Material	h_w	t_w	b_f	t_f	Material
8 mm	5083-H116	100 mm	6 mm	55 mm	8.2 mm	6082-T6

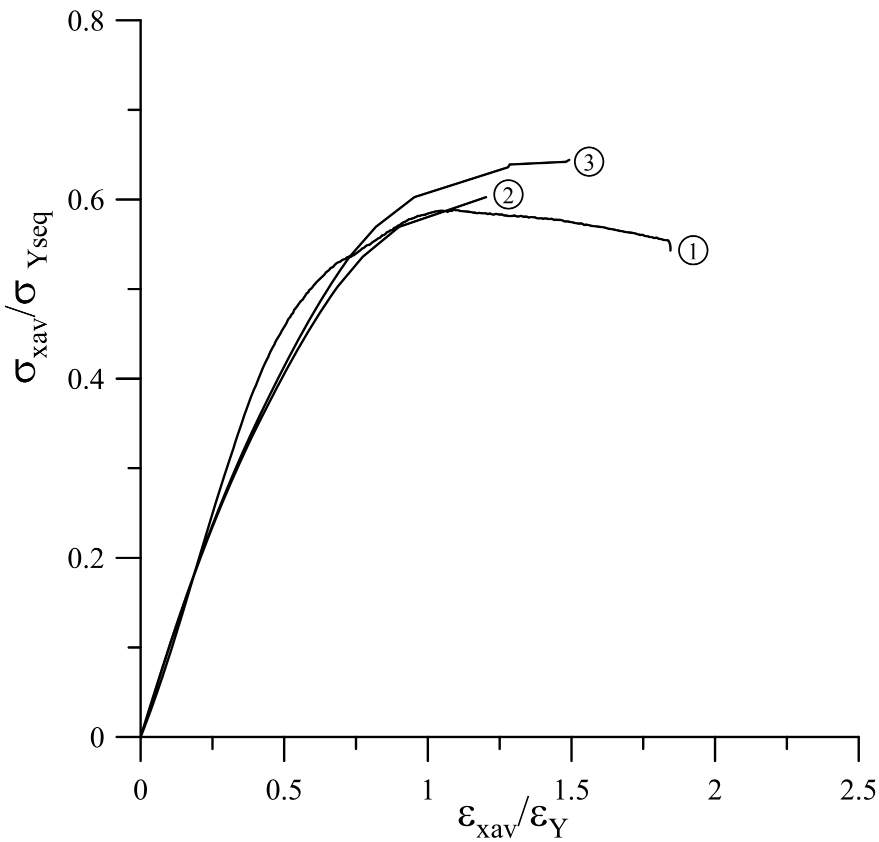

① Exp., collapse mode III (CIP), IV

② 1 bay FEA(PSC-model), collapse mode III (CIP), column type initial deflection with CIP

③ 1 bay FEA(PSC-model), collapse mode III (CIP), column type initial deflection with CIS

Note: CIP = compression in plate side, CIS = compression in stiffener side

Figure 8.77 The load-axial displacement curves for ID74

ID 75

Plate		Stiffener				
t	Material	h_w	t_w	b_f	t_f	Material
8 mm	5383-H116	100 mm	6 mm	55 mm	8.2 mm	5383-H112

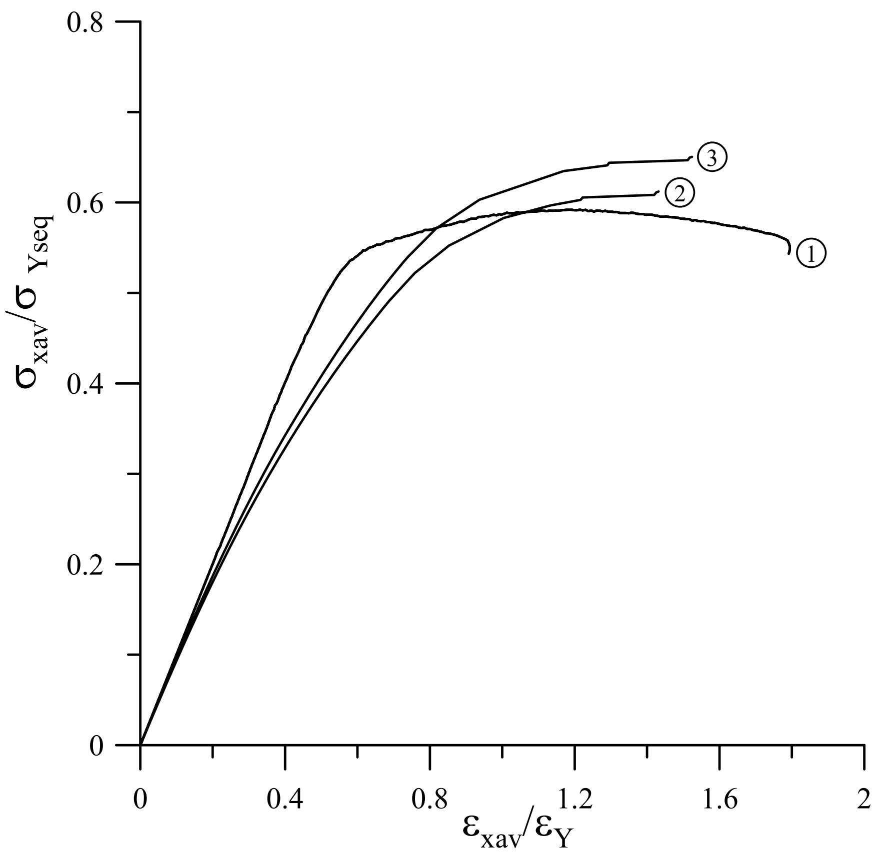

① Exp., collapse mode III (CIP), IV

② 1 bay FEA(PSC-model), collapse mode III (CIP), column type initial deflection with CIP

③ 1 bay FEA(PSC-model), collapse mode III (CIP), column type initial deflection with CIS

Note: CIP = compression in plate side, CIS = compression in stiffener side

Figure 8.78 The load-axial displacement curves for ID75

ID 76

Plate		Stiffener				
t	Material	h_w	t_w	b_f	t_f	Material
6 mm	5083-H116	76.8 mm	4 mm	45 mm	5.6 mm	6082-T6

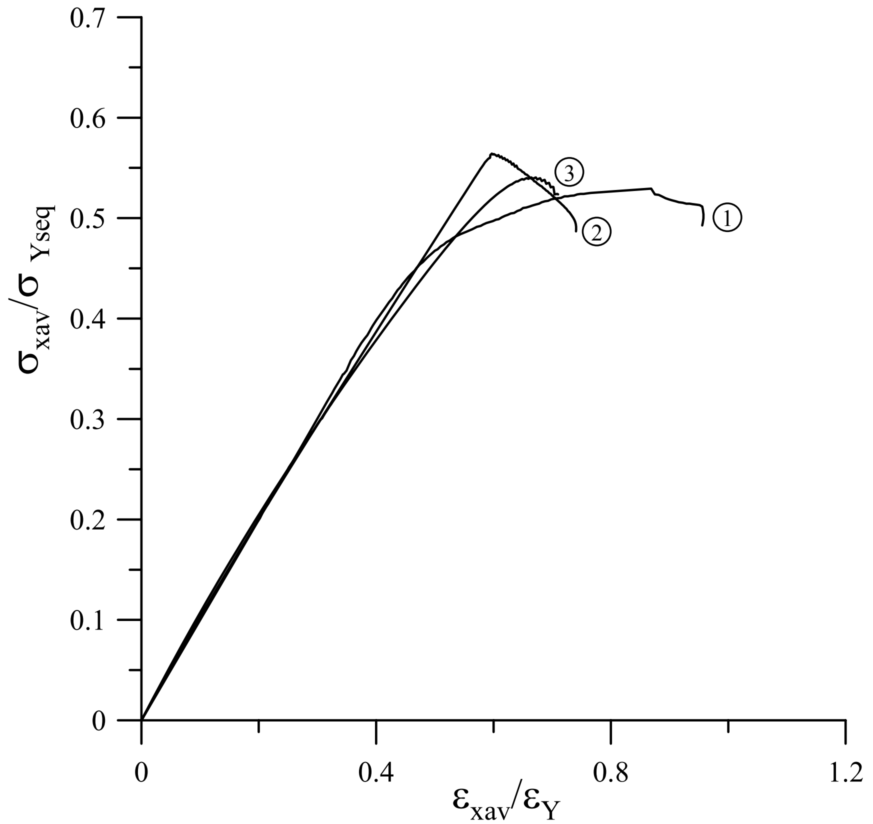

① Exp., collapse mode III (CIP)

② 2 bay FEA(PSC-model), collapse mode III (CIP), column type initial deflection with CIP

③ 2 bay FEA(PSC-model), collapse mode V (CIS), column type initial deflection with CIS

Note: CIP = compression in plate side, CIS = compression in stiffener side

Figure 8.79 The load-axial displacement curves for ID76

ID 77

Plate		Stiffener				
t	Material	h_w	t_w	b_f	t_f	Material
8 mm	5083-H116	100 mm	6 mm	55 mm	8.2 mm	6082-T6

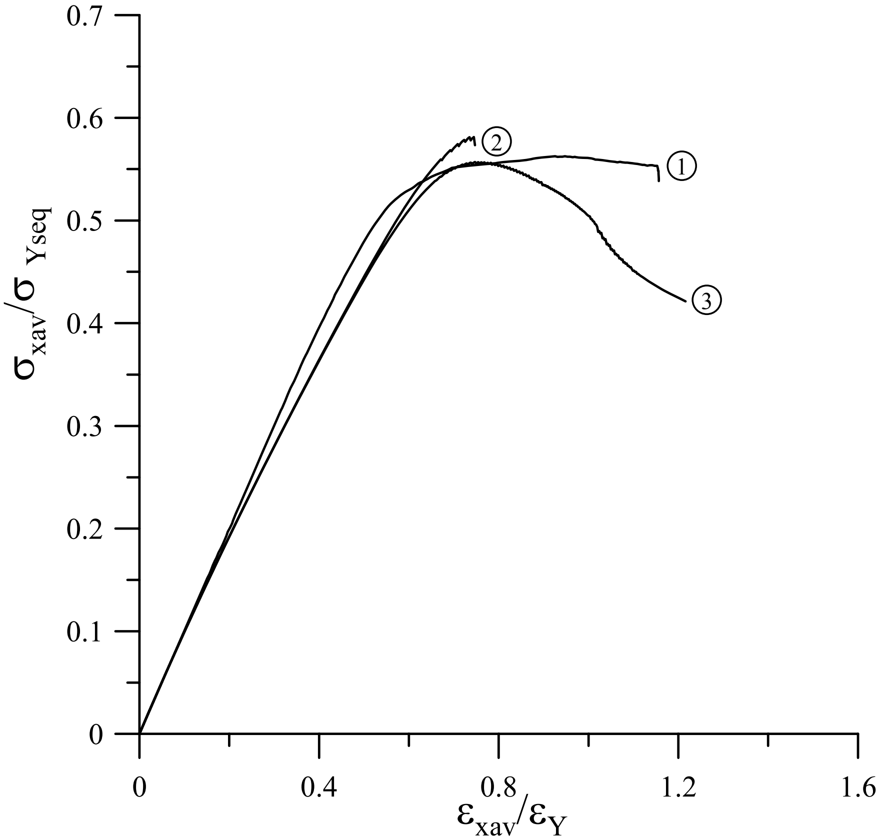

① Exp., collapse mode III (CIP), IV

② 2 bay FEA(PSC-model), collapse mode III (CIP), column type initial deflection with CIP

③ 2 bay FEA(PSC-model), collapse mode V (CIS), column type initial deflection with CIS

Note: CIP = compression in plate side, CIS = compression in stiffener side

Figure 8.80 The load-axial displacement curves for ID77

ID 78

Plate		Stiffener				
t	Material	h_w	t_w	b_f	t_f	Material
8 mm	5383-H116	100 mm	6 mm	55 mm	8.2 mm	5383-H112

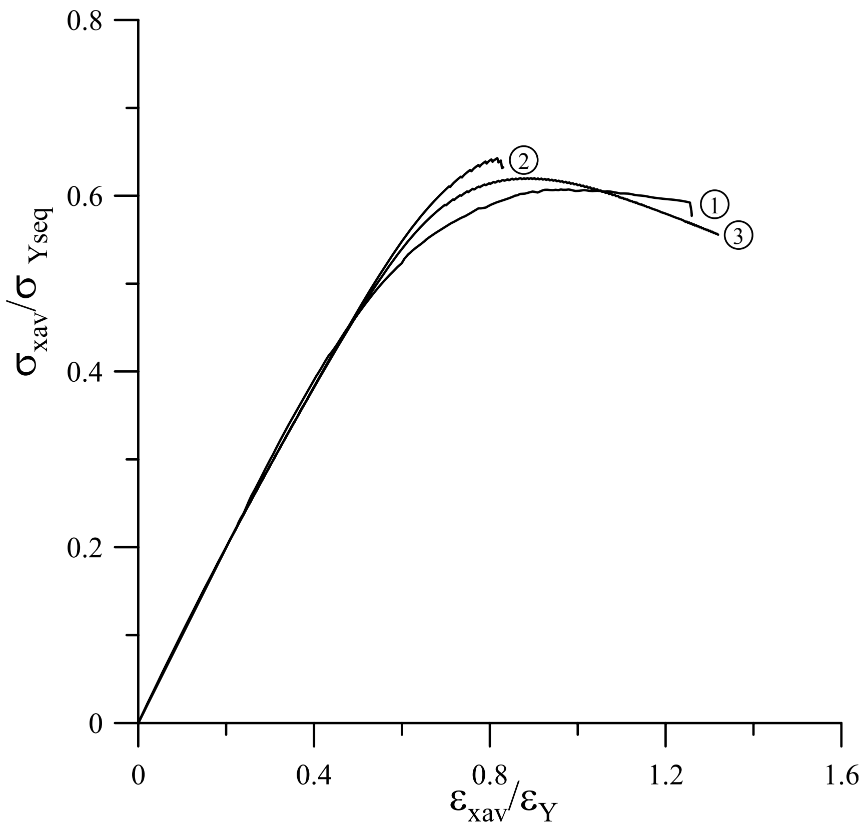

① Exp., collapse mode III (CIP)

② 2 bay FEA(PSC-model), collapse mode III (CIP), column type initial deflection with CIP

③ 2 bay FEA(PSC-model), collapse mode V (CIS), column type initial deflection with CIS

Note: CIP = compression in plate side, CIS = compression in stiffener side

Figure 8.81 The load-axial displacement curves for ID78

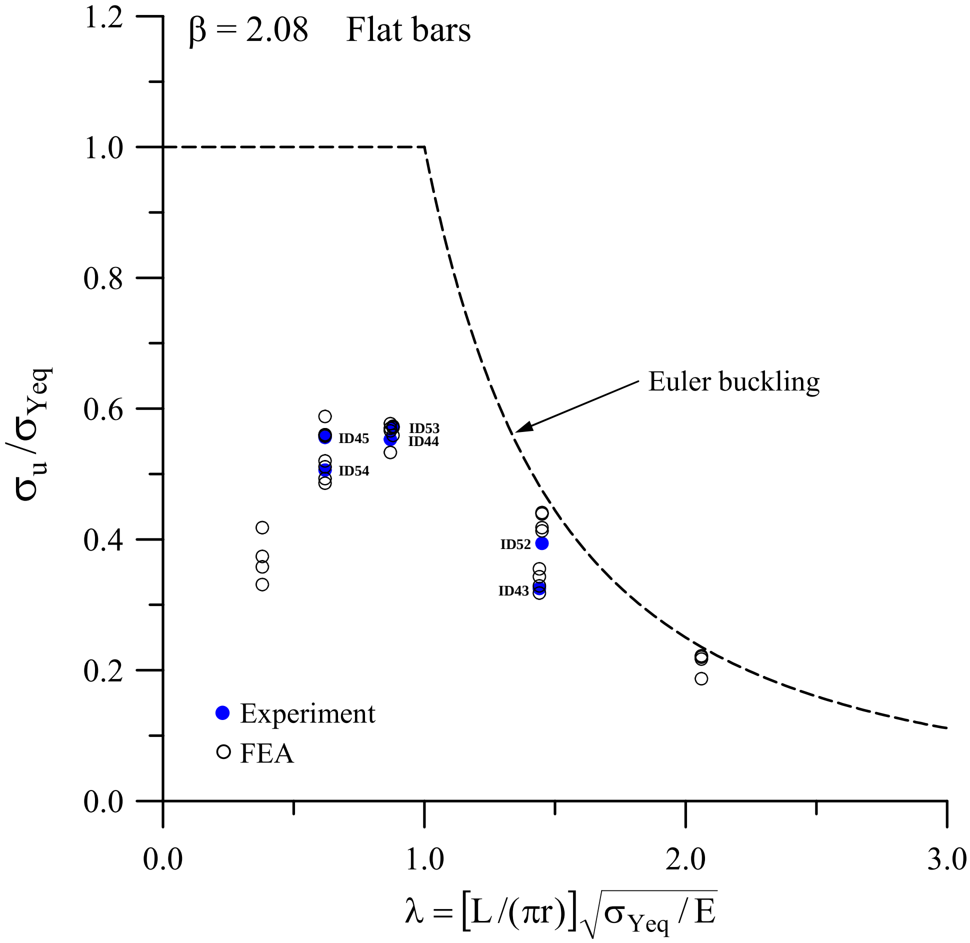

Figure 8.82(a) Variation of the ultimate strength for the test structures with flat-bars, $\beta = 2.08$

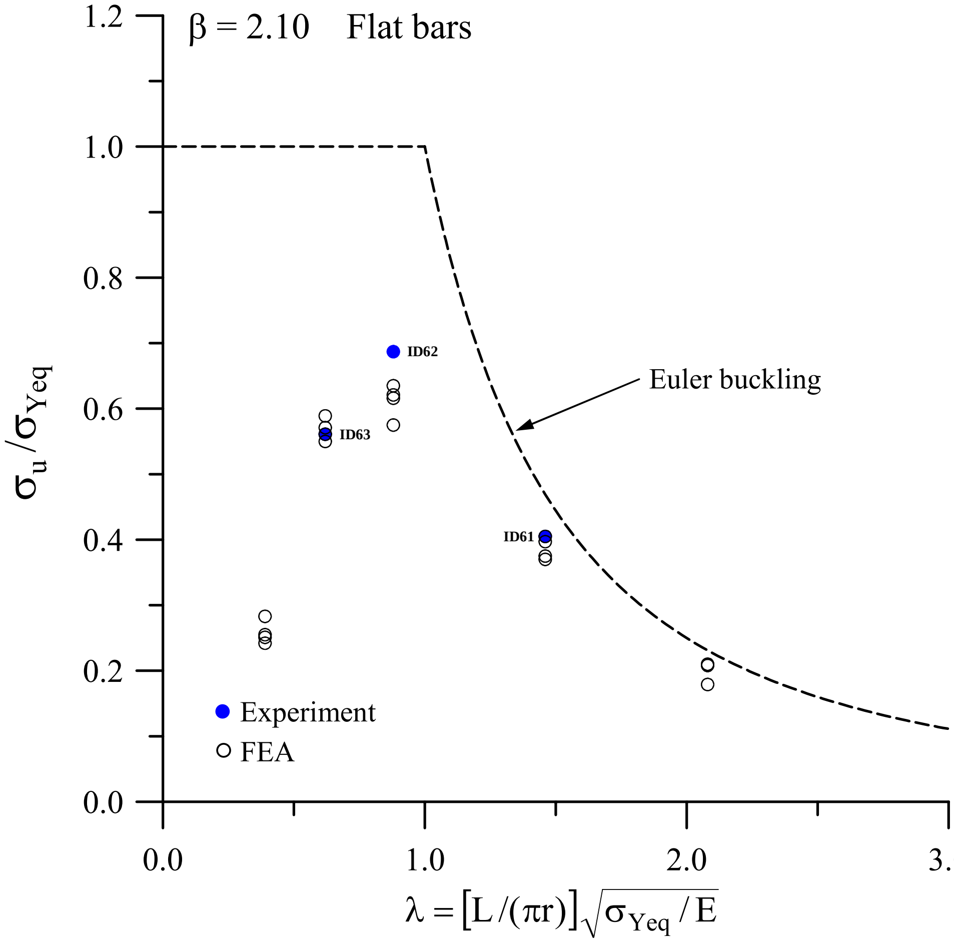

Figure 8.82(b) Variation of the ultimate strength for the test structures with flat-bars, $\beta = 2.10$

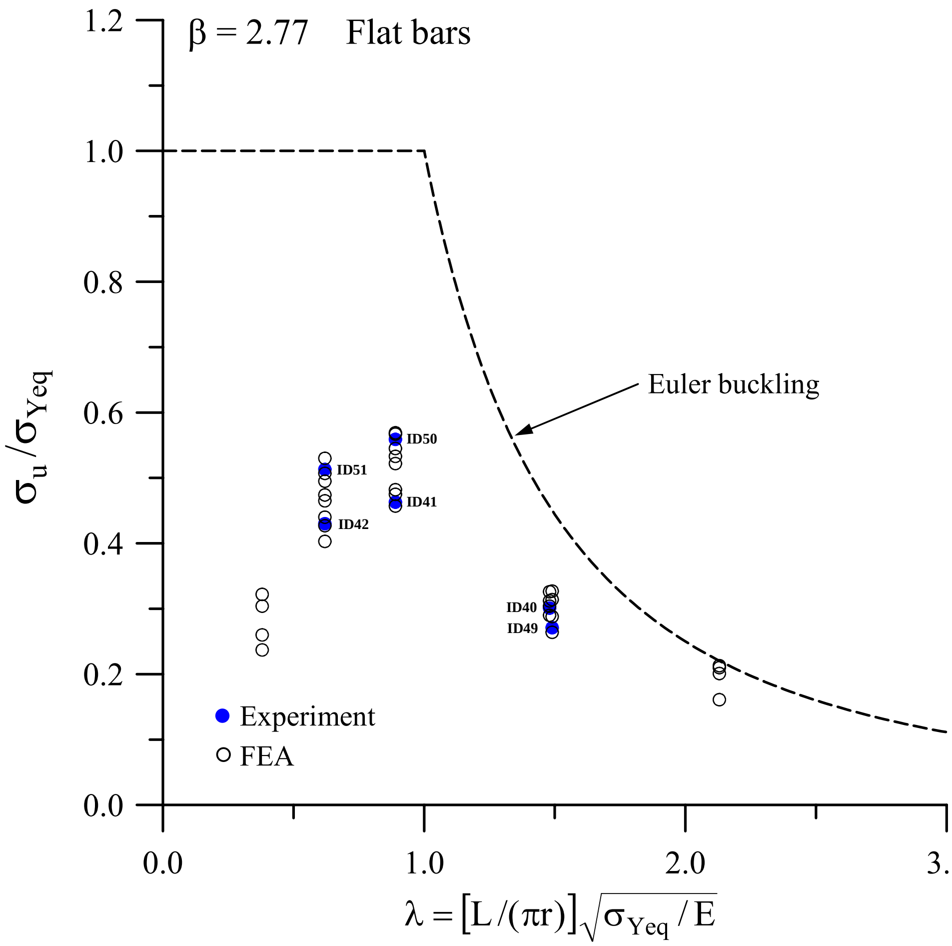

Figure 8.82(c) Variation of the ultimate strength for the test structures with flat-bars, $\beta = 2.77$

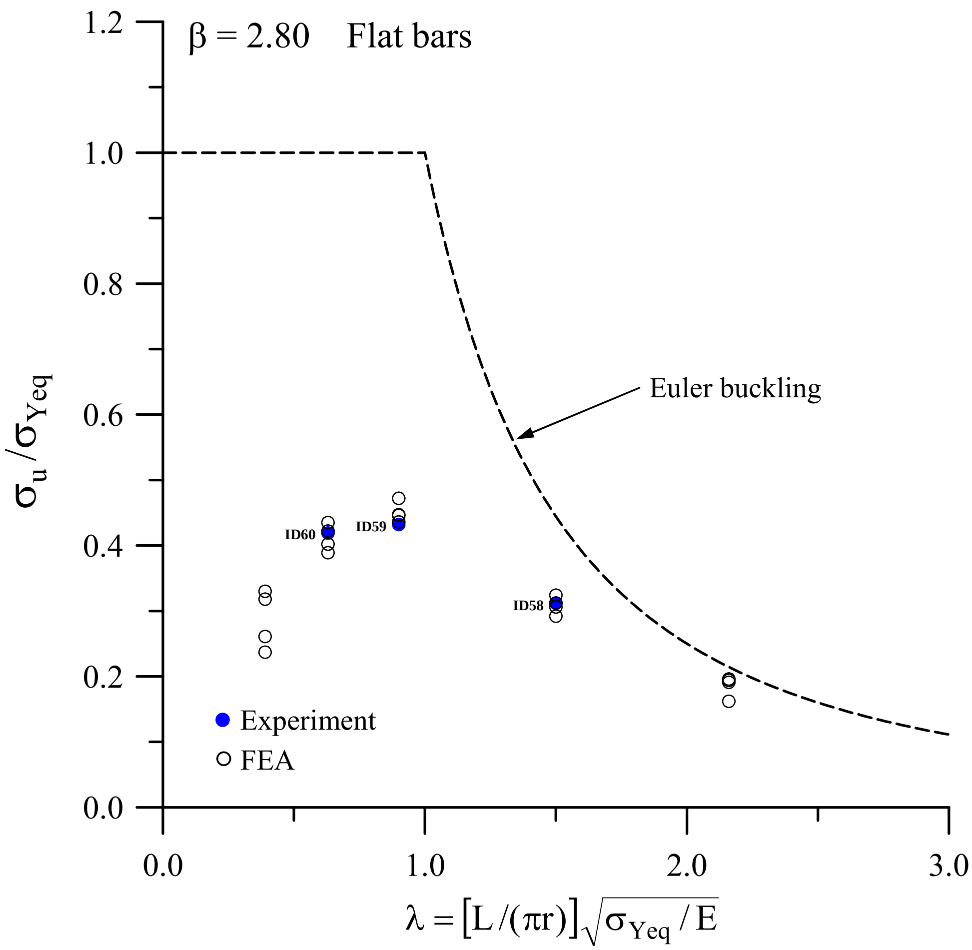

Figure 8.82(d) Variation of the ultimate strength for the test structures with flat-bars, $\beta = 2.80$

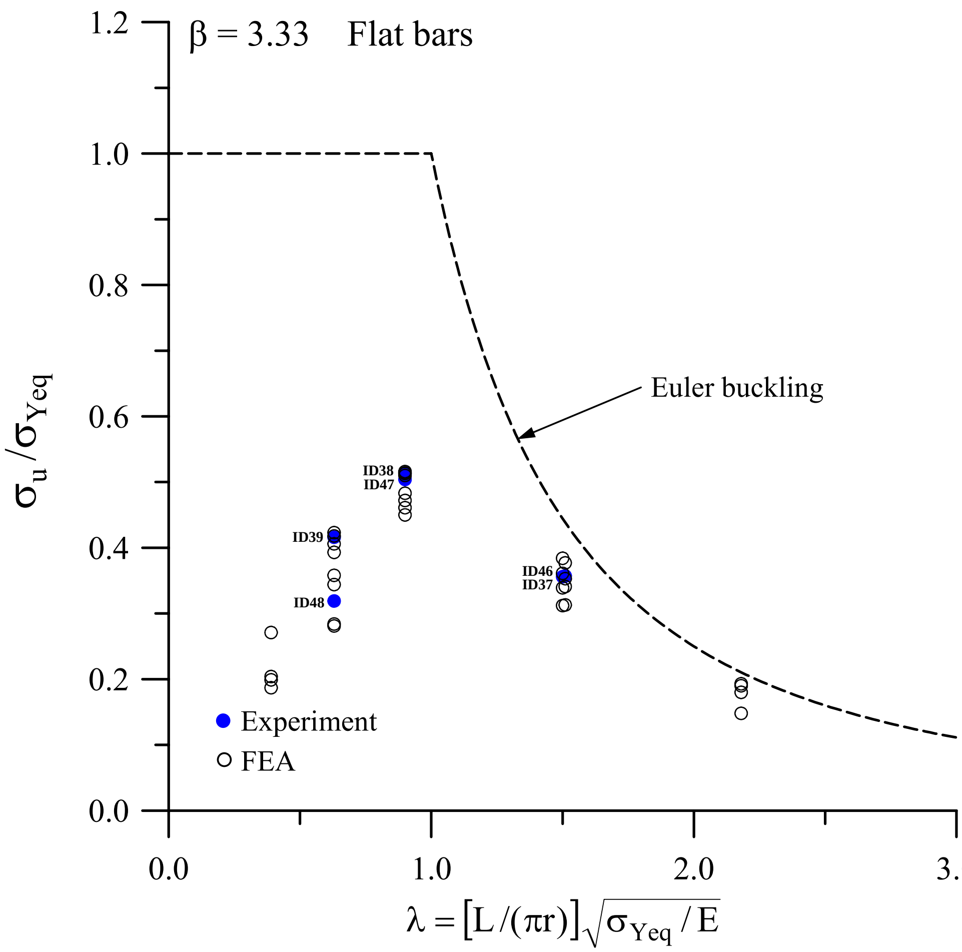

Figure 8.82(e) Variation of the ultimate strength for the test structures with flat-bars, $\beta = 3.33$

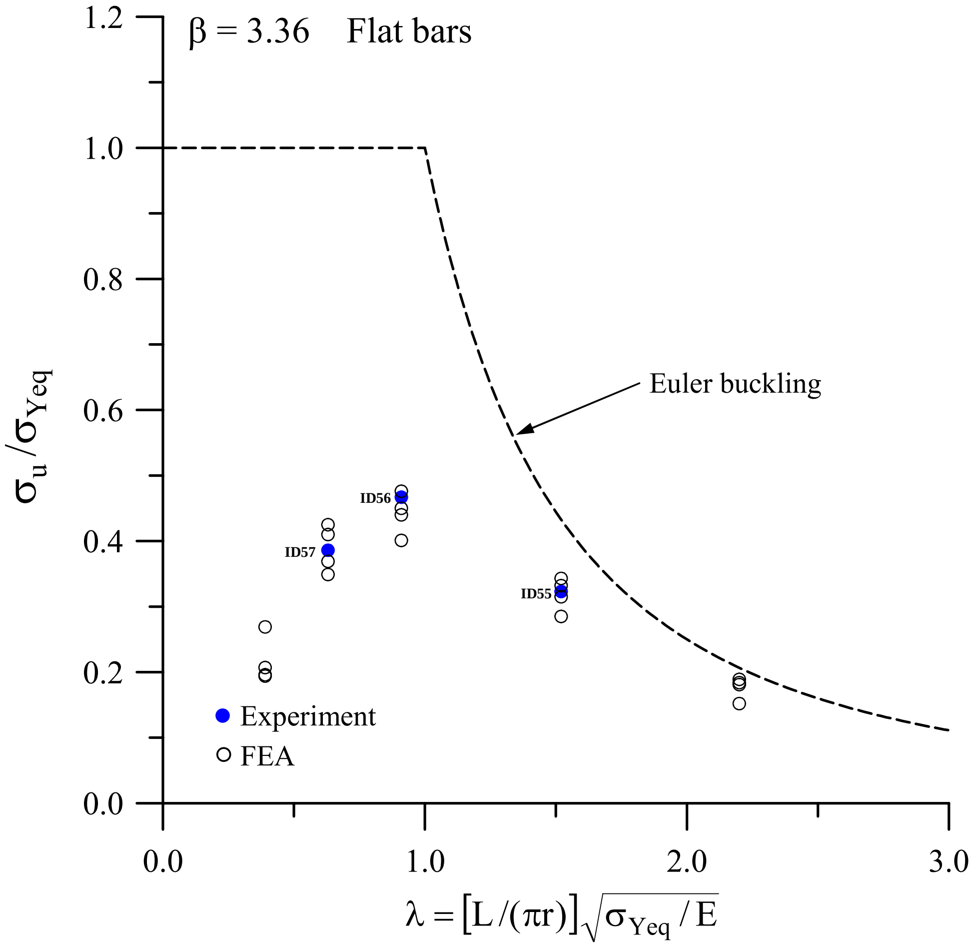

Figure 8.82(f) Variation of the ultimate strength for the test structures with flat-bars, $\beta = 3.36$

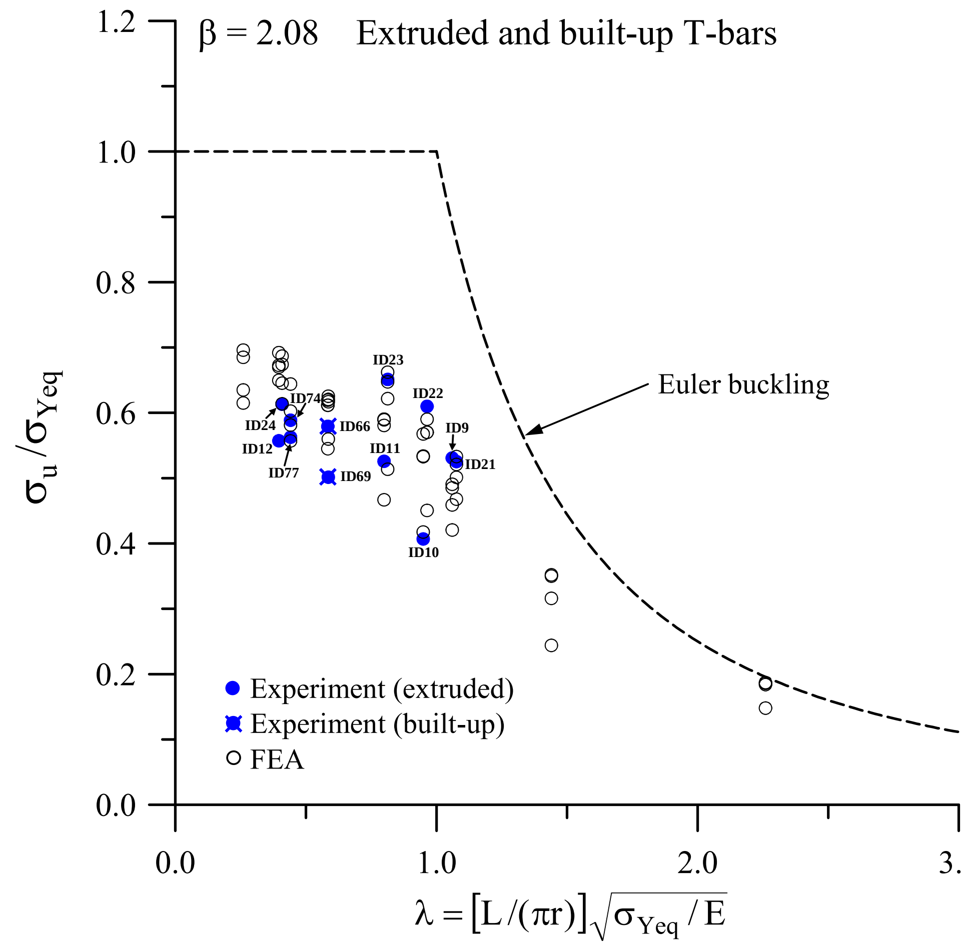

Figure 8.83(a) Variation of the ultimate strength for the test structures with extruded and built-up T-bars, $\beta = 2.08$

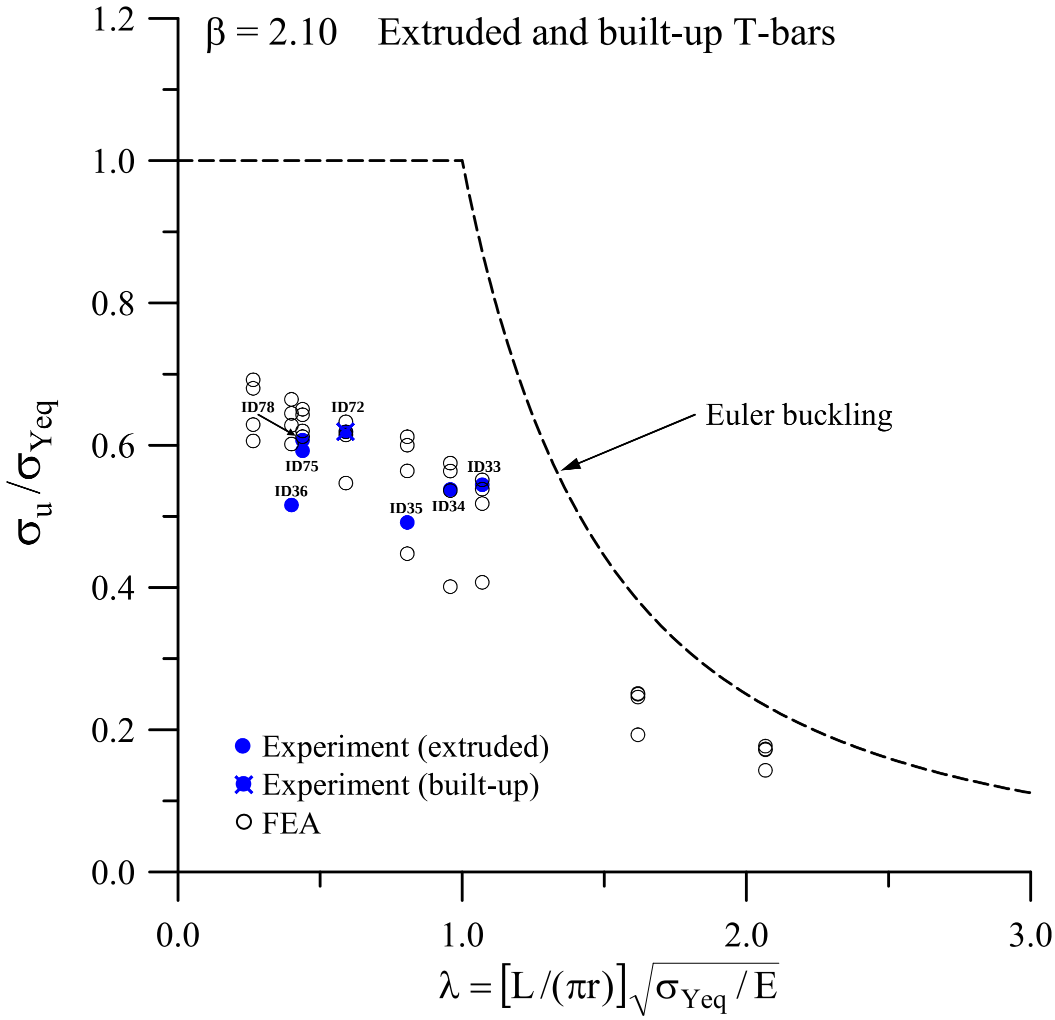

Figure 8.83(b) Variation of the ultimate strength for the test structures with extruded and built-up T-bars, $\beta = 2.10$

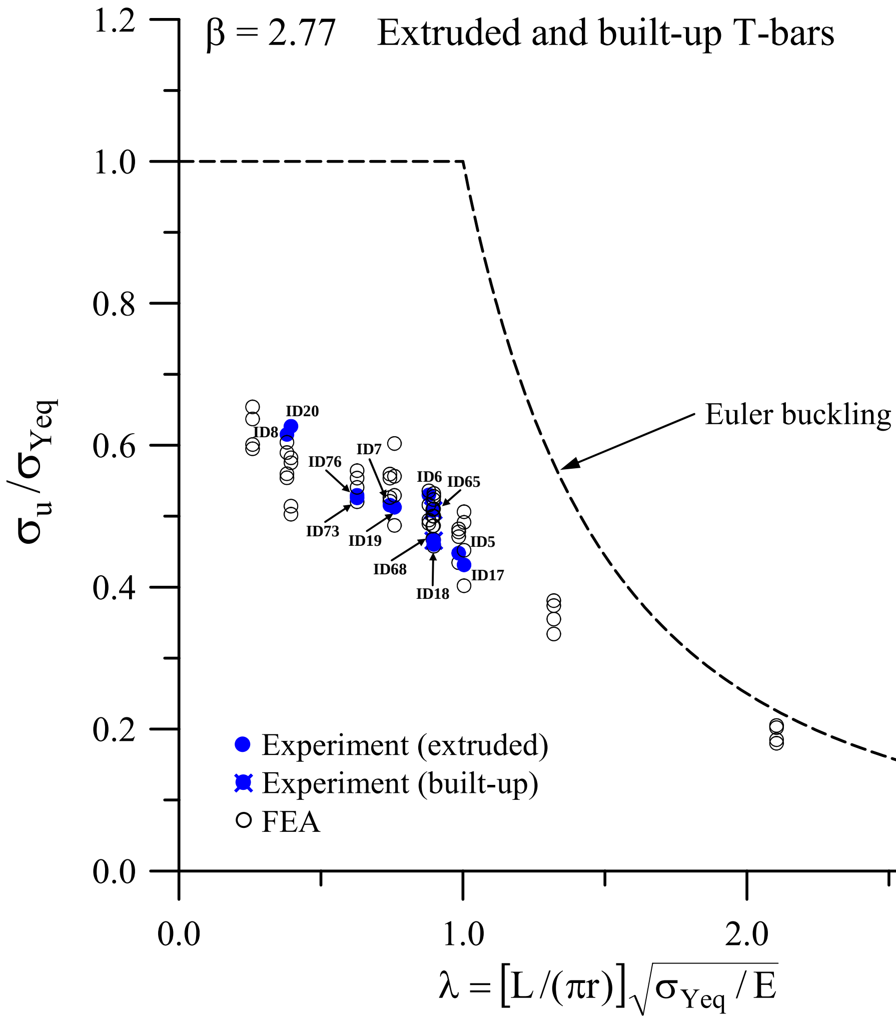

Figure 8.83(c) Variation of the ultimate strength for the test structures with extruded and built-up T-bars, $\beta = 2.77$

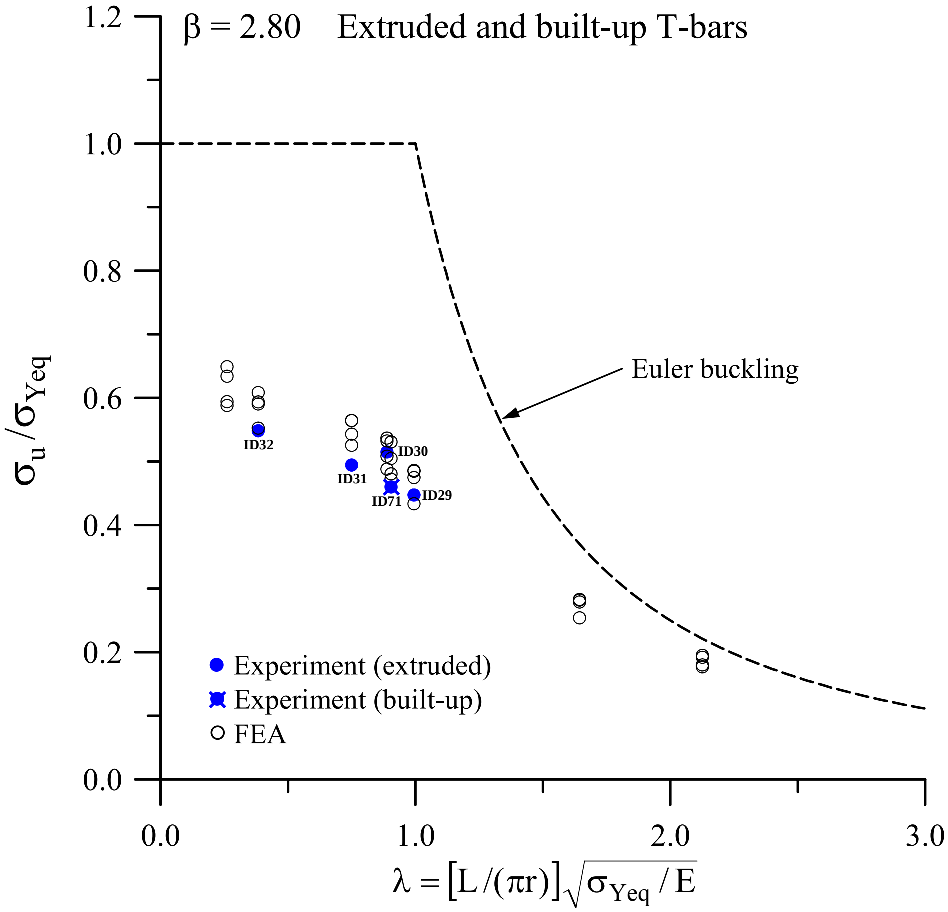

Figure 8.83(d) Variation of the ultimate strength for the test structures with extruded and built-up T-bars, $\beta = 2.80$

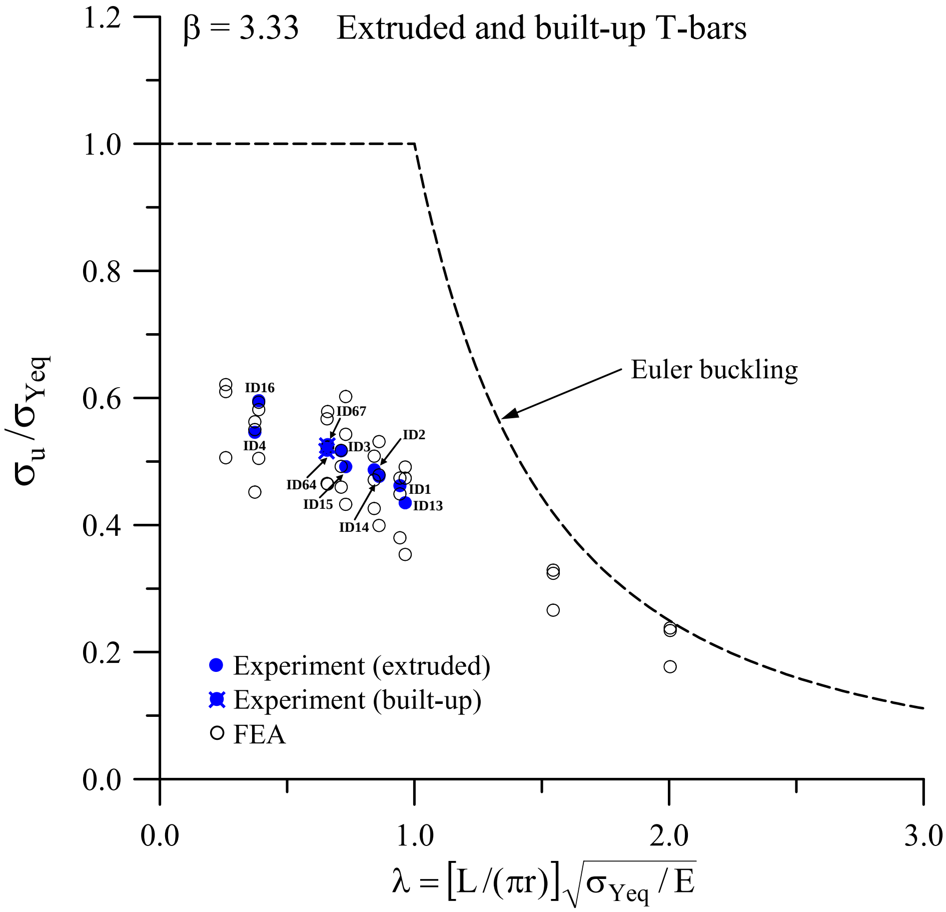

Figure 8.83(e) Variation of the ultimate strength for the test structures with extruded and built-up T-bars, $\beta = 3.33$

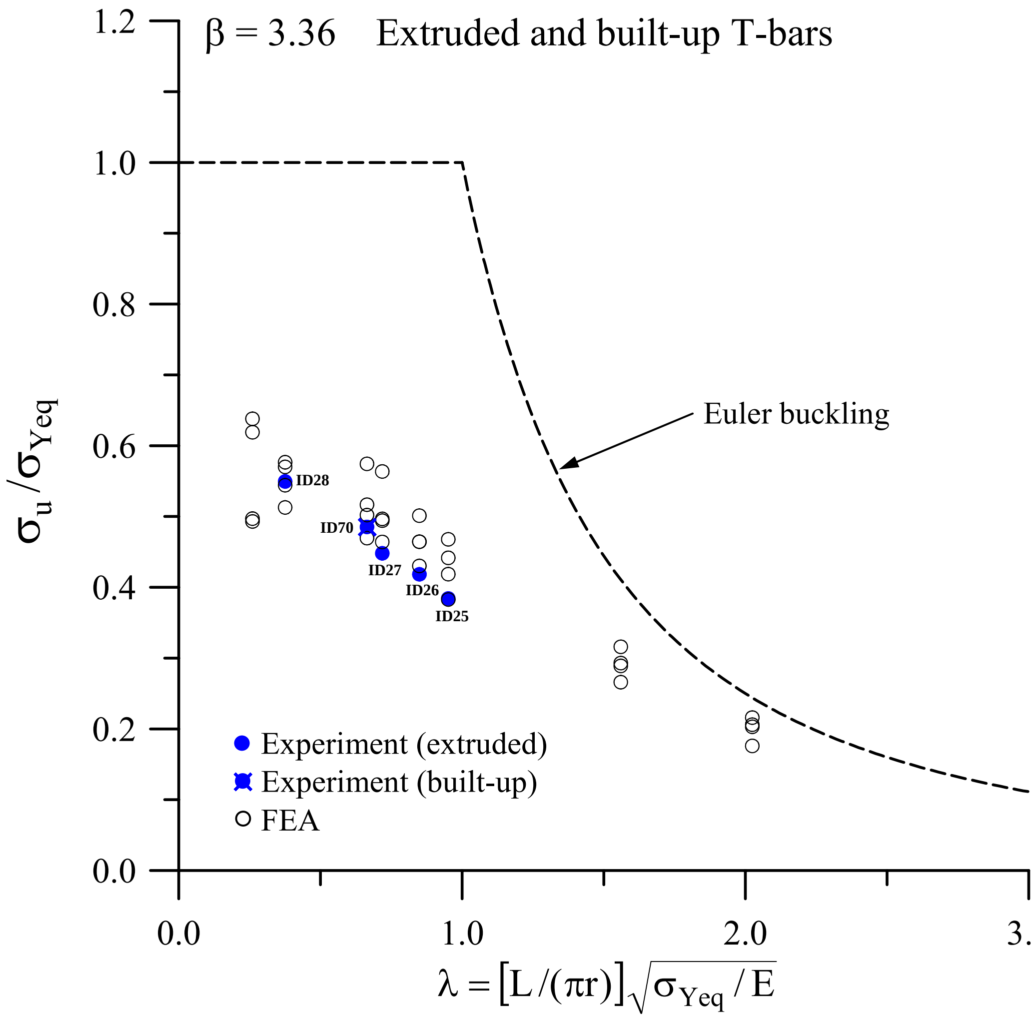

Figure 8.83(f) Variation of the ultimate strength for the test structures with extruded and built-up T-bars, $\beta = 3.36$

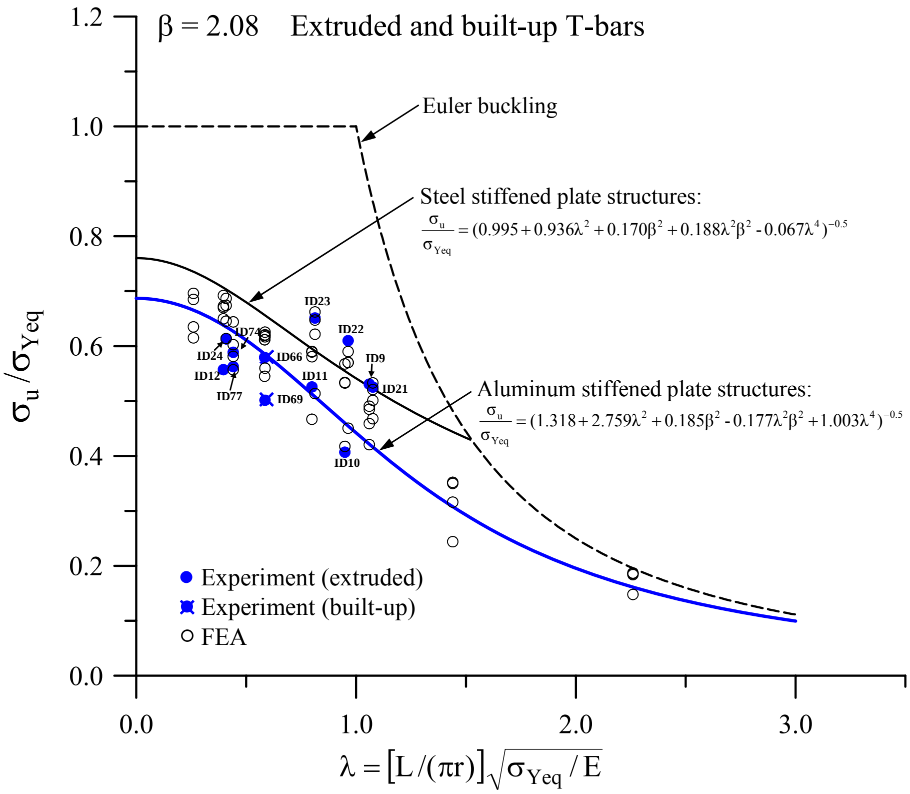

Figure 9.1(a) The accuracy of the closed-form empirical ULS formula, Eq.(9.3), for aluminum stiffened plate structures with T-bars, $\beta = 2.08$

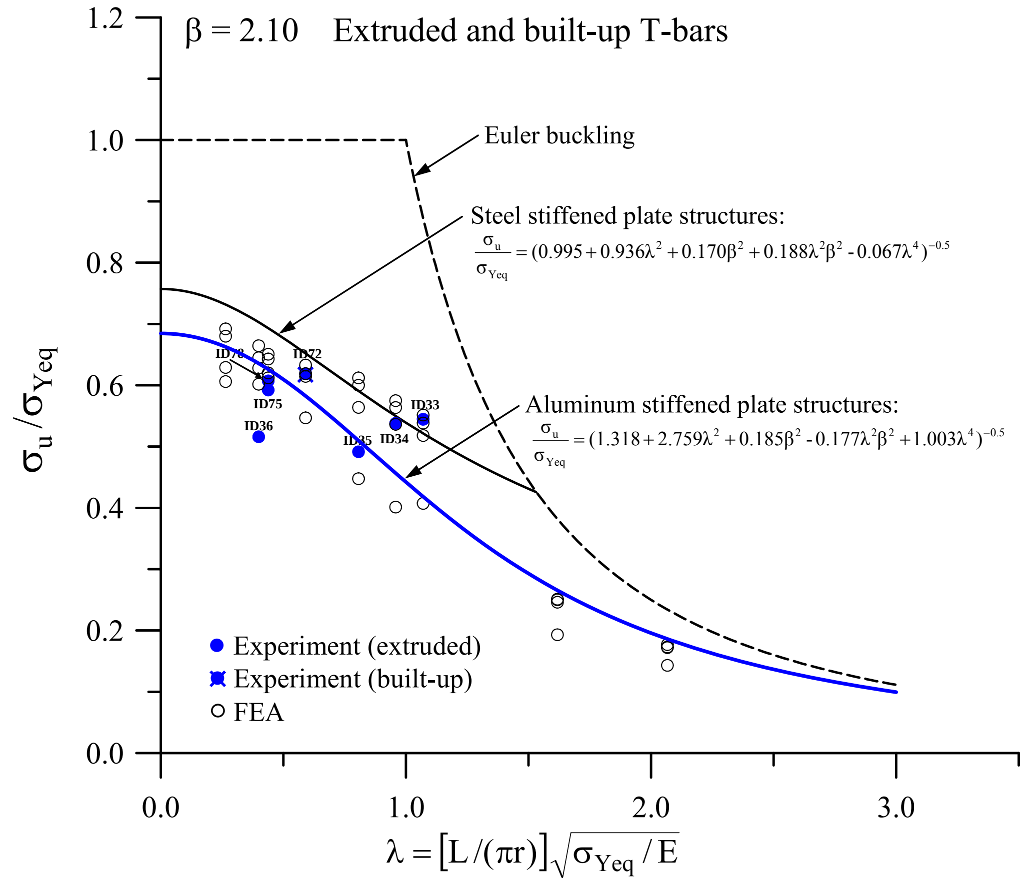

Figure 9.1(b) The accuracy of the closed-form empirical ULS formula, Eq.(9.3), for aluminum stiffened plate structures with T-bars, $\beta = 2.10$

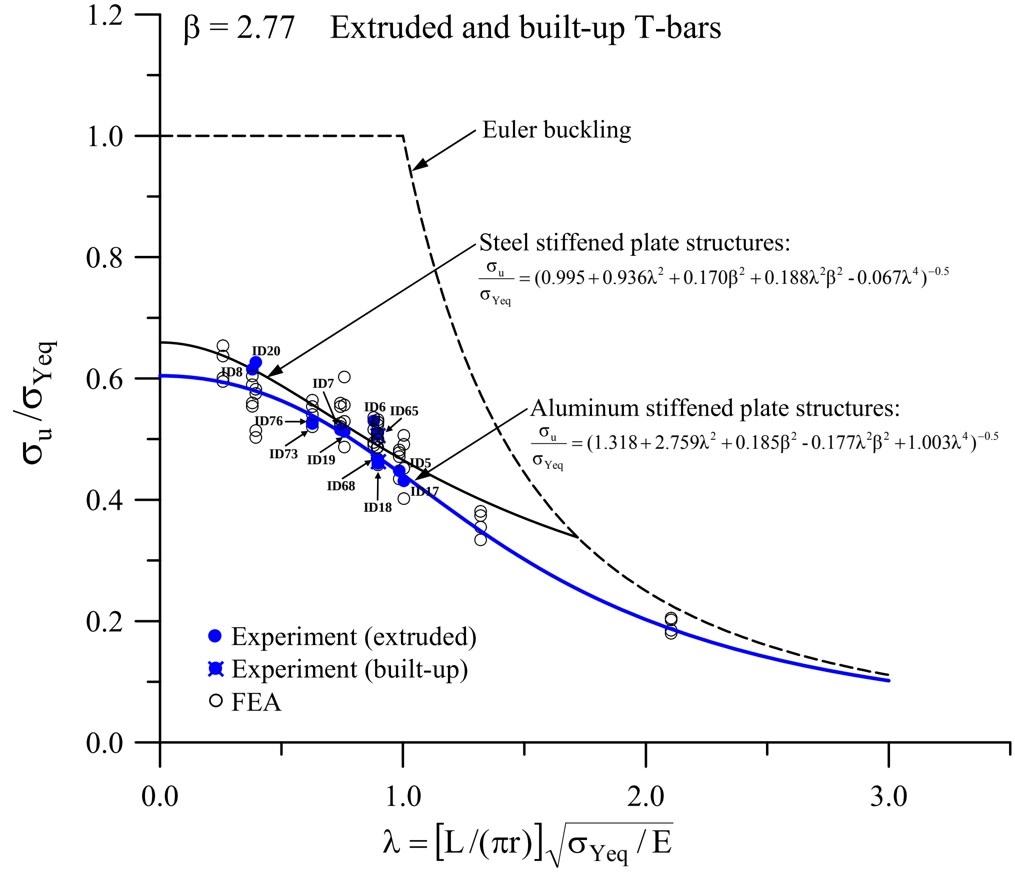

Figure 9.1(c) The accuracy of the closed-form empirical ULS formula, Eq.(9.3), for aluminum stiffened plate structures with T-bars, $\beta = 2.77$

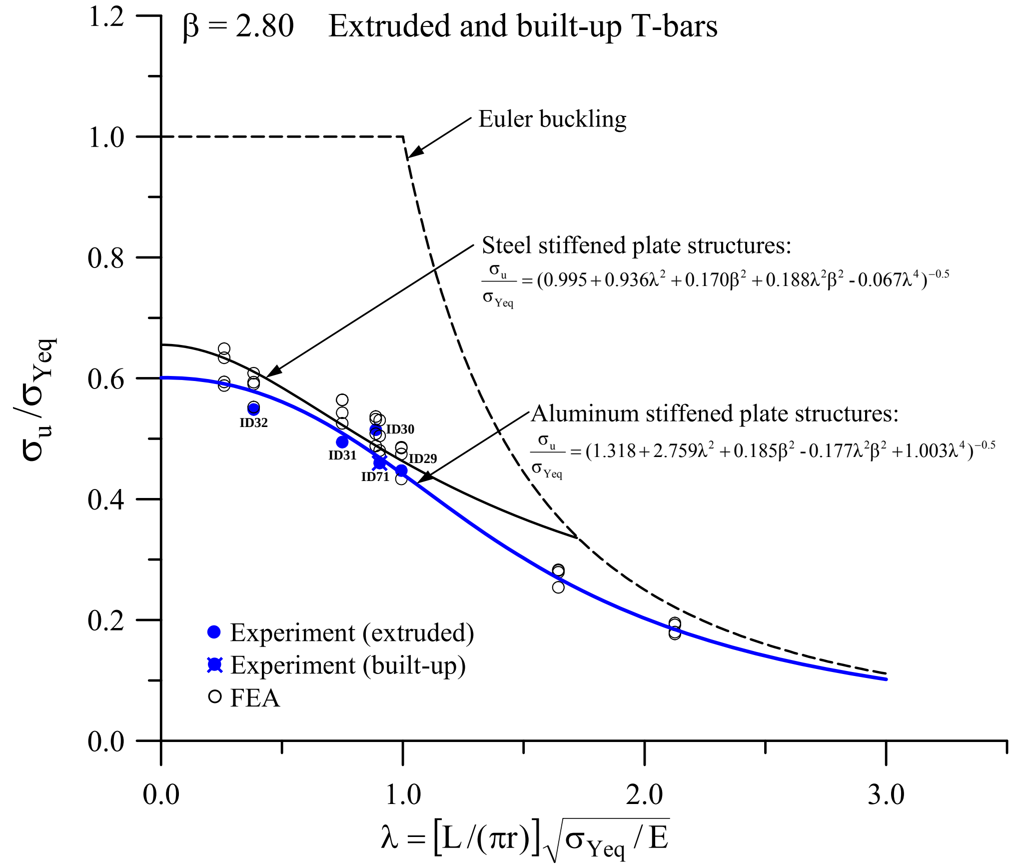

Figure 9.1(d) The accuracy of the closed-form empirical ULS formula, Eq.(9.3), for aluminum stiffened plate structures with T-bars, $\beta = 2.80$

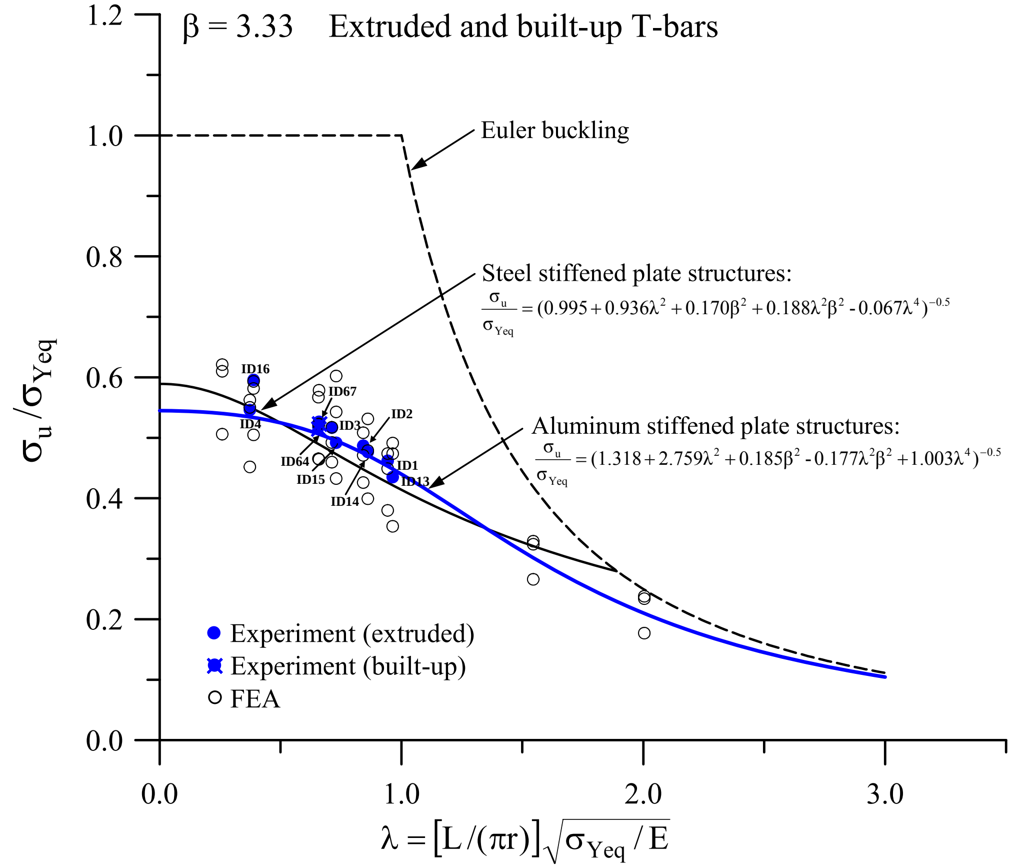

Figure 9.1(e) The accuracy of the closed-form empirical ULS formula, Eq.(9.3), for aluminum stiffened plate structures with T-bars, $\beta = 3.33$

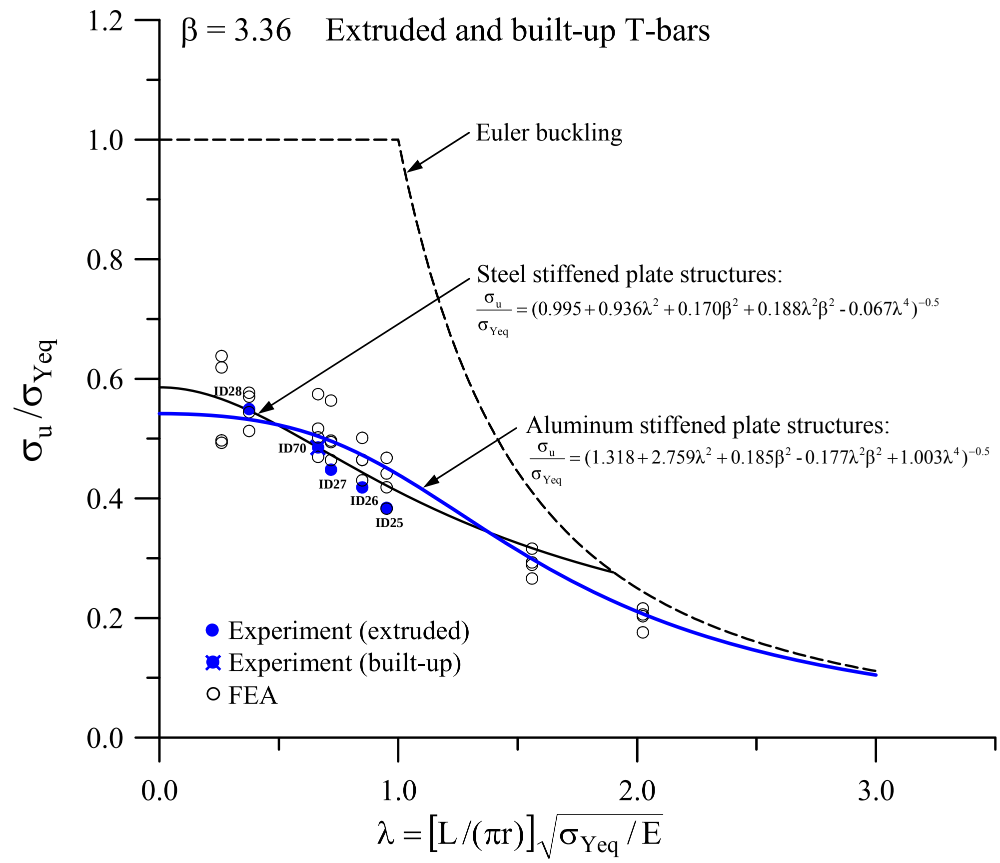

Figure 9.1(f) The accuracy of the closed-form empirical ULS formula, Eq.(9.3), for aluminum stiffened plate structures with T-bars, $\beta = 3.36$

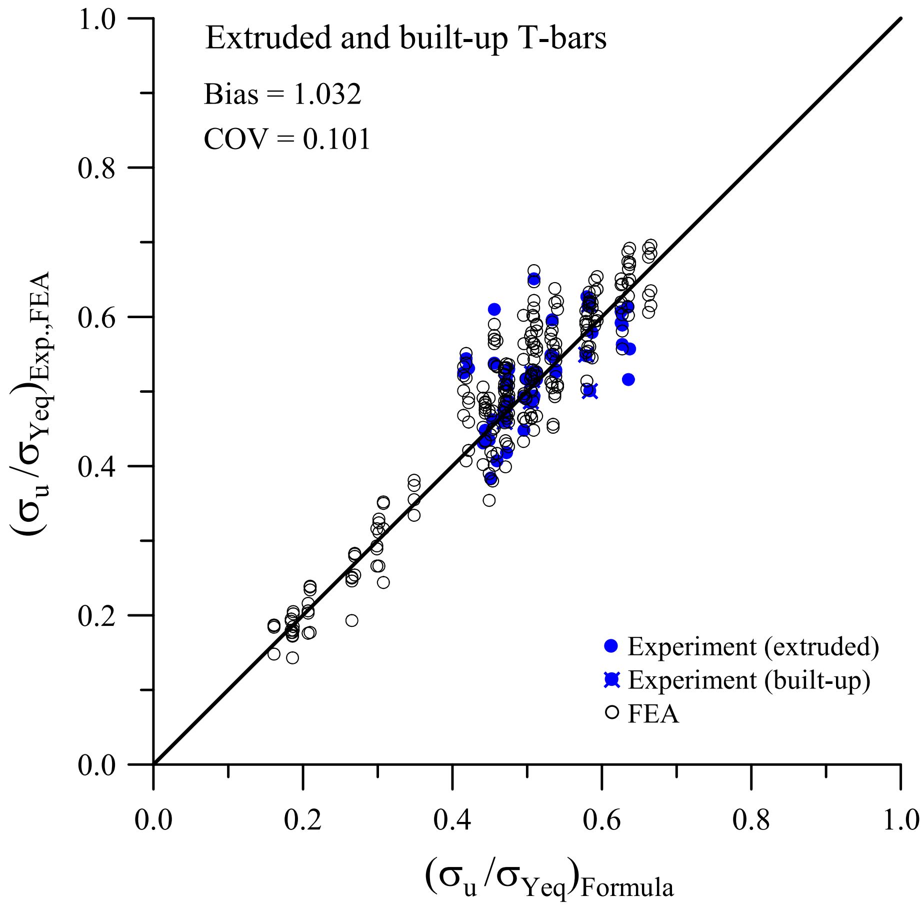

Figure 9.2 The bias and COV for the closed-form empirical ULS formulae, Eq.(9.3), for aluminum stiffened plate structures with T-bars

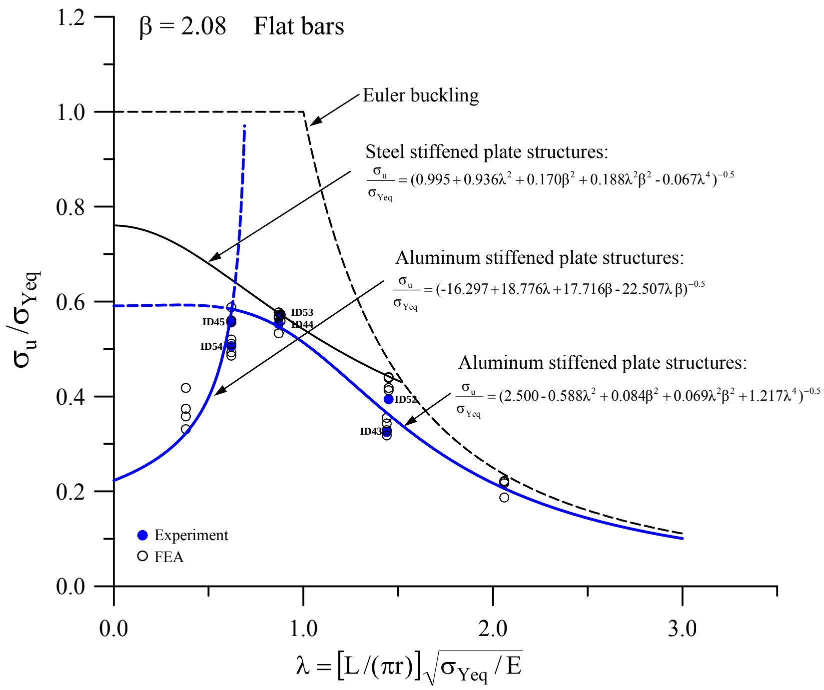

Figure 9.3(a) The accuracy of the closed-form empirical ULS formula, Eq.(9.4), for aluminum stiffened plate structures with flat bars, $\beta = 2.08$

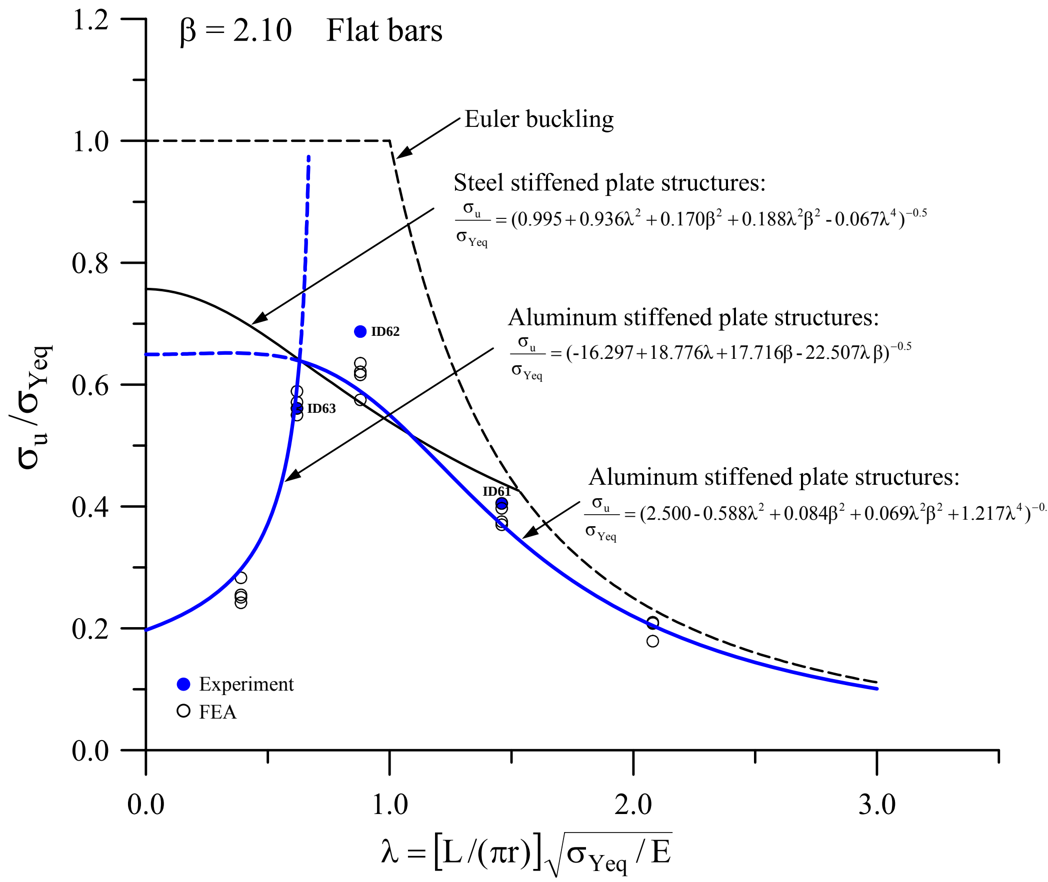

Figure 9.3(b) The accuracy of the closed-form empirical ULS formula, Eq.(9.4), for aluminum stiffened plate structures with flat bars, $\beta = 2.10$

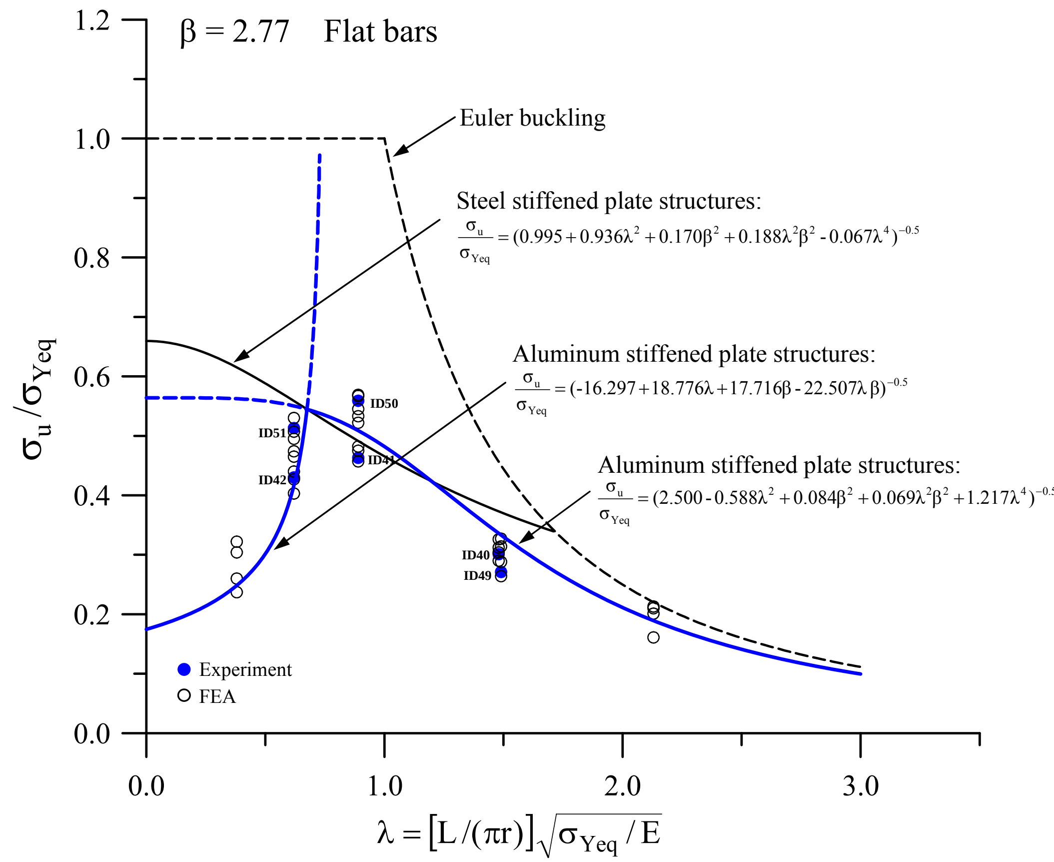

Figure 9.3(c) The accuracy of the closed-form empirical ULS formula, Eq.(9.4), for aluminum stiffened plate structures with flat bars, $\beta = 2.77$

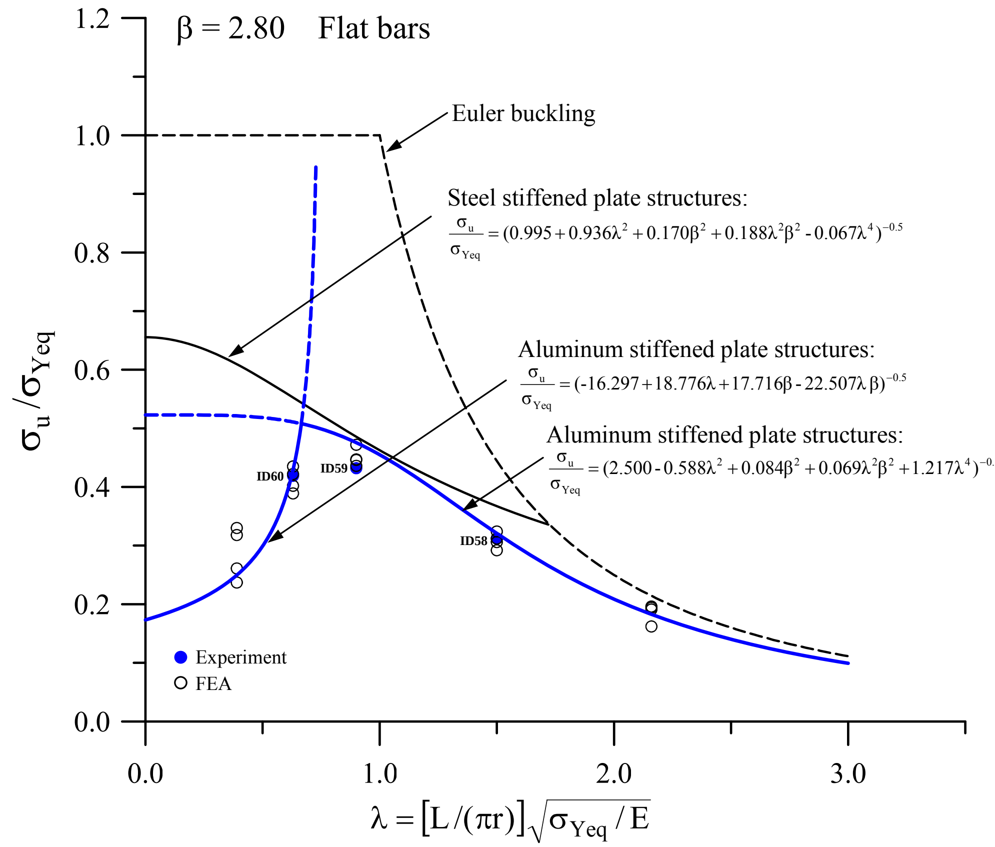

Figure 9.3(d) The accuracy of the closed-form empirical ULS formula, Eq.(9.4), for aluminum stiffened plate structures with flat bars, $\beta = 2.80$

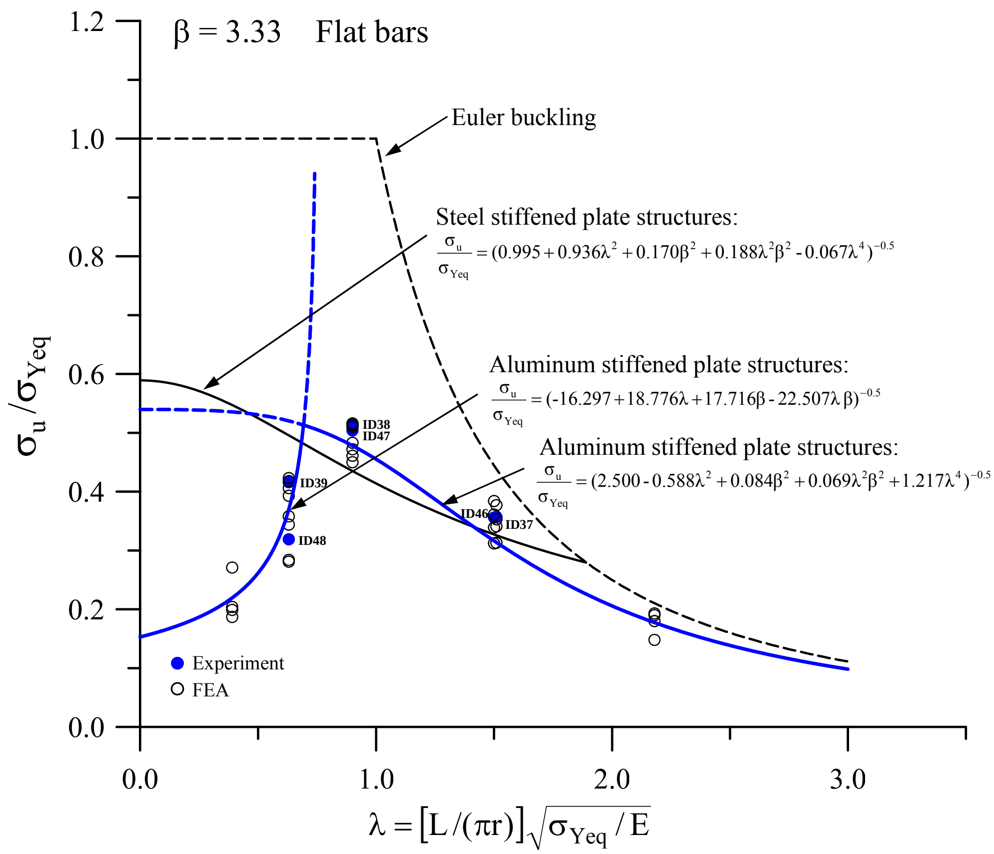

Figure 9.3(e) The accuracy of the closed-form empirical ULS formula, Eq.(9.4), for aluminum stiffened plate structures with flat bars, $\beta = 3.33$

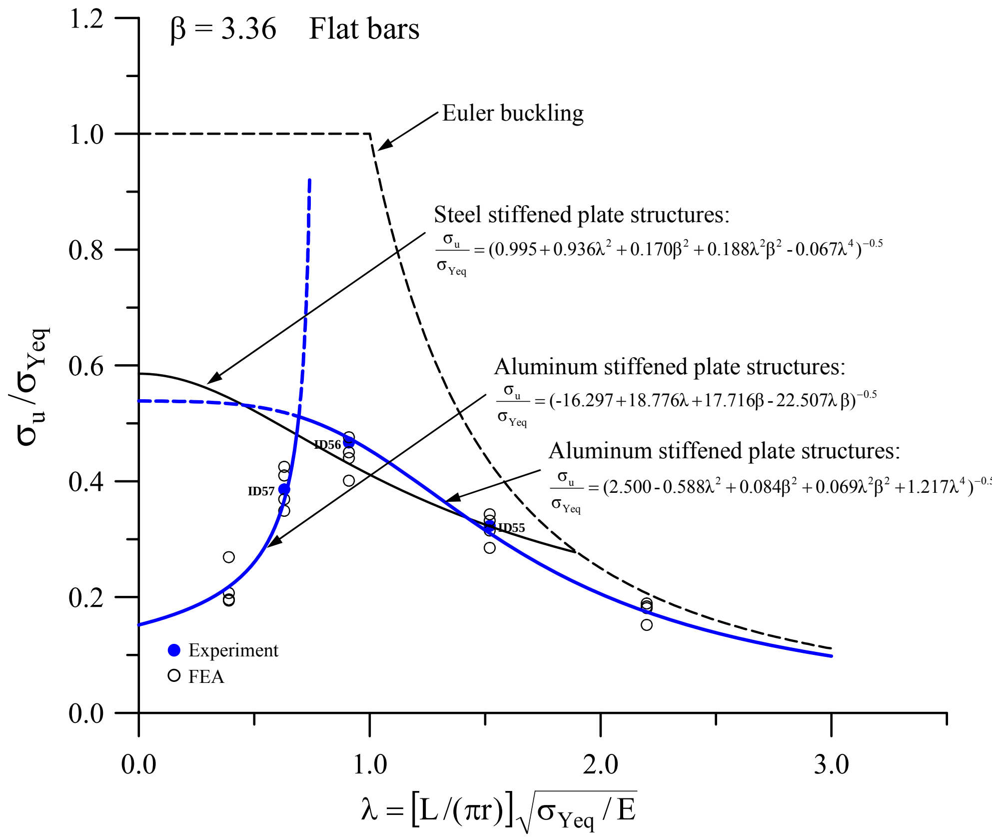

Figure 9.3(f) The accuracy of the closed-form empirical ULS formula, Eq.(9.4), for aluminum stiffened plate structures with flat bars, $\beta = 3.36$

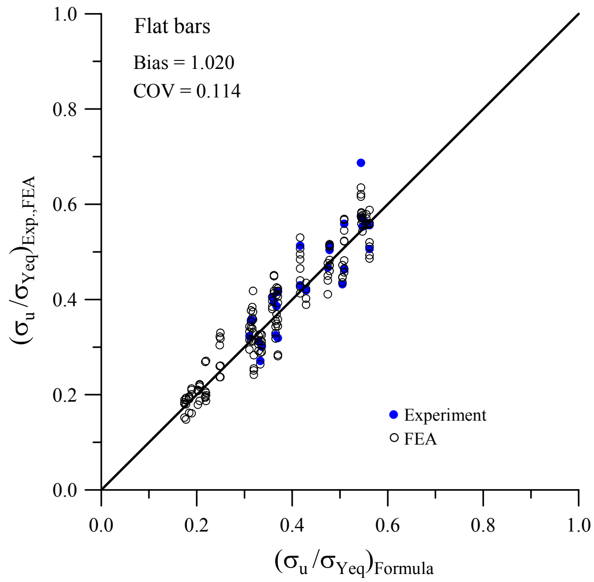

Figure 9.4 The bias and COV for the closed-form empirical ULS formulae, Eq.(9.4), for aluminum stiffened plate structures with flat bars

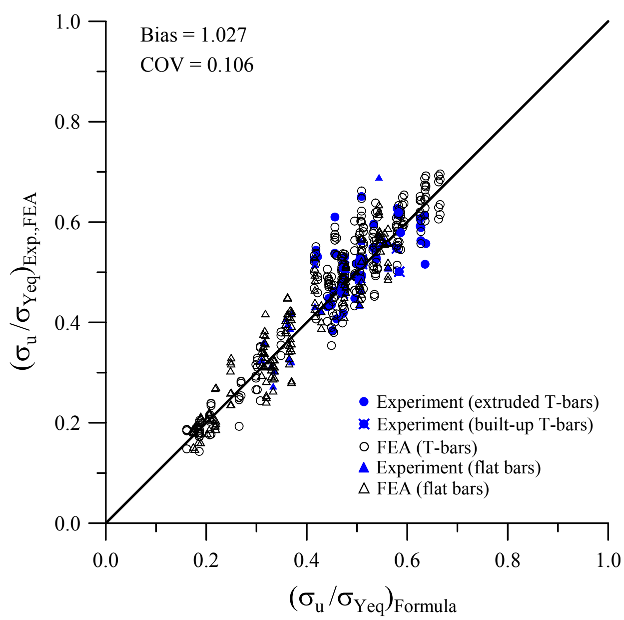

Figure 9.5 The bias and COV for the closed-form empirical ULS formulae, Eq.(9.3) for T-bars and Eq.(9.4) for flat bars, for aluminum stiffened plate structures with T- and flat bars

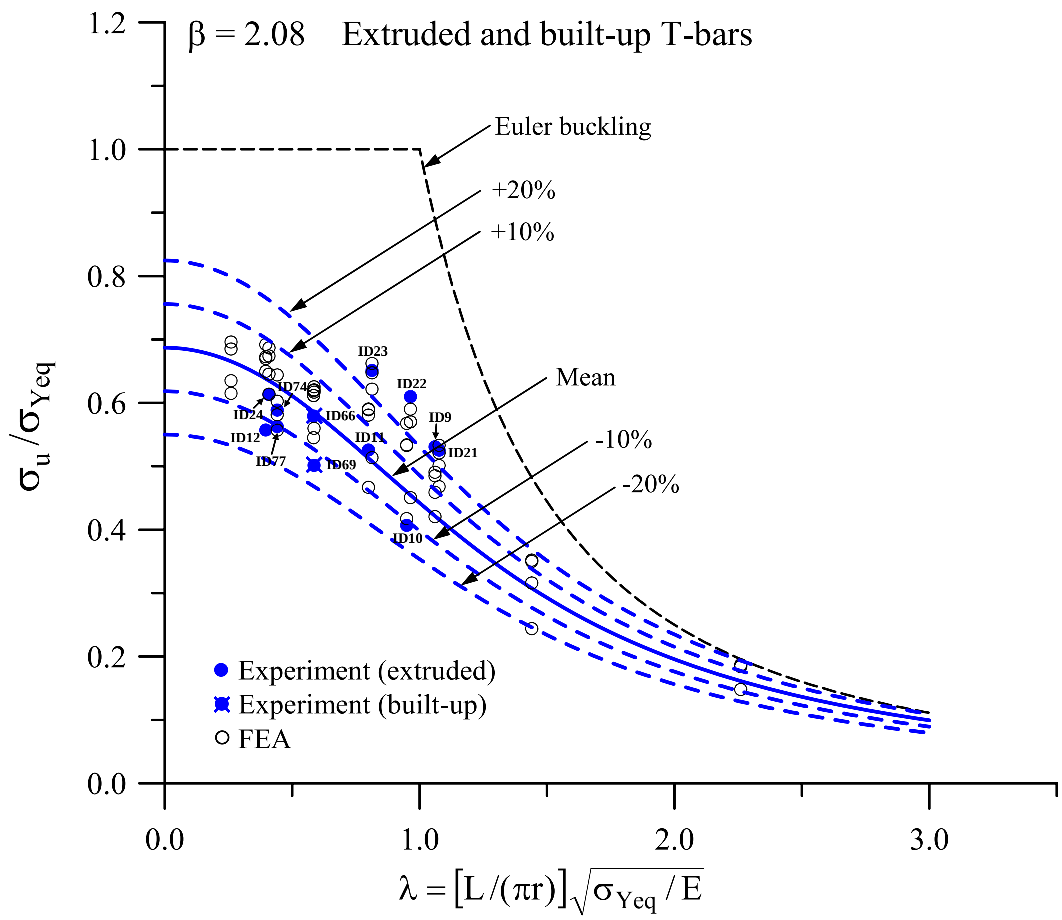

Figure 9.6(a) The aluminum stiffened panel ultimate strength variations with the deviations of $\pm 10\,\%$ and $\pm 20\,\%$, for T-bars, $\beta = 2.08$

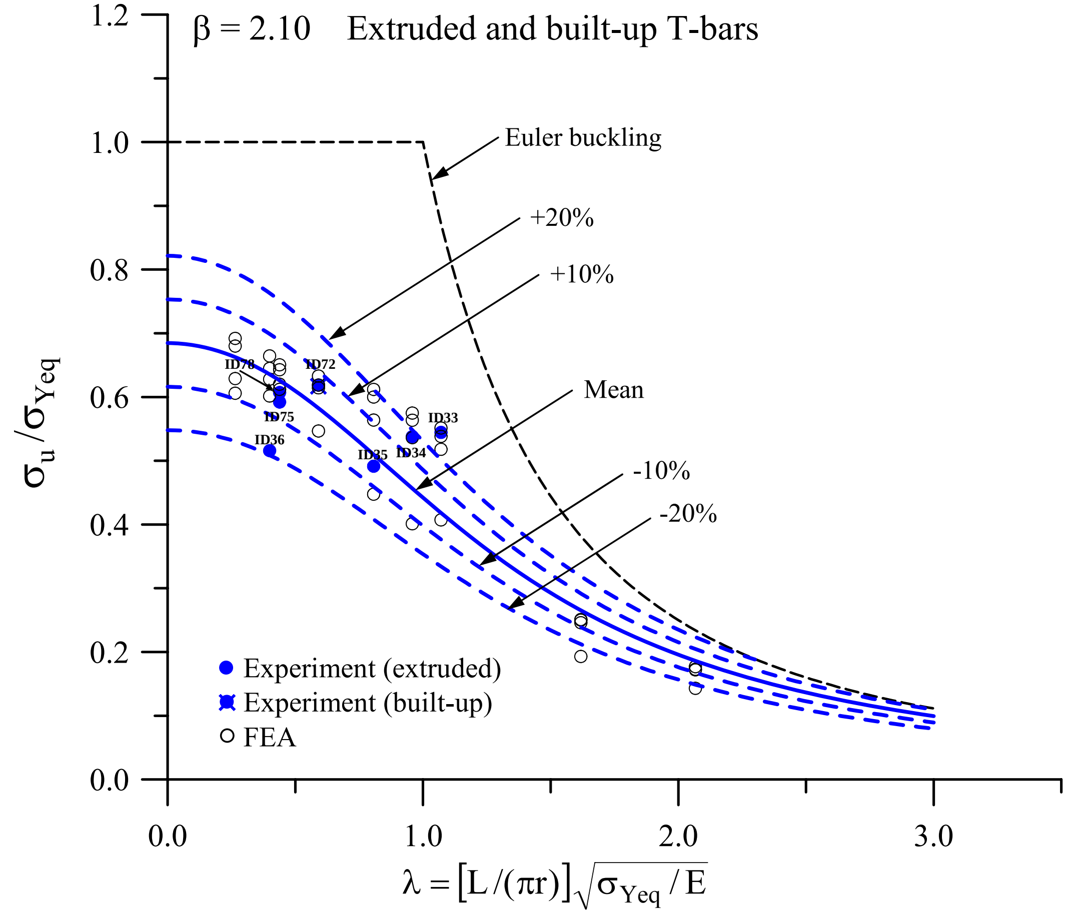

Figure 9.6(b) The aluminum stiffened panel ultimate strength variations with the deviations of $\pm 10\,\%$ and $\pm 20\,\%$, for T-bars, $\beta = 2.10$

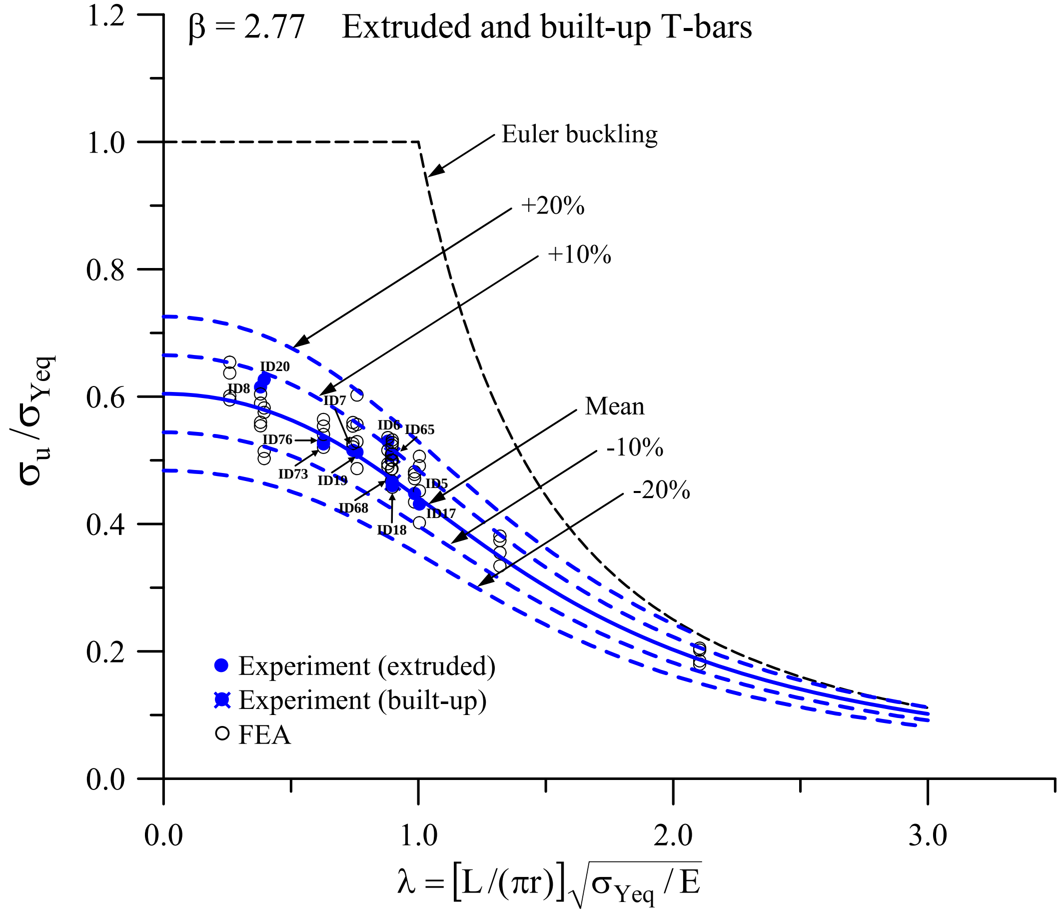

Figure 9.6(c) The aluminum stiffened panel ultimate strength variations with the deviations of $\pm 10\,\%$ and $\pm 20\,\%$, for T-bars, $\beta = 2.77$

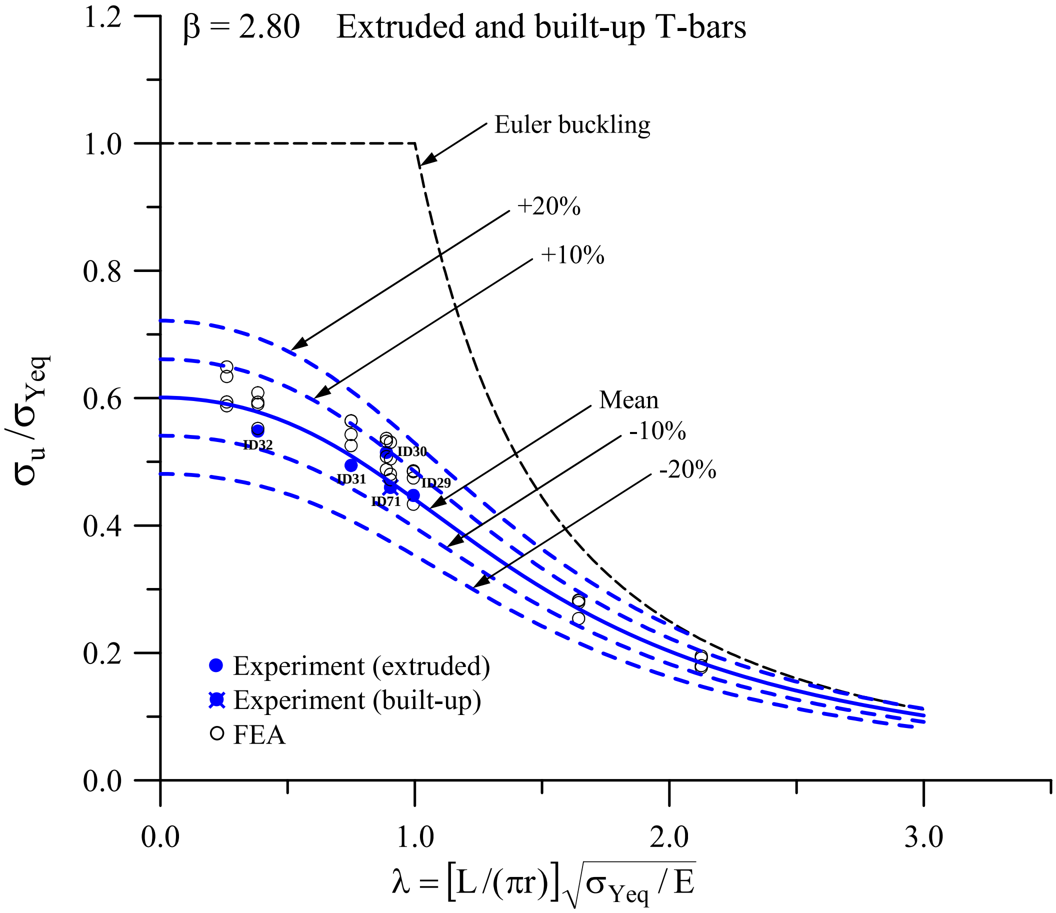

Figure 9.6(d) The aluminum stiffened panel ultimate strength variations with the deviations of $\pm 10\,\%$ and $\pm 20\,\%$, for T-bars, $\beta = 2.80$

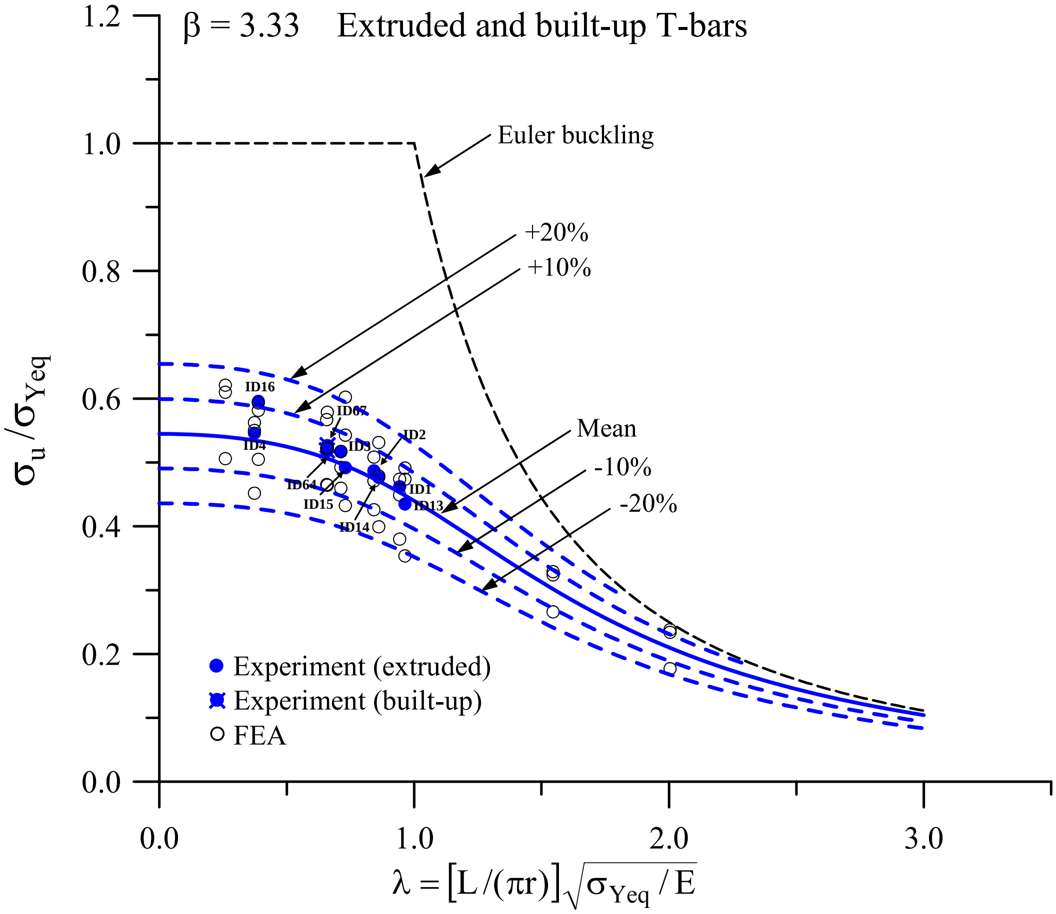

Figure 9.6(e) The aluminum stiffened panel ultimate strength variations with the deviations of $\pm 10\,\%$ and $\pm 20\,\%$, for T-bars, $\beta = 3.33$

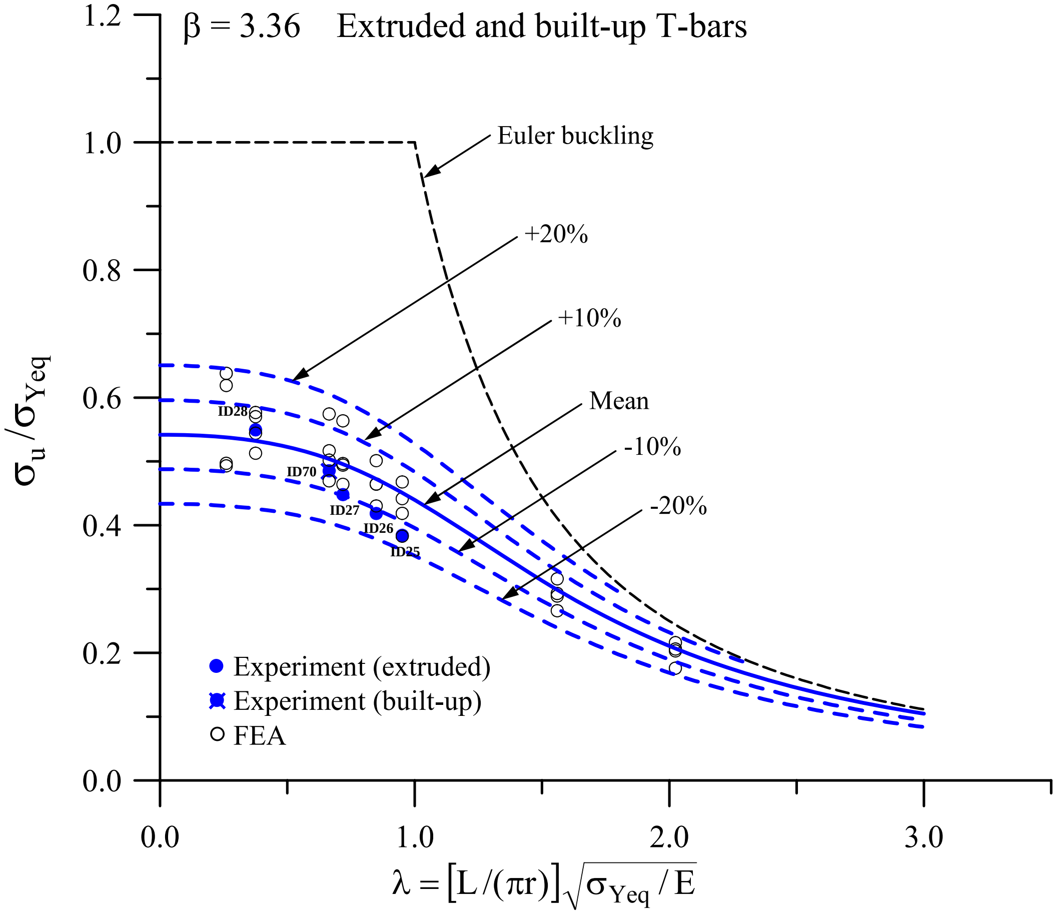

Figure 9.6(f) The aluminum stiffened panel ultimate strength variations with the deviations of $\pm 10\%$ and $\pm 20\%$, for T-bars, $\beta = 3.36$

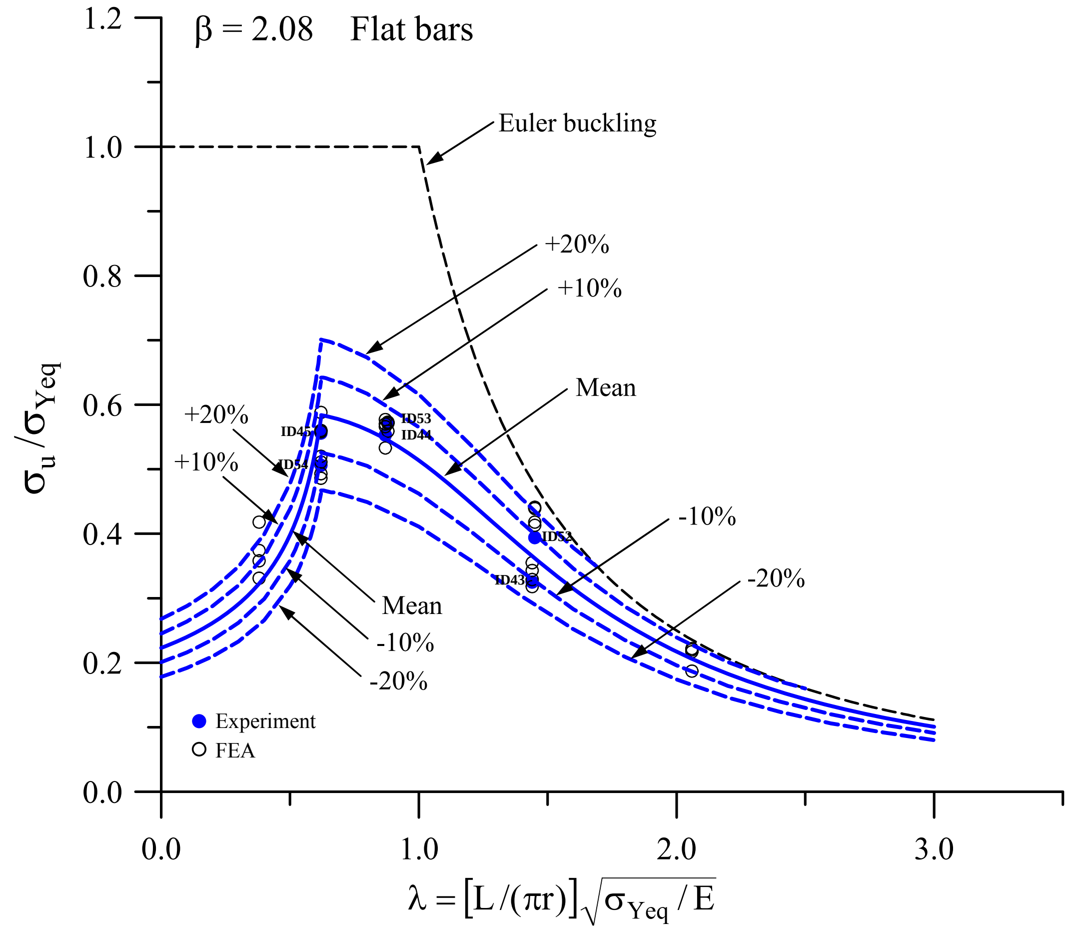

Figure 9.7(a) The aluminum stiffened panel ultimate strength variations with the deviations of $\pm 10\,\%$ and $\pm 20\,\%$, for flat bars, $\beta = 2.08$

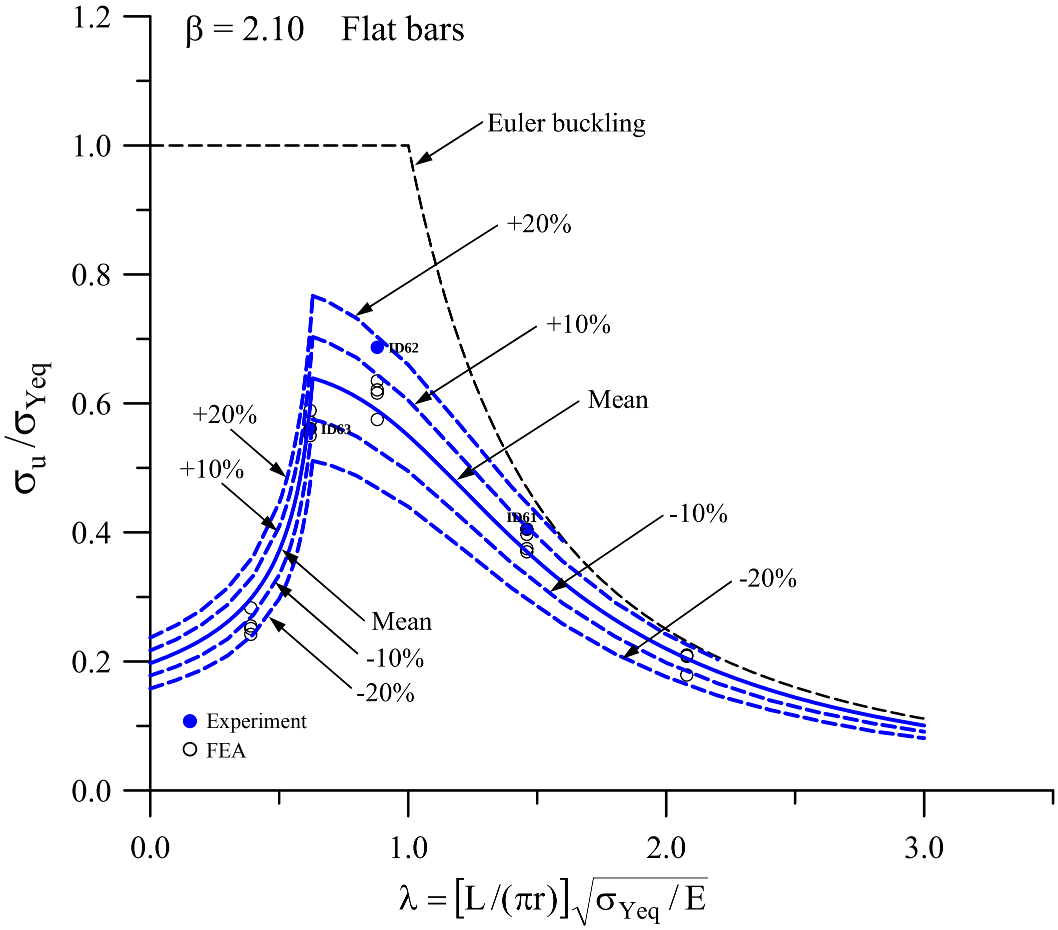

Figure 9.7(b) The aluminum stiffened panel ultimate strength variations with the deviations of $\pm 10\,\%$ and $\pm 20\,\%$, for flat bars, $\beta = 2.10$

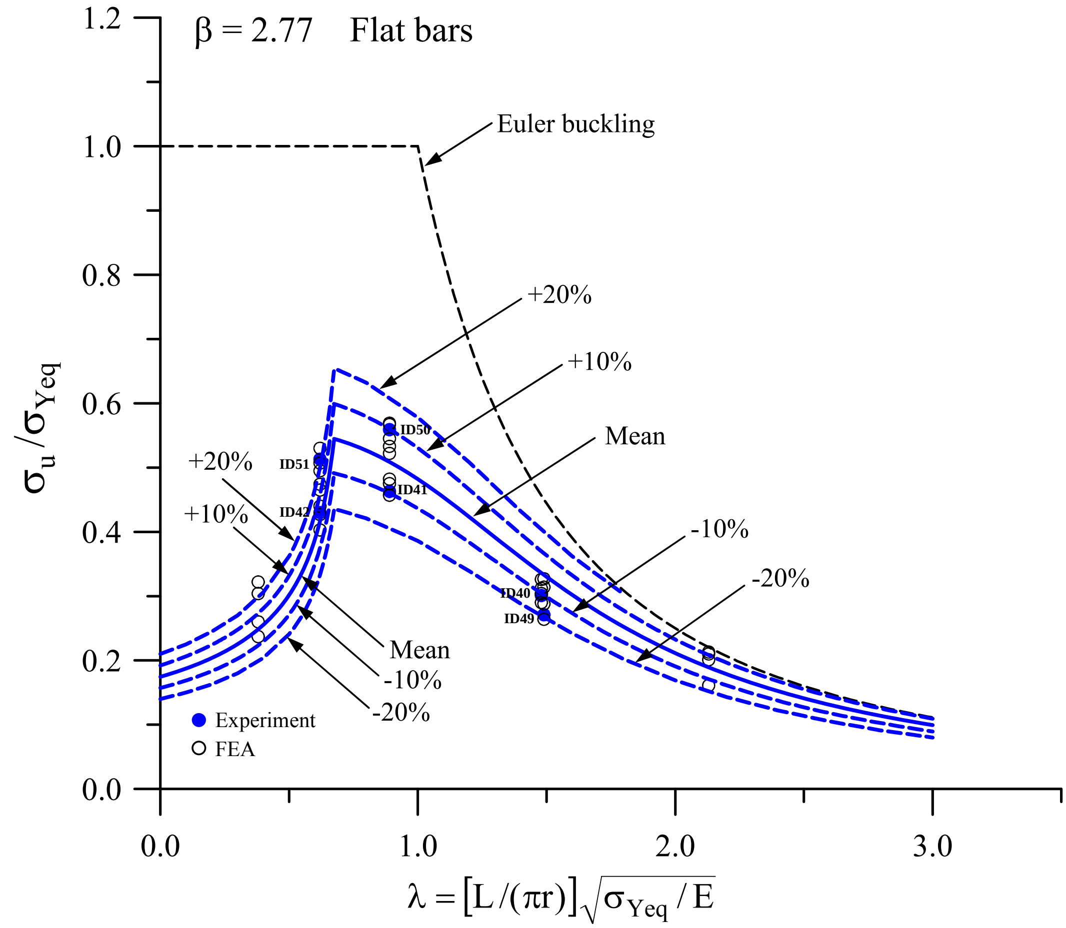

Figure 9.7(c) The aluminum stiffened panel ultimate strength variations with the deviations of $\pm 10\,\%$ and $\pm 20\,\%$, for flat bars, β=2.77

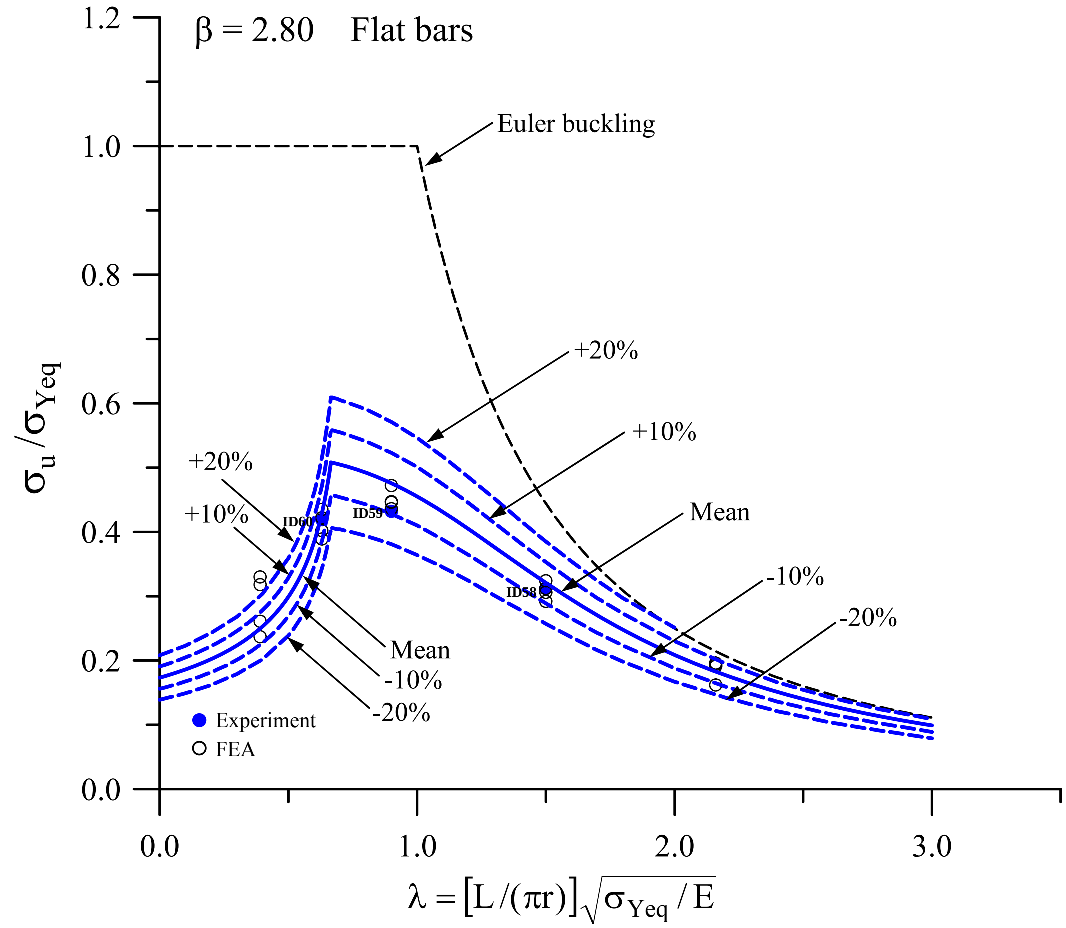

Figure 9.7(d) The aluminum stiffened panel ultimate strength variations with the deviations of $\pm 10\,\%$ and $\pm 20\,\%$, for flat bars, $\beta = 2.80$

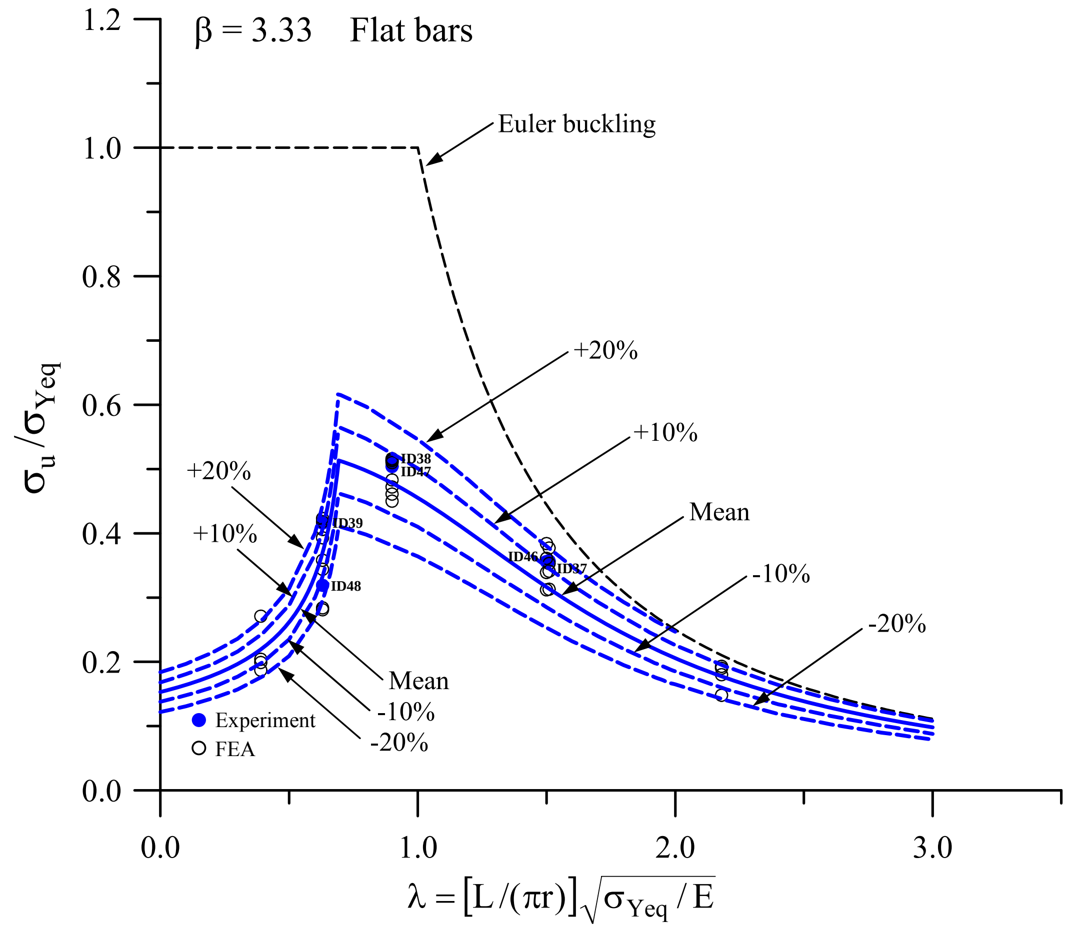

Figure 9.7(e) The aluminum stiffened panel ultimate strength variations with the deviations of $\pm 10\,\%$ and $\pm 20\,\%$, for flat bars, $\beta = 3.33$

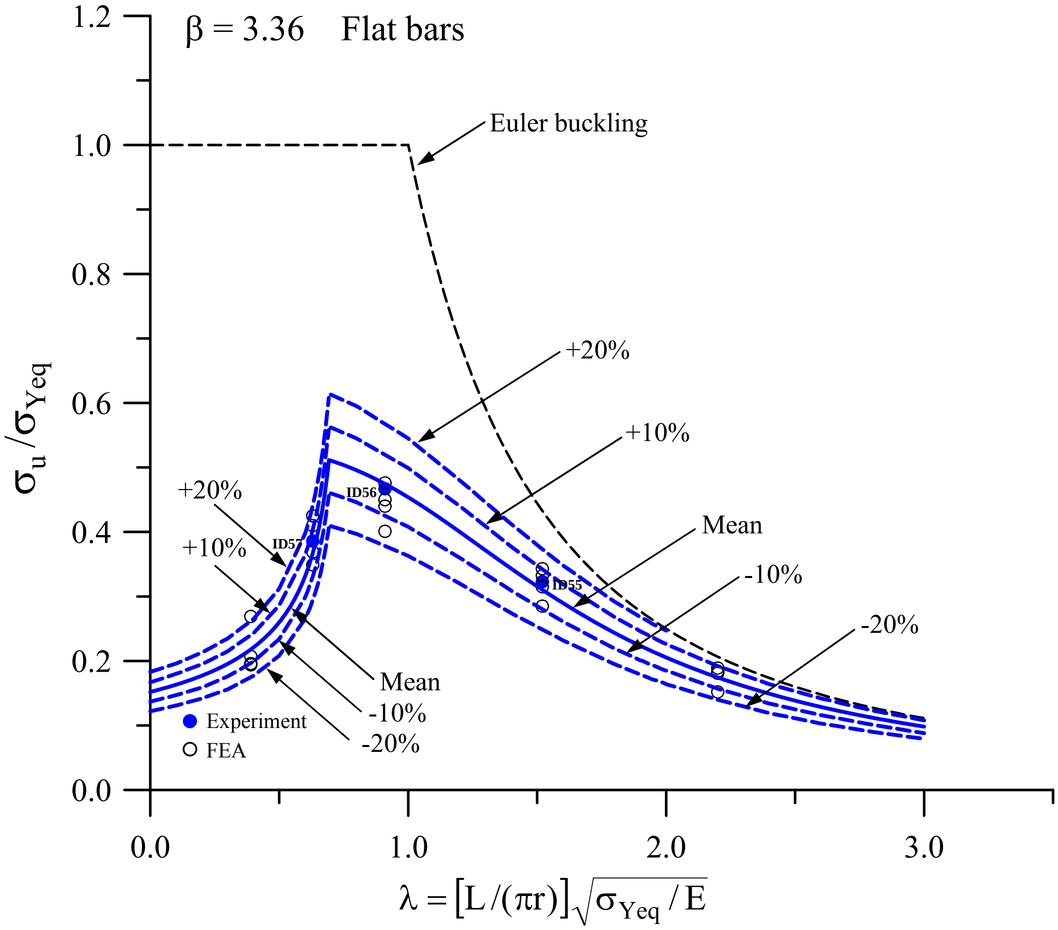

Figure 9.7(f) The aluminum stiffened panel ultimate strength variations with the deviations of $\pm 10\,\%$ and $\pm 20\,\%$, for flat bars, $\beta = 3.36$

References

Aalberg, A., Langseth, M. and Larsen, P.K. (2001). Stiffened aluminum panels subjected to axial compression. Thin-Walled Structures, Vol.39, No.10, pp.861-885.

ANSYS (2006). User's manual (version 10.0), ANSYS Inc., Canonsburg, Pennsylvania, USA.

Antoniou, A.C. (1980). On the maximum deflection of plating in newly built ships. Journal of Ship Research, Vol.24, No.1, pp.31-39.

Antoniou, A.C., Lavidas, M. and Karvounis, G. (1984). On the shape of post-welding deformations of plate panels in newly built ships. Journal of Ship Research, Vol.28, No.1, pp.1-10.

Bradfield, C.D. (1974). Analysis of measured distortions in steel box-girder bridges. Cambridge University Engineering Department, Report CUED/C-Struct/TR42.

Carlsen, C.A. and Czujko, J. (1978). The specification of post welding distortion tolerances for stiffened plates in compression. The Structural Engineer, Vol.56A, No.5, pp.133-141.

Clarke, J.D., Buckling of aluminum alloy stiffened plate ship structure, In: Aluminum structures – Advances, design and construction, Edited by R. Narayanan, Elsevier Applied Science, 1987, pp.81-92.

Clarke, J.D. and Swan, J.W., Interframe buckling of aluminum alloy stiffened plating, Admiralty Research Establishment Dunfermline, AMTE(S) R85104, October 1985.

Collette, M. (2005). Strength and reliability of aluminum stiffened panels. Ph.D. Thesis, University of Newcastle, Newcastle upon Tyne, UK.

Czujko, J. and Kmiecik, M. (1975). Post welding distortions of ship shell plating. Ship Research Institute Report No.4-5, Technical University of Szczecin, Poland.

Czujko, J. (1980). Probabilistic estimation of load carrying capacity of axially compressed plates with random post-welding distortions. The Norwegian Institute of Technology, The University of Trondheim, Norway.

DNV (2003). Rules for ships / high speed, light craft and naval surface craft. Det Norske Veritas, Oslo, Norway.

Ellis, L.G. (1977). A statistical appraisal of the measured deformations in several steel box girder bridge. Journal of Strain Analysis, Vol.12, No.2, pp.97-106.

EN 13195-1 (2002). Aluminum and aluminum alloys: wrought and cast products for marine applications (shipbuilding, marine and offshore). European Standard: French Standard, Association Francaise de Normalisation (AFNOR).

Faulkner, D. (1975). A review of effective plating for use in the analysis of stiffened plating in bending and compression. Journal of Ship Research, Vol.19, No.1, pp.1-17.

Hopperstad, O.S., Langseth, M. and Hanssen, L. (1998). Ultimate compressive strength of plate elements in aluminum: Correlation of finite element analyses and tests. Thin-Walled Structures, Vol. 29, pp.31-46.

Hopperstad, O.S., Langseth, M. and Tryland, T. (1999). Ultimate strength of aluminum alloy outstands in compression: experiments and simplified analyses. Thin-Walled Structures, Vol. 34, pp. 279-294.

Kmiecik, M (1970). The load carrying capacity of axially loaded longitudinally stiffened plates having initial deformation. Ship Research Institute Report No.R80, Technical University of Szczecin, Poland.

Kmiecik, M. (1971). Behavior of axially loaded simply supported long rectangular plates having initial deformations. SFI, Trondheim, Norway.

Kmiecik, M. (1981). Factors affecting the load-carrying capacity of plates. Ship Research Institute Report No.115, Technical University of Szczecin, Poland.

Kmiecik, M. (1986-1987). A review of fabrication distortion tolerances for ship plating in the light of the compressive strength of plates. Lloyd's Register Technical Association, London, Paper No.6.

Kmiecik, M., Jastrezebski, T. and Kuzniar, J. (1995). Statistics of ship plating distortions. Marine Structures, Vol.8, pp.119-132.

Kontoleon, M.J., Preftitsi, F.G. and Baniotopoulos, C.C. (2000). Butt-welded aluminum joints: a numerical study of the HAZ effect on the ultimate tension strength. The paramount role of joints into the reliable response of structures, Edited by C.C. Baniotopoulos and F. Wald, pp. 337-346.

Masubuchi, K. (1980). Analysis of welded structures – Residual stresses, distortion and their consequences. Pergamon Press, Oxford.

Matsuoka, K., Tanaka, Y. and Fujita, Y. (1998). Buckling strength of lightened aluminum hull structures. Proceedings of INALCO'98, International Conference on Aluminum Structural Design, Cambridge, UK, April 15-17.

Mofflin, D.S. (1983). Plate buckling in steel and aluminum. Ph.D. Thesis, University of Cambridge, Cambridge, UK.

Mofflin, D.S. and Dwight, J.B. (1984). Buckling of aluminum plates in compression. In: Behavior of Thin-Walled Structures, Elsevier, pp.399-427.

Paik, J.K. and Thayamballi, A.K. (2003). Ultimate limit state design of steel-plated structures. John Wiley & Sons, Chichester, UK.

Paik, J.K. and Thayamballi, A.K. (2007). Ship-shaped offshore installations: Design, building, and operation. Cambridge University Press, Cambridge, UK.

Paik, J.K., Thayamballi, A.K. and Lee, J.M. (2004). Effect of initial deflection shape on the ultimate strength behavior of welded steel plates under biaxial compressive loads. Journal of Ship Research, Vol.48, No.1, pp.45-60.

Paik, J.K. and Duran, A. (2004). Ultimate strength of aluminum plates and stiffened panels for marine applications. Marine Technology, Vol. 41, No. 3, pp. 108-121.

Paik, J.K., Hughes, O.F., Hess, P.E. and Renaud, C. (2005). Ultimate limit state design technology for aluminum multi-hull ship structures. SNAME Transactions, Vol. 113, pp.270-305.

Raynaud, G.M. (1995). New aluminum products for high speed light crafts. Building High-speed Aluminum Marine Vessels in Victoria – A Feasibility Study, Business Victoria, Melbourne, Australia.

Smith, C.S. and Dow, R.S. (1984). Effects of localized imperfections on compressive strength of long rectangular plates. Journal of Constructional Steel Research, Vol.4, pp.51-76.

Smith, C.S., Davidson, P.C., Chapman, J.C. and Dowling, P.J. (1988). Strength and stiffness of ships' plating under in-plane compression and tension, RINA Transactions, Vol. 130, pp. 277-296.

Somerville, W.L., Swan, J.W. and Clarke, J.D. (1977). Measurement of residual stresses and distortions in stiffened panels. Journal of Strain Analysis, Vol.12, No.2, pp.107-116.

Timoshenko, S.P. and Gere, J.M. (1961). Theory of elastic stability. McGraw-Hill, New York.

Timoshenko, S.P. and Woinowsky-Krieger, S. (1981). Theory of plates and shells. McGraw-Hill, New York.

Tanaka, Y. and Matsuoka, K. (1997). Buckling strength of lightened aluminum hull structures. Proceedings of the 7th International Offshore and Polar Engineering Conference, Vol.4, Honolulu, pp.790-797.

Ueda, Y. and Yao, T. (1985). The influence of complex initial deflection modes on the behavior and ultimate strength of rectangular plates in compression. Journal of Constructional Steel Research, Vol.5, pp.265-302.

Zha, Y., Moan, T. and Hanken, E. (2000). Experimental and numerical studies of torsional buckling of stiffener in aluminum panels. Proceedings of the 8th International Offshore and Polar Engineering Conference, Seattle, pp.249-255.

Zha, Y. and Moan, T. (2001). Ultimate strength of stiffened aluminum panels with predominantly torsional failure modes. Thin-Walled Structures, Vol.39, No.8, pp.631-648.

Zha, Y. and Moan, T. (2003). Experimental and numerical collapse prediction of flatbar stiffeners in aluminum panels. Journal of Structural Engineering, Vol.129, No.2, pp.160-168.

PROJECT TECHNICAL COMMITTEE MEMBERS

The following persons were members of the committee that represented the Ship Structure Committee to the Contractor as resident subject matter experts. As such they performed technical review of the initial proposals to select the contractor, advised the contractor in cognizant matters pertaining to the contract of which the agencies were aware, performed technical review of the work in progress and edited the final report.

Chairman	**H. Paul Cojeen,**	**US Coast Guard**
Executive Director Ship Structure Committee:	**LCDR Jason E. Smith,**	**US Coast Guard**

Members

Paul Hess	Naval Surface Warfare Center Carderock Division (NSWCCD)
Paul Franklin	Bath Iron Works (BIW)
Rune Iverson	Herbert Engineering Consultants
George Wang	American Bureau of Shipping (ABS)
Christina Wang	American Bureau of Shipping (ABS)
Bill Caliendo	U.S. Merchant Marine Academy (USMMA)
William Mish	MR Rosenblatt & Son, AMSEC
Matt Collette	SAIC
Choo Yoo Sang	Singapore National University
Alfred Tunik	U.S. Coast Guard Electronic Logistic Center (ELC)
Ying Mei	Herbert Engineering Consultant
Paul Frieze	Paul A. Frieze & Associates
Sean Brady	U.S. Coast Guard Marine Safety Center (USCG MSC)
Debu Ghosh	U.S. Coast Guard Electronic Logistic Center (ELC)
James Kent	U.S. Navy Military Sealift Command (MSC)
Mike Simbulan	U.S. Coast Guard (HQ)
Al Brown	Virginia Tech University
Jaideep Sirkar	U.S. Coast Guard (HQ)

Ship Structure Committee Liaison Members

Liaison Members

American Society of Naval Engineers	Captain Dennis K. Kruse (USN Ret.)
Bath Iron Works	Mr. Steve Tarpy
Colorado School of Mines	Dr. Stephen Liu
Edison Welding Institute	Mr. Rich Green
International Maritime Organization	Mr. Igor Ponomarev
Int'l Ship and Offshore Structure Congress	Dr. Alaa Mansour
INTERTANKO	Mr. Dragos Rauta
Massachusetts Institute of Technology	
Memorial University of Newfoundland	Dr. M. R. Haddara
National Cargo Bureau	Captain Jim McNamara
National Transportation Safety Board - OMS	Dr. Jack Spencer
Office of Naval Research	Dr. Yapa Rajapaksie
Oil Companies International Maritime Forum	Mr. Phillip Murphy
Samsung Heavy Industries, Inc.	Dr. Satish Kumar
United States Coast Guard Academy	Commander Kurt Colella
United States Merchant Marine Academy	William Caliendo / Peter Web
United States Naval Academy	Dr. Ramswar Bhattacharyya
University of British Columbia	Dr. S. Calisal
University of California Berkeley	Dr. Robert Bea
Univ. of Houston - Composites Eng & Appl.	
University of Maryland	Dr. Bilal Ayyub
University of Michigan	Dr. Michael Bernitsas
Virginia Polytechnic and State Institute	Dr. Alan Brown
Webb Institute	Prof. Roger Compton

RECENT SHIP STRUCTURE COMMITTEE PUBLICATIONS

Ship Structure Committee Publications on the Web - All reports from SSC 1 to current are available to be downloaded from the Ship Structure Committee Web Site at URL: http://www.shipstructure.org
SSC 445 – SSC 393 are available on the SSC CD-ROM Library. Visit the National Technical Information Service (NTIS) Web Site for ordering hard copies of all SSC research reports at URL: http://www.ntis.gov

SSC Report Number	Report Bibliography
SSC 450	Ship Structure Committee: Effectiveness Survey, Buck R. Phillips, M.L., Jones L.M, Jr. 2007
SSC 449	Hydrodynamic Pressures and Impact Loads for High Speed Catamaran/SES, Vorus. W 2007
SSC 448	Fracture Mechanics Characterization of Aluminum Alloys for Marine Structural Applications, Donald J.K., Blair A. 2007
SSC 447	Fatigue and Fracture Behavior of Fusion and Friction Stir Welded Aluminum Components, Kramer R. 2007
SSC 446	Comparative Study of Naval and Commercial Ship Structure Design Standards, Kendrick, A., Daley C. 2007
SSC 445	Structural Survivability of Modern Liners, Iversen R. 2005
SSC 444	In-Service Non-Destructive Estimation of the Remaining Fatigue Life of Welded Joints, Dexter R.J., Swanson K.M., Shield C.K. 2005
SSC 443	Design Guidelines for Doubler Plate Repairs on Ship Structures Sensharma P.K., Dinovitzer A., Traynham Y. 2005
SSC 442	Labor-Saving Passive Fire Protection Systems For Aluminum And Composite Construction E. Greene, 2005
SSC 441	Fire Degradation, Failure Prediction And Qualification Methods For Fiber Composites R. Asaro, M. Dao, 2005
SSC 440	Deterioration of Structural Integrity Due to Chemical Treatment of Ballast Water S. Tiku, 2005